



12th International Conference
Tunnel Safety and Ventilation

ITnA-Reports

Volume 107 | April 16-17, 2024

Series Editor: Helmut Eichlseder

Editor: Michael Bacher

12th International Conference
TUNNEL SAFETY AND VENTILATION

April 16 – 17, 2024

Graz, Austria

ITnA-Reports, Vol. 107

Reports of the Institute of Thermodynamics
and Sustainable Propulsion Systems

Series Editor Univ.-Prof. Dr. Helmut Eichlseder

Editor Dr. Michael Bacher
Cover Verlag der Technischen Universität Graz
Cover pictures
(left to right) 1. Chalabala / Adobe Stock
 2. Helmut Lunghammer
 3. ITnA / TU Graz
 4. Helmut Lunghammer
 5. ÖBB / isochrom
 6. (center) Sakarin Sawasdinaka / Shutterstock.com
Print Haltmeyer.at

2024 Verlag der Technischen Universität Graz
www.tugraz-verlag.at

Print:

ISBN 978-3-85125-996-4

E-Book:

ISBN 978-3-85125-997-1

DOI 10.3217/978-3-85125-996-4



This work is licensed under the Creative Commons
Attribution-NonCommercial 4.0 International (CC BY-NC 4.0) license.

<https://creativecommons.org/licenses/by-nc/4.0/>

This CC license does not apply to the cover, third party material
(attributed to other sources) and content noted otherwise.

SCIENTIFIC COMMITTEE

The Scientific Committee consists of leading experts in tunnel ventilation and safety from around the world, ensuring the highest level of scientific quality.



Rune Brandt, CH



Ignacio Del Rey, ES



Arnold Dix, AU



Norris Harvey, US



Haukur Ingason, SE



Ingo Kaundinya, DE



Bernhard Kohl, AT



René List, AT



Antoine Mos, FR



Günter Rattei, AT



Conrad Stacey, AU



Alan Vardy, UK



Frédéric Waymel, FR



Sonja Wiesholzer, AT

ORGANIZING COMMITTEE

The Organizing Committee is endeavoring to provide an interesting and inspiring conference.

Michael Bacher
Patrik Föbtleitner
Elisabeth Holler
Sabine Minarik

PREFACE

Dear Ladies and Gentlemen,

the proceedings present the papers from the 12th International Conference on Tunnel Safety and Ventilation, which took place in Graz on April 16-17, 2024.

This conference was initiated by Peter Sturm more than 20 years ago and over the years has established itself as an important meeting place to provide a forum for information exchange among operators, users, technicians, scientists and companies involved in the design, construction and equipping of road and railway tunnels and highlights the need for ongoing global research and discussion on these important issues.

The papers in the proceedings provide new and interesting insights into various important aspects of tunnel safety and tunnel ventilation, thus contributing to a positive and sustainable global development in this sector.

During the conference, participants discuss a number of different topics, including railway and road tunnels, alternative propulsion systems, sustainable energy use, tunnel refurbishment, risk analysis, system testing and ventilation.

In today's rapidly changing world, the importance of these issues cannot be overstated. Tunnels and underground infrastructure play an important role in transportation and support economic growth and societal well-being. Therefore, innovation and collaboration are essential to ensure their resilience and sustainability. The knowledge in these proceedings reflects the expertise and commitment of researchers, engineers, policy makers and industry experts. Together, we aim to tackle current challenges and pave the way for safer and more efficient tunnel infrastructure.

The technical visit consists of a tour to the new railway station Wettsmannstätten and the Koralmtunnel, including its ventilation building and a typical technical cross-passage. These facilities show how impressive the safety equipment of railway tunnels can be. In this context, we would like to thank the Austrian Federal Railways (ÖBB) in particular for their support.

We also wish to express our gratitude to our Scientific Committee for its valuable work. We would also like to thank the authors for their hard work in preparing abstracts, papers, and of course their presentations.

Finally, we would like to thank all those who worked tirelessly behind the scenes to ensure that this conference ran smoothly, enjoyable, and effectively for all participants.

Michael Bacher and Organizing Committee

ACKNOWLEDGEMENT



We would like to take this opportunity to express our special thanks to **Peter-Johann Sturm!**

Peter took his well-deserved retirement on October 1, 2023, but he will continue to be available to us with his expertise.

With the International Conference on Tunnel Safety and Ventilation, Peter established an important platform for knowledge transfer between researchers and industry.

Peter embodies the spirit of this event for many participants who have been attending our conference for years and decades as speakers, panellists or exhibitors.

His long-term presence and commitment make him a symbol of the continuity and excellence that characterise our conference.

Thanks to his expertise and passion, Peter has contributed immensely to the success and importance of this event. His name will be intrinsically tied to the success and history of the conference.

Michael Bacher, Helmut Eichlseder

TABLE OF CONTENTS

TUNNEL SAFETY AND VENTILATION
Graz, May 16–17, 2024

Preface

Keynote Speakers

The 33 KM Long Koralm Tunnel – Final Challenges in the Implementation of a Major Project **1**

Klaus Schneider, Helmut Steiner
Austrian Federal Railways, AT

Current Status of the Semmering Base Tunnel **10**

Gerhard Gobiet, Thomas Thaller
Austrian Federal Railways, AT

Tunnel Renovation Program AUSTRIA - Next Level **19**

Andreas Fromm, René List
ASFINAG Bau Management GmbH, AT

Session S1: Energy & Sustainability

Sustainable Energy Consumption **23**

Benjamin Riedl, Johannes Bösl, Ersin Gündogdu
ILF Consulting Engineers Austria GmbH, AT

Energylabel & Ecodesign for Austrian Roadtunnel **31**

Mario Patigler
ASFINAG Bau Management GmbH, AT

Sustainable Tunnel Operation Generation of Electricity Through Thermal and Pressure-Driven Airflows **40**

¹Peter Sturm, ²Dietmar Harbauer, ³Roland Seebacher, ¹Daniel Fruhwirt,
³Klaus Krischan

¹Graz University of Technology, Institute of Thermodynamics and Sustainable Propulsion Systems, AT

²ASFINAG, AT

³Graz University of Technology, Institute of Electric Devices and Machines, AT

Validation of Simplified Variable Speed Control for Road Tunnel Jet Fans **51**

¹Kaito Onoda, ¹Ryoichi Ishizawa, ²Keigo Hatamoto, ³Hibiki Sako,

³Toshiaki Sakaguchi, ⁴Alan Vardy

¹Hanshin Expressway Co., Ltd, JP

²Hanshin Expressway Research Institute for Advanced Technology, JP
Sohatsu Systems Laboratory Inc., JP

⁴University of Dundee, Dundee, Scotland, GB

Session G1: Evacuation

Influence of Acoustic Tunnel Monitoring AKUT on Tunnel Safety	60
¹ <u>Katharina Hoyer</u> , ¹ Regina Schmidt, ¹ Harald Kammerer, ² Franz Graf, ³ Mark Dobrounig, ³ Thomas Kalina ¹ ILF Consulting Engineers, AT ² Joanneum Research, AT ³ ASFINAG, AT	
Evacuation Safety and Human Emotional Responses in Smoke-Filled Tunnels for Machine Learning Insights	69
<u>Miho Seike</u> , Wenhao Li, Akimasa Fujiwara, Makoto Chikaraishi Hiroshima University, JP	
A 3D Parametric Study To Assess the Impact of a Fixed Fire Fighting System on the Evacuation Conditions in Paris La Défense Road Tunnels	77
<u>Nicolas Bourlet</u> , Adrien Host, Florent Jaffier, Florent Guiral, Frederic Waymel EGIS, FR	
Enhancing Evacuation Strategies: A Multifaceted Approach Using Real Time Cognitive Assessment	85
^{1,2} <u>Perez-Jimenez, Christian</u> , ¹ Gary Clark, ¹ Aslan Singh, ³ Martyn Cole, ³ Richard Smith ¹ AtkinsRealis, GB ² Hot Smoke Machines & Demonstrations (HSM) Ltd, GB ³ Heathrow Airport Limited, GB	
Session S2: Railway Systems	
Evaluation of Trackway Ventilation System for the New Metro Line in Singapore	94
<u>Jessleen Chua</u> , Gerald Louis, Linfan Cai, Ernest Poon, Hadi Wijaya, Melvyn Thong Land Transport Authority, SG	
Condensation in Below Ground Metro Stations	104
<u>Paul Jolley</u> , Mark Gilbey, Robert Jones WSP UK Ltd, GB	
Metro Ventilation System in Seismic Areas	112
^{1,2} Romano Borchiellini, ^{1,2} Davide Papurello, ³ <u>Carlo Barbetta</u> ¹ Energy Center, Via Borsellino 38/18, Politecnico di Torino, IT ² Dept. of Energy Galileo Ferraris, Politecnico di Torino, IT ³ Systemair GmbH, Germany/Systemair Srl, IT	
Experiences From Five Years of PM Monitoring in Railway Tunnels of Austrian Federal Railways (ÖBB)	124
¹ <u>Daniel Fruhwirt</u> , ¹ Michael Bacher, ² Helmut Steiner ¹ Graz University of Technology, AT ² Austrian Federal Railways, AT	

Session G2: Commissioning

Rehabilitation of Boston Harbor Tunnel – The “Quarter Duct” Solution 133

^{1,2}Conrad Stacey, ¹Michael Beyer

¹Stacey Agnew Pty Ltd, AU

²Delve Stacey Agnew LLC, US

Commissioning of Tunnels 141

Tor Tybring Aralt

Multiconsult Norge AS, NO

Enhancing Tunnel Fan Reliability Through Advanced Factory Acceptance Test (AFAT) to Prevent Failures 150

¹Justo Suarez, ²Jye Teoh, ³Albert Bach-Esteve

¹S&P-KRUGER Underground Ventilation Division, ES

²KRUGER ASIA Ventilation Group, TH

³SOLER & PALAU Ventilation Group, ES

Advances in the Digital Documentation of Railway Tunnel Inspection 158

¹Matthias J. Rebhan, ²Stefan S. Grubinger, ²Andreas Schüppel,

³Simona Deutinger, ³Gernot Schwarzenberger

¹Graz University of Technology, Institute of Soil Mechanics,
Foundation Engineering and Computational Geotechnics, AT

²recordIT GmbH, AT

³ÖBB Infrastruktur AG, AT

Session S3: Alternative Propulsion Systems

Safety Challenges in an Underground Hyperloop System: A Preliminary Investigation 167

¹Matteo Pachera, ²Maarten Vanneste, ²Thijs Verrecas, ³Bartek Kulig

¹Sweco, BE

²Denys, BE

³Hard-T, NL

Widespread of Electric Vehicles and the Provision of Knowledge About Fire Accidents for Expressway Maintenance Workers in Japan 174

¹Masahiro YOKOTA, ¹Ken-ichiro YAMAZAKI, ²Tetsuya YAMAZAKI,

²Chihiro SGAWARA, ²Toshio SUZUKI

¹Central Nippon Highway Engineering Tokyo Company Limited, JP

²Nippon Expressway Research Institute Company Limited, JP

Preliminary Tests of Mechanical Abuse - Nail Tests of LIBs 183

^{1,3}Papurello Davide, ¹Braghiroli Beatrice, ^{2,3}Bodoardo Silvia, ^{2,3}Amici Julia,

^{1,3}Borchiellini Romano

¹Department of Energy (DENERG), Politecnico di Torino, IT

²Department of Applied Science and Technology (DISAT), Politecnico di Torino, IT

³Energy Center, Politecnico di Torino, IT

Session G3: Simulation

Particle Concentration Levels in a Subway Station - The Effects of Various Locations and Diameters of Relief Shafts in Tunnels 191

Omid Abouali, Erik Östblom, Per Sahlin
Equa Simulation AB, SE

Emission Management in Railway Tunnels With a 1D-3D Simulation Approach 199

¹Evangelos Antoniou, ²Arnaud Colleoni, ³Tom Linden, ¹Francesco Cuzzola
¹Dassault Systèmes Deutschland GmbH, 81541 Munich, DE
²Dassault Systèmes SE, 31770 Colomiers, FR
³Dassault Systèmes AB, 41756 Goteborg Lindholmen, SE

Application of ARTU Software and Multizone Fire Modelling for Risk Analysis: A Road Tunnel Case Study 207

Michele Fronterre, Rugiada Scozzari
Cantene srl, IT

Session S4: Mining & Artificial Intelligence

AI in Roadtunnel – Supporting the Man-In-The-Loop in Roadtunnel (SMaRT) 217

¹Philipp Böhnke, ²Tom Schumann, ²Dirk Kemper, ²Alvaro García Hernandez
¹ave Verkehrs- und Informationstechnik GmbH, DE
²RWTH Aachen University, Lehrstuhl und Institut für Straßenwesen (ISAC), DE

Application of AI to the 1D Ventilation Analysis of a 43KM Complex Road Tunnel Network: Madrid Calle30 225

¹Juan Manuel Sanz, ²Fabián De Kluijver, ²Alberto López, ³Javier Berges,
³Mar Martinez, ¹Guillem Peris
¹Sener, ES
²JVVA, ES
³Madrid Calle 30, ES

Estimating the Seasonal Performance of a Surface Refrigeration Cooling Plant for an Underground Mine 238

¹Jolyon Thompson, ¹Mark Gilbey, ²Hugo Dello Sbarba
¹WSP, GB
²Dello Ventilation, CA

Design of a Ventilation System in a Tunnel Bored With a TBM machine in the Case of Methane Emission From a Rock Mass 246

Marek Borowski, Klaudia Zwolińska-Gładys, Andrzej Szmuk, Zbigniew Kuczera,
Kamil Piech
AGH University of Krakow, PL

Session G4: Risk Analysis

Risk Analysis of Road Tunnels: A Quantitative Risk Analysis Model for Assessing the Effects of Fire **255**

¹Razieh Khaksari Haddad, ²Zambri Harun

¹London Bridge Associates Ltd., GB

²Department of Mechanical and Manufacturing Engineering, Faculty of Engineering & Built Environment, UKM, MY

Some Questions Related to CFD Modeling of Pressurized Tank Burst in Road Tunnels **267**

¹Guillaume Lecocq, ¹Laure Heudier, ¹Benjamin Truchot, ²Antoine Mos,

²Christophe Willmann

¹INERIS, FR

²CETU, FR

Integration of New Energy Carriers in French Specific Hazard Investigations: Overview of Principal Issues **275**

Christophe Willmann, Pauline Charles
CETU, French tunnel study centre, FR

Innovative Approach To Improve the Safety of Tunnels and Tunnel Control Centres **283**

¹Harald Kammerer, ²Anne Lehan, ¹Bernhard Klampfer

¹ILF Consulting Engineers Austria GmbH, AT

²Federal Highway Research Institute, DE

Session S5: CFD Simulation

CFD-assisted Flow Rate Measurements in Ventilation Ducts of long Road Tunnels **291**

¹Diego Angeli, ²Paolo Levoni, ¹Elisabetta Salerno, ³Gioivanni Sebastiano Barozzi,

⁴Paolo Verraz, ⁴Cedric Petitcolin

¹DISMI – University of Modena and Reggio Emilia, IT

²mimesis s.r.l., Modena, IT

³DIEF – University of Modena and Reggio Emilia, IT

⁴TMB-GEIE, Courmayeur (AO), Italy and Chamonix, FR

Jet Fan Installation Factor Correlations for Conventional Jet Fans and Mojets **299**

¹Fathi Tarada, ¹Pier Bertacche, ²Luca Stantero

¹Mosen Ltd, GB

²Risk Design Engineering SRL, IT

CFD Investigation of the Improvement of Smoke Control in a Tunnel Equipped With a Longitudinal and a Transverse Ventilation System **308**

¹Gabriel Remion, ¹Antoine Mos, ²Pietro Salizzoni, ²Massimo Marro,

²Stefano Lanzini

¹Center for Tunnel Studies (CETU), FR

²Laboratoire de Mécanique des Fluides et Acoustique (LMFA), FR

An Analysis of the 3D Critical Region Length in Longitudinally Ventilated Tunnels During Fire Events	316
^{1,2} Ayala, Pablo, ² Amo, Luis, ^{1,2} Cantizano Alexis	
¹ Institute for Research in Technology, ICAI, Comillas Pontifical University, ES	
² ICAI School of Engineering, Comillas Pontifical University, ES	

Session G5: Tunnel Ventilation

Longitudinal Ventilation System for a Long Road-Tunnel: Optimal Design With Batteries of Jet Fans and Challenges To Overcome Extreme Foggy Weather Condition	326
Sunit Kanti Dhar	
Freelance Consulting Engineer -Tunnel Ventilation & Fire Safety and E&M Services, IN	

Advanced Characterisation of a Fan Submitted to Piston Effect	335
¹ Elisa Béraud, ¹ Benoit Houseaux, ² Sydney Tekam	
¹ Eiffage Énergie Systèmes, Ventilation of tunnel & underground spaces, FR	
² Tech'am Ingenierie, FR	

Optimizing Safety in Short High-Slope Road Tunnels: Smoke Propagation and Ventilation System Response	344
¹ Krešimir Ivanek, ² Robert Keser, ¹ Miodrag Drakulić, ³ Željko Špiljar	
¹ CTP PROJEKT d.o.o., Zagreb, HR	
² IN SILICO d.o.o., Zagreb, HR	
³ INVENTO VENTILACIJA d.o.o., Zagreb, HR	

How Information Security Can Be Ensured in Tunnel Systems	352
Gerhard Hudecek	
ASFINAG Maut Service GmbH, AT	

Session S6: Tunnel Ventilation

One-Dimensional Critical Velocity Formulation – An Assessment of the Deficiency of the Current Models and the Introduction of a New Concept	358
J. Greg Sanchez	
TYLin International, US	

Confinement Velocity for Smoke in Tunnels – How to Poke a Stick at it	367
¹ Michael Beyer, ^{1,2} Conrad Stacey	
¹ Stacey Agnew Pty Ltd, AU	
² Delve Stacey Agnew LLC, US	

Design, Refurbishment and Operation of the Ventilation in the Road Tunnel Complex in Prague	384
Jiří Zápařka, Jan Pořízek, Ludvík Šajtar	
Satra spol. s r. o., CZ	

Session S7: Closing Session

Hydrogen Powered Vehicles in a Tunnel Incident – Risks and Consequences	391
¹ Martin Aggarwal, ² Daniel Fruhwirt, ³ Patrik Föbleitner, ⁴ Oliver Heger, ¹ Patrick Pertl, ⁴ Regina Schmidt, ¹ Alexander Trattner ¹ HyCentA Research Ltd., AT ² Graz University of Technology, AT ³ FVT Ltd., AT ⁴ ILF Consulting Engineers, AT	
LeanTech in Road Tunnels	406
¹ Simon Frey, ¹ Rune Brandt, ² Jean-Paul Schnetz ¹ HBI Haerter AG, CH ² jps-conseils, CH	
Looking to the Future From PIARC's Perspective	414
Ingo Kaundinya Federal Highway Research Institute (BASt), Chairman of PIARC TC 4.4 Tunnels, DE	
Reports of the Institute of Thermodynamics and Sustainable Propulsion Systems	421

THE 33 KM LONG KORALM TUNNEL – FINAL CHALLENGES IN THE IMPLEMENTATION OF A MAJOR PROJECT

Klaus Schneider, Helmut Steiner
Austrian Federal Railways, AT

DOI 10.3217/978-3-85125-996-4-01 (CC BY-NC 4.0)

This CC license does not apply to third party material and content noted otherwise.

ABSTRACT

The Koralm railway is a double-track, electrified new railway section between the Austrian provincial capitals of Graz in Styria and Klagenfurt in Carinthia. The maximum operational speed is 250 km/h. The length is about 130 km and its centerpiece, the twin-tube Koralm Tunnel, is around 32.9 km long.

The tunnel construction work began in 2008 and ended with the final tunnel breakthrough in 2020. The railway equipment work began in 2019 and should be completed by the end of 2024. Commissioning will take place in 2025, and regular passenger traffic will begin at the end of that year.

Keywords: Koralm Bahn, Koralm Tunnel, railway tunnel, Trans European Network, Baltic Adriatic rail corridor

1. INTRODUCTION

The so called ‘southern corridor’, which includes the Koralm railway (*Koralmbahn*, “KAB”), is part of the 1’800 km long Baltic–Adriatic rail corridor of the Trans European Network – Transport (TEN–T). It represents the eastern transalpine north-south link and connects the ports and regions in the north (Baltic Sea, Baltic region, Poland) with Central Europe and the ports and regions in the upper Adriatic area [7].

The KAB, with a length of about 130 km, connects the Austrian federal regions Styria and Carinthia, and their capital cities Graz and Klagenfurt. The key element of this new route is the Koralm Tunnel (“KAT”) with a length of 32.9 km and a maximum rock overlying of about 1’200 m. The two single-track rail tunnels are connected via cross-passages every 500 m. These serve as escape routes and also contain the necessary equipment for tunnel operation. An emergency station, approximately 1 km in length, is located between the two tubes near the center of the tunnel. An emergency station, approximately 1 km in length, is located between the two tubes near the center of the tunnel.

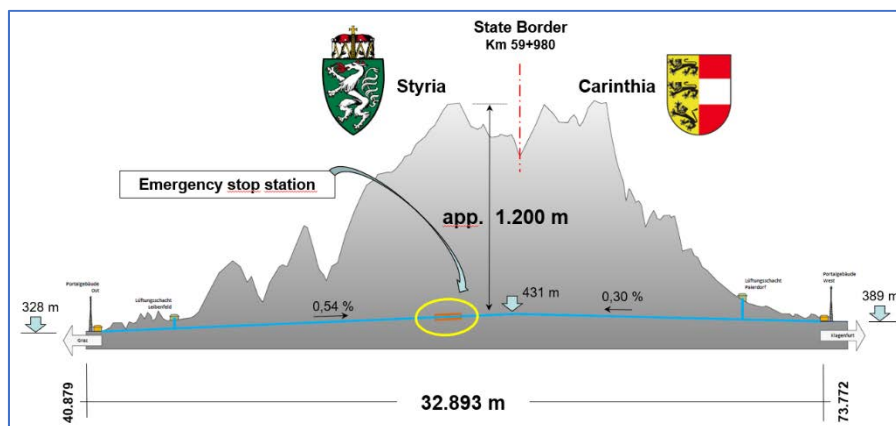


Figure 1: Koralm Tunnel overview – longitudinal cut

2. PROJECT HISTORY – PROJEKT STATUS

2.1. Introduction

Project planning for the KAB began in 1995. From 1997 onwards, the focus was on finding the route and conducting necessary investigations and preliminary studies. Dialogue with stakeholders in the regions was also carried out, and a consensus was reached. Based on this agreement, the necessary official procedures (environmental impact assessment, railway construction permit and numerous other relevant laws) were carried out in the following years. From 2000 to 2007, positive building permits were obtained step by step and in small increments. Construction work began immediately after each building permit was issued. The first new construction section, which serves as a connection to the KAT in Styria, could be put into operation for regional traffic as early as 2010 as a result of this procedure. The structural work will be completed in the following 14 years between 2008 and 2022. The first breakthrough between the east (KAT2) and west (KAT3) sections will take place in the south tube in 2018 and the final breakthrough on June 17, 2020.



Figure 2: Koralm Tunnel – final breakthrough June 17, 2020

This means that 18 years have passed between the first exploratory work in 2002, the start of construction of the three main construction lots KAT1 (2008), KAT2 (2011) and KAT3 (2013) and the final tunnel breakthrough in 2020. Until the planned commissioning in 2025, only 5 years, i.e. one fifth of the previous years, are available for the implementation of the railway equipment [11].

2.2. Railway Technical Equipment

Work on the railway equipment began in 2020, parallel to the ongoing construction. The first step was the construction of the slab track. Prior to or simultaneously with this, 13'000 elastically supported track slabs were produced for the KAT in Lower Austria (NÖ) and transported directly to the KAT in Styria by unit train, where they were laid, set and filled with self-compacting concrete (SCC).



Figure 3: Track support plates transshipment from road to rail / MABA in NÖ, October 2021

After completion of the roadway, the verges and sideways to the left and right of it, as well as all associated cable routes and shafts, were subsequently erected or concreted.



Figure 4: Koralm Tunnel – intermediate state of construction, December 2021

All subsequent activities, such as the transportation of further materials and equipment, as well as the transportation of people, could then only be carried out on rails. The cross passages are equipped with power supply systems, telecom systems, and telecontrol technology to transmit all data to the ÖBB control centers. In this setting, it is also necessary to install a large number of mechanical systems to protect the technical equipment from pressure peaks caused by fast moving trains in the track tubes and to remove the heat losses generated during operation.



Figure 5: Koralm Tunnel emergency station – intermediate state of construction, January 2024

As the KAT is ventilated by ventilation buildings and shafts located near the portal, both in the event of an incident and during maintenance operations, buildings had to be constructed on the surface in parallel with the work in the tunnel. Each building contains two axial fans for overpressure ventilation of the tunnel system.



Figure 6: Koralm Tunnel – West Paierdorf ventilation building, November 2023

Step by step, the entire tunnel is being brought to life and more and more usable and controllable content is being added to ensure reliable rail operations at the time of planned commissioning.

2.3. Logistics

Unlike tunnel construction, the equipment installation phase involves a large number of different trades and professions working simultaneously, either in a very confined space or widely distributed throughout the tunnel, to carry out the installations in the two tubes, the 70 cross-passages and the emergency station. The targeted and timely transportation of materials, starting with the receipt of materials on the construction site installation area, the onward transportation to the various installation points in the tunnel, in combination with the scheduling of useful work steps and processes with each specialist, requires forward-looking and detailed logistics planning across all trades. By continuously monitoring performance against targets, it is possible to quickly implement countermeasures and achieve the performance targets outlined in the construction contract.

The access options for the tunnel are only available through the KAT East and West portals. This presents a logistical challenge for transporting materials and staff. Other tunnel projects, such as the Löttschberg, Gotthard, Semmering, or Brenner base tunnels, have utilized intermediate accesses to create shorter and more accessible equipment sections.

2.4. Commissioning

A fully equipped and functional tunnel integrated into the ÖBB control systems should be available by the end of 2024 / beginning of 2025. The start of measurement runs, test runs and high-speed runs is planned for the beginning of April 2025, which should be successfully completed by summer 2025. In this context, it is important not to forget the "little things" such as the training (local and route knowledge) of more than 1,000 train drivers, dispatchers, emergency and safety personnel as well as future maintenance and repair personnel in this final and all-important phase.

After completing all sub-processes, the Ministry of Climate Action, Environment, Energy, Mobility, Innovation and Technology (BMK) should have all necessary documents, so that a positive operating permit for the KAT and the KAB can be issued in the fall of 2025.

2.5. Project Costs

Effective project management (including risk management and cost management) involves forming appropriate working groups at different decision-making levels to quickly and efficiently respond to changes. So far, KAB has been able to achieve a good balance between continuous change and cost-effective decisions, which is reflected in the fact that project costs have remained stable over the years. This level of stability has been achieved through consistent and continuous tracking of all cost components, ongoing consideration of all project risks, and prior value adjustment. The first cost estimates based on stable route planning were drawn up between 2004 and 2007. Up to one year ago, KAB's costs were kept at the internationally unique and unrivaled level of plus 1 %. Due to the pandemic and unforeseeable inflationary developments, the required project budget for KAB increased from € 5.4 billion to around € 5.6 billion (a 4 % increase). KAT's share of this is approximately 50 %, or € 2.8 billion.

3. SPECIAL PROJECT CHALLENGES AND INNOVATIONS

3.1. Introduction

Projects of this size present numerous challenges, particularly due to their long project duration of 20, 30, or more years. During these periods, laws, guidelines, standards, and the associated engineering and design approaches change. Moreover, the extended project environment can bring global changes in boundary conditions and project objectives, as well as fundamental changes in technology. In addition, it is important to consider the long-term foresight and future visions associated with these projects, spanning 50, 100, or even 150 years. From 1995 to 2024, the Koralm Railway has successfully maintained a balance between all these ongoing changes. This was achieved through the formation of working groups at various decision-making levels.

Some specific challenges will be discussed in more detail below.

3.2. Pressure Loads on Facilities in the Tunnel

The pressure loads in a railway tunnel caused by the continuous operation of the high-speed trains are a great challenge. Due to intensive fundamental research, useful design approaches

have been found, which are now consistently applied to the dimensioning of various objects installed in the tunnel cross-section [3, 9, 10].

In this context, the tunnel doors should be mentioned in particular, as they play a crucial role in many ways. In case of an escape, the emergency exits should be easy to use and reliable. They also serve as a fire compartment between the tunnel and the cross-passage (safe area) and must remain fully functioning for a long period of time (30 to 50 years) with low maintenance and service requirements. In order to verify these requirements, load tests were performed using a servo-hydraulically controlled loading device with 1.5 million load cycles [8].



Figure 7: Emergency exit doors Koralmbahn – load tests in Vienna, March / July 2020

After considering all the advantages and disadvantages, it was decided to use sliding doors as emergency exit doors in all KAB tunnel sections [1, 13].

3.3. Fire Resistance

Tunnel doors often serve as fire barriers. To ensure technical feasibility, numerical CFD simulations were used to calculate potential temperatures and their time profile in the event of an incident.

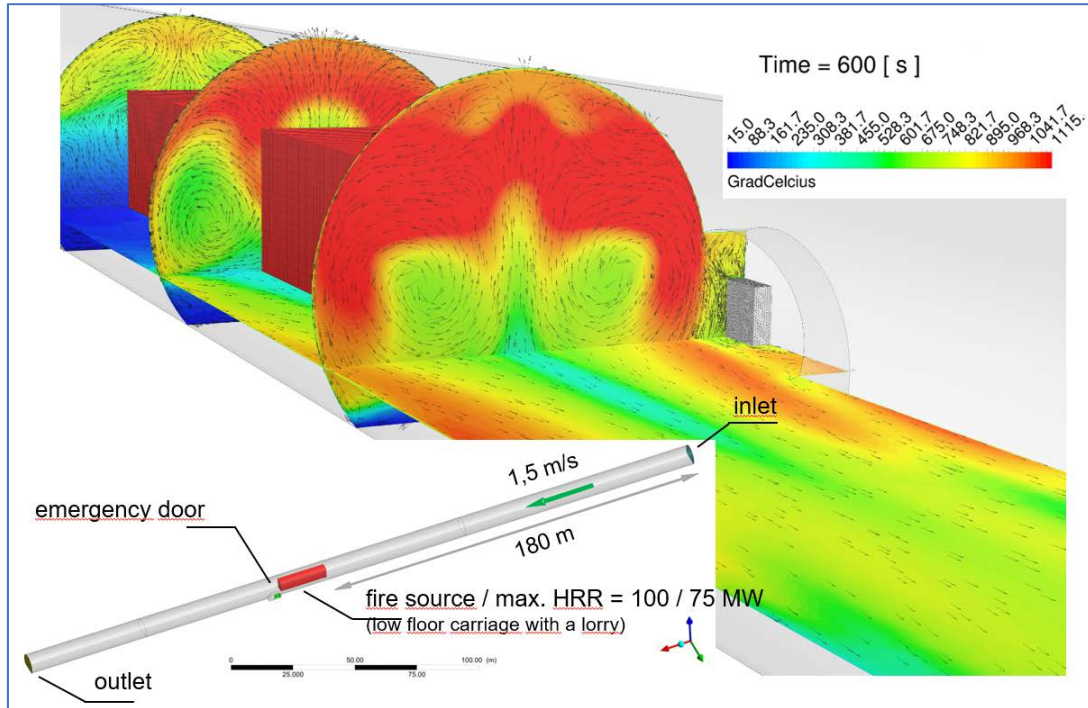


Figure 8: CFD simulation – results for 75 MW heat release rate after 600sec

In close consultation with consultants and experts, the decision was finally made to use the standard temperature/time curve (“ETK”) as the design parameter for the doors of the KAB [5].

3.4. Ventilation and Cooling of Technical Equipment

In the KAT, most technical systems are located in cross-passages, which are then located in separate rooms. These rooms contain power supply switches that convert from medium voltage to low voltage, providing the necessary telecommunications and telecontrol systems for operational management. The heat losses must be removed reliably into the railway tunnels, where they are further distributed and discharged into the atmosphere by the rail traffic.

By considering various factors, including rock temperature and its changes over time, temperature distribution in the railway tubes, seasonal temperature curves at the portals, and global temperature trends, it was possible to develop an overall ventilation concept for the entire tunnel and its specific technical facilities. The decision-making process took into account the target temperature for the technical rooms, considering the system's service life (replacement cycles) that is dependent on temperature, energy consumption, the necessary maintenance and repair activities and the associated costs [2, 4, 6, 12, 14].

3.5. Building Information Modelling / BIM

The final phase of the structural implementation of the KAT utilized the BIM (building information modeling) method for the technical railway equipment. This served as a 3D planning tool to identify structural conflicts or collisions early on and as a data and information carrier during implementation, as well as support for maintenance and repair work required later [15].

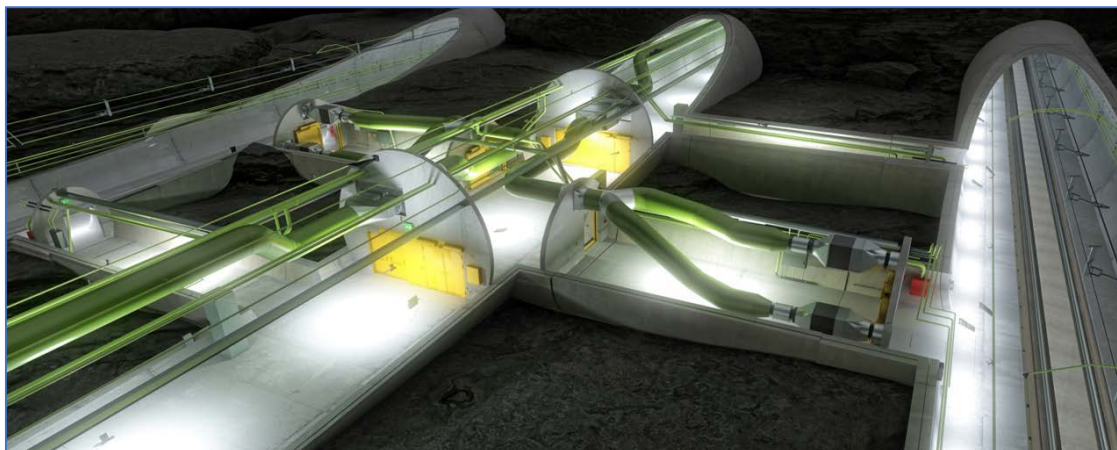


Figure 9: Koralmbahn – BIM method and a 3D view

4. SUMMARY AND CONCLUSION

Projects of this size can only be realized with a tight organizational structure and short, clear decision-making paths. The primary focus should be on identifying issues and making prompt decisions. In this context, decisions that are NOT made should definitely be viewed more critically than decisions that are made but may not be entirely correct.

The Koralm railway is scheduled to be fully operational for freight trains by mid-October 2025 and for passenger trains by mid-December 2025.

5. REFERENCES

- [1] Steiner H.; Reiterer M.; Erste Schritte zur Entwicklung von "neuen" ÖBB-Tunneltüren; Wiener Dynamik Tage 2016
- [2] Steiner H.; Sturm P.-J.; Bacher M.; Fruhwirt D.; Kühlung von Technischen Räumen in Eisenbahntunneln zur Erhöhung der Standzeiten und Minimierung der Wartung: Möglichkeiten der Optimierung am Beispiel Koralmtunnel; STUVA-Tagung 2017; Forschung+Praxis 49; S.335-343
- [3] Kari H.; Steiner H.; Reiterer M.; Baudynamische Analysen bei der Entwicklung von Tunneltüren für die ÖBB: Simulationsberechnungen der Druck- und Sogbelastungen, Stoßspektren, Eigenfrequenzen, Ermüdungsbemessung; STUVA-Tagung 2017; Forschung+Praxis 49; S.393-396
- [4] Fruhwirt D.; Bacher M.; Sturm P.-J.; Steiner H.; Change in thermal conditions during construction and operation of a long railway tunnel - taking the koralmtunnel as an example; 9th Int. Conf. - Tunnel Safety and Ventilation 2018; IVT- Mitteilung; Heft 102; S.30–45
- [5] Steiner H.; Beyer M.; Sturm P.-J.; Requirements for escape doors in the tunnels of the koralm railway line - special focus on thermal loads during fire; 9th Int. Conf. - Tunnel Safety and Ventilation 2018; IVT- Mitteilung; Heft 102; S.19–29
- [6] Scherz M; Fruhwirt D.; Bacher M.; Steiner H.; Passer A.; Kreiner H.; Influence of cross passage temperatures on the life cycle costs of technical equipment; SBE19 - Sustainable Built Environment D-A-CH Conference 2019

- [7] CEF support to Baltic-Adriatic Corridor; Innovation and Networks Executiv Agency, European Union, Brussel, Belgium; May 2020
- [8] Steiner H.; Reiterer M.; Experimentelle Untersuchung der Dauerhaftigkeit von Tunneltüren für schnellbefahrene Bahntunnel der ÖBB; 2. Wiener Dynamik Tage 2021
- [9] Schellander J.; Reiterer M.; Steiner H.; Messtechnische Untersuchungen von druckwellen- und strömungsinduzierten aerodynamischen Belastungen in Hochgeschwindigkeitstunneln; 17. D-A-CH-Tagung 2021 - Erdbebeningenieurwesen und Baudynamik
- [10] Reiterer M.; Steiner H.; Bahntechnische Einbauten in schnellbefahrenen Eisenbahntunnel der ÖBB - Realitätsnahe Belastungsansätze in Theorie und Praxis, Laborversuche und In-situ-Messungen; STUVA-Tagung 2021; Forschung+Praxis 56; S.479–484
- [11] Steiner H.; Gobiet G.; Current status of the two major tunnel projects, Koralm Tunnel and Semmering Base Tunnel, along the new Südbahn Railway line; 11th Int. Conf. - Tunnel Safety and Ventilation
- [12] Fruhwirt D.; Sturm P.-J.; Steiner H.; Methodology for investigations on the tunnel climate in long railway tunnel - optimization of the design process für cross-passage cooling systems; 11th Int. Conf. - Tunnel Safety and Ventilation 2022; ITnA-Reports, Vol 105; S.93–112
- [13] Steiner H., Bacher M.; Egress-doors in ÖBB railway tunnels - basics, decisions, recommendations; 11th Int. Conf. - Tunnel Safety and Ventilation 2022; ITnA-Reports, Vol 105; S.201-209
- [14] Fruhwirt D., Sturm P.-J., Steiner H., Borchiellini R.; Development of a Methodology for Studying Tunnel Climate in Long Railway Tunnels and for Optimizing the Design Process of Cross-Passage Cooling Systems; Tunnel and Underground Space Technology 2023; No. 138
- [15] Mülitzer G.; Niedermoser C.; Ausführungsplanung für die bahntechnische Ausstattung des Koralmtunnels mit BIM – kritische Betrachtungen und Grenzen: Rohbaumodelle, Teil- und Fachmodelle, Qualitätssicherung, regelbasierte Prüfung, Informationsmanagement; STUVA-Tagung 2023; Forschung+Praxis 59; S.354–359

CURRENT STATUS OF THE SEMMERING BASE TUNNEL

Gerhard Gobiet, Thomas Thaller
Austrian Federal Railways, AT

DOI 10.3217/978-3-85125-996-4-02 (CC BY-NC 4.0)

This CC license does not apply to third party material and content noted otherwise.

ABSTRACT

The tunnel construction work for the Semmering Base Tunnel (SBT) is now in its final phase. Approximately 98 % of the required tunneling has been completed and installation of the tunnel equipment has already begun.

The *Gloggnitz* and *Göstritz Ost* drifts are the final tunneling challenges, with around 450 m of highly geologically challenging tunnel excavation remaining in both tracks.

Tunnel lining work in the constructed sections of the Semmering Base Tunnel is progressing rapidly and has even been partially completed (western section of construction lot *SBT2.1*).

The renovation and rebuilding of *Mürzzuschlag* station is now entering in its final phase. To date, new tracks and platforms have been constructed, including platform roofs. A reception building, station forecourt and a large Park & Ride facility on the north side of the station have also been built.

The tender for the track equipment, *SBT4.1 GU Tunnelausrüstung*, was prepared in parallel with the ongoing construction work and is currently in the award phase since its publication in June 2023. The first stage of the tender for the slab track (*SBT5.1*) has also already been published Europe-wide. This will ensure the technical equipment starts in mid-2025 and the slab track is installed by mid-2027.

Keywords: Semmering Base Tunnel, railway tunnel, Trans European Network, Baltic Adriatic rail corridor

1. INTRODUCTION

The Semmering Base Tunnel (SBT) is a crucial component of the new southern line (Vienna – Graz – Klagenfurt), measuring approximately 27 km in length. Located between the stations of *Gloggnitz* (in the east) and *Mürzzuschlag* (in the west), it overcomes a continuous gradient of about 8.4 ‰ and a height difference of about 230 m. It consists of two single-track tubes connected by cross-cuts at least every 500 m and is equipped with an emergency station approximately in the middle of the tunnel (Figure 1).

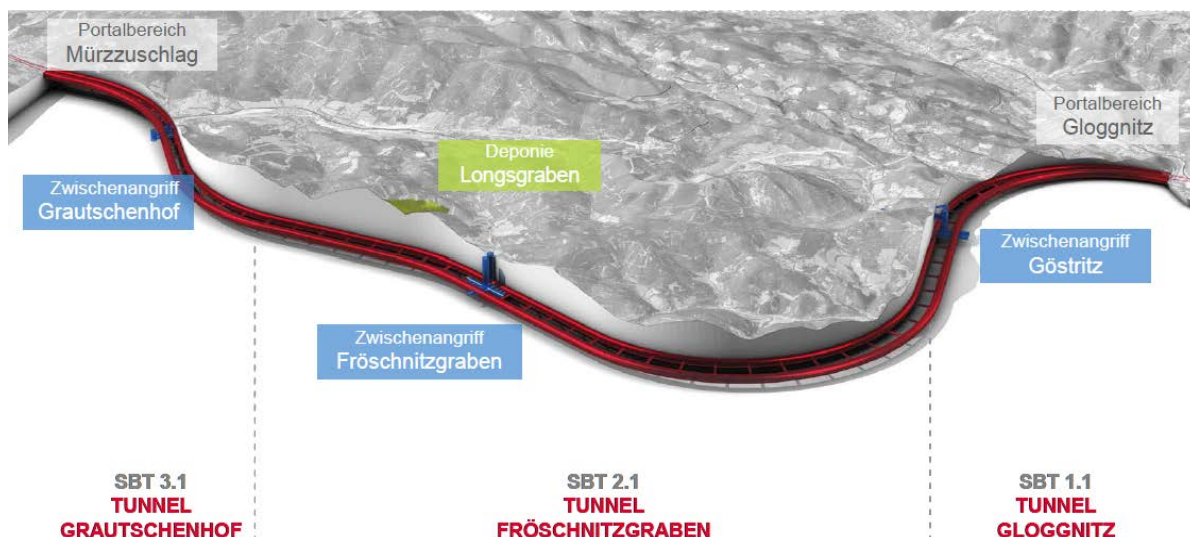


Figure 1: Overview of the Semmering Base Tunnel

In the standard profile, the two tunnel tubes have a clear cross-section of 41.65 m² (cyclic excavation) and 42.71 m² (continuous excavation). The spacing between the two tubes for the track is determined by the geological conditions and route requirements, ranging from 40 m to 80 m.

The tunnel will be constructed in the following phases:

- PGG – *Gloggnitz* portal construction site
- SBT1 – *Gloggnitz Tunnel*
- SBT2 – *Fröschnitzgraben Tunnel*
- SBT3 – *Grautschenhof Tunnel*
- PMZ – Renovation of *Mürzzuschlag* station

The first section, the *Gloggnitz Tunnel*, is approximately 7 km long and starts at the *Gloggnitz* portal. It includes the *Göstritz* intermediate access, which has a 1 km long access tunnel with two 250 m deep shafts and is being built using the conventional NATM tunneling method.

The second tunnel construction lot, *Tunnel Fröschnitzgraben*, is approximately 13 km long. In this construction lot, two 400 m deep shafts were built first, which will serve as tunnel ventilation shafts later. Furthermore, an emergency station approximately 900 m in length was constructed at the base of the shaft. From this point, two TBM excavations of approximately 9 km (in the direction of *Gloggnitz*) and two cyclic excavations of approximately 4 km (in the direction of *Mürzzuschlag*) were carried out. The primary challenge in this construction lot is logistics, as the entire construction site must be served by the two 400 m deep shafts.

The construction lot for the third tunnel, known as *Grautschenhof Tunnel*, is situated in the west and has an intermediate access near the S6 Semmering motorway. Four tunnel excavations, with a total length of approximately 7 km, start from here and are supplied via two shafts, each 200 m deep.

The *Semmering Base Tunnel* will be integrated into the existing structure in the west at *Mürzzuschlag* station. The station will be built using the cut-and-cover method, while rail operations continue. The station will include platforms, station roofs, passenger tunnels, elevator facilities, a heritage-listed reception building, a Park & Ride facility, and a bus station.

2. PROJECT STATUS

Around 98 % of the tunneling work for the Semmering Base Tunnel has been completed successfully to date. Ten of the initial 14 drifts have been finished, with only the *Gloggnitz* and *Göstritz Ost* drifts (both construction lot *SBT1.1*) still under construction.

2.1. Status of the Excavation Work

All excavation works for construction lot *SBT2.1* were successfully completed, i.e., *Fröschnitzgraben West* in February 2021 (track 1) and July 2021 (track 2), and *Fröschnitzgraben East* (TVM excavation) in December 2021 (track 1) and January 2022 (track 2). The *Göstritz West* drift (construction lot *SBT1.1*) was also finished shortly afterwards in June 2022 (track 2) and October 2022 (track 1) with the breakthrough from *SBT1.1* to *SBT2.1*.

In March 2023, the drifts of construction lot *SBT3.1*, *Grautschenhof East* (tracks 1 and 2) were completed with the breakthrough from *SBT3.1* to *SBT2.1*, and the drifts *Grautschenhof West* in June 2023 (track 1) and September 2023 (track 2). Completion of *SBT3.1* to the cut-and-cover method *PMZ2* ended with the breakthrough of the tunnel (Figure 2).



Figure 2: Breakthrough celebration SBT3.1 – PMZ2

This means that only the *Gloggnitz* and *Göstritz East* drifts remain to be bored, with a total length of around 450 m. Due to the so-called Grasberg-Nordrand fault (Lower Austria), which has to be overcome, these drifts are extremely challenging and complex in terms of tunnel construction (Figure 3).

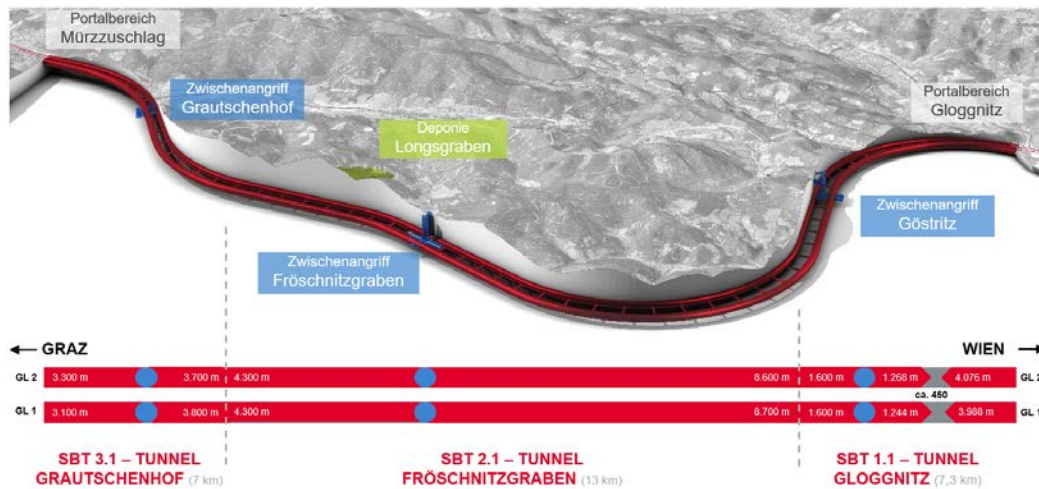


Figure 3: Status of the excavation work, March 2024

2.2. Status of the Tunnel Lining

The tunnel lining (invert filling concrete and invert vault, abutments, sealing and vault) has already started in all three tunnel construction lots and is progressing well everywhere (Figure 4).

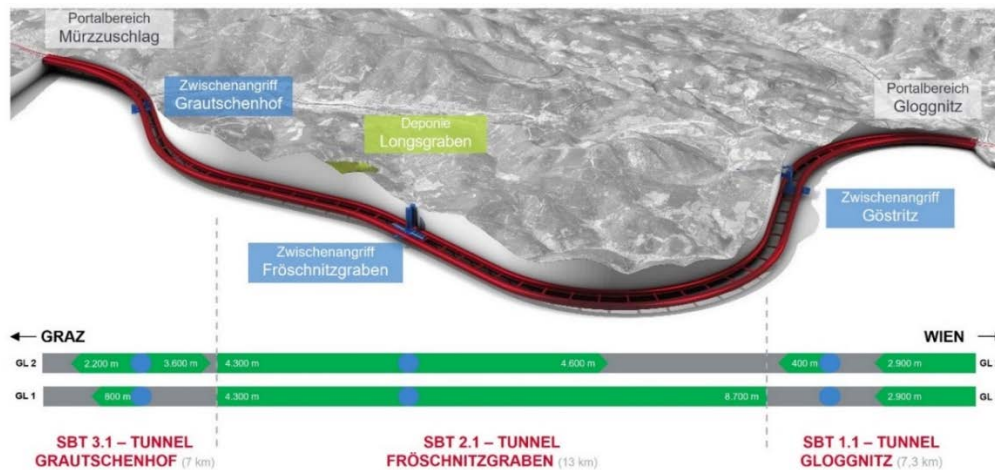


Figure 4: Status of the tunnel lining work, March 2024

2.3. Disposal Site Longsgraben

The *Longsgraben* disposal site was closed in spring 2022 with the completion of the TVM excavation work and the landfiling of approximately 4.25 million m³ of excavated material. This was followed by various dismantling measures, so that the closure of the disposal site was requested from the authorities in December 2022, and the disposal site was able to switch to the post-closure phase. The first planting phase was carried out from April to June 2023.

2.4. Renovation of Mürzzuschlag Station

Between 2021 and 2023, platforms 4/5 including the platform roof and associated track systems were rebuilt. The passenger tunnel under the tracks, including the elevators, was also constructed and put into operation together with the new platforms 4/5 in July 2021 (Figure 5).



Figure 5: Station Mürrzuslag, platform 4/5

The new construction of platform 1 (main platform) with the associated platform roof and reception building started with demolition in 2021. The commissioning of Platform 1 and the associated track systems took place in November 2022.

This was followed by the renewal of the track systems associated with platforms 2/3. The completion and subsequent commissioning of platform 2/3 is scheduled for April 2024.

To accompany the SBT, an ASC (*Anlagen Service Center*) track hall and a Park & Ride facility were built on the north side of the station. The ASC track hall was handed over in October 2021 and the Park & Ride facility for 428 cars (including eight handicapped parking spaces), 110 bicycles and 28 motorcycles was opened in June.

On the south side of the station, the forecourt of the *Mürrzuslag* reception building was redesigned with a reorganization of the bus stops including shelters as well as a Bike & Ride facility and 4 handicapped parking spaces.

The ceremonial opening of the reception building and the station forecourt (Figure 6) took place on May 26, 2023. The Bike & Ride facility was opened in November 2022 and the handicapped parking spaces on the forecourt in early May 2023.



Figure 6: Mürrzuslag station forecourt, reception building and bus stops

2.5. Gloggnitz Station

As part of lot *PGG4*, the ASC will be built on the site of *Gloggnitz* station. This includes the construction of an ASC operations building (office and administration building) with integrated workshops and areas for a rescue unit, as well as an attached two-track storage hall

for rail vehicles (track hall) and a shelter for the rescue train parked outside (rescue train shelter).

The new office building, including the workshops, was ready for use at the end of July/beginning of August 2023. Work is currently underway on the track systems to connect the track hall and the rescue train shelter. The completion of the track hall, the enclosure for the rescue train, the track systems and the outdoor areas and thus the commissioning of the entire ASC site in *Gloggnitz* is planned for April 2024.

2.6. Track Equipment

In the current project phase of construction lots *SBT4* and *SBT5*, planning and the preparation of tender documents as well as the awarding of contracts for services of construction lot *SBT4.1* are taking place.

2.6.1. Construction lot SBT4.1: General Contractor for Tunnel Equipment

The tender for the tunnel equipment for the SBT was completed in mid-2023 and published on June 27, 2023. The detailed tender review is currently underway and the contract award is planned for July 2024.

The track equipment work for the Semmering Base Tunnel is extensive and includes the following key services:

- Construction, operation and dismantling of the temporary construction facilities required for the equipment (construction power supply, construction lighting, construction communication, construction ventilation, ...)
- Complete cabling of the tunnel tube, all cross-passages and the emergency station
- Installation of a water mist system in the emergency station (water pipe and high-pressure water mist system)
- Installation of the systems for operational and emergency ventilation
- Equipping the cross passages and the emergency station with all necessary technical equipment components
- Technical equipment for the 3 operations buildings
- Installation of conductor rails and switchgear for traction current
- Installation of radio equipment including transmitting cables (GSM-R, GSM-P, TETRA, ...)
- Installation of the track vacancy detection system, the marker boards and the balises for ETCS-L2
- Production of the illuminated handrails and the entire lighting in the tunnel tubes, in the cross-passages, in the emergency station and in the ventilation shaft and portal areas
- Installation of all signs
- Connection of socket distributors and emergency call pillars
- Installation of cooling and drying equipment for the technical rooms
- Installation of systems to stabilize the hardness of the drainage water
- And much more

2.6.2. Construction Lot SBT5.1: Slab Track

The *SBT5.1* service will be awarded by means of a negotiated procedure with prior publication: Stage I was published on October 11, 2023 – with a deadline for submission of requests to participate at the end of April 2024. The tender planning and tender preparation for Stage II is currently underway with the aim of publication on June 14, 2024.

The *SBT5.1* will be realized as follows:

- Production and delivery of the track base plates and installation of the slab track,
- Gravel superstructure incl. multiple points installation
- Adaptation of the already constructed bridges over the *Schwarza* river for the slab track
- Closure of the *Mürzzuschlag* trough (construction site access)
- Construction of a retention basin in the *Mürzzuschlag* portal area
- Construction of concrete end walls in 3 cross-connections of the two tunnel tubes
- Rail grinding
- Final tunnel cleaning
- Among other things

3. OUTLOOK

3.1. Tunnel Construction

For construction lot *SBT1.1*, the focus in the near future will obviously be on completing the excavation work in the *Gloggnitz* and *Göstritz East* tunnel sections with the final breakthrough. This breakthrough, and thus the completion of all excavation work for the SBT, is expected to take place in the first quarter of 2025. Once the tunnel lining work, which has already begun, has been completed (around the second quarter of 2026), the tubes from the *SBT2.1* section boundary to the *Göstritz* shaft base will be handed over to the railway equipment.

In 2024, concreting of the vault in the continuous (east) excavation of the *SBT2.1* section will be completed, followed by concreting of the walkway in the two tubes by the end of 2025. This means that the inner lining of the tubes will be completed by early 2026. At the same time, the inner lining (shotcrete) in the emergency station will be constructed and the inner lining of the *Fröschnitz 1* shaft will be installed, so that the underground areas can be handed over to the railway equipment construction lots at the end of April 2026.

Four concreting wagons are currently working on section *SBT3.1*. In 2024, work will begin on the collector pipe, drainage concrete, concrete slab, walkways and crossovers from the *PMZ2* site boundary to *SBT2.1*. In 2025, work will commence to upgrade/deconstruct the caverns at the base of the shafts and backfill the two approximately 100 m depth shafts. In the first quarter of 2026, deconstruction work will commence at the *Grautschenhof* site.

In addition to the completion and commissioning of platform 2/3 planned for April 2024, the completion of the tunnel portal is also on the agenda for construction lot *PMZ2*. This includes the production of the portal blocks and the completion of the filter concrete filling – all in accordance with the requirements of the World Heritage Site.

3.2. Equipping

The equipping work, which will be carried out with the two main construction lots *SBT4.1* and *SBT5.1*, as well as some other smaller lots (e.g., *SBT4.5* cross passage walls and doors), is based on a sophisticated logistics concept.

It is planned to start equipping the *Mürzzuschlag* portal in mid-2025 and then successively move to *Gloggnitz*. The switch to *Gloggnitz* will only take place once the slab track has been installed, around May 2027, also from *Mürzzuschlag*. All work for the technical equipment of the tunnel, such as cabling, equipping the cross-passages, etc., will then be carried out in the

opposite direction, while at the same time the slab track is being installed continuously from *Mürzzuschlag* (Figure 7).

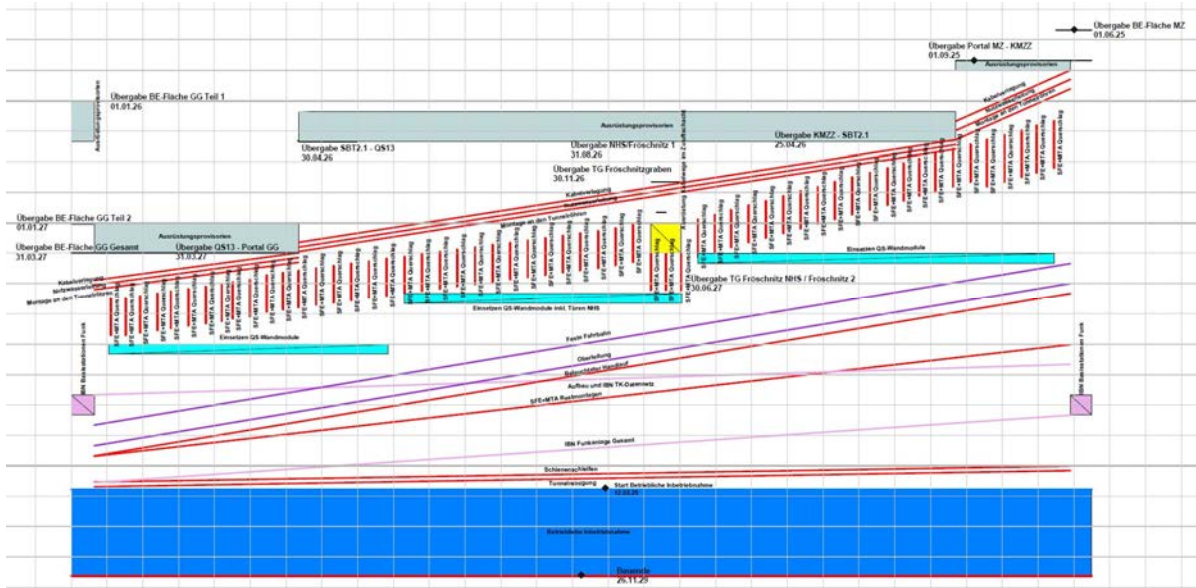


Figure 7: Tunnel equipment process SBT

The advantage of this concept is that all the cabling can be efficiently installed in the completed cable ducts and technical rooms before the slab track is laid, using standard road vehicles. The same applies to the equipment of the technical rooms. The high flexibility of road-bound traffic in the tunnel is only step by step limited once the slab track has been installed.

The equipment work must be fully completed by the start of operational commissioning (construction lot *SBT7*) on March 12, 2029, so that the necessary measurement and acceptance runs can take place as planned and the Semmering Base Tunnel can be commissioned on time.

4. SUMMARY

Construction of the Semmering Base Tunnel is progressing well, with around 98 % of the required excavation work now completed. This means that ten of the original 14 simultaneous drifts have already been successfully completed. The *Gloggnitz* and *Göstritz East* tunnels represent the final challenges of the tunneling project. In total, approximately 450 m of tunnel remain to be excavated.

In the tunnel sections that have been completed from a structural point of view, the inner lining of the Semmering Base Tunnel has begun with the construction of the invert filling concrete and invert vault, abutments, sealing and vault. This work is progressing very rapidly, with the inner lining of the two tunnel tubes in the western section of construction lot *SBT2.1* (cyclic tunneling) already completed.

The renovation and new construction of the *Mürzzuschlag* railway station at the west portal of the Semmering Base Tunnel is nearing completion. In addition to the tracks and platforms, the station building has been built in accordance with the requirements of the monument protection regulations, as well as the station forecourt with a new arrangement of the bus stops, now including turning facilities, and a large Park & Ride facility on the opposite side of the station.

In parallel with the construction work, the tenders for the track equipment – *SBT4.1* general contractor tunnel equipment and *SBT5.1* slab track – have been prepared. They are already in the awarding phase (*SBT4.1*) and in the middle of the tendering phase (*SBT5.1*). This will ensure the planned start of the technical equipment in mid-2025.

Under these conditions, the commissioning of the Semmering Base Tunnel in 2030 is realistic.

TUNNEL RENOVATION PROGRAM AUSTRIA

NEXT LEVEL

Andreas Fromm, René List
ASFINAG Bau Management GmbH, AT

DOI 10.3217/978-3-85125-996-4-03 (CC BY-NC 4.0)

This CC license does not apply to third party material and content noted otherwise.

ABSTRACT

Within the framework of the ASFINAG tunnel renovation and extension program based on the EU directive on road tunnel safety, around 50 individual projects were completed in the TERN network with a total volume of around EUR 1.7 billion. As of April 2019, all relevant projects have been successfully completed on schedule, thus significantly increasing tunnel safety in Austria.

ASFINAG is now facing the next major challenges. These are due to the ageing of facilities, IT security requirements, electricity saving requirements, short life cycles of safety equipment and finally also due to the necessary compliance with the EU directive on road tunnel safety 2029 in Austria's Non-TERN network.

The investment volume required for this is more than EUR 4 billion until 2035 and the actual measures required are still being evaluated on an ongoing basis. This enormous project and investment volume presents ASFINAG with almost insurmountable tasks. These begin with maintaining tunnel availability for users and end with the actual feasibility in cooperation with stakeholders, planning companies, construction companies, authorities, equipment suppliers. It is also questionable whether sufficient capacity is available at suppliers and in the personnel sector.

Keywords: Tunnelsafety, Live cycle, Renovation, Sustainability, Availability

1. INTRODUCTION

Project development at ASFINAG is ensured by the Asset Management activities. Regular reviews and forecasts are carried out to identify refurbishment requirements and necessary improvements to the system. The latest result was published in the Network Status Report 2022. It describes the strategic objectives for the maintenance, the development the condition of the structural, electrotechnical and mechanical installations and provides a long-term outlook about the development of the condition and the resulting financial requirements. [2]

The current plans for the construction projects in the tunnel area include many individual projects and a very high investment requirement. It has been shown that, in combination with the adjustments still required to the „EU Directive 2004/54 – Minimum safety requirements for tunnels in the trans-European road network“[1] am Non-trans-European road network, which are to be implemented by 2029, a new, very comprehensive tunnel safety program is being created.

ASFINAG therefore decided to set up a strategic "Tunnel Task Force" to deal specifically with the feasibility of such a program. A select group of experts and senior project managers from the various specialist areas, such as asset management, operations, infrastructure construction and electromechanical, were nominated for this purpose. A consulting company

specializing in construction processes and construction management provided the content-related support for the task force.

2. TUNNEL TASK FORCE

2.1 Task and Target Definition

The most important task was to analyse the upcoming construction projects regarding the specific number, scope, framework conditions, challenges, and content-related issues. Based on these results, the focus was on the development of strategies and measures to ensure the manageability of this new tunnel program from 2025. The main thrusts were defined as optimizing demand, strengthening expertise, processing efficiency, and making construction projects more attractive for bidders in the construction and service environment.

2.2 Construction volume

The data and cost analysis carried out in the first step showed that around 120 individual construction projects involve investments in tunnel systems. The total investment sum was put at more than EUR 4 billion.

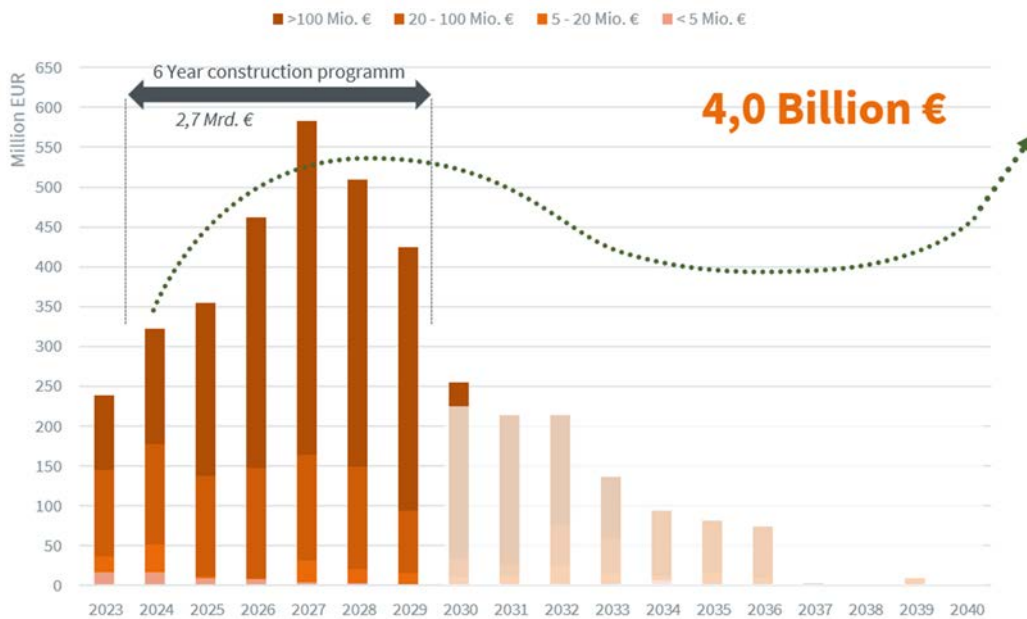


Figure 1: 6 year investment program Tunnels

A further result of the analysis was that, due to the ageing of the system, regular long-term continuous refurbishment and maintenance will be necessary.

A look at the individual projects also shows that very large, extensive projects with long construction periods are due for implementation. These also have high demands on the availability of traffic corridors and the associated impact on traffic flow. The following chart provides an overview of projects with an investment volume of more than 100 million euro for the coming years:

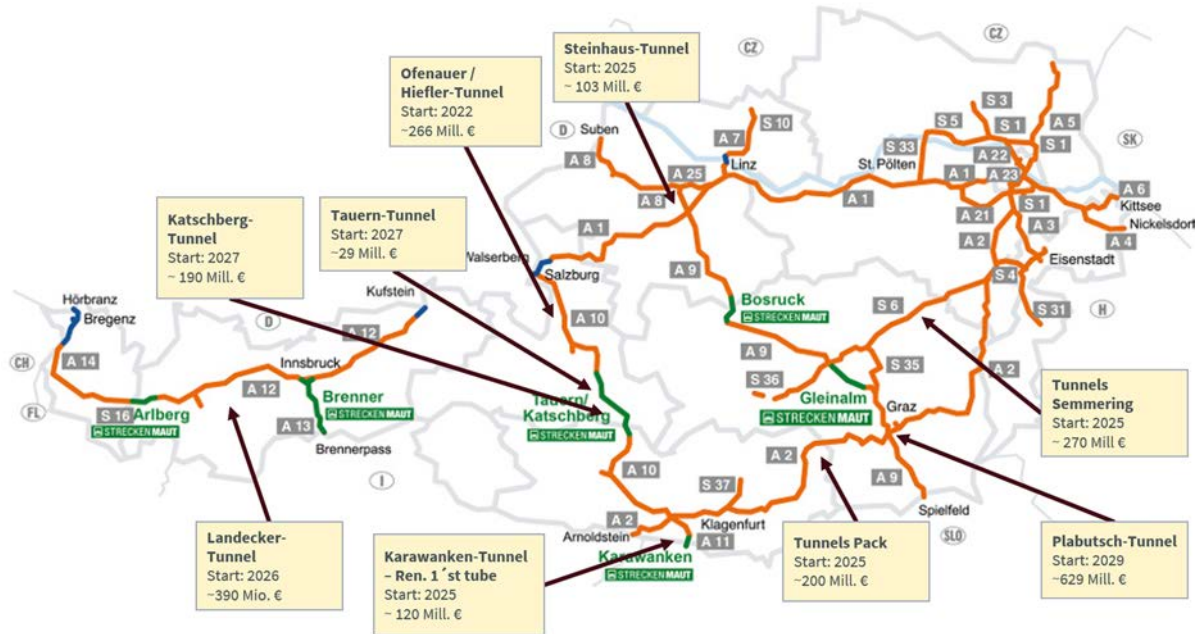


Figure 2: Projects with >100 Mill. € investment volume next years

2.3 Key Challenges and starting Points

The cost forecasts are also problematic in this context due to general conditions such as supply bottlenecks, rising construction costs, rising energy costs and staff shortages. The analysis concludes that the following are the most significant challenges for the coming years and require a very high level of management attention:

- Stability of project content
- Predictability of costs
- Securing the execution of construction projects
- Shortage of personnel and loss of know-how
- Increased attractiveness for the Construction company market

The following possibilities and options were defined as starting points for compensation measures and will be dealt with in greater depth in the coming years:

- Changes to the framework conditions (e.g. legal aspects)
- Extending the service life of systems and equipment
- Optimization or reduction of the scope of construction and renovation work
- Control of the market for construction and consulting
- Adaptation of contract models for construction management
- Optimization of processes and process requirements
- Targeted focusing of existing personnel resources
- Transfer of experience in the field of tunnel renovation

3. SUMMARY AND CONCLUSION

Tunnels are complex structures with high safety requirements and high level of safety equipment. This also results in disproportionately high refurbishment and operating costs, which increase with the age of the facilities. At the same time, the complexity and demands

on construction project management increase for all project partners involved. This means that not only road operators are required to react to these circumstances, but also planning offices and construction companies.

To ensure the feasibility of this Next Level Program, strategic and operational concepts with effective measures are urgently needed. Without these, a sufficient level of safety in Austrian motorway tunnels will not be sustainable in the long term.

4. REFERENCES

- [1] Directive 2004/54/EC of the European Parliament and of the Council of 29 April 2004 on minimum safety requirements for tunnels in the Trans-European Road Network
<https://eur-lex.europa.eu/legal-content/EN/TXT/?uri=CELEX%3A32004L0054>

- [2] ASFINAG Netzzustandsbericht 2022
<https://www.asfinag.at/media/p5tpase5/netzzustandsbericht-2022.pdf>

SUSTAINABLE ENERGY CONSUMPTION

Benjamin Riedl, Johannes Bösl, Ersin Gündogdu
ILF Consulting Engineers Austria GmbH, AT

DOI 10.3217/978-3-85125-996-4-04 (CC BY-NC 4.0)

This CC license does not apply to third party material and content noted otherwise.

ABSTRACT

This paper discusses the importance of implementing photovoltaic systems in tunnels to reduce operating costs and contribute to global climate targets. The amount of electricity consumed in a tunnel depends on various factors, with energy requirements typically highest during the day. Different options for installing PV modules are explored, considering factors such as orientation, sizing, and dimensions. A case study of the Schönberg noise protection gallery in Austria demonstrates how a photovoltaic system can help cover a tunnel’s consumption needs and even generate surplus energy.

Furthermore, the paper explores sustainable cooling methods for electrical rooms in the North Operations Building of the Kramer tunnel in Germany. By utilizing fire water and groundwater as cooling sources, the study aims to enhance energy efficiency and reduce operating costs. The design includes a detailed analysis of cooling load calculations, investment costs, and amortization times for the proposed systems. Results indicate that while initial investment costs for groundwater cooling may be higher, the long-term operational savings make it a more cost-effective and environmentally friendly option. This research contributes to the development of sustainable cooling technologies for electronic infrastructures, with potential applications across various industries.

Keywords: Renewable Energy Sources, Sustainability, Photovoltaic Systems, Cooling Systems

1. INTRODUCTION

In the current period of energy transition, there is great interest in finding ways to sustainably generate electricity from renewable energy sources, especially for public infrastructure. In this context, the use of solar energy to supply tunnel systems, especially enclosures, with electricity, makes a valuable contribution. Another example of how available resources in the vicinity of tunnels can be optimally used, is the use of fire water and groundwater (water from inside the mountain) to cool the electrical equipment in operations buildings.

2. PHOTOVOLTAIC SYSTEMS

The amount of electricity consumed in a tunnel has a major impact on its annual operating costs, not only because of ever-increasing energy prices. Electricity consumption generally represents a high proportion of tunnel operating costs. In order to reduce these costs and also contribute to global climate targets, it is necessary for tunnels to be as self-sufficient as possible in terms of their electricity consumption to cover their own electricity consumption needs as best as possible. There are often many areas around tunnels where it is suitable to install photovoltaic (PV) systems to cover the respective tunnel’s own consumption needs. This paper explains the different options for installing PV modules and the influence of the orientation as well as sizing and dimensions of photovoltaic systems.

2.1. Typical Tunnel Load Profile

The amount of electricity consumed in a tunnel depends on many factors, such as the length of the tunnel, the ventilation concept, traffic monitoring and control, and other technical components. Typically, the amount of energy required is highest during the day and reaches a minimum at night. The amount of energy required for lighting at the tunnel entrance depends in particular on the amount of solar radiation. The higher the level of solar radiation, the more powerful the lighting needs to be in order to maximise the ability of our eyes to adapt to the lighting conditions in the tunnel.

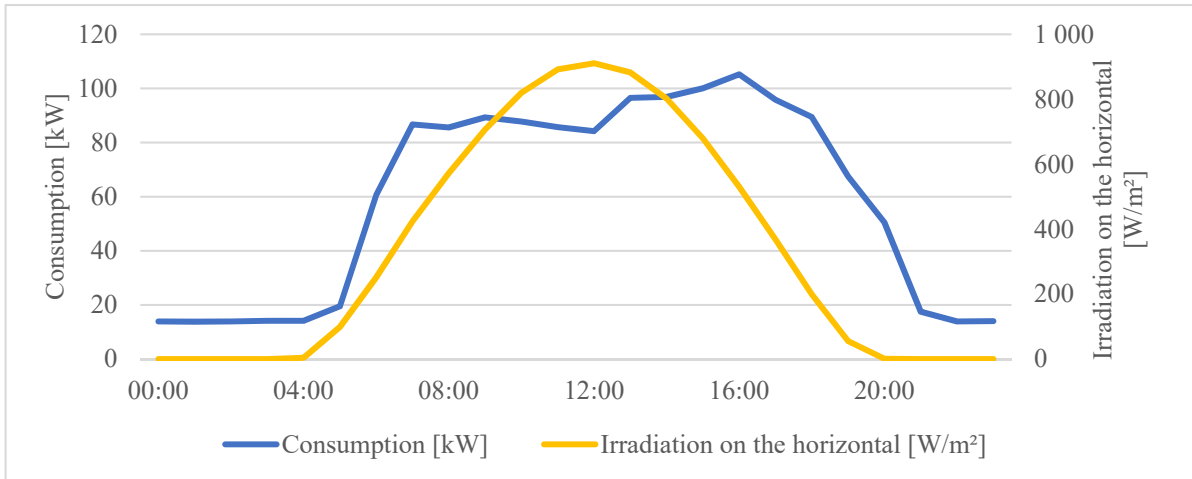


Figure 1: Typical Tunnel Load Profile on a sunny day in June

2.2. PV Module Installation Options for Tunnels

There are a variety of options for installing PV modules in the vicinity of tunnels, a description of which is given in the table below. The options are defined on a project-specific basis according to the local conditions and from an economic, operational and maintenance point of view.

Table 1: Photovoltaic substructures for open spaces

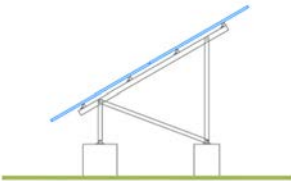
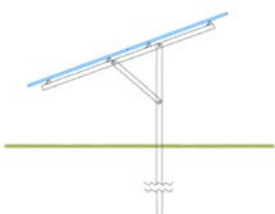
Open Spaces	
	<p>Installation on Concrete Foundations Used in open spaces where there is insufficient cover/overburden to use a rammed system; the substructure is ballasted with concrete foundations.</p> <p>E.g. Cut-and-cover tunnels and galleries</p>
	<p>Rammed Systems Used in open spaces with an inclination of up to 20°, where posts can be driven into the ground.</p> <p>E.g. Areas on top of or in front of tunnels</p>

Table 2: Photovoltaic substructure for slopes and anchor walls

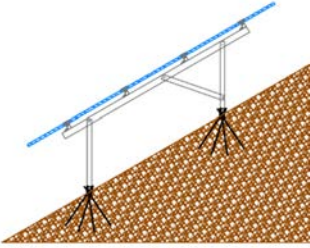
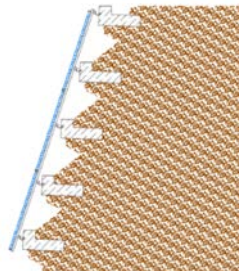

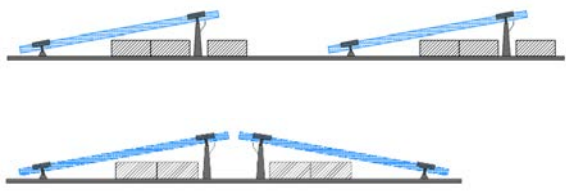


	<p>System with Bored Piles A two-column system with bored piles can be used in open spaces with an inclination of 20° to 40°. This system can also be used in flat areas with difficult ground conditions.</p> <p>E.g. Embankments, slopes</p>
	<p>Installation on Anchor Walls To attach the PV modules to an anchor wall, mounting brackets can be screwed onto the concrete blocks on which a crossbar system is installed for mounting the PV modules.</p>

Table 3: Photovoltaic Substructures for Buildings and Façades

<p>Buildings and Façades</p>	
	<p>Installation on Façades, Noise Barriers, etc. Depending on the type of façade, the substructure is hung, clamped or screwed on. In addition, the PV modules can be mounted either parallel to the building or on top of it (tilted at an angle).</p> <p>E.g. Portal entrances, noise barriers, façades of operations buildings</p>
	<p>Installation on Flat Roofs Modules mounted on top of the building, tilted towards the South or South-East using a ballasted substructure. No roof penetration required.</p>
	<p>Installation on Green Flat Roofs On green roofs, a substructure can be used at a greater distance from the ground to prevent the PV modules from being shaded by vegetation.</p>
	<p>Pitched Roofs Depending on the type of roof covering, pitched roofs can be fitted with roof hooks or clamps; a mounting profile can then be attached to these hooks or clamps.</p>

2.3. Dimensioning and Optimising PV Module Installation

The sizing, dimensions and installation of a photovoltaic system can be planned and designed according to the intended use of the system and the amount of space available. If the load profile is such that more electricity is consumed in the afternoon, the PV modules can be oriented towards the West to better utilize the PV energy, especially in the afternoon. To maximise the specific annual yield, the modules should ideally be tilted directly towards the South.

In order to achieve the most consistent electricity generation possible throughout the year using photovoltaics, PV modules should ideally be installed in a near vertical position. However, this reduces the specific annual yield. When aligning and installing the modules, consideration must be given to neighbouring buildings and resulting possible shadowing.

To determine and implement the best economic option, it is therefore necessary to evaluate all available areas at the site, taking into account the orientation, installation options, size of the available area(s), distance to the feed-in point and possible shadowing. A simulation program can be used to overlay the tunnel’s PV generation and load profile to determine the tunnel’s own consumption, degree of self-sufficiency and amount of surplus energy.

2.4. Example Project

The Schönberg noise protection gallery on the A 13 Brenner motorway in Tyrol, Austria, is 884 m long and approximately 25 m wide. On top of this gallery, a photovoltaic system will be installed to help cover the gallery’s consumption needs. Surplus energy will be fed into the public electricity grid.

The gallery currently uses 503,000 kWh of electricity per year. The gallery roof has been filled with soil and substrate, and grassed. The backfill has been adapted to the terrain profile and the gallery roof. There is a hiking trail as well as a playground and ice-skating rink on the gallery roof. Directly next to the gallery, on the eastern side, is a residential area.

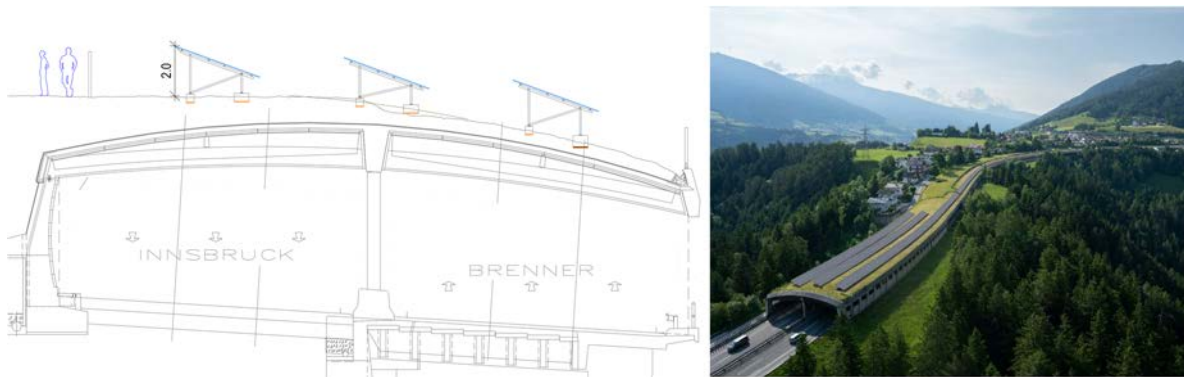


Figure 2: Example project

One of the project requirements is to protect residents from glare from the photovoltaic system. Taking into account the terrain profile of the gallery roof, it was decided that the PV modules will be installed parallel to the road, tilted and oriented between 230° and 310° West.

The PV system – a description of which is given in the table below – is to be installed on the unused parts of the gallery roof.

Table 4: main data example project

Capacity of the PV system	1,025 kWp
Orientation of the modules	230° South-West to 310° North-West
Module inclination	20°
Module area	4,700 m ²
Global radiation	1,242 kWh/year
Specific annual yield	1,020 kWh/kWp
Total annual yield	1,040,000 kWh
Proportion of own consumption	320,000 kWh
Degree of self-sufficiency	63%
Grid feed-in	720,000 kWh

Despite the orientation of the modules deviating from the ideal orientation, it will be possible to achieve a high specific annual yield. The roof area is large enough to generate significantly more power than is needed at the site, despite the need to keep areas free for other uses. The surplus green electricity can be used to help meet climate targets.

Even without any storage facility, the photovoltaic system can already achieve a 63% degree of self-sufficiency.

3. COOLING ELECTRICAL ROOMS USING SUSTAINABLE SOURCES

Cooling of electrical rooms is crucial to maintain an optimal operating temperature for electronic equipment while simultaneously promoting energy efficiency. The Kramer tunnel close to Garmisch Partenkirchen in Germany has a North Operations Building, which houses the necessary technical equipment for the tunnel’s operation. The project explores the application of cooling methods in an Operations Building using two sustainable cooling sources: fire water and groundwater.

The use of fire water as a cooling source provides an innovative solution by utilising the existing infrastructure from fire protection systems. A resource-efficient and cost-effective alternative to conventional cooling systems is being investigated through the targeted diversion and use of fire water to cool electrical installations.

Concurrently, the use of groundwater as a cooling source is also being examined. This method is based on geothermal principles and utilizes the relatively constant temperature of groundwater to keep electrical rooms at an optimal temperature level. This approach minimizes energy consumption and contributes to the sustainability of the cooling process.

Comprehensive experimental testing and modelling is being used for these examinations, with the focus being on developing effective cooling systems that meet the specific requirements of electrical rooms. The aim is to optimize cooling performance while ensuring the reliability and safety of these innovative cooling approaches.

The results are not only intended to help improve energy efficiency in electrical rooms, but will also serve as a guide for the implementation of sustainable cooling technologies in other industries. Overall, this project will make a significant contribution to the development of environmentally friendly technologies for cooling electronic infrastructures.

3.1. Cooling Design of Electrical Rooms

A cooling load calculation according to VDI 2078 [1] has been carried out to determine the total cooling load of the North Operations Building. The calculation includes both the external and internal loads of the Operations Building. The room temperature setpoints listed in Table 3 were used to determine the cooling load.

Two cooling cases have been considered for cooling the electrical rooms in the North Operations Building. Groundwater cooling is used to cool the electrical rooms in the Operations Building. The fire water pipes in the tunnel are used for primary cooling. Secondary cooling (emergency cooling) is provided by groundwater, which is collected in a drainage pipe and discharged from the tunnel. Once its construction is complete, a water collection shaft next to the Operations Building will be used for emergency cooling. In emergency cooling mode, cooling water is extracted from this shaft, then pumped through the system separator (cold exchanger) by a centrifugal water pump and returned to the drainage pipe. During the cleaning process, the cooling system switches between spring water and fire-fighting water. This makes the complete system redundant.

For the primary circuit, the cooling water pipes are laid underground and connected to the fire water pipes. The connections are made in a shaft next to the plant building in which the fire water pipes run. Two connections are provided for the future installation of a water softening system to treat the groundwater. The necessary fittings, regulation, control and measuring equipment will be installed in the technical room in the Operations Building. A heat exchanger will also be installed to separate the cold and cooling water circuits. This heat exchanger has a redundant design so that the cooling system can be operated without interruption during maintenance work.

Depending on the cooling capacity, the indoor units must be installed either on the floor, wall or ceiling.

Table 5: Maximum cooling design parameters

Room	Cooling Design temp. [2]
Low Voltage Room	25 °C
UPS Room	25 °C
Battery Room	20 °C
Communication Room	25 °C
Control Room	25 °C

The calculation includes the external and internal loads for the Operations Building. The cooling load calculation results in a value of 18.3 kW.

An annual average of approximately 37 l/s of water currently flows out of the Main Dolomite section of the rescue tunnel which is built in parallel to the main tunnel. After construction of the main tunnel, a total water volume of approximately 45 l/s is projected to flow out of both tubes. Due to possible fluctuations in the discharge, the study is based on a total annual average (from both tubes) of 40 l/s.

According to water management evidence from September 2013 to February 2018, the following data apply to the groundwater:

Table 6: Groundwater Characteristics

	Average Value	Max. Value	Min. Value
Flow Volume [l/s]	37	57	24
Water Temperature [°C]	8.2	8.5	8.0
pH Value [-]	8.05	8.43	7.53

A water temperature, including losses of approximately 9 °C, was assumed for the calculation. The flow temperature is therefore 10 °C and the return temperature 15 °C. With a spread of 5 Kelvin, a water volume of 1 l/s is required to dissipate the waste heat generated.

3.2. Investment Costs for Cooling Systems

In general, the investment costs for groundwater cooling are higher than for the use of conventional split air conditioning units. However, this is offset by lower operating costs, as the compression process in split air conditioning systems requires more energy.

The estimated investment costs for these two different cooling systems are compared in the following table.

Table 7: Investment Costs for Cooling Systems

Cooling System	Price
Groundwater Cooling	€ 60,000
Split Air Conditioning Units	€ 45,000

The electrical power requirement for a split VRF air conditioning system of the size required in this project is approximately 8 kW. In comparison, the pumps for the groundwater cooling system require a connected electrical load of approximately 1 kW. Two different electricity prices have been used to calculate the energy consumption.

In the following table, the amortization times of the cooling systems are calculated with the assumed electricity prices.

Table 8: Amortization Times

	Electricity Price	
	0.4 €/kWh	0.6 €/kWh
Operating costs for groundwater cooling:	0.4 €/h	0.6 €/h
Operating costs for cooling Split-Air-Conditioning-Unit:	3.2 €/h	4.8 €/h
Difference in investment costs	€ 15,000	€ 15,000
Amortization times [in years]	10.5	7.0

At an electricity price of 0.40 €/kWh, groundwater cooling would be more favourable after 5,750 hours of operation, and at 0.60 €/kWh after 3,833 hours of operation (note: only the investment costs were compared with the operating costs; maintenance costs were not taken into account). The evaluation of the weather data (from WESTE – the Weather Data and Statistics Express of the German Weather Service) at the weather station closest to the project

location revealed that the outdoor temperature was ≥ 21 °C for an average of 507 hours per year (for the years 2013 to 2017). The North operations building is cooled exclusively with fire water or, in an emergency, with groundwater. It is assumed that the electrical components are in operation all year round and generate waste heat. Using fire water or groundwater at an electricity price of 0.40 €/kWh, the cooling system would amortize after 10.5 years, and after 7 years with an electricity price of 0.60 €/kWh.

This does not take into account maintenance, inspection and cleaning costs, as well as interest and any necessary replacement purchases. Taking these aspects into account, the amortization period is further extended.

4. SUMMARY AND CONCLUSION

Photovoltaic Systems

Photovoltaic systems in the vicinity of tunnels are being planned and implemented with increasing frequency. Due to the recent sharp rise in electricity prices, increasing interest is also being shown in installing photovoltaic (PV) modules in other areas close to tunnel portals. In addition to selecting the right areas, planning and designing site-optimised installation and orientation of these PV modules is an essential part of the successful implementation of PV projects. There are a variety of options for installing PV modules. Project examples show that additional aspects, such as light and shadow effects or other constraints from nearby neighbourhoods, also need to be taken into account in order to find the optimized solution for PV module installation. Each of these approaches aims to optimise the energy yield and economic efficiency of the modules by utilising the available space.

Fire water and groundwater cooling

In principle, cooling with fire water and groundwater is possible. From a technical point of view, sufficient cold water is available to cover a tunnel's required cooling load. Even if there is no or insufficient groundwater available for cooling, any tunnel with fire water pipes in a loop design has an already built-in natural cooling source "free of charge", although the operational limitations in case of a leakage have to be carefully considered. The investment costs for groundwater cooling are generally higher than for conventional split air conditioning systems. However, the operating costs are lower as the compression process for split air conditioning systems requires more energy., The amortisation period of such a system is becoming shorter and shorter, especially due to global warming and increased energy prices.

5. REFERENCES

- [1] VDI 2078:2015-06 Calculation of thermal loads and room temperatures (design cooling load and annual simulation)
- [2] DIN EN 16798-1:2022-03 Energy performance of buildings - Ventilation for buildings - Part 1: Indoor environmental input parameters for design and assessment of energy performance of buildings addressing indoor air quality, thermal environment, lighting and acoustics - Module M1-6

ENERGY LABEL & ECODESIGN FOR AUSTRIAN ROAD TUNNEL

Mario Patigler

ASFINAG Bau Management GmbH, AT

DOI 10.3217/978-3-85125-996-4-05 (CC BY-NC 4.0)

This CC license does not apply to third party material and content noted otherwise.

ABSTRACT

With 94 GWh and a share of approximately 75% of the total electrical energy consumption within ASFINAG, its tunnel facilities are the main energy consumers.

This fact motivates to optimize the analysis of energy consumption in ASFINAG’s tunnel facilities. Through standardized equipment we want to develop the comparability of tunnel energy consumption by use of an energy benchmark.

Following the energy classification of electrical devices, the goal is to categorize the tunnels in terms of energy in the future. To achieve this objective, an evaluation system will be developed that focuses on both the quantitative comparability of tunnel facilities and the qualitative assessment based on sustainable or improved equipment.

1. Quantitative quality index

This analysis is based on actual data of energy consumption. The hypothesis is to examine the analogy between equally equipped tunnels by analyzing the energy consumption values of the installed consumers.

2. Qualitative quality index

The quality in terms of sustainable improvements for the consumption of electrical energy is assessed by defining efficiency-enhancing measures in the equipment of technical systems. The hypothesis is based on the fact that higher-quality installations lead to an improvement in the energy balance of the facility.

Keywords: energy efficiency, sustainability, safety systems, energy supply

1. INTRODUCTION

1.1. Sustainability - a means to an end

Austria has a modern, highly technologized and distinctly available transport infrastructure. The establishment of the Autobahnen- Schnellstraßen- Finanzierungs- Aktiengesellschaft (ASFINAG) created the basis for the continuous expansion and modernisation of the high-level transport network. In the heart of Europe, ASFINAG's roads form important connecting routes in the Alpine region due to their partially exposed location.

These routes have 166 road tunnels to enable comfortable passage through the Alpine region. This enables all road users to travel safely at any time of the year and even in poor weather conditions. With Directive 2004/54/EC [1] on minimum safety requirements for tunnels in the trans-European road network and the Austrian Road Tunnel Safety Act [2], these facilities were comprehensively upgraded in terms of safety by 2018 and are among the safest tunnels in Europe [3]. ASFINAG's responsibility throughout Austria and the development of planning premises (ASFINAG planning manuals) have standardised the equipment and functionality of the tunnels. With the expansion, the tunnels were brighter lit and better ventilated. With the additional information systems, information signs, traffic light signalling systems and many sensors and actuators, the facilities have become high-tech systems and guide road users safely

through the tunnels. However, all these safety systems have one thing in common. The components are operated using electrical energy and the safety expansion leads to an increase in the energy consumption of the tunnels. They consume the most electrical energy within ASFINAG. This fact motivates us to optimize our analysis of energy consumption in the tunnel facilities.

In addition to economic aspects, new legal framework conditions such as EU and national requirements and certification measures have led to a sensitisation regarding sustainability and the introduction of regular audits on efficiency and energy consumption within ASFINAG. Due to the rapid development of LED technology, efficiency-enhancing measures with the use of LED tunnel lighting were also considered during refurbishments in parallel with the safety expansion and are now also having an effect as electricity consumption in the tunnels is falling again. In addition, qualitative measures with the expansion of alternative energy generation systems in the tunnel are also leading to a reduction in the purchase of electrical energy.

For the classification we are pursuing the development of an evaluation system that focuses on both the quantitative comparability of tunnel facilities and the qualitative assessment based on sustainable or improved equipment. Electrical energy is one of the most important forms of energy and the best alternative for protecting our environment thanks to the options and chances of sustainable energy generation. *Saving energy is the key to combating climate change and reducing energy dependency* [4]

1.2. Objective

Improving energy efficiency naturally covers many areas in the traffic and transport sector. At ASFINAG, the core topics include:

- Conservation of resources
- **Energy an emission during operation**
- Traffic emissions
- Biodiversity
- Landscape
- Noise protection

Not only the shift towards e-mobility, but also the range of construction measures and the maintenance of operations through sustainable solutions and systems is constantly growing.

1.3. Energy consumption in the operation of our road infrastructure

As an ISO 50001 certified company, ASFINAG is obliged to take measures:

- to improve the CO₂ balance by using resources sparingly and utilising potential for improvement,
- to reduce energy consumption by implementing efficiency-enhancing projects with positive profitability certificates,
- to comply with legal requirements with a positive impact on owners, employees, and customers

To achieve this, the goal of electricity self-sufficiency by 2030 was set. The measures are divided into the qualitative expansion (e.g., to generate 100 MWp of electricity) in the route network and the quantitative analysis of consumption behaviour to reduce energy consumption by 20% per route kilometre. At around 94 GWh, tunnels account for the largest share of total electrical energy consumption within ASFINAG.

1.4. Hypotheses

Analysing the consumption characteristics of electrically operated tunnel safety equipment and electrical equipment leads to worthwhile potential savings in the consumption of electrical energy without compromising safety-related functions. By forming consumption groups, system-specific features can be analysed in a structured manner regarding consumption and innovative and sustainable solutions can be developed in a targeted manner. Sustainable and innovative solutions for increasing efficiency can be argued more easily and further developments are promoted.

- The analysis of measurement data on the consumption behaviour of tunnels leads to a comparability of the Austrian tunnel system. The classification can be based on the energy classes of the EU energy label.
- Improving equipment features that lead to a qualitative improvement in the tunnel systems in terms of sustainability or efficiency can be assessed and can be considered in the planning phase for refurbishments, etc.

1.5. Methodology for development work

The answers to the questions and the development of the evaluation models should lead to a comparability and recognisability of analogies in the 166 tunnels in the high-level Austrian railway network and are analytically carried out by:

a. Literature research

The general basic approaches to the EU energy label [5] are collected for the basic research. The aim is to derive a comparability like that of electrical appliances in general and to develop an understanding of the approach to categorisation. Existing elaborations, e.g., from the Swiss Federal Roads Office (ASTRA), which deal with the energy efficiency of road tunnels, are considered.

b. Quantitative content analysis

To obtain a practical reference or results under real conditions and to be able to compare these with the calculations and theoretical approaches, measurement data from existing tunnels are collected and analysed. The load profiles (15-minute values) of the electricity supply company for the respective tunnel system are primarily used as measurement data. For the verification of data, the existing documents regarding the equipment of the tunnel systems and, if available, the balance sheet design and energy distribution are primarily used. Technical specifications for function, operating mode, hazard classes and operating behaviour are applied based on technical documentation, safety documents, planning premises and guidelines.

c. Qualitative content analysis

The considerations of sustainability-improving measures and equipment in tunnels are included in a catalogue of measures based on procedures and studies on the respective main topic. Calculation approaches are analysed and described using examples for the applicability and allocation of a points system based on quality characteristics and for the presentation of the savings and improvement potential.

2. DEVELOPMENT OF ENERGY LABEL AUSTRIAN ROAD TUNNELS

2.1. Data analysis of the consumption values

The 15-minute load profile values per year for all 166 tunnels are standardised using the existing metering points of the energy supply systems. To ensure comparability, the data was verified for plausibility, traceability and usability. A qualitative and quantitative check was

carried out and transferred into an editable form. The following key exclusion features were identified when checking the usefulness of the data sets:

- Measurement gaps

Data series that are not representative over a longer period (weeks, months with "0" values)

- Supply of several tunnels of a metering point

Data series that show consumption values that cannot be traced or where the supply of several tunnels or other installations lead to an influence due to the circumstances.

After appropriate verification, the data of 53 tunnels >500m (expansion in accordance with the Road Tunnel Safety Act STSG) and 8 tunnels <500m with usable consumption values are available after the inspection of 166 tunnels. The 15-minute power values are converted with a factor of 0.25 to obtain electrical energy values in kWh. The annual energy consumption is calculated by adding the values.

2.2. Development of reference figure for the energy label

In most cases, the key figure in kilowatt hours per year (kWh/a) is used to compare the consumption characteristics of the electrical appliances. Due to different system characteristics, e.g., the length of the tunnel and the number of lanes, considerations were considered during development to obtain as homogeneous a basis as possible for all tunnels and to eliminate their influences. In the initial analysis, the benchmark

$$\frac{kWh}{a * FSm}$$

to quantify comparative approaches, attempts were made to derive analogies based on the analysis of annual energy data by grouping various tunnel characteristics, such as operating mode, hazard classes, geographical evaluation, ventilation system and traffic volume. However, the analysis of this basic data did not lead to a useful result. During further investigations, a reconsideration of the connection with

$$\frac{MWh/a}{FSm}$$

The benchmark used is therefore made up of the annual energy consumption per year (MWh/a) and the sum of all lane lengths in metres or the lane metre (FSm). This correlation enables a more homogeneous categorisation. Here too, the influencing factor of tunnel length and number of lanes is eliminated by referencing the FSm.

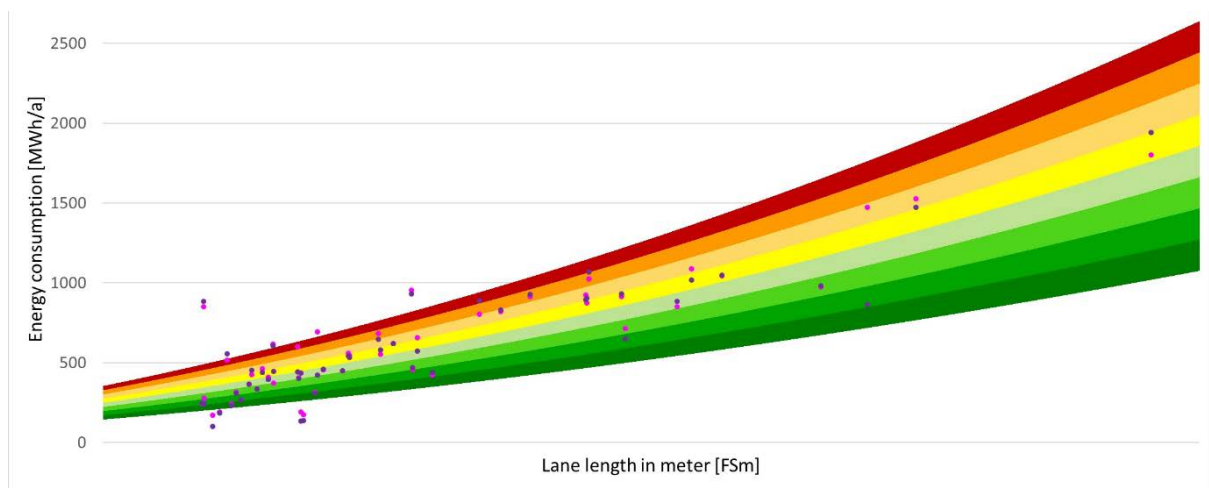


Figure 1: Evaluation of the energy values (MWh/a) in relation to FSm for example longitudinally ventilated directional traffic tunnels

To assign the tunnels to the label classes, the percentage shift in 10% increments was used for the naturally or longitudinally ventilated tunnels selected in Figure 1. For cross-ventilated tunnels, the transition is made in 5% steps. As shown in Figure 1, the result is a largely linear progression and erratic transition areas are eliminated. It is easier to read in consumption data by analysing the annual curve. Further analyses are therefore based on these findings and the use of the representative data sets defined in section 2.5.

Table 1: Evaluation examples for length ranges <7000m lanes with benchmark and category (Energy data base 2022)

F5m Bereich	<2000m		<3000m		<4000m		<5000m		<6000m		<7000m	
Tunnel	Tretting	Bergisel	St. Georgen	Kreuzergegend	Wolfsberg	Flirsch	Niedernhart	Falkenberg	Zederhaus	Noitzmühle	Kalcherkogel	Herzogberg
F5m	1800	1914	2400	2440	3250	3252	4520	4554	6180	6532	7948	7980
MWh/a (22)	101,7	184,3	364,3	453,5	437,4	134,5	534,2	647	886,9	832	893,9	905,2
Kategorie	A+	A+	E	C	C	A+	D	E	G	E	E	E

As can be seen from the selection in Table 1, comparable consumption characteristics can be derived using the annual key figure in MWh/a (based on 2022) and the allocation of lane meters. The significant deviation in the consumption value, for example in the area <4000m from the Flirsch tunnel, is due to the influence of the internal consumption of a small hydroelectric power plant. The consumption behaviour is correspondingly higher but cannot be determined due to the lack of measurement data. In the length range <6000m, the tunnels are very close to the border areas and therefore fall into category E or G.

2.3. Labelling of the tunnel systems based on annual energy values

The energyload profiles and the data from the years 2021 and 2022 were used to derive the data, which was then presented with the category classes based on the EU label. For the 2022 data set, this results in the classification reading to Figure2 for the individual tunnels on the high-ranking Austrian road network.

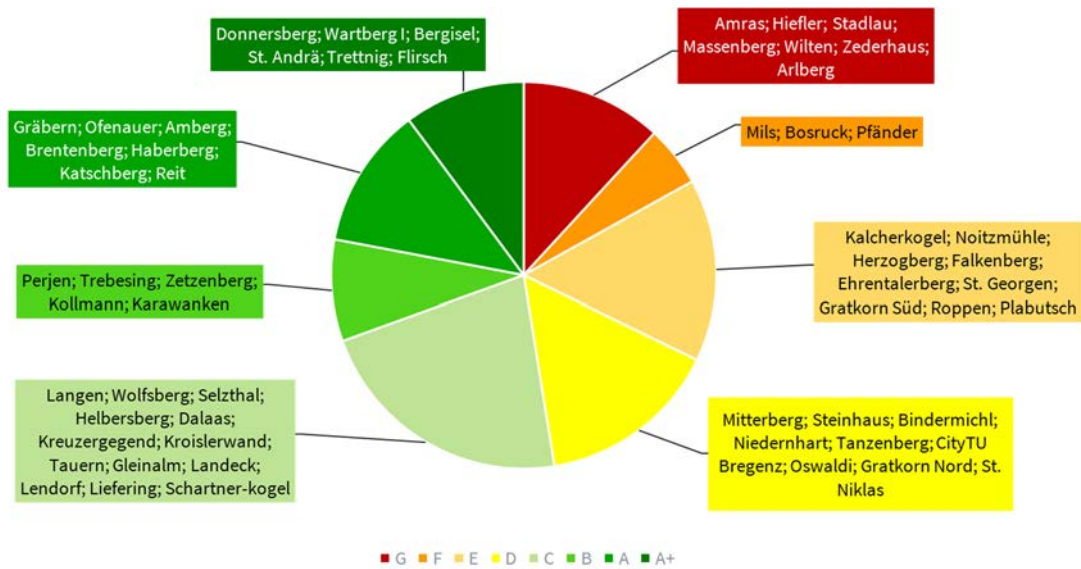


Figure 2: Categorisation and labelling with energy data from 2022

3. „ECODESIGN“ AND EVALUATION OF QUALITATIVE MEASURES

3.1. Quality features of the Austrian tunnelling system for a continuous improvement

The energyload profiles of some tunnel systems could not be used for the quantitative analysis. As described in chapter 2.1, the data was implausible. The causes influencing the measurement results and metering values of the feed-ins were sought by means of questionnaires on the existing plants, checking energy balances or meticulously searching through existing documents. A comparison of the annual energy data revealed striking changes. The supply and self-consumption of alternative energy supply systems can be mentioned here as an example. The unambiguous allocation of consumption, but also of the supply of individual systems, cannot be made due to the lack of consistent individual measured values within a system.

3.2. Evaluation model for the representation of qualitative characteristics in equipment and the operating and safety facilities as consumers of electrical energy

The operational and safety systems must be installed and operated in the tunnels in accordance with the regulations and guidelines. The large number of electrical consumers fulfil a wide variety of tasks. There are systems that are largely only installed in the event of an accident and others that have to be operated permanently during operation. There are also measures that are indirectly related to the electrical consumers. In this respect, the energy requirement due to the large number of safety measures is not necessarily related to the efficiency of the tunnels. The operation of alternative energy sources does not lead to an improvement in efficiency either. A catalogue of points was therefore chosen for the evaluation methodology to assess quality. A selection of criteria can be made for the tunnels and the energy requirement category can be determined using the points model. A standard ASFINAG tunnel is defined as follows:

Table 2: Definition of a standard tunnel in ASFINAG

Control speed	100km/h
Hazard class	III
Ventilation system	Longitudinal
Annual running time ventilation system	10-50h
Fire-fighting system	none
Pressure generation system	Elevated tank
Pumps for water protection systems	< 5kW / < 200h
Other consumer	< 5kW / < 200h

By referencing the characteristics, systems with a high energy requirement defined by criteria such as laws, guidelines, environmental conditions, etc. can be identified. This energy requirement can be improved by operating alternative energy sources. Result categories are:



Figure 3: Result categories

Efficiency-enhancing measures relate to the appropriate optimisation of electrical energy consumption. The improvement is achieved through technical solutions and has a positive and

sustainable influence on the efficiency of the generated benefit. Criteria can be determined in advance using a model calculation and efficiency can be influenced as a result. The following criteria are currently planned:

Table 3: Criteria for increasing efficiency

Transformer losses	Night-time lowering of traffic equipment
Type of uninterruptible power supply	Coolingtype of the electrical operating room
Light source of the lightning system	Frost portection fot the extinguishing water system
Type of luminous flux adjustment	Improvement of the reflexion coefficient of the covering
Condition of the wall coating	Light well glazing in the entrance area
Complete tunnel wash	

Additional criteria to increase efficiency can be added at any time.

3.3. Definition of standardised consumption classes with simulation of consumption values as a planning tool

The analyses of consumption and potential savings make one fact very clear. The derivations can only be made primarily through interpretation, manual allocation of data, analyses of existing documents and raw data. For better comparability, the tunnel consumers were divided into eight consumption groups.

Table 4: Definition of consumption group and manual allocation using energy balances

1	2	3	4	5	6	7	8
Entrance lightning	Lightning for IS / PB / Portal	Ventilation	Heating, ac, ventilation, plumbing	Control system	Safety systems	Traffic systems	others
Entrance	Indor track	Driving area	Ventilation system	Control system	Emergency call	Traffic light	Trace heating
	Brakedown bay	Cross conections	Air conditioning	Network system	Danger detection	Information sys.	Extinguishing water
	Outside portals	Auxiliary drive	Heating system		Video system	Var. traffic signs	Water protection
	Cross conections	Flap drive			Sound system	Guiding system	House installation
	Escape routes				Doors and gates	Height control	Cellular system
					Opening assistan.	Barriers	System lighting
					Radio system		Heater electrical cabinet
					Emergency light		Crane system
					Air quality		Shaft inspection
					Sensors		

By analysing and entering the performance data, it is possible to calculate the energy requirements for the tunnel systems. The analytical and interative approximation of the operating factors and annual seasonality is used to simulate the calculated energy curve over a year. The measured consumption data was then compared for verification and can be plausibly presented as in the example show in Figure 4.

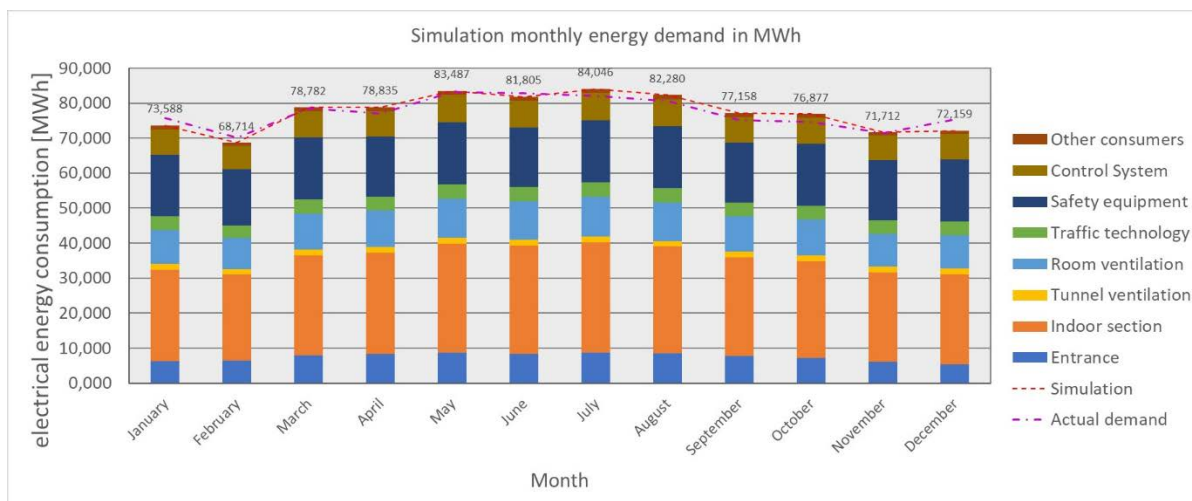


Figure 4: Simulation result of the monthly energy demand in MWh using the example of the Milser Tunnel

4. SUMMERY AND CONCLUSION

The comparability of tunnels via benchmarks and the energy label enable to evaluate and monitor the consumption characteristics of tunnels. In combination with this, the quantitative analysis is expected to further sensitise people to the consumption of electrical energy. The motivation to better record the consumption behaviour of systems in order to make targeted investments in more sustainable systems will be increased. The knowledge gained will also support the goal of establishing an appropriate energy management system. With the planning tools and observation models of the simulation, efficiency-enhancing system features can be taken into account in the run-up to refurbishments and extensions in the future. With the longer lead times, innovative approaches can be better analysed and thus promoted.

4.1. Findings from the studies

For both quantitative and qualitative analyses, there is a need to increase the quality of the input parameters and reduce the theoretical assumptions. This can be done by further checking detailed information, carrying out and expanding measurements and analysing existing data to verify the approaches taken. The quality of the data is particularly important here. Data collection is currently very time-consuming and resource-intensive. Possible solutions are offered by the plans for the expansion of energy management systems and an energy control centre within ASFINAG in order to handle both the expansion of renewable energy and the main consumers. Detailed evaluations of the consumption groups, e.g. by implementing measurement concepts and thus improving monitoring, can lead to functional and operational improvements in addition to energy optimisation. The knowledge gained from this closes the cycle of the continuous improvement process and can in turn be incorporated into planning assumptions.

5. REFERENCES

- [1] E. Parliament, „Minimum safety requirements for tunnels in the Trans-European Road Network,“ 2009.
- [2] „Bundesgesetz über die Sicherheit von Straßentunneln (Straßentunnel-Sicherheitsgesetz –,“ 2014.

[3] „European Pariliament,“ 17 10 2023. [Online]. Available: www.europarl.europa.eu. [Zugriff am 09 01 2024].

[4] S. Moser, „ASFINAG,“ 10 04 2023. [Online]. Available: <https://blog.asfinag.at/>. [Zugriff am 09 01 2024].

[5] „European Commisission,“ 2023. [Online]. Available: https://commission.europa.eu/energy-climate-change-environment/standards-tools-and-labels/products-labelling-rules-and-requirements/energy-label-and-ecodesign/about_en#a-new-generation-of-labels.

SUSTAINABLE TUNNEL OPERATION GENERATION OF ELECTRICITY THROUGH THERMAL AND PRESSURE-DRIVEN AIRFLOWS

¹Peter Sturm, ²Dietmar Harbauer, ³Roland Seebacher, ¹Daniel Fruhwirt, ³Klaus Krischan

¹Graz University of Technology,

Institute of Thermodynamics and Sustainable Propulsion Systems, AT

²ASFINAG, AT

³Graz University of Technology, Institute of Electric Devices and Machines, AT

DOI 10.3217/978-3-85125-996-4-06 (CC BY-NC 4.0)

This CC license does not apply to third party material and content noted otherwise.

ABSTRACT

The energy demand for the operation of a road tunnel is considerable. This results on one hand in high operation costs and – as the production of electricity is not free of fossil fuels – in a significant CO₂ footprint. There is an evident need to reduce energy costs as well as to improve the CO₂ footprint. Due to the high energy costs, alternative options for generating electricity are being considered. The question arises as to whether mechanical ventilation systems can be used in reverse operation to generate electricity in road tunnels when pressure-driven air flows are present.

This paper deals with aspects of pressure-driven air flows in general and their use for generating electricity in electrical machines. As a first step, an analysis was carried out for standard 2-lane tunnels with different lengths and meteorological pressure differences. As a second step, recorded pressure differences between portals or shafts were evaluated for selected Austrian road tunnels.

The calculation of the annual energy quantities for possible electricity generation was based on the actual pressure differences in tunnel systems in the Austrian motorway and expressway network. Based on the available measurement data, those tunnel systems that have a high meteorologically related pressure difference were selected for further consideration. Taking into account the aerodynamic conditions and the expected efficiencies of electricity generation, an expected annual amount of energy can be estimated.

Keywords: sustainable tunnel operation, meteorological pressure differences, electricity generation

1. INTRODUCTION

The operation of road tunnels is energy intense. According to information provided by ASFINAG, the Austrian motorway operator [1], a total of 108 GWh of electricity was consumed in Austria’s motorway tunnels in 2018. This corresponds to 76% of the total electricity consumption of the Austrian motorway network. ASFINAG’s strategic goals for 2030 are to reduce the energy consumption by 20%, cover their own electricity needs independently and increase the production of renewable energies to 100 MWp [1].

Within the framework of the tunnel power plant research project (Future Mobility Funding Program MdZ-VIT, FFG Project 893655), the possibility of generating electricity from meteorologically or thermally induced air flows in road tunnels was to be investigated [2].

Air flows in tunnel systems occur due to pressure differences between the portals. These pressure differences have meteorological causes. To a certain extent, the temperature differences between the air outside and inside the tunnel also contribute to the development of an air flow. Flows generated by the momentum of moving vehicles in the tunnel are not considered further because they are generated by the vehicle itself. Any “use” of this factor would therefore only be a transfer from one energy source (vehicle propulsion system) to another (electricity generation).

In high vertical shafts, such as those found in transverse-ventilated tunnel systems, thermally induced buoyancy flows occur, which can also be superimposed by different barometric pressures.

2. THEORETICAL POTENTIAL FOR ELECTRICITY PRODUCTION FROM AIR FLOWS IN TUNNELS

2.1. Mathematical model

Basically, air flows at higher speeds are turbulent flows. Such flows are usually three-dimensional. In the case of tunnels, however, a one-dimensional channel flow can be assumed due to the very long length of the tunnel. The extended form of Bernoulli's equation is applicable to such flows. Bernoulli's equation is valid for an incompressible, frictionless flow or, more precisely, along a streamline. In order to take friction and other resistances into account, it is extended so that these losses are taken into account by means of characteristic numbers with a quadratic dependence on the flow velocity. For a channel/tunnel with a constant cross section, the extended form of Bernoulli's equation is as follows:

$$\Delta p_{tot} = (\zeta_E + 1) * \frac{\rho}{2} * u_V^2 + \lambda * \frac{l}{D} * \frac{\rho}{2} * u_V^2 + \Delta p_F + \Delta p_T + \Delta p_{Turb}$$

The individual parameters of the equation are:

Δp_{tot} : pressure difference between portals, adjusted according to height

ζ_E : entrance loss for portal, the value 1 within the brackets represents the loss of kinetic energy at the exit

ρ : air density

u_V : air velocity in the tunnel or shaft

λ : wall friction coefficient

l : length of the tunnel or shaft

D : hydraulic diameter

Δp_F : pressure change due to vehicles in the tunnel (can be positive or negative)

Δp_T : thermally induced buoyancy forces in case of inclinations

Δp_{Turb} : pressure loss due to a turbine in generator mode

Thermally induced pressure differences can occur due to the different temperatures between the portal and the inside of the tunnel. They can be approximated as follows:

$$\Delta p_T = \Delta H * \rho * g * \frac{T_V - T_0}{T_V}$$

Where ΔH is the height difference between the portals, ρ is the air density outside the tunnel, g is the acceleration due to gravity, T_V is the mean temperature in the traffic area and T_0 is the absolute temperature of the outside air at the portal of the air inflow.

While thermally induced pressure differences in tunnels are of little relevance for the considerations made here due to the usually relatively small longitudinal gradient, this is very significant for high vertical shafts. Here, the temperature differences between the shaft base and shaft head act as driving forces. If one disregards a possible heat flow via the shaft walls between the surrounding rock and the flowing air, one can assume an almost isothermal behaviour of the air column. The equation shown above remains the same in principle. The driving force is now the difference between the temperature inside (= shaft base) and outside (= surroundings of the shaft head). Further influencing variables, such as wall friction, are small in comparison.

2.2. Theoretically achievable turbine power

The technical work or power of a turbo machine can be calculated as follows, disregarding the effects of friction and changes in external energies (kinetic, potential energy, etc.) and assuming a constant density in accordance with the first law of thermodynamics:

$$P_{Turb} = \dot{m} * \int_1^2 v dp = \dot{V} * \int_1^2 dp = A * u_V * (p_2 - p_1) = -A * u_V * \Delta p_{Turb}$$

The volume flow is calculated by multiplying the tunnel cross section (A) by the average air velocity in the tunnel (u_V). Since the pressure difference in the tunnel utilised by the turbine is quadratic to the air velocity, this results in a cubic dependence of the power on the air velocity.

A maximum value analysis can be used to determine the optimum air velocity at which (theoretically) the maximum power yield is achieved¹.

$$P_{Turb_{opt}} = A \cdot \frac{2}{3} \cdot \sqrt{\frac{1}{3} \cdot \frac{\Delta p_{tot}^3}{k_{Tunnel}}}$$

Whereby k_{Tunnel} represents the resistance of the tunnel multiplied by $\frac{\rho}{2}$.

Applying the above-mentioned equation to a standard two-lane tunnel with a cross section of 55 m² and assuming typical values for air density (1.175 kg/m³), entrance loss (0.85), wall friction (0.016) and efficiency of the turbine (0.7), the theoretically achievable turbine power output can be calculated as a function of pressure difference between the portals and tunnel length.

¹ Thermally and vehicle induced forces neglected

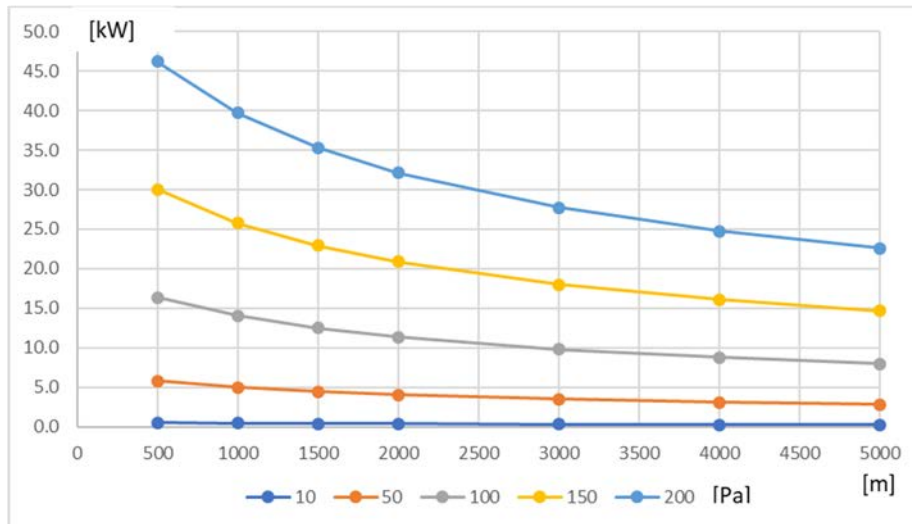


Figure 1: Theoretically achievable turbine power as a function of pressure difference between portals and tunnel length

As shown in Figure 1, a higher turbine power can only be achieved by combining a high pressure difference and a short tunnel length. This is of course diametrically opposed to the real conditions, as the pressure differences between the portals are usually rather small in short tunnels.

3. POSSIBLE APPLICATION TO AUSTRIA'S TUNNELS

Due to Austria's geographical location in the middle of Europe and its mountainous terrain, there are a very large number of road tunnels. According to [3], some 170 tunnels with a total length of around 400 km are currently in operation in the expressway and motorway network alone. As the Alps transect Austria in a west-east direction and act as a weather divide, quite considerable pressure differences can be expected. Since many tunnels are also equipped with a mechanical ventilation system, it can generally be assumed that many of them might be suited to the energetic use of air flows to generate electricity.

3.1. Pressure differences at selected Austrian tunnels

As part of tunnel construction and renovation projects, ASFINAG repeatedly carries out meteorological measurements on tunnel sections within the motorway network. These measurements usually extend over a period of one year (365 days) and concern the usual meteorological parameters such as absolute pressure, wind speed and wind direction distribution as well as air temperature.

In principle, a distinction is made between the two parameters "barometric air pressure" (static pressure) and "wind pressure" (dynamic pressure). Wind speeds (or the dynamic pressure) can in principle be measured with a higher accuracy than the absolute pressure (static pressure) or the resulting pressure difference between the two portals. It should be noted that, depending on the local location of the monitoring sensors and on the measuring conditions, both parameters may be linked. For example, if tunnel portals are located together in the same climatological area (e.g. in the same valley or in basins), a barometric pressure difference automatically acts as wind. Adding these two components would automatically lead to a double assessment in such a case. Simultaneous consideration of both pressures therefore only makes sense if there are decoupled meteorological situations at the two portals, as is the case, for example, with tunnels in the area of major Alpine crossings (usually combined with high overburdens).

As the two portals of tunnels without additional entrances or exits are usually at different altitudes, the measured data of the respective absolute pressure must be corrected in relation to the altitude of the monitoring sensor in accordance with ISO standard atmosphere (ISO 2533).

In a preselection process, data from 18 road tunnels (17 twin tube tunnels, one tunnel with bidirectional traffic) with a length of 1.5 to 14.0 km was selected. These tunnels included longitudinal ventilation systems as well as transverse ventilation systems. The shaft heights of the transverse ventilated tunnels ranged from 80 m to 780 m. Detailed data from all the investigated tunnels as well as details concerning the data processing can be found in reference [4].

In the majority of the road tunnels listed in Figure 2, the portal pressure difference is already below 50 Pa in the 95% percentile. For further exemplary considerations, therefore, only the Kalcherkogel and Semmering tunnels – representative of longitudinally ventilated tunnels – and the long Alpine crossing transverse ventilated tunnels are considered.

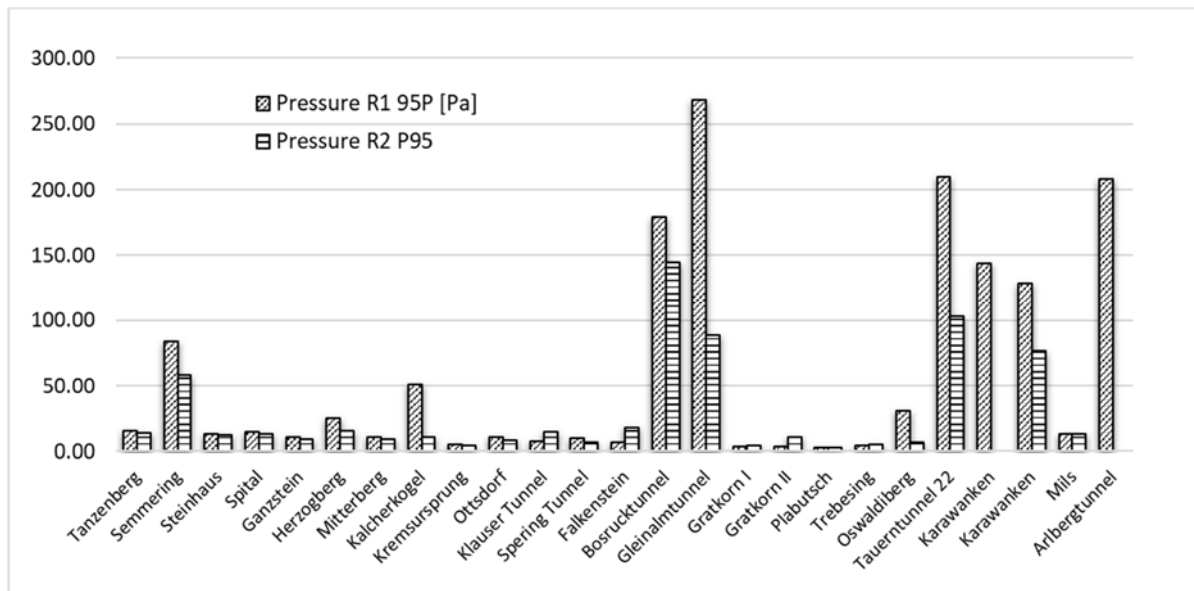


Figure 2: Meteorologically caused pressure difference between portals, 95% percentile values, R1 and R2 denote the different tunnel tubes

Table 1: Meteorologically caused pressure difference between portals

Name	Length [m]	5-P [Pa]	50-P [Pa]	95-P [Pa]	98-P [Pa]
Kalcherkogeltunnel*	2150	1	14	65	78
Semmering*	3062	3	36	99	131
Karawankentunnel**	7864	4	49	144	177
Bosrucktunnel**	5500	8	73	197	232
Arlbergtunnel**	13972	7	66	208	254
Gleinalmtunnel**	8320	7	77	258	308

* Longitudinal ventilation, ** Transverse ventilation

As can be seen on Table 1, the median pressure difference in the selected longitudinally ventilated tunnels is already noticeably below 50 Pa and between 50 and 77 Pa in the long

transalpine tunnels. This already considerably limits the possibilities for utilising pressurised air flows to generate electricity. Table 2 shows the values for selected vertical shafts.

Table 2: Buoyancy caused pressure in vertical shafts

Name	Height [m]	5-P [Pa]	50-P [Pa]	95-P [Pa]	98-P [Pa]
Gleinalm North	366	-30	44	204	299
Arlberg Albona	778	24	148	370	473
Plabutsch North	240	28	101	205	232

3.2. Electromechanical requirements for power generation

Before deploying new electromechanical equipment in the tunnel, the utilisation of the existing ventilation system in reverse mode as a turbine/generator unit shall be considered. The fan of a ventilation system is usually driven by an induction (asynchronous) motor.

General considerations

In order to bring an induction machine into generator operation, the rotating field must rotate slightly slower than the rotor. If the machine is supplied from the mains at a constant frequency, the synchronous speed (zero torque) is determined by the mains frequency and the number of pole pairs of the machine. The turbo machine must therefore change its behaviour at an almost constant speed in order to switch from fan operation to turbine operation. This would at least be conceivable with fans with adjustable blades. In case of a pole changing induction motor, the synchronous speed can be varied in fixed ratios by pole changing.

The rotor speed of synchronous machines is determined by the supply frequency and the number of pole pairs of the machine. Again, a transition from motor to generator operation with a constant frequency supply has to be caused by the load.

The directly grid connected induction machine allows the operation of the machine as a motor as well as a generator. The electrical machine (EM) drives a fan (F) or is driven by a turbine (T) (see Figure 3).

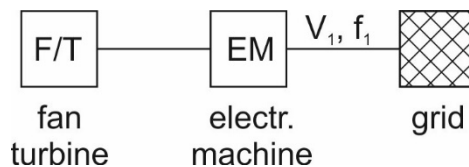


Figure 3: Induction machine directly connected to A/C grid of a certain voltage V_1 and a frequency f_1

If the fan requires a distinct change of speed to operate in regenerative mode, an adjustable speed drive is required. For AC machines this speed variation is achieved by adjusting the amplitude and frequency of the supply voltage. This applies to both the induction and the synchronous design of the AC machine. A DC inverter would be suitable to fulfil this task.

Currently the majority of existing speed-controlled jet fans in Austria are equipped with non-regenerative DC-link inverters, supplied by the grid via an uncontrolled rectifier. In order to supply electrical energy back into the grid, a grid side inverter is required (see Figure 4).

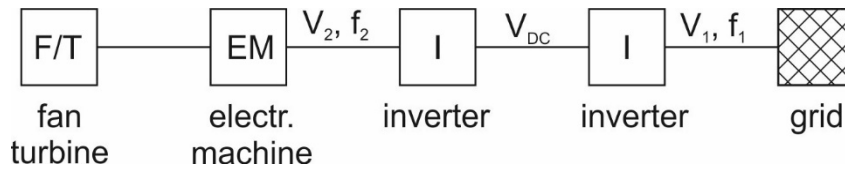


Figure 4: Adjustable speed drive, consisting of AC machine, machine side inverter, DC-link (V_{DC}) and grid side inverter

Existing equipment

The electromechanical equipment in the selected tunnels has the following characteristics:

- Jet fans: induction machines either with direct connection to the mains at 400 V/50 Hz or inverter driven (non-generative) at 400 V/50 Hz or 690 V/50 Hz
- Axial fans in transverse ventilated tunnels: pole-changing induction machines with direct connection to the mains, either 6 kV/50 Hz or 690 V/50 Hz, pitch-controlled. One tunnel is equipped with pitch and inverter-controlled fans, but the inverter is non-regenerative.
- All machines are designed for continuous operation.

4. ESTIMATION OF ANNUAL ENERGY QUANTITIES FROM THE PRESSURE DIFFERENCES

In order to estimate the potential power available for electricity generation, it is necessary to know the pressure differences and the air flow rate through the tunnel. In addition, tunnel-specific data is required in order to establish the tunnel resistance. The following boundary conditions were assumed:

- Cross section and number of jet fans or turbines as in the current situation
- Cross section of air ducts in transverse ventilated tunnels does not change and can be used over the full length of the tunnel
- No changes in tunnel geometry

Table 3: Relevant parameters for the geometry of the considered road tunnels

	Semmer- ing	Kalcher- kogel	Arlberg- tunnel	Bosruck	Gleinalm	Karawan- ken
Cross section jet fan/turbine [m ²]	1.23	2	2	2	2	2
Cross section air duct [m ²]			11.5	12.77	13.69	9
Number of jet fans	14	10	3	10	14	10
Tunnel length [m]	3,062	2,150	13,972	5,500	8,320	7,864

For the consideration of buoyancy driven air flows in the vertical shafts of transverse ventilated road tunnels, the following geometry was used:

Table 4: Relevant parameters for the geometry of the considered tunnel shafts

Tunnel shaft	Gleinalm North	Gleinalm South	Arlberg Albona	Arlberg Maienwasen	Plabutsch North	Plabutsch South
Cross section fresh-air duct [m ²]	17.3	17.3	20	23.5	28	28
Cross section return-air duct [m ²]	13.7	13.7	24.5	28.79	28	28

Hydraulic diameter fresh/return-air [m]	4.2/3.6	4.2/3.6	4.3/4.5	4.5/5.2	je 5.14	je 5.14
Shaft height [m]	366	287	778	260	240	90

For the purpose of comparability, the following assumptions were made for the other necessary input data:

- Available tunnel cross section 48.7 m², hydraulic diameter 6.9 m, air density 1.1 kg/m³, wall friction coefficient 0.016, pressure loss entrance 0.3 (tunnel portal and horizontal air ducts) or 1 (vertical shaft).
- When considering the air flow passing a wind turbine in a road tunnel, it has to be considered that due to the increased air resistance inside the turbine, a considerable amount of air will “bypass” the turbine. According to Betz [5] and [6], a wind turbine is capable of utilising some 60% of the theoretical available energy of a free-flowing wind. This is different to the situation in an air duct, where the full cross section can be utilised for electricity generation.
- Turbine efficiency (isentropic): 0.7
- Efficiency of electrical machines:
 - For those tunnels for which machine data was available, a constant loss according to rated power was assumed.
 - A similar procedure is used for the remaining tunnels, but simplified data values from machines of a similar size were used.
 - The energy losses from the inverters were calculated according to IEC 61800-9-2:2017 for the rated operation point of the electrical machines.
 - A transfer of power into the grid can only happen when the usable power is higher than the power loss by the electrical machine and inverter (for details see [4])

The pessimistic treatment of the electrical losses, in particular, resulted in a “loss” of the power share in the low Watt range. As these power ranges most frequently during a year, the total loss in usable electrical energy is quite considerable. As shown in Figure 5, there is a big difference between the work provided by the turbine (dashed line) and the equivalent delivered into the electrical mains (solid line). But this figure also shows the fact that the required power range of the turbo machine is in the range of a few W to 1.5 kW in the case of the jet fan application, while for the operation in a shaft, the power range is between a few W and 30 kW. Compared to the operation range in fan mode, in both cases this is one to two orders of magnitude higher. This suggests that a simple usage of existing electrical drives for both modes of operation does not seem to be feasible.

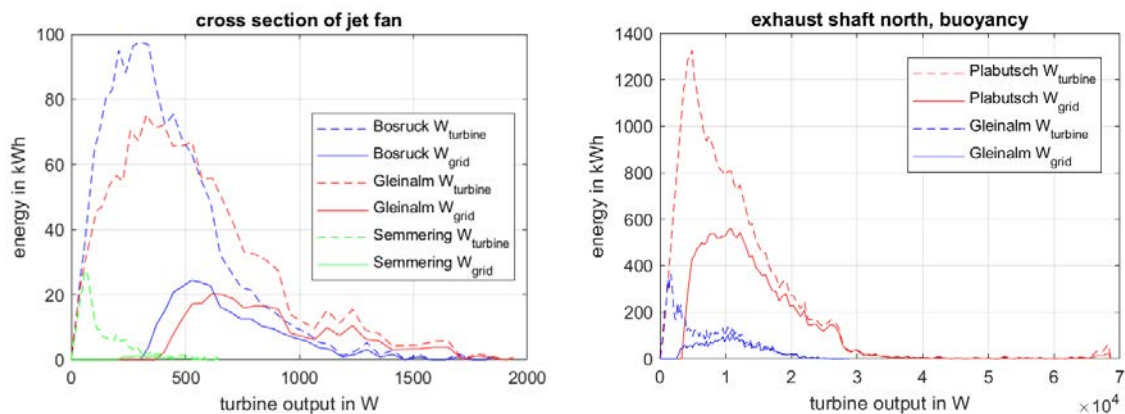


Figure 5: Comparison between work provided by the turbine (dashed lines) and delivered into the electrical grid (solid line) for jet fan application (left) and shaft application (right)

Other influencing variables such as variable flow speed, inertia of the air mass etc. were not taken into account when determining the annual energy quantities. Further details about input and boundary conditions can be found in reference [2] and [4].

4.1. Utilisation of portal-to-portal pressure differences (longitudinal airflow)

In twin-tube tunnels with bidirectional traffic as well as when utilising the horizontal airducts in transverse ventilated tunnels, active operation of the ventilation system during normal operation happens very rarely in the considered road tunnels. Hence the periods with an active longitudinal ventilation system were neglected in the estimation of the yearly achievable electrical energy.

On the basis of the available pressure gradient, the following values for the amount of electrical energy that can be generated annually can be estimated, taking into account the above-mentioned efficiencies and boundary conditions (see Table 2).

As expected, higher meteorologically induced pressure differences only occur in longer road tunnels (with a higher overburden), but these also have a higher pressure loss due to their greater length; these two factors – high barometric pressure differences and long tunnel length – are diametrically opposed. As a result, the power generation potential in the purely longitudinally ventilated tunnels is low, as expected.

Table 5: Generated electrical energy on an annual basis [kWh]

	Per jet fan*	All jet fans*	Utilization of air duct
Kalcherkogel	15.6	156	-
Semmering	10.8	151	-
Arlberg	103.8	313	1943
Bosruck	206.4	2064	5323
Gleinalm	231	3234	5079
Karawanken	85.2	1191	1645

* Generator mode (turbine)

4.2. Utilisation of buoyancy driven air flows in vertical shafts

Transversely ventilated tunnels with a high air intake and exhaust shafts generally have greater potential for utilising buoyancy driven air flows to generate electricity. However, these shafts are also used more or less often during normal operation to ensure the necessary air quality in the tunnel. This is very often the case with a single-tube tunnel such as the Arlberg Tunnel. In twin-tube tunnels - such as the Gleinalm Tunnel - self-ventilation by vehicles is often sufficient so that the shaft fans only rarely need to be used. Such aspects must of course be considered when estimating the potential for electricity generation. This aspect means that the high pressure differences acting in the Arlberg tunnel can only be utilised for about 1/3 of the year, while in the other long double-tube tunnels they can be utilised almost 100% of the time.

Table 6: Generated electrical energy in vertical shafts on annual basis [kWh]

Tunnel shaft	Gleinalm North	Gleinalm South	Arlberg Albona	Arlberg Maienwasen	Plabutsch North	Plabutsch South
Electrical Energy [kWh]	5,545	2,628	19,272	4,380	24,538	5,056

When discussing the values provided in Table 6, it has to be considered that the high availability of the Plabutsch north shaft, combined with a very high volume flow (big cross section), results in the highest achievable amount of generated electrical energy. On the other

side, the low availability of the Albona shaft (which is by far the highest vertical shaft of a road tunnel in Europe) strongly reduces the possibility of electricity generation in this shaft.

5. SUMMARY AND CONCLUSION

The effort to reduce the high energy consumption (and CO₂ footprint) of Austria's road tunnels and to achieve cost reductions leads to the investigation of innovative concepts for electricity generation. In one of these concepts, the question arose as to whether mechanical ventilation systems can be used in reverse operation to generate electricity in road tunnels when pressure-driven air flows are present.

The power of a turbo machine is proportional to the volume flow rate through this machine and the pressure drop across the machine. This means that in a duct flow there is a cubic relationship between air speed and machine power. It can also be expressed as a relationship between machine power and the acting pressure difference to the power of 3/2 and a proportional factor dependent on the tunnel resistance. From this relationship, it can be deduced that the higher the pressure differences between the portals or across shafts and the shorter the tunnel/duct, the higher the electrical power that can be generated.

This contradicts reality, as high meteorologically caused pressure differences only occur in tunnels that cross under a large mountain range. With thermally driven flows, shafts with appropriate heights are required in order to be able to convert a relevant amount of energy.

The use of existing fans in generator operation is contradicted by the fact that the power requirement in fan operation is orders of magnitude higher than in generator operation. The currently installed electrical machine part is therefore unsuitable for economical generator operation due to the high inherent losses.

The calculation of the annual amounts of energy that can be utilised to generate electricity was based on the actual pressure differences in tunnel systems in the Austrian motorway and expressway network. Based on this data, the tunnel systems with high meteorologically-generated pressure differences were selected for further consideration. For the respective tunnels, it was assumed that the existing ventilation equipment shall be used in reverse mode for electricity generation.

When considering the longitudinal ventilated tunnels, the reverse operation of the turbo machines would lead to an electricity production in the range of 160 kWh. Using the turbo machines in the existing transverse ventilated tunnels results in an electricity production in the range of between 1,620 kWh to 3,230 kWh. As the transverse ventilated tunnels offer the possibility to use the air duct (above the false ceiling), an annual electricity production in the range between 1,645 kWh and 5,320 kWh would be achievable.

When utilising the big vertical shafts of transverse ventilated road tunnels, the availability of such a shaft is of high importance. In single-tube tunnels with bidirectional traffic, the ventilation is quite often used during normal operation. This is totally different for Austria's double-tube tunnels with unidirectional traffic. In those tunnels additional mechanical ventilation during normal operation is in most cases not needed. The latter is the case e.g. when considering the Plabutschunnel north shaft. Here an annual electricity production up to 24,540 kWh would be achievable.

In order to be able to classify the values listed above correctly, they can be compared with the average annual electricity consumption of an Austrian two-person household. This amounted in 2022 to almost 3,100 kWh.

However, for all the investigated cases, it must be mentioned that the numbers given above are rough estimations and can vary in both directions. The following restrictions need to be mentioned:

- Simplifying assumptions were made regarding efficiencies in the power generation chain (from the turbine to the power grid interface). Values were assumed that must at least be achieved in accordance with normative specifications. Lower losses are to be expected in real electrical systems, which means that a higher annual output per system can be expected.
- The benchmark refers to a theoretical machine choice. When installing small wind turbines specifically tailored to the existing performance potential, a higher yield may be achieved.
- The results relate to optimised, low-resistance flow conditions in air ducts and shafts. For example, inflow losses via any air damper, deflections in the air path etc. were not taken into account in the estimates. Such considerations would require detailed project planning.

Generally speaking, it can be concluded that a simple upgrading of existing engine and turbo machine combinations (ventilation systems) by means of additional electrical equipment such as inverters will not be sufficient to end up with an economically feasible electricity production system. The installation of additional wind turbines, in combination with all the required civil works for improving the air path, would be required. Whether such an effort is economically and also ecologically feasible has to be decided on a project-by-project basis. However, the investigations showed that at best, high buoyancy driven air flows in high vertical shafts could be used to generate electricity to a feasible extent, provided they are not occupied by ventilation for normal operations.

6. REFERENCES

- [1] List R.: The way to sustainable and efficient road tunnel operation, International PIARC Seminar on “Advances in Design, Construction and Operation of Tunnels, Dehradun, India, April 19th 2023
- [2] FFG MdZ: <https://projekte.ffg.at/projekt/4429532>, access Dez. 28th 2023
- [3] BMK: Statistik Straße und Verkehr, Federal Ministry, Republic of Austria, Climate Action, Environment, Energy, Mobility, Innovation and Technology, Bundesministerium für Klimaschutz, Umwelt, Energie; Vienna, June 2023
- [4] Sturm P., Fruhwirt D., Seebacher R., Krischan K.: Möglichkeit von Stromerzeugung aus meteorologisch oder thermisch bedingten Luftströmungen in Straßentunneln, ITnA Bericht Nr. I-30/23/PSt/V&U Inst_21/014/1640, <https://doi.org/10.3217/0aa6q-c0k47>, Graz University of Technology
- [5] Betz, A.: Das Maximum der theoretisch möglichen Ausnützung des Windes durch Windmotoren. *Zeitschrift für das gesamte Turbinenwesen*, Band Heft 26, 1920
- [6] Schaffarczyk, A.P.: Introduction to Wind Turbine Aerodynamics, Springer Verlag Berlin, 2014

VALIDATION OF SIMPLIFIED VARIABLE SPEED CONTROL FOR ROAD TUNNEL JET FANS

¹Kaito Onoda, ¹Ryoichi Ishizawa, ²Keigo Hatamoto, ³Hibiki Sako, ³Toshiaki Sakaguchi,
⁴Alan Vardy

¹Hanshin Expressway Co., Ltd, JP

²Hanshin Expressway Research Institute for Advanced Technology, JP

³Sohatsu Systems Laboratory Inc., JP

⁴University of Dundee, Dundee, Scotland, GB

DOI 10.3217/978-3-85125-996-4-07 (CC BY-NC 4.0)

This CC license does not apply to third party material and content noted otherwise.

ABSTRACT

In 2010, the first variable speed control system for tunnel jet fans was installed in the Kobe Nagata Tunnel in Japan. Its purpose was to achieve energy savings in comparison with constant speed control. The original installation, which was based on a 3-level inverter, became due for replacement after more than a decade of successful use. The decision was made to replace it with a system based on a 2-level inverter with the aim of improving space factors, weight, and maintainability. The present paper deals with the entire replacement process that began with the development and verification of the simplified (i.e. 2-level) variable-speed control, followed by validation tests during the migration from the original system. The functionality and effectiveness of the new system are described and future potential is discussed.

Keywords: jet-fan inverter control, advantages of 2-level inverters, replacement and validation of jet-fan control system

1. INTRODUCTION

In 2009, Nakahori et al [1] confirmed an earlier revelation by Bopp [2] that energy savings in jet-fan operations could be achieved by running groups of jet-fans at a low speed instead of fewer fans at full speed. They compared the performance of 2-level and 3-level inverters and concluded that the superior performance of 3-level inverters would be needed for this purpose despite disadvantages of increased capital costs and space requirements.

In a simultaneous development, described later by Kawabata et al [3], a powerful new noise filter known as a distance free surge absorber (“DFSA”) was shown to be capable of greatly reducing all kinds of electrical noise that could be caused by the use of inverters in road tunnels. This opened the door to enabling the use of long distances between the inverters and the jet fans that they were to control and hence avoiding the need to have inverters in the tunnel space.

A combination of 3-level inverters and DFSA was adopted for the control of five (5) jet-fans at the Kobe Nagata Tunnel in 2010, and led to energy savings reported by Kanazawa et al [4]. Since then, more than 130 jet-fans in 15 tunnels in Japan have been operated successfully by the jet-fan inverter control. Furthermore, the use of inverter control outside Japan is receiving increasing interest for similar reasons – e.g. the E4 Tunnel in Stockholm [5].

Developments in inverter technology have now progressed to an extent that makes a compact and lightweight 2-level inverter a potentially standard product for use in tunnel ventilation. To take advantage of this progress, a combination of 2-level inverters and DFSA has been assessed and refined in an extensive development program. Importantly, it has been found

that, by increasing the carrier frequency from 5 kHz to 8 kHz, it is possible to use identical DFSA designs for both 3-level and 2-level inverters. This versatility has been verified in full-scale factory tests reported by Sako et al [6] in which 2-level and 3-level inverter control of a jet fan were assessed. In the tests, the noise reduction performance of the 2-level inverter control system was as strong as that for the 3-level inverter system.

The lifetime of the general-purpose inverter for the road tunnel varies from supplier to supplier. The 3-level inverter systems adopted at the Kobe Nagata Tunnel were deemed ready for replacement after more than ten (10) years and the decision was taken to replace it with the newly developed 2-level system. This was done over a period of three (3) years, thereby enabling experience of actual operation to be gained gradually. Most of the remainder of this paper is a description of the whole replacement process at the tunnel including validation tests in a comparative study of the noise-elimination performance of the old and new systems. A summary of future installation plans for inverter control of jet-fans is then given and key conclusions drawn from the paper are summarized.

2. INSTALLATION OF INVERTER CONTROL IN THE KOBE NAGATA TUNNEL

2.1. Outline of inverter control in the Kobe Nagata Tunnel

The Kobe Nagata Tunnel is 4.0 km long and is located on the Kobe Yamate Line of the Hanshi Expressway No. 31. Figure 1 shows an overview of the tunnel, with the part labelled ‘south extension’ being added to the original tunnel in December 2010. The concentrated exhaust longitudinal ventilation has three ventilation stations in the tunnel (Hasumiya, Myohoji, and Chuo). The south extension has portal leakage suppression control by the five jet-fans. A comparative study between inverter-based variable-speed control and constant speed control for the jet-fans was conducted at the time of installation [4]. Then, after a period of operation, the *measured* power consumption of inverter-controlled fans was found to be much smaller than that predicted in simulations based on constant-speed control. It was concluded that this is partly because the inverter control has a high rate of operation as the Kobe Nagata Tunnel is located at the center of the Kobe City and conveys more than 20,000 vehicles/day.

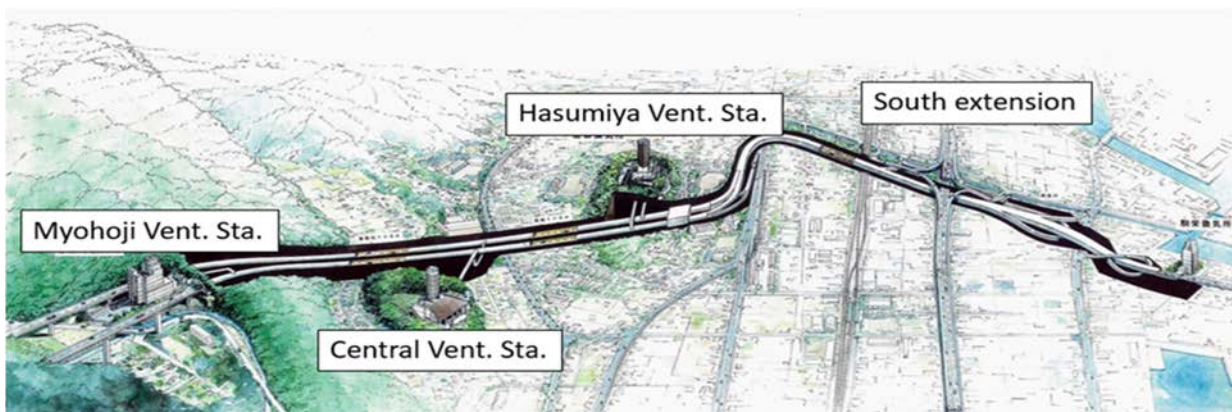


Figure 1: Overview diagram of the Kobe Nagata Tunnel

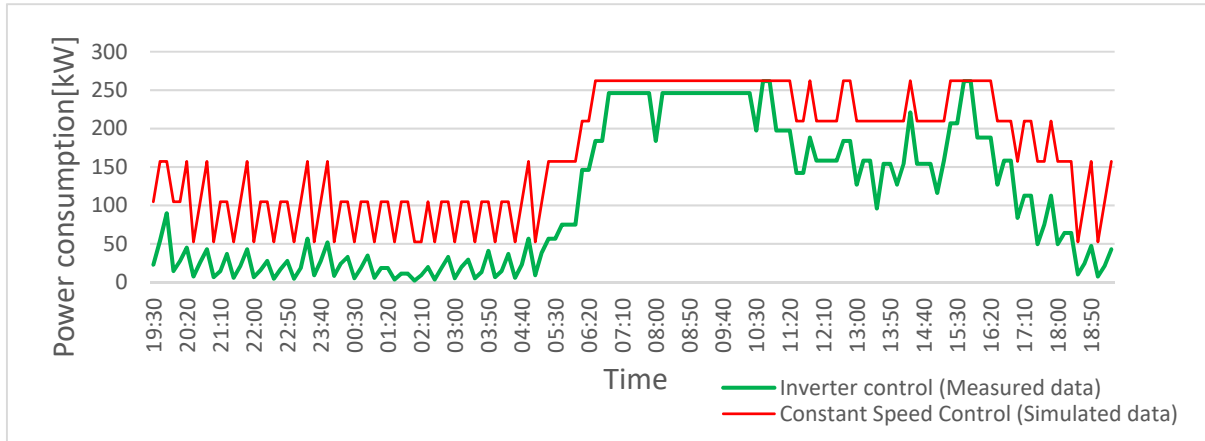


Figure 2: Comparison of power consumption between inverter-based variable and constant speed control

2.2. Demands for replacement of inverter control

The industry standard design life of inverters, capacitors and PLCs in the original variable-speed control panels was approximately 10 years, whereas that of the reactor and transformer was at least 20 years. As the time for replacement approached, it was decided to replace only the components with the shorter lifetime such as inverter unit, capacitors and PLC, and to remove damping resistors in the DFSA filter, thereby saving cost and minimizing disruption. This work was carried out in 2020 and the opportunity was taken to take advantage of progress in the development of a simplified control system using 2-level inverters instead of the original 3-level inverters.

3. REPLACEMENT OF INVERTER CONTROL IN THE KOBE NAGATA TUNNEL

3.1. Verification of the simplified variable-speed control

Table 1 gives a comparison of the 3-level and 2-level inverters. It shows that 2-level inverters have important advantages over 3-level ones

Additionally:

- 2-level inverters excel in size, weight, and efficiency.
- The carrier frequency in 2-level inverter can be up to 8 kHz, whereas that for 3-level inverters is 5 kHz. This has the additional benefit of enabling the DFSA filter to be smaller than is required for 3-level inverters.

The acceptability of electrical noise generated by 2-level inverters has already been verified in factory tests [6]. However, it was considered necessary to validate it in actual tunnel tests.

Table 1: Comparison between 3-level and 2-level inverter of 50 kW

Items	3-level inverter	2-level inverter
Width x Depth x Height	450×348×725 mm	264×335×543 mm
Weight	90 kg	39 kg
Efficiency	~97%	~98%
Carrier frequency	Up to 5 kHz	Up to 8 kHz

3.2. Validation test of the simplified inverter control prototype

The factory tests [6] clarified the magnitude of the zero-phase current, the prime source of noise. They showed that little difference exists between the performance of the two types of inverters when DFSA filters are used. The zero-phase current, however, varies depending on many factors such as power cable length, power cable type, electrical power receiving/transforming equipment, grounding circuit, inverter operating frequency, and jet-fan motor characteristics. Therefore, a test to compare the zero-phase current of the existing 3-level inverter control and the new simplified inverter control prototype was conducted with the jet-fan #1 which is controlled with the longest cable of 800 m from the control room.



Figure 3: Prototype control

The power cable for the jet-fan #1 was disconnected from the existing 3-level inverter control panel and temporarily connected to the 2-level prototype control panel shown in Figure 3 to

conduct a validation test. The zero-phase currents of the two inverter controls were measured at 20, 30, 40, 50 and 60 Hz of the power frequency with the results shown in Figure 4. The zero-phase current of the 2-level inverter control indicated a larger magnitude than 3-level control in the lower frequency region such as 20, 30, and 40 Hz. The reasons of the large magnitude are considered due to the operating principles which differ in the 2-level and 3-level inverter such as the pulse amplitude and modulation method. A trial was tested to see an impact of increasing the zero-phase inductance by adding one more reactor on the zero-phase current. As expected, the zero-phase current became smaller as is shown in Figure 4. It has been confirmed that enhancing the zero-phase reactor (using two reactors for example) reduces the zero-phase current. The zero-phase current of the prototype control was the maximum of 220 mA at 20 Hz with the simplified design. This is far smaller than 1,000 mA which is considered as the acceptable upper limit of the zero-phase current [7]. Accordingly, it was decided that no enhancement of L_z (zero-phase reactor) was required in the DFSA filter.

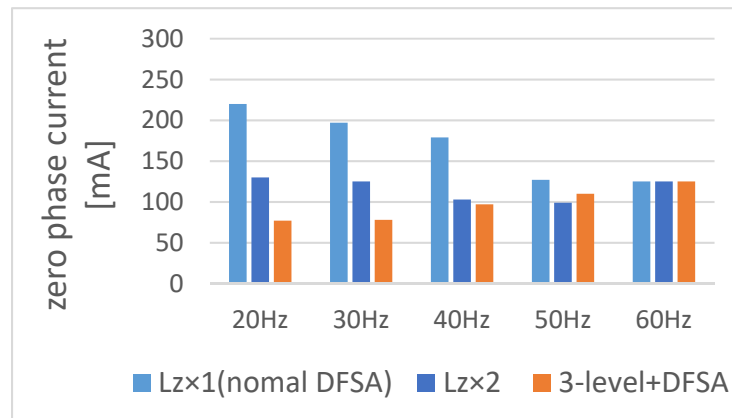


Figure 4: Comparison of zero-phase currents when zero-phase reactor is

3.3. Validation test with one unit of the simplified speed control

After installation, a long-term test (> a year) of the simplified inverter control system was conducted to assess the approach of replacing major parts of the inverter panel instead of the entire panel. Jet-fan #1 was selected for this purpose. The inverter unit, capacitor, PLC unit and other miscellaneous parts of the existing inverter control for the jet-fan #1 were replaced. Figure 5, 6 and 7 show the replacement of the inverter unit and illustrate the potential for

reduction in the size of future control panels. This can be important when (as usual) space in control rooms is at a premium.



Figure 5: 3-level inverter unit in the control



Figure 6: Exchanging the inverter unit



Figure 7: 2-level inverter unit installed in the control

During this test period, the inverter controls for jet-fans #2, #3, #4 and #5 remained as before. All five (5) inverter controls were operated through the existing PLC for 3-level inverters and, to enable this, an additional “PLC for conversion” was installed to pass the control signals to the 2-level inverter. The replaced 3-level inverter unit was held on standby in case of any need to respond urgently to an emergency. The system configuration for this long-term reliability test was shown in Figure 8. As expected, all five jet-fans operated interconnectedly without any issues throughout one year period of the long-term reliability test and no electrical noise troubles were caused by the new simplified inverter control.

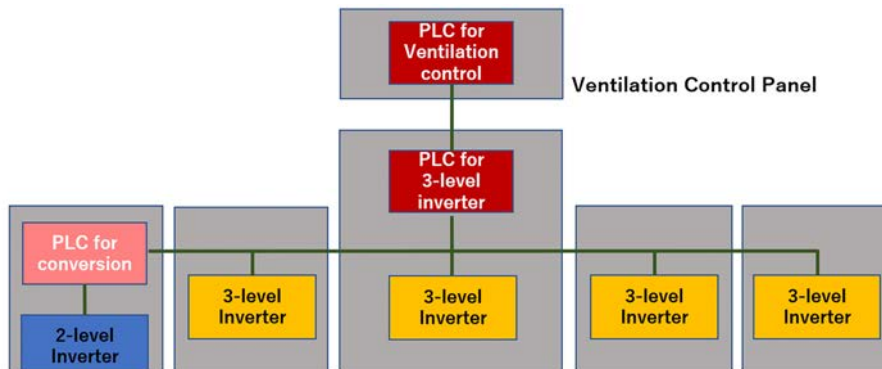


Figure 8: Control system including added “PLC for conversion”

3.4. Validation test with complete replacement

Following the success of the test for the inverter panel #1, the remaining four inverter panels were upgraded using the same approach for parts replacement. To minimize the total cost of construction and operation, this was carried out in two stages, in each of which two panels were upgraded. In addition, the interconnecting control PLC unit for 3-level inverter was replaced with a new one due to it reaching the end of its design life.

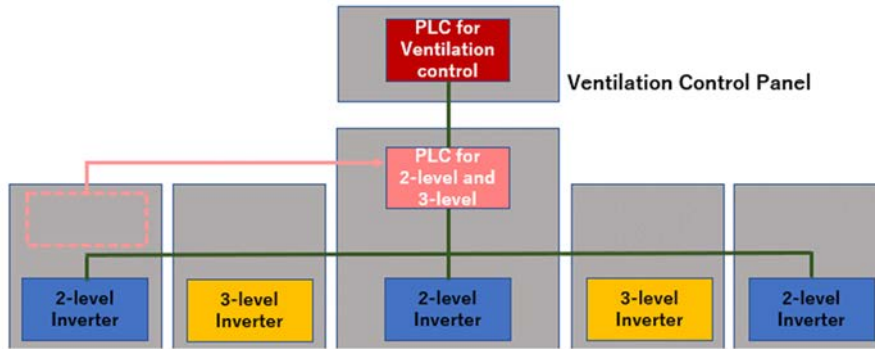


Figure 9: Inverter control system at the Stage 1 of replacement

Stage 1: In the first stage, the control software for the 3-level and 2-level inverters was installed in the “PLC for conversion” that already controlled jet fan #1, and the old interconnecting PLC was replaced by the “PLC for conversion”. The relevant components of the two inverter panels #3 and #5 were replaced to make them simplified inverter controls. The operation of the new interconnecting “PLC for conversion” with 2-level and 3-level software, and three 2-level and two 3-level inverter controls were confirmed by measuring the electrical parameters of voltage and current. The whole inverter control system then resumed normal operation. Figure 9 illustrates the control system configuration at the end of Stage 1.

Stage 2:

After a short period allowed to confirm that everything was operating correctly, inverter panels #2 and #4 were replaced in the same manner as above. This completed the migration from 3-level to 2-level and, as a final step, the “PLC for conversion” loaded the software for the 2-level inverters, replacing the 3-level software. Figure 10 illustrates the control system configuration at the end of Stage 2. The operation of the new interconnecting PLC for 2-level inverters, and five 2-level inverter controls was confirmed by measuring the electrical parameters of voltage and current and the whole inverter control system again resumed normal operation.

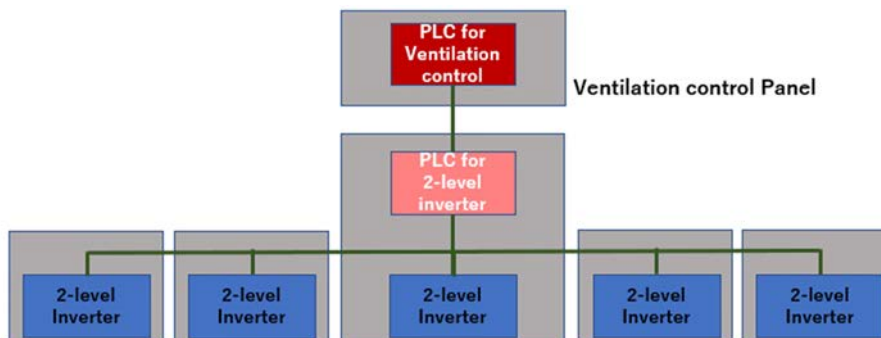


Figure 10: Inverter control system at the Stage 2 of replacement

3.5. Comparison of the 3-level and 2-level inverter controls

(1) Efficiency of the inverter control

So far, the performance of the control system has been discussed primarily with a focus on stability and the suppression of unacceptable electrical effects. However, the power efficiency of the inverter units is also important. Accordingly, this was measured at jet fan #1, giving results shown in Figure 11. The figure compares the 2-level performance with that of the 3-level inverters before their replacement and, for this purpose, ‘efficiency’ is defined as the ratio of output power to input power. By inspection, the new 2-level units actually

outperformed the original 3-level ones, albeit by only about 2% over the range used in practical operation. Somewhat greater improvement (approximately 8%) was obtained at a frequency of 20 Hz, but the absolute efficiencies are then smaller than at higher frequencies.

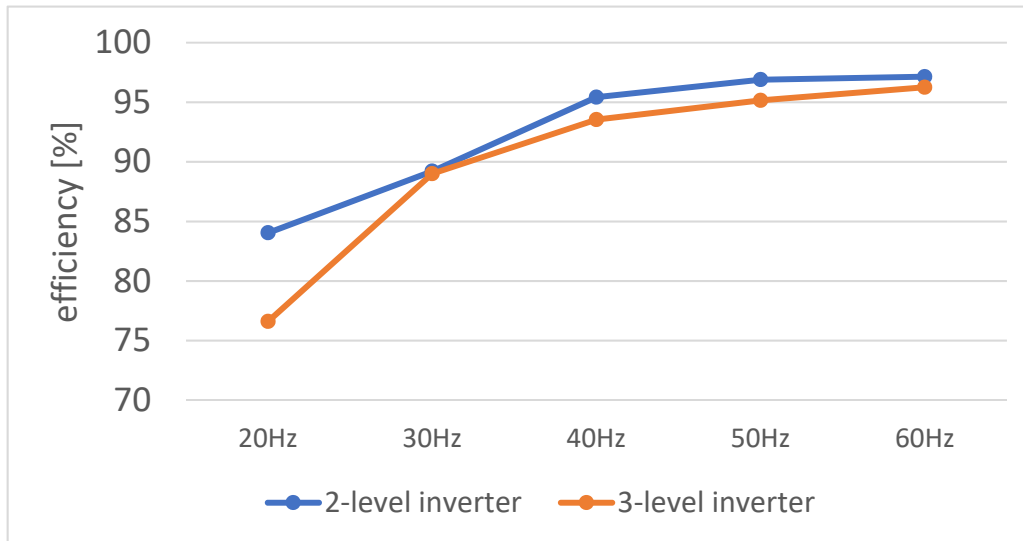


Figure 11: Comparison of 2-level and 3-level inverter control efficiency

(2) Zero-phase current

It is well known that various forms of electrical noise caused by inverters can have negative effects on the operation of jet-fan motors and other tunnel devices such as AM radio, sensors, and communication equipment. The standard LC filter is effective in reducing the surge voltage, but it does not restrict the zero-phase current. In contrast, the DFSA filter [3] does limit the zero-phase current and it performs better than various other types of filters assessed by Weicker et al [7],

Measurements of the zero-phase current at jet fan #1 have been described in Section 3.2, in which it is shown that the values for the 2-level unit are greater than those for the 3-level unit, but nevertheless far smaller than the acceptability limit of 1000 mA. Corresponding measurements for all five jet fans are shown in Table-2. It is seen that the current increases with increasing cable length. This is to be expected but, importantly, it may be inferred that the use of significantly greater cable lengths would also be acceptable. For completeness, this expectation is assessed in Figure 12, which shows maximum zero-phase currents measured in 15 tunnels in Japan in which inverter-driven speed control is used for jet-fans. Figure 12 shows a clear dependence on tunnel length and it also shows that, for the 3-level inverters, the dependence tends to reduce with increasing length. The measurements for the 2-level inverters in the Kobe Nagata Tunnel are at the upper end of the range of measurements for 3-level inverters, but it is too early to know whether their dependence on cable length will also begin to reduce with increasing length.

Table 2: Maximum value of the zero-phase current of the inverter control at the Kobe Nagata Tunnel

	Jet fan#1	Jet fan#2	Jet fan#3	Jet fan#4	Jet fan#5
Cable length(m)	800	800	650	650	500
Zero phase current(mA) 3-level inverter	125	110	98	91	77
Zero-phase current(mA) 2-level inverter	220	201	174	134	133

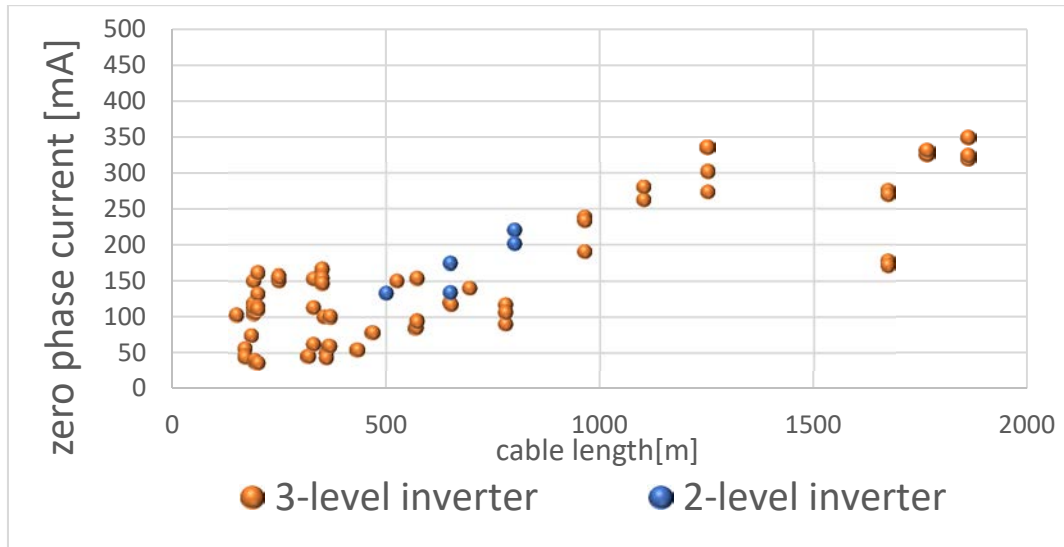


Figure 12: Correlation between cable length and maximum zero-phase current

4. NEXT STEPS TOWARD WIDER INSTALLATION

Tunnel operators and designers must consider financial cost as well as efficiency even in times when climate change demands ever-increasing attention. For these purposes, it is necessary to acknowledge that the initial capital cost of inverter control systems exceeds that of constant-speed systems. It is therefore of considerable interest to predict life-cycle costs that include both capital and operational costs. Such a study has been undertaken to predict life-cycle costs for the proposed replacement of 3-level control by 2-level control in the Shorenjigawa Tunnel in Japan. Figure 13 shows predicted total life-cycle cost in twenty years for 34 fans including (i) initial construction and installation, and parts replacement at the end of ten years of operation, (ii) electrical power requirements and (iii) maintenance. This shows that a break-even point occurs after about half of the design life of inverter units (and hence about a quarter of that of other components). Furthermore, it is to be expected that the longevity of jet-fans and their motors will be greater in the variable-speed mode. Thus, the increased flexibility of variable-speed control – in response to incidents as well as in routine operation – is achieved simultaneously with reduced life-cycle costs and reduced detriment to the environment. None of these benefits is game-changing, but their potential collective influence is nevertheless compelling.

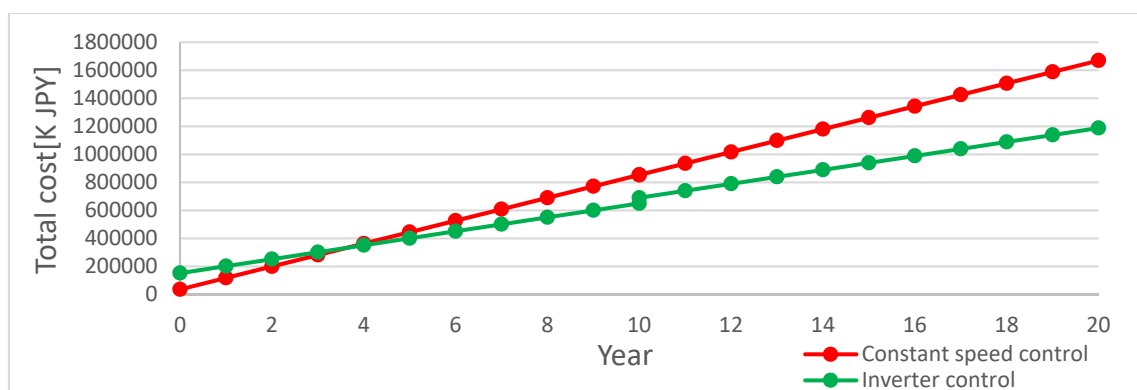


Figure 13: Comparison of Life-Cycle Cost between inverter control and constant speed control at the Shorenjigawa Tunnel

5. CONCLUSION

The paper has assessed the practical potential of using 2-level inverter speed-control for tunnel jet-fans instead of 3-level control, thereby reducing costs and also reducing space demands in control rooms. Inevitably, to enable the assessment to be made on the basis of actual measurements, it has been necessary to focus on a particular tunnel in which direct comparisons could be made. However, the inferences drawn from the measurements have been interpreted generically. Particular attention has been given to assessing electrical noise such as zero-phase current that is strongly-dependent on the method of filtering the inverter output. It has been shown that, when used in conjunction with DFSA filters, the zero-phase current caused by 2-level control exceeds that for 3-level control, but is nevertheless far below acceptability limits even with cable lengths as large as 800 m. It has also been shown that power efficiencies in the desired frequency range are similar for both methods. Furthermore, it has been shown that life-cycle costs of inverter-driven control of jet fans is significantly smaller than that of constant-speed systems even though the initial capital costs are greater.

6. REFERENCES

- [1] I Nakahori, T Ato, K Murakami, D Araki, T Kanatani, A Vardy, “The use of inverter-driven jet-fans to reduce tunnel ventilation costs”, BHR Group, 13th ISAVVT, pp69-80, 2009.
- [2] R Bopp, “Energy-optimized ventilation of road tunnels by speed control of jet fans”, *Proc 1st int conf on Tunnel Control and Communication, Basel Switzerland*, ITC Ltd, 219-229, 1992.
- [3] T Kawabata, I Nakahori, “Variable speed driving equipment for the jet-fan induction motors in road tunnel”, Japan Patent No. 5300775, registered on June 26, 2013.
- [4] K Kanazawa, H Hara, A Tsurumaki, H Fujimoto, H Kurano, I Nakahori, T Ato, “Application of inverter-driven jet-fans to the Kobe Nagata Tunnel”, BHR Group, 14th ISAVT, pp91-102, 2011.
- [5] R Brandt, S Lucchini, “Ventilation of the E4 Stockholm Bypass”, Conference Proceedings on 16th Australasian Tunneling Conference, Sydney, Australia, 2017.
- [6] H Sako, T Sakaguchi, S Abe, A Vardy, “A strong advance in variable-speed control of road tunnel jet fans”, BHR Group, 20th ISAVFT, Brighton, UK, pp389-40, 2022.
- [7] M Weicker, G Bello, D Kampen, A Binder, “Influence of system parameters in variable speed AC-induction motor drives on parasitic bearing currents”, EPE’20, ECCE Europe, pp1-10, 2020.

INFLUENCE OF ACOUSTIC TUNNEL MONITORING AKUT ON TUNNEL SAFETY

¹Katharina Hoyer, ¹Regina Schmidt, ¹Harald Kammerer, ²Franz Graf, ³Mark Dobrounig,
³Thomas Kalina
¹ILF Consulting Engineers, AT
²Joanneum Research, AT
³ASFINAG, AT

DOI 10.3217/978-3-85125-996-4-08 (CC BY-NC 4.0)

This CC license does not apply to third party material and content noted otherwise.

ABSTRACT

The acoustic tunnel monitoring system AKUT is used in Austrian motorway tunnels since 2015 to detect critical events during tunnel operation. Through the automatic acoustic detection of unusual noises, the system detects potentially dangerous conditions or abnormal noises. By increasing detection possibilities, detection times can be reduced and subsequent traffic control as well as safety and rescue measures can be implemented faster. This can reduce the risk potential in case of an accident.

Since the first installation of AKUT the detection times have been recorded in an event database, which is continuously updated. On this basis the detection times with and without AKUT can be objectively evaluated and the safety benefit of the system can be determined:

- Faster event detection allows for faster activation of safety equipment.
- Faster activation of traffic lights at the portal prevents people to enter hazardous zones.
- Faster activation of warning systems can reduce the subsequent accident rate after vehicle breakdowns and accidents.

Based on the event data, an approach for the tunnel risk model TuRisMo has been developed. This has included establishing statistical fatalities numbers for the model tunnels selected through detailed fire simulations. Subsequently, reduction factors for application in the standard risk analysis model have been extracted. In this paper, the influence and changes to the event tree of the Austrian instruction RVS 09.03.11 will be presented.

The result of the study allows a data-based quantitative consideration of AKUT as an additional safety measure in road tunnels.

Keywords: acoustic monitoring system, detection system, detection time, accelerated event response, risk assessment approach

1. INTRODUCTION

Fast detection of critical incidents in tunnels is essential for triggering emergency measures and evacuating people who have been involved in an accident in the tunnel. This enables operators in the traffic management centre to take immediate action and leads to a reduction of dangerous situations and consequently reduces related consequences corresponding to tunnel users and to infrastructure. Acoustic monitoring in tunnels has shown to significantly reduce detection times [3]. AI-based detectors recognise the abnormal noises in real time and assign them to predefined noise classes.

The advantage of acoustic detection is that AKUT can react directly to the critical incident (e.g. accident noises after a collision). This means that AKUT can trigger an alarm in the traffic management centre in less than 1 second after the occurrence of an incident. Other safety systems usually recognise the consequences of an accident indirectly (e.g. slow drivers, traffic jam, etc.) and therefore require a longer time to trigger an alarm.

The following sound classes are currently recognised: (i) accident/tyre blowout, (ii) tyre squeal, (iii) door slam, (iv) horn honking, (v) voices/shouting.

After the development of the system, the first pilot system was installed in the network of the Austrian highway operator ASFINAG in 2010. Following clearly positive evaluation results in 2014, ASFINAG started to gradually equip all tunnels of hazard classes 3 and 4 with AKUT. Currently, the acoustic monitoring system is installed in 35 tunnels with approx. 2.100 microphones. Around 177 km of tunnels in the ASFINAG network are currently acoustically monitored. Over the next few years, another 21 tunnels in Austria will be equipped with the system. In recent years, it has become apparent that many critical events in the tunnels were recognised very quickly by AKUT.

However, there has not been a comprehensive analysis and no approach has been recognised as to how the rapid incident detection of AKUT effects the risk assessment of a tunnel and what advantages can result from it.

Consequently, the highway operator ASFINAG initiated a study to develop an approach for the evaluation of acoustic monitoring in risk analysis based on the evaluation of a large number of real incidents in tunnels.

Focus points for the study have been potential benefits in risk assessment, such as for instance a reduction in the fire risk through faster activation of safety equipment (e.g. activation of red lights at the portal, ventilation, loudspeakers, lighting, water mist system) or a reduction in subsequent accident rates (following breakdowns and accidents).

2. DATA ANALYSIS

In order to obtain a basis for assessing the performance of acoustic monitoring, incidents in a one-year period have been evaluated as part of this analysis. The ASFINAG incident database [1] and the alarm lists of the individual tunnel control servers [2] have been used as the data basis for the analysis.

2.1. ASFINAG Incident Database (IDB)

The analysis is based on the entries in the ASFINAG incident database (IDB). The IDB has been operated by ASFINAG for many years. In case of an incident, the operators enter the incident data into the IDB. This basis thus represents an optimal starting point for the evaluation.

The following data is entered into the IDB for each incident in a tunnel: tunnel name and route number, date and time of the incident, exact location of the incident, tunnel area (entrance, inner area, exit), vehicles involved, verbal description of the incident, etc.

2.2. Tunnel alarm lists

In addition to the IDB, the alarm lists of the individual tunnel control servers were used to analyse the individual incidents. The alarm lists were exported from the respective tunnel control servers and made available by ASFINAG in the form of MS Excel files. These alarm lists contain the following data:

- Date and time stamp of the alarm that occurred or the action performed by the operator (e.g. switching traffic lights to red)
- Text of the message (alarm)
- Description of the alarm
- Time stamp of the acknowledgement by the operator

In agreement with ASFINAG, the events of an entire year were analysed, namely 1 September 2021 to 31 August 2022.

2.3. Procedure for analysing the incidents

Based on the alarm lists and the entries in the IDB, the following procedure has been pursued. For each individual incident in the IDB, based on the timestamp, the matching incident in the alarm lists has been identified. As soon as corresponding alarms were found in the alarm lists, these were extracted and (i) the date of the incident, (ii) the timestamp of the alarm and (iii) the description of the alarm were saved.

Because the exact timestamp of the alarms is particularly relevant for the analysis, the time stamps of the first, second and third alarms have been extracted for each incident.

2.4. Analysed tunnels

The analyses has been carried out for 28 tunnels in the ASFINAG road network encompassing a total distance of 156.7 kilometres.

2.5. Incident distribution across the tunnels selected

A total of 168 events were analysed over a period of one year. Of these 168 events, 126 events could be analysed beyond any doubt. This corresponds to 75 % of the total number of events. For the remaining 42 events, a clear allocation was not possible. These cases reflected situations with a traffic jam, resulting in a relatively high number of alarm messages making it (often) not possible to clearly assign them to a specific incident. These events were therefore not further analysed.

2.6. Data analysis of first alarms in case of incidents

One of the most important aspects with critical incidents in tunnels is the time of detection and resulting alert in the tunnel control centre. For each incident, the sequence in the alarm chain was analysed and it was determined which safety system in the tunnel provided the first, second and third alarm according to that incident.

Figure 1 shows the distribution of which system sent the first alarm to the tunnel control centre. In 68% of the incidents AKUT sent the first alarm to the tunnel control centre, 29.7% of the incidents were first reported by the video detection system and the remaining 2.3% were first reported by induction loops.

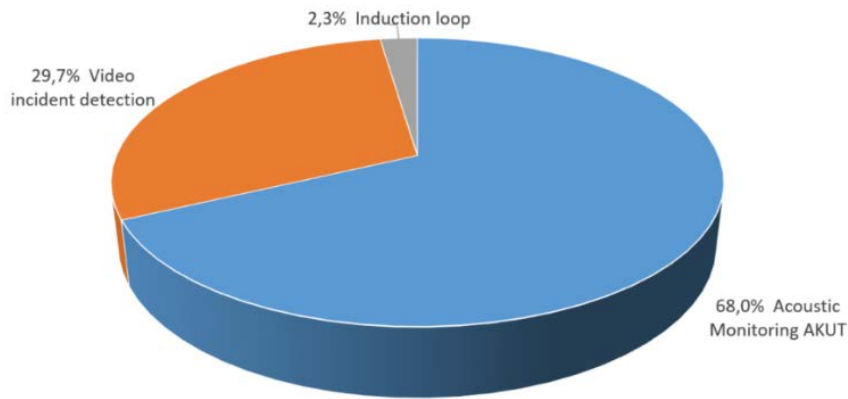


Figure 1: Overview of which safety system sent the first alarm to the tunnel control centre

2.7. Time advantage of AKUT alarms

Time differences between the first and the second alarms triggered have been analysed. The second alarms triggered in all 87 events in which AKUT detected first have been categorised in six-time categories. Figure 2 shows the time advance of AKUT against other detection systems.

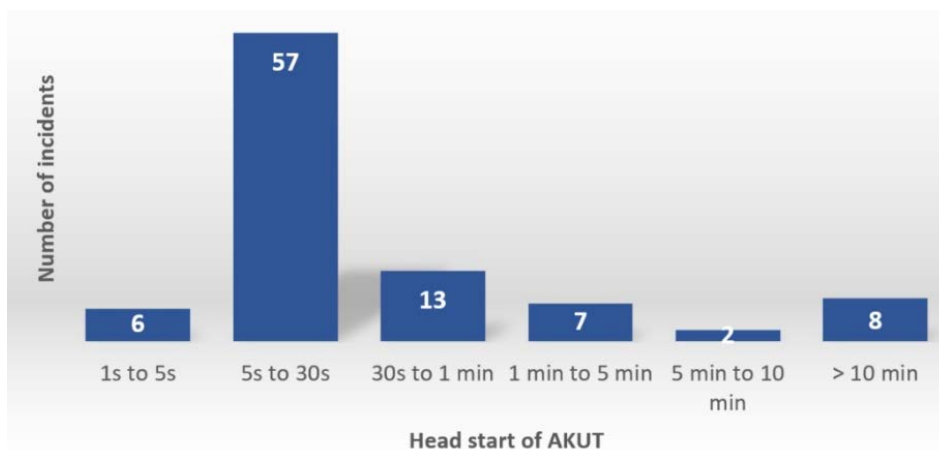


Figure 2: Time advance provided by AKUT compared to other tunnel safety systems

All time differences between first and second alarms triggered have been determined, ordered by size and their Median value calculated. According to this data set analysis, the time advantage of AKUT could be identified to amount to 23 seconds.

2.8. Data analysis in case of secondary incidents

The analysis has shown that the database unfortunately contains too few events to be able to make a well-founded statement regarding the influence of AKUT on the accident rate following initial incidents (so-called secondary incidents). Therefore, other data bases and valuation methods were used (see chapter 3.1).

3. DEVELOPMENT OF AN ASSESSMENT APPROACH

3.1. Valuation approaches for the risk model

Faster detection time (extent of damage model)

The Austrian tunnel risk model consist of both an event tree-based probability analysis and a consequence model to determine statistical number of fatalities. The consequence model is further differentiated into a detailed smoke propagation simulation and an agent-based evacuation simulation. The advantages of AKUT are relevant for both of these simulation parts, as faster detection times lead to faster activation of safety equipment (ventilation, tunnel closure) and faster start of the evacuation (play-back tunnel-user information).

To be able to quantify this logic, two different simulation approaches have been used for the individual model tunnels selected:

1. Without AKUT: Absolute detection time of 37 seconds is applied according to the previous data basis (simulation approach adopted in accordance with RVS 09.03.11).
2. With AKUT: Values adapted for an absolute detection time of 14 seconds (37 seconds – 23 seconds faster detection due to AKUT = 14 seconds detection time for tunnels with installed AKUT system).

The detection times of 37 and 14 seconds represent solely the event being detected. In both cases, additional time periods must be added for which the following has been considered: 15 seconds for response time of operating personnel, 8 seconds for the system reaction time, 30 seconds for the time until the red light signal is respected (in accordance with RVS 09.03.011). Further reaction times of critical safety systems, such as activation of the ventilation and start of the evacuation process have been considered as detailed in table 1:

Table 1: Time line for key parameters

	Tunnel without AKUT	Tunnel with AKUT
Absolute detection time	37 seconds	37 – 23 = 14 seconds
Tunnel closure	90 seconds	90 – 23 = 67 seconds
Activation of fire ventilation	120 seconds	120 – 23 = 97 seconds
Alert time	150 seconds	150 – 23 = 127 seconds

Reduction factors have been determined based on comparison of the fatalities or consequence numbers for both simulations of each of the tunnel studied. These factors are subsequent applied to the precalculated consequence values of the standard risk analysis to account for an installed AKUT system.

Accelerated closure time (event tree – frequency of incidents)

Faster detections lead to faster activation of safety devices; this also influences tunnel closure time (traffic light). As a result, fewer vehicles enter the tunnel and consequently the number of vehicles stopping after a traffic disruption is reduced, which also reduces the number of vehicles that can cause a rear-end collision.

This effect can be considered in the frequency analysis by adjusting the percentage of subsequent accidents after accidents and breakdowns and is determined as follows (value C2 of event tree, in accordance with RVS 09.03.11):

$$C2 = A1 \cdot B1 \cdot \bar{N} \cdot p_{A,P} + A1 \cdot B2 \cdot \bar{N} \cdot p_{A,U}$$

Where $p_{A,P}$ and $p_{A,U}$ are the probability for one vehicle to be involved in a rear-end collision after a breakdown or after an accident respectively. \bar{N} defines the average number of vehicles queuing up behind the incident vehicle and is determined as follows:

$$\bar{N} = \left(\frac{t_{SP}}{3600} + \frac{L_{TA}}{2 \cdot v_{max}} \right) \cdot \frac{JDTV}{24}$$

With values A1, B1 and B2 of event tree, in accordance with RVS 09.03.11; in addition the tunnel length without additions L_{TA} , maximum permitted speed v_{max} and AADT (annual average daily traffic), the closure time t_{SP} is also included here.

This assessment approach influences all secondary events in the tunnel – occurring after accidents and breakdowns, thus influencing the fire risk and the mechanical risk.

Reduced probability for rear-end collisions after break downs or accidents

Faster detection leads to faster activation of safety devices; consequently, the warning facilities in the tunnel are also activated more quickly. This increases the attention of tunnel users and reduces the probability of a vehicle being involved in a rear-end collision. That effect can be considered in the frequency analysis by adjusting the value C2 in the event tree. The value C2 represents the subsequent accidents after accidents and breakdowns and is determined as follows (in accordance with RVS 09.03.11):

$$C2 = A1 \cdot B1 \cdot \bar{N} \cdot p_{A,P} + A1 \cdot B2 \cdot \bar{N} \cdot p_{A,U}$$

The Austrian RVS specifies values for both probabilities, $p_{A,P}$ and $p_{A,U}$. These values have been determined on the basis of the ASFINAG event database. However, as mentioned before, it is not possible to derive adapted subsequent accident probabilities (after breakdowns or accidents) when using AKUT in tunnels on the basis of the current ASFINAG event database due to the low number of incidents.

Nevertheless, in order to account for the positive effect, it would be possible to define reduction factors for the two probabilities mentioned above on the basis of expert judgement. A general reduction factor f_{AKUT} or two specific reduction factors for breakdowns $f_{AKUT,P}$ and for accidents $f_{AKUT,U}$ could be incorporated into the formula for C2 as follows

$$C2' = A1 \cdot B1 \cdot \bar{N} \cdot p_{A,P} \cdot f_{AKUT,P} + A1 \cdot B2 \cdot \bar{N} \cdot p_{A,U} \cdot f_{AKUT,U}$$

This assessment approach influences all secondary events in the tunnel – occurring after accidents and breakdowns, thus influencing the fire risk and the mechanical risk.

3.2. Representative model tunnels

Determining the influence of AKUT for all possible tunnel types for which consequence numbers are available in RVS 09.03.11 would have considerably exceeded the scope of the research project. For this reason, several representative motorway tunnels have been selected for the analysis. Among other things, the focus was on tunnel types with AKUT in the ASFINAG network for which a risk assessment with the standard risk model could be relevant:

Table 2: Selection of representative model tunnels

Operation	Tunnel length	Ventilation type	Longitudinal inclination	Distance of emergency exits
Uni-directional (no traffic congestion)	0.7 km	Natural ventilation	-3.0%	233m
				350m
			+3.0%	250m
				350m
	1.5 km	Longitudinal ventilation	-3.0%	250m
				500m
			+3.0%	250m
				500m
	4.0 km	Longitudinal ventilation	-3.0%	250m
				500m
			+3.0%	250m
				500m

The detailed risk analysis has been carried out for three model fires (5 MW, 30 MW and 100 MW) and for two fire scenarios, primary events and secondary events. Events involving congested traffic (tertiary events) have not been considered.

Tunnels with bi-directional traffic, special structural properties or traffic characteristics (e.g. congestion) were not considered, as in these cases the standard model is often not applicable.

3.3. Detailed risk analysis for model tunnels selected

Methodological framework

The TuRisMo risk model [4] is a system-based quantitative risk analysis model. It allows a systematic and quantitative risk assessment and takes into account all relevant incident scenarios in a road tunnel.

The risk model considers the personal risk of tunnel users and results in an expected risk value for the group of tunnel users. Therefore, all data used in the risk model refers to accidents with personal injury. The method consists of the following two basic elements:

1. Quantitative frequency analysis (event tree analysis)
2. Quantitative consequence analysis which consists of two simulation parts – the smoke propagation simulation and the evacuation simulation

Results

The model tunnels selected are all uni-directional tunnels and are equipped in accordance with the guidelines. Therefore, small fires (5 MW) result in negligible consequences, both for primary and secondary events. This can, for the most part, be explained by the relatively low fire load. Accordingly, the difference in the resulting consequence numbers is too small to be able to determine a factor related to the effectiveness of AKUT.

For the large fire scenarios, 30 MW and 100 MW, differences in the consequence numbers for the primary scenarios are too small to determine an improvement factor for AKUT. This is mainly caused by the favorable spread of smoke in traffic direction for uni-directional tunnels, protecting the tunnel users in the traffic jam behind the fire location. Factors for the effectiveness of AKUT can only be defined for both of these fire sizes in case of secondary scenarios. These scenarios represent a fire related accident in the traffic jam combined with the spread of smoke in traffic direction. Under these circumstances, tunnel users in front of

the fire location could be effected by smoke. The improved detection time by AKUT causes a reduction in the consequence numbers.

Reduction factor for standard risk model

In order to establish an improvement factor for the consequence numbers used in the standard risk analysis, the absolute difference of the respective consequence numbers has been calculated. The aim was to obtain as few representative factors as possible in order to ensure simple applicability. In the following, the resulting reduction factors according to the three model tunnels selected and only for secondary events will be presented and discussed:

- Tunnel without mechanical ventilation

The resulting reduction factors differ roughly in terms of fire load and longitudinal inclination. For this reason, no further simplification is possible and individual factors are required in each case.

Table 3: Reduction factor for unidirectional tunnels without mechanical ventilation for secondary events

	30 MW -3%	30 MW +3%	100 MW -3%	100 MW +3%
Reduction factor AKUT	0.7	0.8	0.4	0.6

- Tunnel with longitudinal ventilation

Contrary to the model tunnels with natural ventilation, it is possible to further reduce the number of reduction factors for the tunnels with longitudinal ventilation systems.

This is firstly due to the relative small differences between model tunnels with a positive or negative gradient, reflecting that the ventilation system is designed for the respective longitudinal inclination and the fires can therefore be controlled. Secondly, the factors for different fire sizes can be summarized, as the differences become negligible due to the positive influence of the installed ventilation system. In addition, the damage extent values of the model tunnels with 1.5 km and 4.0 km show only minor differences. This means that the tunnel length factor can be neglected in case of longitudinal ventilation.

Hence, it was possible to limit the number of reduction factors and to define only one generally valid factor for unidirectional traffic with longitudinal ventilation, namely **0.5**.

4. SUMMARY AND CONCLUSION

It is undisputed that AKUT - as a safety measure - provides an advantage for the safety level in road tunnels. However, until now there has been no measurable and therefore quantifiable factor in the tunnel risk assessment. This means that the benefit for the tunnel operator cannot be taking into account during the risk analysis.

To develop such an approach, an extensive data analysis of the event database and the recordings of the tunnel control servers was carried out. It was found that AKUT is often the first system to detect an event, highlighted by a first detection in almost 70% of the tunnel incidents recorded. Moreover, analysis has shown that AKUT can accelerate the detection time in these case by around 23 seconds.

The faster detection time can be taken into account in the risk model in both the event tree based frequency analysis and in the fatalities or consequence analysis:

- For the evaluation in the frequency analysis, individual adjustments must be made in the event tree with regard to the subsequent accident rate (secondary events). These relate firstly to a reduced number of vehicles entering the tunnel due to faster activation of tunnel closure and secondly to a reduced probability of collision after breakdowns and accidents due to faster activation of warning devices in the tunnel.
- In the Austrian guideline RVS 09.03.11 two different risk models are available for analyzing the fire consequences: A standard risk analysis model, for which the RVS specifies the consequence numbers, and a detailed risk model, for which individual simulation calculations are required for each tunnel. For the evaluation of AKUT, an approach was provided for both risk models:
 - When evaluating AKUT with a detailed risk analysis and only when the tunnel is similar to the model tunnel parameters, the reduction factors can be applied to the individually determined consequences. In most cases, however, the individual time parameters have to be adjusted in the risk analysis. For tunnels with installed AKUT, a doubling of the simulation effort has to be taken into account. A set of simulations representing 70% of cases with the detection time, time for tunnel closure, activation time of ventilation or loudspeaker announcements reduced by 23 seconds. The second set of simulations represent the remaining 30%, using the standard time parameters.
 - In order to evaluate AKUT with the standard risk model, the defined reduction factors can be applied to the precalculated consequence numbers (RVS 09.03.11). Depending on the specific tunnel under investigation, the installation of AKUT reduces the secondary fire consequences by 20% to 60%.

5. REFERENCES

- [1] ASFINAG, „Ereignisdatenbank 2018 bis 2022“.
- [2] ASFINAG, „Tunnelkopfdaten 2021 bis 2022“
- [3] Joanneum Research, „Auswertung der Ereignisse der ASFINAG-Ereignisdatenbank; September 2021 bis August 2022,“ 2023
- [4] Austrian guidelines, RVS 09.03.11 – Tunnel Safety; Tunnel risk model; 04/2015

EVACUATION SAFETY AND HUMAN EMOTIONAL RESPONSES IN SMOKE-FILLED TUNNELS FOR MACHINE LEARNING INSIGHTS

Miho Seike, Wenhao Li, Akimasa Fujiwara, Makoto Chikaraishi
Hiroshima University, JP

DOI 10.3217/978-3-85125-996-4-09 (CC BY-NC 4.0)

This CC license does not apply to third party material and content noted otherwise.

ABSTRACT

To clarify the relationship between emotion and walking behavior in tunnel fires, we conducted evacuation experiments using model-scale tunnel with smoke and investigated participants’ emotions, physiological signals, and walking speed. For applying machine learning to recognize emotions during evacuation in the future, we estimated the causal relationship using structural equation modeling and found that heart rate, systolic blood pressure, and standard deviation of N-N interval influenced the walking speed to be faster, while diastolic blood pressure influenced the walking speed to be slower.

Keywords: Emotion, physiological signal, walking speed, smoke, tunnel fire.

1. INTRODUCTION

When a fire occurs in a tunnel, which is an enclosed space, smoke fills the tunnel easily and users need to evacuate a long distance with reduced visibility due to smoke. In this situation, the users are at a high risk of becoming a victim. For future real-time evacuation guidance in a tunnel fire, understanding the psychological state and evacuation behavior of evacuees is considered as one of the important factors. Recently, studies on emotion recognition using machine learning have been conducted [1–3], however, there were no studies on emotion recognition during evacuation in our searching. In this study, we focused on the case of evacuation in smoke, classified emotions by combining heart rate with blood pressure, and investigated the relationship between emotions, physiological signals, and evacuation speed.

2. LITERATURE REVIEW

2.1. Emotion recognition by machine learning

Studies on negative emotion recognition using machine learning have been conducted [1–3] (Table 1). These studies used movies, documentaries, and TV shows to evoke participants’ emotions. Subsequently, the type and degree of emotions were labeled by participants’ self-report (subjective evaluation) [1–2] or by others such as the staff (objective evaluation) [3]. Finally, these studies used physiological signals such as electrocardiogram (ECG) to recognize emotions.

Table 1: Previous studies on negative emotion recognition by machine learning

Author(s)	Methodology	Labeled by	Recognition tool
Jang et al. [1]	Movie Documentary TV show	Self-report	Electrocardiogram, electrodermal activity, skin temperature, and photoplethysmography
Park et al. [2]	Movie Documentary TV program	Self-report	Electrocardiogram, electrodermal activity, skin temperature, and photoplethysmography
Takeshita et al. [3]	Movie	Behavior observation by staff	Heart rate variability

2.2. Emotion measurement

Early studies have been conducted to investigate the relationship between emotions and physiological responses such as heart rate (*HR*) and systolic (*SBP*) and diastolic (*DBP*) blood pressure [4–9].

Adstee et al. [4] reported that participants’ *HR* and *SBP* had increased and *DBP* remained constant when the staff had judged them as anxious via the implications in the conversation as well as direct statements, and the observations of their gestures, facial expressions, blocking, and slips of the tongue, etc., in the stressful interviews. Nyklíček et al. [5] reported that *DBP* had increased in the anxiety by music and noise listening experiments. The anxiety state was determined by combining a pre-experiment investigation which emotion the music and noise had evoked, and the participants’ self-report after the experiment.

Ax [6] conducted experiments which participants were asked to listen to music in a relaxed state to investigate physiological differences between those who with and without hypertension. Firstly, the staff had given the electric shocks to the participants, and then the sparks by the high-voltage short circuit had been shown to induce fear. Ax [6] reported that their *HR* had increased in fear state. Schwartz et al. [7] conducted walking-experiments which participants had been instructed to imagine a fearful situation from their past or future. The fear was determined by the participants’ self-report and the staff’s observation of the participants’ behavior, such as facial expressions and body postures. Schwartz et al. [7] reported that their *DBP* had decreased in fear state.

Berntson et al. [8] proposed a quantitative bivariate model for chronotropic control of the heart in humans and mentioned an increase in *HR* when feeling stress. Sloan et al. [9] conducted experiments to measure participants’ 24-hour electrocardiograms and found that when participants self-reported that they felt stress, their heart rate variability (HRV) decreased.

Zhang et al. [10] classified emotions by extracting key words from people’s talk. Before classification, they referred to Bhargava and Polzehl [11] and determined that the heart rate should be in the range of 40–70 bpm in sadness and 80–150 bpm in anger. However, these studies were conducted in a stationary condition, such as in sitting.

In this study, we targeted the smoke-filled tunnel fire evacuation scenario and attempted to label emotions via physiological responses by the previous studies’ results for future machine learning studies of emotion recognition in the evacuation.

3. EXPERIMENTS

3.1. Model tunnel

As same as Li et al. [12–13], a model tunnel (10 m long, 2 m wide, and 2 m high, with pitch-black interior) was used for the experiments (Figure 1). To set up evacuation routes, four check points (CP) were placed at a height of 1.5 m in the tunnel. Two smoke generators (PORTA SMPKE PS-2005, Dainichi) were placed diagonally at each end of the tunnel and three smoke density (extinction coefficient) measurements (laser sensor, LV-NH100, Keyence) were placed at 3 m intervals on the tunnel ceiling.

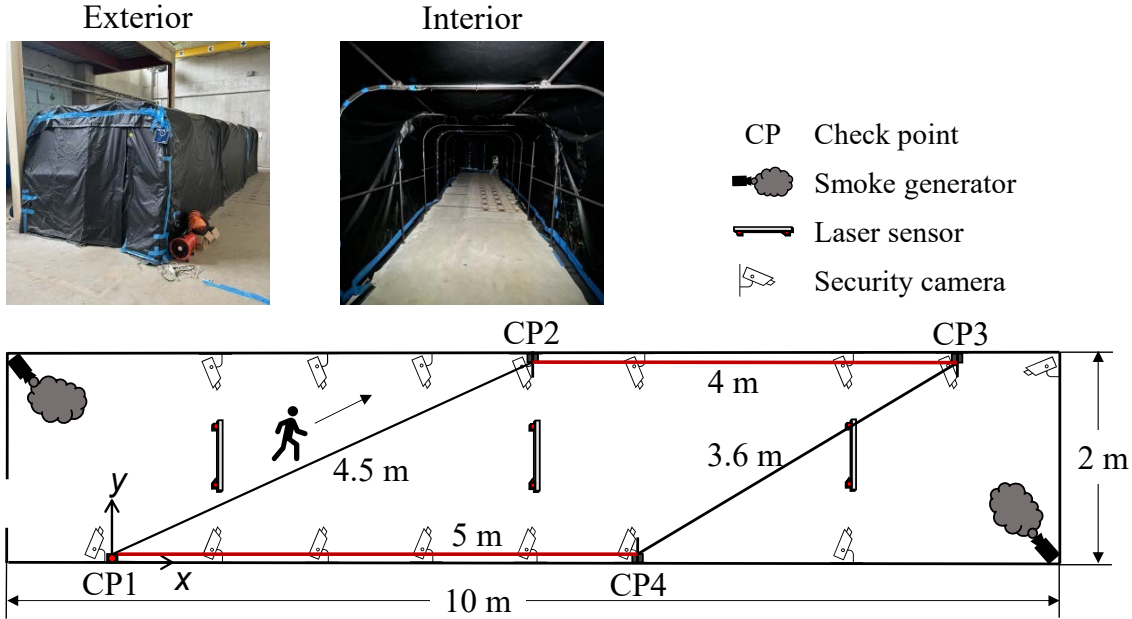


Figure 1: Model tunnel, evacuation route, and equipment

3.2. Methodology

Each participant evacuated a total of five times in different extinction coefficients (1st time: no smoke, 2nd to 5th times: light to dense). Walking speed was calculated by the evacuation time and distance, and extinction coefficient (C_s) was calculated using the following Lambert-Beer equation. We used the average value by the three measurements, for each route (from one CP to the next).

$$C_s = -\frac{1}{l} \ln \left(\frac{IL}{IL_0} \right)$$

where IL_0 is the incident light intensity (non-smoke), IL is the intensity of light transmitted through the smoke, and l is the distance traveled by the light through the smoke ($l = 0.8$ m).

Before the evacuation, participants were provided with the following instructions: ‘‘A fire has occurred in the tunnel, and the space has become completely dark and filled with smoke. Please evacuate urgently (in Japanese).’’

3.3. Participant

A total of 132 participants (91 males, age range: 20–64, mean age: 35.8; 41 females, age range: 20–63, mean age: 29) participated in the experiments. All the participants wore and used helmets, safety vests, masks, knee and elbow pads, small flashlights, and stopwatches.

3.4. Emotion definition

Proulx [14] proposed a stress model of decision-making in fires and mentioned that evacuees in a fire initially feel low-stress; subsequently, the emotion degree increases and transitions to stress, fear, worry (anxiety), and confusion. Based on this model, we focused on anxiety, fear, and stress, as same as Li et al. [12–13]. In addition, we defined as low-stress those that were excluded in anxiety, fear, or stress (see Table 2).

We defined the emotions using *HR*, standard deviation N-N interval (*SDNN*) (as one of the indicators of HRV), *SBP*, and *DBP*, by referring to the previous studies listed in Section 2.2 [4–9]. *HR* was recorded via a Wahoo Tickr WF124 heart rate monitor and *SDNN* was calculated from the standard deviation of *HR*. *SBP* and *DBP* were measured using an Omron HEM-6324T blood pressure monitor.

Table 2: Emotion definition in the present study

Indicator	Description	Anxiety	Fear	Stress	Low-stress
<i>HR</i> change rate	Ratio of <i>HR</i> during / before the experiment	> 1 [4]	> 1 [6]	> 1 [8]	Others
<i>SDNN</i> difference	Difference of <i>SDNN</i> during – before the experiment			< 0 [9]	
<i>SBP</i> change rate	Ratio of <i>SBP</i> after / before the experiment	> 1 [4]			
<i>DBP</i> change rate	Ratio of <i>DBP</i> after / before the experiment	≥ 1 [4–5]	< 1 [7]		

4. RESULTS

4.1. Walking speed vs. smoke by emotion

Figure 2 shows the results of walking speed vs. smoke density by emotion. To investigate the relationship between the walking speed and smoke density by emotion, we divided smoke

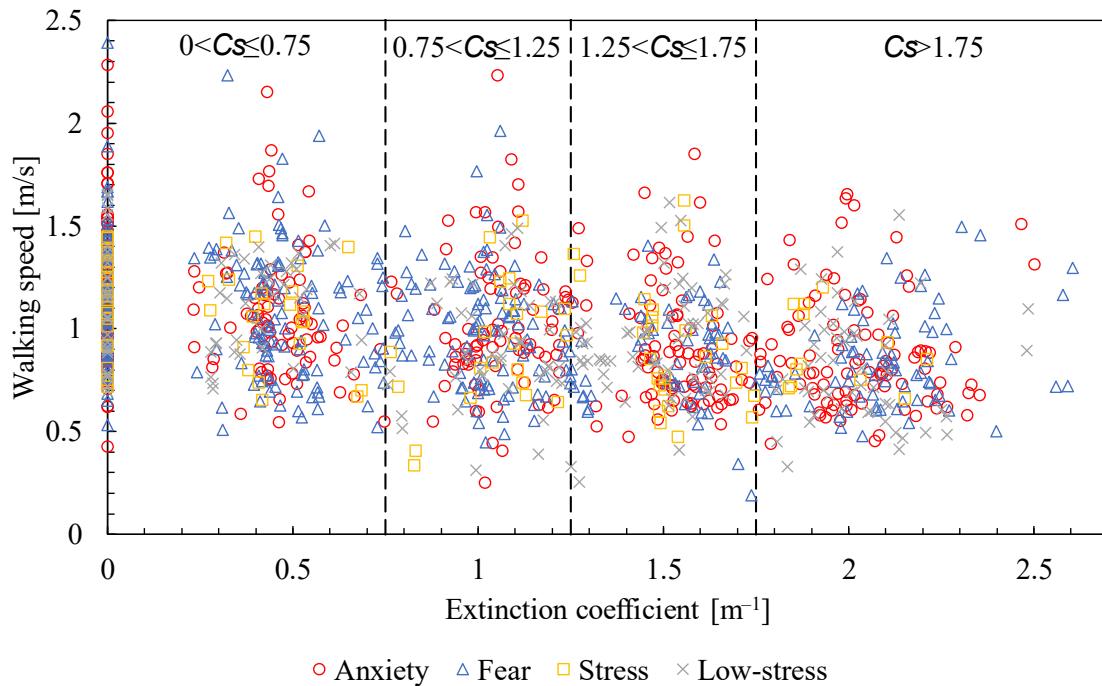


Figure 2: Walking speed vs. extinction coefficient by emotion

density into five ranges. Figure 3 displays the mean, maximum, and minimum walking speeds by emotions at each range. As smoke density increased, the mean walking speed decreased. The mean walking speed difference between the four emotions in five ranges were 0–0.10 m/s. The maximum and minimum walking speeds were always observed from anxiety and fear, but the maximum speed attenuation with smoke density increase in anxiety and fear was larger than in stress and low-stress.

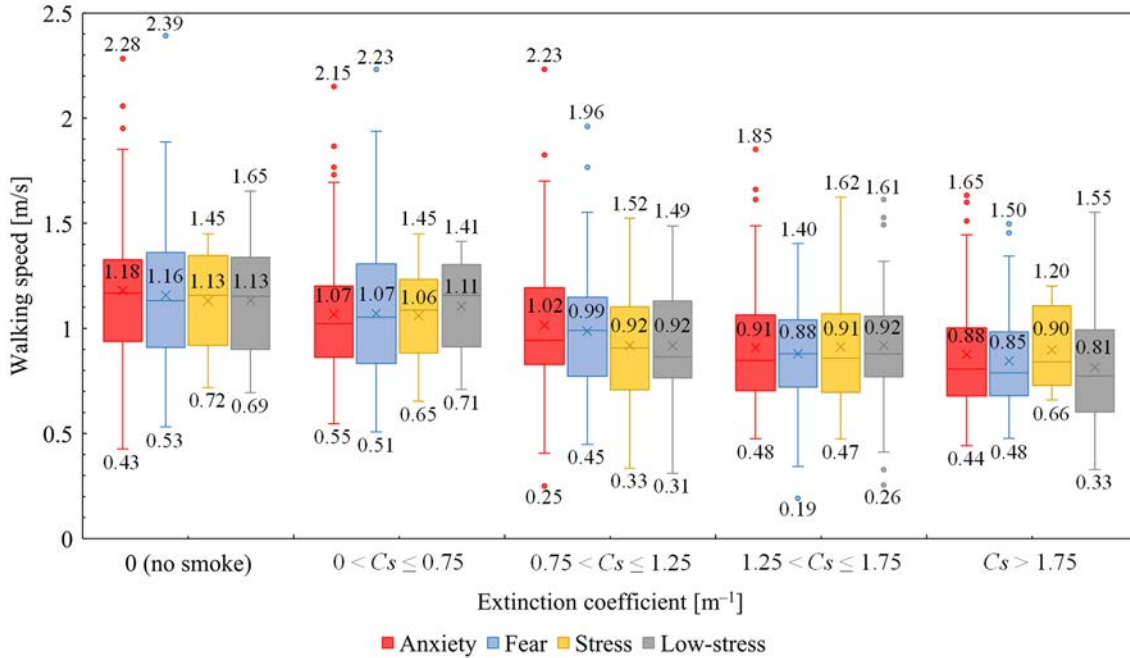


Figure 3: Mean, maximum, and minimum walking speeds at each smoke density range by emotion

4.2. Structural equation modeling

Applying the collected data to machine learning, we used Structural Equation Modeling (SEM) to investigate the causal relationship between emotions, physiological signal changes by emotions, and walking speed.

SEM comprises structural and measurement equations [15]. Structural equation analyzes the relationships between latent variables; measurement equation determines the impact of latent variables on the observed variables. In this study, we explored and verified the relationships between observed variables by regression equation.

The results are shown in Figure 4. GFI (Goodness of Fit Index, 0.870) and AGFI (Adjusted GFI, 0.725) indices showed that the model structure was acceptable.

Hypothesis H1: Physiological signals impact walking speed

The relationship between physiological signals and walking speed (W) considering smoke density (C_s) was calculated by the following regression equation.

$$G_{W,n} = \sum_j B_{j,W} \cdot Z_{j,n} + B_{C_s,W} \cdot Z_{C_s,n} + e$$

where G , Z , and B are the observed dependent and independent variables and the parameter, in regression equation, respectively; $j \in \{HR \text{ change rate: } 1, SBP \text{ change rate: } 2, DBP \text{ change rate: } 3, SDNN \text{ difference: } 4\}$; n is the n th sample; and e is the error term.

$B_{1,W}$ was 0.099 ($p < 0.001$) and accepted at the 0.1% level, while $B_{2,W}$ and $B_{4,W}$ were 0.057 ($p = 0.037$) and 0.059 ($p = 0.027$), respectively, and accepted at the 5% level. $B_{3,W}$ was -0.027 ($p = 0.320$) but the hypothesis was rejected based on the significance test.

Hypothesis H2: Emotions impact on physiological signals

The relationship between emotions and physiological signals was calculated by the following measurement equation.

$$F_{j,n} = \sum_i \lambda_{ij} \cdot \xi_{i,n} + e$$

where F , ξ , and λ are the observed dependent and latent exogenous variables and the parameter, in measurement equations; and $i \in \{\text{Low-stress: 1, Stress: 2, Fear: 3, Anxiety: 4}\}$. The reference for emotion was set as low-stress.

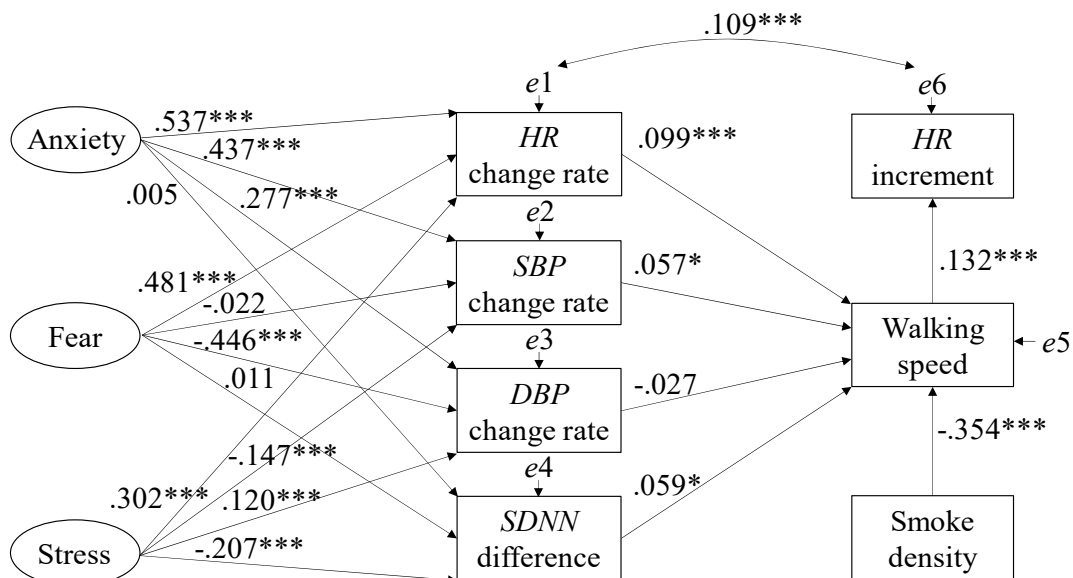
Anxiety ($i = 4$) impacts HR ($j = 1$), SBP ($j = 2$), and DBP ($j = 3$)

Focusing on HR , SBP , and DBP in anxiety because of the definition in Table 2. $\lambda_{4,1}$ (0.537), $\lambda_{4,2}$ (0.437), and $\lambda_{4,3}$ (0.277) were positive and accepted at the 0.1% level ($p < 0.001$). Hence, anxiety influenced HR , SBP , and DBP increase, which consistent with the previous studies’ report [4–5], and had the largest impact on HR increase compared with fear and stress.

Fear ($i = 3$) impacts HR and DBP

Focusing on HR and DBP in fear, $\lambda_{3,1}$ (0.481) was positive and $\lambda_{3,3}$ (-0.446) was negative and accepted at the 0.1% level ($p < 0.001$). Hence, fear influenced HR increase and DBP decrease, which consistent with the previous studies’ report [6–7]. Schwartz et al. [7] reported that HR had increased approximately 10 bpm on average when imaging a fearful situation in a sitting condition. The mean HR increase in the present fear was 11.8 bpm, almost the same as Schwartz et al. [7].

Stress ($i = 2$) impacts HR and SDNN ($j = 4$)



GFI=.870, AGFI=.725
 $***p < 0.001$, $**p < 0.01$, $*p < 0.05$

Figure 4: Standardized estimation results obtained through SEM

Focusing on *HR* and *SDNN* in stress, $\lambda_{2,1}$ (0.302) was positive and $\lambda_{2,4}$ (−0.207) was negative and accepted at the 0.1% level ($p < 0.001$). Hence, stress influenced *HR* increase and *SDNN* decrease, which consistent with the previous studies’ report [8–9].

By combining the results of hypotheses H1 and H2, the indirect impacts from emotions on walking speed via physiological signals could be represented by $\lambda_{i,j} \cdot B_{j,w}$. Therefore, anxiety increased walking speed via *HR* (0.053) and *SBP* (0.025) and decreased walking speed via *DBP* (−0.007), fear increased walking speed via *HR* (0.048) and *DBP* (0.012), and stress increased walking speed via *HR* (0.030) and decreased walking speed via *SDNN* (−0.012).

Hypothesis H3: *HR* increase by emotion is larger than that by walking exercise

To verify this hypothesis, we defined *HR* increment (*HRI*) as the walking exercise-induced *HR* increase. Here, *HRI* is the difference between the *HR* at the start CP (instantaneous value) and the mean *HR*, for each route. The influence of emotions on *HR* change rate ($\lambda_{4,1}$, $\lambda_{3,1}$, and $\lambda_{2,1}$) was larger than the influence of walking speed on *HRI* ($B_{w,HRI}$ (0.132, $p < 0.001$)), consequently, hypothesis H3 was accepted.

5. DISCUSSION AND CONCLUSION

In this study, we conducted evacuation experiments using a model-scale tunnel filled with smoke, targeting a tunnel fire. The causal relationship between emotions, physiological signals, and walking speed was modeled and investigated by structural equation modeling with the aim of applying it to machine learning in the future. The results showed that *HR*, *SBP*, and *SDNN* influenced the walking speed to be faster, while *DBP* influenced the walking speed to be slower. And emotion-induced *HR* increase was larger than that induced by walking exercise. Hence, the next behavior might be able to predict from *HR* or *BP* via the present SEM and the optimal operational technical support or design decision to prevent the irrational behavior could be recommended.

Similar to the stress model of decision-making in fires proposed by Proulx [14], the present influence of emotions on *HR* were anxiety (0.537) > fear (0.481) > stress (0.302). As a future prospect, by setting the thresholds for increased *HR*, recognizing the emotion and predicting the next behavior might be possible. Accumulating and combining data such as physiological signals of evacuees recorded by their smartwatches and their evacuation behaviors from security cameras installed in tunnels, in actual tunnel fires, machine learning can be used to optimize the evacuation process and promote and help safe and rapid evacuation in the future.

The results of this study were obtained from evacuation experiments using a model-scale tunnel, further investigations such as full-scale tunnel experiments and further physiological signals such as LF/HF during an actual tunnel fire accident are needed in the future.

6. ACKNOWLEDGMENTS

This study was supported by The Kyoto Technoscience Center (Research Development Grant 2021), JSPS KAKENHI (20K15006, 23H01532, and 23K17806), JST FOREST (JPMJFR215L), and JST SPRING (JPMJSP2132). We express our sincere gratitude to all the participants in the experiments.

7. RESEARCH ETHICS

Ethical Committee for Epidemiology of Hiroshima University, E-2457.

8. REFERENCES

- [1] Jang, E. H., Park, B. J., Kim, S. H., Sohn, J. H., 2012. Emotion classification based on physiological signals induced by negative emotions: Discrimination of negative emotions by machine learning algorithm. Proceedings of 2012 9th IEEE International Conference on Networking, Sensing and Control, Beijing, China, 283-288.
- [2] Park, B. J., Yoon, C., Jang E. H., Kim, D. H., 2017. Physiological signals and recognition of negative emotions. 2017 International Conference on Information and Communication Technology Convergence (ICTC), Jeju, Korea (South), 1074-1076.
- [3] Takeshita, R., Shoji, A., Hossain, T., Yokokubo, A., Lopez, G., 2021. Emotion Recognition from Heart Rate Variability Data of Smartwatch While Watching a Video. 2021 Thirteenth International Conference on Mobile Computing and Ubiquitous Network (ICMU), Tokyo, Japan, 1-6.
- [4] Adsett, C. A., SCHOTTSTAEDT, W. W., Wolf, S. G., 1962. Changes in coronary blood flow and other hemodynamic indicators induced by stressful interviews. *Psychosomatic Medicine*, 24(4), 331-336.
- [5] Nykliček, I., Thayer, J. F., Van Doornen, L. J., 1997. Cardiorespiratory differentiation of musically-induced emotions. *Journal of Psychophysiology*, 11(4), 304-321.
- [6] Ax, A. F., 1953. The physiological differentiation between fear and anger in humans. *Psychosomatic Medicine*, 15(5), 433-442.
- [7] Schwartz, G. E., Weinberger, D. A., Singer, J. A., 1981. Cardiovascular differentiation of happiness, sadness, anger, and fear following imagery and exercise. *Psychosomatic Medicine*, 43(4), 343-364.
- [8] Berntson, G. G., Cacioppo, J. T., Quigley, K. S., 1993. Cardiac psychophysiology and autonomic space in humans: empirical perspectives and conceptual implications. *Psychological bulletin*, 114(2), 296.
- [9] Sloan, R. P., Shapiro, P. A., Bagiella, E., Boni, S. M., Paik, M., Bigger Jr, J. T., Steinman, R. C., Gorman, J. M., 1994. Effect of mental stress throughout the day on cardiac autonomic control. *Biological psychology*, 37(2), 89-99.
- [10] Zhang, W., Meng, X., Lu, Q., Rao, Y., Zhou, J., 2013. A Hybrid Emotion Recognition on Android Smart Phones. 2013 IEEE International Conference on Green Computing and Communications and IEEE Internet of Things and IEEE Cyber, Physical and Social Computing, Beijing, China, 1313-1318.
- [11] Bhargava, M., Polzehl, T., 2013. Improving automatic emotion recognition from speech using rhythm and temporal feature. Proceedings of ICECIT-2012, 139-147.
- [12] Li, W., Seike, M., Fujiwara, A., Chikaraishi, M., 2022. Experimental study on gender difference in mental stress and walking speed during tunnel fires. 11th International Conference Tunnel Safety and Ventilation, Graz, Austria, 136-143.
- [13] Li, W., Seike, M., Fujiwara, A., Chikaraishi, M., 2023 (accepted). Structural equation modeling of negative emotion and walking behavior by smoke-filled model-scale tunnel experiments. *Safety Science*.
- [14] Proulx, G., 1993. A stress model for people facing a fire. *Journal of Environmental Psychology*, 13(2), 137-147.
- [15] Jöreskog, K. G., & Sörbom, D., 1993. LISREL 8: Structural equation modeling with the SIMPLIS command language. Scientific software international.

A 3D PARAMETRIC STUDY TO ASSESS THE IMPACT OF A FIXED FIRE FIGHTING SYSTEM ON THE EVACUATION CONDITIONS IN PARIS LA DÉFENSE ROAD TUNNELS

Nicolas Bourlet, Adrien Host, Florent Jaffier, Florent Guiral, Frederic Waymel
EGIS, FR

DOI 10.3217/978-3-85125-996-4-10 (CC BY-NC 4.0)

This CC license does not apply to third party material and content noted otherwise.

ABSTRACT

Techniques and technologies that aimed at limiting the risks and consequences of fires in road tunnels are regularly developed and optimized. In this context, Fixed Fire Fighting Systems are increasingly seen as a method capable of ensuring user safety and infrastructure protection.

The objective of the study presented in the paper is to evaluate in a parametric and comparative manner the influence of Fixed Fire Fighting Systems in Paris la Défense tunnels, on environmental conditions encountered by the users during their evacuation. One of the subjects is also to ensure their compatibility with other safety provisions such as the emergency ventilation system.

For this, a 3D CFD prototype representing a generic section of Paris la Défense tunnels has been developed. Several scenarios are carried out to take into account different structure geometries, different configurations of smoke extraction principles (longitudinal, transverse or natural), different types of fire size, different configurations of sprinkler systems as well as different initial longitudinal air speeds in the tunnel.

A conclusion is then drawn based on a qualitative multicriteria analysis including the sensitivity of the parameters studied on the evacuation conditions of users, distinguishing the zone close to the fire (zone of action of the sprinklers) from the zone further away.

Keywords: Fixed Fire Fighting Systems, Tunnels, Ventilation, Evacuation.

1. INTRODUCTION

Major fires in road tunnels have significant consequences for users, tunnel infrastructure, and, on a larger scale, the road network. Techniques and technologies aimed at limiting the risks and consequences of fires in road tunnels are regularly developed and optimized.

Fixed Fire Fighting Systems (FFFS) are increasingly considered as a method capable of ensuring the safety of users and the protection of infrastructure and can be used as a risk reduction measure. However, their use is not widespread for various technical, economic, political, and social reasons. FFFS may not necessarily be the most appropriate measure to adopt in all circumstances or locations.

The given study is an excerpt from a larger comparative study assessing the impact of sprinkler systems on the evacuation conditions of users for different smoke extraction ventilation configurations, different structure geometries, different types of fire sources, and different sprinkler system configurations.

The main objective was to characterize the influence of existing and projected sprinkler systems in the tunnels of PARIS LA DEFENSE on the ambient conditions experienced by people during their evacuation, to ensure their compatibility with other safety provisions such as smoke extraction or the position of emergency exits.

2. SIMULATION ASSUMPTIONS

2.1. Modelling softwares

Simulations are carried out with:

- 3D-type calculations to model the three-dimensional effects of smoke propagation and the effects of sprinkling on these smokes in relation to evacuation conditions. These simulations are carried out using FDS software (version 6).
- 1D-type calculations to calibrate the boundary conditions of 3D models. These calculations are performed using CAMATT2 software (distributed by CETU) to determine the intensity and direction of longitudinal air velocity in an unmeshed network.

2.2. Evacuation simulations

The evacuation simulations are carried out using a specific tool developed by EGIS Tunnels to meet the requirements of [3].

2.3. Geometrical assumptions

The study entrusted to EGIS aimed to comparatively assess the impact of Fixed Firefighting Systems (FFFS) on the evacuation of people in a tunnel section representative of several tunnels in PARIS LA DEFENSE. Consequently, certain elements such as road infrastructure (sidewalks, barriers) or the tunnel slope were not considered in the modeling, as they would provide specific results for a limited linear section of the tunnel.

Thus, a model aimed to simulate a long section of approximately 400 m of a tunnel in PARIS LA DEFENSE called the "Sculptors' Lane".

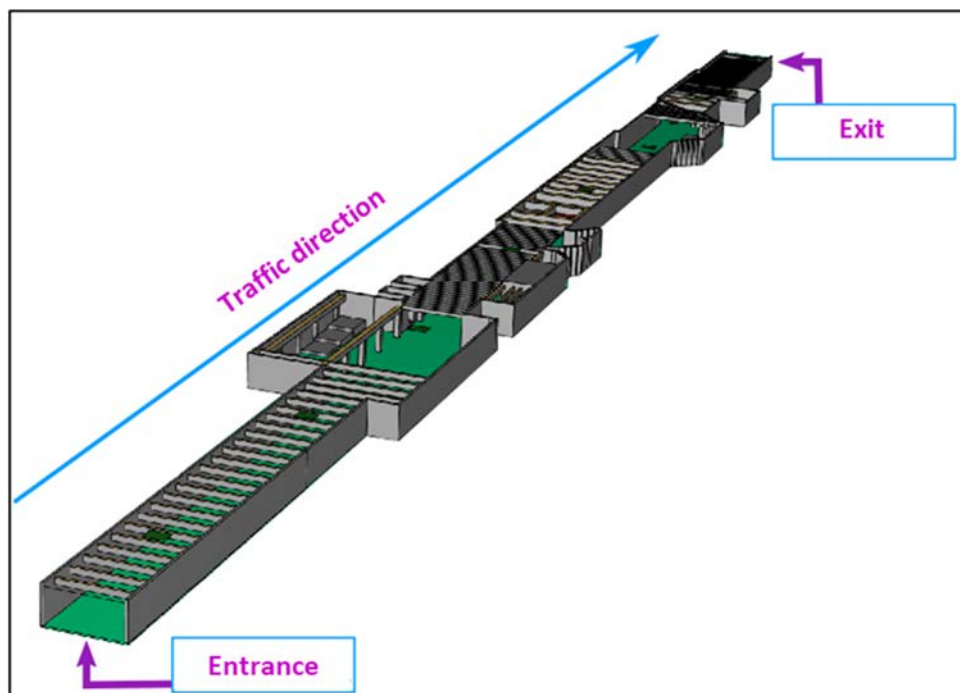


Figure 1: FDS model of the tunnel

2.4. Fire assumptions

The majority of tunnels in PARIS LA DEFENSE being restricted to vehicles weighing less than 19-ton, the ignition sources for various scenarios in this study were based on a 19-ton heavy goods vehicle (HGV).

A third-party provider commissioned by PARIS LA DEFENSE was tasked with defining the mitigation of a Fixed Fire Fighting System (FFFS) on the fire power of a 19-ton HGV.

Three types of fire sources were deemed relevant: an unmitigated source reaching 37 MW in 300s (“Scenario 1”); a mitigated source from a covered fire reaching 35 MW in 300s (“Scenario 2”); and a mitigated source from an open fire depending on the activation time of SFLIs, reaching 5,7 MW in 50s (not part of this paper).

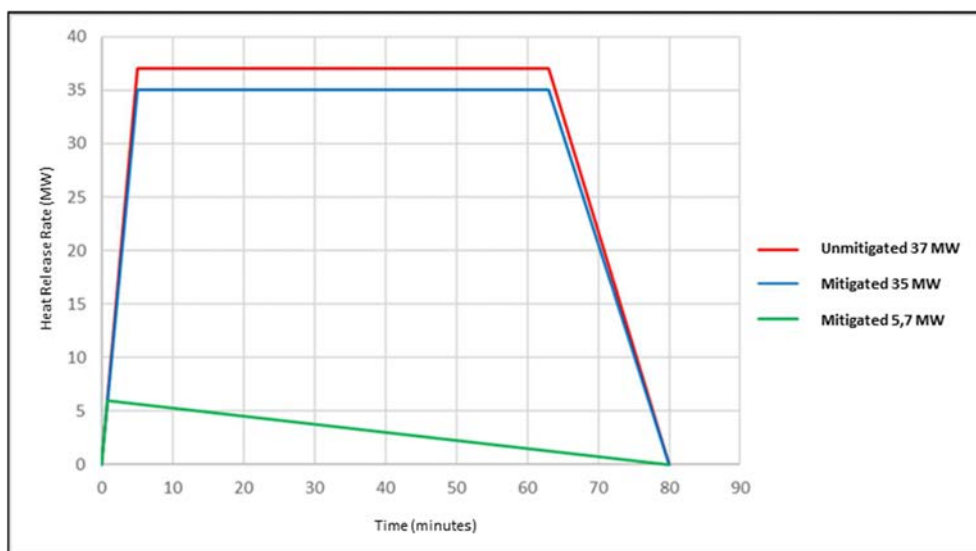


Figure 2: Heat Release Rate of fire sources

The choice of modeling the fire in the FDS software was as follows:

- 1) A prescribed pyrolysis model of HRRPUA type (Heat Release Rate Per Unit Area).
- 2) A "Simple Chemistry" combustion model, with a reactant of type $C_xH_yO_z$

The chemical reaction used for the fire was calibrated according to the production rates defined by [3].

2.5. Traffic assumptions

The low number and speed of vehicles in the structures of Paris La Défense lead to the consideration that the piston effect they generate is negligible. The traffic assumptions taken into account are 9 cars stopped upstream of the fire and 2 cars stopped downstream of it (calculated based on an average daily flow).

2.6. Aerodynamic assumptions

2.6.1. Wind effects

No counter-pressure related to the effects of external wind was taken into account in this simulation.

2.6.2. Initial air velocity

The studied tunnel having low traffic flow (2200 vehicles per day), the initial speed criterion of the air was not considered as an essential parameter for this study.

2.7. Smoke extraction assumptions

Transverse ventilation strategy is used in the tunnel. The extraction flow rate of the tunnel was set in accordance with the current French tunnel regulations [2]:

$$Q_{ext} = 80 \text{ m}^3/\text{s} + 1,5 \times S_{tun}$$

As the cross-sectional area of the tunnel is variable, the chosen reference section S_{tun} [m²] is the one located at the fire, which is 60,75 m². Therefore, the total smoke extraction flow rate has been set to 171 m³/s (distributed over 8 extraction points with a volumetric flow rate of 21,4 m³/s each).

2.8. FFFS assumptions

2.8.1. Characteristics of individual sprinkler

A third-party provider commissioned by PARIS LA DEFENSE recommended using a tunnel application rate of at least 10 l/min/m², with a sprinkler K factor of a minimum of 115L/min/bar^{0,5} and an involved surface area of approximately 300 m², considering coverage over the entire width of the tunnel. These values have been chosen for the simulation.

The activation temperature of the sprinklers is set at 72°C with a response time index of 50 $\sqrt{(m.s)}$.

Regarding the 3D modeling, a conical-shaped spray filled entirely with water droplets was considered.

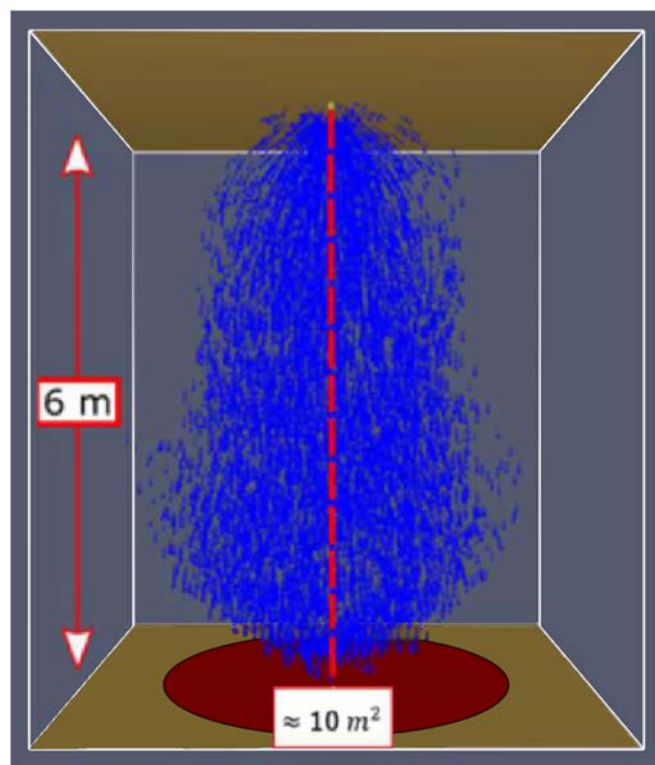


Figure 3: Individual coverage area of a single sprinkler

An individual coverage area at ground level of approximately 10 m² per sprinkler has been chosen for the entire tunnel. To achieve this :

- The two angles of the cone are set to 0° and 90°
- The discharge velocity of the droplets is set at 10 m/s

The operating pressure at the sprinkler head was calculated considering the formula:

$$Q = K \times \sqrt{P} \text{ [L/min]}$$

where Q is the operating flow rate in m^3/s , K is the orifice coefficient (known as K-factor) in $L/min/bar^{0.5}$, and P is the operating pressure at the sprinkler nozzle head in bar .

The considered operating flow rate is derived from the pro-rata between the application rate imposed on each sprinkler ($L/min/m^2$) and the individual ground level coverage area ($10 m^2$).

2.8.2. Positioning

The coverage of the modeled tunnel is ensured by 3 sprinkler heads (spaced 3.5m apart) on the transverse axis distributed throughout the entire length of the tunnel, totaling 328 sprinklers.

3. RESULTS

3.1. 3D Slice

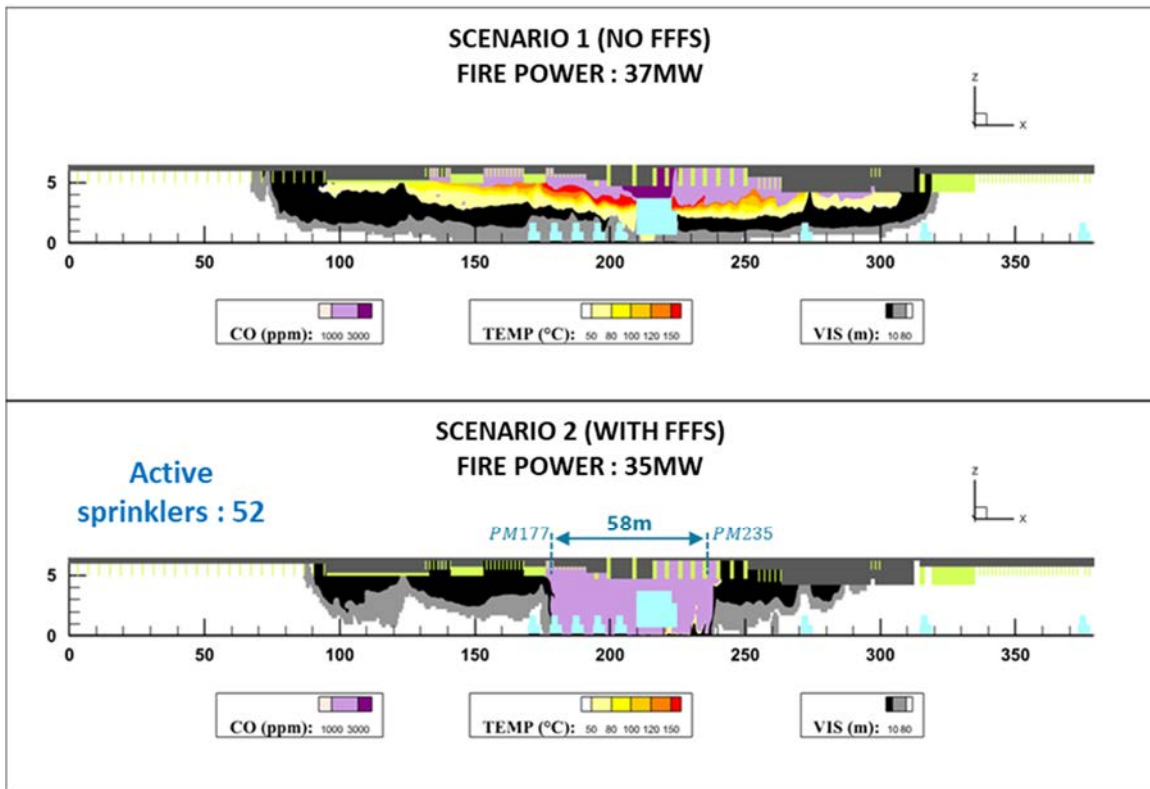


Figure 4: 3D Slice at simulation time = 600 s

The comparison between Scenario 1 and Scenario 2 revealed that the FFS coverage area (58m at the end of the simulation, 52 active sprinklers) leads to significant degraded evacuation conditions. This is because the operating sprinklers induce smoke destratification through the entrainment effect of water droplets on the smoke layer. Consequently, the hot and toxic smoke in the upper part is destratified, increasing the CO concentration and temperature at human height while decreasing visibility.

Nevertheless, outside the SFLI coverage area, evacuation conditions are greatly improved.

The sprinklers' cooling effect also reduces the smoke propagation speed on both sides of the fire.

3.2. Space-time diagrams

The space-time diagrams below depict the state of the main section of "Voie des Sculpteurs" over time, at 1.80 meters above the ground, for the different studied scenarios. These scenarios are associated with evacuation diagrams highlighting the potential paths of individuals affected by the fire.

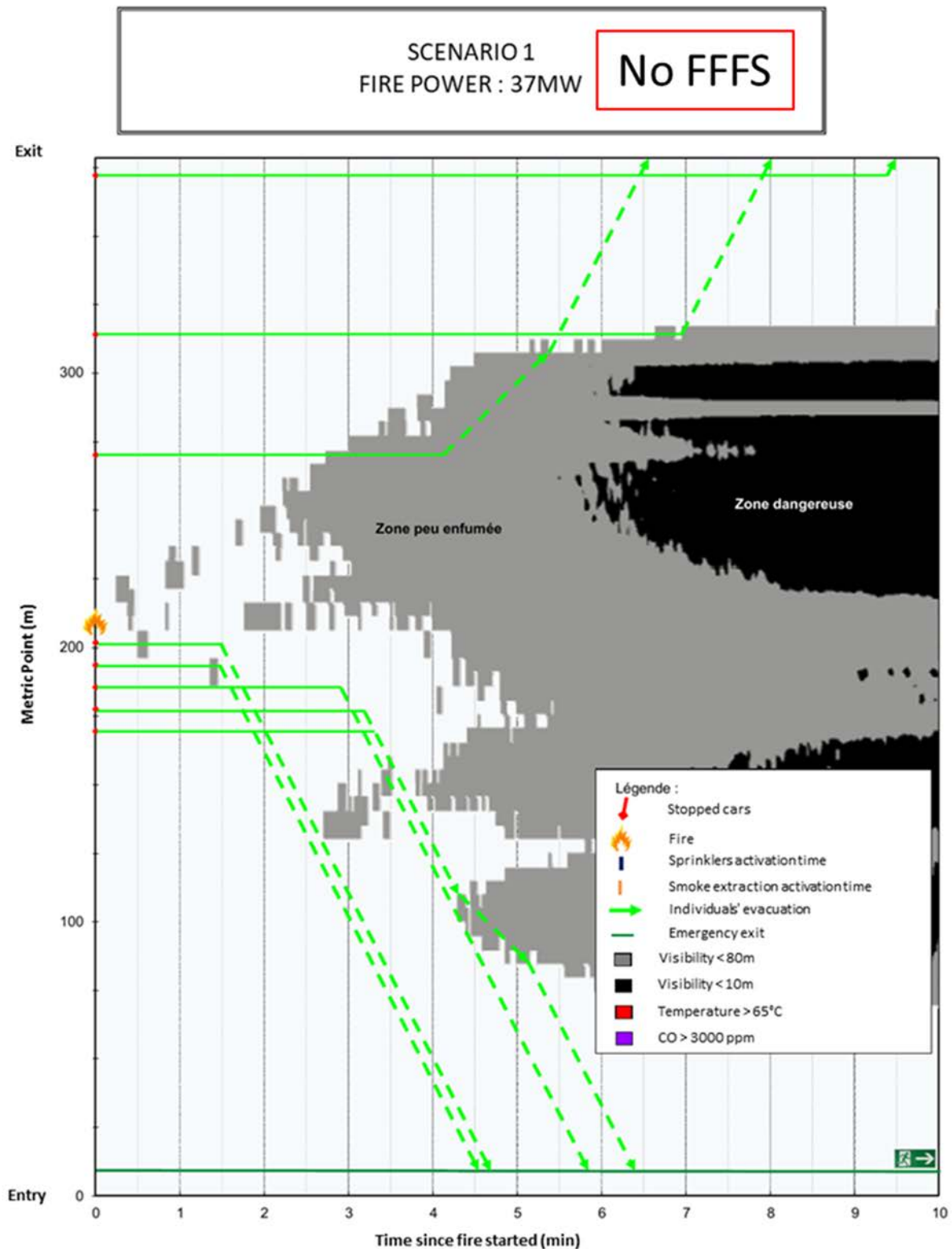


Figure 5: Space-time diagrams without FFFS

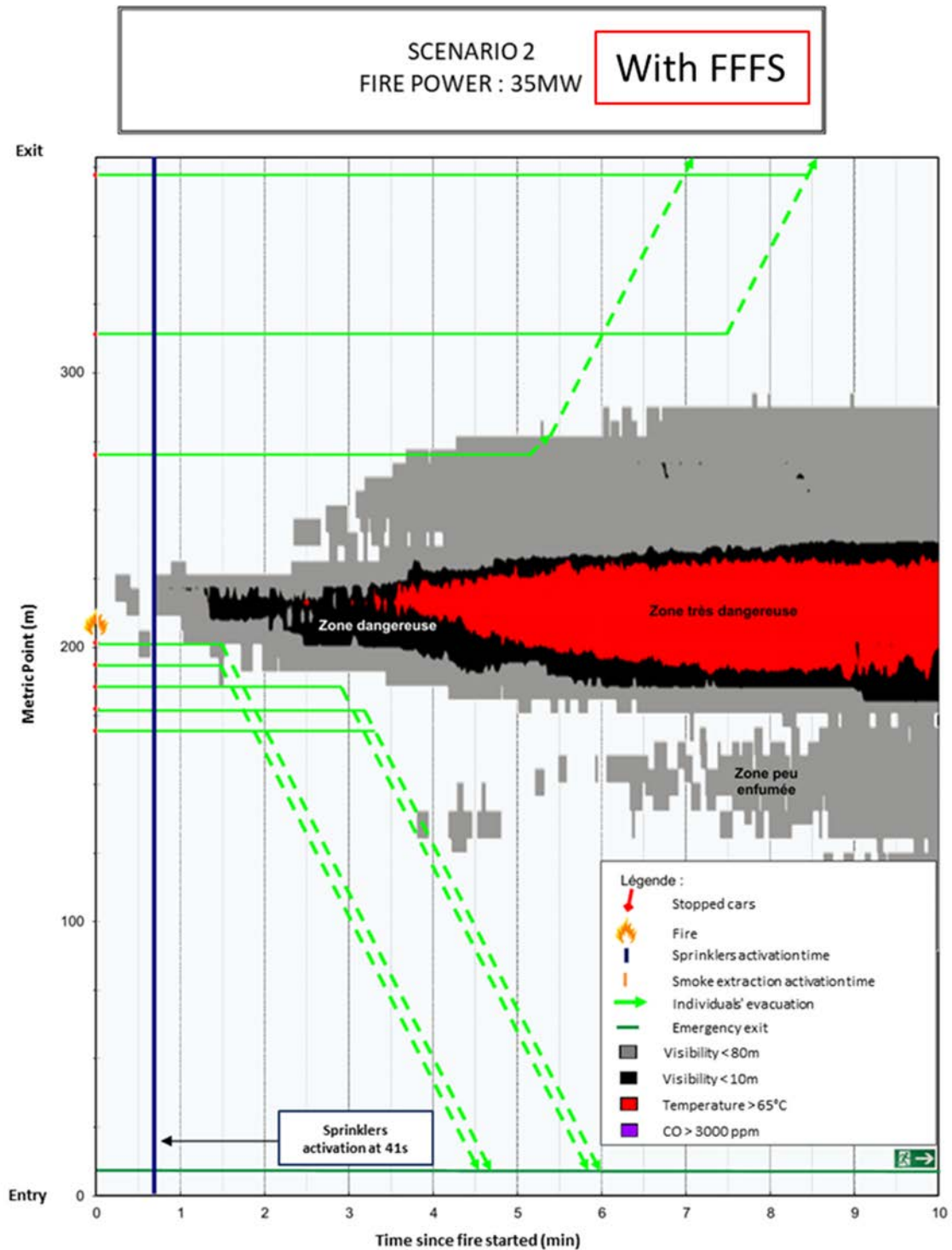


Figure 6: Space-time diagrams with FFFS

These graphs have revealed that the use of a Fixed Fire Fighting System does not worsen the evacuation of users within its coverage area as users close to the fire (within the coverage area) have sufficient time to evacuate through the emergency exits before the fire reaches high intensity.

Additionally, evacuation conditions outside this area are improved.

4. FFFS IMPACT EXTENDED STUDY

The present study was part of a larger comparative study aiming to highlight the impact of implementing a Fixed Fire Fighting System (FFFS) on the evacuation conditions of users. This was done for various smoke extraction ventilation configurations, different structure geometries, various fire scenarios, and diverse sprinkler system configurations.

In Table below is presented a multi-criteria summary making it possible to qualitatively evaluate the sensitivity of the parameters used in our study on the tenability criteria (Temperature, Radiation, CO concentration and Visibility) in the near focus zone or in the distant. In addition, a column is added to evaluate the evacuation conditions of users with the use of FFFS.

- 0** : the use of the FFFS could not highlight any change
- +** : the tenability criterion concerned has improved
- ++** : the tenability criterion concerned has been greatly improved
- : the tenability criterion concerned has deteriorated
- : the tenability criterion concerned has been greatly degraded

Table 1: Summary on the tenability criteria and evacuation of users

		TENABILITY CRITERION				
Type of smoke extraction	Area	VISIBILITY	TEMPERATURE	TOXICITY	RADIATION	EVACUATION OF USERS
TRANSVERSAL	CLOSE Sprinkled Area	--	0	-	+	+
	DISTANT Non-Sprinkled Area	+	++	++	++	++
LONGITUDINAL	CLOSE Sprinkled Area	-	+	0	++	+
	DISTANT Non-Sprinkled Area	0	++	++	++	++
NATURAL (without ventilation)	CLOSE Sprinkled Area	-	+	-	+	+
	DISTANT Non-Sprinkled Area	+	++	++	++	++

5. REFERENCES

- [1] Fire Dynamics Simulator_Technical Reference Guide_Volume 1: Mathematical Model
- [2] IT n°2000-63 : Annexe 2 du 25 Août 2000 relative à la sécurité dans les tunnels du réseau national
- [3] Guide ESD du CETu : Fascicule 4 : Les études spécifiques de danger
- [4] 2nd International Symposium on Tunnel Safety and Security: Mars 2006

6. ACKNOWLEDGEMENT

EGIS thanks Paris la Défense for having placed its trust in carrying out this study.

ENHANCING EVACUATION STRATEGIES: A MULTIFACETED APPROACH USING REAL TIME COGNITIVE ASSESSMENT

^{1,2}Perez-Jimenez, Christian, ¹Gary Clark, ¹Aslan Singh, ³Martyn Cole, ³Richard Smith

¹AtkinsRealis, GB

²Hot Smoke Machines & Demonstrations (HSM) Ltd, GB

³Heathrow Airport Limited, GB

DOI 10.3217/978-3-85125-996-4-11 (CC BY-NC 4.0)

This CC license does not apply to third party material and content noted otherwise.

ABSTRACT

This paper introduces an inventive method using real-time cognitive technology to aid tunnel operators in evaluating and enhancing evacuation strategies and safety provisions in tunnels during fire incidents. By integrating eye tracking, face emotion recognition technology, and warm smoke tests into emergency exercises, this approach highlights improvement potential in the emergency procedures (self-evacuation) as well as identifying mitigation measures and assessing the benefit of implementing them. Unlike prior studies [1], [2], [3] focusing on human attributes in evacuations, this approach emphasizes the operator's control over evacuation systems and actions, crucial in improving the safety level during an evacuation process.

This study details the application of this approach in a private UK road tunnel during a live exercise involving over 20 evacuees. Special attention is given to how safety is perceived within the bus, incident zones, cross-passages, non-incident areas, as well as at the tunnel portals and how findings were used to define mitigation measures and assess their impacts on evacuation.

Keywords: Live exercise, smoke test, evacuation process, cognitive technology, 3D modelling, eye tracking, face emotion recognition.

1. INTRODUCTION

The tunnel, as part of its overall tunnel upgrade works, instigated a project intended to explore and investigate how pre-defined emergency strategies/actions, existing life safety systems and staff competence combine to support the tunnel users (evacuees) and influence their evacuation process. While reported studies [1], [2], [3] are typically focused on the impact of human demographics, physical attributes, and other related parameters on the evacuation process, these parameters are mostly fixed in a real emergency based on the nature/use of the infrastructure. Therefore, the tunnel operator has little control over them. However, the tunnel operator does have control of how/when to deploy the different elements of the evacuation strategy (including safety provisions and actions). Understanding the impact of such actions on human behaviour is a key factor to enhance the success of the evacuation process. This paper describes an innovative approach, its application and results in a UK road tunnel to support understanding of how the tunnel safety provisions and tunnel operator actions are perceived, interpreted from the point of view of the evacuee and used by them to make (wrong or right) decisions during the evacuation process.

2. UNDERSTANDING THE TUNNEL

This UK tunnel was constructed by a combination of bored and cut and cover methods. It is a twin bore tunnel with a single lane in each bore of 6.0m width. Its total length is around 1400m with a total bore width of 8.1m and a maximum height clearance of 4.7 m.

The tunnel is provided with a longitudinal ventilation system for both pollution and smoke control. The ventilation system consists of twenty-four fully reversible roof-mounted jet fans in each bore spaced at intervals through the tunnel. Control of the ventilation system is automatic for pollution control and semi-automatic in case of fire. In addition, it is provided with other safety systems such as CCTV, lighting, emergency points, emergency telephones, cross-passages, and way-finding, but no public address/ voice alarm system.



Figure 1: Tunnel layout: Cut & Cover portal and single lane layout.

3. OBJECTIVES AND METHODOLOGY

3.1. Objectives

The main objective of this study is to get a deeper insight to how pre-defined emergency strategies/actions, existing life safe systems and staff training capabilities impact on the evacuation process in case of emergency (fire). Special attention is paid to:

- Understanding how tunnel users perceive and interpret the tunnel environment, tunnel operator actions and messages (including signalling) and use this information to decide on how to react.
- Identifying potential improvement measures (operational and systems related).
- Quantitatively assessing the potential evacuation process optimization level (benefit) of addressing/implementing those improvement measures.

3.2. Methodology

Step 1: Defining the emergency scenario (live exercise), see Section 4.

Step 2: Technology set up and instrumentation, see Section 5.

Step 3: Live exercise and smart evacuation monitoring, see Section 6.

Step 4: Analysis and recommendations - the results, see Section 7.

Step 5: Assessing the potential evacuation process optimization, see Section 8.

4. STEP 1: DEFINING THE EMERGENCY SCENARIO (LIVE EXERCISE)

4.1. Emergency event

The emergency event consisted of a tunnel fire due to a vehicle crash within the tunnel. Figure 2 represents the set-up for the live exercise. The location of the vehicle crash, and therefore, location of the smoke machine, was located at 300 m from the East portal (between cross-passages 8 & 9). One bus full of passengers and one small vehicle were placed upstream of the location of the smoke machine. The bus was located next to the smoke machine to represent a worst-case scenario as smoke is supposed to reach this location at early stages and therefore compromising the evacuation of the passengers.

4.2. Tunnel users’ distribution

The bus, full of passengers, and one small car were placed upstream of the location of the smoke machine to simulate vehicles unable to exit the tunnel. Participants were not aware of the nature and objective of the exercise, and the only instruction they received was to act/react as they were trained to do or as they would do in a real scenario. The following demographic participated in the exercise:

- Bus driver: 1 (male).
- Passengers: 20 (16 males / 4 females).
- No families or persons with reduced mobility were available for this exercise.

4.3. Instrumentation set up.

Nine fixed cameras were located at strategic points along both the incident and non-incident bore to capture the smoke propagation/behaviour as well as the evacuation process in real time. One thermocouple was located at the outlet of the smoke machine to monitor the smoke temperature. The location and orientation of these sensors are shown in the Figure 2.

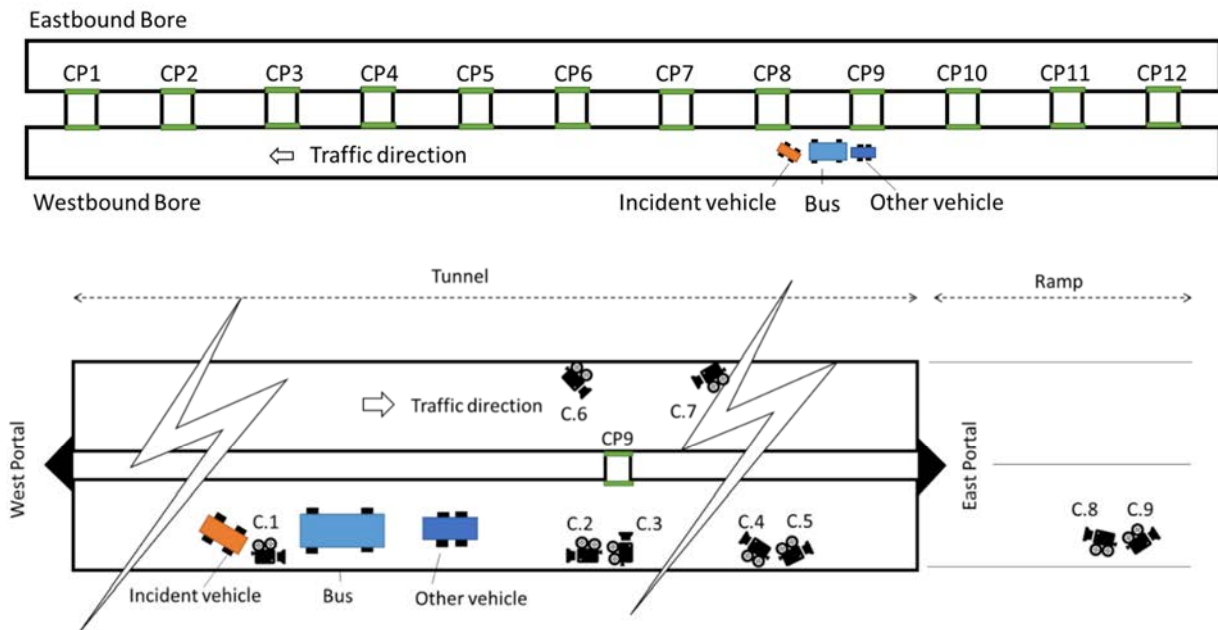


Figure 2: hot smoke machine (incident vehicle) location & the set-up for the live exercise

5. STEP 2: TECHNOLOGY SET-UP AND INSTRUMENTATION

5.1. Smoke Technology

An innovative high performance smoke generating machine (SGM), developed under a R&D framework, was deployed to create realistic and representative fire conditions and challenge the human response under low visibility conditions. During the exercise, the temperature and smoke flow at 2.1 m above the ground was set at 70°C and 25m³/s, respectively.

5.2. Eye tracking technology and Gaze detection, EGT

Eye tracking is the process of measuring the motion of an eye relative to the head. In this project, eye tracking technology is used with the purpose to detect the point of gaze (where one is looking, what is drawing his/her attention and for how long) during the evacuation process. Information from this stage is used to assess whether, which and how the available safety measures are perceived and interpreted by the evacuee to support their decision-making. Figure 3 shows the evacuee detecting a tunnel system during the live exercise. The red square represents the location at which the evacuee is looking (the “gaze”) while eye tracking is represented in red and green.

5.3. Facial expression recognition, FER

Facial Emotion Recognition is the technology that analyses facial expressions from both static images and videos to reveal information on one’s emotional state. The approach is to detect a variety of face expression patterns allowing evaluation of the emotions expressed by the evacuee during the evacuation. Information from this stage is used to assess uncertainty, confusion and decision-making moments during the evacuation. Figure 3 shows the face emotion recognition process during the live exercise.



Figure 3: Eye and Gaze tracking and face emotion recognition during the live exercise. Gaze Detection Software v1.0 developed by HSM Ltd.

6. STEP 3: LIVE EXERCISE & SMART EVACUATION MONITORING (SEA)

6.1. Overview

This section describes the evacuation process during the live exercise taking insight from the instrumentation (Section 4.1), the smart monitoring system, **SEA = EGT+ FER**, (section 5.2 & section 5.3) fitted to one of the participants, and post-exercise interviews. The evacuation assessment is split in the following phases: **a)** Phase 1: Within the bus, **b)** Phase 2: Near the bus, **c)** Phase 3: Incident bore, including access to the cross-passage **d)** Phase 4: Non-incident bore and Exit portal. For clarity in the following sections “evacuee” refers to the passenger fitted with the smart evacuation monitoring device and “passenger” refers to the other tunnel users.

6.2. Phase 1: Within the bus.

The exercise started at 00:55:00. At the same time, smoke was released. Initially, the passengers were calm and relaxed. At 00:57:30, the evacuee observed the presence of smoke propagation outside the bus (Figure 4-a). In-tunnel visibility was quickly reduced to zero. The initial calm and relaxed ambience faded as the passengers became more aware of the situation. Passengers were confused with regards what to do. Some of them were sharing their concerns among other passengers. The evacuee was expecting instructions. After 3:20 mins (00:58:20), the bus driver reacted and decided to start the evacuation. He opened the door of the bus and instructed the passengers to evacuate. Smoke entered the bus door alerting passengers and the evacuee creating confusion and delay to the evacuation process (Figure 4-b).

6.3. Phase 2: Near the bus.

The passengers exited the bus to a low visibility environment. No bottlenecks were observed at the bus door. Landing in a low visibility environment provokes a feeling of uncertainty and confusion on where to go and what to do. Some of the passengers were exploring around the bus, even heading towards rather than away from the smoke source. The control room was aware of the event and the ventilation system was activated (00:59:40), clearing the smoke away from the bus location. Adequate visibility levels were recovered and helped the bus driver to instruct the passengers on the next step. However, passengers waited in this zone for around 60 secs for instructions (Figure 4-c). The bus driver was able to instruct (01:00:03) the passengers to evacuate toward to the next SOS sign located at around 60 m upstream of the bus (Figure 4-d).

6.4. Phase 3: Incident bore, including access to the cross-passage.

At 01:00:05, all passengers started to walk to the nearby SOS points taking around 40 seconds to reach this place (Figure 4-e). Cross-passage number 9 was located next to the SOS sign. Passengers remained next to the cross-passage without accessing. Some passengers tried to open the door, but they did not dare access the unfamiliar environment (Figure 4-f). After a 01:00:58 sec, one passenger took the decision, and the rest of the passengers followed him to the non-incident bore. During this phase, the bus driver was near the bus, and he was not able to aid them during this evacuation stage.

6.5. Phase 4: Non-incident bore and exit portal.

Passengers reached the non-incident bore at 01:01:20. Uncertainty on which direction to evacuate was observed. One passenger as well as the evacuee took the decision to explore the nearby area while the rest were still exiting the cross-passage. The evacuation direction was decided based on nearby wayfinding (Figure 4-g). The exit portal was reached 5.5 mins later (Figure 4-h). During this time, it was observed that the evacuee was regularly looking back

and forward as he was worried about potential oncoming traffic. In addition, the evacuee was looking for tunnel signs to reassure the decision taken on which direction as well as to understand how far from the point of safety they were. During this stage, the evacuation was done in a relaxed and calm way as no major hazards were perceived by the passengers and evacuee. Once the passengers reached the portal, the group began to disperse. There was not a clear point of rendezvous for the passengers.

7. STEP 4: ASSESSMENT OF THE EVACUATION PROCESS

7.1. Timeline of events.

- Start of the exercise: 00:55:00am
- Start of releasing smoke: 00:55:00am.
- Start of the evacuation (from the bus): 00:58:53am.
- Ventilation system activation: 00:59:34am.
- Last passenger leaving the bus: 00:59:40am.
- Time to reach cross-passage: 01:00:45am.
- Time to reach non-incident bore: 01:01:20am.
- Time to reach exit portal: 01:06:50am.

7.2. Relevant findings.

The identification of the relevant findings was done by analysing the fixed cameras footage, the smart evacuation monitoring data as well as by set of interviews after the exercise. Thus,

- Passengers tended to rely on the bus driver as he was considered to have a better understanding of how to react in emergency scenarios. This resulted in 3.20 mins waiting time even if FER showed that smoke was observed by the passengers at the beginning of the exercise.
- Passengers proved to be unfamiliar with tunnel environment and emergency protocols. During the exercise, there was no clear idea on what to do at the cross passage area or where to go (from FER: “What is this door?”, “Where does it go?”, “Are we supposed to use it?”).
- In the absence of a PA system, clear instructions from tunnel systems and personnel (bus driver) to passengers are crucial to reduce any waiting time/decision time. Around 258 sec from the total evacuation time (720s) was time in waiting for instructions and decision making.
- Well-trained personal and accurate pre-defined messages/instructions will support on improving the evacuation. Personnel escorting the passengers may have a positive effect. Specific located signs may encourage passengers to take faster decisions at those places where confusion was detected such as at cross passages.
- Wayfinding has a reassuring effect on passengers not only on the selected route but also with regards how far the exit was.
- From SEA, emotions during this exercise ranged between “confusion”, “nervous” which prove that passengers were in an unfamiliar environment and uncertain on how to react but also “happiness” (smiling) which indicated that they are aware that this was a controlled exercise.

8. STEP 5: POTENTIAL OPTIMISATION STRATEGIES

8.1. Selected strategies and applied methodology.

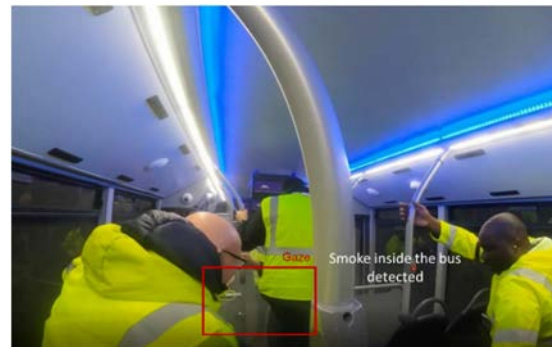
Based on the findings from section 7, this section is intended to assess the potential evacuation process optimisation of the current live exercise. Two main areas are identified: a) Updated communication strategies (Strategy 1) which represents a scenario where all passengers are clearly informed on what to do and where to go before leaving the bus and b) Trained Staff with updated communication strategies (Strategy 2) which represents a scenario where the bus driver reacts faster, and passengers are clearly informed on what to do and where to go before leaving the bus.

A like-for like comparison is made between the live exercise and strategies 1 and 2. For that purpose a set of 3D evacuation analysis are performed with Pathfinder. The main working assumptions are summarized below:

- Demographic distribution: as per live exercise (section 4.2).
- Walking speed: as per live exercise, defined based on the total evacuation time and evacuation distance (calculated around 1.0 m/s -1.5m/s).
- Pre-movement time: For strategy 1, the pre-movement time replicates the live exercise (3.20 mins). For strategy 2, it is based on the bus driver awareness time. 60 sec is considered at this study which corresponds to the time smoke covers the length of the bus.



a) 00:57:30. Evacuee sitting on the bus



b) 00:58:20. Evacuation starts



c) 01:00:00. Passenger waiting outside bus



d) 01:00:03. Bus driver instructions



Figure 4: Timeline of events from the live exercise – eye and gaze tracking visualization

8.2. Optimization level estimation

The following results are observed from the like-for-like comparison between the virtualized live exercise and strategy 1 and strategy 2:

- Regarding the evacuation process to point of safety: it is observed that the evacuation time from bus to cross-passage is 387 sec, 311 sec and 135 sec for the virtualized live exercise, strategy 1 and 2, respectively. Therefore, the potential optimisation of the evacuation ranges from around 15% to 65% for strategy 1 and 2, respectively
- Regarding the evacuation process to ultimate point of safety: It is observed that the total evacuation time (from bus to exit portal) is 720 sec, 663 sec and 487 sec for the virtualized live exercise, strategy 1, and strategy 2 respectively. Therefore, the potential optimisation of the evacuation ranges from around 10% to 35%.

Figure 5 represents the evacuation from the virtualised live exercise, strategy 1 and strategy 2. The images are taken at the same simulation time ($t=720$ sec).

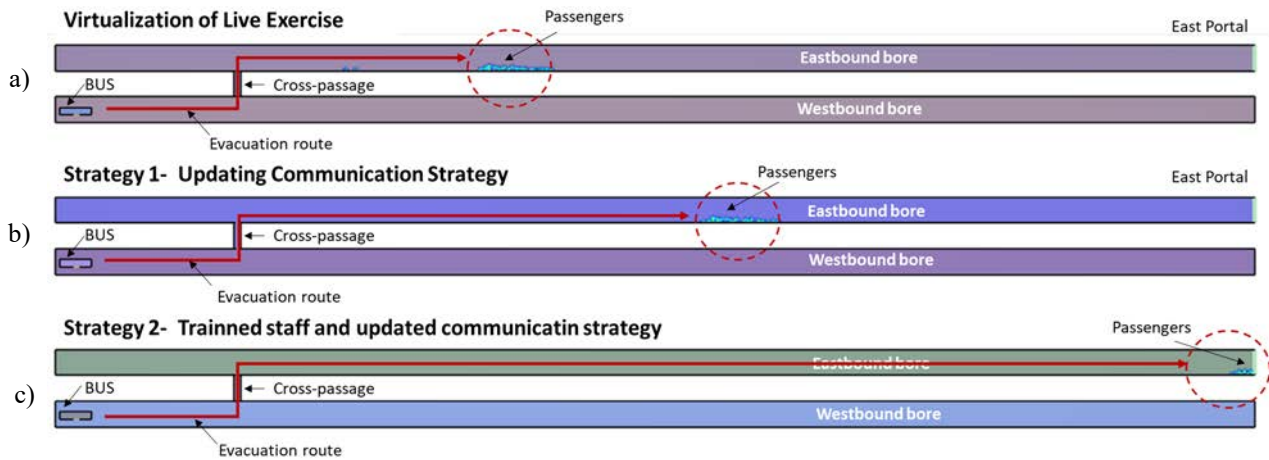


Figure 5: a) Virtualised live exercise, b) Strategy 1, c) Strategy 2. Simulated results at $t=720$ s.

9. SUMMARY AND CONCLUSION

An innovative approach to get a better insight to how actions from the tunnel operator and safety provisions are perceived and interpreted by the evacuees has been performed during a live exercise. Cognitive technology based on eye-gaze tracking and face emotion recognition has been proven to improve the pre-defined evacuation strategy by understanding why and how passengers react in one way or another. SEA can provide a continuous follow up of the evacuation process and allows detection of moments of concern, waiting time, and decision points from tunnel users for further assessment. Simple mitigation measures such as pre-defined messages from driver, strategically located signs etc were proved to have a significant impact on the evacuation. The impact of the mitigation options can be assessed by a like for like comparison of the 3D virtualized scenario. Results can support tunnel operator investment decisions - e.g., PA design and implementation.

10. REFERENCES

- [1] SFPE Handbook of Fire Protection Engineering, 2016.
- [2] Jin, T., and Yamada, T., Irritating Effects of Fire Smoke on Visibility, Fire Science & Technology, 5:1, 1985, pp. 79-89.
- [3] Seike, M., et al., Experiments of Evacuation Speed in Tunnel Filled Smoke, Tunnelling and Underground Space Technology Vol. 53, 2016, pp. 61-67.

EVALUATION OF TRACKWAY VENTILATION SYSTEM FOR THE NEW METRO LINE IN SINGAPORE

Jessleen Chua, Gerald Louis, Linfan Cai, Ernest Poon, Hadi Wijaya, Melvyn Thong
Land Transport Authority, SG

DOI 10.3217/978-3-85125-996-4-12 (CC BY-NC 4.0)

This CC license does not apply to third party material and content noted otherwise.

ABSTRACT

Maintaining acceptable temperatures within the tunnels of underground metro systems is crucial particularly in countries with tropical climates like Singapore and the trackway ventilation system plays a vital role in achieving this. As the performance of the train air-conditioning (A/C) system is affected by the temperature in the tunnel, it is important to have a properly designed and effective trackway ventilation system to extract heat dissipated by the trains when they are dwelling at the stations.

Underground stations for the existing metro lines in Singapore are equipped with an Under-Platform Exhaust (UPE) system at each platform to extract the heat dissipated from the train air-conditioning system condensing units which are mounted at the train undercarriages. However, the UPE system may not be effective for extraction of the heat from the train a/c systems for the Cross-Island Line (CRL) because the A/C unit condensing units of the CRL trains are mounted on the roof of the train carriages.

In this paper, Computational Fluid Dynamics (CFD) is used to evaluate the effectiveness of the three types of trackway ventilation systems, namely the UPE, Over-Track Exhaust (OTE), and the combined OTE and Under-Platform Air Supply (UPAS) systems for adoption in the CRL underground stations. Results show that the combined OTE and UPAS system is the most effective in maintaining the lowest inlet air temperatures at the A/C units. It also has the least impact on the station A/C system during train dwelling at the stations.

Keywords: Tunnel Ventilation System (TVS), Over-Track Exhaust (OTE), Under-platform Air Supply (UPAS), Under-platform Exhaust (UPE)

1. INTRODUCTION

The underground metro network serves as a convenient mode of transportation for commuters, facilitating travel between places and helps alleviate traffic congestion, especially during peak hours. During peak periods when more trains are in operation, it is important to control the temperature within the tunnels to ensure the functionality of both train-borne equipment and equipment installed inside the tunnels. As trains traverse the tunnels, significant amounts of heat can be generated during acceleration and braking, and the operation of the air-conditioning (A/C) system. If the heat is not effectively removed by the tunnel ventilation system, it can result in elevated temperatures within the tunnel, potentially causing passenger discomfort if the performance of the A/C system is adversely affected. The trackway ventilation system, a component of the tunnel ventilation system (TVS) plays a vital role in helping to maintain acceptable temperatures within the tunnels. This is achieved by extracting significant amounts of heat dissipated from the train propulsion, braking and air-conditioning systems when dwelling at the station trackway.

Trains on the existing metro lines are equipped with the condensing units of the A/C system located underneath the train carriage. All underground stations are provided with platform screen doors (PSD) along the edge of the platforms, to isolate the platform from the tunnel,

thereby maintain the station environment by minimizing exchange of air between the tunnel and station platform public area. The stations are equipped with an Under-Platform Exhaust (UPE) system, which comprises two or more UPE fans and a concrete duct with sliding plate dampers evenly distributed beneath each platform.

For the upcoming Cross-Island Line (CRL), the train A/C units are mounted on the roof of the train carriages instead of underneath. This change may result in the UPE system currently used in the existing lines being less effective for the CRL. Therefore, the objective of this study is to evaluate different variations of the trackway ventilation system and determine the most effective option for the CRL. The trackway ventilation systems studied were the Under-Platform Exhaust (UPE) system, Over-Track Exhaust (OTE) system and the combined Under-Platform Air Supply (UPAS) and Over-Track Exhaust (OTE) system.

2. LITERATURE REVIEW

Various studies have been conducted on the use of different types of trackway ventilation systems to aid in removal of the heat from the trains while at the stations. However, majority of the studies focused on the use of the OTE and/or UPE system, as underground metros worldwide typically employ a UPE and/or OTE trackway ventilation system, depending on the location of the equipment [1]. Alaa Hasan et. al. studied the effectiveness of the UPE system [2]. Wang & Li found that the heat removal efficiency of the OTE was positively correlated with the commuter density in the train, but the UPE had little effect on heat removal [3]. Liu et. al compared the effects of air distribution and thermal comfort in a subway station by applying three types of ventilation schemes [4].

The objective of this study is to evaluate different variations of the trackway ventilation system and determine the most effective option for the CRL. The evaluation focused on two main criteria: the average temperature at each condenser air intake, and the volume of air exchange at the PSD openings, using the commercial CFD software, ANSYS FLUENT. The design criteria of the TVS during normal and congested operations is to maintain the average temperature below 45°C at the air intake of the A/C condensers to ensure the functionality of the A/C units. If the temperature exceeds 45°C, the A/C units may start unloading, and subsequently result in uncomfortable conditions for the commuters inside the trains [3].

3. METHODOLOGY/APPROACH

3.1. Physical Model

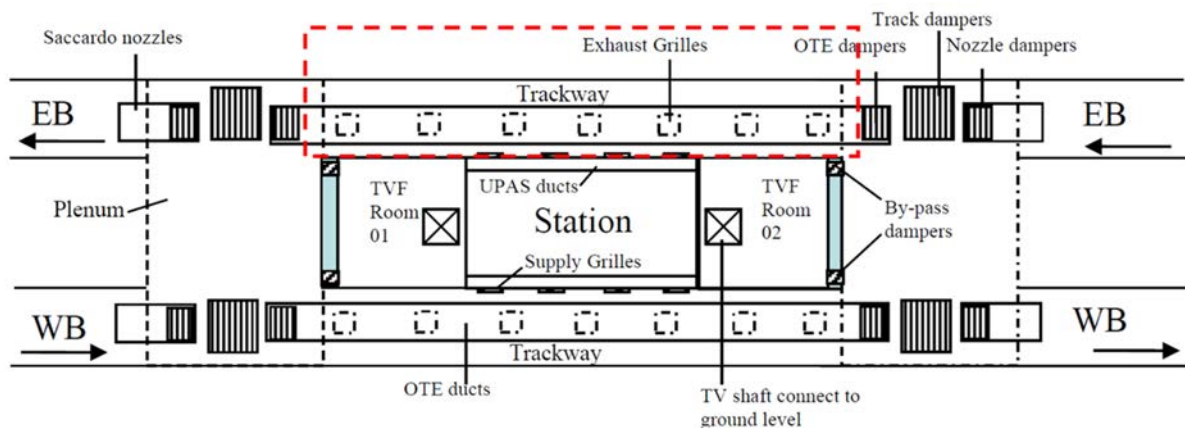


Figure 1: Typical TVS Arrangement in a CRL Station

Figure 1 shows the typical TVS arrangement in a CRL station. As the focus of this study is on the trackway ventilation system, the computational domain that was included in this study is depicted in red in Figure 1. The trackway ventilation system comprised of 32 numbers of 1.25m (L) x 1m (W) exhaust grilles along the OTE duct, located 0.5m away from the tunnel wall, and 64 numbers of 0.8m (L) x 0.5m (H) supply grilles along the UPAS duct below the platform. For the UPE system, the UPAS openings were replaced with UPE openings.

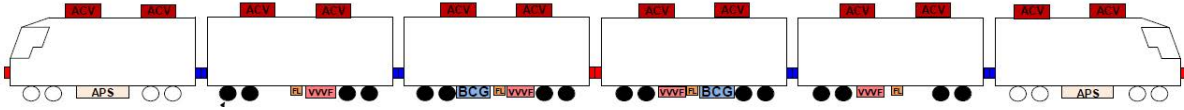


Figure 2: Heat Emitting Equipment on Train

Figure 2 shows the schematic of a six-car train, approximately 138.5m (L) x 3.2m (W) x 3.76m (H), together with the heat dissipating equipment. The equipment consisted of A/C units (ACV) located on the roof of the train carriages, and other equipment such as traction inverter (VVVF), filter inductor (FL), traction motor, auxiliary power supply system (APS), and battery charger (BCG) located on the underneath the train carriages. Heat dissipation from the abovementioned equipment can be found in Table 1 and the air flowrates for the A/C unit and the different trackway ventilation systems can be found in Table 2 respectively.

Table 1: Equipment Heat Dissipation

Equipment	Quantity per train	Heat Dissipation per train (kW)
ACV	12	162
VVVF	4	55.2
FL	4	128.8
Traction Motor	16	257.6
APS	2	39.8
BCG	2	3.6

Table 2: Flowrate of each Equipment

Equipment	Total Area (m ²)	Total Air Flowrate (m ³ /s)
ACV	40	24
OTE	40	40
UPAS	25.6	40
UPE	25.6	40

4. NUMERICAL MODEL

4.1. Computational Domain and Boundary Conditions

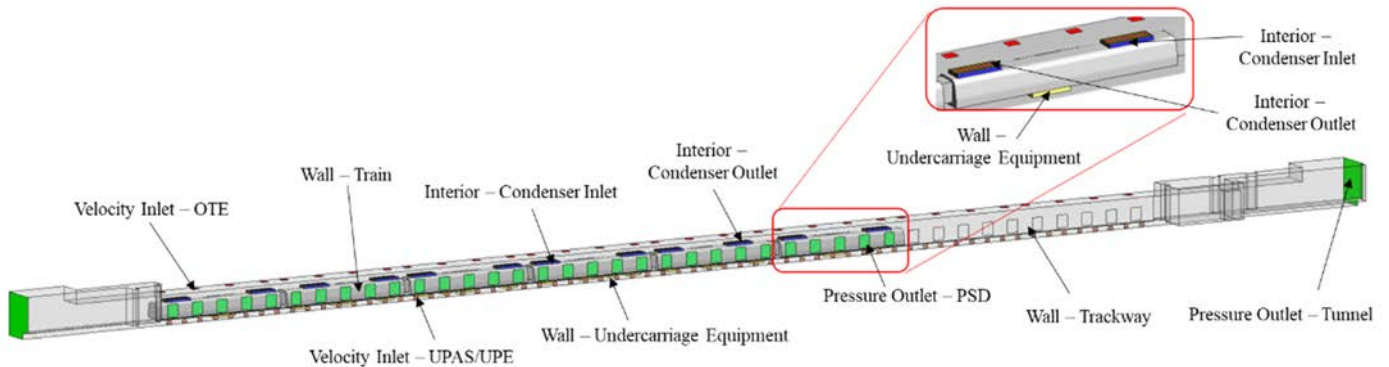


Figure 3: 3D view of Computational Domain

Although CRL stations are designed to cater for eight-car trains, six-car trains would be employed during the initial phase. Hence, PSD doors for the last two carriages at the station tail wall would remain closed. Figure 3 shows the computational domain of a typical station trackway with a six-car train located within the station trackway. Each train carriage has five numbers of doors, and they are aligned with the 30 numbers of PSDs indicated in light green. The OTE exhaust openings are indicated in red and the UPAS or UPE openings is reflected in orange. It should be noted that although the PSDs corresponding to the last two train carriages were closed, the supply and/or exhaust grilles for the OTE/UPAS would remain open and operate as intended. The A/C units have side air intakes depicted in blue, and top air discharge as shown in pink. On the underside of the train carriages, heat emitted from the equipment is shown in yellow.

Figure 3 also shows the boundary conditions that were used. The OTE, UPAS and UPE openings would be prescribed with *velocity inlet* as per Table 2. The end of the trackways indicated in dark green as well the PSD openings would be prescribed with the *pressure outlet* boundary condition. Backflow temperatures at the ends of the tunnel and PSDs were assumed to be 32°C and 25°C respectively. Heat emitted from equipment located along the undercarriages would be prescribed as *walls* with their respective heat fluxes. Finally, the A/C unit was modelled as fluid domains, prescribed with fixed values and energy sources to correspond with the fan and heat from the A/C unit.

The air flow was assumed to be independent of time, i.e., steady state and air was assumed to be non-viscous and density changes were accounted for by the incompressible ideal gas law.

4.2. Grid Independence Study

A grid independence test was performed by keeping the global mesh sizes constant while refinement to the local mesh sizes were half of the previous. Three sets of computational grids were produced as shown in Table 3. To ascertain grid independence, area-weighted average temperature and velocity at the 13th PSD openings were compared. Mesh types B and C produced similar results within 10% discrepancy. Hence, numerical analyses for this study would be performed with the use of mesh type B.

Table 3: Grid Independence Study

Mesh Type	A	B	C
Mesh Count	1,764,164	2,709,693	3,227,694
Temperature at 13 th PSD (°C)	304.54	303.26	303.06
Error (%)	0.42	-	-0.07
Velocity at 13 th PSD (m/s)	0.26	0.13	0.21
Error (%)	34.75	-	7.47

5. RESULTS AND DISCUSSIONS

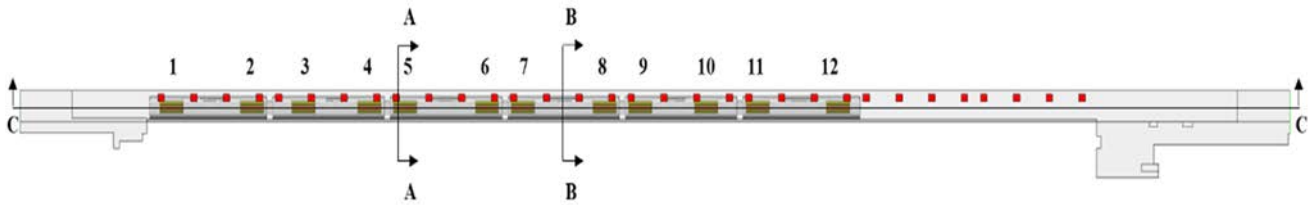


Figure 4: Cutting Plane Locations of Results (Plan View)

Results for the trackway ventilation systems are discussed in this section. Figure 4 shows the locations where results would be presented, and the numbers indicated correspond to the naming convention of the A/C units. Section A-A corresponds to a vertical section indicating the flow of air through the OTE and/or UPAS or the UPE, as well as the PSD openings. Section B-B cuts across a typical section of the PSD opening, away from the A/C units. Section C-C cuts across the exhaust openings of the A/C units.

5.1. Under-platform Exhaust (UPE)

Results for the UPE system is discussed in this section. The velocity vector at section A-A in Figure 5 indicates air was exhausted through the UPE openings, but some of the heat from the A/C unit was recirculated back into the air intake openings on the two sides. Figure 6 shows that in areas away from the A/C unit, the air flow might be relatively stagnant, as indicated by low air velocity of no more than 0.2m/s. In both illustrations, train A/C units drew most of air into the tunnel via the open PSDs.

Figure 7 and Figure 8 show the temperature contours along sections A-A and B-B respectively. Based on the results, it is evident that the A/C units drew air into the tunnel via the open PSD doors as the air temperatures near the PSD were between 25°C and 27°C. Although the UPE is effective in removing some of the heat from the undercarriage, the air temperatures within the tunnel are mostly at 45°C and above. Based on Figure 7, it seems that the air drawn into the tunnel by the train A/C units was wasted, as it was exhausted through the UPE openings, while cool air from the station platform area passed through the gap between the train and PSD. Figure 8 also shows that some of the heat could be trapped within the tunnel between the UPE openings due to limited air movement. Figure 9, which shows the temperature contour along section C-C, suggests that inadequate removal of heat within the tunnel led to the longitudinal propagation of heat, resulting in the temperature at the roof of the train carriages rising to 45°C and above, potentially causing A/C units to unload.

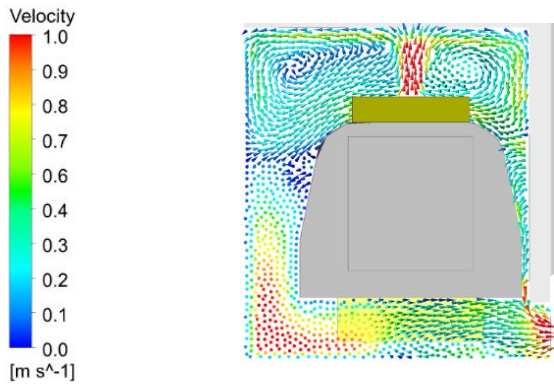


Figure 5: Velocity Vector of Air Distribution across Profile across Section A-A

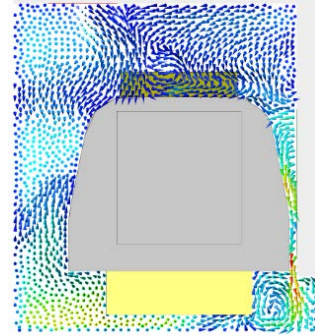


Figure 6: Velocity Vector of Air Distribution across Profile across Section B-B

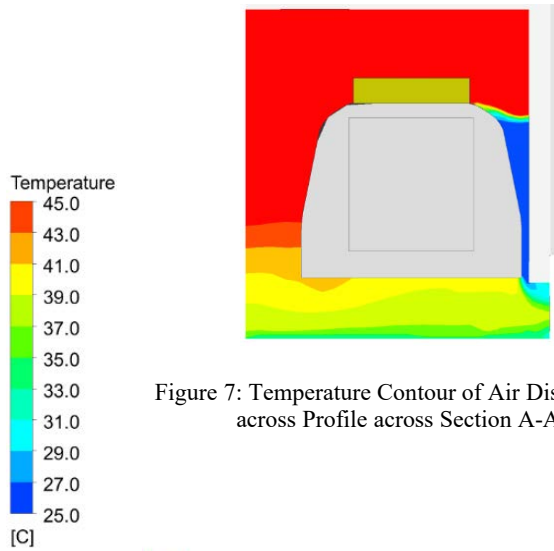


Figure 7: Temperature Contour of Air Distribution across Profile across Section A-A

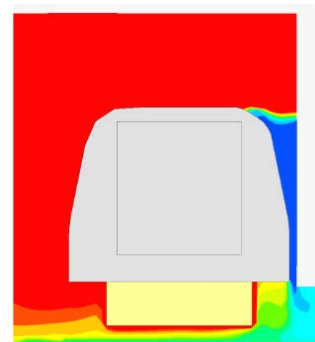


Figure 8: Temperature Contour of Air Distribution across Profile across Section B-B

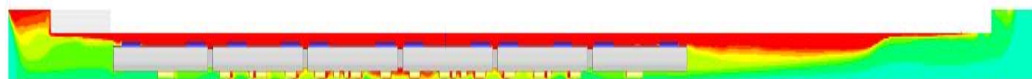


Figure 9: Section View of Temperature Contour across Section C-C

5.2. Over-track Exhaust (OTE)

This section discusses the results of the OTE system. Figure 10 and Figure 11 show the velocity vectors at Sections A-A and B-B respectively, while Figure 12 and Figure 13 show the corresponding temperature contour plots. Figure 10 shows that air from the A/C unit and undercarriage travels upwards and was then exhausted by the OTE. The OTE system shows higher air velocity in the tunnel as compared to the UPE system, as depicted in Figure 11. Like the UPE system, both Figure 10 and Figure 11 show that some air from the tunnel infiltrated into the station public area through the open PSD doors.

Figure 12 and Figure 13 show that the cool air drawn from the station public area assisted in maintaining the temperature within the tunnel to no more than 41°C at the top of the tunnel, except at localised areas near the exhaust openings. The results in Figure 14 demonstrated a similar trend, indicating that the tunnel temperatures can be maintained below 35°C.

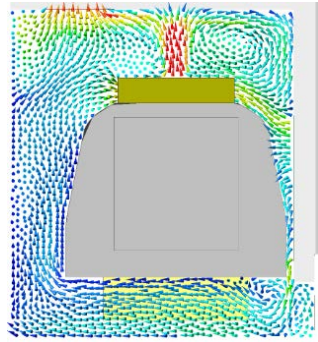
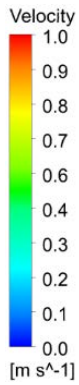


Figure 10: Velocity Vector of Air Distribution across Profile across Section A-A

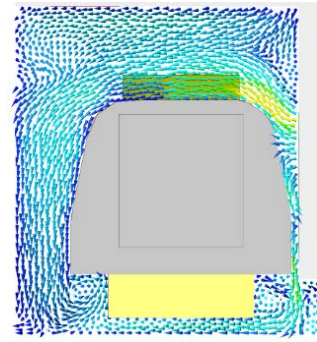


Figure 11: Velocity Vector of Air Distribution across Profile across Section B-B

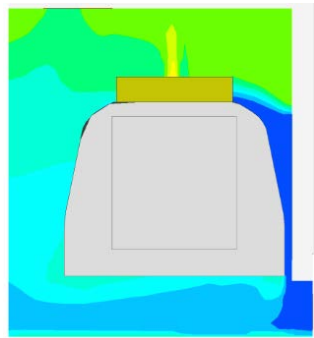
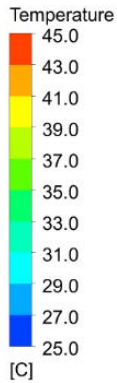


Figure 12: Temperature Contour of Air Distribution across Profile across Section A-A

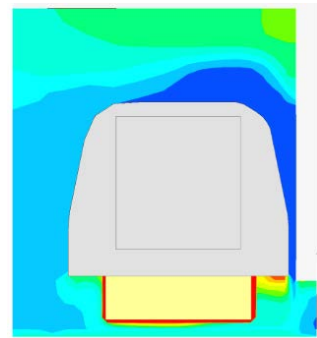


Figure 13: Temperature Contour of Air Distribution across Profile across Section B-B

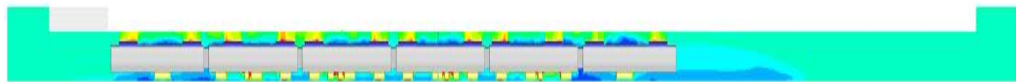


Figure 14: Section View of Temperature Contour across Section C-C

5.3. Combined Over-track Exhaust (OTE) and Under-Platform Air Supply (UPAS)

Airflow patterns for the combined OTE and UPAS system in sections A-A and B-B show that air from the UPAS openings pushes the heat from the undercarriage away from the PSD, before being exhausted through the OTE. Unlike the earlier two systems, a portion of the air from the A/C unit was drawn into the tunnel at low levels, while some of the warm air, ranging from 35°C to 37°C enters the station through the open PSD at high levels as shown by temperature contours in Figure 17 and Figure 18 respectively. However, it should be noted that some recirculation of heat from the discharge back to the intake of the A/C system is observed, particularly at the air intake near the PSD. This could be due to the OTE openings located off-centred, away from PSD. However, results in Figure 19, along section C-C, shows that although heat accumulation occurs at localised areas near the vicinity of the condensers, temperature throughout the tunnel is largely maintained below 35°C.

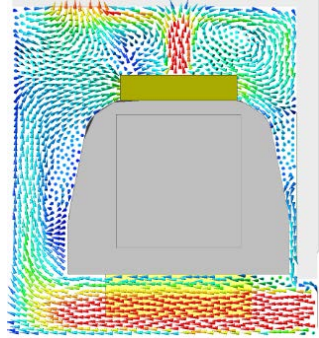
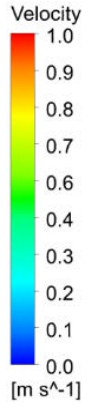


Figure 15: Velocity Vector of Air Distribution across Profile across Section A-A

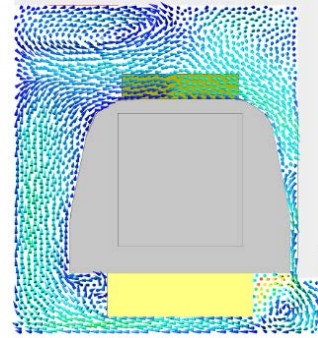


Figure 16: Velocity Vector of Air Distribution across Profile across Section B-B

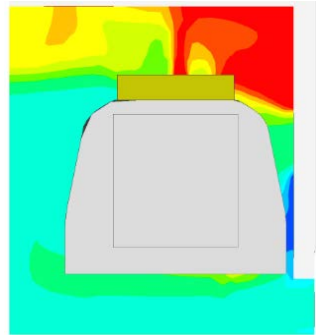
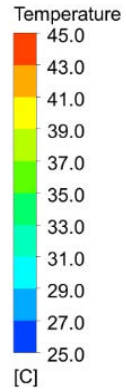


Figure 17: Temperature Contour of Air Distribution across Profile across Section A-A

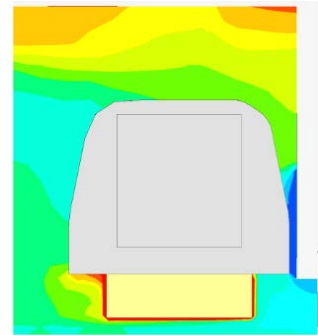


Figure 18: Temperature Contour of Air Distribution across Profile across Section B-B

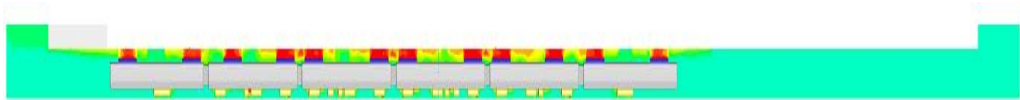


Figure 19: Section View of Temperature Contour across Section C-C

6. SUMMARY AND CONCLUSION

This section summarises the results presented in the earlier sections. Table 4 shows the average air inlet temperature at the respective train A/C unit condensers.

Table 4: Area-Weighted Average Inlet Temperature for Each Condenser

Condenser Location	Temperature (°C)		
	UPE	OTE	OTE & UPAS
1	59.20	32.90	37.49
2	65.34	31.85	38.24
3	68.31	32.71	39.44
4	68.96	33.92	40.47
5	69.08	32.99	40.18
6	69.32	31.84	40.45
7	69.28	31.52	40.15
8	68.76	32.85	40.56
9	68.18	31.35	40.22
10	67.04	31.60	40.56
11	64.27	29.99	38.72
12	58.66	31.07	37.99

For the current CRL train configuration with the A/C units located on the roof of the carriages, the conventional UPE system was not effective as it was unable to maintain the temperatures at the air inlet of the A/C unit condenser below the design criteria of maximum 45°C, thus potentially causing the A/C units to trip.

Both the OTE and the combined OTE and UPAS systems were able to maintain the temperatures at the air intake of the A/C unit condensers below 45°C. However, the temperatures at the condenser air intakes were generally lower for the OTE when compared to the combined OTE and UPAS system.

Table 5 shows the amount of air exchange through the PSD for the three systems. Positive and negative values indicate exfiltration of cool air from the station into the tunnel and infiltration of hot air from the tunnel into the station respectively. It is evident from Table 5 that both the UPE and OTE systems have significantly higher exfiltration of station cool air into the tunnel but smaller infiltration of tunnel hot air into the station as compared to the combined OTE and UPAD system. Conversely, the combined OTE and UPAS system resulted in a reduced pressure differential between the tunnel and station as compared to both the UPE system and the OTE system, thus reducing the overall air exchange through the open PSDs.

Table 5: Air Infiltration and Exfiltration at the Tunnel through Open PSDs

	Volume Flow Rate (m ³ /s)		
	UPE	OTE	OTE & UPAS
Exfiltration	22.66	26.73	4.06
Infiltration	-3.50	-1.53	-4.99

In conclusion, the UPE system is not effective for the CRL as it cannot maintain the temperature in the tunnel within the design criteria of maximum 45°C and there was significant exfiltration of cool air from the station into the tunnel. Conversely, while the OTE system can maintain the lowest average temperature at the air intakes of the train A/C unit condensers, there would be significant exfiltration of station cool air into the tunnel through the open PSD. Although the combined OTE and UPAS system may result in higher air intake temperatures at the train A/C unit condensers as compared to the OTE system, the temperatures were well below the design criteria of maximum 45°C. Additionally, the OTE

and UPAS system reduced the overall air exchange through the PSDs, which in turn led to impact to the A/C system of the station. Hence, in conclusion, the combined OTE and UPAS system would be the preferred trackway ventilation system for the CRL.

7. FURTHER STUDIES

This paper only studied the effects of the trackway ventilation systems during train dwelling at the stations. However, other factors could also be explored. This includes the use of 1D and 3D simulation tools to ascertain the infiltration and exfiltration rates due to the piston effects as trains ply between stations. The overall effect on the power consumption on the station A/C system due to infiltration of tunnel warm air and exfiltration station cool air could also be further evaluated.

8. REFERENCES

- [1] S. Kuman and S. Sharma, "Tunnel Ventilation System for the Underground Corridor of Delhi Mass Rapid Transit System," in *International Seminar on Emerging Technologies & Strategies for Energy Management in Railways*.
- [2] A. Hasan, T. ElGammal, P. S. Amano and E. E. Khalil, "Flow Patterns and Temperature Distribution in an Underground Metro Station," in *Proceedings of the ASME 2018 Power & Energy Conference and Exhibition*, Florida, 2018.
- [3] W. Chunwang and L. Xiaofeng, "Measurement-based investigation of subway station tunnel thermal environment," *Journal of Building Engineering*, vol. 57, 2022.
- [4] L. Changping, L. Angui, Y. Changqing and Z. Wenrong, "Simulating Air Distribution and Occupants' Thermal Comfort of Three Ventilation Schemes for Subway Platform," *Building and Environment*, vol. 125, pp. 15-25, 2017.

CONDENSATION IN BELOW GROUND METRO STATIONS

Paul Jolley, Mark Gilbey, Robert Jones
WSP UK Ltd, GB

DOI 10.3217/978-3-85125-996-4-13 (CC BY-NC 4.0)

This CC license does not apply to third party material and content noted otherwise.

ABSTRACT

Metro systems with significant water ingress can create conditions where condensation forms on surfaces. This may present safety issues (such as trips, slips, and falls), lead to costly asset degradation and look unsightly for passengers.

Modelling condensation in buildings is well understood, where temperatures change slowly, and air velocities are relatively low. However, modelling condensation formation in a station environment where train driven airflows can cause high air velocities and fast fluctuations in temperatures, presents a greater challenge. This paper demonstrated how 1D modelling can be used to assess the formation of condensation in existing metro stations with significant tunnel water ingress. Using this analysis method, this paper will show that if the leakage cannot be prevented, a heated supply system gives an effective mitigation against condensation.

Keywords: Metro, Condensation, Humidity, Station Ventilation, SES.

1. CONDENSATION IN A METRO STATIONS

Condensation forms when humid air meets cool surfaces. More specifically, it forms when the surface temperature is lower than the dew-point temperature of the air. The dew point temperature can be determined using the following formulae [1] by calculating the vapor pressure of the air, then using an iterative technique to determine the temperature for which the calculated vapor pressure is a saturated vapor pressure.

$$p_v = \frac{p_a g}{f_s(0.62197 + g)}$$

$$\log p_s = 30.59051 - 8.2 \log(\theta + 273.16) + 2.4804 \times 10^{-3}(\theta + 273.16) - [3142.31/(\theta + 273.16)]$$

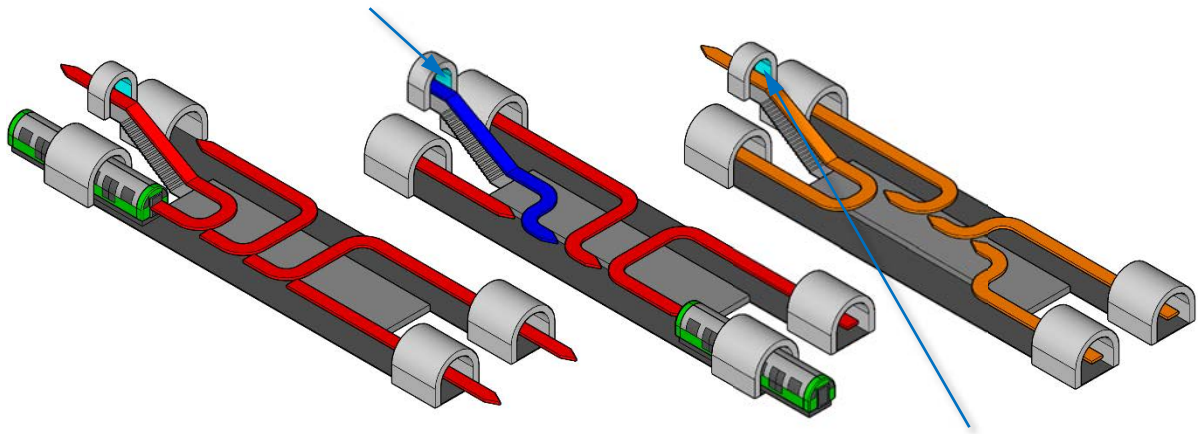
p_v = vapor pressure (kPa), p_a = atmospheric (barometric) pressure (kPa),

g = humidity ratio (kg/kg), f_s = a dimensionless enhancement factor,

p_s = saturated vapor pressure (kPa), θ = air temperature (°C)

The humidity of air increases due to the addition on water into the air (thus increasing ‘g’). In metros water is added by passengers due to exhalation or sweat, but in our experience, evaporation of seepage water is a key factor in causing condensation. Metro tunnels can run through ground containing a significant amount of water, especially where they run under rivers. This water can seep through the tunnel lining into the tunnel. Older brick-lined and newer immersed tube tunnels can be particularly prone to leakage. This seepage water can create either damp surfaces, standing water or even flowing water along the tunnel. The water ingress, unless channeled, tends to evaporate into the air. The rate of evaporation can be exacerbated if the water is warmed by the tunnel walls, themselves warmed by the long-term accumulation of heat from train operations. The warmer tunnel air also has a higher capacity to hold water. Figure 1 shows three stages in which this water can meet cold surfaces to form condensation.

Cold outside air cools the station exit surfaces.



At night condensation occurs where warm tunnel air meets the cool station exit surfaces.

Figure 1: Train arriving (left), train leaving (middle), night-time with no trains (right).

- In the leftmost pane air from the tunnel is pushed out of the station by the piston effect of an arriving train. This causes warm humid air to encounter cooler surfaces at the upper part of the station.
- In the middle pane the piston effect caused by leaving trains draws cold air into the station, cooling the walls and increasing the propensity for condensation to form.
- In the right pane, during the night (with no piston effect) the warmer tunnel air evaporates the seepage water and increases in moisture content. The warm and humid tunnel air can then rise due to buoyancy and contact colder surfaces forming condensation. Humid air is also less dense than dry air (for example, the molecular mass of water (18 g/mol) is lower than the molecular mass of dry air (29 g/mol) so at a temperature of 15°C, the air density at 50 %RH and 1013.25 hPa is 1.221 kg/m³; however, at 100 %RH and 1013.25 hPa, it is 1.217 kg/m³).
- In the morning the process loops back to the left pane. The condensation can become quite pronounced when the trains start operating in the morning as the air leaving the tunnels can be very humid.

While this paper focuses on temperate climates, condensation can occur in tunnel systems in tropical climates as well. For tropical climates, in summer hot and humid air can be drawn into tunnels and encounters surfaces that have been cooled by colder ground conditions.

Condensation manifests as water build-up on surfaces, and if sufficient condensation occurs this water can run off surfaces to affect other areas. In any environment, regular exposure to water where it isn't planned for can cause many issues. Probably the most important impact of condensation is the possibility to increase the number of trips, slips, and falls for passengers and staff. Condensation has been seen to form on tiled walls and floors on stairs leading from platforms, these areas are heavily trafficked and standing water could be a significant hazard. Safety should always be a priority to a metro operator, so reducing or preventing water build-up on walking surfaces should be a primary consideration.

Not all surfaces within a metro station may be designed to handle regular exposure to water, and condensation can form on hidden surfaces. An example could be where steel cladding has been used, and the visible surface has been treated, but the reverse surface has not. In dry conditions, this would not be an issue. However, if humid air could contact both sides of the cladding, condensation could form on the untreated surface causing significant degradation. Furthermore, this degradation would not be visible and could go unnoticed until it has become

a much greater problem. This effect on assets could create an increased burden for inspection and maintenance.

Humid air can find its way into any unsealed area and hence there may be the possibility of condensation forming on or close to electrical equipment. This could cause short circuits, damaging equipment, causing service outages, or even presenting a fire risk. If condensation occurs, it is likely that to limit any of the issues discussed, increased cleaning would be required to remove excess water in a station, especially if it was causing issues with passenger and staff safety. This will increase operational costs.

The most obvious mitigation to avoid condensation, to stop the seepage, can be very expensive and difficult, particularly for older structures and tunnels. Compensation grouting can tend to simply move the water ingress to other locations. The next most obvious mitigation would be to increase the extent of overnight ventilation to dilute the humidity. However, some existing railways may not have significant tunnel ventilation facilities, nor much space available to install large plant or create new ventilation shafts to platform level. Direct dehumidification by mechanical or chemical methods can be considered but may be very energy intensive due to the amount of water vapor that would need to be removed.

Our case study is based on an existing metro with little ability to reduce seepage and little tunnel ventilation. We therefore considered mitigations that would take up minimal space and address the two key factors in condensation formation: the reduction in relative humidity in the station and the increase of wall temperatures (to above dew point) in the location where condensation was occurring. Any mitigation would ideally achieve both.

2. ANALYSIS OF CONDENSATION

2.1. General

Evaluation of condensation risk would ideally be built into the analysis of both old and new metros. This would include the ability to estimate or predict how much water flows into the airways; how large the free surfaces areas of any water would be; the temperature and vapor pressure of the water; the undertaking of a mass transfer analogy between convection and evaporative heat exchange, a short time-step simulation capability for all hours of the year, and accurate prediction of wall surface temperatures for complex wall assemblies. At present we do not know of an industry standard way of either accurately and reliability parameterizing the preceding factors into a model a priori, nor a standard tunnel ventilation model that could directly predict the outcomes.

Our experience of dealing with condensation has mainly been in the form of mitigating an existing problem caused by water ingress above and beyond what was foreseen and could be managed. Fortunately, in such cases it is normally possible to obtain measured data to allow better estimates of evaporation rates and wall surface temperatures. If using existing data, as a minimum, air and wall temperature and air humidity data should be obtained over several weeks for the tunnels, outside the station and in the area where condensation is occurring. Furthermore, peak train driven air velocities should be recorded.

2.2. Starting air conditions

The analyses of the risk and mitigations were assessed against what we had observed and measured to be representative starting conditions of 15°C at 95 %RH for the tunnel air conditions at night, 5°C at 70%RH for outside air conditions and station wall/surface temperatures of 11.5°C.

2.3. Starting wall surface temperature

From analysis of recorded temperature data, it was estimated that the wall surface temperatures/local air temperatures at the wall surface in the station were correlated to outside and tunnel air temperatures. For example (as shown in Figure 2) the starting wall surface temperature could be calculated by taking the average of a fixed tunnel air temperature (15°C in this example) and outside air temperature and adding on a factor (in this case 1.5K). For other stations where recorded data was available, similar relationships could be found.

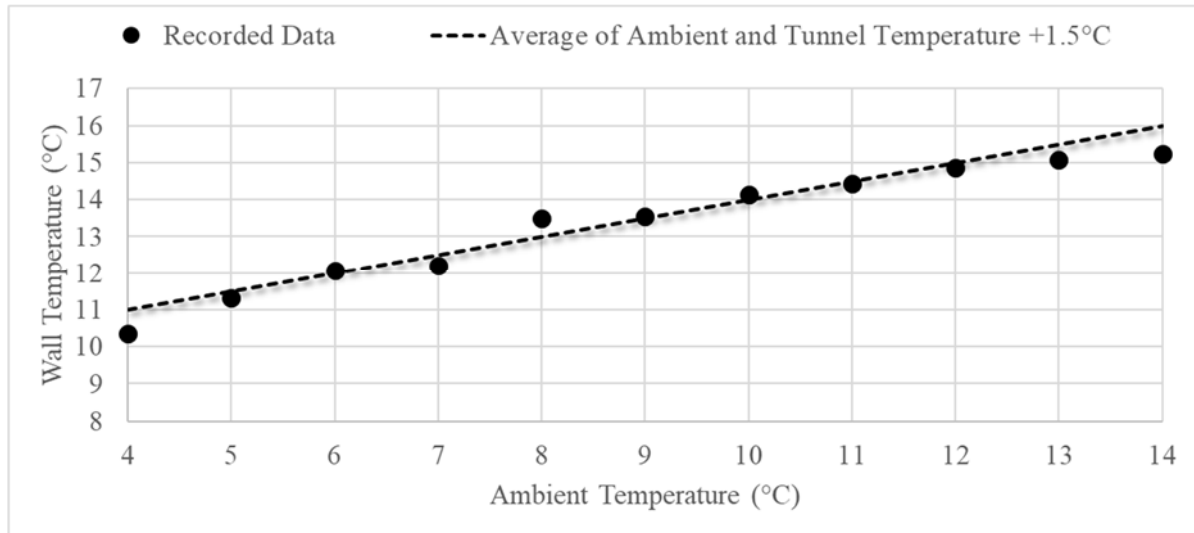


Figure 2: Relationship between ambient air temperature and wall temperature at the area of interest

2.4. 1D analysis to include tunnel airflows

Predicting the air exchange between the tunnels and the station and associated walls was an important part of the analysis. SVS/SES (a well-known and validated one-dimensional model) was used to predict the transport of tunnel air temperatures, humidities, and airflow [2,3,4,5].

By modelling the station and tunnel geometry, along with train movements and initial conditions, we could predict the fluctuations in temperature, humidity, and air flow throughout the station for a period including the last few hours of service in the evening, the hours over night where trains were not running and the first few hours of service in the morning.

2.5. 1D analysis of station surface temperatures

While we could have assumed that station surface temperatures would not change much over this relative short period, some of the mitigations relied on warming of the walls at night. Whilst there is strong confidence in the ability of SES to predict tunnel air temperatures, it has lower predictive capability for short-term transients. We therefore also used a one-dimensional numerical solver, Dynamo, that is specialized in transient tunnel wall heat transfer calculations to model how the station surface temperatures may change over the period where no trains were running. Dynamo was developed by WSP to aid in complex ground/tunnel air transient heat exchange problems. It has been well validated against exact analytical solutions to cyclic transient heat transfer and used by WSP in several applications [6,7,8,9].

2.6. Methodology

The overall process used was to:

1. Place the far-field (tunnel and outside conditions) at the SES model boundaries and use this to calculate the bulk thermal conditions and airflows, including the airflows caused by piston effect, buoyancy, and the additions of any fans.
2. Initialize a Dynamo model representing the station walls between the outside and the tunnels and use this model to calculate second-by second wall and air temperatures and humidities.
3. Use the results of the first two steps in spreadsheets along with the Chartered Institution of Building Services Engineers (CIBSE) formulae to predict dewpoint and evaluate the condensation risk.

Four key cases were analyzed:

1. Base case to verify measured condensation formation could be replicated.
2. Use of exhaust fan located at the station upper levels to draw warm tunnel air up through the station to warm the walls before the morning.
3. Use of supply fan located at the station upper levels to stop humid air rising from the tunnels at night and condensing.
4. As above but with heating of the air at the supply fan to also warm the walls.

For the cases with the fans added at the upper level, the station entrance doors were shut at night to be confident that the resulting airflows did not short-circuit directly to outside.

2.7. Base case results

Figure 3 shows these results for the base case. The trains were modelled as stopping at 02:15 and the analysis focused on the overnight to morning period since this was when condensation was most prevalent.

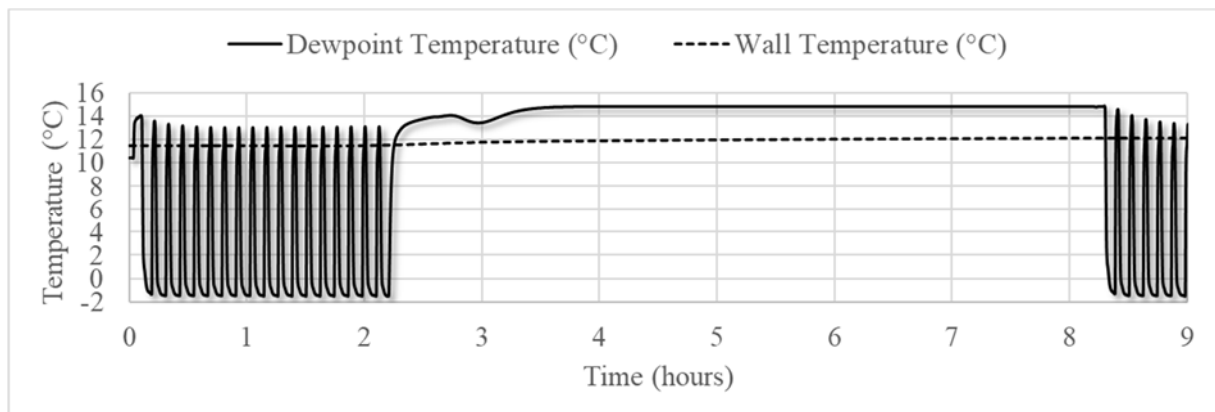


Figure 3: Dewpoint temperature and wall temperature plotted against time for the area of interest

The figure shows that the dewpoint temperature fluctuated during the last few hours of train service as the air is alternately drawn from outside and then pushed from the tunnels. The dewpoint temperature is typically below the wall temperature but for only very short durations and hence condensation is unlikely to form.

During the night, where the trains are not running, the figure shows that the dewpoint temperature rises above the wall temperature and stays there until service resumes in the morning. It is also noted that there is a small rise in wall temperature during this period. During the evening period there was no piston effect to dilute the moisture concentration in the air

and hence the still/stagnant air increased in relative humidity due to the seepage coming in from the tunnel walls and floor. Once service resumes in the morning, the dewpoint temperature returns to the same pattern as in the evening reducing the likelihood of condensation forming.

2.8. Mechanical exhaust results

A 5 m³/s fan was adopted drawing air through the station from the tunnels at night. This was a low-capacity fan in recognition of the spatial constraints at the station. The main goal of this mitigation was to see if this could warm the station walls, by virtue of the warmer tunnel air, sufficiently to prevent condensation. Figure 4 shows the analysis results.

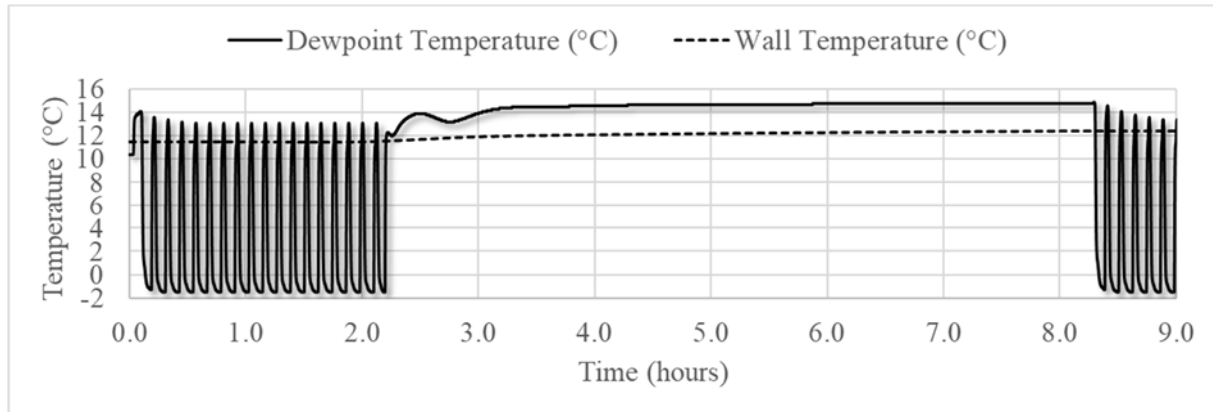


Figure 4: Dewpoint temperature and wall temperature plotted against time for night-time exhaust through station

The station walls were predicted to warm slightly compared to the base case, but not enough to prevent condensation. The temperature rise on the walls was also considered small enough that the cooling effect during the day would cancel it out, so no greater benefit would be seen over several days.

2.9. Mechanical supply results

A 5 m³/s fan supplying outside air through the station at night was assessed to prevent the warm humid air from rising through the station at night and condensing. It was thought that while the air outside may have a high relative humidity, due to its low temperature, its water content would be low and, therefore, have a dewpoint temperature below the wall temperature. Figure 5 shows the predicted results.

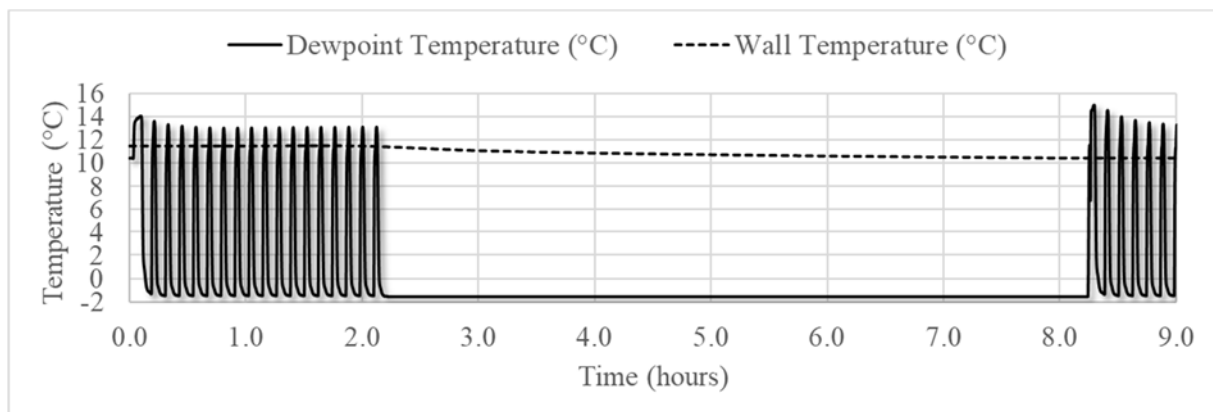


Figure 5: Dewpoint temperature and wall temperature plotted against time for night-time supply through station

Due to the low water content of the cold outside air, the dewpoint temperature is significantly lower than the wall temperature at night, predicting that condensation would be suppressed at night. However, due to the cold temperature of the outside air, the wall temperature was predicted to drop throughout the night, increasing the likelihood of condensation forming first thing in the morning when train service resumed. Spikes of wall temperature below dewpoint temperature can be seen in the right-hand side of the image.

2.10. Heated mechanical supply results

A 2.5 m³/s supply fan was assessed. A heat input of 120 kW was adopted giving a supply temperature at the fan of 45°C. A lower flow rate was used so that a higher air temperature could be achieved for a given heat input (the best permutation of flow and temperature was iterated, but for brevity those results are omitted from the paper). Figure 6 shows the predicted results.

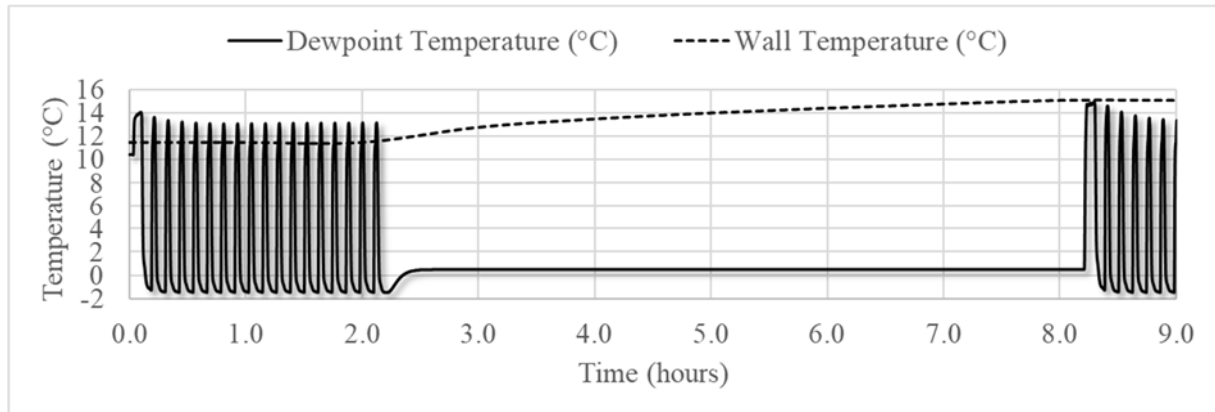


Figure 6: Dewpoint temperature and wall temperature plotted against time for heated night-time supply through station.

The dewpoint temperature of the air in the station during the night was predicted to be much lower than the wall temperature. Furthermore, due to the added heat, the wall temperature was predicted to increase noticeably to the extent that when service resumes in the morning the wall temperature is greater than the predicted air dewpoint temperature. This mitigation, therefore, has the potential to prevent condensation occurring in the morning as well. The control of the heated supply air system requires careful consideration. Ideally the system would be initiated seasonally in advance of cooler periods where condensation is likely. By doing so the walls may be progressively heated, reducing the maximum required capacity of the system.

Clearly this is an energy intensive way of mitigating the issue; however, with an inability to practicably reduce or further channel the seepage, and constraints on airflow capacity, this remains the most practicable alternative. An important factor is to find innovative ways to reduce either the heating capacity and/or energy usage. For example, in tunnels where there is significant seepage water there may also be significant water ingress into sumps. The water temperature may be considerably warmer than the outside air temperature. If this water can be collected and pumped up through the station it could be combined with a water-source heat pump to allow the required heating to be provided with greater energy efficiency.

3. CONCLUSION

By using one dimensional modelling it is possible to predict the formation of condensation within a below ground metro station. Furthermore, it is possible to use these models to predict the effectiveness of possible mitigations against the formation of condensation. However, condensation formation is strongly correlated to the rate of water ingress, and this is very

difficult to estimate in advance of construction of any tunnels. Therefore, the use of one-dimensional models will likely rely on some site data and measurements to be valid.

The preferred mitigation for condensation is a little different for tunnels than for general building mitigations, i.e., reduce water ingress and increase ventilation. For this application neither could practicably change. Of the mitigations we assessed, a heated supply system was predicted to be the most effective at minimizing condensation. This was achieved by reducing the dewpoint of the air in the station to below the wall temperature and allowing the heated air to further increase the wall temperature. Heating energy may also be reduced if it is possible to intercept some of the seepage water that is common to such tunnels with condensation issues and using this in combination with a heat pump.

4. REFERENCES

- [1] CIBSE, Guide C Reference data (2007)
- [2] U.S. Department of Transportation. Subway Environmental Design Handbook, Volume I Principles and Applications (2nd Edition), Research and Special Programs Administration John A. Volpe National Transportation Systems Center, Cambridge, MA 02142-1093
- [3] Parsons Brinckerhoff, 2014, Subway Environment Simulation User's Manual.
- [4] Bradbury W.M.S, Gilbey M.J, Temperature management on London Underground, 13th International symposium on aerodynamics, ventilation and fire in tunnels, New Jersey, 2009.
- [5] Lightfoot A., Clark G. Hunt K., Tunnel ventilation modelling for normal operations of London Underground, 3rd International symposium on aerodynamics, ventilation and fire in tunnels, New Jersey, 2009.
- [6] Thompson J.A., Missenden J.F. Gilbey M.J. and Maidment G.G., Response of wall heat transfer to steady and transient flows along a cylindrical cavity, Int. Symp. Aero. & Vent. Vehicle Tunnels, New Brunswick 2009
- [7] Thompson J.A., Dynamo – Enhancing tunnel ventilation modelling, Network, Issue 78, Parsons Brinckerhoff, December 2014
- [8] Thompson J.A., Gilbey M.J. and Legg M., Application of heat recovery to long tunnels, 16th International symposium on aerodynamics, ventilation and fire in tunnels, Seattle, 2015
- [9] Thompson J.A., Kemp S. and Gilbey M.J., Heat waves and their influence on tunnel environments, 15th International Symposium on Aerodynamics, Ventilation and Fire in Tunnels, Barcelona 2013

METRO VENTILATION SYSTEM IN SEISMIC AREAS

^{1,2}Romano Borchiellini, ^{1,2}Davide Papurello, ³Carlo Barbetta

¹Energy Center, Via Borsellino 38/18, Politecnico di Torino, IT

²Dept. of Energy Galileo Ferraris, Politecnico di Torino, IT

³Systemair GmbH, Germany/Systemair Srl, IT

DOI 10.3217/978-3-85125-996-4-14 (CC BY-NC 4.0)

This CC license does not apply to third party material and content noted otherwise.

ABSTRACT

Globally more people live in urban areas than in rural areas. By 2050 67% of the world's population is projected to be in urban areas. This demographic datum clearly shows that future megalopolis will have to face a challenge in the urban traffic and surely the underground metro network will expand. The paper analyzes the main Countries in the world that have seismic risk and their codes/standards that are locally used. The analysis is carried out where a full document is available. Major attention will be placed on Europe where a common approach is available with Eurocode 8 (EN 1998-1 Design of Structures for Earthquake Resistance). The focus will be on the Italian Code NTC 2018, which is in line with Eurocode 8. The paper focuses on non-structural components and analysis of the equipment of the ventilation system concerning the seismic forces. Comments on the seismic forces in underground soil and analysis of data. General information regarding seismic tests on the vibration table is given to understand the feasibility of a seismic qualification of equipment. Where seismic requirements are limited to stability a static analysis is sufficient or a dynamic one still feasible, conversely where a functionality or operational status is required the preferred route leads to a seismic test.

Keywords: Seismic codes, Seismic areas, Underground, Seismic qualification

1. INTRODUCTION

Globally, more people live in urban than rural areas: in 2014, 54% of the world's population lived in urban areas (in 1950, 30% of the world's population was urban). In 2050, 67% of the world's population will be urban [1]. Of course, today's figure of 54% is not constant worldwide: North America 82%; Latin America and the Caribbean 82%; Europe 73%, conversely Africa 40% and Asia 48%. All regions are expected to urbanise further in the coming decades. Africa and Asia will urbanise faster than the other regions and are expected to reach 56% and 64% by 2050. These demographics clearly show that future megacities (> 10 M people) will face an urban mobility challenge: new vehicles powered by environmentally friendly engines and the metro network will expand for public transportation. Additional attention must be addressed and placed in seismic areas. The seismic design approach certainly focuses on the structural elements, but attention must also be paid to the "non-structural elements" that are sometimes crucial to the operation and safety of structures. Indeed, in the event of an earthquake, the functionality of facilities and equipment is a major issue. Ventilation systems for subways in earthquake zones fall into this context, especially because of the large number of people involved and located in confined spaces.

2. SEISMIC AREAS

2.1. Non-EU Countries

A global view provides an overview of the technical approach to seismic design. Each country has its own "Seismic Code" that guides how to approach seismic design. A focus on the non-European level is given in the following table:

Table 1: Seismic codes for non-EU Countries

Country	Code	Notes
USA	ASCE/SEI 7-10 [2]; ASCE/SEI 7-05[3]; ASHRAE-2019 Handbook Application Chapter 56 (see comments) [4]; International Building Code IBC (ICC 2009) [5]; SMACMA 2008 [6]; FEMA 412-413-414 (Federal Emergency Management Agency) [7-9]	
CANADA	NRC-IRC 2010 [10]	National Building Code for Canada
CHILE	NcH 2369-Of2003 [11]	Diseño Sísmico de Estructuras e Instalaciones Industriales
AUSTRALIA, NEW ZEALAND	AS 1170.4-2007 [12] and NZS 1170.5-2004 [13]	Common base AS/NZS 1170.2-2002
JAPAN	kyu-taishin building codes [14]	
CHINA	GB 50011-2010 [15]	Chapter 14 (Underground Buildings), Section 14.1.1, states that this chapter does not apply to urban subways and highway tunnels; this means that there is a separate document covering subways.

This global overview is not exhaustive but shows only examples from some Countries; it should be noted that sometimes these codes in the preamble and/or in the initial part of the text refer to other standards, consequently, a complete analysis is extremely complex and beyond the scope of the paper. Structural components are primarily discussed and refer to building construction and thus are outside our scope. The focus is on non-structural elements, in our case HVAC equipment used in subway ventilation systems. The following table provides a brief comparison of the various Codes and the technical requirements that must be adopted to meet the application of the standard. The equipment and its fixings are analysed in the Codes where it is possible to have the complete document and thus be assured of a correct view and interpretation.

Table 2: Comments on the codes for non-EU Countries

ASCE/SEI 7-10	<p>(i)Table 1.5-1. Buildings and other structures that failure of which could pose a substantial hazard to the community (similar to NTC 2018 later shown).</p> <p>All chapter 13 (Seismic Design Requirements for non-structural components) gives precise information on action to be taken.</p> <p>(ii)Paragraph 13.1.3 Numbers 1 and 3. Essential components for safety, continuous operation purposes.</p> <p>(iii)Paragraph 13.1.6. Letter c. Fixings of components.</p> <p>(iv)Table 13.2.1. Applicable requirements for mechanical and electrical components.</p> <p>(v)Paragraph 13.2.2. Components for continuous operation after earthquake. Qualification by analytical approach.</p> <p>(vi)Paragraph 13.2.5 &6. Certification of component as alternative to analytical approach.</p> <p>(vii)Paragraph 13.6.1. Mechanical and electrical components fixings.</p> <p>(viii)Paragraph 13.6.3. Critical mechanical components (grade $I_p > 1$)</p>
---------------	---

ASHRAE 2019 Handbook Application Chapter 56	(i) in the preamble equipment that is to be restrained must also have the necessary strength to remain attached to the restraint. (ii) Paragraph 1. The importance of the equipment and system affected should be understood for code application to include those items that must be functional after the seismic event
AS 1170-4 2007	(i) Paragraph 8.1.4-part (b) letter (viii). Reciprocating or rotating equipment. (ii) paragraph 8.2 & 3. Non-structural components and their attachments shall be designed to resist the earthquake forces. The Acceleration method or the simple method is used.

2.2. EU Countries

If we now look at Europe, we can see that seismic zones are limited to five areas with significant seismic risk: Italy, Greece, Turkey, the northern Balkan area (Romania) and Iceland, see the following figure.

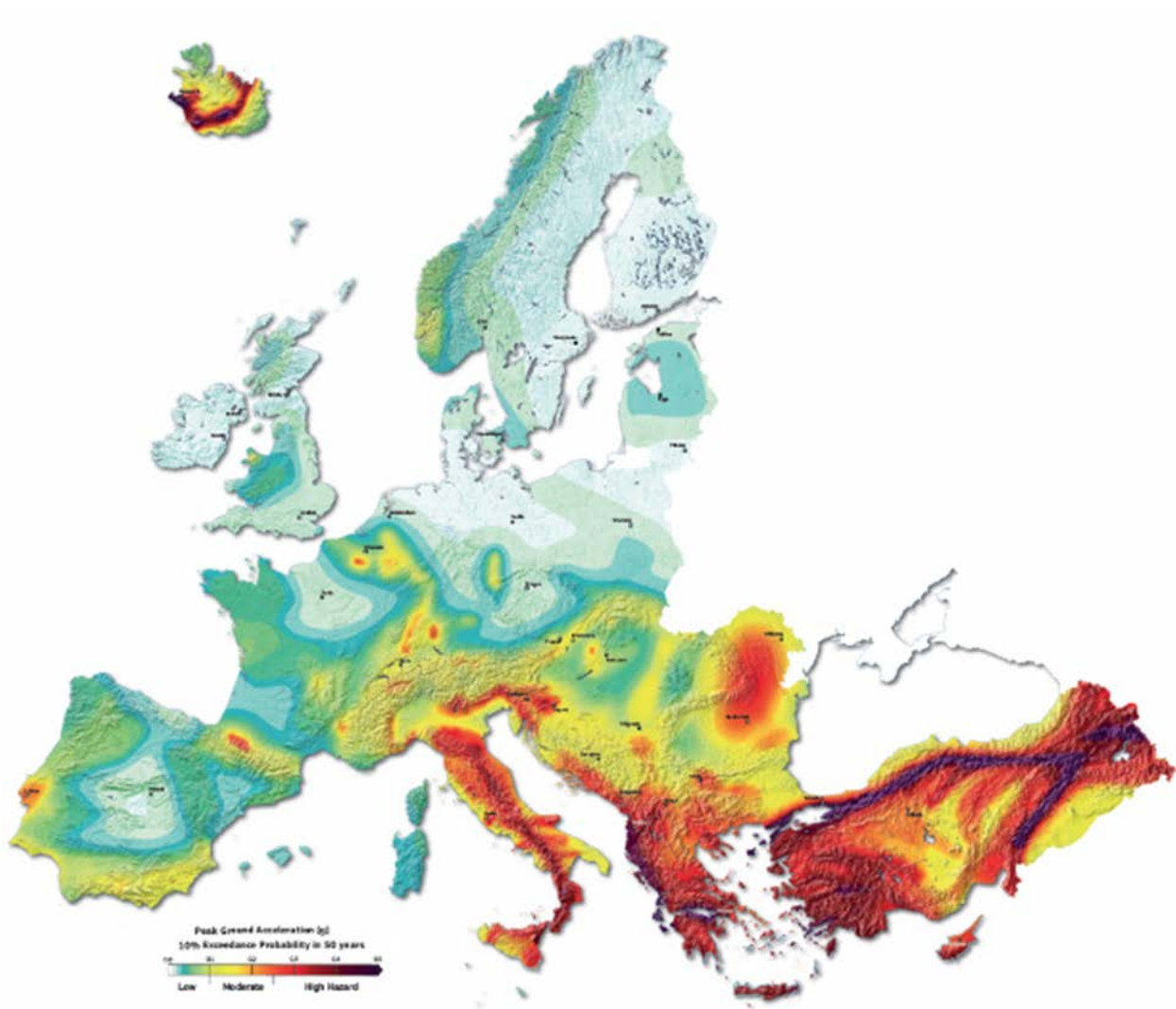


Figure 1: European seismic hazard map [16].

A common code called the Eurocode was issued in Europe in early 2000; the structural Eurocode program includes the following standards, generally consisting of several parts:

- EN 1990 Eurocode: Basis of structural design
- EN 1991 Eurocode 1: Actions on structures
- EN 1992 Eurocode 2: Design of concrete structures
- EN 1993 Eurocode 3: Design of steel structures
- En 1994 Eurocode 4: Design of composite steel and concrete structures
- EN 1995 Eurocode 5: Design of timber structures
- EN 1996 Eurocode 6: Design of masonry structures
- EN 1997 Eurocode 7: Geotechnical design
- EN 1998 Eurocode 8 Part 1: Design of structures for earthquake resistance
- EN 1999 Eurocode 9: Design of aluminium structures

The following table shows the essential elements of Part 8 and the “Basis of structural design (EN 1990)”, document from which the National Standards are derived.

Table 3: Comments of the EN1998-1 [17] and EN 1990 [18]

EN 1990	<p>(i) Paragraph 1.5.1.1 Construction works define not only building but also civil engineering work. “It refers to the complete construction works comprising structural, non-structural and geotechnical elements.”</p> <p>(ii) Paragraph 1.5.1.2 gives some examples related to buildings and civil works</p> <p>(iii) Annex B. Table B1. Construction classes. Metro should be in CC3. In any case, EN 1998-1 under 4.2.5 Table 4.3 is clearer.</p>
EN 1998-1	<p>(i) Eurocode 8. Design of structures for earthquake resistance.</p> <p>(ii) Paragraph 1.1.1. Letter (1) P. Structures important for civil protection remain operational. Note every EU Country can define different seismic risks.</p> <p>(iii) Paragraph 1.1.2. Norm applies to buildings and civil engineering works in seismic regions.</p> <p>(iv) Paragraph 2.1.1(P). Structures in seismic regions shall be designed and constructed with the requirements of no-collapse and damage limitation.</p> <p>(v) Paragraph 2.2.2.6(P). The ultimate limit state is designed. It shall be verified that under the design seismic action, the behaviour of non-structural elements does not present risks to persons and does not have a detrimental effect on the response of the structural elements.</p> <p>(vi) Paragraph 4.2.5. It is defined the importance class for buildings, and the underground train is in class IV.</p> <p>(vii) Paragraph 4.2. Table 4.3. Importance class for buildings. Class IV buildings whose integrity during earthquakes is of vital importance.</p> <p>(viii) Paragraph 4.3.5.1 Letter (1) P. Non-structural elements equipment that might, in case of failure, cause risk to persons or..... services of critical facilities, shall together with their supports, be verified to the design seismic actions. Letter (2)P..... the seismic analysis shall be based on realistic models.</p> <p>(ix) Paragraph 4.3.5.2. Verification of non-structural components.</p>

The Eurocode standards recognize the responsibility of local authorities in each EU member country to safeguard their right to determine values according to national levels, as these may vary from time to time, based on seismic risk, and from state to state.

The following table shows the different standards or codes found in various European Countries:

Table 4: Seismic codes for EU Countries

Country	Code	Notes
Greece	EAK-2000 [19]	Greek Code for Seismic Resistance Structures
Turkey	TEC-2007 [20]	National norm recently updated in 2019
Spain	NCSE-02 [21]	National norm General y edificación (Norma de Construction Sismorresistente)
Portugal	National decreto Lei 235/83 (RSAEEP) [22]	National Decreto
Romania	P100 series [23]	National norm that follows also the ASCE standards of USA
Bulgaria	Regulation RD-02-20-2 of January 2012 [24]	the Regional Ministry approved a methodology for seismic risk assessment
Austria	The National Annex ÖNORM B 1998-1 (2017) [25] to Eurocode 8 (2004) was firstly introduced in 2009.	
Iceland	the Standardization Council of Iceland is preparing a National Application Document (NAD) in conjunction with adoption of Eurocode 8	
Switzerland	SIA Norms from 260 to 267 compliant to Eurocode 8; SIA 269,269-1, 269-8 the last one relevant to seismic conservation and seismic safety; ASTRA 13020-2021 V1.01 (mainly dedicated to energy supply in tunnels); ESTI 248 version 1220i (electrical plants and seismic fixings).	Even if is not part EU the approach is inspired by Eurocode 8.

2.3. Italian approach

The regulatory framework in Italy includes various documents such as Standards, Directives, Laws, L.D., Regional Laws, and Guidelines. They have been issued over the years and some of them refer to international documents. We can mention the Official Gazette No. 108 of May 11, 2006, which establishes the territory in four seismic zones (acceleration with a 10% probability of exceedance in 50 years ag):

- Zone 1 – $0.25 < ag < 0.35$ g
- Zone 2 – $0.15 < ag < 0.25$ g
- Zone 3 – $0.05 < ag < 0.15$ g
- Zone 4 - ≤ 0.05 g

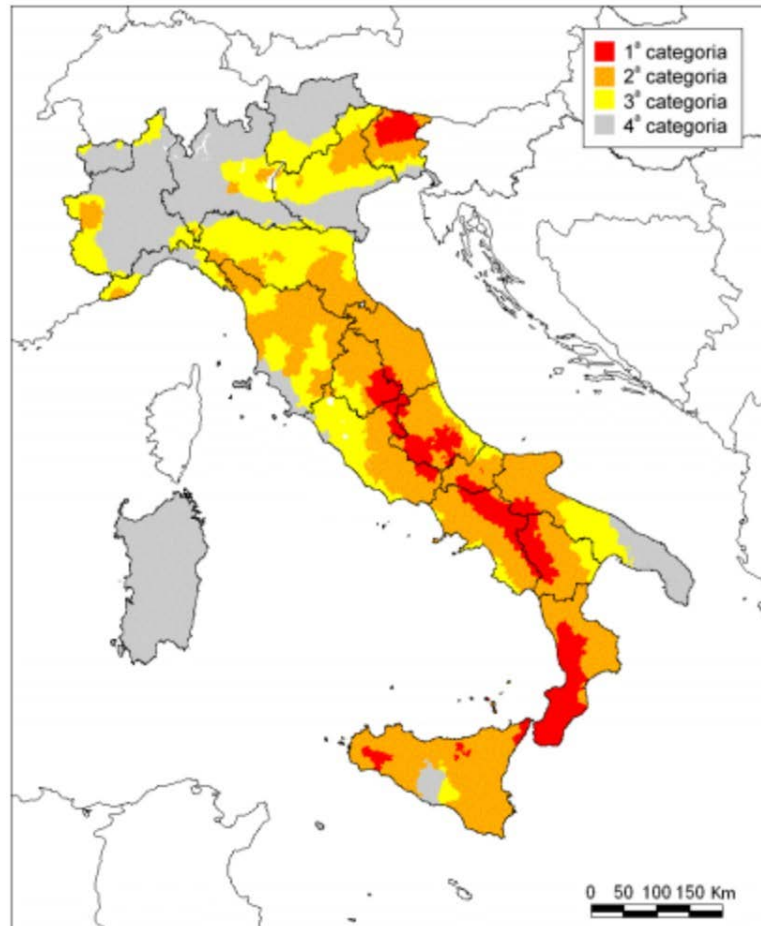


Figure 2: Peak ground acceleration According to "PCM Ordinance No. 3519-2006" [26]

Seismic acceleration ranges from 0.35 to 0.05 g. The main and essential document for seismic design is the NTC 2018 (Norme Tecniche per le Costruzioni) issued in “Gazzetta Ufficiale” No. 42 on February 20, 2018. This document is derived from EN 1998-1. This document is mandatory and currently in force, also used for the design of non-structural elements. To have a complete view, it is also necessary to consider the DM (Ministerial Decree) of October 21, 2015, which stipulates that fans for ventilation systems in subways must be certified for 400 °C/90 minutes. Therefore, the legislature considered the operation of fans essential for safety reasons during fires.

2.3.1. Focus on NTC 2018

Within NTC 2018 are the updated technical standards for construction. In Article 2, the scope, also provides for public works or public utilities, of course, subways fall within this context. The works and structural components must be designed, executed, tested, and maintained to enable the intended use with the expected level of safety. Requirements related to strength, durability, fire safety, safety against operating limit states, and safety against ultimate limit states are identified. The last two states refer to the construction, both considering structural elements, but also non-structural elements and systems. Buildings are divided into classes, the "metro" being in class IV, in which the use coefficient will be 2. This coefficient is used to obtain the reference period in which seismic actions on buildings are evaluated. Regarding the presence of structures within the metro, a static (to verify the stability) or dynamic analysis of them (to verify the functionality) can be carried out. This analysis is useful for determining the effects of seismic action. For all primary and secondary structural elements, non-structural

elements and structures, it must be verified that the value of each design demand is less than the corresponding design capacity value. Thus, as can be seen from Table 7.3.III of the NTC text [27], verifications of facilities are carried out in terms of operation and stability, obviously depending on the class of use. It should also be remembered that the fans installed inside the subways, must be F400 certified, so they are considered vital for safety. Complexity in modelling easily leads to seismic testing.

3. METRO VENTILATION SYSTEMS

In the fan system the main equipment is the fan, and the other components are part of the system; all are described and discussed from sections 3.1 to 3.4. In seismic terminology, it is considered a "non-structural component," but this does not mean that it is not important. Non-structural seismic design, such as ventilation systems, cannot be forgotten or given less attention; it is not normally considered a priority like structural components. Typically, ventilation systems are push-pull in that they push fresh air in and suck out exhausted air to create a safe escape route for people. A general ventilation plant layout is shown in the following figures.

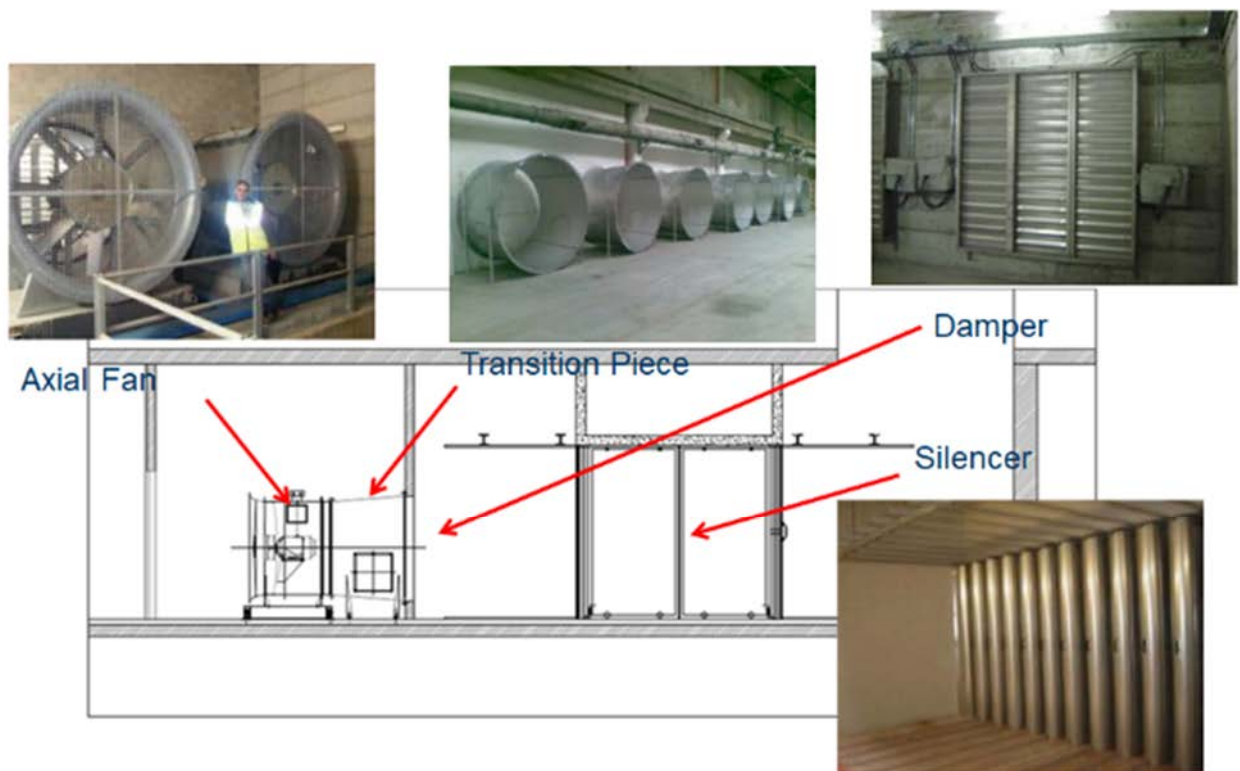


Figure 3: Typical ventilation chamber arrangement – courtesy of Systemair

3.1. Fans

The fans are mainly axial type horizontally installed in a plant room. They are also reversible and have a diameter of 1800 to 2500 mm with a motor power up to 350 kW. In Italy, they are also certified to operate as F400. The air volume is divided into 2 or more fans in parallel to have a safe redundancy. In some cases, jet fans in the metro tunnel are present to keep control the smoke spread. Fans can also be fixed on an inertial basement, which is intended to lower the centre of gravity and consequently achieve greater operational stability. Adding mass also results in less transmission of vibration to the surrounding ground. As a rule, adding mass reduces the natural frequency, while stiffening the structure increases the natural frequency.



Figure 4: Fan with seismic anti-vibrators – courtesy of Systemair and Mecanocaucho [28]

To complete the fan analysis, we can mention the natural blade frequencies are sufficiently higher than seismic normal frequencies (0.1 to 20 Hz). A typical fan of 2000 mm, 4 pole motor at 50 Hz shows a blades natural frequency of 46 Hz [29]. Furthermore, for an axial fan of 1600 mm (diameter) suitable for a 4-pole motor at 50 Hz, it was reported a casing natural principal frequency of 187 Hz with 1.927 m/s^2 ; with also two other frequencies at 237 Hz and 293 Hz [29].

3.2. Antivibration mountings

They can be rubber or spring-loaded and selected to have maximum isolation efficiency at the rated rotational frequency of the impeller. In seismic zones, it is necessary to select components that limit horizontal displacement and have resistance to the seismic forces present. The market offers seismic constraints (bumpers) that limit movement in only one direction; there are also multidirectional seismic dampers (snubbers) that can be used in conjunction with vibration-damping mounts [4]. It is recommended to use anti-vibration mounts that include the ability to operate in a seismic environment and have a low natural frequency, in some cases close to 1 Hz (lower than the normal earthquake excitation frequency, e.g., 2-3 Hz); these can hold the displacement that is quite considerable and continue to function as a normal anti-vibration mount; seismic tests have shown a reduction of up to 25 percent of the seismic forces transmitted to the fan [30]. On the other hand, when you are forced to increase the natural frequency and go up to 25 Hz, the anti-vibration mounts are still in place, but as a last resort, as it is a poor vibration insulator. The component is not an accessory, but it is an important piece that ensures the stability and operation of the fan, so it is recommended that the manufacturer be involved from the beginning. Fasteners are normally designed using the equivalent static force method acting on the fan's center of gravity. For design in Italy, NTC 2018 applies, while in Europe, EN 1998-1 and EN 1992-4 apply.

3.3. Transformation ductwork and silencers

The fan/fans are connected via a round-to-square transformation diffuser to the on/off dampers. Silencers are generally installed after the dampers as shown in figure 3. These components are static ones so they can be statically designed to withstand the load of seismic forces, ground fixing is normally enough to reach the scope. As above NTC or EN are used.

3.4. On/Off dampers

The dampers consist of a frame (static part) and blades that open and close (dynamic part) via an actuator. The dampers are fixed on a partition wall which is certainly also a non-structural element, so care must be taken to check the seismic resistance of both. Dampers can be as much as 15 m² so an appropriate seismic evaluation should be performed.

The actuators can be of various types: electrical, pneumatic, electro-pneumatic, spring return etc. There are available types already certified in the seismic environment [31] the mentioned one should be connected to a one-quadrant gear. Also, actuators already suitable for dampers application as quarter turn are seismically approved [31]. Integral controls have to be evaluated in seismic applications.

4. SEISMIC ACCELERATION IN THE UNDERGROUND

The main data in the seismic design is PGA (Peak Ground Acceleration) and the Ground Elastic Response Spectrum; in the usual building with many floors the last one can increase up to 3 times with respect to the one measured at ground (should the building oscillate in the first mode e.g. upside-down pendulum); in case of the underground metro network we have a hypogeal construction (below the ground level) and it happens an opposite effect: acceleration decreases. Recently at a PIARC Conference it was presented a paper that for the first time, as far as we know, considers the seismic design in road tunnels [32], tunnels generally respond better during an earthquake than structures located at the surface. Ground seismic data are typically established at the ground surface. Tunnels, however, are located at some depth below the ground surface. For seismic evaluation of the tunnel construction and structure and non-structural components, ground seismic data must be obtained at the height of the tunnel. Since seismic data decreases with depth, the underground data is less than the surface data [33,34].

The ratio of tunnel depth/ground surface data is shown in the following table:

Table 5: Ground motion attenuation with depth [33]

Tunnel depth (m)	Ratio of ground motion at tunnel depth to motion at ground surface
≤ 6	1.0
6 -15	0.9
15 -30	0.8
≥ 30	0.7

Since the reduction is also influenced by soil type [35] a site depth-specific dynamic response analysis should be performed (1D response) or with spatial coordinates (2 or 3D response). Normally a 1D analysis is enough to have coherent data.

5. SEISMIC QUALIFICATION

So far, as far as we can understand, there are no cases where seismic qualification by vibration test rig (shake table) have been done regarding the main components of the metro ventilation system. Most seismic Codes ask for a static or analytical approach, if modelling is required it is specified that has to be realistic. Case studies are not available and consequently no data can be evaluated as examples. In Italy the NTC 2018 asks for stability and operation so for the latter one only a modeling is applicable; but again, the mathematical net of elements is very heavy and practically leads us to consider the seismic test. There is exhaustive literature and documentation relevant to seismic test for nuclear application. For the considered case studied, the technical requirements are lower and therefore the approach should be easier. There are many norms for seismic testing but mainly focus on nuclear applications (e.g. IEEE 344 and IEC 60980). Currently, the Norms that should be applied to the ventilation equipments are: ICC ES AC 156 (2020) of the International Code Council and IEEE 693 (2018). The process is quite complex and not fully explained in this paper; the Laboratory will handle the horizontal and vertical seismic forces with relevant frequencies and with an appropriate mathematical manipulation will determine the required technical inputs to be used during the test. This part is the core of the seismic qualification.

The test is performed on a multi-axial shake table with the following main data

Table 6: multi-axial shake table / main data

Plate dimensions	4.8m x 4.8 m
Movements	longitudinal/transversal/vertical/yaw/roll/pitch
Stroke (X, Y, Z axes)	±500mm/±500 mm/+90 mm, -50 mm
Velocities (X,Y axes)	2 m/s
Velocity (Z axis)	0.5 m/s
Acceleration (X, Y, Z axes)	±15 m/s ² ; ±15 m/s ² ; ±12 m/s ²
Max. longitudinal/transverse force	1400 kN static
Max. payload	30 t
Frequency range	0.1-50 Hz nominal



Figure 5: Multi axial shake table - courtesy of EUCENTRE [36]

6. CONCLUSION

Depending on the complexity, and the type of plant section, the designer, installer and supplier will have to find the best way to fit the plant and the tool identified. The choice of the best procedure to be able to comply with the regulations is linked to the type of component, whether a static analysis is sufficient or a dynamic analysis is also necessary. In this context, the possible alternatives are as follows: in the case of stability, static calculation, or modelling (static only) may be sufficient, whereas for functionality, dynamic modelling is very complex and, in any case, would then have to be validated with ad hoc tests, so the preferred route concerns the use of seismic testing. An example of structural and fatigue strength analysis for a tunnel damper (5650x3600x300 mm) can be cited to highlight the complexity. For the fatigue strength analysis alone for a passive component, 793622 elements with a high computational cost were used [37]. Another damper manufacturer approaches the problem in a different way: the number of elements changes during the process of modelling so the damper is divided into parts and consequently in sub-models to be separately calculated. This approach leads to reduce the modelling complexity [38].

7. ACKNOWLEDGEMENTS

The Authors wish to thank EUCENTRE Foundation Pavia (Italy) for the permission to show the picture of shake table and the relevant technical data [36].

8. REFERENCES

- [1] U.P. Division, World urbanization prospects 2018: highlights, UN, 2019. <https://digitallibrary.un.org/record/3828520> (accessed October 18, 2023).
- [2] American Society of Civil Engineers, ASCE/SEI 7-10 Minimum Design Loads for Buildings and Other Structures, (2010).
- [3] ASCE, Minimum Design Loads for Buildings and Other Structures, ASCE/SEI 7-05, Minim. Des. Loads Build. Struct. ASCESEI 7-05. (2013) i–xxxii. <https://doi.org/10.1061/9780784408094.fm>.
- [4] ASHRAE, Description 2023 ASHRAE Handbook—HVAC Applications. Chapter 56 Seismic., (n.d.). <https://www.ashrae.org/technical-resources/ashrae-handbook/description-2023-ashrae-handbook-hvac-applications> (accessed October 18, 2023).
- [5] 2009 International Building Code (IBC), (2009). <https://codes.iccsafe.org/content/IBC2009> (accessed October 23, 2023).
- [6] SMACNA, Seismic Restraint Manual Guidelines for Mechanical Systems, (2008). <https://store.smacna.org/seismic-restraint-manual-guidelines-for-mechanical-systems> (accessed October 23, 2023).
- [7] Building Science Resource Library, FFEMA 412, Installing Seismic Restraints for Mechanical Equipment, (2021).
- [8] Building Science Resource Library, FEMA 413, Installing Seismic Restraints for Electrical Equipment, (2021).
- [9] Building Science Resource Library, FEMA P-414, Installing Seismic Restraints for Duct and Pipe, (2021).
- [10] TR.31.2.4 Canadian Seismic Code (NRC) - 2010, (n.d.). https://docs.bentley.com/LiveContent/web/STAAD.Pro%20Help-v13/en/STD_DEFINE_NRC_2010.html (accessed October 23, 2023).
- [11] Chilean Standard NCh2369.Of2003: Earthquake-Resistant Design of Industrial Structures and Facilities, (2016). <https://doi.org/10.1061/9780784413647.ap02>.
- [12] AS 1170.4-2007 Amd 2:2018 | Standards Australia, (n.d.). <https://store.standards.org.au/product/as-1170-4-2007-amd-2-2018> (accessed October 23, 2023).

- [13]NZS 1170.5:2004 (Includes Amdt 1) :: Standards New Zealand, (n.d.).
<https://www.standards.govt.nz/shop/nzs-1170-52004-includes-amdt-1/> (accessed October 23, 2023).
- [14]Y. Ishijama, Introduction to Earthquake Engineering and Seismic Codes in the World, Yuji Ishijama, New Research Lab. Co. Ltd, February 2011., in: 2011.
- [15]GB 50011-2010(2016) English Version, GB 50011-2010(2016) Code for Seismic Design of Buildings (2016) (English Version) - Code of China, (n.d.).
[https://www.codeofchina.com/standard/GB50011-2010\(2016\).html](https://www.codeofchina.com/standard/GB50011-2010(2016).html)
 (accessed October 23, 2023).
- [16]Mapping Europe’s earthquake risk | Research and Innovation, (2014).
<https://ec.europa.eu/research-and-innovation/en/horizon-magazine/mapping-europes-earthquake-risk> (accessed October 18, 2023).
- [17]European Union, EN 1998-1 Design of structures for earthquake resistance, (2004).
- [18]EN 1990 (2002): Eurocode - Basis of structural design, (2002).
- [19]Greece, Greek Code for Seismic Resistant Structures (EAK 2000), (n.d.).
- [20]Turkish Earthquake Code 2007 - EN, (2007).
- [21]Spanish Seismic code NCSE-02, (2005).
- [22]Decreto-Lei n.º 235/83 | DR, (n.d.). <https://diariodarepublica.pt/dr/detalhe/decreto-lei/235-1983-451672> (accessed October 23, 2023).
- [23]Romanian seismic design code: for earthquake resistant design. Design provisions for buildings. P100-series, (n.d.).
- [24]RD-02-20-2-BG, 2012 - Seismic strengthening measures. Bulgaria., (n.d.).
- [25]A. Standards, ÖNORM B 1998-1: 2017 07 01 - Eurocode 8: Design of structures for earthquake resistance - Part 1: General rules, seismic actions and rules for buildings - National specifications concerning ÖNORM EN 1998-1 and national comments, (2017).
https://shop.austrian-standards.at/action/en/public/details/606415/OENORM_B_1998-1_2017_07_01 (accessed October 23, 2023).
- [26]Mappa di pericolosità sismica del territorio nazionale, (n.d.).
http://zonesismiche.mi.ingv.it/mappa_ps_apr04/italia.html (accessed October 18, 2023).
- [27]NTC - Aggiornamento delle «Norme tecniche per le costruzioni». 2018, (2018).
- [28]wegetit | wegetit.eu, 10 AMC ANTISISMICI, (n.d.). <https://www.mecanocaucho.com/it-IT/prodotti/antivibranti-a-molla/Supporti-antisismici-10-AMC/> (accessed October 24, 2023).
- [29]Systemair GmbH, R&D Laboratory., Natural Frequency Procedure. Internal document., (n.d.).
- [30]Eucentre Foundation, Seismic Certification Laboratory. Seismic test, European Patent n° 3512803, DAFIRes®, (n.d.). <https://www.eucentre.it/laboratory-tests/?lang=en>.
- [31]Auma Riestler GmbH&Co.KG, Operational Instructions SAN 07.2-SAN16.2 - Actuators SQ 05.2/SQ12.2 Test Report 5212-00., (n.d.).
- [32]B. Khaleghi, Lecture: “Seismic And Tsunami Resilience Assessment of Roadway Tunnels In Earthquake Prone Regions”. PIARC 2nd International Conference and Safety & VIII Spanish Tunnel Symposium., in: Granada, Spain, 2022.
- [33]C.J. Hung, J. Wisniewski, J. Monsees, N. Munfah, National Highway Institute (U.S.), Technical Manual for Design and Construction of Road Tunnels - Civil Elements, 2009.
<https://rosap.ntl.bts.gov/view/dot/50019> (accessed October 19, 2023).
- [34]J.E. Luco, H.L. Wong, C.-Y. Chang, M.S. Power, I.M. Idriss, Engineering characterization of ground motion. Task II: Soil structure interaction effects on structural response, (1986).
<https://www.osti.gov/etdweb/biblio/20479139> (accessed October 19, 2023).
- [35]D.W. Sykora, Y. Moriwaki, J.A. Barneich, Measured Variation of Peaks Acceleration and Peak Particle Velocity with Depth at Soil Sites, Elsevier Elev. World Conf. Earthq. Eng. (1996).
- [36]EUCENTRE., (n.d.). <https://www.eucentre.it/>.
- [37]NORM TEKNİK, SimuTek, Norm teknik tunnel damper Finite Element Analysis - Report, under FlowPro license, (2021).
- [38]SIROCCO Luft und Umwelttechnik, GmbH, Austria. www.siricco.at, (n.d.).

EXPERIENCES FROM FIVE YEARS OF PM MONITORING IN RAILWAY TUNNELS OF AUSTRIAN FEDERAL RAILWAYS (ÖBB)

¹Daniel Fruhwirt, ¹Michael Bacher, ²Helmut Steiner

¹Graz University of Technology, AT

²Austrian Federal Railways, AT

DOI 10.3217/978-3-85125-996-4-15 (CC BY-NC 4.0)

This CC license does not apply to third party material and content noted otherwise.

ABSTRACT

Railways are considered a green transport system due to a high degree of electrification. However, due to abrasive- and wear processes railways do emit non-exhaust particles. On the one hand these particles represent a special concern related to the consequences on human's health and the environment. On the other hand, particles emitted from railways comprise a high share of conductive material, which potentially causes issues in the operation of railway infrastructure. In order to gain more information about the quantity of emissions and PM loads in railway tunnels, extensive measurement campaigns have been conducted in Austrian railway tunnels. The results show large differences in the hourly and daily average PM concentrations, which result from differences in the tunnel characteristics, traffic volume and the position in the tunnel. Iron, copper and manganese have been identified to represent the major share in the emitted particles. Furthermore, PM filter service life has been evaluated in an in-situ installation. The nominal end of filter service life was achieved within a period of two to three months.

Keywords: non-exhaust emissions, particulate matter, railway Tunnel, filter service life, Koralmbahn, Koralmtunnel, railway operation

1. INTRODUCTION

Particle emissions from road transport are well investigated and subject to strict regulations. In particular, this refers to the particle emissions from combustion processes, but non-exhaust emissions are also the focus of research, legislation and industry. The emissions from railways are not investigated in the same level of detail, although some researchers [1][2][6][9][11] carried out investigations in order to quantify the emission. However, depending on the applied methodology, PM₁₀ emission factors vary by a factor of 10 (0.2 g/km to 23 g/km). Brakes, wheels, rails as well as the contact strip and the contact wire represent the main sources of non-exhaust particle emission in rail transport.

In a tunnel environment, the PM concentrations can be expected high, due to a limited dilution of pollutants. This expectation is confirmed by many studies which identified metro systems to be the highest polluted urban places. [4] investigated the PM loads in the metro system in Milan and determined daily average concentrations up to 300 µg/m³. Similar results were obtained in the study of [10] who investigated the air quality in Barcelona's metro system.

PM loads in railway tunnels were assessed by [3], who conducted measurements in the Arlanda airport tunnel in Stockholm. During rush hour the PM₁₀ concentration reached values up to 260 µg/m³. Due to a lack of information an assignment to exhaust and non-exhaust emissions cannot be made. However, these results show that particle emissions from rail transport can cause a severe problem due to the particles conductive properties and the quantity of emitted particles.

Long subsurface structures become more and more often part of modern transport infrastructure. A safe and reliable operation of such structures requires a variety of technical installations. Some of these installations release significant off-heat, which has to be removed in order to keep room air temperatures on an acceptable level [5]. Hence, cooling systems are required, which most commonly utilize tunnel air for re-cooling. In case of a mechanical ventilation system, the tunnel air is directly guided into the utility rooms. Another option is to use means of air conditioning in order to avoid from a direct utilization of polluted tunnel air. However, the re-cooling unit as well has to be protected from the dust loads. Thus, in both cases tunnel air has to be specially treated by the utilization of filter systems that are characterized by a service life, which depends on the collected particle mass.

In order to determine the PM filter service life in a railway tunnel environment, extensive PM monitoring has been conducted in recent years. This includes the observation of PM mass-concentrations, the derivation of PM emission factors, chemical analysis of particle composition and in-situ testing of PM filters in order to determine the service life. This paper summarizes the experiences and the main findings from the past five years.

2. KORALMBAHN AND KORALMTUNNEL

In the future the Austrian Federal railways will face the issue of dust loads, as three very long (longer than 27 km) railway tunnels (Koralmtunnel / KAT; Semmering Base Tunnel / SBT; Brenner Base Tunnel / BBT) will be set in the next 10 to 15 years into operation.

The so called ‘southern corridor’, which includes the Koralm railway (Koralmbahn / KAB – see Figure 1), is part of the 1,800 km long Baltic–Adriatic rail corridor of the Trans European Network – Transport (TEN-T). The KAB, with a length of about 130 km, connects the Austrian federal regions Styria and Carinthia, and their capital cities Graz and Klagenfurt.

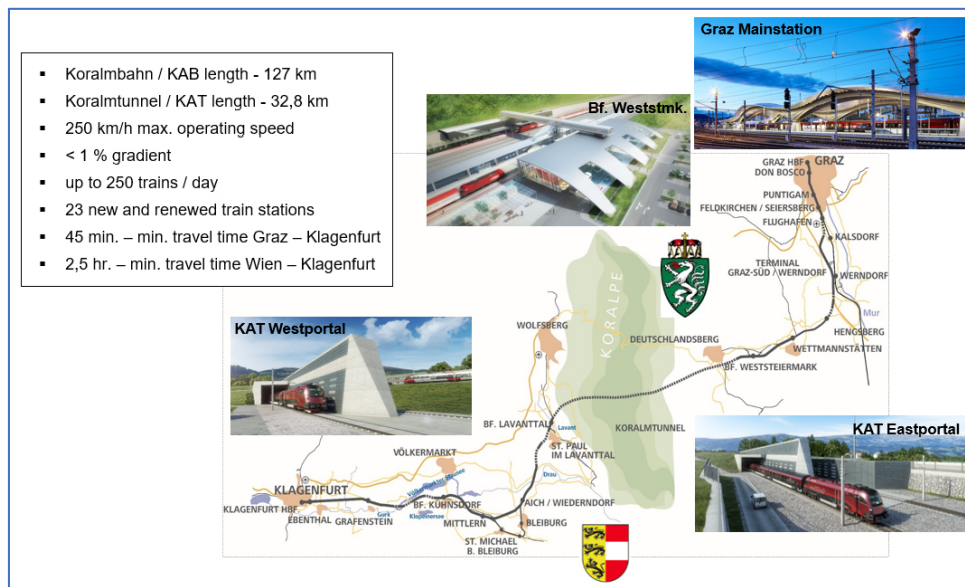


Figure 1: Overview of the Koralmbahn (KAB) Graz - Klagenfurt

The key element of this new route is the Koralm Tunnel (KAT) with a length of 32.9 km and a maximum rock overburden about 1,200 m. The two single-track rail tunnels are connected via cross-passages every 500 m. These serve as escape routes and also house the necessary equipment required for tunnel operation. An emergency stop station with a length of about 1 km is situated between the two tubes roughly in the middle of the tunnel. Both the tunnel (KAT), and the railway line (KAB) should be completely ready for operation by the end of 2025.

3. TEST SITES AND MEASUREMENT SETUP

3.1. Test-sites

Three different test sites have been selected for the PM monitoring. The selection was made based on the tunnel characteristics, which is mainly expressed by the length of the tunnel, the traffic volume and the speed limit. In order to obtain information about the range of PM loads tunnels with different characteristic have been selected. Table 1 shows the tunnel test-sites including their characteristic. All tunnels are single-bore double track tunnels equipped with a solid track (slab track). The tunnels cross-section are similar ($\sim 65\text{m}^2$). Figure 2 shows the location of the test sites on the Austrian railway network.

Table 1: Test-sites including information of tunnel characteristics.

Tunnel	Length [m]	Traffic volume [# /day]	Speed limit [km/h]
Tunnel Unterwald	1.075	50 – 85	100
Burgstaller Tunnel	2.500	160 -210	250
Münsterer Tunnel	15.990	80 – 135	250

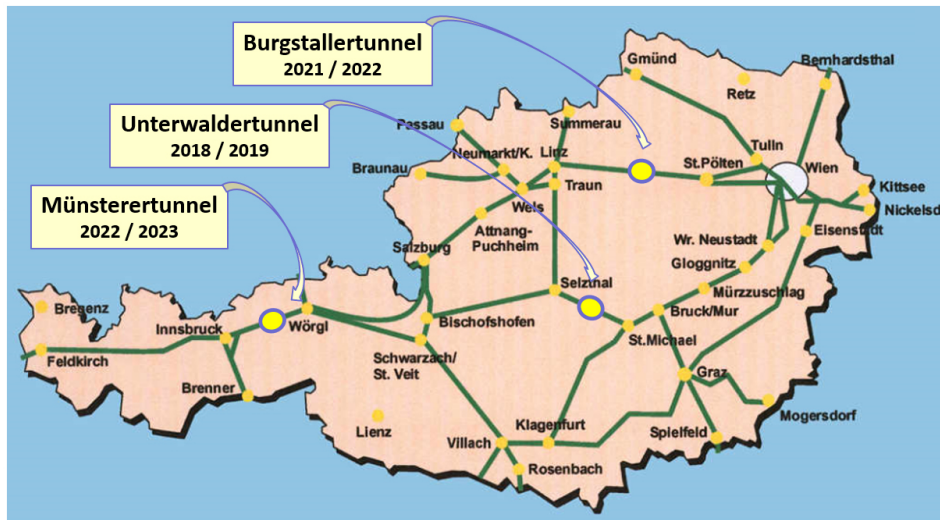


Figure 2: Location of test sites on the Austrian railway network.

3.2. Measurement setup

The measurement setup differed slightly between the measurement campaigns. In particular, the test setup in the tunnel Unterwald (Figure 3) had a special design, as the PM monitoring was implemented in supply air system that was used for cooling purposes. This system was designed to extract tunnel air ($0.25\text{ m}^3/\text{s}$) and to guide the supply air via ventilation ducts into a dedicated utility room. The PM monitor was located in the egress way and extracted the sample flow from the supply air duct. Isokinetic extraction was applied in order to minimize particle losses. However, due to several fittings, redirections and the length of the supply air system ($\sim 15\text{ m}$), particle losses due to deposition could not be prevented. A tapered element oscillating micro balance monitor (TEOM 1400i) was employed to continuously monitor the TSP concentration in the supply air duct. TEOM 1400i uses a gravimetric principle to determine changes of collected particle mass on a filter.

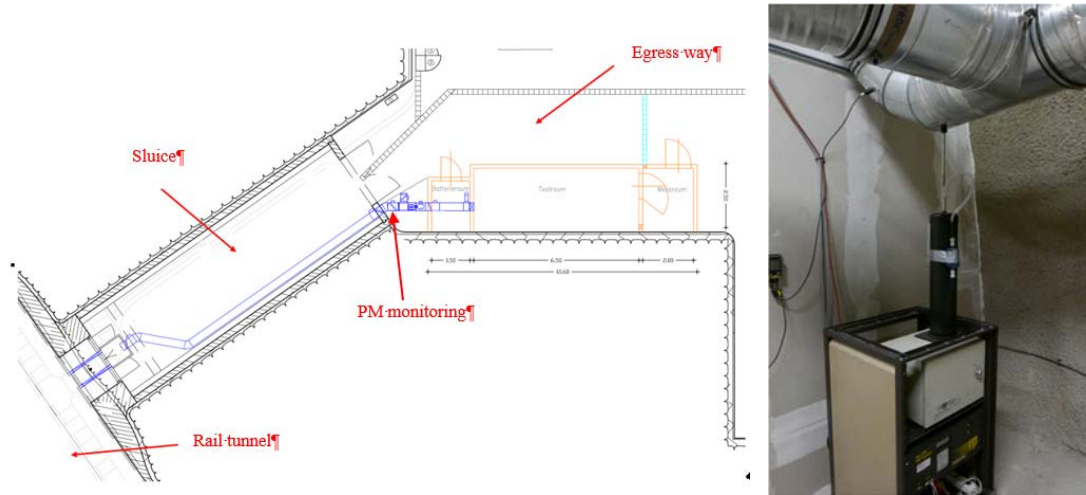


Figure 3: left - scheme of the test setup at Unterwalder Tunnel, right – position of the TEOM 1400

In contrast, in Burgstaller- and Münsterertunnel the PM monitors were situated directly in the rail tunnel, thus, providing more precise information about the PM loads in the tunnel. In both tunnels two PM monitors were employed, which use different measurement principles. One is an optical particle monitor (EDM180), which uses light scattering technique to count particles in the size range of 250 nm to 32 μm . An internal algorithm transforms the particle count into information of particle mass concentration. Hence, a certain particle density has to be applied, which by default is set at a level of 2.6 to 2.8 g/cm^3 in order to account for ambient aerosols. In a railway tunnel environment, the share of heavy metals in the aerosol is expected much higher, thus requiring the application of a density correction. For this reason, in both tunnels a sequential air sampler PARTISOL Plus, which uses a gravimetric principle was operated in parallel for a period of one month. The drawback of a gravimetric device is the limitation related to the resolution in time, which depends on the collected particle mass on the filter. In order to overcome this issue, daily average values were determined and compared to the results of the EDM180 monitor, which gives information about the PM concentration every sixth second. Subsequently, the data of EDM180 were corrected by the quotient of daily average values (PARTISOL/EDM180). Figure 4 shows the PM monitoring positions in both Burgstall- and Münster Tunnel as well as an image of the installed PM monitors.

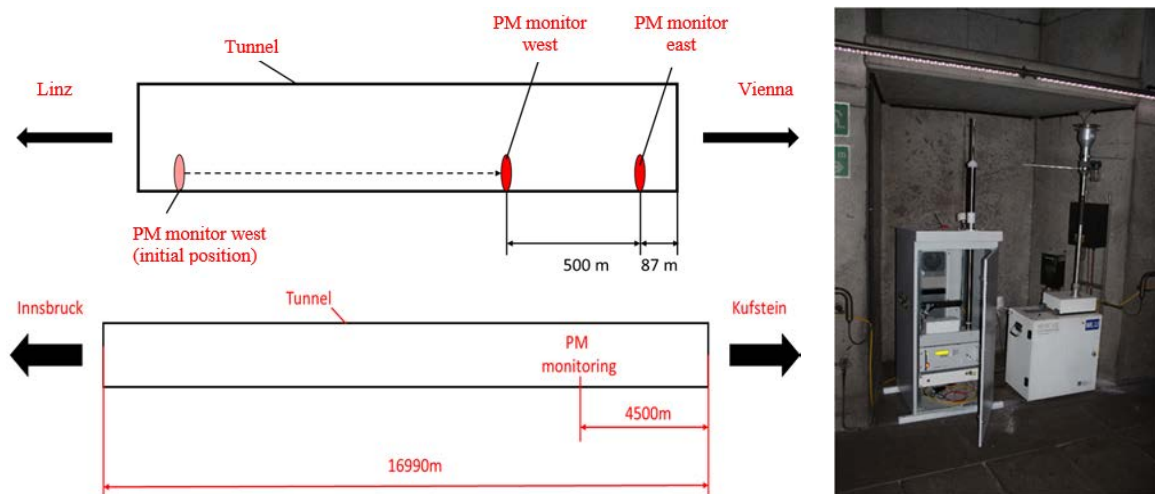


Figure 4: top left - scheme of the test setup in the Burgstaller Tunnel, bottom left - Scheme of the test setup in the Münsterer Tunnel, right – installation of PM monitors in the Tunnel Burgstall

In addition to the monitoring of PM concentrations, the service life of PM filters in a railway tunnel environment has been evaluated. For this reason, a supply air system comprising a supply air fan, ventilation ducts, fittings and a two-stage filter were installed in the Münster tunnel. This installation was operated for half a year, thus, enabling the sequential testing of three filter sets. These filter sets (coarse dust and PM filter) were covered in a filter box. Figure 5 shows the installation in a niche next to the PM monitoring station. There was no fan control in dependency on the air flow. However, the initial supply air flow was set slightly higher than the nominal air flow ($1 \text{ m}^3/2$) through the filters. With increasing particle mass on the filters, the total pressure difference across the filters increased as well, thus, leading to a decrease of air volume flow. This effect was negligible for most of the time, but with very high pressure differences, the air flow decreased to $0.85 \text{ m}^3/\text{s}$. The observed quantities comprised the supply air speed and the pressure difference across every filter stage.



Figure 5: Tunnel Münster - installation of ventilation system including double-stage filter.

4. RESULTS

4.1. Particle mass-concentration in the railway tunnels

The observation of PM concentrations in three different ÖBB railway tunnels showed large differences that result from different tunnel characteristics as well as from different monitoring positions in the tunnels. Figure 6 illustrates these differences in a comparison of daily average particle mass-concentrations for selected periods. In addition, data from tunnel Burgstall and tunnel Münster show a comparison of mean PM₁₀ concentrations recorded by EDM180 (optical device) and PARTISOL Plus (gravimetric device). One can see that daily average particle mass-concentrations in a short tunnel (Unterwald) and in a monitoring position close to the portal (Burgstall) are significantly lower compared to a monitoring position away from the portal of a long tunnel (Münster). Furthermore, daily average concentrations varied by a factor of 10 – 15 in every tunnel. The main reasons for that are variations in the daily traffic volume as well as the influence of precipitation. The latter causes a reduction of background concentrations as well as of particle emissions from trains. In humid conditions, it is more likely that the particles will settle on the floor as well as on the surfaces of the train. Hence, precipitation has a strong impact that in particular can be observed in short tunnels as well as in portal regions.

A second aspect to be mentioned are the deviations between optical and gravimetric measurements, which were different at tunnel Burgstall and tunnel Münster. While the daily average values recorded by EDM180 covered 64% of the collected particle mass of

PARTISOL Plus, in the tunnel Münster the share was only 32%. These deviations are a result of differences in the effective density of the tunnel aerosols. In this context it is important to understand the influence of ambient air in tunnel sections close to the portals and in some distance to the portals. Moving trains will cause ambient, thus lower polluted air to enter the tunnel in driving direction and reaches PM monitoring stations close to the portal. In contrast, some time is required in which ambient air will reach tunnel sections in some distance to the portals. In longer single tube tunnel characterized by bi-directional traffic, it is most likely that another train will enter the tunnel from the opposite side. The piston effect of trains in both directions, cause highly polluted tunnel air to remain inside the tunnel for a long time. Thus, in average, PM loads are higher in the tunnel centre than close to the portals. This statement is confirmed by the results depicted in Figure 6, as PM loads in tunnel Müntser are significantly higher than in tunnel Burgstall, although, the traffic volume usually is higher in tunnel Burgstall.

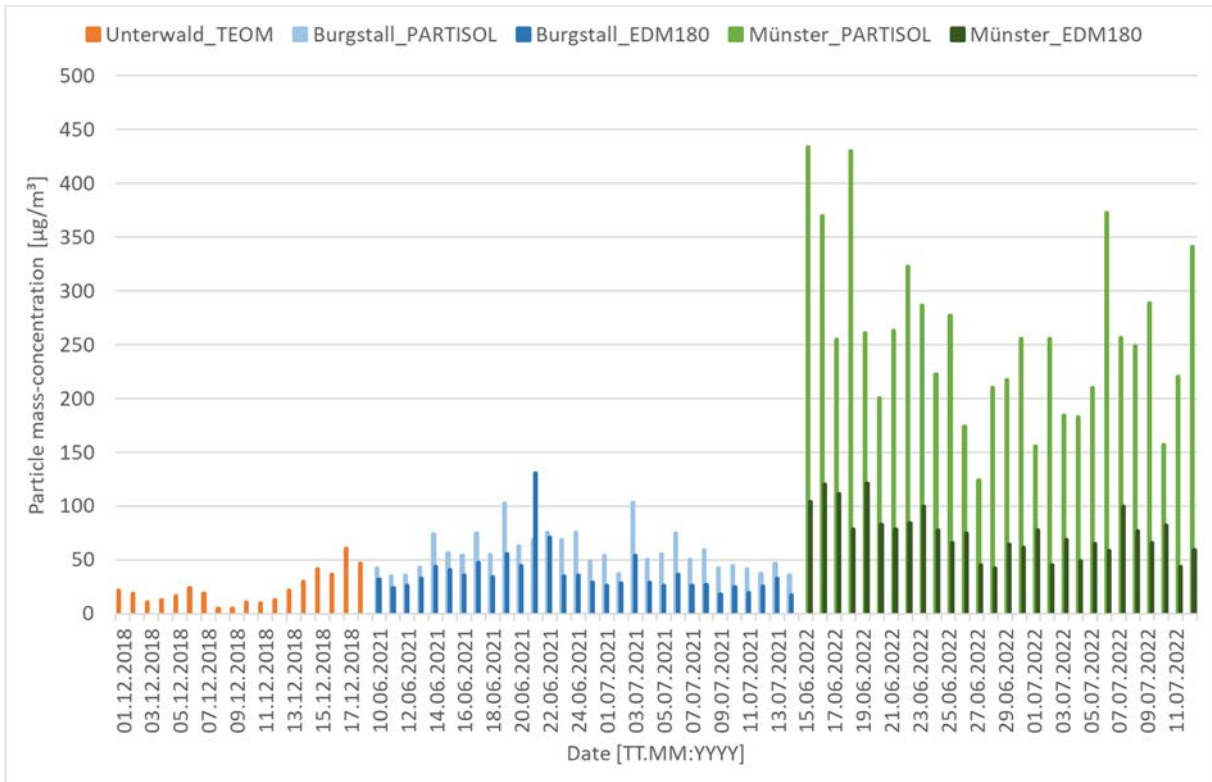


Figure 6: Daily average TSP (Unterwald) and PM10 (Burgstall and Münster) concentrations.

In order to quantify aforementioned differences, Table 2 shows the average particle mass-concentration of the entire monitoring period for each of the tunnels. In addition, minimum and maximum daily average values of the monitoring periods are added. The average PM10 concentration in the tunnel Münster was roughly six times higher than in tunnel Burgstall and roughly 19 times higher than in Tunnel Unterwald. While the minimum value is five times lower compared to the average value, the maximum daily average value is three times higher. Similar relations could be observed as well for tunnel Unterwald and tunnel Burgstall.

Table 2: Comparison of daily mean PM concentrations at every test-site

	Münster			Burgstall	Unterwald
	PM10	PM2.5	PM1	PM10	TSP
Average	407.3	215.1	126.2	70.8	22.5
Minimum	80.5	60.2	44.0	21.2	4.7
Maximum	1297.9	479.5	240.2	205.3	60.7

4.2. Monitoring of filter service life

Obviously, the PM loads have an impact on the filter service life of PM filters. In order to extend the service life of a PM filter, usually a coarse dust filter is arranged in front of the PM filter. Such an arrangement has been tested in the tunnel Münster. The filter status has been monitored by recording the total pressure differences across each filter stage. Figure 7 illustrates the development of pressure differences across each filter stage as well as the total pressure difference for three filter sets, which were tested sequentially. Additional information is provided by the daily average PM10 concentrations during the test period. The end of service life is indicated by a total pressure difference of 450 bar (defined by manufacturer), which was reached after 1.5 to 2 months. One aspect to be emphasized is the development of the pressure difference across the PM filter. After some time, the expected increase of pressure difference turned into a decrease. This decrease was a result of massive particle mass collected on the coarse dust filter, which caused smaller particles as well to be caught by the coarse dust filter. Hence, the decrease of volume flow led to a reduction of the pressure difference across the PM filter.

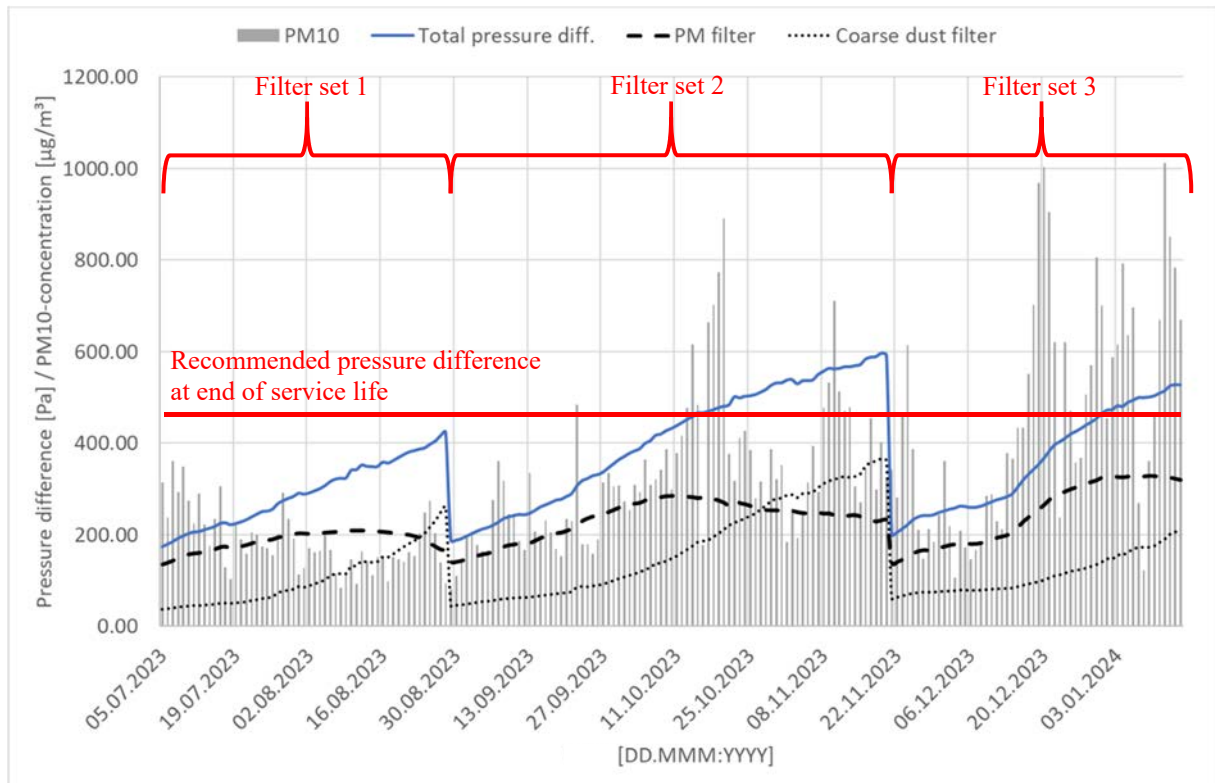


Figure 7: Development of Pressure difference across 2 stage filter and daily average PM10 concentrations – Münster Tunnel

4.3. Particle composition

Ultimately, filter samples collected by PARTISOL PLUS air sampler were analyzed for the heavy metal and total carbon mass deposited on them. The information gained by this analysis shows the mass-fractions of selected elements in the total PM10 mass collected on the filter samples. These mass-fractions are expressed as average values of 32 filter samples for each of the tunnel sites. As one could assume, iron, carbon, and carbon represented the major shares in the collected particle mass. Furthermore, copper, chromium, manganese, magnesium and nickel were identified to represent minor shares of the particle mass. It has to be mentioned that the analysis was made for selected elements and does not provide full information about the particle composition. However, a comparison of mass-fractions determined individually for each of the test tunnels (see Table 3) shows differences in the particle composition. On the

one hand these differences are caused by the already mentioned differences related to the influence of ambient air and on the other hand the emission of the rolling stock as well as other railway components (e.g. contact wire) may varies dependent on the utilized materials. As an example, contact wires usually consist of pure copper or copper and alloy additives such as magnesium or silver. Hence, there are local variations in the non-exhaust emission of moving trains.

Table 3: Results of chemical analysis of particle composition – (mass %)

	TC	Cr	Cu	Fe	Mg	Mn	Ni
Unterwald **	29.20	1.38	0.45	48.16	<<	0.51	0.103
Burgstall	*	0.01	1.12	25.09	3.18	0.15	0.94
Münster	10.44	1.10	9.20	38.00	<<	0.30	0.11

* not analyzed

<< below detection limit

**already published in [7]

5. SUMMARY AND CONCLUSION

The presented study provides information about OM loads in railway tunnels caused by non-exhaust emissions from moving trains. The provided data are derived from extensive measurement campaigns in tunnels of Austrian Federal Railways, which were carried out for more than five years. The aim of the study was to determine the PM loads, to derive PM emission factors (see [8][12]), to gain information about the particle composition as well as to determine the service life of PM filters in a railway tunnel application. The main findings can be summarized as follows:

- PM loads in railway tunnels depend on the traffic volume, the tunnel characteristics as well as on the position inside the tunnel. Test results show that the latter is dominant over the other parameters.
- In tunnel sections close to the portals significantly lower PM loads could be observed compared to tunnel sections in some distance to the portals. In particular, this conclusion is valid for single-bore double-track tunnels.
- Due to significant changes in the effective particle density, data from optical particle monitors have to be corrected in a railway tunnel environment.
- The service life of two-stage particle filters at an air flow of 1 m³/s could be determined by 1.5 to 2 months (away from tunnel portals).
- The main mass-fractions in the PM10 fraction are iron and carbon. Smaller amounts of copper, chromium, manganese, magnesium and nickel were identified as well.
- The particle composition will vary dependent on the impact of ambient air (position inside the tunnel) and differences in the utilized materials in the rolling stock as well as in additional railway components such as rails and contact wires.

6. ACKNOWLEDGMENTS

The research activities presented in this paper were funded by the Austrian Federal Railways.

7. REFERENCES

- [1] Abbasi, S., Jansson, A., Sellgren, U., Olofsson, U., 2013. Particle Emissions From Rail Traffic: A Literature Review. *Critical Reviews in Environmental Science and Technology* 43, 2511–2544. <https://doi.org/10.1080/10643389.2012.685348>
- [2] Abbasi, S., Olander, L., Larsson, C., Olofsson, U., Jansson, A., Sellgren, U., 2012. A field test study of airborne wear particles from a running regional train. *Proceedings of the Institution of Mechanical Engineers, Part F: Journal of Rail and Rapid Transit* 226, 95–109. <https://doi.org/10.1177/0954409711408774>
- [3] Cha, Y., Olofsson, U., 2018. Effective density of airborne particles in a railway tunnel from field measurements of mobility and aerodynamic size distributions. *Aerosol Science and Technology* 52, 886–899. <https://doi.org/10.1080/02786826.2018.1476750>
- [4] Colombi, C., Angius, S., Gianelle, V., Lazzarini, M., 2013. Particulate matter concentrations, physical characteristics and elemental composition in the Milan underground transport system. *Atmospheric Environment* 70, 166–178. <https://doi.org/10.1016/j.atmosenv.2013.01.035>
- [5] Fruhwirt, D., Sturm, P., Steiner, H.; Borchiellini, R.; 2023; Development of a methodology for studying tunnel climate in long railway tunnels and for optimizing the design process of cross-passage cooling systems; *Tunneling and Underground Space Technology*, Volume 138; <https://doi.org/10.1016/j.tust.2023.105194>
- [6] Fridell, E., Ferm, M., Ekberg, A., 2010. Emissions of particulate matters from railways – Emission factors and condition monitoring. *Transportation Research Part D: Transport and Environment* 15, 240–245. <https://doi.org/10.1016/j.trd.2010.02.006>
- [7] Fruhwirt D., 2022. NON-EXHAUST PM EMISSIONS FROM RAILWAYS – IN-SITU MEASUREMENTS AND PARAMETER STUDY.; Air Quality Conference 2023, Thessaloniki, Greece; June 2022
- [8] Fruhwirt, D., Sturm, H., Steiner, H., 2021. Partikelemissionen des Schienenverkehrs – Ergebnisse aus in-situ Messungen in Tunnelanlagen/PM emissions from railway traffic – results of in-situ measurements in tunnels. *GrdL* 81, 225–233. <https://doi.org/10.37544/0949-8036-2021-05-06-71>
- [9] Heldestab J., Kljun N., 2007. PM10-EMISSIONEN VERKEHR Teil Schienenverkehr (No. 1492A-SYNTHESESBERICHT-070108.DOC). INFRAS AG, Bern.
- [10] Moreno, T., Pérez, N., Reche, C., Martins, V., de Miguel, E., Capdevila, M., Centelles, S., Minguillón, M.C., Amato, F., Alastuey, A., Querol, X., Gibbons, W., 2014. Subway platform air quality: Assessing the influences of tunnel ventilation, train piston effect and station design. *Atmospheric Environment* 92, 461–468. <https://doi.org/10.1016/j.atmosenv.2014.04.043>
- [11] Richter F., Schmidt Sch., Wolf P., 2012. Emissionen des Schienenverkehrs in Sachsen Schriftenreihe, Heft 2/2012. Sächsisches Landesamt für Umwelt, Landwirtschaft und Geologie (LfULG), Dresden.
- [12] Sturm, P., Fruhwirt, D., Steiner, H., 2022. Impact of dust loads in long railway tunnels: In-situ measurements and consequences for tunnel facilities and operation. *Tunnelling and Underground Space Technology* 122, 104328. <https://doi.org/10.1016/j.tust.2021.104328>

REHABILITATION OF BOSTON HARBOR TUNNEL – THE “QUARTER DUCT” SOLUTION

^{1,2}Conrad Stacey, ¹Michael Beyer

¹Stacey Agnew Pty Ltd, AU

²Delve Stacey Agnew LLC, US

DOI 10.3217/978-3-85125-996-4-16 (CC BY-NC 4.0)

This CC license does not apply to third party material and content noted otherwise.

ABSTRACT

Structural rehabilitation of the Sumner Tunnel under Boston Harbor will be finalised in late 2024. Associated with the structural work, the in-tunnel parts of the ventilation system had to be re-constructed. Conceived as a structural project, the base requirement was for the reconstructed ventilation to be no worse than existing. However, reconstructing the 1930s scheme carried significant schedule risk and uncertainty in the ability to achieve the Owner’s Quality requirements. In addition, it would have missed an opportunity to dramatically improve the smoke management. Working within strict project constraints, an innovative reimagining of the ventilation ducts’ operation improved smoke control performance using existing ventilation plant capabilities, and with only a quarter of the previous duct being rebuilt. Testing of the ventilation system before and after rehabilitation qualitatively and quantitatively demonstrated the improvements made to the smoke management. Insights from the iterative concept development, and details of the testing procedure are provided. An innovative Ventilation Test Vehicle was used to perform environmentally friendly warm smoke tests with very little demand on tunnel closure time. The ventilation concept dramatically improved fire safety, minimised change to pre-existing operations, and saved construction time, and tunnel closure time.

Keywords: Commissioning, rehabilitation, re-construction, tunnel ventilation system

1. INTRODUCTION

The Sumner Tunnel was first opened to bidirectional traffic in 1934 and currently carries unidirectional highway traffic travelling from East Boston to Boston under Boston Harbor. It’s approximately 5,650 feet (1.72 km) long from portal to portal.

The tunnel configuration includes rectangular sections (box sections) of about 400 feet (122 m) in length near both portals of the tunnel, and a circular section that runs about 4,850 feet (1.48 km) in length beneath the harbour. The portal sections were constructed using cut and cover construction techniques. The circular section between them was bored/shield-driven to form a 31-foot (~9.5 m) diameter tube, using steel liner plate support with a cast in place reinforced concrete secondary lining.

Given its age and constant use, the Sumner Tunnel concrete arch, roadway deck, ceiling (exhaust duct floor), electrical, drainage, lighting, and CCTV systems needed repair and upgrading. The scope of work includes both design and construction of the reconstruction of the Sumner Tunnel. This includes the reconstruction of the roadway deck superstructure and pavement, tunnel concrete arch, and ceilings. In addition, the project is upgrading the life safety systems including lighting, fire standpipe, CCTV cameras, communications, and fire alarm systems. Reconstruction of the concrete arch and ceiling brought the in-tunnel parts of the ventilation system into the project. The benchmark on the ventilation performance was based on the existing system and the objective was to provide a solution that is equal to or better than the status quo. The base case was for the duct to be rebuilt to match the original design intent.

One of the challenges was to use the existing ventilation plant capabilities. Changes to the surface plant, buildings, and fan plant were prohibited by the Contract. A further tremendous challenge was that the entire project, including adjustments to the in-tunnel ventilation equipment had to be constructed during limited weekend closures, and a single 80-day summer shutdown.

2. PRE-EXISTING VENTILATION SYSTEM

Figure 1 shows the long section of the existing tunnel configuration with the boundaries of the operating modes of the ventilation system. From the East Boston Portal, the tunnel goes down under Boston Harbor with an approximate downgrade of 4%, is nearly flat for a central section, and comes up on the other side with approximately the same 4% grade. There are two ventilation shafts connected to ventilation buildings approximately 300 m into the tunnel from either portal. The shafts are connected to an exhaust duct created by a false ceiling above the roadway, and separately to a supply air duct between the invert and the roadway deck. Both ducts run along the tunnel with distributed permanently open slots along the ducts, providing continuous extraction or air supply in longitudinal direction of the tunnel. The slots were adjusted, seeking to make the supply or extraction reasonably uniform over the length. A bulkhead in both ducts at the low point of the tunnel separated the ventilation of the eastern tunnel section from the western tunnel section. There are 4 supply fans and 5 exhaust fans in each ventilation building. Under normal conditions, the tunnel is operated under the lowest speed on each fan. There were three fire modes that could be activated, depending on the fire location. Those modes are mostly reused in the new scheme, minimizing change for the operations. A fire in the first 1/3 of the tunnel after the entry portal was dealt with in Mode 1, where both ventilation buildings run all exhaust fans at the maximum speed, and the supply fans are turned off and isolated. Mode 2 addresses fires in the middle third of the tunnel which is nearly flat. In Mode 2, the ventilation building on the entry end turns off the exhaust fans and runs all supply fans at maximum speed, and the ventilation building on the exit end stays in the same full exhaust function, creating a push-pull effect and moving smoke to the exit side ventilation building. The final Mode 3 has both ventilation buildings running supply fans at the maximum setting with the exhaust fans turned off and isolated. For fires in the last third of the tunnel, this effectively pushes smoke out of the exit portal.

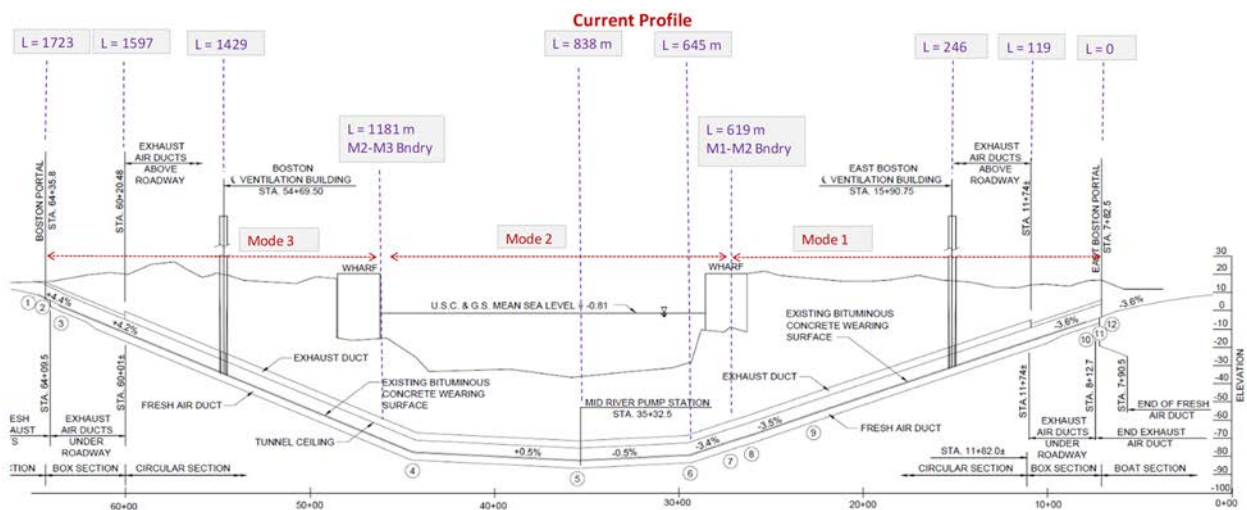


Figure 1: Long section of the pre-upgrade tunnel configuration with tunnel ventilation mode boundaries.

The existing tunnel’s transverse ventilation system was originally established when the tunnel carried bi-directional traffic. However, in a unidirectional road tunnel, a primary aim of smoke control is to prevent smoke moving against the traffic direction and engulfing motorists held

behind the fire. Against that aim, preliminary modeling of the system showed ventilation performed acceptably for fires occurring along most of the tunnel, but was poor on the downgrade section west of the East Boston Ventilation Building. It predicted extremely poor performance towards the bottom of the downgrade section, where the transition from Mode 1 to Mode 2 response was programmed. Mode 1, by design, has zero longitudinal flow somewhere near the tunnel midpoint, and so becomes progressively less effective as the fire location moves in that direction. On the other hand, Mode 2 (push-pull operation) is most effective for fires near the midpoint, and loses effectiveness either side of that. In the critical area near the bottom of the downgrade (around the mode transition point), Mode 1 had lost all effectiveness, while Mode 2 had not yet achieved a useful longitudinal air speed (see dashed lines in Figure 5). While that was the performance benchmark of the project’s requirements, the ventilation response was not acceptable to the designers from a fire life safety responsibility perspective. So, there was a need to improve the ventilation response in the first half of the tunnel (downgrade section), all within the constraints that had not envisaged significant change.

During the final design, the Delve Stacey Agnew team performed on-site aerodynamic measurements to validate the preliminary modelling and establish the baseline performance of the existing tunnel prior to construction, but also to record the flow capacities of the ventilation buildings in different modes. These measured capacities allowed the team to refine the initial modelling to align with existing performance. That model in turn was the base for finalising elements of the ventilation concept to enhance the ventilation performance.

Figure 2 shows the achievable cold air velocities in the tunnel before the project, based on on-site measurements for the different fire modes. Figure 2 shows that the achievable velocity at the end of the planned Mode 1 zone was actually negative, pushing smoke back over the waiting traffic. Even if the Mode 1 to Mode 2 transition had been selected optimally, the achievable cold flow was only 0.5 m/s, and likely to again be negative for a hot fire.

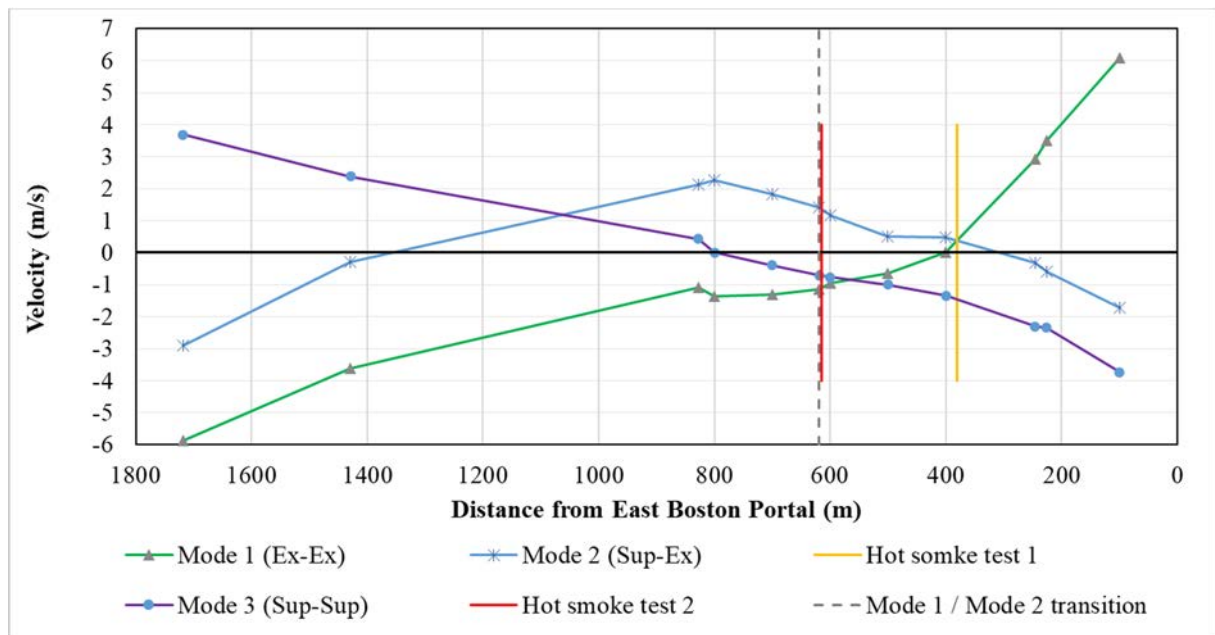


Figure 2: Achievable cold air velocities of the pre-existing ventilation system for Mode 1, 2 and 3 resulting from on-site aerodynamic measurements.

3. THE QUARTER DUCT SOLUTION

Early in the design phase, different options were on the table and discussed. Installing jet fans in the tunnel in addition to the existing ventilation plant would have been an obvious and efficient solution in terms of constructability and flexibility in the ventilation operation. Removing the false ceiling and installing 3 pairs of jet fans near each portal, in addition to providing point extraction at the bottom of the ventilation shafts, would have pushed the achievable air speed onto the fire high enough to prevent smoke backlayering at any location in the tunnel. However, jet fans were not acceptable to the tunnel owner. A further option would have been the construction of a Saccardo nozzle system at the East Boston shaft, using the existing supply fans. Calculations showed that the existing ventilation capacity (pressure) was just a bit too low to pursue that option. An entry portal Saccardo nozzle plant was also considered but was ruled out by heritage considerations.

The key to the enhanced design solution was revealed during the design team’s analysis, when it was realised that a partially reinstated ceiling assisted in meeting the goal of improved smoke control, while simultaneously not changing the emissions at either portal. To do so, a new extraction point was created via the partially reinstated ceiling duct (about 25% of the previous duct length). The new extraction point is located near the bottom of the downgrade, at the ‘Quarter Point’ Station 27+90.75 (612 m or 2,008 ft from the entry portal). This allows extraction from both East Boston Ventilation Building (EBVB) and Boston Ventilation Building (BVB) to be applied more effectively for fires anywhere from the entry portal to the ‘Quarter Point’.

In the new design, with only a quarter of the duct rebuilt, the Boston Vent Building extracts directly from the tunnel, with only a short ceiling section for maintenance and to protect the traffic from anything falling from higher in the building. The EBVB can extract from the end of the ‘Quarter Duct’ alone or use the Quarter Duct intake in combination with extraction directly at the base of the EBVB using a damper. Using the ‘Quarter Duct’ alone cannot take advantage of the maximum exhaust rate from the installed EBVB fans. The damper improves the ventilation response for fires between the entry portal and the EBVB, by using all the flow available. Use of that damper creates a new mode, called “Mode 0” to preserve the naming of the re-used modes and the numbering order. The schematic design, with the profile view and cross section of the ‘Quarter Duct’ is shown below in Figure 3. Figure 4 lists the fire modes for the different sections.

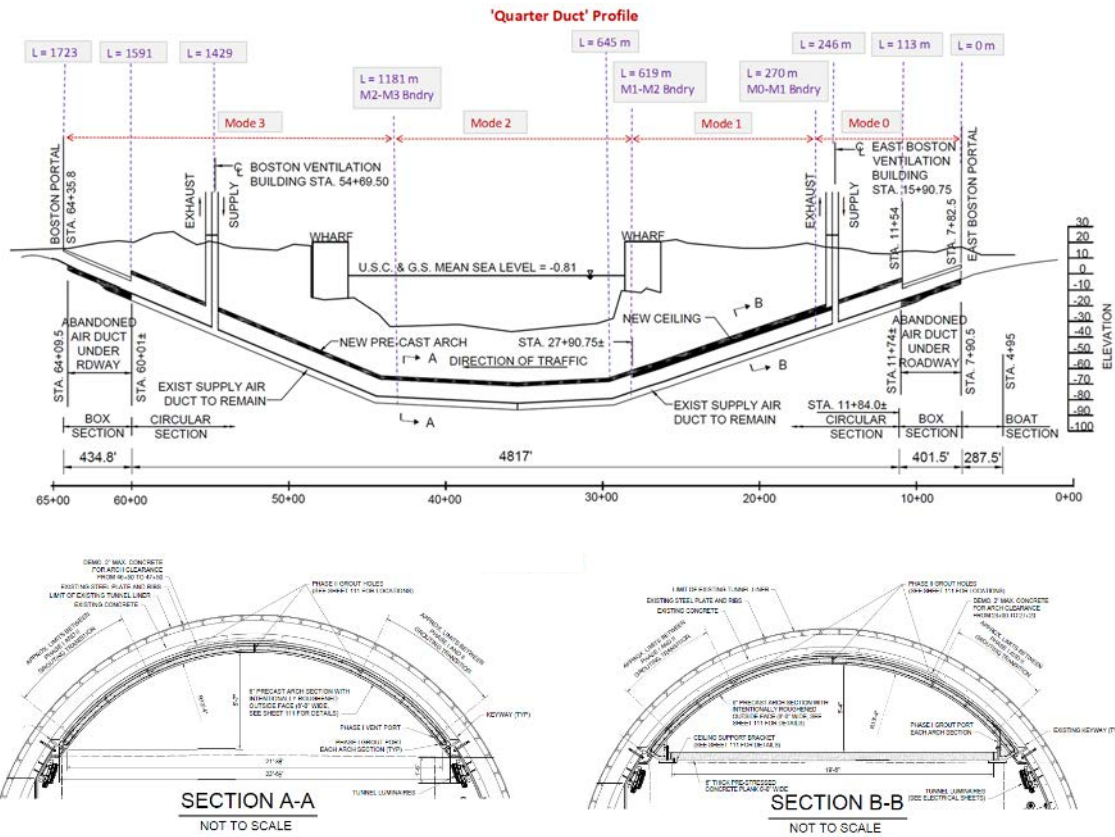


Figure 3: Quarter Duct design for Summer Tunnel, with only approximately 1,200 feet of the ceiling reinstated. Long section shows the mode boundaries and the extent of the new ceiling, with the detail of the profile shown in the cross sections.

Mode	BVB	EBVB	EBVB Damper
Mode 0	Emergency	Emergency	OPEN
Mode 1	Emergency	Emergency	CLOSED
Mode 2	Emergency	Pressurize	CLOSED
Mode 3	Pressurize	Pressurize	CLOSED

Figure 4: Fire modes with ‘emergency’ (exhaust fans at maximum speed) and ‘pressurise’ (supply fans at maximum speed) operations at each shaft.

While Figure 2 showed the measured cold flows achievable, the flow that is really sought is the flow onto the 30 MW design fire, including the buoyancy effects. That is assessed by 1D simulation using the model calibrated for the cold flow measurements. Figure 5 shows the predicted achievable air velocity onto a 30 MW fire for different fire locations in the tunnel. The dashed lines are predictions for the ventilation system as it was performing prior to the upgrade, and the solid lines are after the upgrade.

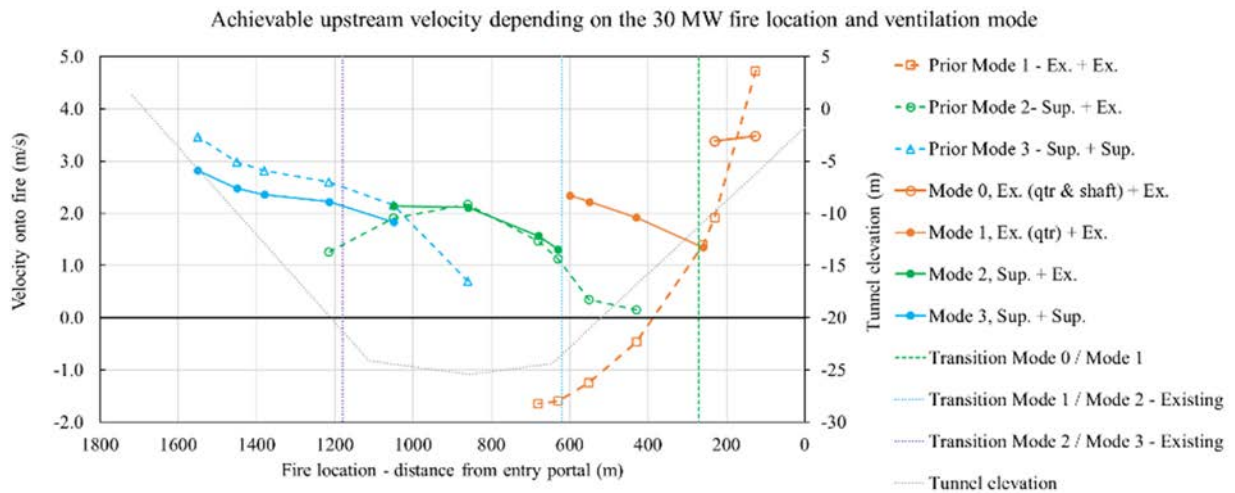


Figure 5: Modelled achievable upstream velocity throughout tunnel with a 30 MW fire in Modes 1, 2, and 3 for the existing system and in fire Modes 0, 1, 2 and 3 for the ‘Quarter Duct’ design.

The improvement in the performance for the region between 280 m into the tunnel and the end of the ‘Quarter Duct’ (600 m in) is dramatic. Previously the velocity onto the fire was less than 0.3 m/s for a significant section of the tunnel. That is a result from a 1D model. Acknowledging the 3-dimensional reality of a 30 MW fire, velocities that low, at 4% downgrade, would result in rapid uncontrolled backlayering, and engulfment in smoke of people uphill of the fire.

With the Quarter Duct solution, modelled achievable velocities in that section of tunnel are generally around 2 m/s, with the lowest being 1.4 m/s. While that is still not meeting critical velocity, it is a dramatic improvement. It would likely manage smoke for the early stages of a fire, permitting evacuation back upgrade.

4. MEASURED RESULTS

Two test sessions at the completion of construction changes to the ventilation system showed the end result. Of course, the air speeds are recorded without the 30 MW design fire, but they can be compared against the same cold flow records from before the upgrade. That is done in Figure 6. The dramatic improvement in the downgrade section between the East Boston Ventilation Building (246 m) and the end of the Quarter Duct (612 m) is clear from the plot.

The ‘Quarter Duct’ scheme not only addressed the very poor ventilation performance between roughly 250 m and 600 m into the tunnel, it also allowed increased extraction flowrates at the Boston Ventilation Building by eliminating all the exhaust duct in the western end of the tunnel. This would also have assisted the result in the mid-section of the tunnel (610 m to 1180 m) where Mode 2 applies. As Mode 3 only involves the supply system, which was not upgraded, no significant change was expected in the air speeds achieved in the western third of the tunnel. Further, by removing the ceiling in the three quarters of the tunnel (from approximately 600 m into the tunnel up to the box section at the Boston Portal (except for the very short section at the bottom of the BVB shaft) an additional smoke reservoir was created, still keeping the air speed in that section almost the same. During the Mode 0 test, only four of the five EBVB fans ran. The intention was that all five would run, but that doesn’t seem necessary.

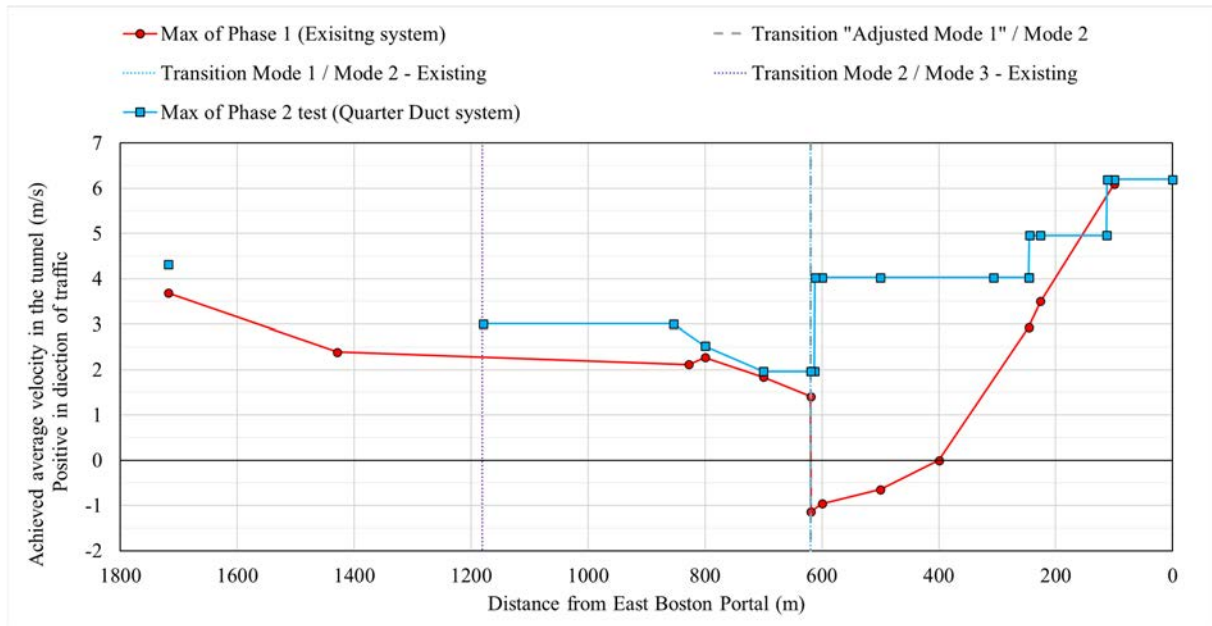


Figure 6: Achieved 'cold flow' velocities in the tunnel for the programmed emergency modes. Red line depicts the results of the ventilation system obtained during pre-upgrade testing, and the blue line depicts final results with the Quarter Duct system fully commissioned.

5. WARM SMOKE TESTS

You can wave anemometers till the cows come home, and publish the most carefully analysed models of ventilation response, but for achieving a common (whole project team) clarity of understanding about what is going on in the different modes, there is nothing quite like watching buoyant smoke in the tunnel itself. Delve Stacey Agnew's Ventilation Test Vehicle (aka Smoke Bus) was mobilised for both the before and after tests, with some images given below. The Smoke Bus was driven into position and a large quantity of harmless buoyant 'smoke' could be created within minutes. When the programmed ventilation response is implemented, and the smoke goes backwards, the need becomes clear. Besides creating a video record of the smoke behaviour, the use of the Smoke Bus facilitated the discussions around the ventilation performance.



Figure 7: Images of the Delve Stacey Agnew Smoke Bus at various stages of different tests, producing copious quantities of hot ‘smoke’ in service of demonstrating visually the ventilation system performance.

6. COMMENTARY AND CONCLUSION

The testing results, and the hot smoke tests, showed that the ventilation response, and therefore the smoke management during a tunnel fire, was significantly improved by the project. It is noted also that the cross section of the tunnel is larger without a smoke duct, giving more room for any layering smoke in the arched tunnel obvert. Even if the velocities had stayed the same, the larger, taller smoke reservoir would improve the chances of successful egress in a fire, from those areas in which the duct was not rebuilt.

Referring to Figure 6, there is a similar air speed in the western (upgrade) section, and a slightly improved air speed in the ‘flat’ (mid-tunnel) section. The problem before the project was with the flow in the downgrade section. The achievable “cold flow” velocity in the problematic downgrade section is dramatically higher with the Quarter Duct system using the existing fans.

At the outset, the project had not envisaged upgrading the ventilation, so there was not time or cost allowance for doing so. There were also significant constraints, both physically and organisationally. The unacceptability of jet fans, and the impossibility of Saccardo nozzles eliminated those two obvious options, and so greater creativity was called for. The Quarter Duct design was a very successful innovation generated within the project, achieving improved ventilation results with greatly simplified re-construction (replacement of only a quarter of the previous duct), which enabled the project to be completed within the time allowed by the Contract and the budget established at Tender, while giving the tunnel owner a dramatic improvement they had not asked for in the documents.

COMMISSIONING OF TUNNELS

Tor Tybring Aralt
Multiconsult Norge AS, NO

DOI 10.3217/978-3-85125-996-4-17 (CC BY-NC 4.0)

This CC license does not apply to third party material and content noted otherwise.

ABSTRACT

Commissioning starts with approval of design documents, and ends with user acceptance test. In between is FAT and SAT. Planning must prepare for confirmation of fulfilment. The main success factor is that it is possible to identify and verify all demands. SAT must be planned and performed by the owner himself or someone representing him, and should not be left to the contractor

Keywords: Factory Acceptance Test, Site Acceptance Test, commissioning

1. INTRODUCTION

This paper is intended to help tunnel operators to minimize problems during commissioning and is primarily a field report, based on 27 years of practical and personal experience.

The contract and close coordination with the planner or operator before and during implementation are essential for smooth commissioning. In this way, a lengthy troubleshooting and incorrect product selection can be minimized. Some examples of ambiguities, wrong decisions and possible solutions are listed and described in more detail below. The public road authority defines the following test for a tunnel. FAT (Factory acceptance test), EET (Contractor’s verification of delivered system), SAT (tunnel owner test before acceptance of delivery, or Site Acceptance Test) and UAT (Road traffic central confirmation that they can take supervise the tunnel). UAT is the last test before request for safety approval.

2. AUTOMATION AND SAFETY EQUIPMENT DESIGN FROM CONSULTANT

2.1. Hardware

There are different approaches toward the design of an automatic system. Two main “schools” exist: Centralized software and decentralized software.

2.2. Centralized software

All software is located in one computer, of course with a hot backup. The benefit is that you only have one place to connect to adjust the software, and it is easy and cheap to make as simulator for testing and training of operators monitoring the tunnel. The drawback is that everything is running in the same computer, and an error in communication could have drastically impacts on safety. And the actual PLC (Programmable Logical Controller) able to do the job is very expensive.

Since one PLC is to monitor everything, scan time might be in seconds, and not milliseconds.

2.3. Decentralized software

The main focus is that the software should be performed as close to the equipment as practical. For example, the software controlling a barrier must be performed in the local control cabinet

to satisfy safety regulations for the machine. Drawback, if too much is decentralised it is difficult and more expensive to make a good simulator. Decision of many small PLC, or RIO (Remote In Out unit for signals, connected to PLS by network) should be made during design, not by supplier. It affects demands for software and descriptions for how to avoid unnecessary alarms.

2.4. Demands for Software from consultant.

Very often the designers / planners do not clearly define the requirements but refer to standard documents. However, general documents are almost never meaningful enough to map all specifications in detail. The planner should therefore endeavour to identify all requirements in the descriptions, as only these can then be checked. It is important that all demands can individually referred to as demand number x.y.z, and that you know how to test it. Examples for can be found in ref 1.

3. COMMISSIONING OF THE TUNNELS, GENERAL EXPERIENCE

3.1. Design documents

The work of commissioning starts when you approve the design documents for installation.

If these consist primarily of references to standards, many details stay unclear. Here you need to ask the designer / planner for detailed specifications and information. This problem shall be explained below, based on the requirements for the emergency call centre.

3.2. Emergency control panel

The standard gives limited number of commands for the panel.

Command Close tunnel: This command closes the tunnel. Red stop signals turn on, all associated speed and traffic regulating signs are activated. Escape lights are activated. Other lights in the tunnel are lit and the barrier is lowered after the agreed time regarding, among other things, speed limits and stop distances.

Back to normal: The command opens the tunnel. Boom raised, red stop signal Extinguishing and traffic control signs return to their normal position. Lights and fans are set in "Normal" and escape lights go out. The tunnel is now back to normal operation with VTS as Monitors.
Lamp test: Functional test of the lamps in the panel.

During Site Acceptance Test (SAT) this rarely works satisfactorily.

If the tunnel is to be closed, but the barrier is set to manual opening in the local control, first problems can arise. Should the barrier be set from manual to automatic and then close immediately or is this procedure incorrect? If subsequent changes are necessary, the contractor will ask: 'Where in the contract does it say so?'. Last observed during SAT Ryggedalstunnel

The consultant should deliver a drawing of the emergency control panel and a detailed functional description.

For example, like this:

If it is a reset of the PLC, then the emergency tableau must be put into automatic response.

If the push button "close the tunnel" is pressed, the tunnel must close for traffic, and status word for open/close tunnel must show that the command was given from emergency control panel. The button must activate all the same procedures as if the command was given by the operator.

If the button for “return to automatic” is pressed, then it must be written in detail what should happen. Do you regard “return to automatic” as a command to “open the tunnel”, or just as a command that you give away control. This must be described for the contractor. Otherwise, there is a 50% chance that it is wrong.

3.3. Factory Acceptance test (FAT)

It is important to do a thorough FAT, in several stages. The supplier will normally write the test procedures for FAT for each part to test. The design documents must contain demands for FAT, and for minimum testing of FAT. Any deviation detected at this project stage / during FAT can easily be fixed without significant additional costs.

3.4. Barriers

For a barrier normally current loops are used to detect if a vehicle is blocking the barrier to close. Some of the current loop detector units have a default setting where detection fades out after approximately five minutes. If it has this setting activated, the barrier will come down on a car that stopped below the barrier after 5 minutes. A demand for complete setup of barrier with control cabinet connected all the way to Scada during Factory Acceptance Test (FAT) will enable you to discover this error at an early stage. But you still must test it during SAT.

If the light on the barrier fails, you would like to have an error message to maintenance. Then you must test it. In the control cabinet, disconnect the +48V_{dc}, and half the time, no error message received. If you disconnect ground (0V_{dc}) nearly never an error message is received. It will not work, and the operator does not know that it is not working.

Is it possible to close the barrier before, or without a red light on? Did you test this? The juridical closing of the tunnel is the red light. Not even manually, it is legal to close the barrier without a red light on Experience shows us that this is not always safety applied. Then we have the standard status word for a barrier, showed in Table 1. It of course exists a defined command word as well.

Table 1: status word for a barrier

		Description	
0	1	Barrier open	
1	2	Barrier closed	
2	4	Fault on barrier	Barrier has no fault
3	8	Vehicle preventing to clos	No vehicle
4	16	Alarm from vehicle under barrier blocked	Not blocked
5	32	Fault message blocked	Fault message not blocked
6	64	Directly control from road traffic central (VTS)	Controlled by automatic response or in local control cabinet
7	128	Controlled by local control cabinet	Controlled by automatic response or in from VTS
8	256	Faulty current loop	Current loop working
9	512	Error message fault current loop blocked	Error message not blocked
10	1024	Faulty warning lights on barrier	Warning lights has no fault
11	2048	Faulty warning lights on barrier blocked	Faulty warning lights on barrier not blocked

3.5. Alarm philosophy

The road traffic central in Bergen supervises approximately 270 tunnels. The tolerance for false or unnecessary alarms is extremely low. As an example: ‘Alarm’ for a stopped vehicle should not occur until the stop lasts for 15 seconds. If the stop is shorter, it can be neglected. This reduces the number of false/unnecessary alarms drastically. If a system gives one false alarm pr km pr day, it is worthless. We have been able to reduce it to between one and two pr km pr week in some tunnels. The goal is to reduce more. Several tunnels will give far too many alarms, especially in congestion areas or during wintertime when snow is dropped from vehicles.

As an example, The Arnanipa tunnel, 2km long, has less than one false alarm a week for stopped vehicle. During commissioning we do not accept false alarms on a closed tunnel. This tunnel is two-way traffic, approximately 12000 vehicles a day. But during winter the number of false alarms increase drastic.

False alarms from fire extinguisher removed are not tolerated at all. It is treated by the tunnel as confirmed fire and closing, and fire ventilation starts by automatic response. The operator must then think and open, not think and close. To avoid false alarms, for this it is important that strict demands for quality are part of the tender and confirmed during commissioning.

Where we often discover major errors are when we trigger a fuse in the technical buildings. We accept a maximum of 3 alarms for one fuse. If the main circuit breaker in a technical building is triggered, we accept the following alarms.

- Main circuit breaker triggered.
- UPS running in battery mode.

No other alarms accepted. All other must be filtered by the PLC.

If UPS power fails, only the alarm UPS power failure, and 1 communication error is acceptable.

The PLC and main switches should of course have double power supplies, one from UPS and one from normal power. If not, we will only have “communication failure”.

When PLC fails it is only acceptable with communication failure.

For JET fans we sometimes have two alarms, if circuit breaker for control power fails, which is on UPS we will have the alarm for control power to the jet fan, and communication error to the soft starter/motor starter. These alarms must be filtered away if the UPS power has failed.

For communication failures the system defines “short time loss of connection” which is a maintenance alarm given if communication is down for more than one to three seconds. If the communication is gone for more than 30 seconds, it is changed to “communication error” and is given to the operator. This protects the operators from unnecessary alarms.

When power to an emergency phone is gone, do you really want an alarm for “handset not in position”, or is “phone error” to maintenance enough. Remember that when the tunnel is equipped with AID, you already have an alarm for stopped vehicle, and a camera located on the area on screen if it is a real situation.

Time before an error or alarm is reported to Scada is a critical definition. An operator will normally use 90 seconds from alarm to activating response. If operator load is high, this time will increase. Does the operator need to know if a technical error exists for 20 seconds? Or is that just noise? EN62682 give that one operator should not have more than 6 alarms pr hour as the normal workload. The road traffic central operates on more than 30 as average.

3.6. Site acceptance test (SAT)

If the SAT is planned and performed by the contractor, the test will confirm what he has delivered, not what you ordered. That is why it is often performed User Acceptance Test (UAT) after the SAT. In Norway UAT is a short test, and confirmation of stability. SAT is planned and performed by the tunnel owner, or a representant for tunnel owner, and not by the contractor.

During commissioning we start by entering the technical building. Here take out circuit breaker for circuit breaker. This will show us if the network is according to plan, since it is designed with several small subnets. If circuit breaker Q12 takes out power to cabinet AS01, 03 and 05 I should lose communication only to these cabinets. If I have any other errors design plans are not followed. We cannot accept errors on anything under these cabinets.

This often gives us a communication error to the phone, the camera, and the fire extinguisher supervised by the cabinets that lost communication. If the road central receives all these alarms, then the cause of the alarms will be drowned by the secondary alarms. They will on SCADA see what is affected, and the alarm list will show the cause of the problem.

The reason we start with this is that this is where we nearly always find major errors. And quite often, things do not start up again as they should after power is returned.

During SAT we also monitor the log for communication to PLC’s and RIO’s and other critical equipment. If we discover unexpected loss of communication or other communication errors this is reported as major errors, that must be fixed before approval. We will also not accept that it takes more than 3 seconds before we receive the alarm for “loss of connection”.

It has been discovered that some switches reboot too often, and thereby cause loss of connection. The only way to discover this is to analyze the system over time.

4. COMMISSIONING OF E39 SVEGATJØRN-RÅDAL

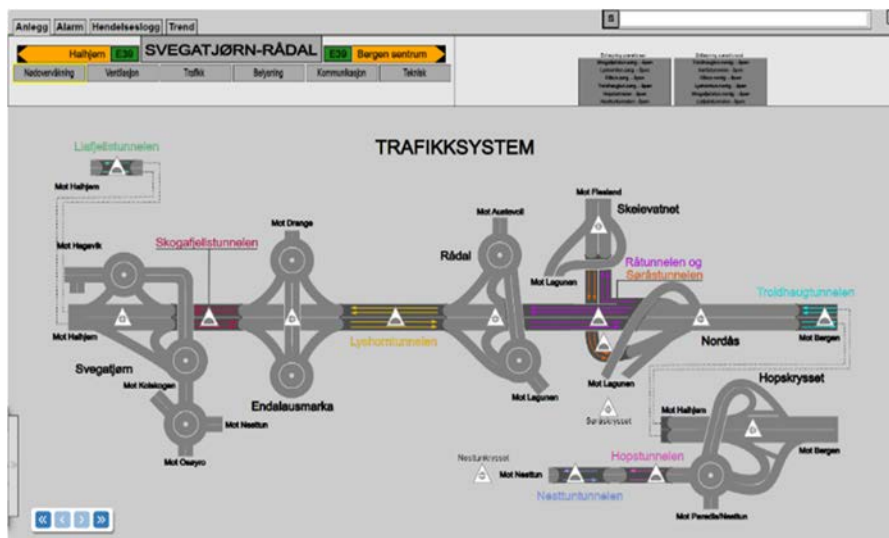


Figure 1: Overview of the project in Scada

The New tunnels is Skogafjellstunnelen 1500m. Lyshorntunnel 9300m, Råtunnel 2200 and Søråstunnel 2600m. Installations affected 7 junctions, which was also affected by 6 old tunnels. The “worst sign” had 20 different predefined pictures depending on which tunnels was closed.

All together it is approximately 5300 objects like camera, signs, communication control etc.

We did a thorough testing of traffic plans in simulator long before they finished installation. This way we could find minor errors in plans and software installation in an early stage.

All together it was more than 130 tables for traffic management, with large variations in size. They varied from approximately 10 cells to 20000 cells.

For each VMS sign for a given situation it was a cell containing the position the VMS should show. This can be adjusted from a web interface, and then downloaded to responsible PLC.

In simulations we could test traffic plans, illegal combinations of traffic plans, and closing of tunnels.

Table 2: Close Skogafjell tunnel northbound

Objekt SS_NL	Command sends to next level				
Kommando received from	SN_1	SN_2	SN_3	SS_SL	S_OS_Nord
AID	x	x	x		x
Lokal - Close	x	x	40		x
Lokal - Open	x	x	x		x
VTS - Close	x	x	40		x
VTS – Emergency close	x	x	x	x	x
VTS-Open	x	x	x		x
Fireplan – emergency close	x	x	x	x	x
High pollution -close	x	x	x		x
Emergency clos for southbound tube	x	x	x		x

X- send the message. If a number, wait n second before transmitting the message

Table 3: level 2 for closing tables.

Rutine SN_1	Command forwarded to			
Command come from	S_AS1001	S_AS1004	S_AS1005	TP_SN_1
SS_NL and SL_NL pone	1	1	1	off
SS_NL closed SS_SL open	2	2	2	activate
SS_NL open SL_NL closed	3	3	3	off
SL_NL, SS_NL closed	4	4	4	activate

ASxxxx are control cabinets for VMS and barriers. TP_SN_1 is a specialized lane signal plan for use when the tunnel is closed, to avoid “green arrows” visible from upstream the barriers

Table 4: Final level for closing tables, controlling the actual signs

Rutine S_AS1001	Object to position		
Command come from	VV10003	OG10003	
SN_1=1	101	101	
SN_1 =2	2	2	
SN_1 =3	3	2	
SN_1 =4	2	2	

In Table 2 we list the different ways a tunnel might be closing. The next level can then be one of the columns. SN1 is a level two, and is an area with different control cabinet (ASxxx) who is controlling different VMS(VV) and barriers (YV) and yellow light (OG). This table might have an input from different tunnels. In SN1 we see that it is two tunnels that activates the area. One of the control cabinets are AS_1001. Routine AS_1001 will then put the sign to different positions depending of input. Position 101, is release control to other traffic plans, which enables us to set at lane signal plan, when the tunnel is closed, to ensure that it goes directly to this position when the tunnel opens for traffic. If now other plan is active 101 gives position 1.

It is all together nearly 140 tables of varying size for the project. The largest are for use of lanes signals and contained approximately 20 000 cells. All combination tested thoroughly on simulator. All together 14 different commands for close a tunnel in one direction affect the overall system. The “worst” VMS has 20 predefined positions. In addition, we had some illegal combinations of the use of lane signals and closing of tunnels, causing automatically closing of the next tunnel.

For all traffic control tables, it is a WEB-configuration for the position we would like the sign to show. During test by simulator, we could see that signs changed position as expected. During SAT we discovered that perception of distances is not the same on drawings as in reality. Quick changes in WEB-interface, and new test, without needing to change software was implemented. The road traffic central do not look on a single VMS, unless an error is reported. They never change position on a single sign manually. But maintenance can do this from Scada, when needed for maintenance purpose.

During SAT we closed tunnels and combinations of tunnels to confirm that all tables worked as intended.

For testing of traffic plans, we first confirm that status of VMS and lane signals to SCADA is correct. When we trust on the positions shown in SCADA, we don't need people in the field during test of the major traffic plans.

4.1. Factory Acceptance Test (FAT)

For the project E39 Svegatjørn-Rådal with 585 control cabinets the first FAT was performed with an empty control cabinet. Here the material experts used an x-ray gun to control steel quality. The contract demanded ANSI 316 for all parts. But for the first FAT hinges, screws and nuts were made of ANSI304. This was not approved, and we could point to numbered demands in the contract that not was satisfied.

We were able to find good solutions for excess fiber coil storage, improve design of installation of cabinets in wall elements. These problems were identified on the prototype of an empty control cabinet. Imagine the cost if this was discovered after production of 585 cabinets, already installed on site.

FAT of VMS signs and lane signals. Here it is of major importance to work together with the PLC supplier and the software engineers. Especially since we ordered them with a Modbus TCP/IP interface. With nearly 700 lane signals in one contract, we asked for three signals to be delivered to PLC supplier early. They could then test their software and the communication to the signals early. In the beginning it didn't work. After replacing firmware in the lane signals more than once, it worked in the laboratory. For the large VMS signs, we brought the PLC supplier to the factory. When Modbus communication didn't work, we left the software engineers from the two companies alone and tested other things. When we got back, they had solved the problems.

4.2. Test of Traffic objects

For each type of object to Scada a definition of data words to be sent to Scada exist. This is a good basis for a test plan for all objects.

After we tested status to Scada for all positions for all signs, we return to 10% of the control cabinets (60 cabinets) to an extended test. Starting with taking the power to the control cabinet. Did we have only expected communication errors? Very often you will discover unexpected alarms and reactions in the system.

Then we start to test with deliberate errors to see that consequence of the error we introduced is as expected. This is time consuming testing, but very important for stability in use of the tunnel.

4.3. Main problems during SAT

All together it was registered 1270 deviations from how thing should work during SAT of automation and safety systems.

Disturbance from late finishing asphalt work is common during SAT, and just something you have to expect.

During SAT we has a major focus on unnecessary/false /alarms error messages to Scada.

One thing we often discover, is that during normal operation of VMS and barriers it is an error messages lasting for 1 to 5 seconds during normal operation. For example, a barrier used 11 second to close, when it was expected to use 10 seconds, an alarm for undefined position is reported. This is not acceptable. Deley before error message increased to 30 seconds. Problem solved.

A major problem in many projects, including this, is alarm for grounding error. Suppliers should be informed about this early in the project.

It was several emergency phones standing error when they reported ready for SAT. Difficult to demand best emergency phones in open tenders. EEC regulations, when followed, makes it difficult to evaluate quality in a tender.

A very common error is, when a control cabinet has more than one VMS, and you are in the control cabinet and put one VMS status in "local", alle the others signs switch to "local" as well. This is never acceptable.

In several signs the graphic shown in Scada was wrong. The reason is an unsatisfactory communication with company implementing Scada.

Profibus DP communication to motor starters for JET-fans was not done right, so when we took the circuit breaker for control power to one motor starter, we lost communication to all. One minor circuit breaker caused a section of JET fans to be unavailable. When we discovered this in the first two technical buildings, we stopped testing until it was reported fixed.

5. SUMMARY AND CONCLUSION

All design must be done considering verification. Truth tables for all traffic signs must be made during design, and not by contractor.

For one project we are involved in, we are writing detailed tests plans for EET as part of the tender. We believe this will reduce the problems. Extra costs can be reduced by detailed descriptions for the software, where it is possible to refer to all functional demands and hardware demands, as demand number x y z. And that the supplier must sign that each functional demand is fulfilled and verified during EET.

It must be a demand that is exist no critical errors, and strict demands for number of minor errors. Short time errors defined to be shown to traffic operators are not tolerated at all. For each project it should be decided in the tender number of stable traffic errors that can be tolerated. Large project with 20000 signals will always have some errors, so "0 errors" are not realistic. For small two-way traffic tunnel (2km), zero errors should be possible.

6. REFERECES

- (1) Norwegian Public Road administration, tender number 2016/132787 with associated drawings and papers
- (2) SAT report: 616039-RIEAut-RAP-010-SAT, Multiconsult ASA for Norwegian Public Road administration
- (3) SAT report: 615971-RIEAu-RAP-004 SAT Arnanipatunnelen

ENHANCING TUNNEL FAN RELIABILITY THROUGH ADVANCED FACTORY ACCEPTANCE TEST (AFAT) TO PREVENT FAILURES

¹Justo Suarez, ²Jye Teoh, ³Albert Bach-Esteve

¹S&P-KRUGER Underground Ventilation Division, ES

²KRUGER ASIA Ventilation Group, TH

³SOLER & PALAU Ventilation Group, ES

DOI 10.3217/978-3-85125-996-4-18 (CC BY-NC 4.0)

This CC license does not apply to third party material and content noted otherwise.

ABSTRACT

This paper introduces the concept of the Advanced Factory Acceptance Test (AFAT) and highlights its potential to mitigate tunnel fan failures.

Conventional Factory Acceptance Test (FAT) primarily focuses on basic performance criteria, such as flow, pressure, efficiency, and noise level for axial fans and thrust and noise level for jet fans. It often falls short in identifying and addressing potential issues that may lead to post-installation fan failures. AFAT takes into account additional critical factors to guarantee fan reliability and durability. These factors encompass structural integrity, material quality, vibration analysis and thermal performance.

AFAT can detect latent defects, design inconsistencies, and manufacturing deviations that often go unnoticed during a conventional FAT. Through AFAT, stakeholders in a tunnel ventilation project can reduce the risk of unexpected fan failures, enhancing operational safety and minimizing costly downtimes.

This paper proposes AFAT as a best practice to be promoted in the tunnel ventilation industry.

Keywords: tunnel ventilation, fan failures, Advanced Factory Acceptance Test.

1. INTRODUCTION

Testing is a powerful tool to assure the performance of the Tunnel Ventilation System (TVS) within designed parameters, and to prevent failures in the Tunnel Ventilation Equipment (TVE). As the tunnel ventilation is a critical system for ensuring the safety and comfort of users, a comprehensive testing approach on the ventilation equipment must be executed during the implementation of any underground infrastructure project. As extensively explained by Dr. G. Leoutsakos and others [1], the objective, through various levels of testing, is to prove and verify the quality and functionality of components, subsystems and the overall system and to transfer it into fully operational conditions. Therefore, it is needed to perform tests at different stages of the project, as follows:

1. Factory Acceptance Tests (FAT)
2. Installation Tests (IT)
3. Site Acceptance Tests or Stand Alone Test (SAT)
4. System Integration Tests (SIT)
5. System Performance Tests (SPT)
6. Trial Runs (TR)

Among all ventilation equipment, fans require special attention as they, along with the dampers, are the most critical equipment in the Tunnel Ventilation System. Fan components

are subjected to quality assurance trials during manufacturing, but the first level of actual testing for the whole fan unit is the Factory Acceptance Test (FAT).

FAT is typically a contractual obligation for the fan supplier, and a significant milestone in a tunnel ventilation project. During FAT, key stakeholders, including Client, Consultant, Contractor and Supplier gather at testing facilities, usually located at manufacturer’s premises or at independent laboratories, to witness a series of tests on the tunnel fans. In addition to critical commercial terms, such as partial payments or releasing bank guarantees, linked to successful FAT completion, the primary objective of FAT is to verify that fan performance and its constructive parameters comply with the project specifications.

Under the generic term of FAT are included a wide range of possible fan factory testing activities. The basic and most conventional FAT involves verifying fan performance parameters, that is flow, pressure and efficiency for the axial fans, thrust for the jet fans and noise level for both of them. However, there are projects requesting very demanding factory testing procedures, which are also referred as FAT.

This paper introduces the concept of Advanced Factory Acceptance Test (AFAT) to define a standardized and comprehensive series of tests to be conducted on the tunnel fans before delivery. AFAT includes the conventional FAT, focused in verifying performance parameters, plus additional tests, mostly oriented to guarantee the mechanical and electrical integrity of the tunnel fans.

Furthermore, this paper addresses the weakness of conventional FAT in preventing potential tunnel fans failures and explores how AFAT could lead to a more reliable and robust TVS.

2. SYSTEM AND EQUIPMENT FAILURES IN TUNNEL VENTILATION

The failures in tunnel ventilation can be classified into system failures and equipment failures, with fan failures being the primary concern. These two types of failures are closely interconnected, as system failures often lead to equipment failures, but also, equipment failures can result in system failures.

Based on fan manufacturers’ records and general database of industrial equipment and components, such as the Nonelectronic Parts Reliability Data (NPRD) reports [2], the most frequent system and equipment failures in tunnel ventilation are listed in Table 1.

System failures arise from mismatches between the actual performance of the Tunnel Ventilation System and the performance needed to ensure a safe environment in the underground infrastructure. These failures have an aerodynamic root cause, either due to mistakes in the ventilation design or the inability of the selected tunnel fans to reach the specified performance parameters.

Equipment failures, primarily fan failures, are associated with electromechanical breakdowns.

While failures linked to a wrong tunnel ventilation design cannot be identified during factory testing, those related to performance, mechanical or electrical issues in the fans can be identified. Once identified, these issues must be fixed prior to equipment delivery.

On the other hand, system and equipment failures resulting from defective onsite installation and/or a lack of maintenance are not the subject of this paper, as they cannot be identified during factory testing. They shall be treated separately and prevented through rigorous verification and continuous control of these two activities.

Table 1: Failures in Tunnel Ventilation

No.	Description	Root Cause	Type
01	TVS is not able to perform to ensure a safe environment in the underground infrastructure	Wrong TVS Design	SYSTEM FAILURES
02	Axial fans do not achieve the required Flow & Pressure	Performance Issue	
03	Axial fan is in stall	Performance Issue	
04	Fan motors exceed specified power consumption values	Performance Issue	
05	Jet fans do not provide the requested nominal thrust	Performance Issue	
06	Tunnel fans do not reach specified acoustic levels	Performance Issue	
07	Tunnel fans under high vibration levels	Mechanical Issue	EQUIPMENT (FAN) FAILURES
08	Tunnel fans under vibration resonance due to natural frequencies	Mechanical Issue	
09	Reversible tunnel fans do not withstand dynamic forces due to consecutive cycles of reversal operation	Mechanical Issue	
10	Impeller’s damages under peak operation stress	Mechanical Issue	
11	Impeller comes into contact with the fan casing	Mechanical Issue	
12	Blade design or material does not withstand mechanical stresses while full speed operation at high temperature	Mechanical Issue	
13	Motor overheating during fan continuous operation	Electrical Issue	
14	Fan electro-mechanical integrity or performance fails while full speed operation at high temperature	Mech & Elect Issue	

3. CONVENTIONAL FAT TO IDENTIFY FAN PERFORMANCE ISSUES

3.1. First Article Inspection (FAI)

Before to proceed with any kind of factory acceptance testing procedure a First Article Inspection (FAI) shall be conducted. FAI consists in a visual and dimensional verification along with a materials certifications review of a fan sample selected by the customer among a quantity of units manufactured as per project’s requirement.

3.2. Aerodynamic performance test for tunnel axial fans

This test is conducted to verify the duty point (Flow & Pressure) and efficiency of axial fans. It is usually performed according to standards ANSI/AMCA 210-16 [3] or ISO 5801:2017 [4]. Through the test, ambient temperature, fan speed and pressure values must be recorded, at a minimum of 10 operating points. Adjustments to the auxiliary fan at the test bench, the Variable Speed Drive (VSD) and/or auxiliary damper are made accordingly.

The test shall cover the full operational speed of the fan, from maximum flow to zero flow. This is essential for verifying the stability of fan operation along the entire characteristic curve and identifying how external factors, such the piston effect, could potentially shift the fan operation into stall. Tunnel fans with stall-free characteristics curves ensure safe operation under all conditions.

Passing criteria (as per point 10.1.2.1 of AMCA 211-23 [5]):

- ✓ Airflow tolerance $\pm 5\%$ of specified values
 - ✓ Pressure tolerance $(1-0.05)^2 \leq P \leq (1+0.05)^2$
 - ✓ Power tolerance $\pm 7.5\%$ of specified values
- NOTE: Tolerance applies along the whole fan curve

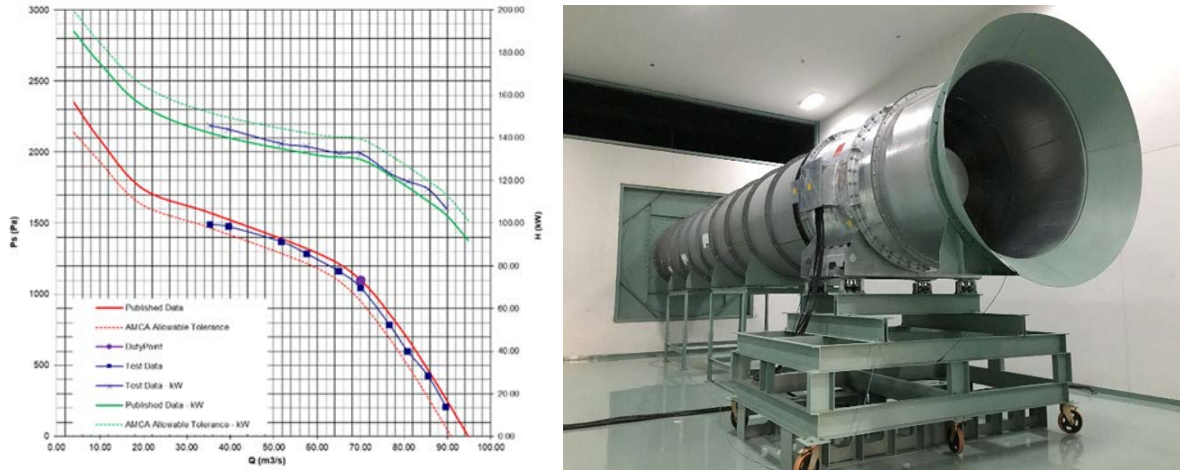


Figure 1: Stall-free characteristic curve and photo of tunnel axial fan under aerodynamic performance test

By conducting this test, the following failures (as numbered in Table 1) are prevented:

- Failure No. 2: In case the axial fan is not able to reach the specified flow and pressure values, the TVS will not perform as designed, compromising the tunnel safety.
- Failure No. 3: When the axial fan is in operation during certain time beyond its stall limit, a catastrophic impeller breakage may happen.
- Failure No. 4: The fan motors exceeding the specified power consumption values could lead to frequent tripping out on the electrical installation. Additionally, the operational cost related to higher power consumption will be increased.

3.3. Thrust force test for tunnel jet fans

This test verifies the nominal thrust of jet fans. It is typically conducted in accordance with standards ANSI/AMCA 250-22 [6] or ISO 13350:2015 [7]. The jet fan shall run for 10 minutes for stable readings of thrust force, temperature and speed.

Passing criteria (as per point 10.3.2.1 of AMCA 211-23 [5]):

- ✓ Thrust force tolerance - 6 % of specified values.
- ✓ Input power tolerance + 5 % of specified values.

By conducting this test, the following failures (as numbered in Table 1) are prevented:

- Failure No. 5: Verifying the specified nominal thrust during testing ensures that, once installed in the tunnel, the jet fans will generate the critical velocity to prevent smoke backlayering in case of fire. A failure on this point will compromise the performance of the longitudinal ventilation system, leading to an unacceptable level of risk in the tunnel.
- Failure No. 4: Similar consequences to those explained in section 3.2 regarding this failure.

3.4. Sound test for tunnel fans

This test verifies the sound power level of tunnel fans. It is typically conducted according to standards ANSI/AMCA 300-14 [8] or ISO 13347-2:2004 [9]. The sound test is performed after the fan’s aerodynamic performance test has established the exact duty point and operating speed.

Sound Power Level (SWL) must be measured for each of the 8 octave band frequencies. The fan’s overall SWL is not representative of its actual acoustic characteristic and does not provide sufficient data on sound attenuators’ outcomes.

Passing criteria (as per AMCA 311-16 [10]): Measured SWL values of the tested fan shall not exceed the published SWL values by more than 6dB in the first octave band of frequency and 3dB in any other octave band.

By conducting this test, the following failure (as numbered in Table 1) is prevented:

- Failure No. 6: Excessive noise level from tunnel fans can impact the health and well-being of residents near the tunnel portals or the ventilation shafts of the underground infrastructure. Furthermore, in emergency conditions, when the fans are operating at full speed, the noise should not exceed specified values to prevent voice messages or other acoustic signals from being heard by users of the underground infrastructure during evacuation.

4. AFAT TO IDENTIFY FAN MECHANICAL AND ELECTRICAL ISSUES

4.1. Vibration test

The purpose of the vibration test is to assess and verify that the fan operates within acceptable vibration levels, ensuring structural integrity, minimizing potential damage, and guaranteeing reliable long-term performance. This test is typically conducted according to standards ANSI/AMCA 204-20 [11] or ISO 14695:2003 [12].

Passing criteria (as per tables “6.1- Fan application Categories for Balance and Vibration” and table “8.2 – Vibration Limits on Factory Test” of ANSI/AMCA 204-20 [11]):

- ✓ For tunnel Axial fans ≤ 75 kW is requested category BV-3
- ✓ For tunnel Axial fans ≥ 75 kW is requested category BV-4
- ✓ For tunnel Jet fans is requested category BV-4

NOTE: An upgrade into category BV-5 will improve fan’s longevity.

By conducting this test, the following failure (as numbered in Table 1) is prevented:

- Failure No. 7: As extensively reported in many technical documents, excessive vibration levels in tunnel fans can lead to major failures in short or medium terms. Additionally, high vibrations reduce the operational life of the fan in the long term.

4.2. Natural frequency test

Natural frequency is an object’s innate vibration rate when excited. Applying a force at this frequency creates a resonance effect, potentially leading to structural failure due to escalating oscillations.

The natural frequency test verifies that the fan blade’s natural frequencies are outside of the fan’s operational range. The impact test is one of the most commonly used methods to identify natural frequencies. It is carried out with an impact hammer applying a minor force in the fan blade to identify frequencies where oscillations are amplified.

Passing criteria: No natural frequency shall occur from 0 to 300 % of the fan operating speed. For example, in a fan with an operating speed of 1,500 rpm (25 Hz) there should not be any natural frequency between 0 and 75 Hz.

By conducting this test, the following failure (as numbered in Table 1) is prevented:

- Failure No. 8: In the event of vibration resonance generated by natural frequencies, there is a serious risk of catastrophic impeller disintegration.

4.3. Reversal test

This is an operational test to be conducted on reversible fans. The procedure involves running the fans at full speed during 7 consecutive periods of 30 minutes, alternatively in forward and reverse, to complete a total operation time of 3 hours and 30 minutes. The insulation resistance of the motor winding is measured before and after the test to verify that there is not any drop or change due to the heat generated during reversal operations.

Passing criteria: The fan must run smoothly for every operational cycle, remaining securely intact and maintaining mechanical integrity on all its parts throughout the test.

By conducting this test, the following failure (as numbered in Table 1) is prevented:

- Failure No. 9: The mechanical integrity of the fan could be compromised if it has not been designed with sufficient mechanical robustness to withstand the demanding dynamic forces created during reversal maneuvers. Special attention is required in cases where the fans are operated with direct starting or autotransformer, as a pick of up to 7 times the rated current is supplied to motor over 15-30 seconds and the heat generated in short period could have a negative impact in winding insulation. Alternatively, soft-starter or inverter provide a soft motor starting and reversibility.

4.4. Overspeed test

The overspeed test is conducted to verify that the impeller can withstand centrifugal forces and stresses beyond its full operational speed with a sufficient safety margin. Typically, the overspeed test is performed at 125 % of the normal operating speed.

Passing criteria: Blade measurements are compared before and after the test. Tip clearance and blade angle must remain unchanged, with an allowable measurement tolerance of ± 1 mm for tip clearance and ± 1 degree for blade angle.

By conducting this test, the following failures (as numbered in Table 1) are prevented:

- Failure No. 10: The impeller may experience peak mechanical stresses beyond its nominal speed, particularly in situations like the piston effect in the tunnel. This can result in serious damages, including catastrophic disintegration.
- Failure No. 11: Peak mechanical stresses on the impeller can lead to elongation or deformation on the fan blades, reducing the tip clearance between the impeller and the fan casing. In the event that the impeller, rotating at its maximum speed, comes into contact with the fan casing, it will break.

4.5. Tri-Axial strain gauge test

The Tri-Axial strain gauge test for an impeller involves measuring strains under operating conditions by attaching sensors at tip and middle position of the blade, and at the hub. The strains are measured while the impeller is running for five to ten minutes and using formulas and standards to calculate the stress experienced by the blade.

Passing criteria: The stress found on the blades and impeller hub shall not exceed 60% of the material yield strength at specified operational high temperature (i.e. 250°C, 300 °C, 400 °C).

By conducting this test, the following failure (as numbered in Table 1) is prevented:

- Failure No. 12: During fan operation at emergency mode, the high temperatures reduce the mechanical strength of the blade material, typically aluminum alloy. If the actual operational stresses exceed the blade’s mechanical resistance at high temperature, it leads to impeller breakage and subsequently to a major failure on the TVS during the most critical emergency situation.

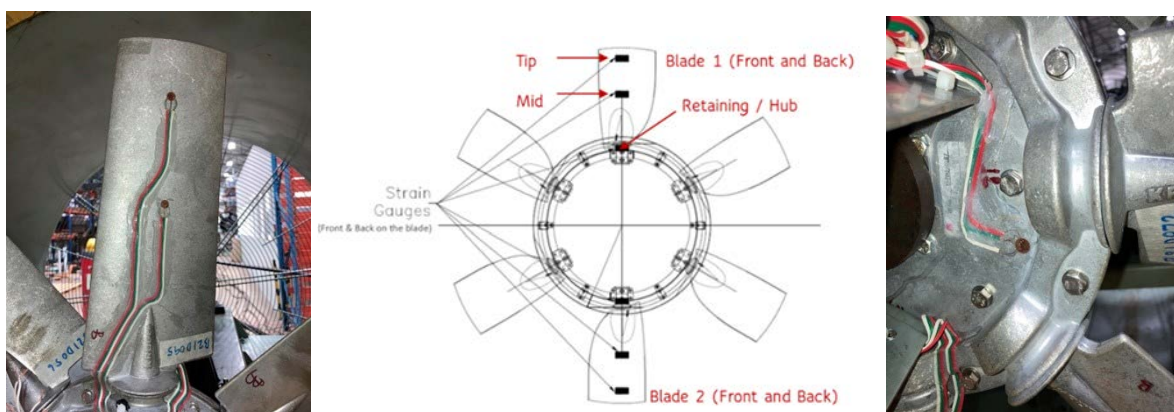


Figure 2: Tri-axial strain gauge test. Photos and impeller layout with sensors location

4.6. Run-in 24 hours test

Similarly to the reversal test, the run-in 24 test is an endurance operational test consisting of running the fan continuously at ambient temperature for 24 hours. Reversible fans shall operate 12 hours in forward and 12 hours in reverse.

Passing criteria: Motor fan shall not overheat. The motor temperature shall rise within the allowable limit as per its insulation class. Additionally, the fan shall remain securely intact.

By conducting this test, the following failure (as numbered in Table 1) is prevented:

- Failure No. 13: In case of motor overheating during continuous fan operation, the lifetime of the motor will be reduced. Additionally, it could lead to the motor burn out.

4.7. High temperature test

Besides of high temperature certificates to be provided for tunnel fans, it is recommended, especially in major projects, to perform high temperature tests on the actual fans intended for installation. These “ad hoc” tests ensure the fan’s resistance and performance in case of a fire. Tests shall be conducted as per Annex C4 of the standard EN 12101-3:2015 [13] where a dual-purpose fan shall go through warm up, heat up and high temperature test phases.

Passing criteria: Testing temperature shall be maintained within 0 and +25 °C. Static pressure difference (corrected according to air density) shall remain within -20 % +50 % of the measurement taken at the end of warm-up cycle. Additionally, fans must be inspected after the test and all parts must remain physically intact.

By conducting this test, the following failure (as numbered in Table 1) is prevented:

- Failure No. 14: A fan failure under emergency operation at high temperature, is the worst possible event for the safety of any underground infrastructure, as the evacuation

of users and the intervention of fire brigades and emergency services will be compromised. Hence, all possible measures must be taken to prevent this scenario.

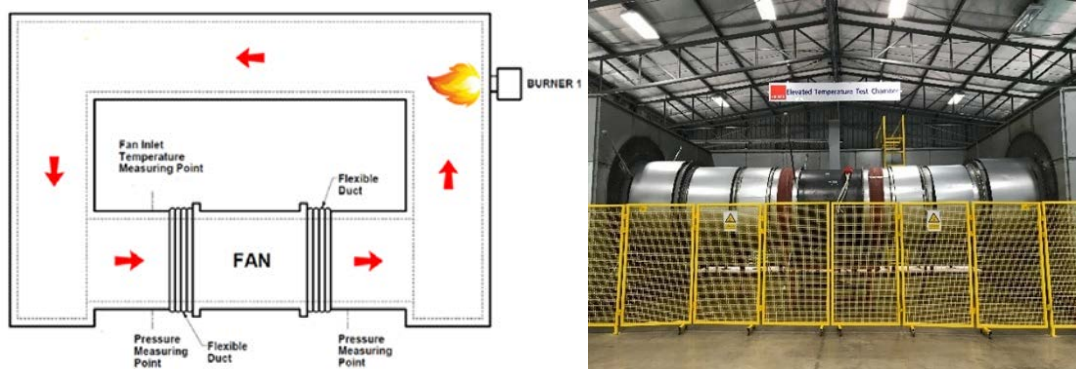


Figure 3: High temperature test for tunnel axial fans. Test bench layout and actual photo

5. SUMMARY AND CONCLUSION

FAT is defined on project basis and its level of testing varies for each project. However, conventional FAT is not enough to guarantee fan quality and reliability. AFAT (Advanced Factory Acceptance Tests) is a standardised factory testing procedure comprising 10 tests. AFAT not only verifies fan performance parameters as in conventional FAT, but also conducts additional tests to secure the mechanical and electrical integrity of fans.

6. REFERENCES

- [1] Leoutsakos G., Kouropalatis A., Filis P. “Testing and Commissioning of Metro Tunnel Ventilation Systems”. 19th International Symposium on Aerodynamics, Ventilation and Fire in Tunnels. Brighton (UK) 28th-30th September 2022.
- [2] “NPRD-2023. Nonelectronic Parts Reliability Data”. Quanterion Solutions Incorporated. 2023.
- [3] ANSI/AMCA 210-16 /ASHRAE 51-16 “Laboratory Methods of Testing Fans for Certified Aerodynamic Performance Rating”.
- [4] ISO 5801:2017 “Fans – Performance testing using standardized airways”.
- [5] AMCA 211-23 “Certified Ratings Program – Product Rating Manual for Fan Air Performance”.
- [6] ANSI/AMCA 250-22 “Laboratory Methods of Testing Jet Fans for Performance”.
- [7] ISO 13350:2015 “Fans – Performance testing of jet fans”.
- [8] ANSI/AMCA 300-14 “Reverberant Room Method for Sound Testing of Fans”.
- [9] ISO 13347-2:2004 “Industrial fans – Determination of fan sound power levels under standardized laboratory conditions. Part 2: Reverberant room method”.
- [10] AMCA 311-16 “Certified Ratings Program – Product Rating Manual for Fan Sound Performance”.
- [11] ANSI/AMCA 204-20 “Balance Quality and Vibration Levels for Fans”.
- [12] ISO 14695:2003 “Industrial fans – Method of measurement of fan vibration”.
- [13] EN 12101-3:2015 “Smoke and heat control systems – Part 3: Specification for powered smoke and heat control ventilators (Fans)”.

ADVANCES IN THE DIGITAL DOCUMENTATION OF RAILWAY TUNNEL INSPECTION

¹Matthias J. Rebhan, ²Stefan S. Grubinger, ²Andreas Schüppel, ³Simona Deutinger,
³Gernot Schwarzenberger

¹Graz University of Technology, Institute of Soil Mechanics, Foundation Engineering and
Computational Geotechnics, AT

²recordIT GmbH, AT

³ÖBB Infrastruktur AG, AT

DOI 10.3217/978-3-85125-996-4-19 (CC BY-NC 4.0)

This CC license does not apply to third party material and content noted otherwise.

ABSTRACT

Like other infrastructure, railway tunnels require inspection to ensure their safety and to detect damages at an early stage, representing a major challenge for those involved. Thus, in addition to the inspection, the tunnel down time can be a major disruption in operation. Under economic aspects, the inspection itself with all the subsequent work required is very time-consuming. In the area of rail networks, comprehensive preparations are necessary to be able to plan track barriers and bypass measures accordingly to minimise any undue influence on availability. This paper presents the results of an initial test phase of using a digital documentation solution in order to generate a rapid localisation and a corresponding time advantage when carrying out the inspection activities. By offering the use of a multitude of bases, a standardisation of damage patterns is carried out and a collaborative cooperation of multiple inspection personnel is possible. Depending on the data stock, digitised as-built models in the form of a plan, digital plan documents and existing or generated digital twins can be used. Thus, making it possible to locate the damages already in the course of the inspection and therefore enable a comprehensible documentation of the inspection activity and an automated generation of inspection reports.

In the course of a series of field tests along four tunnels of the Tauern Line of the Austrian Federal Railways, the digital procedure was validated in form of a pilot project. Within this paper the first results, together with the advantages of a digital inspection are presented.

Keywords: inspection, digital twin, digitalization, tunnel safety

1. RAILWAY TUNNEL INFRASTRUCTURE IN AUSTRIA

The entire route network of the Austrian Federal Railways has a length of 4,965 km with 1,032 stations and enables a saving of 4 million tonnes of CO₂ (for 2022) through rail transport [1] compared to transport by road. In addition to a large number of properties and tracks together with the railway stations, there are also a large number of civil engineering structures (assets) which are required for the construction and routing based on the topography and the alignment. In addition to bridges and retaining structures, there are also 254 tunnels [2] along the entire railway network. These have an average age of 45 years and a target service life of 141 years on average. A relatively high number of 150 tunnels and tunnel-like structures have already reached an age of 100 years or more, of which 63 tunnels are already more than 150 years old and date back to the intensive construction period around 1850. These include the tunnels along the Semmering line, which were recognised as a UNESCO World Heritage Site in 1998 [3]. Figure 1 shows the location of tunnels along the Austrian Federal Railways network. It can be seen that they are distributed across the entire railway network. However,

it can also be clearly seen that tunnels (the blue dots in Figure 1) are more frequent in the Alpine areas of Austria as well as in the vicinity of major cities or transport hubs.

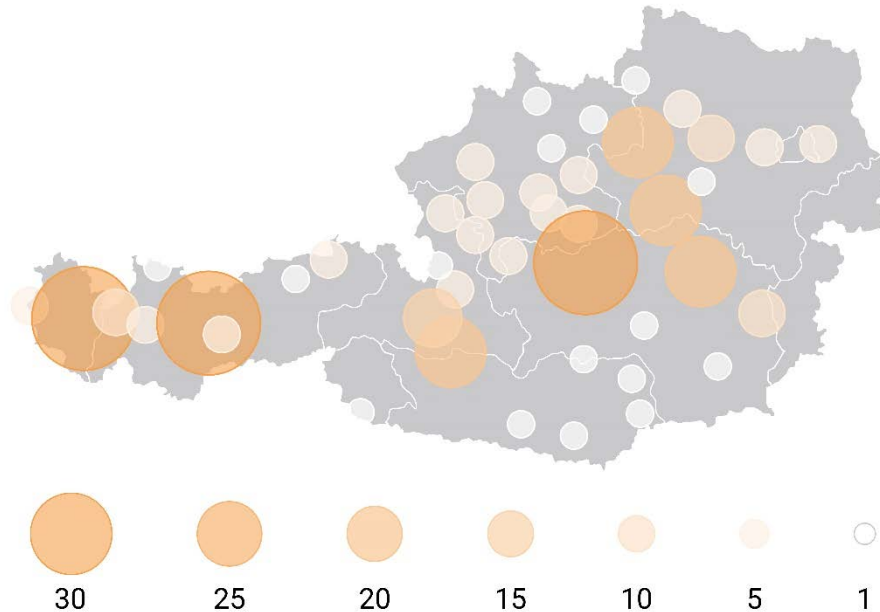


Figure 1: Tunnels along the Austrian railway network

Due to their position within the network, its linear extension and the lack of diversions and bypasses, tunnels have a significant influence on the availability of the route and thus to the operation of the railway, making them a key factor for a smooth operation.

2. STATE-OF-THE-ART IN INSPECTION OF RAILWAY TUNNELS, DAMAGES AND DAMAGE SYMPTOMS

The inspection of structures is a challenging, demanding, and highly responsible task for civil and geotechnical engineers. In general, a distinction is made between the inspection of buildings and industrial structures (object safety inspection according to the standard ÖNORM B 1300 [4] and ÖNORM B 1301 [5]) and civil engineering structures. The latter are regulated in the guidelines of the RVS 13.03 series – Quality Assurance for Structural Maintenance, Monitoring and Inspection of Engineering Structures. The focus lays generally on a visual inspection, which includes all relevant and non-relevant components and structural elements required for traffic safety. Inspection activities are carried out periodically and conclude with a report or assessment. This provides information on the state of preservation, defines further steps for maintenance and serves as the basis for subsequent inspection intervals.

2.1. State-of-the-art in inspection of civil-engineering structures focus on tunnels

Planning documents usually constitute the basis for every inspection activity, especially for civil-engineering structures. These form the basis for the scope of inspection and provide the necessary structural and safety-related information on a structure, which defines the tasks for the inspection personnel. Furthermore, these documents provide the basis for recording information of the inspection during the field work. Examples of this are damaged areas, image numbers, changes compared to preliminary inspections or changes in the state of preservation. Such documents are usually available digitally in the form of drawings (usually

As shown in Figure 3, damage to the inner lining of the tunnel is usually recorded, documented and assessed during a visual inspection of the structure. In the case of tunnels in Austria, a distinction can be made between damage to masonry linings (Figure 3 top) and damage to concrete segments or a shotcrete lining (Figure 3 bottom).

3. DIGITAL INSPECTION SOLUTIONS

Digitalization is one of the main topics in research and development in the construction industry. Currently, the focus here is on new constructions and, above all, the integration of the BIM process in all project phases from planning to utilisation and maintenance. Only limited attention is currently being paid to the application of digitalisation measures to existing buildings and civil engineering structures. However, digital solutions for building inspection can bring a number of advantages here, which are of course associated with possible disadvantages. A brief summary of these is provided in Table 1.

Table 1: Advantages and disadvantages of digital solutions for tunnel inspection (overview)

Advantages	Disadvantages
Time saving	User reluctance
Reduced downtime and inspection effort	Modification of processes required
Data utilization for evaluation	Digital model of the structure required
Intuitive and self-explanatory usage	Missing usability
Integration into inspection databases	Ongoing standardisation required
Transfer of inspection results	
Multiple user applications	
Virtual inspection	

As Table 1 shows, a number of advantages can be generated through the digitalization of inspections, especially for civil engineering structures. The biggest and usually most decisive point is the saving potential in terms of on-site time. Time can for example be saved, by using an existing inspection documentation from previous tasks, which can generate a considerable advantage, especially when documenting damaged areas and defects. In addition to the monetary savings, this can result in shorter closure times (track barriers), especially when inspecting railway infrastructure due to the fact of missing bypass possibilities. This can result in a reduced need for total closures and an improvement in track availability. In addition, a software solution used on-site creates a standardised and less error-prone inspection, from which reports, a documentation and an assessment can be created with little effort. Furthermore, information and characteristic values as well as a periodical documentation can be further processed digitally. In addition, the current condition of a structure can be depicted more comprehensively using pictures, allowing a comparison between inspection periods.

In addition to these advantages, there are also disadvantages associated with a digitalization - or generally a change and adaptation of an existing process using digital solutions. On the one hand, these relate to usability and the utilisation of a digital solution by users. However, an appropriate approach (UX and UI design) can remedy this. On the other hand, the pervasive and sustainable use of digital solutions often requires adjustments to databases, data structures and standardisation in general. In Austria, there is currently a lack of specifications in the area of inspection regulations, relating to the use of digital processes for inspections.

One of the main advantages of digitalization from a practical point of view, as mentioned in Table 1, is the fact that several users can use the solution at the same time on the same project. In addition to time-saving, this leads to a possible division of tasks with regard to the expertise

of the inspection personnel. It has also been shown that this results in a standardisation of processing - through consistent standardisation. Such an approach can also lead to a transfer of expertise - in the form of an exchange of experience. This is particularly the case with a periodic and recurring use of inspection documents and the data and information from inspections by different personnel or changing subcontractors for the inspection.

4. WORKFLOW FOR A DIGITAL INSPECTION AND EXAMPLES FROM A SERIES OF INITIAL FIELD TESTS

In addition to the advantages offered by digitalization, it is also important to adapt working methods and processes to the newly created possibilities in order to generate a corresponding increase in time-saving and quality improvement. Preparation remains essential, but the approach will take a different form. For the most part, the collection of inventory data will no longer be necessary and a stronger focus on existing issues and damages will be possible. However, it is not only the preparation that changes, the form of inspection also changes when digital solutions are used. For example, due to standardisation and the use of former inspection results, inspection personnel will receive a much stronger role as a controlling element. This results from the fact that a software-supported inspection already specifies or can specify defects or damages from former on-site inspections and thus can provide a framework for the documentation on-site whilst conducting the inspection. As an introduction to the workflow described in chapter 4.5, the respective basic principles are described below.

4.1. Master files and data preparation

Master data for structures is generally stored in a database after it has been entered once and is reused in identical form for every inspection. The already existing and standardised assessment bases also provide a basis for assessing and reporting that can be used and evaluated in the same way for subsequent inspections.

4.2. Drawings, sketches and other documents

Similar to the master data, planning bases are also implemented (normally) only once, which enables comparability and, in addition, usability of the information and data generated during subsequent inspections. This allows a "single point of truth" to be created for the inspection, making the digital inspection software a valid source of information for managing recurring inspections, but also for maintenance, refurbishment or adaptation. Examples of plan/drawing bases range from scans or photos, as shown in Figure 2, to the use of 3D models from terrestrial and mobile laser scanning images [6] or extracted from BIM models.

4.3. Annotate / Asses / Localise

Using a software, annotation (the addition of comments) and the allocation of facts can be carried out directly on-site using a pre-defined methodology. This means that the results can be compared with a certain degree of standardisation and the inspection personnel is able to select and allocate damages or information quickly. In addition, the ongoing experience of the inspection personnel - with regard to the increase in damage patterns and defects - can also be incorporated, resulting in a continuous improvement of the inspection quality.

4.4. Integration of results and findings

The integration of the collected and recorded information into databases can be largely automated. This eliminates the otherwise time-consuming task of transferring data and information and also offers the creation of more comprehensive reports.

4.5. Workflow for digital inspection of structures

The contents described in chapters 4.1 to 4.4 are part of a comprehensive process that is used both for non-digitalized inspection and for the application of a digital solution - albeit in partially different approaches. This is summarized in Figure 4 - with a focus on the digital implementation of the process.



Figure 4: Schematic workflow for an inspection and documentation of inspection works and damages with emphasis on the use of a digital inspection methodology (adapted from [6])

It can be seen that a database can be used as a central element, which must initially be filled with documents, data, and information and then supplemented by the damages, facts, and information as well as pictures of the inspection. Furthermore, this forms a cumulative possibility to derive maintenance measures as well as the necessary output options for reports and the safety assessment of the civil-engineering structure.

4.6. Inspection of railway tunnels using digital tools

As already mentioned, the usability and involvement of the inspection personnel in the development process of a digital solution for the inspection of tunnels is one of the decisive criteria for the success of a process as described in chapter 3. It is therefore necessary to include the practical on-site inspection processes in addition to pure software development. For this reason, comprehensive testing and subsequent improvement under real-life conditions is necessary. In the following, some constraints for the inspection of tunnels along the Austrian Federal Railways network are briefly described and the design criteria for a software solution developed for this task are briefly described.



Figure 5: Inspection and documentation of the lining of a tunnel

The images in Figure 5 show some circumstances that must be dealt with when inspecting tunnels for railway operation - and similarly for road operation. On the one hand, as shown in the left-hand image, climbing aids and transport equipment are required in order to be able to inspect the entire lining of the tunnel visually. In the case of railway tunnels, this is significantly influenced by the requirements for rail-bound solutions and the presence of overhead lines. On the other hand, a more comprehensive survey of the damaged areas, as shown in the picture on the left, must also be carried out as a rule in order to record and assess their effects on the load-bearing capacity and traffic suitability of the tunnel.

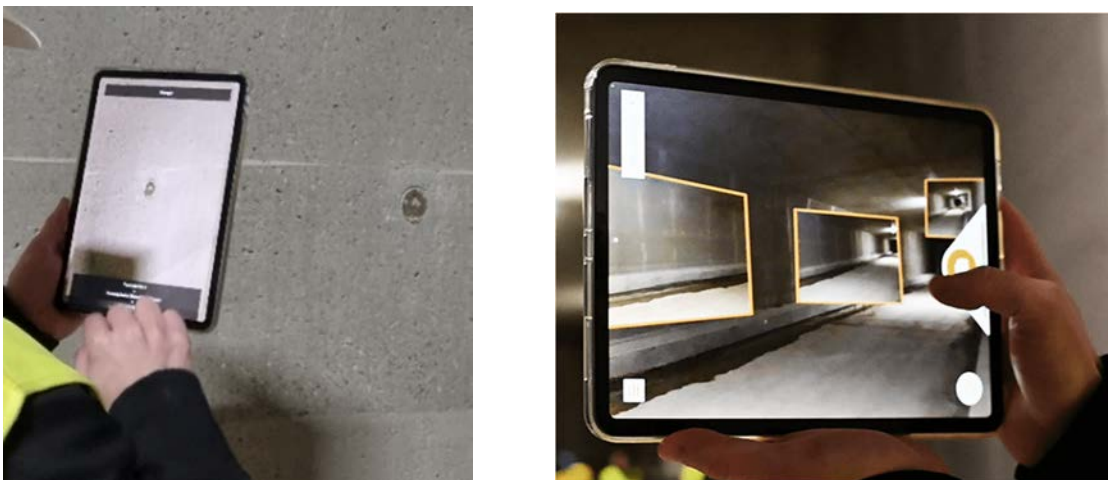


Figure 6: Examples of annotation and localisation of damage and defects, recording including annotation (left), integration of virtual reality to display existing inspection results (right)

Such requirements must be taken into account in software development and, above all, in UX (User Experience) and UI (User Interface) design. For example, as shown in Figure 6 on the left, selection boxes in the software must be of the appropriate size, so that they can be operated easily and under restricted handling conditions e.g. while wearing gloves. In addition, especially for recurring inspections, technologies such as virtual reality and augmented reality, as shown in Figure 6 on the right, can help to ensure that inspections can be carried out more quickly and thus reduce the duration of the inspection and the workload for the inspection personnel.

4.7. Use of digital inspection on other railway infrastructure

In addition to the tunnels mentioned in this article, the Austrian Federal Railways network also includes a large number of other structures to which the workflow described in this article can be applied. The aim here is to reduce the workload of the inspection personnel and, above all, to reduce track-barrier durations while maintaining a sufficient safety level.



Figure 7: Example of assets along the Austria railway lines, retaining structures (left), noise-protection constructions (centre), natural hazard-protection structures (right)

The examples in Figure 7 show a small selection of the existing structures on the Austrian railway network. Currently there are 8,363 retaining structures (Figure 7 left), 933 km of noise barriers (Figure 7 centre) and a vast number of protective structures against natural hazards (Figure 7 right), which must be inspected and assessed in accordance with the maintenance obligation (§19 Eisenbahngesetz 1957 i.e the railway legislation [7]).

5. SUMMARY AND CONCLUSION

This paper attempts to provide a brief insight into the requirements for the implementation of a software for the inspection in particular of civil structures of tunnels with focus on railway tunnels. In addition to the procedure and workflow for the implementation of digital processes, the integration of practice-relevant questions and handling are also shown. These were developed together with the future users of the Austrian Federal Railways and tested in a field study. From a technical point of view, the added value of a digital solution could be demonstrated, which lies primarily in the reduction of track downtimes and the reduction of workload for the inspection personnel. There is certainly potential for further development, for example to directly integrate digital models (e.g. 3D scans or BIM) and enable a more comprehensive utilization of data and information with regard to the maintenance strategy. In addition, such digital solutions can also be used to create a comprehensive data pool in order to drive forward solutions for image recognition and/or automatic information extraction from images. However, the aim behind such developments must always be to reduce downtimes of the infrastructure in order to ensure that the railway network can be operated economically and as smoothly as possible.

Furthermore, the realization of these developments showed that for a useful development of software solutions, it is necessary to ensure a close cooperation between the inspection personnel, the maintenance department and the software development to enable a comprehensive view and corresponding ensure the applicability of the solutions developed.

6. REFERENCES

- [1] ÖBB (2022); Zahlen Daten Fakten ÖBB-Infrastruktur AG, ÖBB-Infrastruktur AG Stab Kommunikation, 2. Ausgabe / 1. Auflage.
- [2] ÖBB (2022a); Netzzustandsbericht 2022, ÖBB-Infrastruktur AG GB Asset Management und Strategische Planung, Version 1.0.
- [3] <https://www.unesco.at/kultur/welterbe/unesco-welterbe-in-oesterreich/semmeringeisenbahn>
- [4] ÖNORM B 1300, 2018. Objektsicherheitsprüfungen für Wohngebäude - Regelmäßige Prüfroutinen im Rahmen von Sichtkontrollen und zerstörungsfreien Begutachtungen - Grundlagen und Checklisten. Austrian Standards. Wien.
- [5] ÖNORM B 1301, 2016. Objektsicherheitsprüfungen für Nicht-Wohngebäude - Regelmäßige Prüfroutinen im Rahmen von Sichtkontrollen und Begutachtungen - Grundlagen und Checklisten. Austrian Standards. Wien.
- [6] Grubinger et. al., 2023. Digitalisierungspotential der Prüfung geotechnischer Bauwerke, Beiträge zum 37 Christian Veder Kolloquium, Technische Universität Graz, Institut für Bodenmechanik, Grundbau und Numerische Geotechnik, Graz.
- [7] EisebG (1957). Bundesgesetz über Eisenbahnen, Schienenfahrzeuge auf Eisenbahnen und den Verkehr auf Eisenbahnen, BGBl. Nr. 60/1957, Fassung vom 02.12.2023.

SAFETY CHALLENGES IN AN UNDERGROUND HYPERLOOP SYSTEM: A PRELIMINARY INVESTIGATION

¹Matteo Pachera, ²Maarten Vanneste, ²Thijs Verrecas, ³Bartek Kulig
¹Sweco, BE
²Denys, BE
³Hard-T, NL

DOI 10.3217/978-3-85125-996-4-20 (CC BY-NC 4.0)

This CC license does not apply to third party material and content noted otherwise.

ABSTRACT

A new link between the train station and the airport of Rotterdam in the Netherlands is under study to increase the passengers’ capacity and reduce travel time. One of the proposed solutions is an hyperloop tunnel that travels under the city for about 2 km. This article provides an overview about the safety challenges of an underground hyperloop system. In case of fire on board or sudden loss of cabin pressure, tenability conditions deteriorate quickly due to the small size of the vehicle. The preferred option is to travel to the next station and evacuate passengers from there before they become incapacitated. In case two stations are too far apart, additional evacuation routes are required: through the tunnel or in separate evacuation stations. In the first case the tunnel should be equipped with ventilation (for pressurization and smoke confinement) and evacuation routes. In the second case smaller stations are necessary. Alternatively, additional safety measures can be installed on board (water suppression and oxygen masks) to increase the time passengers can stay in the vehicle. The integration of the different safety measures should be further investigated following the development of the project and of the hyperloop technology.

Keywords: Hyperloop, evacuation, high-speed, vacuum.

1. INTRODUCTION

The hyperloop concept was first described by Elon Musk in a white paper in August 2013 [1]. This system is made of a capsule traveling at high speed in a vacuum tube and it was proposed as a cost-effective alternative to high speed rail and aviation [2][3]. Several routes are currently under-study [4] and a test rig was inaugurated at the European Hyperloop Center in 2023 [5].

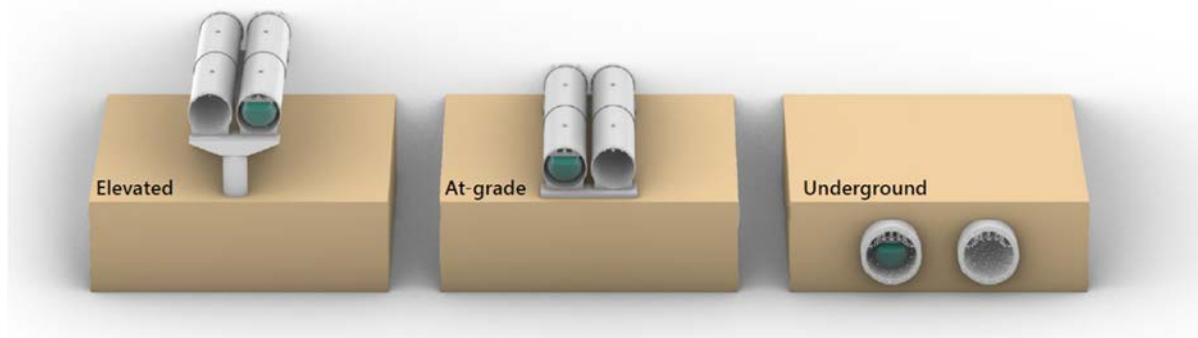


Figure 1: Different tube’s configurations

Different configurations for the tubes have been proposed, both above ground and underground. For above ground configurations, each section is separated from the others with

airlocks every 500 m. In case of emergency a section is isolated by closing the airlocks and it is pressurized, so passengers can evacuate via the tube. This solution is not applicable to underground configurations, which will be later addressed in this article. Hyperloop’s safety has been already investigated in few publications [6][7][8] mostly with focus on the safety systems available on the vehicle. Alternative standards applicable for metro systems could be also applied to hyperloop [9][10], however their solutions can’t be implemented directly.

2. SAFETY ISSUES IN HYPERLOOP TUNNELS

A hyperloop system shares some of safety issues of aircrafts and metro systems. The vehicle travels at very low pressures (near vacuum) to limit friction losses and allow higher cruise speed, like a plane. This environment is created with vacuum pumps that remove most of the air from the tube to a pressure of 100 Pa, or 0.1% of atmospheric pressure. The vehicle however travels underground in a closed structure (the tunnel) as a metro train.

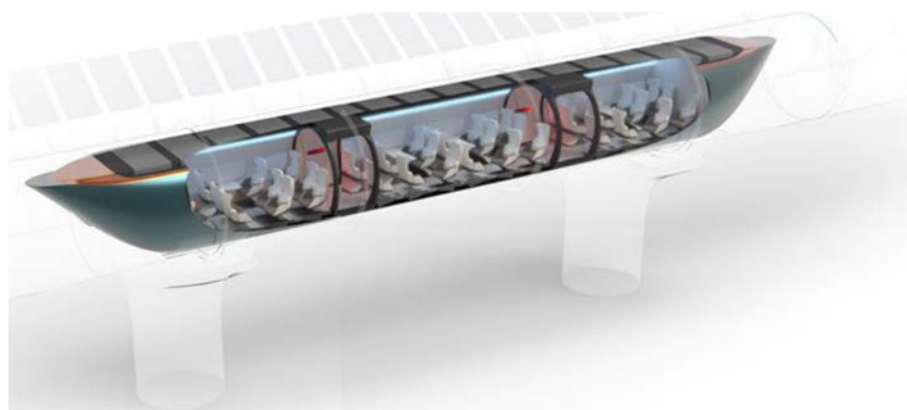


Figure 2: Schematic view of the hyperloop vehicle.

In case of an accident the system must face critical conditions, both related to the underground environment and to the low pressure. The main threats for passengers’ life safety are:

- Fire on board: passengers are exposed to heat and toxic smoke.
- Loss of pressure on board: passengers are exposed to low pressure and low levels of oxygen.

In case of fire on board passengers can become incapacitated by the effect of smoke’s toxicity and high heat. This is especially relevant due to the small size of the vehicles. The vehicle under study is 24 m long with an outer diameter of 2.5 m [11], Figure 2. The total capacity of the vehicle is 40 seats. Such a vehicle is sealed to keep ambient pressure inside, therefore in case of fire the vehicle can quickly fill with smoke. Based on a preliminary analysis with a luggage fire on board, (medium ground fire with peak HRR of 0.5 MW after 103 s) the time to incapacitation is calculated using FED and FED_{th} [12]. FED reaches a value of 0.3 at 2 m high after 430 s and at 1 m high (assuming passengers are seat) after 450 s. FED_{th} reaches a value of 0.3 at 2 m high after 155 s and at 1 m high (assuming passengers are seat) after 180 s. These times give an idea of the available time to evacuate passengers, about 2-3 minutes, before they become incapacitated and unable to self-evacuate.

In case of loss of pressure passengers can be incapacitated due to low oxygen concentrations, critical hypoxia. These conditions are achieved when the pressure reaches 50% of the initial pressure [13]. The time required to reach this limit value is function of the size of the leakage and the volume of the vehicle (175 m³). For normal leakages there is no risk of depressurization of the vehicle, however in case of accidents (collision with objects, structural defect) the pressure can drop faster due to larger leakages, Figure 3.

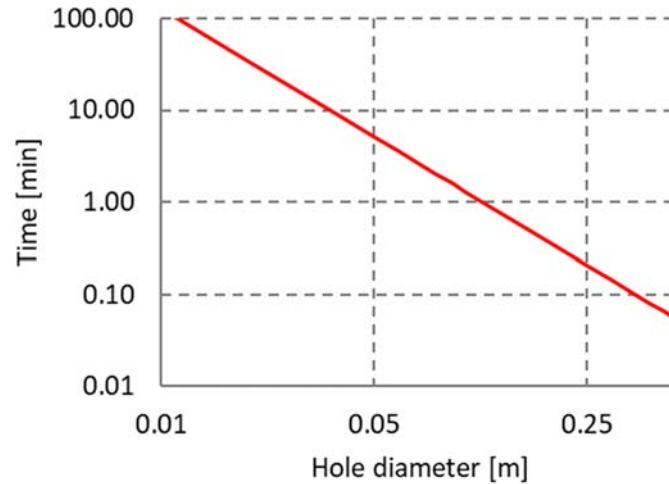


Figure 3: Time to critical pressure as function of the hole size

Based on the analyses above the time to reach critical conditions inside the vehicle can be short in case of fire, therefore the passengers should be promptly evacuated. Different approaches are proposed for passengers’ evacuation:

- Evacuation in the station
- Evacuation in the tunnel
- Evacuation in an emergency station

2.1. Stations

In case of detection of smoke or low pressure on board, the vehicle must travel to the next station to evacuate the passengers into the station. Once the vehicle arrives at the station, it passes through an airdock, where the pressure is reset from the tunnel pressure level to the atmospheric level. Then the vehicle enters the station where passengers can quickly evacuate using 6 emergency doors (4 embarking and 2 emergency doors). The total time to leave the vehicle is around 10-20 s for 40 passengers using 5 out of 6 exits in case of emergency. The different phases of the evacuation process are described in Table 1.

In case the fire is not detected or not detected yet the vehicle arrives to the station in a similar way, but the breaking, pressurization and debarking operations are slower (not in emergency mode).



Figure 4: Example of a vehicle in a station

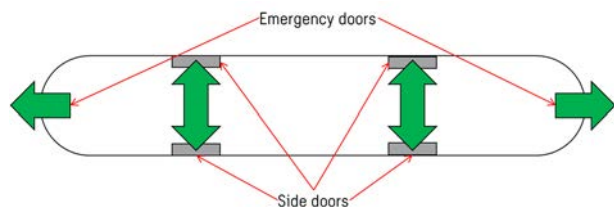


Figure 5: Evacuation scheme from the vehicle

Table 1: Evacuation phases in a station

	Vehicle	Operator	Station	Passengers
Timeline ↓	Accident detection			
		Accident verification		
		Start of station emergency procedure		
	Vehicle reaches the station		Activation of the emergency procedures in the station	
			Pressurization of the airdocks	
	Opening of the emergency doors of the vehicle			
				Evacuation from the vehicle into the station

In case of long routes, the longest delay before the evacuation starts is the travel time required to reach the station. A vehicle travels at 700 km/h at cruise speed and in case of emergency it can brake with a deceleration of 0.8 g. This implies that the vehicle requires about 50 s to stop and given the limited time for incapacitation, the total time before doors open should not exceed 2 minutes. Therefore, the vehicle can drive at full speed for about 60 s before reaching a new station, which leads to a travel range of about 11.7 km. This value is only indicative because of the uncertainty about the possible fire scenarios and operational speed of the vehicle. In this scenario it is also assumed that once the doors are open the ventilation is activated to dilute and cool the smoke (as the fire is still relatively small), so passengers are not in life danger anymore. If additional time is required to emergency procedures, pressurization and evacuation procedures, the travel range is further limited. In case the travel time exceeds the time before passengers are incapacitated alternative solutions must be implemented to guarantee an acceptable safety level.

2.2. Ventilation in the tunnel

In case the vehicle is unable to travel to the next station because the travel distance is too long, or the vehicle is damaged, the passengers can leave the train and evacuate through the tunnel. The tunnel should be then equipped with ventilation system to reset the pressure and to confine the smoke with a push-pull approach. The ventilation system should be designed to pressurize the tunnel quickly (less than 50 s) and to confine the smoke only on one side of the vehicle, Table 2. Additional emergency exits and evacuation routes should be added to the tunnel sections to allow a safe evacuation. The distance between doors should be estimated based on the time required by passengers to reach the door without risk of incapacitation.

Table 2: Emergency procedures in tunnel

	Vehicle	Operator	Tunnel	Passengers
Timeline ↓	Accident detection			
		Accident verification		
		Start of tunnel emergency procedure		
	Vehicle comes to halt		Pressurization of the tunnel via ventilation	
	Opening of the emergency doors of the vehicle		Switch to longitudinal ventilation	
				Evacuation from the vehicle into the tunnel and towards emergency exits

This evacuation strategy allows for the maximum flexibility because the vehicle can stop anywhere in the tunnel, and it is less affected by the reliability of the vehicle. However, this solution requires additional evacuation corridors, evacuation shafts and ventilation shafts. These additional installations create new leakage paths to the tunnels, increasing the extraction rate for the vacuum pumps.

2.3. Evacuation stations along the tunnel

An alternative solution to evacuation in tunnel is the creation of additional evacuation stations that can be installed in long routes where the travel time is longer than the time to incapacitation. The evacuation station is like a normal station, there is a pressurization zone and after that the passengers can leave the train using all doors, Table 3. The evacuation station can be equipped with ventilation system to confine the smoke and guarantee a tenable environment for passengers once out of the vehicle.

Table 3: Evacuation phases in an evacuation station

	Vehicle	Operator	Evacuation station	Passengers
Timeline ↓	Accident detection			
		Accident verification		
		Start of station emergency procedure		
	Vehicle reaches the evacuation station		Activation of the emergency procedures in the evacuation station	
			Pressurization of the airdocks	
	Opening of the emergency doors of the vehicle			
				Evacuation from the vehicle into the station

As seen above these stations can be placed at regular intervals (~11.7 km), but this solution requires a higher reliability for the traction system of the vehicle.

2.4. Additional safety systems on board

The three solutions proposed above try to minimize the time required to leave the vehicle. An alternative approach is to increase the time that passengers can stay in the vehicle. Different safety systems can be installed on board of the vehicle to mitigate a fire or a sudden loss of cabin pressure.

- Active water suppression system
- Additional oxygen masks

The presence of a water suppression system on board can prevent the development of small fires into larger one. In case the fire size is limited or suppressed the smoke temperature can be effectively mitigated and the vehicle can drive longer towards the stations. The vehicles are designed without personnel onboard; therefore, the system should be operated automatically or from remote.

The presence of oxygen masks can also increase the travel range of the vehicle to a station because passengers are not exposed to large quantities of toxic gasses in case of fire or low oxygen concentrations in case of pressure loss.

3. CONCLUSION AND FUTURE STEPS

This article provides an overview about the safety challenges and possible solutions associated with an underground hyperloop system. Due to the small dimensions of the vehicle a fire on board can lead to untenable conditions in very short time, thus passengers shall leave within 2-3 minutes. Considering the high speed of the vehicle (700 km/h) this can cover long distances in short time and reach the station of destination where passengers can evacuate. However, in case the next station is out of reach, passengers shall evacuate directly in the tunnel or in evacuation stations along the route. These solutions require additional installations, ventilation and evacuation shafts in the tunnel, or the construction of additional small stations.

Alternatively, the tenability conditions inside the vehicle can be improved with the installation of water suppression systems that can confine the fire and limit smoke temperature. Oxygen masks can be also installed in the vehicle (as in airplanes) to mitigate the effects of toxic smoke or hypoxia.

These different solutions can be combined, and they should be further investigated considering their effectiveness, reliability, and financial impact on the project. Further research is also required to understand the possible fire scenarios that could occur and define a standard fire scenario that could be later used for the design of the different safety systems.

4. REFERENCES

- [1] E., Musk, “Hyperloop Preliminary Design Study Technical Section”, Tesla [Hyperloop Alpha \(tesla.com\)](https://www.tesla.com/hyperloop-alpha)
- [2] Hard-T, “Mode comparison”, [Hyperloop Progress Paper \(hardt.global\)](https://www.hardt.global/hyperloop-progress-paper)
- [3] Hard-T, “Hyperconnected Europe” [Hyperconnected Europe \(hardt.global\)](https://www.hardt.global/hyperconnected-europe)
- [4] Hard-T, “Studies” [Studies \(hardt.global\)](https://www.hardt.global/studies)
- [5] Hyperloop development program, “European Hyperloop Center marks its kick-off in Veendam”, [European Hyperloop Center marks its kick-off in Veendam — European Hyperloop Center](https://www.europeanhyperloopcenter.com/news/european-hyperloop-center-marks-its-kick-off-in-veendam), 2023
- [6] TÜV SÜD, “Hyperloop Application Generic Guideline for Design, Operation and Certification”, 2017.
- [7] J. J. ter Kuile and M. L. M. Beek, “Safety Framework for the European Hyperloop Network,” Delft Hyperloop, Delft, 2020.
- [8] Mateu, Jose M., Pablo Martínez Fernández, and Ricardo Insa Franco. “Setting safety foundations in the Hyperloop: A first approach to preliminary hazard analysis and safety assurance system.” Safety science 142 (2021): 105366.
- [9] NFPA 130, “Standard for Fixed Guideway Transit and Passenger Rail Systems,” National Fire Protection Association, 2014.
- [10] Gemeente Amsterdam Dienst Infrastructuur, Verkeer en Vervoer , “Amsterdamse Leidraad Integrale Veiligheid ondergrondse tram- en metrosystemen (ALIVs),” Amsterdam , 2005.
- [11] Hard-T, “Vehicles”, [Hyperloop Progress Paper \(hardt.global\)](https://www.hardt.global/hyperloop-progress-paper)
- [12] Daniel J. O’Connor et al. “Guide to Human Behavior in Fire.” SFPE handbook of fire protection engineering, 2019.
- [13] A. J. Higgins, “Vacuum Exposure, How long will it take a spacecraft to decompress?,” <https://web.archive.org/web/20090208103930/http://geoffreylandis.com/higgins.html>.

WIDESPREAD OF ELECTRIC VEHICLES AND THE PROVISION OF KNOWLEDGE ABOUT FIRE ACCIDENTS FOR EXPRESSWAY MAINTENANCE WORKERS IN JAPAN

¹Masahiro YOKOTA, ¹Ken-ichiro YAMAZAKI,
²Tetsuya YAMAZAKI, ²Chihiro SGAWARA, ²Toshio SUZUKI
¹Central Nippon Highway Engineering Tokyo Company Limited, JP
²Nippon Expressway Research Institute Company Limited, JP

DOI 10.3217/978-3-85125-996-4-21 (CC BY-NC 4.0)

This CC license does not apply to third party material and content noted otherwise.

ABSTRACT

In October 2020, the Japanese government declared “carbon neutrality by 2050” and set out a policy to take comprehensive measures to achieve 100% electric vehicle sales in new passenger car sales by 2035. On the other hand, the world situation is changing rapidly, and the spread of electric vehicles is changing due to economic conditions, resource, and energy supply systems, etc., and the impact on Japan must also be predicted. Furthermore, the spread in Japan of electric vehicles is expected to change further due to future technological innovations, electricity demand, and infrastructure development trends. Therefore, it is necessary to prepare to maintain safe and comfortable expressway function without panic even when that stage is reached.

In this paper, we conducted a domestic and international survey on the spread of BEVs, fire accidents and their characteristics, and specific measures to reduce these risks. In addition, by confirming the current awareness of expressway maintenance worker regarding electric vehicle fire accidents, we have summarized the knowledge, issues, countermeasures, equipment, etc. necessary for future tunnel fire safety.

Keywords: expressway maintenance, maintenance worker, knowledge, BEV fire, fire extinguishing.

1. INTRODUCTION

Expressways prioritize user safety and aim to provide a safe and comfortable expressway space 24 hours a day, 365 days a year. To achieve this goal, maintenance work includes inspections of structures and facility equipment, improvement work, reinforcement, and disaster prevention measures to prepare for disasters, recovery, and repair work in the event of accidents, and countermeasures against traffic jams. Checks are constantly made to ensure that expressway functions are maintained and improved.

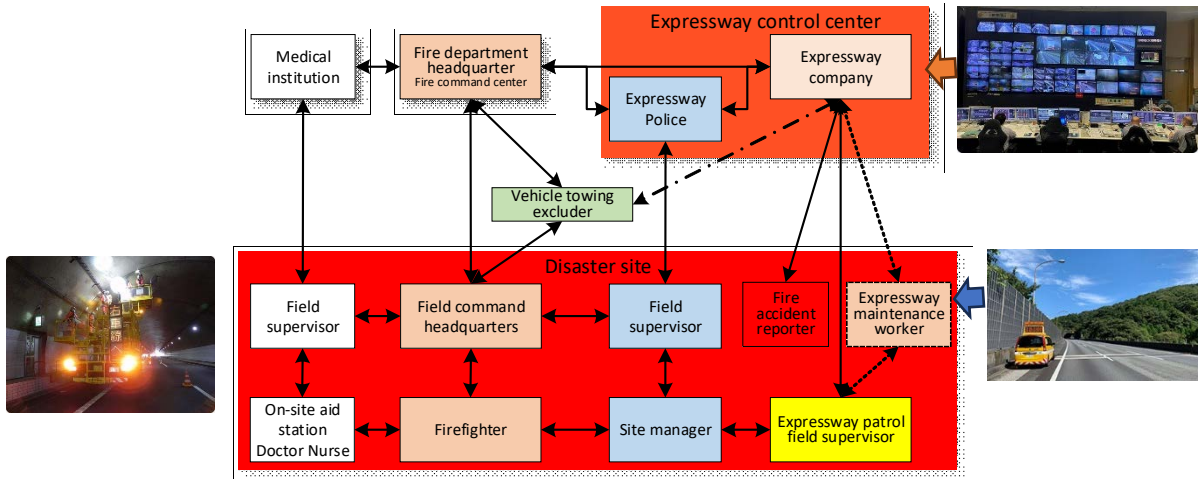


Figure 1: Collaboration with related organizations during expressway accidents and fires

Figure 1 shows the coordination system in case those engaged in maintenance worker an accident or fire while on the move. Currently, maintenance worker needs to minimize the decline in expressway functionality by collecting accurate information quickly and responding promptly and in collaboration with related parties.

Tunnels are special closed spaces that generate smoke, harmful gases, and heat in the event of a fire, so knowledge of emergency response is also required.

2. SPREAD OF ELECTRIC VEHICLES

2.1. Domestic situation

Currently, electric vehicles in Japan are classified into four types: HEV: hybrid vehicle, PHEV: plug-in hybrid vehicle, BEV: electric vehicle, and FCEV: fuel cell vehicle. This section summarizes domestic trends from 2018 to 2022. As shown in Figure 2 and Table 1, the number of electric vehicles in use in Japan is 9.86 million, overwhelmingly HEV, with both BEV and PHEV on the rise, with PHEV at around 200,000 and BEV around 165,000.

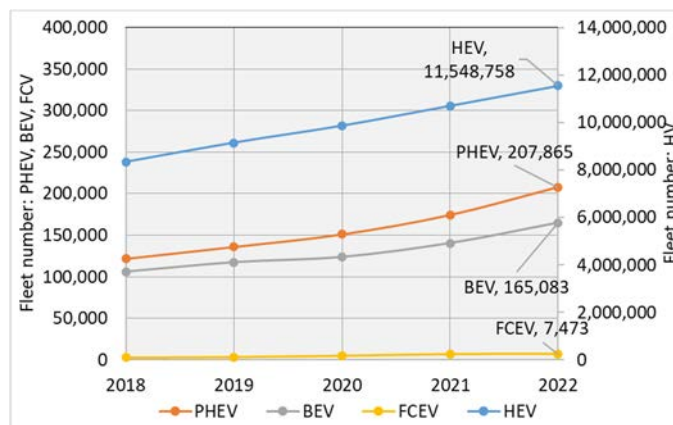


Figure 2: Changes in the number of electric vehicles (passenger cars) owned [1]

Next, as shown in Table 1, the number of registered passenger cars in 2022 will be about 62 million, with HEVs accounting for 19% and BEVs and PHEVs accounting for about 0.3%.

Table 1: Number of registered electric vehicles (passenger cars) and occupancy rate [1]

2022	Passenger cars fleet	61,953,135		
HEV	PHEV	BEV	FCEV	Total
11,548,758	207,865	165,083	7,473	11,929,179
18.6%	0.34%	0.27%	0.01%	19.3%

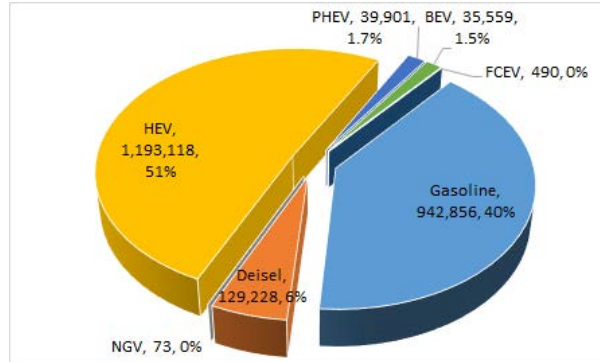


Figure 3: Percentage of passenger car sales by drive type (2022) [2]

Next, Figure 3 shows the percentage of passenger car sales in 2022 [2]. The share of sales is 40% for gasoline cars and 6% for diesel cars, while HEVs account for 51%, BEVs 1.5%, and PHEVs 1.7%. Although the sales volume of BEV and PHEV is on the rise, their market share is still low.

2.2. Comparison with other countries

Figure 4 shows the BEV and PHEV sales volume and the sales ratio of BEV and PHEV from 2018 to 2022 extracted from the literature [3] for data on major countries. The BEV and PHEV sales ratio will be on a slight downward trend from 2021 to 2022.

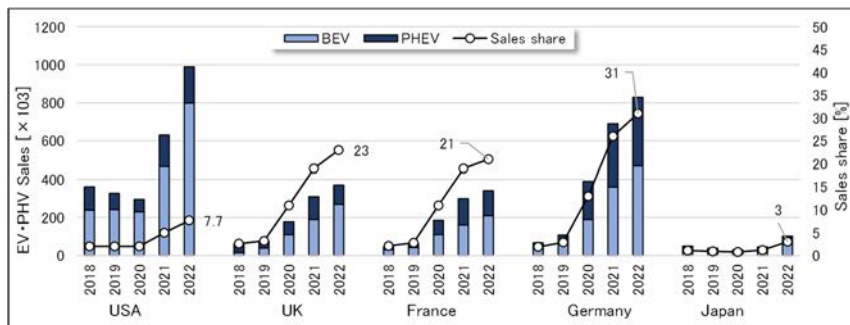


Figure 4: Trends in BEV/PHEV sales volume in each country from 2018 to 2022 [3]

In contrast, the ratio of BEVs and PHEVs in Japan is still low, but the trends are clearly different, with HEV sales in 2022 being about 1.2 million units (Figure 3), and the number of vehicles owned being just over 11.5 million units (Table 1).

2.3. Future trends

According to the electric vehicle spread targets for each country [4] compiled by Japan's Ministry of Economy, Trade and Industry, the target years are slightly different (see Table 2). Additionally, HEVs and PHEVs are handled differently in the EU and in Japan. However, on March 25, 2023, the EU, which had been the first in the world to shift to electric vehicles (EVs) by completely banning internal combustion engines, underwent a major change in

policy. The EU has announced that it will allow vehicles powered by e-fuel, an environmentally friendly synthetic fuel that does not rely on fossil fuels.

Table 2: Electrification targets of each country [4]

Country/Region	Target	Share				
		FCEV	BEV	PHEV	HEV	ICEV
Japan	2030	~3%	20~30%		30~40%	30~50%
	2035	100%				Not applicable
EU	2035	100%		Not applicable		
USA	2030	50%			50%	
China	2025	20%				
	2035	50%				Not applicable
UK	2030		50~70%			Not applicable
	2035	100%		Not applicable		
France	2040	100%		Not applicable		
Germany	2030		15 million			

3. BEV FIRES

3.1. BEV fire characteristics determined through experiments.

In BEV fire experiments conducted in Japan so far [5], differences in vehicle heat generation rate and lithium-ion secondary battery (hereinafter referred to as “LIB”) charging rate were ascertained. It was also confirmed that the combustion behavior was like that of a gasoline-powered vehicle, except for the flame eruption caused by LIB thermal runaway.

However, it was suggested that the charge rate affects the characteristics of the erupting fire, that it takes a long time to dispose of residual flames, and to cool the LIB pack, and that continuous cooling is necessary to prevent re-ignition after the fire is extinguished.

3.2. Domestic BEV fire cases

There are very few cases of BEV fires in Japan, so we referred to the past five years of vehicle recall, and defect information published by the Ministry of Land, Infrastructure, Transport and Tourism [6]. This is because this information includes not only recall information, but also accidents, fire events, and their causes. As shown in Table 3, the number of fires occurring is high in HEVs.

Table 3: Status of passenger car fires in the past five years [6]

Fire accidents	2018	2019	2020	2021	2022	Total
BEV	1	0	0	2	1	4
PHEV	1	0	3	1	0	5
HEV	42	33	15	22	26	138
Total	44	33	18	25	27	147

Next, Table 4 shows the causes of fire occurrence. None of the causes of fires in the HEVs, PHEVs, and BEVs we identified were due to accidents, and most HEV fires were caused by modifications (installation of aftermarket lights). Other than that, there are no major differences from conventional vehicles, such as oil leaks and exhaust system issues. Three cases have been reported regarding the causes of BEV fires: a case in which LIB short circuit due to submergence is suspected, a case in which a fire broke out from a cable during charging, and a case in which a fire of unknown cause occurred and completely burned down. Furthermore, on September 21, 2022, a complete fire incident was added, but the cause was said to be an external heat source that caused the fire. As described above, there is very little information on BEV fire accidents and their characteristics in Japan, but fortunately, no events that pose a social problem have occurred.

Table 4: Causes of fires in electric vehicles (passenger cars) over the past 5 years [6]










Cause of fire	engine oil leak	brake fluid leak	exhaust system	tire burst	aftermarket lamps	headlight	aftermarket light	wiring system	charging adapter wiring	suspected battery	fire spread	Cause unknown	Total
BEV									1	2	1		4
PHEV	2		2					1					5
HEV	40		6	1	2	19	55	8		6		1	138
Total	42	0	8	1	2	19	55	9	1	8	1	1	147

3.3. Typical cases of BEV fires

Typical characteristics and points to note are shown below, as determined from BEV accident and fire case studies in other countries [7], [8].

- 1) Flames and smoke are suddenly emitted from LIB: Do not touch or approach, prepare for emission of harmful gas, prepare a blower, etc.
- 2) A large amount of water is required to extinguish LIB: Cooling methods such as immersion containers and simple water storage banks, fire blankets, etc.
- 3) Risk of electric shock due to LIB residual power, repeated ignition: Water spray method, secure water source
- 4) Prolonged firefighting work: Road closures for long periods of time
- 5) Prevention of re-ignition when transporting the affected vehicle: Movement and transport methods
- 6) Isolated space for the storage area of the affected vehicle: Fire spread prevention and monitoring device in the event of a re-ignition
- 7) The fire incidence rate of BEVs, which are becoming more popular, appears to be lower than that of gasoline and diesel vehicles.

Table 5: Examples of fire cases and fire extinguishing methods

Examples of BEV fire accident cases [7]			
 Fire after collision with garage	 Reignition during loading	 Fired again during storage	
Examples of fire extinguishing measures in case of BEV fire [8]			
 Water storage levee	 Lance	 Water sprinkler	 Rosenbauer
 Fire blanket	 Fireproof bag		




It is necessary to coordinate among organizations that work together in the event of an expressway fire on the equipment necessary to respond to these incidents. In addition, the knowledge and actions required for maintenance workers in the event of an accident or fire are as follows.

- a.) Thoroughly check and ensure your own safety: do not go downwind of the vehicle, do not approach, or touch it, be careful of electric shock
- b.) Collect information: location (route direction, kilometer posts, lanes, etc.), traffic conditions, vehicle type (passenger, cargo, electric vehicle, etc.), accident/fire situation (single, multiple, etc.), presence of injuries, etc.
- c.) Provide accurate information to the road control center
- d.) Prevent secondary disasters: Alert following vehicles, implement simple regulations, etc. (prioritize the safety of disaster victims and yourself)
- e.) Wait calmly for the expressway police, emergency fire brigade, and towing service vehicle to arrive.

3.4. Road tunnels and BEV fires

In Japan, experiments have been conducted at the laboratory level to understand the fire characteristics of BEVs, and harmful exhaust gases and heat generation characteristics have been ascertained. However, in tunnels, which are closed spaces, not enough consideration has been given to the necessary equipment, effective fire extinguishing methods and equipment, the impact on the structure, the environmental impact, and methods for removing, transporting, and storing vehicles involved in disasters. These matters need to be addressed before the rapid spread of BEVs is expected in the future. To this end, the information obtained from advanced research examples [9], [10], [11] shown in Table 6 is extremely useful.

Table 6: Examples of technical documents published in recent years.

Alternative Fuel Vehicles in Tunnel [9]	BRAFA [10]	EV Fire Safety in Enclosed Spaces [11]
		
<ul style="list-style-type: none"> • Tunnel research highlights for traditional fuels • Research Summary in Tunnels; Fire cases, experiments, modeling, etc. related to BEV, NGV, PV, FCEV 	<ul style="list-style-type: none"> • BEV potential hazards, FCEV, risk modeling • Effect of fire on tunnel • LIB/vehicle fire experiments in tunnels, fire extinguishing training, contamination issues, etc. 	<ul style="list-style-type: none"> • Data on the few causes of BEV fires and points to note regarding handling and risks. • Fire in closed spaces, early detection of fire, fire extinguishing equipment, space, and structure, etc.











4. KNOWLEDGE AND EQUIPMENT NECESSARY FOR BEV ACCIDENT/FIRE RESPONSE

4.1. Advancement of fire brigade rescue techniques and prevention of electric shock.

The Fire and Disaster Management Agency has published a document [12] regarding the advancement of technology for responding to accidents and fires for next-generation vehicles, including BEVs. This report shows that, in response to the changing times, technological innovations in next-generation vehicles and mutual cooperative relationships with automobile manufacturers are necessary for firefighters to carry out firefighting and rescue operations safely. It is also shown that training through basic knowledge and practical skills is necessary.

It also introduces the dangers and necessary equipment during the initial response; when expressway maintenance workers encounter an accident or fire, it is difficult to conduct full-scale extinguishing and rescue operations like a fire brigade. However, this knowledge is extremely effective when trying to reduce damage and prevent secondary disasters. For reference, Table 7 shows examples of insulating protective equipment as personal protective equipment to prevent electric shock during rescue operations, as well as examples of main countermeasures against gas, heat, smoke, etc. emitted by accident vehicles.

Table 7: Examples of main insulating protective equipment and equipment [12]

Electric insulation equipment				
 Helmet	 Gloves	 Boots	 Clothing	 Pants
Hydrogen gas detector	Thermal imaging camera	Blower	Explosion proof light	Tools
				

4.2. Current knowledge of maintenance workers

4.2.1. Knowledge survey of maintenance workers

(1) Survey method and target audience

To survey the current state of knowledge, we conducted a simple questionnaire targeting two of our 10 offices that handle expressway maintenance and management work (27 people in total) and the research and design department at our head office (14 people).

(2) Questionnaire items

The questionnaire asked respondents to answer the following questions based on the premise that they encountered an accident or fire while driving a maintenance vehicle for work.

Question 1) Ensuring the safety of disaster victims: “Do you take measures (simple regulations), reporting, rescue, fire extinguishing, evacuation, etc. to ensure the safety of disaster victims?”

Question 2) Vehicle type confirmation: “Do you like to confirm the vehicle type at that time? (Conventional vehicle, BEV, etc.)”

Question 3) Points to note by vehicle type (knowledge): “Do you know that there are points to be noted depending on the type of vehicle (electric shock, harmful gas ejection, explosion, etc.)?”

Question 4) Willingness to acquire knowledge: “Do you want to know how to respond in the event of an accident or fire involving new energy vehicles in order to protect yourself and victims?”

(3) Survey results

Table 8 shows the overall results of the questionnaire. Regarding question 1, “Ensuring the safety of disaster victims,” almost all respondents answered that they would do so. However, over 40% of respondents answered that they did not confirm the vehicle type in question 2.

Regarding question 3, “Points to note by vehicle type,” just under 30% answered that they did not know. Regarding question 4, “Willingness to acquire knowledge,” all participants were willing.

Table 8: Knowledge survey results

Questions and answers		A- operation office	B- operation office	Headquarter	Total
Question 1	Execute	22	4	14	40
	Not execute	1	0	0	1
Question 2	Confirm	10	1	12	23
	Do not confirm	13	3	2	18
Question 3	I know	16	4	10	30
	I don't know	7	0	4	11
Question 4	I want to know	23	4	14	41
	I don't want to know	0	0	0	0

5. CONCLUSION

In this article, we have conducted a survey on the spread of BEVs in Japan and overseas, as well as accidents and fires, and have compiled the necessary information from the perspective of those involved in expressway maintenance work.

On the other hand, the world situation is changing rapidly, and there appears to be a shift to BEVs due to economic conditions, resource, and energy supply systems, etc., and we must also anticipate the impact on Japan.

However, the BEV shift is expected to change further due to future technological innovations, electricity demand, and infrastructure development trends. Therefore, it is necessary to prepare to maintain safe and comfortable expressway functions without panicking each time.

For this reason, it is necessary to continue collecting and maintaining information for a wide range of expressway maintenance workers to acquire knowledge on basic responses and to improve equipment and devices. In addition, our mission is to “maintain safe and secure expressways” by “knowing correctly and fearing correctly” to prevent secondary disasters and protect one's own life, in cooperation with related organizations. And they are just beginning.

6. REFERENCES

- [1] Automobile Inspection & Registration Association of Japan, “Statistics on the number of automobiles owned”, <https://www.airia.or.jp/publish/book/d1consent.html> (in Japanese).
- [2] Japan Automobile Dealers Association, “Statistics data”, <http://www.jada.or.jp/data/> (in Japanese).
- [3] International Energy Agency, “Global EV Data Explorer”, <https://www.iea.org/data-and-statistics/data-tools/global-ev-data-explorer>.
- [4] Agency for Natural Resources and Energy, “The current state of “decarbonization” of automobiles (Part 1) - What is Japan's strategy? How many electric cars are sold? “ https://www.enecho.meti.go.jp/about/special/johoteikyo/xev_2022now.html.
- [5] Watanabe N, et al, “Combustion Behavior of a Small Electric Vehicle Equipped with a Prismatic Lithium-Ion Battery”, Proceedings of the 2014, Japan Association for Fire Science and Engineering, May 2014.
- [6] Ministry of Land, Infrastructure, Transport and Tourism, “Accident/fire information search”, <https://renrakuda.mlit.go.jp/renrakuda/cgi-bin-search.html> (in Japanese).
- [7] National Transportation Safety Board, “Safety Risks to Emergency Responders from Lithium-Ion Battery Fires in Electric Vehicles”, NTSB/SR-20/10, PB2020-101011.

- [8] Onderzoek dompelcontainers, "Een beoordeling van de dompelcontainer en mogelijke alternatieven, Nederlands Instituut Publieke Veiligheid", 6 February 2023.
- [9] SANDIA REPORT, "Alternative Fuel Vehicles in Tunnels", SAND2020-5466, Sandia National Laboratories, Printed May 2020 (in Japanese).
- [10] INSTITUT FÜR VERBRENNUNGSKRAFT- MASCHINEN UND THERMODYNAMIK BRAFA, "Brandauswirkungen von Fahrzeugen mit alternativen Antriebssystemen, Bericht" Nr. I-21/21/PSt-V&U Inst-18/13/640 vom 08.09.2021.
- [11] Jonna Hynynen, et al, "Electric Vehicle Fire Safety in Enclosed Spaces", RISE Report 2023: 42.
- [12] Japanese Fire Department, "Report of the Study Group for the Advancement of Rescue Technology, Regarding the sophistication of activity technology for next-generation automobile accidents, etc.", March 2021 (in Japanese).

PRELIMINARY TESTS OF MECHANICAL ABUSE - NAIL TESTS OF LIBS

^{1,3}Papurello Davide, ¹Braghiroli Beatrice, ^{2,3}Bodoardo Silvia, ^{2,3}Amici Julia, ^{1,3}Borchiellini Romano

¹Department of Energy (DENERG), Politecnico di Torino, IT

²Department of Applied Science and Technology (DISAT), Politecnico di Torino, IT

³Energy Center, Politecnico di Torino, IT

DOI 10.3217/978-3-85125-996-4-22 (CC BY-NC 4.0)

This CC license does not apply to third party material and content noted otherwise.

ABSTRACT

Current tunnel safety concepts are based on the experience of conventional fuel vehicle accidents. The transition in the coming years will involve the use of alternative fuels such as hydrogen, natural gas and the use of electric vehicles. Among them, it seems that in the near future medium-sized and small vehicles will be powered electrically by lithium-ion batteries (city cars). The main problem of electric vehicles with Lithium-Ion batteries (LIBs) lies in the heat release rate (HRR), and toxic compounds released by LIB fire. Thermal runaway to a fire can be triggered by temperature, electricity, and mechanical abuse. The latter is more complex to manage via the Battery Management System (BMS) or cell architecture. In the present work, preliminary results of LIBs tested by nail test, inside a calorimeter are shown. The LIB cell tested and modelled is a SAMSUNG INR-18650-29E. Such a cell was tested at 100% SOC reaching temperatures above 800 °C and a maximum pressure value of about 4 bar. The concentration of CO inside the chamber was measured. The measured CO level ranged from 3000-4000 ppm(v), comparable to other research. The model implemented on COMSOL consists of two components: a 1D model that aims to simulate the electrochemical behaviour of the battery through a pseudo-two-dimensional (p2D) model, while the 3D model simulates heat transfer only.

Keywords: LIB; BEV; HRR; Toxic release

1. INTRODUCTION

Lithium Ion Batteries (LIBs) have become one of the most popular energy storage technologies in recent years, powering a wide range of devices and applications, from Portable Electronic Devices (PEDs) to Electric Vehicles (EVs) [1]. Electric vehicles are defined according to IEC 61851-1 [2]. EVs are defined, according to the Standard IEC 61851-1 and the main rechargeable storage systems considered are LIBs. The market increase is linked to the ongoing clean energy transition. In fact, with the possibility of using renewable energy to charge EVs, even locally, and zero emissions during operation, EVs are seen as a viable way to substitute conventional Internal Combustion Engine (ICE) vehicles. Moreover, EVs are characterized by up to four times higher energy efficiency than ICE vehicles [3], which is also possible to further increase by using regenerative braking. As the use of batteries has increased [4], a greater demand has been placed on their safety and management. Whether the application, safety of batteries is of paramount importance to manufacturers and integrators, especially in the event of external mechanical stress or Thermal Runaway (TR). Abuse testing is a crucial aspect of LIBs safety and reliability, as it helps to understand battery failure mechanisms, identify potential hazards and improve safety measures [5–7]. Abuse tests are divided into mechanical, electrical and thermal [8]. Among different abuse tests, nail penetration is a common mechanical test that consists of the penetration of the battery using a

sharp object [9]. This type of test is helpful to study the mechanical crash via an internal short circuit. To reduce the number of experimental tests, as they are destructive and can be expensive, it is important to model the abuse process. Furthermore, this can help to develop a predictive capability of the TR battery's response to mechanical impacts and, consequently, develop prevention and mitigation approaches to ensure the safety of the battery system. These results will be used in future activities aimed at larger vehicles (scale effect).

2. MATERIAL AND METHODS

The nail penetration test is an industry-standard method for simulating an Internal Short Circuit in a cell (ISC). It is performed by using an electrically conductive pointed rod to pierce the battery perpendicularly to the battery. Typical nail diameters range from 3 mm to 8 mm, depending on the standard considered, and the penetration speed is typically 8 cm/s [9–13]. The test is considered successful if the cell does not explode or burn. Several variables can be considered such as: State Of Charge (SOC), chemistry, geometry, nail speed, penetration depth, position, nail material, nail diameter, and cell orientation. Some of the previous variables can affect the fire release, as demonstrated by [14]. The nail penetration tests have been performed using the Thermal Hazard Technology EV+ Accelerating Rate Calorimeter (ARC, THT, UK) provided with the auxiliary option called Nail Penetration and Crush Option (NPCO) present at the Energy Center facility.

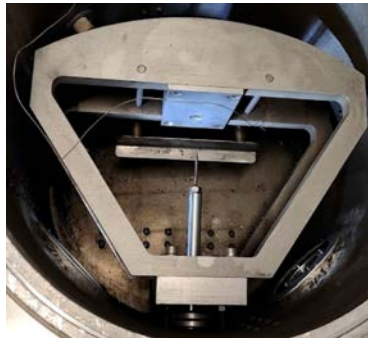


Figure 1: NPCO at the Energy Center.

Table 1 shows the main properties of the INR18650-29E battery model tested. It is produced by Samsung SDI Co., Ltd.

Table 1: Details for the LIB 18650 tested

Specification	INR18650-29E[15]
Type (-)	Cylindrical
Diameter (mm)	18
Height (mm)	65
Nominal capacity (mAh)	2850
Nominal voltage (V)	3.65
Charging voltage (V)	4.2 +/- 0.05
Charging method (-)	CC-CV
Charging current (mA)	1375 (Standard)
Charging time (hours)	3
Discharge Cut-off Voltage (V)	2.5
Cell weight (g)	48
Operating temperature (°C)	25 °C

The cathode is made of Nickel Manganese Cobalt (NMC) coated onto an aluminium current collector, while the anode is made of graphite. The electrolyte is liquid and based on LiPF₆ and organic solvents. The CC-CV method was used to reach the SOC 100%. The battery is positioned in the holder to ensure the penetration in the centre of the battery. All tests have been performed using an AISI 316 stainless steel nail, with a diameter equal to 4 mm that penetrates the battery at a nail speed equal to 80 mm/s starting 35 mm from the battery. The battery is kept in the ARC until a small enough temperature is reached (Cool temperature equal to 35 °C), after which it is possible to open the calorimeter with precaution. The test is repeated twice for each battery. IR camera (THT, UK) is used to monitor the temperature distribution, while a k-type thermocouple (Tersid srl, Italy) is placed near the centre of the battery. A pressure transducer is mounted in the calorimeter with a pressure range of 0 – 200 bar and a resolution of 0.005 bar, precision of 0.02% and accuracy of 0.05% [16]. Gas exhausts are measured in the canister using the Testo 330 (Testo SE & Co. KGaA, Germany) to monitor the CO production (CO 0 – 10000 ppm(v), +/- for 5% 200 – 2000 ppm(v) and +/- 10% for 2000 – 10000 ppm(v) with 4 s of reaction time).

The model has been implemented into COMSOL Multiphysics® software v6.0 using the Battery Design Module functionalities coupled to the Heat Transfer in Solids interface. The model consists of a coupled p2D electrochemical-3D thermal.

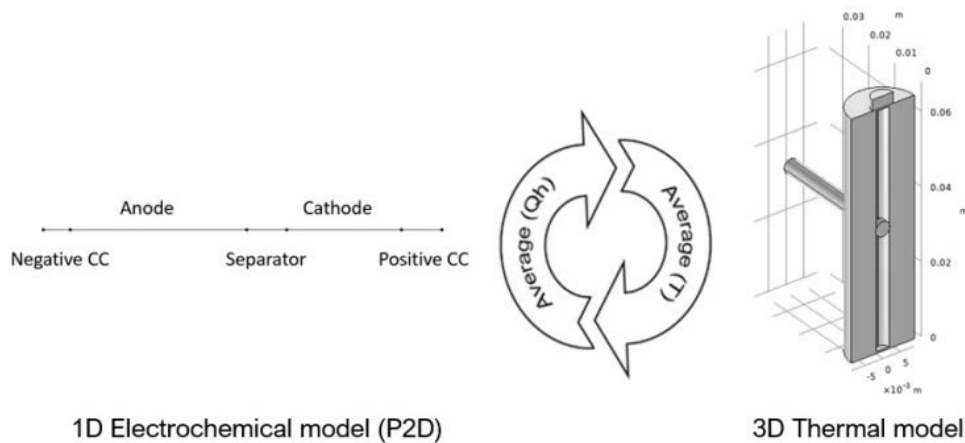


Figure 2: Model structure and schematic representation.

A 1D component is used to solve the P2D model, while a 3D component solves the thermal equations. This separation between electrochemical and thermal equations is carried out to obtain faster computational times with lower CPU requirements concerning a fully 3D electrochemical-thermal model.

3. RESULTS AND DISCUSSION

3.1. Experimental test abuses

During the tests, the temperature and pressure of the sample and their rate of change are recorded over time. The data obtained for all tests are analysed and compared. The test starting temperature is set at 20 °C. The maximum temperatures reached are 469 °C and 584.3 °C for Test3_29 and Test4_29, respectively. The graphs show a sharp increase after about one second, followed by a rapid decrease until a plateau is reached. Test 3_29E and Test 4_29E (in blue and orange in the graph, respectively) have a very similar shape: the temperature rises sharply, then appears to slow down but then rises rapidly again reaching its peak in about 1 minute.

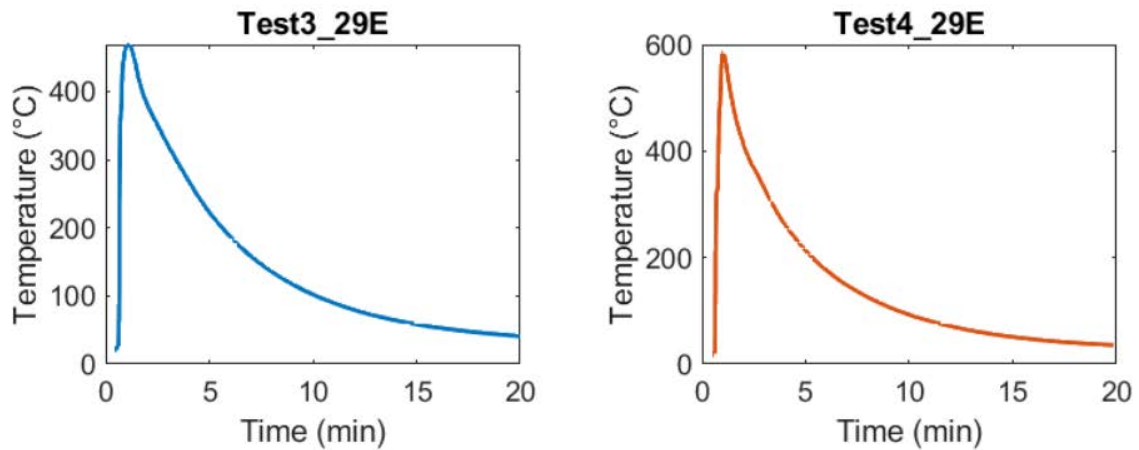


Figure 3: Battery 29E results in terms of temperature.

The IR camera was used to see the TR evolution in time (5 s per frame), see the following figure. It is possible to see the nail penetrated and the instantaneous increase of the temperature. Being an IR camera, it is only possible to appreciate the qualitative increase in thermal energy of a rapid process. This aspect is important to emphasize the need to improve data acquisition time.

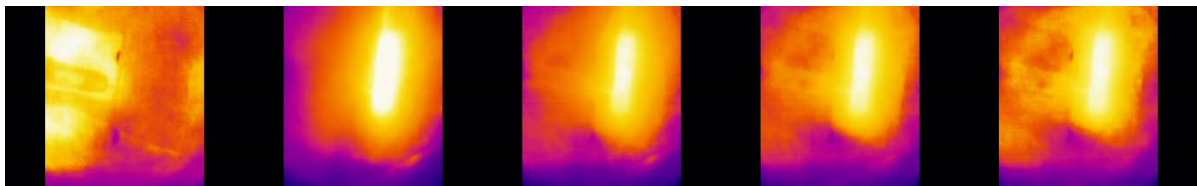


Figure 4: battery 29E IR camera, TR evolution, each frame was recorded every 5s.

The abuse test led to the TR being observed, causing the battery to explode, see the figure below.



Figure 5: battery 29E after the nail penetration test.

The tests reported above show rapid changes in pressure, followed by an almost stable state condition. The highest-pressure value recorded was 3.57 bar.

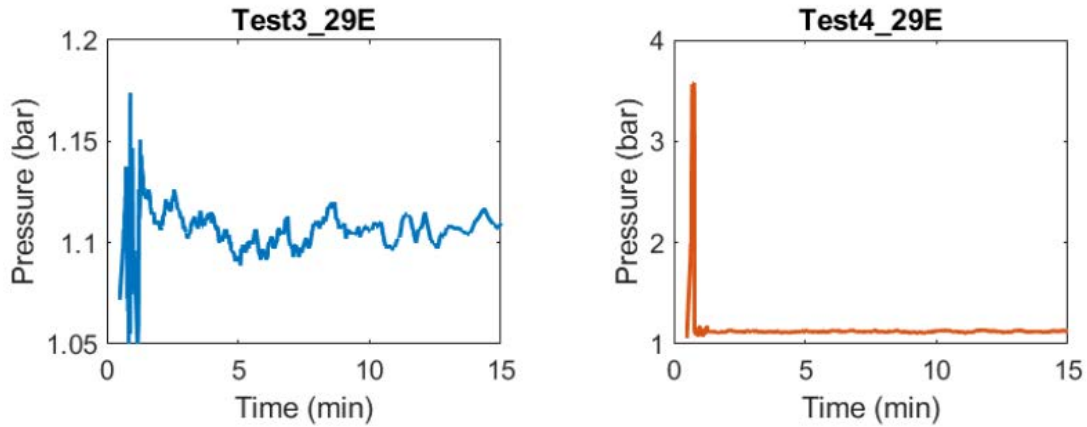


Figure 6: Battery 29E results in terms of pressure.

The following figure shows the trend of CO emitted during the TR. A maximum CO value of about 4000 ppm(v) was reached, and similar results have been published in the literature [17]. The development of CO is related to the establishment of incomplete combustion as a result of thermal runaway of the battery.

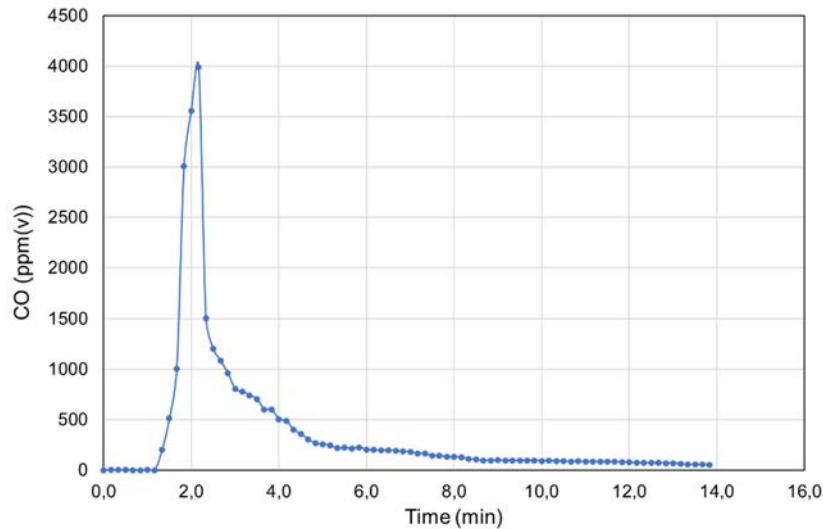


Figure 7: Battery 29E results in terms of CO release (Test3_29E).

3.2. Model results

The model implemented on COMSOL consists of two components: a 1D model that aims to simulate the electrochemical behaviour of the battery through a p2D model, while the 3D model simulates heat transfer only. To implement the TR phenomenon the parameters used are reported in the following table.

Table 2: Exothermic reaction parameters

Reaction	H (J/Kg)	W (Kg/m ³)	A (s ⁻¹)	E (J mol ⁻¹)
SEI decomposition	2.57×10^5	610	1.14×10^{14}	1.35×10^5
Anode-Electrolyte	1.714×10^6	610	7.18×10^{13}	1.35×10^5
Cathode-Electrolyte	3.14×10^5	1120	6.66×10^{13}	1.41×10^5
Electrolyte decomposition	1.55×10^5	406.9	5.12×10^{15}	1.75×10^5

The nonlocal coupling operator was used to couple the 1D electrochemical model and the 3D model. As shown in the figure below, the temperature starts to rise around the nail, generating a hot spot. After about 30 s, the temperature reached is homogeneous.

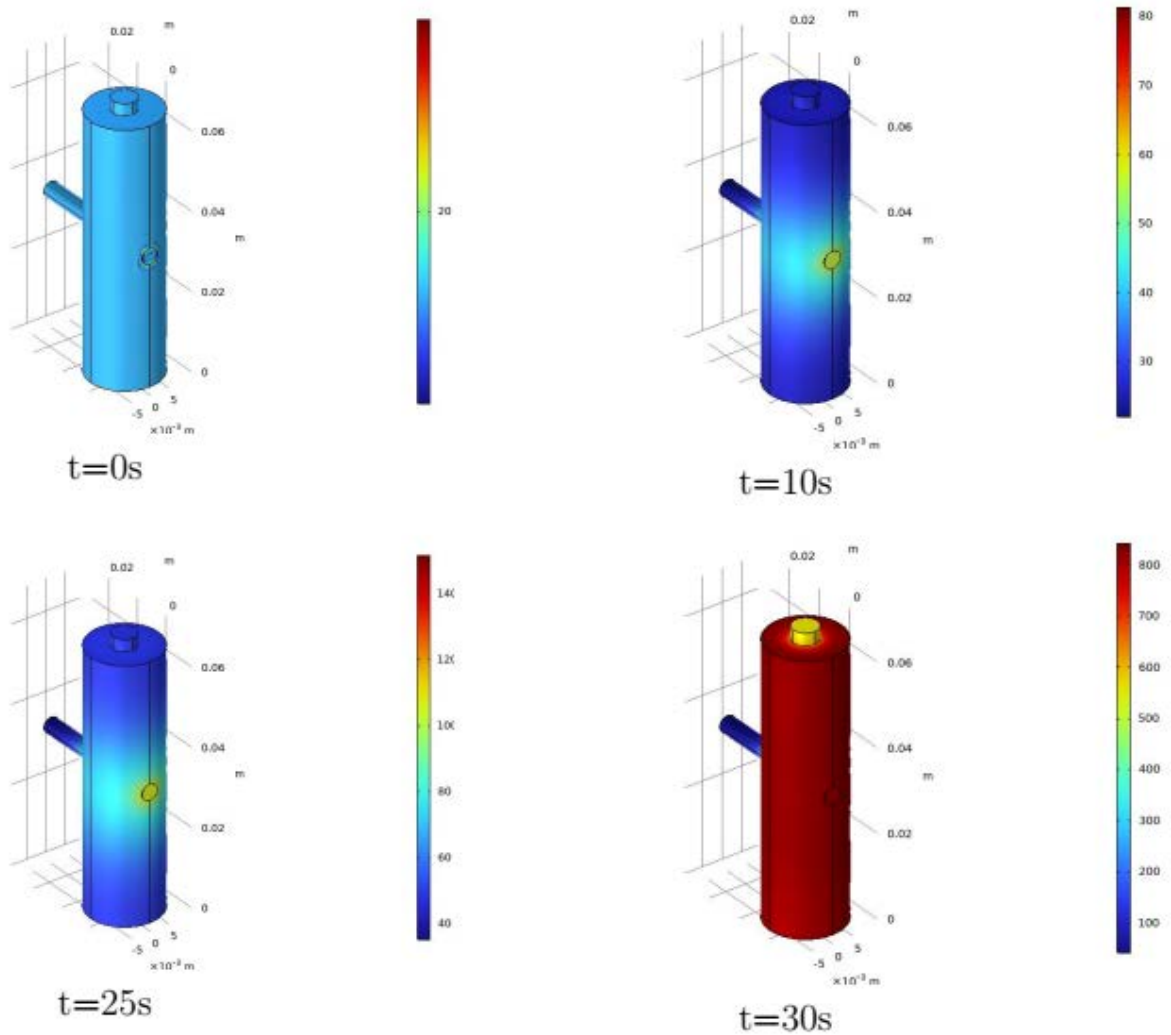


Figure 8: Nail penetration test modelled with Comsol (Test3_29E).

The maximum temperature monitored during the reported experimental tests is approximately over 600 °C, while the maximum temperature reached by the model is just over 700 °C. The experimental variability of the maximum temperature value is very high. An increase in the number of samples tested could improve the validity of the data by improving the validation of the model.

At this point considering the structure of the battery and the data sheet provided by the manufacturer [15], it is possible to assess the power generated during mechanical abuse, by following these equations:

$$Q_{heat} = \rho \cdot C_p \cdot \frac{\partial T}{\partial t} \text{ (eq.1)}$$

$$\rho_{batt} = \frac{\sum L_i \rho_i}{\sum L_i} \text{ (eq.2)}$$

$$C_{p, batt} = \frac{\sum L_i C_{p, i}}{\sum L_i} \text{ (eq.3)}$$

Where: ρ is the weighted density (kg/m^3) for the LIB material, C_p is the heat capacity (kJ/K), $\partial T/\partial t$ is the thermal gradient recorded during the experimental test and L_i is the i -layer considered.

The results show that the single battery with a nominal capacity of 2.85 Ah can produce up to a maximum heat output of 300 W during the nail test. This value is not an outlier because of the rapid reaction of the TR, but it will be necessary to refine the collection of times to seconds as an order of magnitude to collect more data.

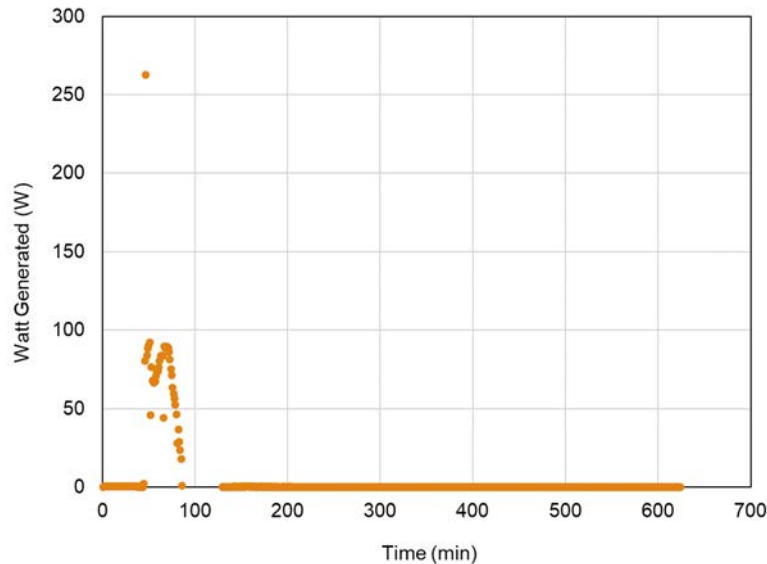


Figure 9: Thermal power generated during the nail test.

4. CONCLUSION

The nail test was investigated as the mechanical abuse condition for a commercial Lithium ion cell. The experimental results were used to monitor the temperature, pressure and the gas exhausts released. The maximum temperature recorded experimentally vary from 400 to above 600 °C, while the model implemented show a maximum temperature roughly around 700 °C. The experimentally recorded maximum temperature ranges from 400 to over 600 °C, while the implemented model shows a maximum temperature approximately around 700 °C. The experimental activity should be improved by increasing the number of trials to reduce the temperature variability. Regarding the SOC effect, the higher the SOC, the greater the battery response, in terms of peak temperature. In terms of nail speed, a higher nail speed generally means a higher temperature. Also, in terms of voltage, the decrease to zero occurs faster with a higher nail speed. Experimental results obtained at a preliminary level will be used to validate models closer to real conditions. Gas analysis to detect the main toxic compounds (HF, HCl, HCN etc.) will have to be implemented. These results will be used to assess performance under battery pack abuse conditions, thus scaling up to higher electrical capacity sizes.

5. REFERENCES

- [1] S. S. Rangarajan, S.P. Sunddararaj, A.V.V. Sudhakar, C.K. Shiva, U. Subramaniam, E.R. Collins, T. Senjyu, Lithium-Ion Batteries—The Crux of Electric Vehicles with Opportunities and Challenges, *Clean Technologies*. 4 (2022) 908–930. <https://doi.org/10.3390/cleantechnol4040056>.
- [2] E. Standards, BS EN IEC 61851-1:2019 Electric vehicle conductive charging system General requirements, <https://www.en-standard.eu>. (n.d.). <https://www.en-standard.eu/bs-en-iec-61851-1-2019-electric-vehicle-conductive-charging-system-general-requirements/> (accessed November 16, 2023).
- [3] R.T. Yadlapalli, A. Kotapati, R. Kandipati, C.S. Koritala, A review on energy efficient technologies for electric vehicle applications, *Journal of Energy Storage*. 50 (2022) 104212. <https://doi.org/10.1016/j.est.2022.104212>.
- [4] Trends in batteries – Global EV Outlook 2023 – Analysis, IEA. (n.d.). <https://www.iea.org/reports/global-ev-outlook-2023/trends-in-batteries> (accessed November 16, 2023).
- [5] P.A. Christensen, Z. Milojevic, M.S. Wise, M. Ahmeid, P.S. Attidekou, W. Mroziak, N.A. Dickmann, F. Restuccia, S.M. Lambert, P.K. Das, Thermal and mechanical abuse of electric vehicle pouch cell modules, *Applied Thermal Engineering*. 189 (2021) 116623. <https://doi.org/10.1016/j.applthermaleng.2021.116623>.
- [6] C.F. Larsson, Lithium-ion Battery Safety - Assessment by Abuse Testing, Fluoride Gas Emissions and Fire Propagation, Chalmers University of Technology, 2017. <https://research.chalmers.se/en/publication/251352> (accessed October 3, 2022).
- [7] F. Larsson, P. Andersson, B.-E. Mellander, Lithium-Ion Battery Aspects on Fires in Electrified Vehicles on the Basis of Experimental Abuse Tests, *Batteries*. 2 (2016) 9. <https://doi.org/10.3390/batteries2020009>.
- [8] X. Feng, M. Ouyang, X. Liu, L. Lu, Y. Xia, X. He, Thermal runaway mechanism of lithium ion battery for electric vehicles: A review, *Energy Storage Materials*. 10 (2018) 246–267. <https://doi.org/10.1016/j.ensm.2017.05.013>.
- [9] B. Mao, H. Chen, Z. Cui, T. Wu, Q. Wang, Failure mechanism of the lithium ion battery during nail penetration, *International Journal of Heat and Mass Transfer*. 122 (2018) 1103–1115. <https://doi.org/10.1016/j.ijheatmasstransfer.2018.02.036>.
- [10] A.V. Shelke, J.E.H. Buston, J. Gill, D. Howard, K.C. Abbott, S.L. Goddard, E. Read, G.E. Howard, A. Abaza, B. Cooper, J.X. Wen, Characterizing and predicting 21700 NMC lithium-ion battery thermal runaway induced by nail penetration, *Applied Thermal Engineering*. 209 (2022) 118278. <https://doi.org/10.1016/j.applthermaleng.2022.118278>.
- [11] X. Gao, Y. Jia, W. Lu, Q. Wu, X. Huang, J. Xu, Mechanistic understanding of reproducibility in nail penetration tests, *Cell Reports Physical Science*. 4 (2023) 101542. <https://doi.org/10.1016/j.xcrp.2023.101542>.
- [12] N. Mao, S. Gadkari, Z. Wang, T. Zhang, J. Bai, Q. Cai, A comparative analysis of lithium-ion batteries with different cathodes under overheating and nail penetration conditions, *Energy*. 278 (2023) 128027. <https://doi.org/10.1016/j.energy.2023.128027>.
- [13] J. Diekmann, S. Doose, S. Weber, S. Münch, W. Haselrieder, A. Kwade, Development of a New Procedure for Nail Penetration of Lithium-Ion Cells to Obtain Meaningful and Reproducible Results, *J. Electrochem. Soc.* 167 (2020) 090504. <https://doi.org/10.1149/1945-7111/ab78ff>.
- [14] Z. Huang, H. Li, W. Mei, C. Zhao, J. Sun, Q. Wang, Thermal Runaway Behavior of Lithium Iron Phosphate Battery During Penetration, *Fire Technol.* 56 (2020) 2405–2426. <https://doi.org/10.1007/s10694-020-00967-1>.
- [15] INR18650-29E datasheet, (n.d.). <https://datasheetspdf.com/pdf-file/821874/Samsung/INR18650-29E/1> (accessed November 21, 2023).
- [16] EV+ Accelerating Rate Calorimeter | Thermal Hazard Technology, (n.d.). <https://www.thermalhazardtechnology.com/battery-products/ev-plus-accelerating-rate-calorimeter> (accessed November 22, 2023).
- [17] P. Ribière, S. Grugeon, M. Morcrette, S. Boyanov, S. Laruelle, G. Marlair, Investigation on the fire-induced hazards of Li-ion battery cells by fire calorimetry, *Energy Environ. Sci.* 5 (2012) 5271–5280. <https://doi.org/10.1039/C1EE02218K>.

PARTICLE CONCENTRATION LEVELS IN A SUBWAY STATION - THE EFFECTS OF VARIOUS LOCATIONS AND DIAMETERS OF RELIEF SHAFTS IN TUNNELS

Omid Abouali, Erik Östblom, Per Sahlin
Equa Simulation AB, SE

DOI 10.3217/978-3-85125-996-4-23 (CC BY-NC 4.0)

This CC license does not apply to third party material and content noted otherwise.

ABSTRACT

In this article, we investigate how ventilation shaft diameter and placement in a subway tunnel can influence the concentration of particulate matter (PM) in stations. The trains' rolling and braking systems have been considered the particles' source. The stations have two large escalators, and their doors are open. The airflow in the studied systems is driven exclusively by the piston effect of the moving trains. The IDA Tunnel version 2 software package has been utilized for the simulations.

The results indicate significant fluctuations in PM levels on subway platforms. The average PM concentration on a platform associated with single-track tunnels is almost 5 percent lower than on a platform connected to double-track tunnels, considering similar headway and relief shaft geometry. In the case of single-track tunnels, the shaft location plays a less critical role, while the impact of shaft diameter is more pronounced. For double-track tunnels, the shaft location becomes more crucial. A single relief shaft placed near the stations primarily increases the PM level on the platform, making a shaft location at the tunnel center preferable. The variation in PM levels on the platform for single- and double-track tunnels is approximately 13 percent across shaft locations and cross-sectional areas.

Keywords: Tunnel ventilation- Particulate matter- Subway station, Relief shaft

1. INTRODUCTION

Poor air quality has become a major issue of modern life. In Europe today, air pollution poses a higher health risk than tobacco smoking. Problems with air quality in subway systems have received minimal attention for many years. However, recent studies indicate poor air quality inside these systems, with higher PM concentrations than in the streets above them. The generation and distribution of hazardous particles inside the subway system can severely affect the health of vulnerable groups such as children or older people. Subway particles can be eight times more genotoxic and four times more likely to cause oxidative stress in the lung cells than particles in a busy urban street [1].

Raut et al., 2009 reported that PM₁₀ and PM_{2.5} concentrations in subway stations in Paris were 5–30 times higher than the outdoor air [2]. Johansson and Johansson's measurements at an underground station in Stockholm revealed that concentrations of PM₁₀ and PM_{2.5} were 5 and 10 times higher, respectively, than levels observed in one of the busiest streets in central Stockholm [3]. Martins et al. (2015) demonstrated that average PM_{2.5} concentrations in a subway station in Barcelona exceed those in the surrounding outdoor air [4]. Tu et al. investigated the impact of train type on airborne particle concentrations by analyzing field measurements from six underground metro platforms in Stockholm between 2016 and 2020 [5]. The predominant element in subway particles is iron [6], with brake pads, catenary systems, and abrasion of rail tracks and wheels identified as the primary sources [7]. Three distinct particle size categories exist, with a peak diameter of approximately 100 nm for ultra-fine particles, 0.35 µm for fine particles, and 3–6 µm for coarse particles [8]. In a study closely

related to the present paper, Qu et al. (2022) conducted recent field measurements in two stations with Platform Screen Doors (PSDs) from two different subway lines and four air shafts in their connecting tunnels in China [9]. They assessed the effective ventilation and particulate matter discharge efficiency of these air shafts.

Most prior numerical studies have focused on assessing the impact of ventilation systems on thermal comfort and smoke removal. The flow field within a subway system is inherently complex, influenced by both the movement of trains (piston effect) and, if present, the ventilation system [10]. There are very few 3D numerical simulations specifically examining particle transport within subway stations induced by the piston effect. Izadi et al. (2021) investigated the wear particle dispersion due to the train piston effect representing the first 3D numerical investigation into particle distribution due to train braking within a subway system [11]. Another recent study explored the influence of ventilation systems, both with and without under-platform exhaust, on the concentration of braking micro-particles within the subway system [12]. Despite the detailed 3D Computational Fluid Dynamics (CFD) simulations providing valuable information, their coverage is constrained to a specific time interval, typically representing a train's movement between two stations. This limitation stems from the considerable computational cost and time associated with 3D CFD simulations of train motion using dynamic mesh techniques. As previously mentioned, PM measurements within subway stations in Sweden and globally underscore the significance of this issue, rendering it a major concern. Consequently, reducing particle concentrations has become a crucial objective in the design of recently developed subway lines in Sweden. To address this concern and enable the study of particle concentration over a realistic time duration in a subway line, this article employs a 1D numerical simulation. Using the IDA Tunnel version 2 software package, the study investigates how the diameter and placement of ventilation shafts in a tunnel impact PM concentration in stations. Both typical types of single and double-track tunnels have been studied.

2. SIMULATION MODEL

2.1. Model description

Two single- and double-track tunnel models (Figures 1 and 2) are developed and studied here. Both consist of four 40-meter-deep stations with platforms measuring 145 m x 15 m x 5 m. Each platform includes two symmetrical escalators (70 m length, 15 m² cross-section) to the ground level, with open doors. The tunnels are 2 km in both models. The double-track model comprises five tunnels (40 m² cross-section), connecting stations and the portals at the ground level. The single-track model includes ten 2 km tunnels with a 25 m² cross-section. In both models, each tunnel is equipped with a relief shaft. The shafts have a height of 40 meters. The cross-sectional area of all shafts is 10 m². These shafts are positioned at the tunnel center, except for the tunnels between the second and third stations, where a parametric study introduces variations. In this section, the placement of the shaft shifts from a short distance to the neighboring stations (15 m) to the center of the tunnel. The cross-sectional area of the shaft changes, ranging from 5 to 20 m².

2.2. Boundary conditions and train data

Mass, momentum, energy, and particle mass conservation equations have been solved by the IDA Tunnel version 2 software package [13]. Standard atmospheric pressure and the ambient temperature of 10°C were assumed for portals and all shafts' grills. The train's relevant parameters include a length of 140 m, a front area of 9 m², a perimeter of the front area at 13 m, a nose drag coefficient of 0.5, and a skin friction coefficient of 0.012 aligning closely with the geometrical data of the C20 train. The total mass of the train, including occupants, is 306

tons. The particle source is the train's rolling and braking systems. The mass flow rate of the emitted particles from the train to the tunnel and platform depends on the train velocity, braking, and traction force. Two coefficients, k_b and k_r (g/kWh) play a crucial role in determining the quantity of released particles, and they can be calibrated individually for each metro line. In this study, the values $k_b = 0.234$ g/kWh and $k_r = 0.378$ g/kWh were assumed to achieve an almost equal share of particle concentration on the platform to see the effects of particles released from both braking and rolling systems. The particles corresponding to braking are released only during effective braking. The train headway in each route is 5 minutes, but stochastic delays were introduced to train departures to disrupt perfect adherence to timetables. The maximum velocity of the train in the tunnels is 72 km/h, with acceleration and deceleration rates of 1 and -1 m/s², respectively. The number of trains passage per hour is 24 on both routes.

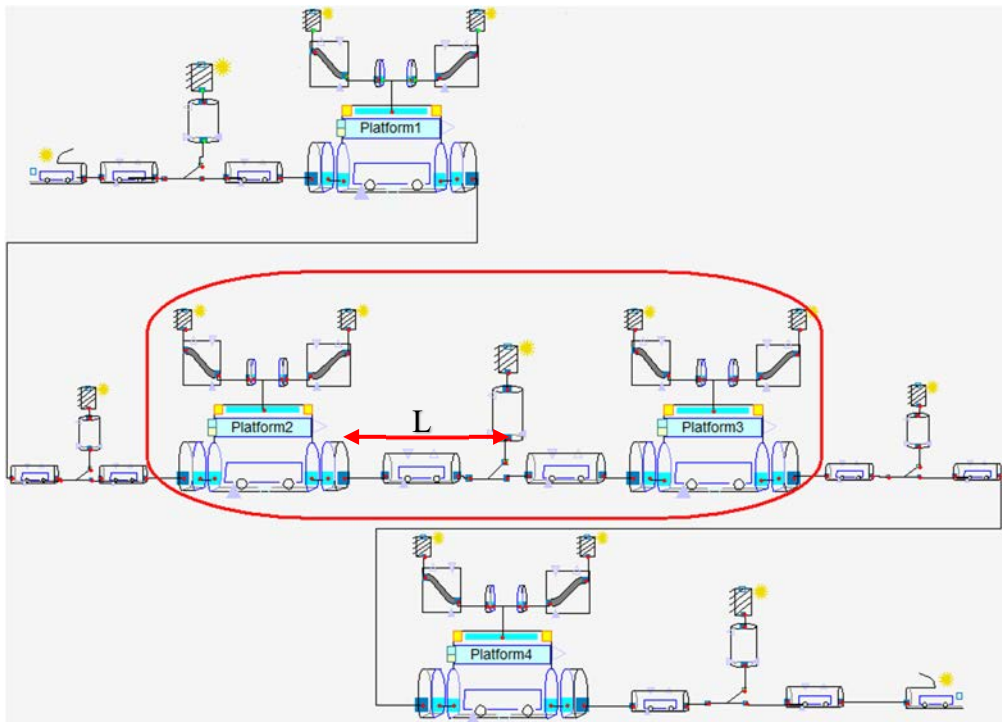


Figure 1: Model for simple metro line with double track tunnels

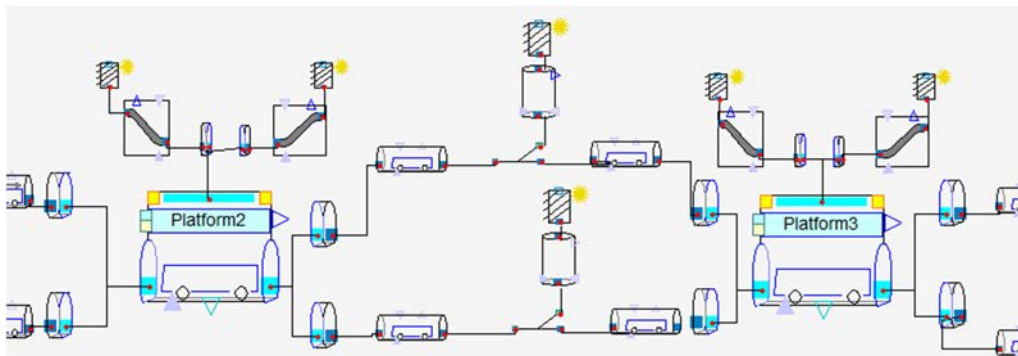


Figure 2: Model for simple metro line with single-track tunnels
(Only the second and third stations with connecting tunnels are shown)

3. RESULTS

Due to the stochastic nature of train departures and the varying airflow caused by the train piston effect at the platform, particle concentrations fluctuate significantly on the platforms. Fig.3 shows a sample of the results for the platform in station 3 for the double-track tunnel

model. The simulation is performed for 6 hours. Since the simulation commences with zero concentration in the tunnels and stations, it takes nearly two hours to reach a stationary condition in the platform PM level. The graph also displays a moving average with a time scale of one hour. The average PM level for the final four hours of the simulation is calculated and serves as the basis for comparing the different scenarios studied. Testing revealed that extending the time duration did not significantly alter the statistical average and the trend of the results.

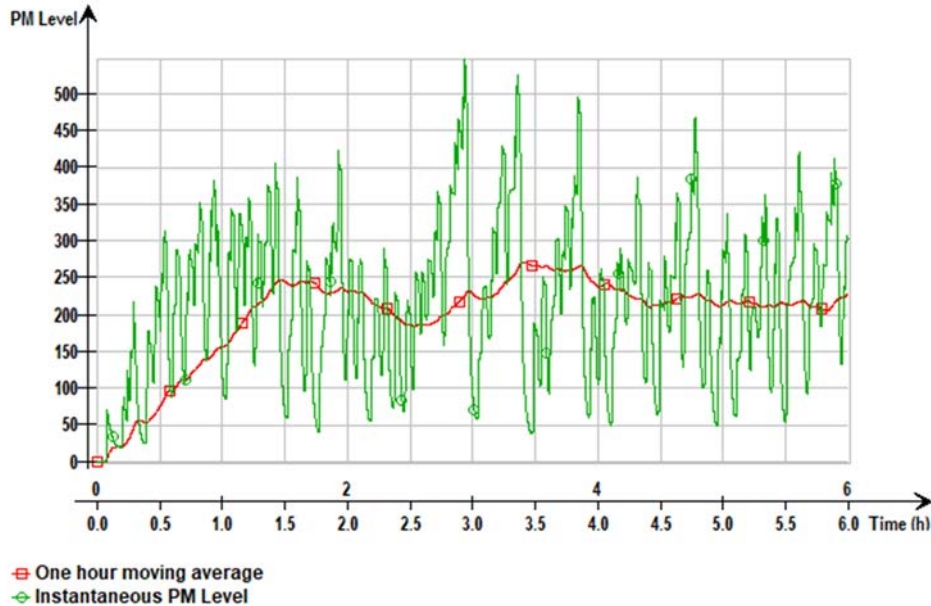


Figure 3: A sample of variation of PM level in the platform for one of the studied cases

The parametric run module of IDA Tunnel 2 is used to study the effects of shaft placement and diameter on the level of particle concentration in the platforms. In this module, the range of the parameters and the number of data points in each range are defined, and the software package performs the simulation for all cases defined in this parametric study.

The shaft cross-sectional area has been varied within the 5-20 m² range. Furthermore, the shaft placement shifts from 15 meters from the train departure side of the stations to an equivalent distance on the train arrival side of the next station. Changes in the shaft cross-sectional area and placement necessitate adjustments in corresponding parameters, like shaft diameter or tunnel segment length, which are executed using IDA Tunnel2's graphical script feature.

In presenting the results, the focus has been on the platforms of stations 2 and 3, as well as the relief shafts in connecting tunnels (Figures 1 and 2). While a particular shaft location may reduce the particulate matter (PM) level on one platform, it may increase it at the neighboring station; thus, this study compares the average PM levels at these two stations across various scenarios.

The presentation and discussion of results begin with the double-track tunnel model. The data in Table 1 have been arranged in ascending order from the minimum to the maximum PM level on the platforms. Table 1 provides a detailed breakdown of exhaust and intake air through the relief shaft, along with the PM mass entering and exiting the shaft, and the PM mass exhausted from the station escalators.

Generally, a shaft farther from the adjacent stations correlates with a lower platform PM level. The results highlight that shaft placement significantly influences PM levels, outweighing the impact of shaft size. Even with the smallest studied cross-sectional area of the shaft (5 m²), a low particle level is achieved when it is positioned at the tunnel center. In this scenario, the

particle level is only 3 percent higher than when the shaft size is 20 m². Conversely, a shaft close to the station can elevate the particle level by more than 13 percent compared to the central shaft position. Interestingly, increasing the shaft's cross-sectional area can further elevate the PM level on the platforms when the shaft is placed near the stations.

Qu et al. [9] introduced a PM discharge efficiency for the air shaft, denoted as $\eta = (M_{in} - M_{out}) / M_{in}$. In this equation, M_{out} represents the PM mass expelled through the outer opening of the air shaft connected to the grill during the exhaust process per train run, and M_{in} is the intake PM mass from the tunnel through the inner opening of the air shaft connected to the tunnel during the exhaust per train run. However, this definition appears problematic, as it yields 100 percent efficiency when no particle mass is exhausted from the shaft grill. In this study, we propose an alternative definition for the PM discharge efficiency of the air shaft.

$$\eta = M_{exh,sh} / M_{int,sh}$$

where $M_{exh,sh}$ and $M_{int,sh}$ mirror the concepts of M_{ou} and M_{int} in Qu et al.'s work [9], but are considered over an extended time duration (for instance, a couple of hours, where the PM mass existing in the relief shaft at a given moment becomes negligible compared to the total exhaust mass from the shaft). Additionally, we introduce the exhaust/suction air volume ratio, denoted as Q_{exh} / Q_{suc} . This ratio reflects the capacity of the shaft to discharge polluted air relative to its capacity to intake air from the outside. Table 1 presents the PM discharge efficiency and the exhaust/suction air volume ratio for various studied cases.

The results show a strong inverse correlation between the PM level on the platforms and both the exhaust/suction ratio, and the PM mass expelled from the shaft. However, there is no discernible correlation between the shaft's PM discharge efficiency and the platform's PM level. Notably, both the maximum and minimum cases of PM level in the platform have the same PM discharge efficiency. Therefore, this efficiency alone is insufficient to define the PM level conditions on the platforms. One important physical aspect of the relief shaft that one must know is the PM that remained in the shaft at the last moment of the airflow exhaust. This PM returns to the tunnel during the suction phase of the outside air. This return of PM occurs with each train run, and the difference between the first and second columns for the PM mass exhaust in Table 1 approximates the total mass of PM returning to the tunnel from the relief shaft over four hours. The proportion of returned mass relative to the total exhaust from the tunnel to the shaft varies between 12-20 percent for different studied cases.

The same analysis was conducted for the single-track tunnel model, with similar ranges considered for shaft placement and diameter as in the double-track tunnels. The results are presented in Table 2. Notably, the PM level on the platforms is nearly five percent lower for the single-track model. An important distinction arises between the single- and double-track models: for the single-track model, the shaft cross-section is considerably more influential than the shaft placement (excluding cases with very close proximity to the downstream station). As evident in Table 2, the platforms exhibit the lowest PM levels when the shaft has the maximum cross-sectional area. Neither the PM discharge efficiency nor the exhaust/suction air ratio of the relief shaft correlates with the PM level on the platforms. A crucial observation is that a relief shaft positioned near the train-arriving side of the station, a configuration typical in existing metro lines, exhibits poor overall performance. The PM level on the platform for this case ($L=1985$ m) is higher than in all other scenarios. The PM mass expelled from the relief shaft is higher than in other cases, but this doesn't translate to a lower PM level on the platform. The primary reason is that the exhaust PM mass from the escalators of the stations is significantly lower in this case. This aligns with the logical consequence of the piston effect of the train entering the station being less pronounced when the relief shaft is placed directly on the train-arriving side of the station. In simpler terms, fewer particles

enter the platform, however, the low exhaust airflow through the station's escalators results in a higher PM concentration on the platforms. Additionally, the volume of fresh air intake to the tunnel from the shaft is significantly reduced when the relief shaft is placed at the train-arriving side of the station. It's crucial to emphasize that the discussion here centers around the PM level perspective.

Table 1: Results for double-track tunnel model. The results are summed or averaged for the last four hours of each simulation.

L (m)	A _{sh} (m ²)	PM Platform (µg/m ³)	The volume of air through the shaft (m ³)		PM mass exhaust from (µg)			Shaft PM discharge efficiency	Exh/Suc air ratio
			discharge	intake	Shaft to outside	Tunnel to shaft	Station to outside		
1000	20	234,6	309330	2,97E5	4,09E7	4,95E7	3,83E8	0,83	1,04
1000	15	235,6	270480	2,65E5	3,88E7	4,59E7	3,84E8	0,84	1,02
1000	10	237,4	212658	2,15E5	3,62E7	4,18E7	3,87E8	0,86	0,99
1500	20	239,8	300897	2,90E5	4,50E7	5,37E7	3,79E8	0,84	1,04
1500	15	239,9	259780	2,54E5	4,19E7	4,95E7	3,81E8	0,85	1,02
1500	10	240,8	201128	2,02E5	3,74E7	4,38E7	3,85E8	0,85	1,00
1000	5	241,0	125736	1,31E5	3,15E7	3,57E7	3,95E8	0,88	0,96
500	10	241,2	200452	1,91E5	3,78E7	4,38E7	3,85E8	0,86	1,05
500	15	241,5	260719	2,41E5	4,21E7	4,92E7	3,79E8	0,86	1,08
500	20	242,0	302221	2,77E5	4,45E7	5,26E7	3,76E8	0,85	1,09
500	5	243,2	115002	1,15E5	2,99E7	3,44E7	3,96E8	0,87	1,00
1500	5	243,5	117706	1,21E5	2,99E7	3,42E7	3,95E8	0,87	0,97
15	5	253,1	73915	9,63E4	1,46E7	1,71E7	4,04E8	0,85	0,77
15	10	253,4	135540	1,73E5	2,33E7	2,79E7	3,88E8	0,84	0,78
1985	5	255,0	76369	9,75E4	1,59E7	1,83E7	4,06E8	0,87	0,78
1985	10	256,6	139633	1,76E5	2,52E7	2,95E7	3,91E8	0,85	0,79
15	15	257,1	182838	2,36E5	2,80E7	3,40E7	3,81E8	0,82	0,77
1985	15	259,4	187887	2,42E5	3,00E7	3,57E7	3,83E8	0,84	0,78
15	20	262,2	218732	2,89E5	3,04E7	3,77E7	3,78E8	0,81	0,76
1985	20	263,8	224730	2,97E5	3,21E7	3,88E7	3,80E8	0,83	0,76

In the single-track tunnel model, the airflow pattern is easily predictable since the trains move only in one direction. As the cross-sectional area of the shaft increases, both the intake and exhaust flow through the shaft also increase. With the increase of the shaft distance from the train-leaving side of the station, the intake airflow decreases, and the exhaust airflow increases. The minimum exhaust/suction air ratio occurs when the shaft is at the train-leaving side of the station. This ratio then increases as the shaft is positioned further from this station and reaches its maximum when the shaft is placed close to the train-arriving side of the next station. The proportion of the exhaust PM from the tunnel to the shaft that returns to the tunnel during the suction phase is notably higher than in double-track tunnels, varying between 13 to 35 percent for different studied cases.

Table 2: Results for single-track tunnel model. The results are summed or averaged for the last four hours of each simulation.

L (m)	A _{sh} (m ²)	PM Platform (µg/m ³)	The volume of air through the shaft (m ³)		PM mass exhaust from (µg)			Shaft PM discharge efficiency	Exh/Suc air ratio
			discharge	Intake	Shaft to outside	Tunnel to shaft	Station to outside		
15	20	223,8	7,32E4	4,40E5	1,09E7	1,60E7	4,28E8	0,68	0,17
1000	20	226,6	1,78E5	2,29E5	3,33E7	4,28E7	3,84E8	0,78	0,78
500	20	227,8	1,39E5	3,12E5	2,23E7	3,16E7	4,00E8	0,70	0,44
1000	15	227,9	1,63E5	2,14E5	3,23E7	3,95E7	3,83E8	0,82	0,76
15	15	229,8	6,37E4	3,73E5	1,02E7	1,43E7	4,15E8	0,72	0,17
500	15	229,8	1,28E5	2,82E5	2,20E7	2,92E7	3,95E8	0,75	0,45
1000	10	231,8	1,37E5	1,86E5	2,85E7	3,35E7	3,80E8	0,85	0,74
1500	20	233,9	2,00E5	1,42E5	4,15E7	5,16E7	3,54E8	0,80	1,41
1500	15	234,6	1,80E5	1,36E5	3,86E7	4,65E7	3,57E8	0,83	1,32
500	10	234,7	1,08E5	2,33E5	1,99E7	2,48E7	3,88E8	0,80	0,46
1500	10	237,1	1,46E5	1,23E5	3,27E7	3,82E7	3,61E8	0,86	1,19
15	10	237,7	4,93E4	2,84E5	8,56E6	1,15E7	3,98E8	0,75	0,17
1000	5	241,9	8,70E4	1,25E5	1,93E7	2,19E7	3,73E8	0,88	0,69
1985	20	242,1	2,34E5	9,16E4	5,58E7	6,58E7	3,15E8	0,85	2,55
1985	15	244,2	1,95E5	8,28E4	4,74E7	5,52E7	3,23E8	0,86	2,35
500	5	244,6	6,85E4	1,50E5	1,35E7	1,62E7	3,77E8	0,84	0,46
1500	5	245,2	9,02E4	8,70E4	2,12E7	2,42E7	3,63E8	0,88	1,04
1985	10	247,6	1,44E5	6,93E4	3,58E7	4,13E7	3,33E8	0,87	2,08
15	5	248,2	2,78E4	1,66E5	5,21E6	6,80E6	3,80E8	0,77	0,17
1985	5	253,0	7,84E4	4,59E4	1,99E7	2,29E7	3,46E8	0,87	1,71

4. SUMMARY AND CONCLUSION

The impact of the placement and cross-sectional area of relief shafts on particle concentration in the platforms of two subway line models has been examined. Both single- and double-track tunnels were investigated, considering a naturally driven flow resulting from the trains' piston effects. Each station has two large escalators with their doors kept open. The sources of the particles under study were the rolling and braking systems of the trains, and particle levels were compared between the two models.

The key findings of the current study are outlined below.

- In double-track tunnels, the placement of the relief shaft is more important, whereas for single-track tunnels, the size of the cross-sectional area of the shaft plays the same role. The optimal placement for double-track tunnels is in the middle of the tunnel.
- In double-track tunnel model, the PM level on the platforms exhibits a strong inverse correlation with the exhaust/suction air ratio and the total exhaust PM mass discharged outside of the relief shaft. However, there is no correlation between the PM discharge efficiency and the PM level on the platforms.
- For single-track tunnels, neither the exhaust/suction ratio nor the PM discharge efficiency of the shaft correlate well with the PM level in the platforms. The only weak correlation observed is with the total PM mass exhausted from stations and shafts, which correlates to some extent with the PM level on the platforms.

- A relief shaft placed very close to the train-arriving side of the station results in higher particle levels on the platforms. While this placement reduces the mass of entering particles on the platform, it also decreases the exhaust air from the stations, consequently increasing the PM concentration.

4.1. Limits

In the current 1D model, the entire platform is treated as a control volume with a single value for the PM level, disregarding local variations in particle concentration on the platform. The complex 3D geometry of the station might lead to a high regional variation in the PM level. Additionally, the model excludes consideration of flow driven by temperature differences and mechanical ventilation, focusing solely on naturally driven flow resulting from the train piston effect. Assumptions include typical sizes for tunnels and stations, train and rail specifications, and a typical train headway, all based on a subway line in Sweden. Additionally, it was assumed that the two large escalators in each station are always open during the simulation, so the results should not be interpreted for cases where the escalators occasionally have open doors.

5. REFERENCES

- [1] Karlsson HL, Nilsson L, Möller L., 2005. Subway particles are more genotoxic than street particles and induce oxidative stress in cultured human lung cells. *Chem. Res. Toxicol.* 18, 19–23.
- [2] Raut, J.-C., Chazette, P., Fortain, A., 2009. Link between aerosol optical, microphysical and chemical measurements in an underground railway station in Paris. *Atmos. Environ.* 43, 860–868.
- [3] Johansson C, Johansson PÅ, 2002. Particulate matter in the underground of Stockholm. *Adv. Air Pollut.* 11:541–549.
- [4] Martins, V., Moreno, T., Minguillon, M.C., Amato, F., de Miguel, E., Capdevila, M., Querol, X., 2015. Exposure to airborne particulate matter in the subway system. *Sci. Total Environ.* 511, 711–722.
- [5] Tu, M., Olofsson, U., 2021. PM10 in underground stations from different types of trains. *Transp Res D Transp Environ.*, 95, 102867.
- [6] Sitzmann, B., Kendall, M., Watt, J., Williams, I., 1999. Characterisation of airborne particles in London by computer-controlled scanning electron microscopy. *Sci. Total Environ.* 241, 63–73.
- [7] Querol, X., Moreno, T., Karanasiou, A., Reche, C., Alastuey, A., Viana, M., Font, O., Gil, J., Miguel, E.d., Capdevila, M., 2012. Variability of levels and composition of PM 10 and PM 2.5 in the Barcelona metro system. *Atmos. Chem. Phys.* 12, 5055–5076.
- [8] Abbasi, S., Wahlstrom, J., Olander, L., Larsson, C., Olofsson, U., Sellgren, U., 2011. A study of airborne wear particles generated from organic railway brake pads and brake discs. *Wear.* 273, 93–99.
- [9] Qu, H., Jianbin Z.ang, Yan W. 2022. Field Measurement and evaluation of effective ventilation and particulate matter discharge efficiency of air shafts in subway tunnels. *Atmosphere.* 13, no. 7.
- [10] Izadi T, Mehrabian MA, Abouali O, G. Ahmadi, 2019. 3-D numerical analysis of train-induced flow inside four ventilated underground subway stations and connecting tunnels. *J. Wind Eng. Ind. Aerodyn.* 193, 103974.
- [11] Izadi T, Mehrabian MA, Ahmadi G, S. Sadrizadeh, S., Abouali, O., 2021. Numerical analysis of the micro-particles distribution inside an underground subway system due to train piston effect. *J. Wind Eng. Ind. Aerodyn.* 211, 104533.
- [12] Izadi T, Mehrabian MA, Sadrizadeh S, Olofsson, U., Abouali, O., 2022. The effect of ventilation system with and without under-platform exhaust on the concentration of braking micro-particles inside the subway system. *Tunn. Undergr. Sp. Technol.* 128, 104638.
- [13] IDA Tunnel, Theoretical Reference, 2017. EQUA Simulation AB, Stockholm, Sweden

EMISSION MANAGEMENT IN RAILWAY TUNNELS WITH A 1D-3D SIMULATION APPROACH

¹Evangelos Antoniou, ²Arnaud Colleoni, ³Tom Linden, ¹Francesco Cuzzola

¹Dassault Systèmes Deutschland GmbH, 81541 Munich, DE

²Dassault Systèmes SE, 31770 Colomiers, FR

³Dassault Systèmes AB, 41756 Goteborg Lindholmen, SE

DOI 10.3217/978-3-85125-996-4-24 (CC BY-NC 4.0)

This CC license does not apply to third party material and content noted otherwise.

ABSTRACT

Railway tunnel maintenance involving grinding operations poses a significant challenge due to the emission of hazardous exhaust gases and dust, making the tunnel an unsafe working environment for personnel. To address this issue, simulations become crucial for designing and operating an efficient tunnel ventilation system, essential to mitigate these risks. The simulation workflow outlined in this paper brings together a fast and quasi-real time 1D systems model approach with a detailed 3D Computational Fluid Dynamics (CFD) simulation. This approach not only predicts the duration required for the dust and exhaust levels to reach acceptable safety thresholds, but also assesses the energy consumption of a given ventilation system. This study eventually underlines the ease and speed with which different scenarios can be tested, emphasizing how accessible this approach is without requiring extensive simulation expertise from end-users.

Keywords: CFD, system modelling, railway tunnel emission management, railway tunnel ventilation, rail-grinding

1. INTRODUCTION

Rail grinders are track maintenance vehicles used to restore the profile of rails and eliminate irregularities, contributing to prolonging the lifespan of rails and improving the overall performance of trains. However, when operating within tunnels, these vehicles emit exhaust and dust, posing health risks to workers. The variety of diesel and petrol-powered vehicles, machinery, and tools used in such scenarios emit harmful emissions that can lead to severe respiratory and cardiovascular diseases [1]. In addition, maintenance activities on the ballasted superstructure generate hazardous dust emissions, including mineral and quartz dust, potentially leading to lung disorders such as silicosis or even lung cancer [1]. Prioritizing the safety and well-being of tunnel personnel requires the ability to predict the duration needed for emissions to diminish within the tunnel environment, while utilizing a ventilation system. Furthermore, accurately estimating the energy consumption requirements for a ventilation system is crucial in mitigating these risks efficiently.

In this context, simulation emerges as a key tool in the design and operation of an efficient ventilation system, especially in cases where conducting experiments on a large number of tunnels is not feasible; such as in the case of the expansive German railway tunnel infrastructure spanning over 33,500 km [2]. The proposed 1D-3D simulation approach stands as a sophisticated methodology to address the challenges posed by rail grinder emissions in tunnels. While 1D simulations offer speed and simplicity, they may lack accuracy without proper calibration derived from measurement or simulation data, making it challenging to obtain reliable results. On the other hand, 3D simulations provide high-fidelity results with reasonable computational effort in areas in proximity to the train, which can be used to calibrate 1D models. By combining the strengths of both 1D and 3D simulations, both

resources are used efficiently, ensuring a balance between computational effort and accuracy of results. This approach not only offers an intelligent solution for railway tunnel design and operation, but also makes final simulation tool accessible to individuals without extensive simulation expertise, thereby promoting a more inclusive and democratized approach to simulation.

This paper begins with an overview of the 1D-3D concept, followed by a comprehensive case study that thoroughly outlines each step of the workflow. Finally, the conclusion and summary of this work are drawn in the last section.

2. CONCEPT

An overview of the simulation workflow is shown in Figure 1. In the first stage, SIMULIA PowerFLOW®, a Lattice Boltzmann Method (LBM) solver, is employed to generate a 3D CFD model. LBM solver operates by solving the mesoscopic Boltzmann equation to predict macroscopic fluid dynamics. This solver is high-fidelity transient and compressible, exhibiting very low numerical dissipation. Additionally, the LBM solver is equipped with an integrated Lagrangian particle simulator that can simultaneously track millions of particles with highly detailed models. Transient particle trajectory tracking is crucial, as it facilitates the mixing of particles, captures airflow fluctuations, and ensures accurate dispersion analysis. Following the 3D simulation, an advanced post-processing analysis follows. This step allows to extract volumetric and surface results essential for the proper calibration of the 1D model.

The third step involves the development of a calibration model in CATIA Dymola®, which utilizes Modelica®, an open-source object-oriented language for modeling complex physical systems. Replicating the 3D scenario in a 1D model and obtaining precise calibration parameters, the workflow processes for preparing and executing the 1D long tunnel model. In the fourth step, a realistic simulation scenario of a long tunnel and its ventilation system is defined, which is executed in a matter of seconds, allowing rapid tuning and testing of the model in a short time frame. Upon completing the 1D simulation, the workflow moves to the fifth step, wherein the results are post-processed to estimate the development of emissions over time and assess power consumption attributed to the ventilation system. The final step includes the option to rerun the 1D model for different simulation scenarios. This can be achieved either using CATIA Dymola® or within the 3DEXPERIENCE® platform, which offers a comprehensive business and product development framework, enabling non-experts to leverage an advanced simulation process such as the one outlined in this paper.

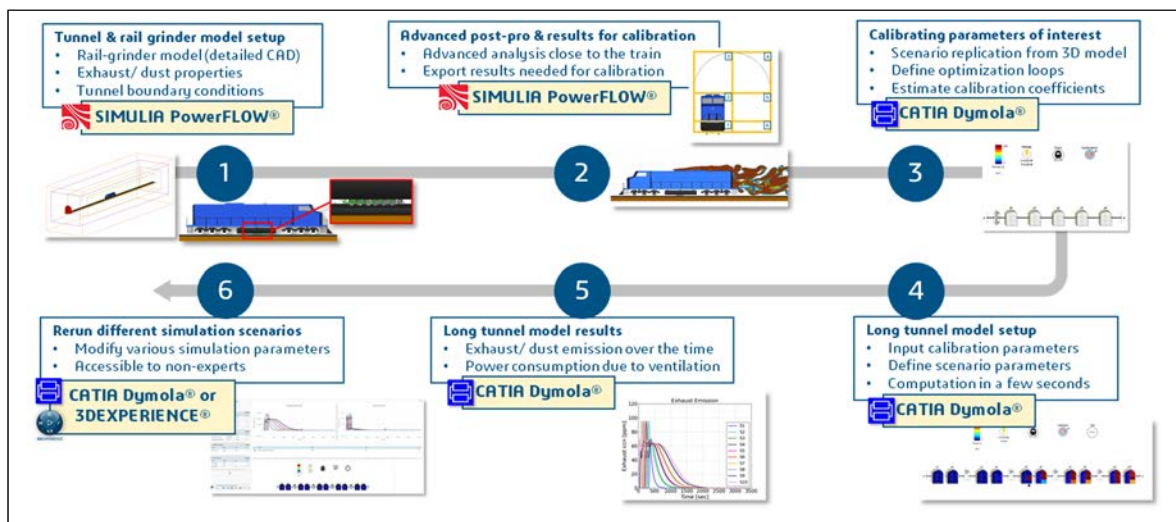


Figure 1: 1D-3D simulation approach overview

3. CASE STUDY

This section presents step by step a case study of a railway tunnel during grinding operations, demonstrating its applicability and effectiveness in real-world scenarios.

3.1. 3D CFD model: Tunnel & rail grinder model setup

An overview of 3D CFD tunnel and rail grinder model is shown in Figure 2. In this particular use case, a detailed 3D CFD simulation is prepared for a 200 m long tunnel. This includes a train model equipped with a grinder featuring 6 cylinders representing grinding stones, operating at a speed of 10 km/h. At the tunnel entrance, the inlet velocity boundary condition is set at 4.95 m/s, considering the airflow generated by the ventilators. This condition assumes a uniform flow distribution in the tunnel, neglecting potential flow concentration near the ventilators as well as velocity variations from top to bottom of the tunnel. To simulate exhaust emissions, vapor water scalar transport modelling is chosen, which is coupled with the flow solver. The mass flow rate of the exhaust emissions at the outlet is set to 27 g/s. For dust emissions, particle modeling is employed, incorporating two types of dust particles, A- and E-dust, characterized by mean diameters of 1.5 and 6.25 μm , respectively. The dust emission rate is determined to be 12,000 particles per second. To properly discretize the domain, 6 variable resolution (VR) levels are used, as shown in Figure 3, whose resolution is increased by a factor of two compared to the neighboring area, with the finest resolution applied at the emitter area and exhaust outlet equivalent to 6 mm.

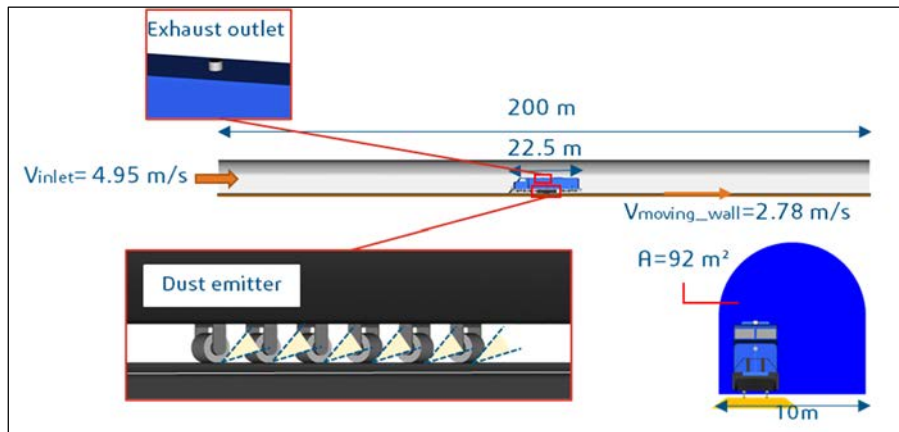


Figure 2: Overview of 3D CFD model.

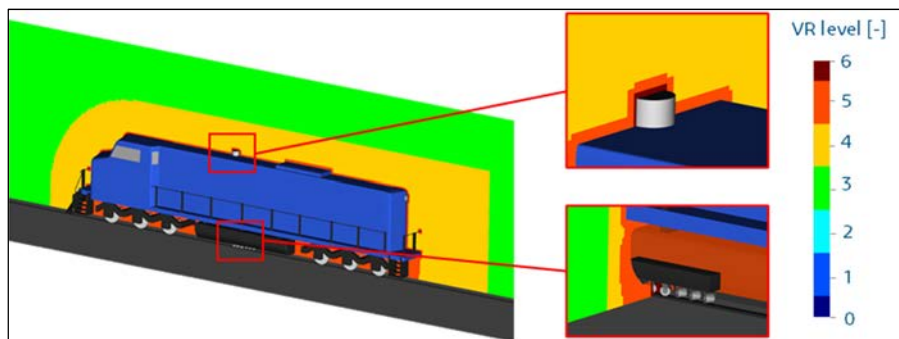


Figure 3: Close-up view of variable resolution (VR) levels.

3.2. 3D CFD model: Advanced post-pro & results for calibration

Figure 4 shows an example of the comprehensive post-processing analysis that provides insights into the dispersion of emissions in close proximity to the train. First, plotting the total

pressure plane across the train helps to understand the wake dynamics. To complement this, an iso-surface plot provides a more intuitive representation of its structure. The accurate prediction of the train's wake is essential for understanding the dispersion and transportation of exhaust gases and dust particles within the surrounding airflow. This region significantly influences the propagation patterns of these particles, thus affecting their distribution and motion. Moreover, instantaneous results of the exhaust gas mass fraction are shown through both cut plane and volumetric representations. Additionally, similar to exhaust emissions, to offer a more intuitive understanding of the dust dispersion, volumetric results of particle volume ratio are presented.



Figure 4: Advanced post-processing of 3D CFD analysis.

Regarding the calibration of the 1D model, certain quantitative results have to be extracted from the 3D CFD simulation that capture the main flow patterns. These results include volumetric mean data of the total concentration of exhaust and dust emissions across 18 volumes shown in Figure 5, as well as, surface results of mean mass flow and static pressure on the interfaces between the volumes for mean mass flow and static pressure. The results of the mass flow and exhaust gas concentration are given as examples in Table 1 and Table 2 respectively.

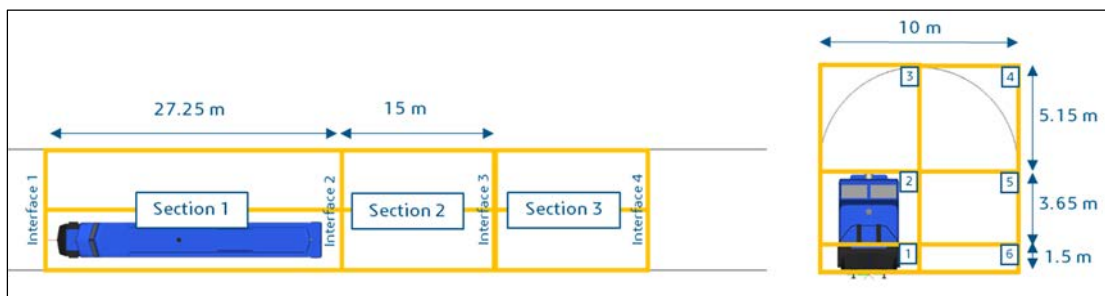


Figure 5: Sections and interfaces to extract results needed for calibration.

Table 1: Mean mass flow [kg/s]

Surface	Interface 1	Interface 2	Interface 3	Interface 4
1	40.7	14.6	26.1	30.2
2	104.0	81.7	92.5	98
3	123.5	138.9	133.4	129.6
4	126.0	140.5	134.3	132.2
5	111.7	126.0	119.8	118.3
6	44.9	49.7	45.1	43.0

Table 2: Mean exhaust emission concentration [ppm]

Surface	Section 1	Section 2	Section 3
1	7.2	183.0	242.4
2	158.4	348.2	290.4
3	104.3	22.5	21.6
4	0.1	0.1	0.3
5	0.1	2.9	5.2
6	0.1	4.4	23.9

3.3. 1D system model: Calibrating parameters of interest

Implementing the 1D model for parameter calibration requires the replication of the 3D use case scenario, which is essential for achieving a consistent correlation between two distinct approaches. Figure 6 shows the 1D system modeling of the tunnel used to calibrate the parameters of interest. In this process, each segment of the 1D model corresponds to a specific part of the 3D model. Within each 1D slice, 6 nodes are defined, facilitating flow in different directions while identifying the exact locations where exhaust or dust emissions occur. Defining boundary conditions similar to those in the 3D model involves configuring inputs, such as train speed and airflow ventilation. These elements play a critical role in ensuring the match between the 1D and 3D models.

The technical complexities of the calibration process include identifying specific parameters to be adjusted. Parameters of interest include flow coefficients, not only for the main flow but also for perpendicular directions, the train's wake length, and the rate at which dust and exhaust emissions dissipate. To fine-tune and optimize the model, a series of iterative optimization loops are deployed. These loops are essential in calibrating and adjusting pressure dynamics, the distribution of mass flow, and the overall quantity of dust suspended in the air.

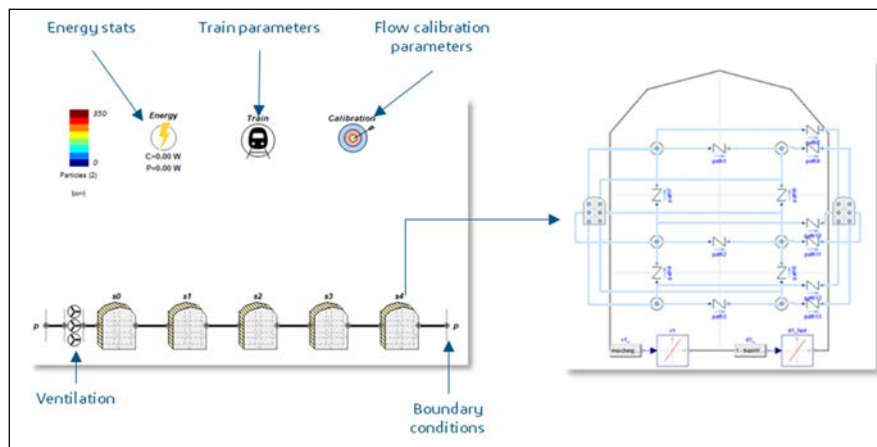


Figure 6: 1D system modeling of the tunnel for calibration flow parameters.

3.4. 1D system model: Long tunnel model setup

The 1D system model for a long tunnel scenario is subsequently developed. Figure 7 shows a schematic representation of 1D model of the long tunnel case. Here, the model employs 4 ventilators distributed across the 1 km long tunnel, with each 1D segment representing a 100 m section. Boundary conditions are defined at the entrance and exit of the tunnel, and specific inputs for the train, such as its length, speed, and rates of dust and exhaust emission, are

incorporated, along with the calibration parameters estimated from the previous step.

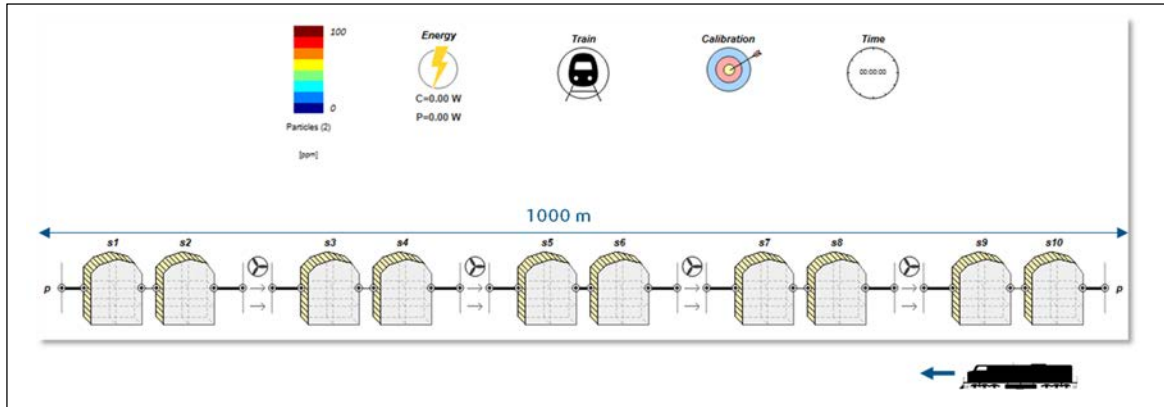


Figure 7: 1D system model of the long tunnel model.

3.5. 1D system model: Long tunnel model results

Monitoring exhaust and dust emissions across various tunnel sections over time is crucial as it helps to ensure a safe working environment. Figure 8 shows the exhaust and dust emissions over the time per tunnel slice. In particular case, it takes approximately 30 minutes for the exhaust gas concentration to diminish significantly, reaching a notably low level within this timeframe. However, the dust concentration tends to decrease at a faster rate, due to gravity. Furthermore, an additional aspect under consideration is the estimation of the energy consumption attributed to ventilation, which for approximately half an hour of operation in this case is estimated at 3.64 kWh. This assessment broadens the scope of understanding regarding the operational costs and environmental impacts associated with maintaining optimal air quality in such infrastructure.

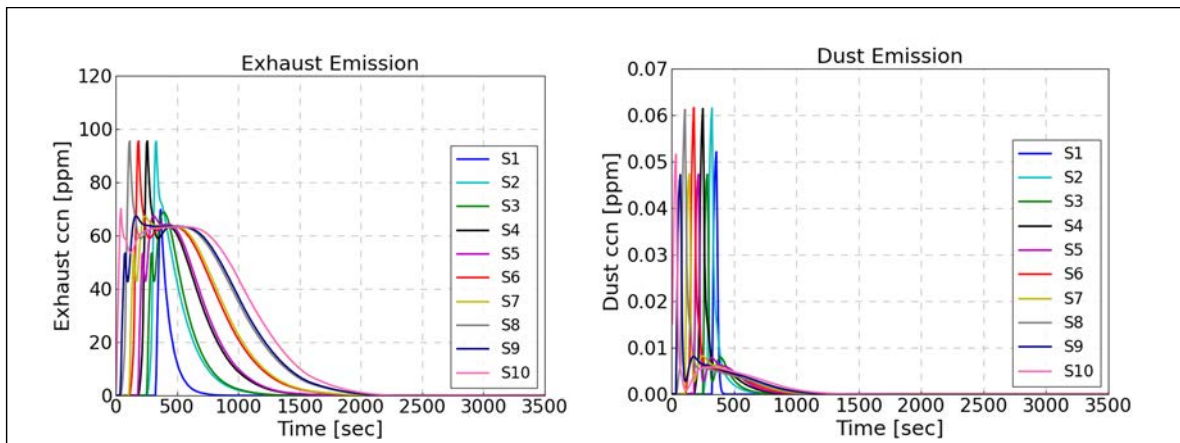


Figure 8: Exhaust and dust emission concentration over the time per tunnel slice.

3.6. 1D system model: Rerun different simulation scenarios

As previously highlighted, the end-user has the capability to efficiently rerun the 1D long tunnel model within a matter of seconds in CATIA Dymola® or the 3DEXPERIENCE® platform. Particularly in the platform through the dedicated role System Simulation Design, users can easily interact with the model. This allows them to modify various parameters such as train length, speed, dust and exhaust rates, rerun simulations, and review the results.

Therefore, the challenge in enabling non-experts to take full advantage of the capabilities of an advanced simulation process can be achieved in the platform through a streamlined approach including the following key aspects:

- **Effortless access:** Using the platform is as simple as opening a web browser, eliminating the need for complex software installations.
- **User-friendly interface:** A sophisticated, user-friendly cockpit displays only the essentials for easy navigation. Figure 9 shows an overview of the simulation dashboard within the platform.
- **Simplified parameter selection:** Selecting model variables, aligned with non-expert understanding, empower users to define only crucial parameters without complexity.
- **Simplified post-processing:** Graphical representations provide clear insights, such as emissions per tunnel segment and power consumption, without overwhelming technical details.



Figure 9: Web-based railway tunnel simulation dashboard on the 3DEXPERIENCE® platform.

4. CONCLUSION

In summary, this work shows the effectiveness of a combined 1D-3D simulation approach to address the complex problem of managing exhaust and dust emissions in railway tunnels during grinding operations. The 3D CFD simulation not only provides insights into exhaust and dust dispersion in proximity to rail grinder, but also plays a crucial role in calibrating the 1D model properly. The 1D system simulation proves instrumental in estimating tunnel cleaning duration and determining the energy consumption of ventilation system in a 1 km long tunnel scenario. Notably, leveraging the 3DEXPERIENCE® platform is an excellent example of democratizing simulation, making it accessible to a wider audience. While the presented case study focuses on a specific ventilation and tunnel design, a key future step involves employing 3D CFD to model multiple layout scenarios alongside well-tuned 1D models. This comprehensive approach would enable non-experts to explore a variety of tunnel and ventilation designs, thereby significantly enhancing tunnel performance in terms of both safety and energy efficiency. Furthermore, the assumption of a uniform flow distribution in the 3D CFD model setup, discussed in Section 3.1, lays the groundwork for future exploration, potentially expanding this approach to analyze ventilator spacing. Looking ahead, the focus is on acquiring measurement data to further refine and validate the simulation models against

experimental data, marking the next step in enhancing the accuracy and reliability of the simulation approach.

5. REFERENCES

- [1] V. Voicu and A. Draghici: Mitigating risks in railway tunnel maintenance: A pilot study on air quality management during drainage flushing. *Cogent Engineering* 10, 1 (2023) 2244767.
- [2] Statista.de, Länge des Schienennetzes der Deutsche Bahn AG in den Jahren 2000 bis 2022, 2023. URL: <https://de.statista.com/statistik/daten/studie/13349/umfrage/laenge-vom-schienennetz-der-db-ag>.

APPLICATION OF ARTU SOFTWARE AND MULTIZONE FIRE MODELLING FOR RISK ANALYSIS: A ROAD TUNNEL CASE STUDY

Michele Fronterre, Rugiada Scozzari
Cantene srl, IT

DOI 10.3217/978-3-85125-996-4-25 (CC BY-NC 4.0)

This CC license does not apply to third party material and content noted otherwise.

ABSTRACT

In the previous editions of the Graz Tunnel Conference (2020 and 2022), the ARTU software was presented through a case study (a 6 km tunnel with longitudinal ventilation). ARTU calculates the societal risk related to fire in tunnels combining probabilistic and deterministic approaches and different sub-models: fluid dynamics, queue formation, egress, interaction between environment and people.

The current release of ARTU incorporates a multizone fire model - developed along with Lund University - that permits a better description of the smoke stratification and back-layering, compared to 1D fluid dynamic model.

In the present paper the current version of ARTU is presented through the results of the risk analysis of a 3 km road tunnel with jet-fans and smoke extraction shafts. Risk analysis results are expressed by means of FN curve and damage expected value. The results are compared with the ones obtained by the previous version of ARTU, which was based on 1D fluid-dynamic and did not include multizone fluid-dynamic model.

In order to analyze the effect of the back-layering phenomenon on the overall risk, a sensitivity analysis is done modifying longitudinal velocity and observing how this impacts the results obtained through the multizone fluid-dynamic model.

An in-depth study is performed about the smoke layer height, using CFD simulations to check the stratification prediction made by the multizone model.

Keywords: Tunnel risk analysis, 2004/54/EC, 1D fluid dynamics, zone modelling, Multi-Zone Fire model.

1. INTRODUCTION

Since the publication of the Directive 2004/54/EC of the European Parliament, related to tunnels within the Trans-European Road Network which are longer than 500 meters [1], risk assessment has become an integral part of tunnel design [2]. Furthermore, an appropriate risk assessment of existing and new facilities can be a useful tool to assess tunnel safety levels and inform decision makers and designers upon solutions to be adopted [3].

Based on these premises, Cantene developed a tunnel risk analysis tool called ARTU (acronym in Italian for Risk Analysis in Tunnels) [4][5]. ARTU performs the risk assessment of a tunnel simulating a large number of scenarios. Each scenario involves the fire in a different position and with a different HRR (Heat Release Rate) curve. Furthermore, scenarios vary for what concerns number and characteristics of people inside the tunnel. Each scenario returns a certain number of fatalities, the results are cumulated and plotted on a FN diagram. ARTU combines probabilistic and deterministic approaches, including different sub-models: fluid dynamics, queue formation, egress, interaction between tenability conditions and people. The fluid-dynamics is represented by means of 1D and zone models. One-dimensional (1D) models include geometrical data and characteristics of the ventilation system, representing the system under analysis as a network made by branches and nodes. 1D models returns time-varying air temperature, air velocity, and volume airflow by means of one value for each

variable at a set distance from the fire, representing an average over the cross-section of the branch. As a consequence, 1D models are not suitable to simulate the fluid behaviour in regions characterised by high temperature or velocity gradients, typically close to the flames or in the regions where well-defined smoke stratification is found [3].

Zone models are promising because they make it possible to represent phenomena like stratification and back-layering, keeping the computational cost relatively low. Nevertheless, when applying control volume equations to tunnel fires, consideration should be given to the unique nature of some fire phenomena in tunnels: (i) the ratio between length and height of the simulated domain; (ii) the representation of ventilation devices used in tunnels, such as jet-fans, that may require dedicated model input calibration efforts [3].

ARTU implements a zone modelling tool originally developed by Lund University, called the Multi-Zone Model [6]. The tool has been improved by the developers with the contribution of the authors of this paper, in order to make it suitable to the tunnel fire application. The model represents the entire enclosure through several smaller computational volumes (zones), for which the conservation of mass and energy are applied. Fire is specified as a heat release rate and empirical models are used to represent the plume and the ceiling jet [7]. A dedicated model validation for tunnel applications has been conducted through benchmarking against experimental data. Model results were also compared against results from the Fire Dynamics Simulator (FDS) [10]. The results of the benchmarking indicate that the Multi-Zone Fire model performs well 50–200 m away from the fire for heat release rates of 5–20 MW and moderate longitudinal ventilation flows [7]. Taking into account these results, currently the Multi-Zone Model is used in ARTU as an additional model to determine tenability conditions in the vicinity of fire during the initial phase of emergency.

The tool is still under development in order to improve its modelling capabilities and accuracy for tunnel fires. As an example, the Multi-Zone Fire model uses an empirical plume model that does not account for the effect of forced ventilation on the plume air entrainment. Another aspect that needs to be improved is the fact that the Multi-Zone Fire model does not include the turbulent mixing between zones and this could be an issue if the longitudinal ventilation flow is high [7]. Furthermore, the accuracy in the momentum conservation needs more efforts. More details about ARTU and the Multi-Zone Fire can be found in references [4][5][6][7][8]. This paper introduces a tunnel case study in which the use of ARTU is demonstrated while using its Multi-Zone component. The effect of the use of Multi-Zone model in the assessment of risk is presented. Then, a particular case is discussed, when the tunnel operates in maintenance configuration. As discussed in the following, in this case the risk predicted using 1D model is fictitiously equal to 0 and the Multi-Zone Model becomes crucial in risk assessment, due to its capability to represent stratification and back-layering. To further test the Multi-Zone approach, this is hence compared to a Computational Fluid Dynamics approach (e.g. using the Fire Dynamics Simulator, FDS) for the investigation of smoke stratification, and theoretical formula for the back-layering representation.

2. CASE STUDY

The case study is a bidirectional, urban, single-bore, 3190m long tunnel. The cross-section varies along the tunnel length from 55 to 165m². The tunnel is provided with 2 intermediate entrance ramps. The ventilation strategy is based on the smoke extraction by means of a vent near the fire (see a schematic drawing in Figure 1). Jet-fans are used to balance the pressure in order to assure a near-zero longitudinal velocity next to the fire. This in order to prevent smoke moving along the tunnel instead of being pulled out from extraction vent.

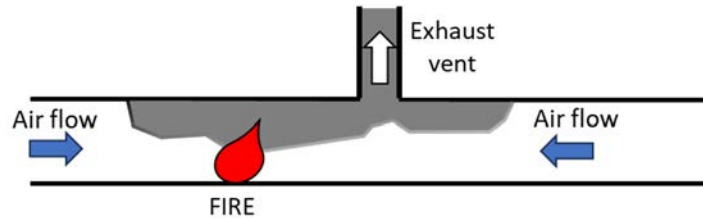


Figure 1: Single point extraction system

Figure 2 shows the longitudinal profile of the tunnel and the position of jet-fans, smoke extraction vents and entrance ramps.

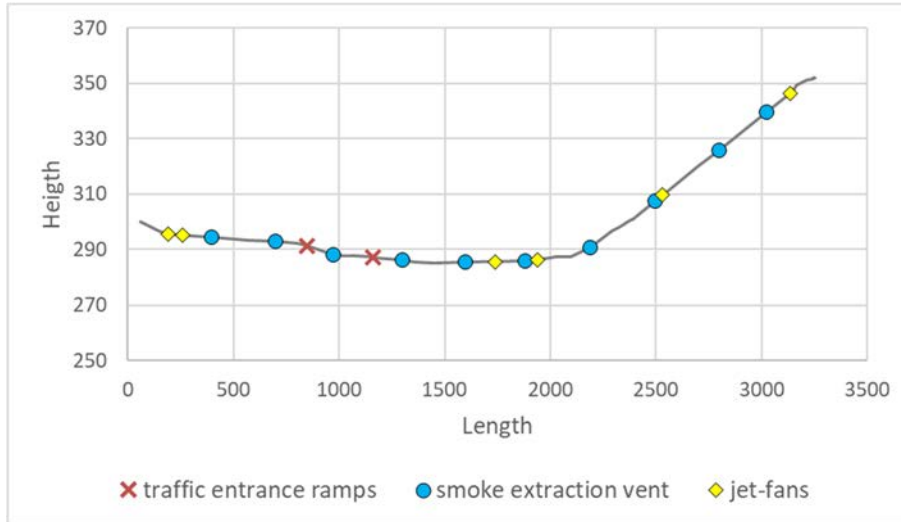


Figure 2: Longitudinal profile of the tunnel

2.1. Results of ARTU risk analysis

ARTU risk analysis has been performed both including and not including the Multi-Zone Model. Figure 3 shows the FN curves and the expected value of damage (EV), i.e., the integral of the FN curve.

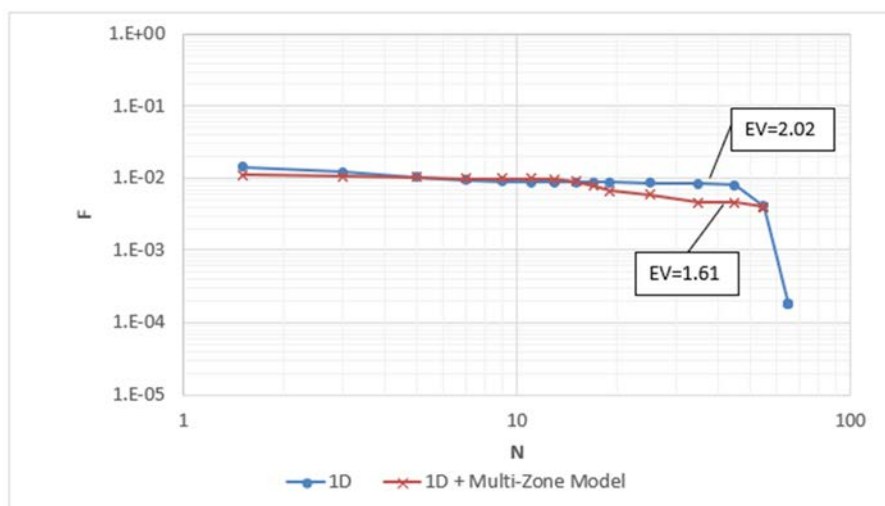


Figure 3: FN curves

Table 1 shows the results in terms of percentage of fatalities and chemical FED (Fractional Effective Dose) among all the analyzed scenarios used to create the FN curve. FED allows to quantify the interaction between people and smoke, taking into account the presence of

toxicant, asphyxiant gases and hypoxia. FED equal to zero corresponds to no interaction. FED can be used in relation to different thresholds (e.g. incapacitation or lethal doses). FED incapacitation equal to one means that half of the population would be expected to be incapacitated [9].

Table 1: Maximum and average scenarios results

	1D		1D + Multi-Zone Model	
	maximum	average	maximum	average
Fatalities	7%	0.09%	5%	0.05%
Chemical FED	0.63	0.04	0.45	0.02

Both the FN curves of Figure 3 and results of Table 1 show that the risk level estimated using the Multi-Zone Model is lower than the one based solely on 1D model. This is due to the fact that near the fire the 1D model does not take into account the stratification of smoke. 1D model considers the smoke as homogeneously distributed in the cross section of the tunnel. As a consequence - in the cases in which a stratification exists and hot smoke are confined in the upper part of the tunnel - a conservative estimation of the interaction between people and smoke is made above human height.

Since the capability to represent the smoke layer is a crucial point in the development and validation of the tool, an example of the smoke layer representation in the Multi-Zone Model is given in the chapter 3.

2.2. Temporary operation mode

When maintenance works are planned, the case study tunnel operates in temporary operation mode. Only the first section of the tunnel (from the lower portal to the first ramp at ~800m length) is opened to traffic (see Figure 4, left image). Traffic is monodirectional from the ramp to the portal. In case of emergency, a longitudinal ventilation mode is operated by jet-fans, pushing smoke through the portal.

Before the ventilation system activates, the smoke naturally tends to move toward the highest portal due to the tunnel slope. Nevertheless, the smoke velocity generated by the chimney effect in the first phase of fire is presumably lower than the critical. As a consequence, the traffic queue located downwards the fire (see Figure 4, image on the right) is exposed to the smoke back-layering. After the mechanical ventilation is activated, smoke are confined downstream the fire.

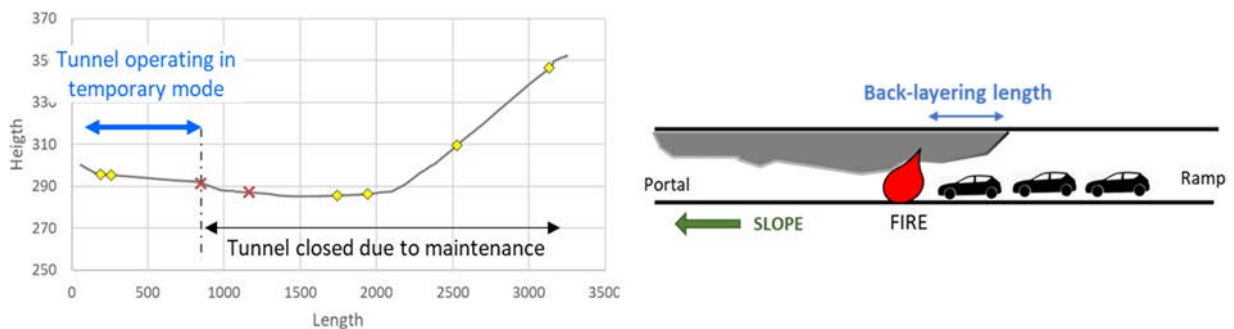


Figure 4: Tunnel (left) and smoke dynamic (right) in temporary operation mode

In this case, the expected value of risk calculated by means of the 1D model is equal to zero, because back-layering cannot be represented in 1D models (Figure 5).

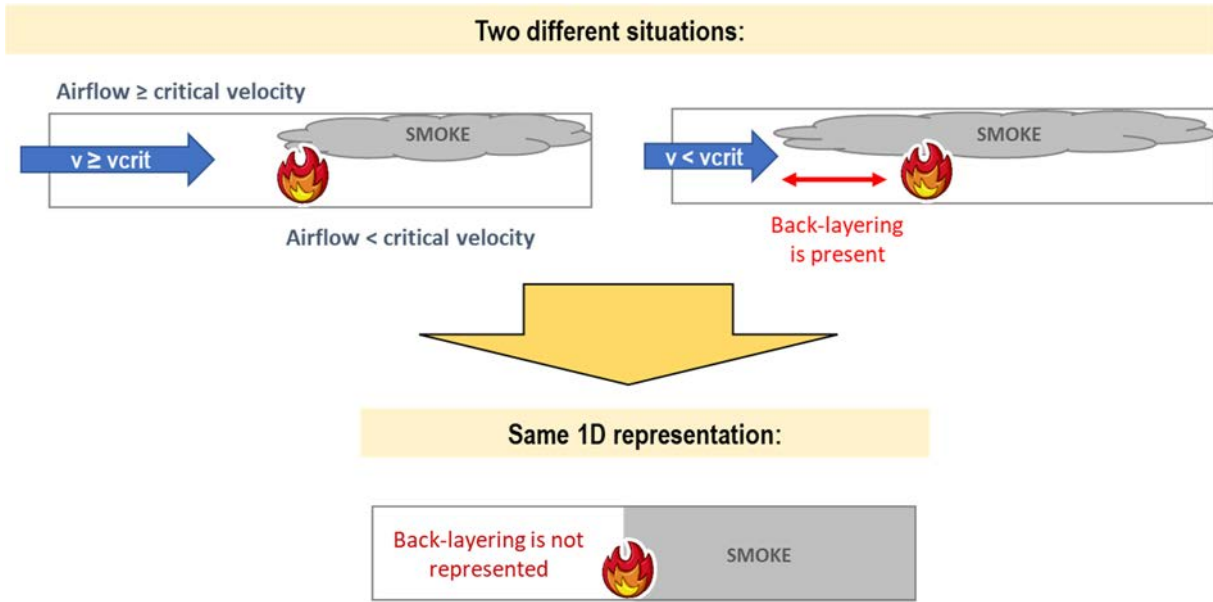


Figure 5: 1D representation of cases with different longitudinal ventilation

In this case, the use of Multi-Zone model is crucial for a proper assessment of the risk. An in-depth analysis of the back-layering representation in the Multi-Zone Model is given in chapter 4.

3. SMOKE STRATIFICATION REPRESENTATION IN THE MULTI-ZONE MODEL

To evaluate the capability of the Multi-Zone Model to address the representation of a smoke layer, a simple case test is analyzed with both the Multi-Zone Model and FDS. FDS (Fire Dynamic Simulator) [10] is a computational fluid dynamics model of fire-driven fluid flow that solves numerically the Navier-Stokes equations. Even though some issues arise when applying FDS to tunnels ([11][12][13]), this is a well-established and widely used model in fire engineering and tunnel ventilation design.

A simple test tunnel is used, in order to better appreciate the smoke stratification dynamic. This is different than the case study presented above. The tunnel is 200m long, with 80m² rectangular cross section shape (height 8 m, width 10m), no slope and no mechanical ventilation. The fire source has a constant heat release equal to 8MW and is located in the center of the tunnel.

Figure 6 and Figure 7 show the distribution of temperature on a vertical plane in correspondence to the tunnel longitudinal axis, at two different time steps.

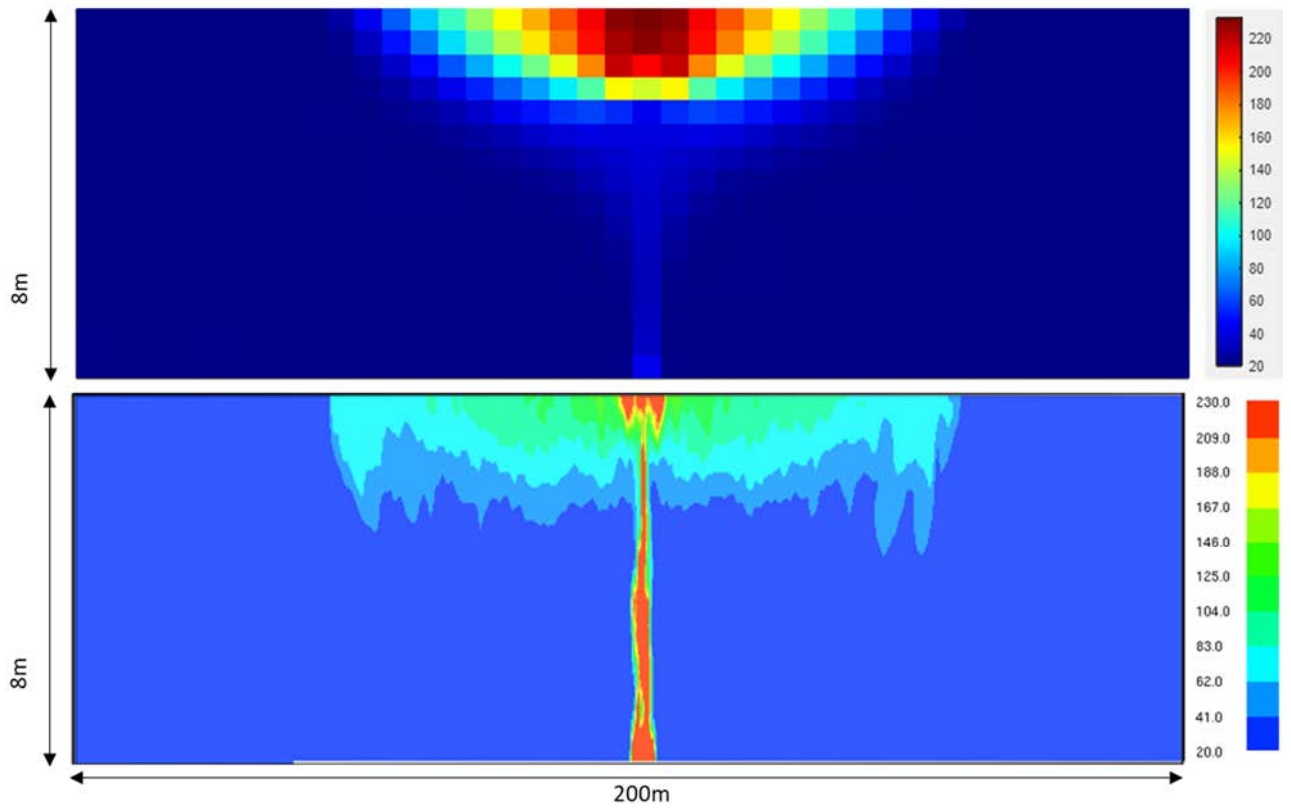


Figure 6: Stratification comparison between MZ (up) and FDS (down), 30s from ignition

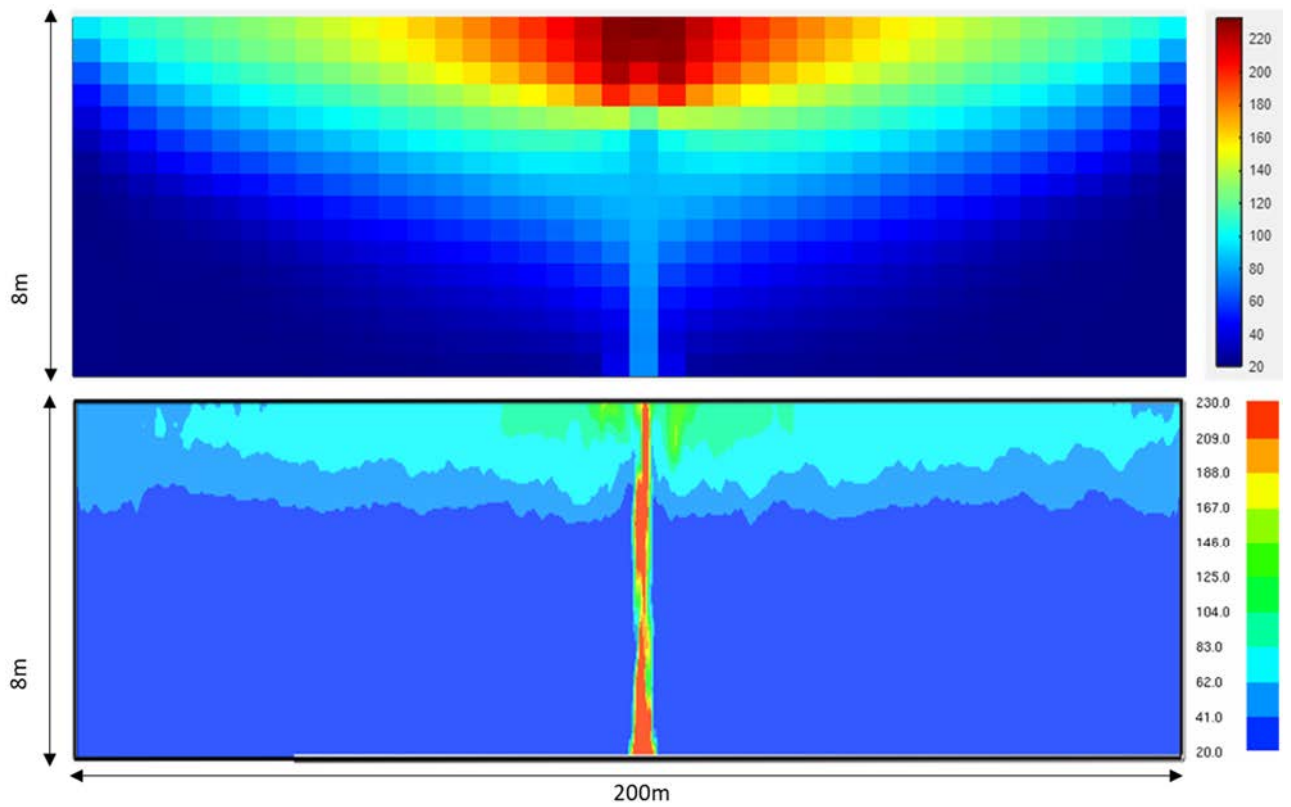


Figure 7: Stratification comparison between MZ (up) and FDS (down), 300s from ignition

At 30 seconds (Figure 6), when the smoke has not yet reached the portals, the extension of the area affected by smoke is the same in the Multi-Zone Model and FDS. Both the figures show that the Multi-Zone Model tends to overestimate temperature and the thickness of the smoke layer, in particular far from the portals. In general, a slower smoke propagation has been observed in the Multi-Zone Model respect to FDS simulations.

The main difference between the two models is the representation of the plume. In FDS the plume is fully represented by means of the solution of Navier-Stokes equations. In the Multi-Zone Model, an empirical model is used (Heskestad [14]). The fire plume rises until it hits the ceiling, entraining air and hot gases from the zones that it passes through. To account for momentum conservation when a fire plume hits the ceiling and a horizontal flow created, an empirical ceiling jet model is used. The ceiling jet velocity is introduced as a hydrodynamic pressure term in the model [7]. This aspect is crucial in the application of the Multi-Zone Model to tunnels respect to the application in large enclosures, and needs to be further investigated in order to assure that the momentum is conserved throughout the length of the domain.

4. BACK-LAYERING LENGTH ESTIMATION

In general, ventilation systems are designed to avoid back-layering. Longitudinal ventilation systems push the smoke downstream the fire. Transverse and semi-transverse ventilation systems push the smoke in a specific area of the tunnel, next to the extraction point (smoke confinement). Nevertheless, there are some situations in which the confinement of smoke is not achieved. This happens for example 1) in the first phase of fire since the ventilation system has not been activated yet, 2) in tunnels that are not provided with mechanical ventilation, 3) in case of ventilation system failure. In these cases, when back-layering arises, the use of 1D models could lead to an under-estimation of the interaction between people and fire products. The Multi-Zone Model indeed has a crucial role in the estimation of risk level.

The back-layering length is defined as the length of the smoke back-layering upstream of the fire when the ventilation velocity is lower than the critical, and can be expressed by the correlation proposed by Li et al. [16]. Li et al. carried out two series of tests in model-scale tunnels based on a dimensional analysis, and found that the back-layering length increases with the HRR for low HRRs and is nearly independent of HRR and dependent only on the ventilation velocity at higher HRRs. It is shown that the relationship between the ratio of longitudinal ventilation velocity to critical velocity and the dimensionless back-layering length approximately follows an exponential relation. [15]. Li et al. correlation is reported below.

$$L_b^* = \frac{L_b}{H} = \begin{cases} 18.5 \ln \left(0.81 \frac{Q^{*\frac{1}{3}}}{u^*} \right) & Q^* \leq 0.15 \\ 18.5 \ln \left(\frac{0.43}{u^*} \right) & Q^* > 0.15 \end{cases}$$

$$Q^* = \frac{\dot{Q}}{\rho_0 c_p T_0 g^{\frac{1}{2}} H^{\frac{5}{2}}} \quad u^* = \frac{u}{\sqrt{gH}}$$

Where g is the gravitational acceleration (m/s^2), H is the tunnel height (m), ρ_0 is the ambient density (kg/m^3), u is the velocity (m/s). \dot{Q} is the total heat release rate (HRR) (kW), c_p is the heat of capacity ($\text{kJ}/(\text{kg K})$), T_0 is the ambient temperature.

In order to evaluate the capability of the Multi-Zone Model in representing the back-layering phenomenon, a comparison is made between the values obtained from the model and the formula reported above. Table 2 shows the back-layering length estimated for the simple 200m long tunnel presented in previous chapter, in which a 8MW fire is located. The critical velocity is estimated by the following formula [14] and is equal to 2.5m/s.

$$u_c^* = \begin{cases} 0.81Q^{*1/3} & Q^* \leq 0.15 \\ 0.43 & Q^* > 0.15 \end{cases}$$

Estimation of back-layering length by the Multi-Zone Model is made taking into account the temperature vs tunnel length in the upper zone. Zones are 5m long (along the longitudinal axis of the tunnel), 2.5m width and 0.5 high.

Figure 8 shows the temperature vs tunnel length in correspondence of the zone next to the ceiling, at steady-state conditions, estimated by the Multi-Zone Model. It can be seen that the higher the velocity, the lower the temperatures both downstream and upstream the fire.

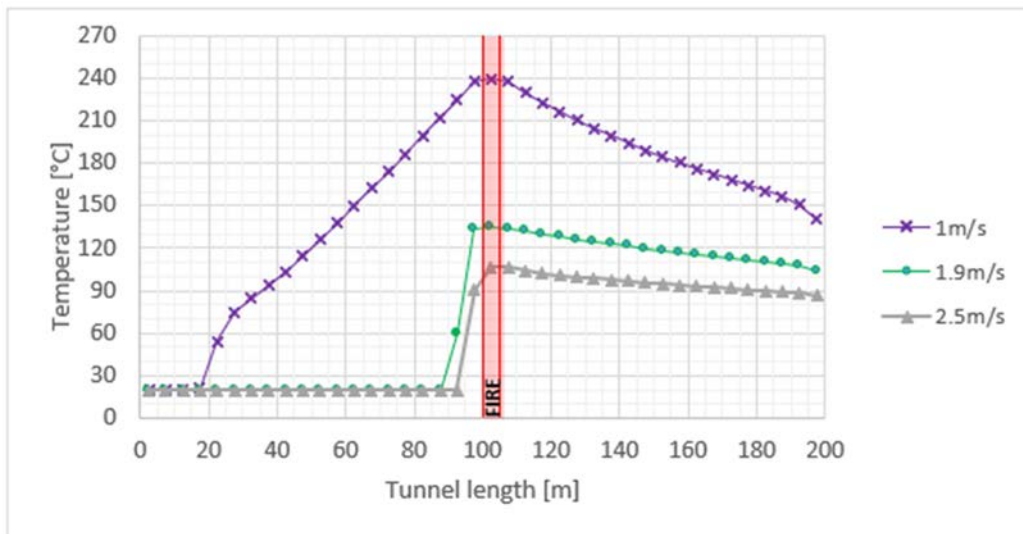


Figure 8: Back-layering representation in the Multi-Zone Model

Table 2 summarizes back-layering length obtained by formula presented above and Multi-Zone Model.

Table 2: back-layering length (formula vs Multi-Zone Model)

Longitudinal velocity	Formula	Multi-Zone Model
1.0m/s	103m	80m
1.9m/s	43m	10m
2.5m/s	0m	5m

The back-layering length estimated by means of the formula is higher than the one estimated by the Multi-Zone Model, when the longitudinal velocity is lower than the critical value. In the case in which the longitudinal velocity is equal to the critical value, the Multi-Zone Model shows a back-layering equal to 5m. It must be noted that the model resolution in the longitudinal axis is equal to 5m.

In general, the back-layering length is under-estimated by the Multi-Zone Model, and the accuracy increases when the ratio between critical velocity and actual longitudinal velocity is higher.

In the risk analysis, the Multi-Zone tool is used in the first phase of fire, when the longitudinal velocity is low. This is the phase in which the Multi-Zone tool prediction of back-layering is most accurate.

5. SUMMARY AND CONCLUSION

The Multi-Zone Model - which development is on-going thanks to the collaboration with Lund University - shows promising results in the accuracy of smoke dynamic representation. Typical three-dimensional phenomena that cannot be represented by means of 1D models, can be depicted using the Multi-Zone Model. This expands the possible range of applicability of the software ARTU, including tunnels which safety strategy is based on the stratification of smoke (transverse and semi-transverse ventilation systems, naturally ventilated tunnel with low slope). In these cases, the 1D model cannot represent the stratification, and over-estimation of fatalities occurs. On the other hand, the possibility to predict the back-layering length solves the 1D blindness to the diffusion of smoke at low velocity, typical during first phase of fire when ventilation system has not reached the target velocity, or in case of ventilation system failure. This makes the Multi-Zone tool suitable for increasing accuracy in the risk assessment of tunnel with longitudinal ventilation.

The accuracy gain in the estimation of risk depends on the type of tunnel and ventilation strategy. It is higher for naturally ventilated tunnels with low slope and tunnels with exhaust vents. The current version of the Multi-Zone Model shows in general a conservative estimation of smoke layer thickness and temperature, compared with the Fire Dynamics Simulator, and an under-estimation of the back-layering length especially for velocity near to the critical value, compared with analytical formula. Further development of the Multi-Zone Model will be aimed at addressing these issues.

6. ACKNOWLEDGEMENT

The authors thank Nils Johansson and Enrico Ronchi, both at Lund University, for the fruitful discussions regarding tunnel fire risk assessment and multi-zone modelling.

7. REFERENCES

- [1] The European Parliament. (2004). DIRECTIVE 2004/54/EC. Official Journal of the European Union.
- [2] Kohl, B., Botschek, K., & Hörhan, R. (2007). Austrian Risk Analysis for Road Tunnels. Development of a new Method for the Risk Assessment of Road Tunnels. First International Tunnel Safety Forum for Road and Rail. Lisbon, Portugal.
- [3] Beard, A. (2010). Tunnel safety, risk assessment and decision-making. *Tunnelling and Underground Space Technology* 25, 91-94.
- [4] Application of in-house risk assessment tool on the analysis of a tunnel in the new Gronda di Genova highway. M. Fronterre, R. Scozzari. (2020) 10th International Conference ‘Tunnel Safety and Ventilation’, Graz
- [5] The application of zone modelling in the risk analysis of tunnels with ARTU software. Fronterre M., Scozzari R. (2022) 11th International Conference ‘Tunnel Safety and Ventilation’, Graz
- [6] Johansson, N. (2021). Evaluation of a zone model for fire safety engineering in large spaces. *Fire Safety Journal* 120.

- [7] Johansson N., Ronchi E., Scozzari R., Fronterre M., (2023) The use of multi-zone modelling for tunnel fires, *Tunnelling and Underground Space Technology*, Volume 134, <https://doi.org/10.1016/j.tust.2023.104996>.
- [8] Sandin, K., Grenberg, K., Husted, B. P., Scozzari, R., Fronterre, M., Ronchi, E. (2019). *Verification and Validation of the ARTU (Tunnel Fire Risk analysis) tool*. Lund, Sweden: Lund University, Department of Fire Safety Engineering.
- [9] Purser, D., & McAllister, J. (2016). *Assessment of Hazards to Occupants from Smoke, Toxic Gases, and Heat*. In M. Hurley, *SFPE Handbook of Fire Protection Engineering*, 5th edition (pp. 2308-2428). Springer Science+Business Media.
- [10] McGrattan K.B., McDermott R. J., Weinschenk C. G., Forney G. P. (2013) *Fire Dynamics Simulator, Technical Reference Guide, Sixth Edition*
- [11] Ang C., Rein G. und Peiro J. (2020), *Unexpected Oscillations in Fire Modelling Inside a Long Tunnel*, "Fire Technology, Nr. 56, pp. 1937-1941, 2020.
- [12] McGrattan K. und McDermott R (2022) *Response to "Unexpected Oscillations in Fire Modelling Inside a Long Tunnel" by Ang et al*, "National Institute of Standards and Technology, Gaithersburg, Maryland, USA, 2022.
- [13] *Backlayering and changes with grid resolution, discussion started in 2023 on FDS issue tracker* (<https://github.com/firemodels/fds/issues/11495>)
- [14] Heskestad, G., 1983. *Virtual origins of fire plumes*. *Fire Safety Journal* 5 (2), 109–114.
- [15] Ingason H., Li Y. Z., Lönnemark A. (2015). *Tunnel Fire Dynamics*. Springer
- [16] Li YZ, Ingason H (2014) *Position of Maximum Ceiling Temperature in a Tunnel Fire*. *Fire Technology* 50:889–905

AI IN ROADTUNNEL – SUPPORTING THE MAN-IN-THE-LOOP IN ROADTUNNEL (SMART)

¹Philipp Böhnke, ²Tom Schumann, ²Dirk Kemper, ²Alvaro García Hernandez
¹ave Verkehrs- und Informationstechnik GmbH, DE

²RWTH Aachen University, Lehrstuhl und Institut für Straßenwesen (ISAC), DE

DOI 10.3217/978-3-85125-996-4-26 (CC BY-NC 4.0)

This CC license does not apply to third party material and content noted otherwise.

ABSTRACT

This paper gives an overview about the latest research results of ave company together with the RWTH Aachen University in the field of AI based incident detection. The presented approaches and results were mainly gained in the context of the research project “Supporting the **Man-in-the-loop** in **Roadtunnel** (SMaRt)” funded by the German Federal Ministry of Education and Research (BMBF).

The workload of tunnel operators is constantly increasing, leading to overloads and affecting safety. Today's systems for traffic monitoring and incident detection in road tunnels usually follow a two-stage approach. A sensor bases automated incident detection system is followed by “final detection” and/or the cause of the incident by the tunnel operator. Depending on the reliability of the incident detection system used, this means more or less "extra" work for the "man-in-the-loop" – the tunnel operator.

Within the 3-year project SMaRt (2021-2024) AI based methods are developed to improve incident detection and thereby to reduce the workload of the operators. AI is used on three levels, namely the sensor- (“Intelligent Induction Loops” and video), the data fusion- and the GUI-level.

The results show that AI algorithms can help combine loop and video technology to take advantage of both technologies.

Keywords: AI based incident detection; support for tunnel operators; increasing tunnel safety

1. INTRODUCTION

Even in an increasingly digitalized world, many decisions are still made manually, i.e. with the direct involvement of a person. Highly complex technical systems and processes are monitored by so-called operators, the people responsible for the process. In the event of a malfunction or alert, the technical system automatically provides the operators with information that enables them to quickly assess the current status of the process, but the operator is still responsible for selecting the necessary and appropriate countermeasures and initiating them. This approach, also known as "man-in-the-loop", is used in various areas of application. In many of these areas, however, the large flood of information and insufficiently adaptive evaluation of the information leads to a constant overload of operators and thus to a reduction in safety. Particularly in the field of public infrastructure, e.g. road tunnels, the approaches used today are still too often based on classic, i.e. non-learning algorithms that no longer reflect the state of the art.

In Germany, but also in Europe, automatic incident detection systems are mainly based on optical (video, infrared, etc.) or electromagnetic (induction loops, etc.) technologies. Both technologies have specific advantages and disadvantages, which are basically due to the underlying physical measuring principles. For example, the "Intelligent Induction Loop"

electromagnetic sensor used in the SMaRt measures very reliably, but has a spatial resolution that corresponds to the distance between two neighboring measurement cross-sections (here: 330-480m). The optical video system used, on the other hand, has a very high spatial resolution, but is not as reliable with regard to shadowing.

Aim of the research project SMaRt is to use innovative artificial intelligence (AI) algorithms to significantly improve the working conditions for operators in road tunnels. This is done by a three-level approach. Therefore, AI should be used namely on

- Sensor level (“Intelligent Induction Loop” and video)
- Data fusion level
- Graphical user Interface (GUI) / operator level

2. RESEARCH PROJECT SMART

The SMaRt project is funded by the German Federal Ministry of Education and Research (BMBF) within the funding directive “KMU-innovativ: IKT”.

Goal of the funding is to strengthen the innovation potential of small and medium-sized enterprises (SMEs) in the field of cutting-edge research and to increase the attractiveness of research funding under the “IKT Fachprogramm”. This funding measure is intended to help SMEs establish themselves in the information and communication technology (ICT) market and become more competitive. The aim is to support SMEs that are active in the field of ICT or want to expand and strengthen their business area through the use of ICT [1]. During the 36-month project (July 2021 to July 2024) a test area was set up near the city Aschaffenburg, which includes parts of the tunnel-like noise protection housing “Einhausung Goldbach-Hösbach” on the motorway A3, in the following called Hösbach tunnel (Figure 1).

The SMaRt project team consists of the “ave Verkehrs- und Informationstechnik GmbH”, “Lehrstuhl und Institut für Straßenwesen (ISAC) der RWTH Aachen” and, as an associated partner, the “Die Autobahn GmbH des Bundes – Niederlassung Nordbayern”. This means that a SME as a developer and manufacturer of automatic incident detection systems, a research institution and an infrastructure provider are represented, so that the entire chain from research to development and implementation to operation is covered.



Figure 1: “Einhausung Goldbach-Hösbach”,
Source: www.google.de/maps; www.wikipedia.org/wiki/Einhausung_Hösbach

Acronym	SMaRt
Full name of the project	Supporting the Man-in-the-loop in Roadtunnel
Project duration	July 2021 bis July 2024
Funding directive	KMU-innovativ: IKT
Funder	German Federal Ministry of Education and Research (BMBF)
Project Management Agency	DLR Projektträger
Project partners	ave Verkehrs- und Informationstechnik GmbH RWTH Aachen University, Lehrstuhl und Institut für Straßenwesen (ISAC)
Associated project partner	Die Autobahn GmbH des Bundes – Niederlassung Nordbayern

3. DESCRIPTION OF THE APPROACH

3.1. Test area Hösbach tunnel

The test area in the Hösbach tunnel consists of three measuring cross-sections with intelligent double induction loops according to TLS Type2 [2]. These three measuring cross-sections form two measuring sections of about 480m and 330m, each of which is limited by two neighboring measuring cross-sections. This covers a total length of approx. 810m of the tunnel with three main lanes and hard shoulder as well as in section 1 an exit and in section 2 an access road (Figure 2).

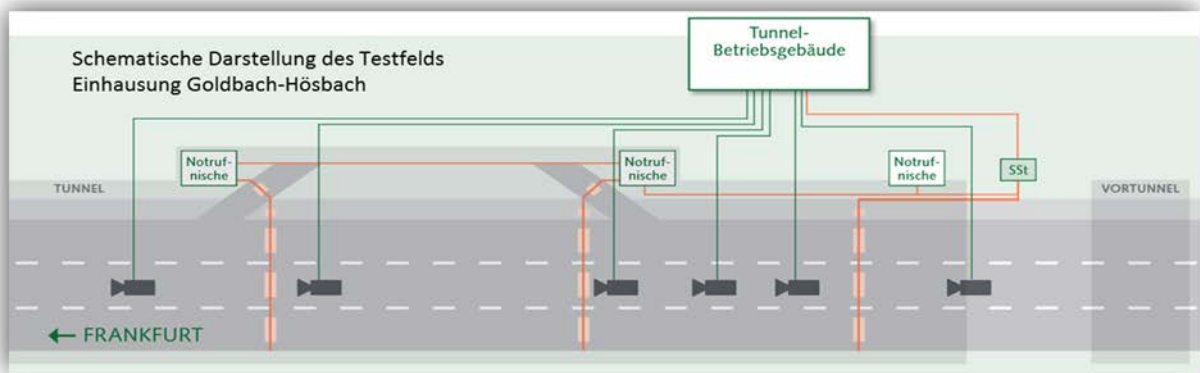


Figure 2: Schematic layout - test area Hösbach tunnel

In addition, various video cameras are installed in the Hösbach tunnel which provides a good visual overview of the whole tunnel, including the test area.

3.2. Used electromagnetic sensor “Intelligent Induction Loop”

As electromagnetic sensors a MAVE[®]-tun R&D system based on the measuring principle of the “Intelligent Induction Loop” was chosen. This sensor enables to collect both local and section-related traffic data as well as local and section-related alerts. Possible alerts are broken down/stationary and slow driving vehicle on the measuring cross section (local) as well as in

the measuring section (section-related). In addition it allows also detecting wrong-way driver and traffic jam.

For the section-related alerts, two neighboring measuring cross-sections are logically combined into one measuring section (Figure 3). As soon as a vehicle enters the measuring section via the entrance cross section, an electromagnetic pattern of the vehicle is recorded. When leaving the measuring section, a second electromagnetic pattern is detected at the exit cross section. By pattern recognition both patterns were correlated. An essential feature of this measuring procedure is to guarantee privacy. This means it is for system-related reasons impossible to identify individual vehicles or drivers [3].

The time difference between the time stamps of the two patterns corresponds to the travel time of the vehicle. As the distance between entrance and exit cross section is structurally defined and known. Thus, the travel speed through the section can be calculated easily. Since the method is applied continuously for each vehicle, the number of vehicles in the section can also be measured. This also enables the calculation of the traffic density. All collected traffic data as well as the resulting alerts are available nearly in real time.

Alerts are detected by comparing the travel time of the individual vehicle with the travel time of the surrounding traffic. Significant differences are an indicator for incidents like broken down, slow or wrong driving vehicles. All significant events cause an immediate change in the current traffic flow. Hence, the detected results indicate an incident of any cause, e.g. a car break down, an accident or a person on the road at a very early stage.

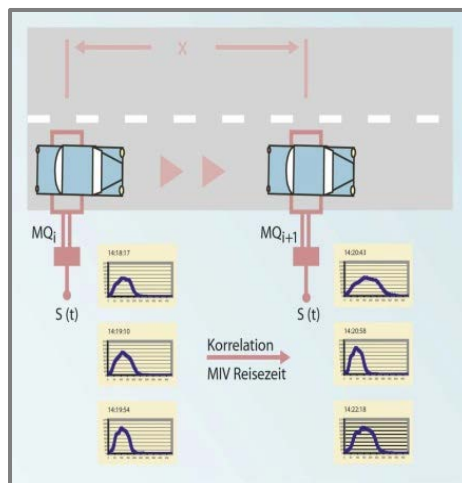


Figure 3: Intelligent Induction Loop technology - measuring principle

Due to the physical measuring principle and its implementation in the Hösbach tunnel the electromagnetic sensor data has a spatial resolution of about 330-480m and a temporal resolution that corresponds to the current travel time for the section.

Even though the conventional MAVE[®]-tun system already works very well and delivers very good results, new detection and evaluation algorithms based on AI are developed within the research project. One aim of SMarT is to investigate if and if yes to which extent the MAVE[®]-tun system based on the ‘‘Intelligent Induction Loop’’ can be further improved through the use of AI at sensor level.

3.3. Used optical sensor ‘‘Videocamera’’

In order to keep this system cost efficient the developed methods are designed to be applicable to various different camera systems and run on the preinstalled cameras also used by the operators. The test area itself is supplied with full-hd and hd-ready cameras covering the entire tunnel. All video-streams are firstly downsampled to 320 x 320 pixels to keep the

computational cost low while ensuring the proposed system's usability on a wide variety of camera systems.

Due to the relative efficiency and reliability of the induction loop based system the development of the vision based system was centered on effectively validating pre-alerts. As described in chapter 3.1.2 the induction loop alerts are generated if there is an unexpected deviation in traveling times between multiple vehicles e.g. single vehicles having stopped. Due to the time critical nature of the reaction of the operators to potential dangers being caused by incidents in the tunnel [4] this system is designed to detect anomalies as quickly as possible once being triggered. To achieve this task while being energy efficient a two stage system is proposed. The first stage continuously extracts sequences of video frames from the video streams. Using this method a ring buffer of the last five minutes is stored, of which only the last 30 seconds are used for the incident detection.

The optical systems second stage is in its default state on standby, waiting to be triggered by an alert. Once an alert is received a background estimation method is performed on the last seconds of the ring buffer. The estimated background as well as the individual frames are used as input for different anomaly detection methods. The anomaly detection method is derived from [5]. A pre-trained deep neural network is used to extract features given an input image. In a following step the distribution of these deep features is estimated for each camera position and raw frames and background estimated frames. The anomaly score of each image is derived from its feature representations probability in this distribution. Additionally a novel neural network architecture is developed and tested on the dataset. Both architectures are especially suited to work in conjunction with a loop based system.

3.4. AI Approach

In the SMarT research project, AI is to be used to find new solutions that help to speed up the detection of significant anomalies in the traffic flow and thus significantly support the operators - the man-in-the-loop. To detect these anomalies, both the "Intelligent Induction Loop" sensor from the company ave and the video detection/ CCTV system from RWTH / ISAC are used. Innovative AI solutions can be found on three different levels in three different project phases:

- Phase 1: Stand-alone AI - on sensor level
- Phase 2: Connected AI (partly) - on fusion level
- Phase 3: Connected AI (mainly) - on GUI / operator level.

While AI is still independent at the sensor level for the two sensor systems used, the results are connected at the fusion level. The aim here is to confirm or reject early "pre-alerts" from the Intelligent Induction Loop system as quickly as possible, i.e. faster than is possible with the Intelligent Induction Loop system alone, using the video system. If this is possible, time can be saved and road safety increased (Figure 1).

Finally, at the GUI and operator level, the personal preferences of different tunnel operators with regard to alerting by means of AI should be analyzed and taken into account. Not every tunnel operator in every tunnel sees similar anomalies in the traffic flow in the same critical way and wants them to be displayed. For example, slow-moving trucks in underwater tunnels can be "normal" and therefore "undesirable" due to gradients, but in mountain tunnels without a significant gradient they can indicate an "alerts-worthy anomaly" and therefore be "desirable".

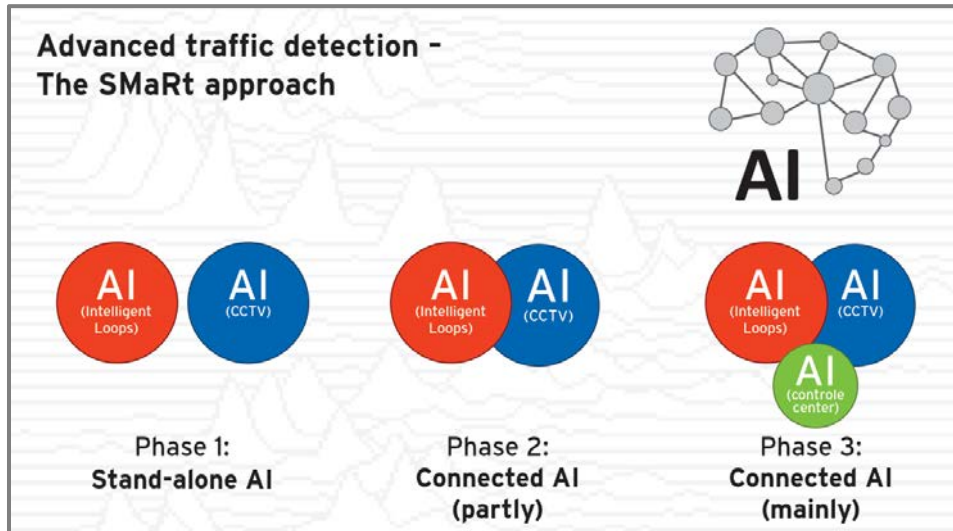


Figure 4: AI the SMaRt approach

4. RESULTS

4.1. Sensor level

Within SMaRt the sensors Intelligent Induction Loop and video / CCTV are used.

4.2. Intelligent Induction Loop

AI is used at the sensor level of the Intelligent Induction Loop sensor for pattern respectively vehicle recognition to reduce the dimensions of 1-dimensional vehicle patterns to 8-16 essential dimensions.

The process uses an encoder to generate a coded pattern with lower dimensions from the initial vehicle pattern, which is then decoded into a reconstructed vehicle pattern using a decoder.

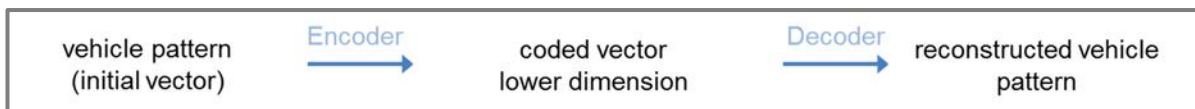


Figure 5: Encoder – Decoder

By comparing the initial vehicle pattern with the reconstructed vehicle pattern, a degree of error is calculated which needs to be optimized (Figure 6).

In a further step, the coded patterns of lower dimensions of the input and output measurement cross-sections are compared with each other and assigned. AI is also used here.

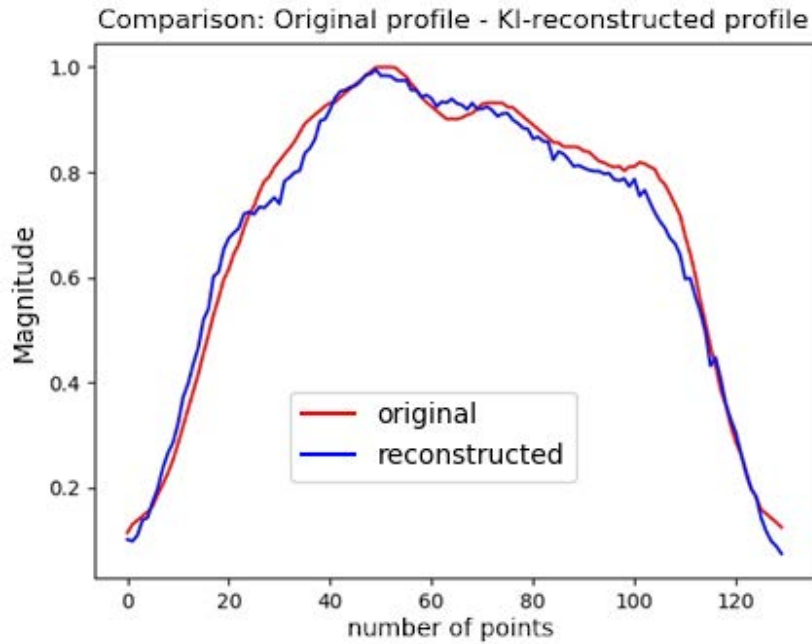


Figure 6: Comparison between initial and reconstructed vehicle pattern

4.3. Video

The dataset used for the experiments consists of 30 hours of video material of 10 cameras in the 500 m long test area as an input. Data was extracted over five different days while covering all times of day and night. The dataset used for these experiments has been recorded during normal traffic. It consists of almost exclusively ordinary traffic situations and does not include a significant number of incidents for a quantitative evaluation. The only incident that is present in the dataset reaches the highest anomaly score within the entire dataset using the Pre-Trained Deep Features based Anomaly Detection. The same video also shows very promising anomaly scores using our self-developed anomaly architecture. Both methods meet the speed requirement by reaching under 0.1 second response times for current anomalies in all ten cameras simultaneously and a under 1 second response time while detecting anomalies in the past 30 seconds. Both systems do not show a significant correlation between anomaly score and vehicle count in the frame and can be a reliable addition to an induction loop based system.

4.4. Fusion level

On the fusion level first results have shown that all alerts forwarded by the loop based system were classified correctly by the video detection system. The experiments ran for a very limited time of a few weeks. During this time there was 1 true positive alert and less than 10 false positives alerts.

4.5. GUI / Operator level

Up to now, no results are available for this level. Due to the complex real-time data collection of e.g. desired and undesired alarms, which would have to be carried out by the operators on site, this level will have to be worked on theoretically in large parts at the end of the project.

5. SUMMARY AND CONCLUSION

The first results of the research project SMaRt are promising. It appears that a combination of different sensor types (here Intelligent Induction Loop and video) based on physically different measurement principles can be very useful in terms of accuracy and speed of the generated alerts. The use of AI can also help to improve such a system on various levels.

However, it remains to be seen whether the use of different, partly redundant sensor systems for alert detection can be operated economically and thus find a market.

6. REFERENCES

- [1] KMU-innovativ: IKT; Forschungsprogramm des Ministeriums für Bildung und Forschung im Bereich Informations- und Kommunikationstechnologien (IKT), https://www.bmbf.de/bmbf/de/forschung/innovativer-mittelstand/kmu-innovativ/kmu-innovativ-ikt/kmu-innovativ-ikt_node.html
- [2] TLS 2012; Technische Lieferbedingungen für Streckenstationen; Ausgabe 2012; Herausgeber: Bundesministerium für Verkehr, Bau und Stadtentwicklung; Berlin 2012; https://www.bast.de/DE/Publikationen/Regelwerke/Verkehrstechnik/Unterseiten/V5-tls-2012.pdf?__blob=publicationFile&v=1
- [3] P. Böhnke, P.L. Böhnke, „Intelligente Induktionsschleifen zur automatischen Detektion von Störfällen“, Zeitschrift Straßenverkehrstechnik Ausgabe 01/2018, Kirschbaum Verlag GmbH Bonn (Organ der FGSV Köln, BSVI München, FSV Wien), Germany
- [4] J. Versavel, "Road safety through video detection," Proceedings 199 IEEE/IEEJ/JSAI International Conference on Intelligent Transportation Systems (Cat. No.99TH8383), Tokyo, Japan, 1999, pp. 753-757, doi: 10.1109/ITSC.1999.821155.
- [5] O. Rippel, P. Mertens, E. König and D. Merhof, "Gaussian Anomaly Detection by Modeling the Distribution of Normal Data in Pretrained Deep Features," in IEEE Transactions on Instrumentation and Measurement, vol. 70, pp. 1-13, 2021, Art no. 5014213, doi: 10.1109/TIM.2021.3098381.

APPLICATION OF AI TO THE 1D VENTILATION ANALYSIS OF A 43KM COMPLEX ROAD TUNNEL NETWORK: MADRID CALLE30

¹Juan Manuel Sanz, ²Fabián De Kluijver, ²Alberto López,

³Javier Berges, ³Mar Martinez, ¹Guillem Peris

¹Sener, ES

²JVVA, ES

³Madrid Calle 30, ES

DOI 10.3217/978-3-85125-996-4-27 (CC BY-NC 4.0)

This CC license does not apply to third party material and content noted otherwise.

ABSTRACT

Madrid Calle 30 ring road tunnels are a very complex road tunnel network, with a total extension of 43 km opened in 2007. In order to update the ventilation control algorithms, it has been necessary to analyze the records of all sensors and ventilation equipment since inauguration with the objective of characterize the current capacity of the system, the influence of the different parameters and learn from the analysis of past events. Due to the extension and complexity of the network, and the huge amount of field data available, an Artificial Intelligence (AI) system (Respira®, from SENER) has been used to evaluate the current performance of the system.

In parallel, a 1D simulation model of the whole ventilation system (as a digital twin) has been generated. The uncertainty in some parameters of the 1D model, and its size and complexity, has driven the design team to automatize its calibration. A surrogate model of the 1D model was built on Python by training it with a sample of 3,000 1D simulations, where uncertain parameters were modified randomly within ranges given by expert knowledge. Differential Evolution method is used for calibration [1], obtaining a set of parameters that minimizes an error function between the model prediction and the field data.

With this calibrated digital twin, it has been possible to optimize the ventilation algorithms for the different events foreseeable in the different areas of the M30.

Keywords: Algorithms, ventilation, Artificial Intelligence, simulations.

1. INTRODUCTION

The tunnels of Madrid Calle30 form a complex road network over 43 km long, with 938 fans, 85 ventilation shafts, 430 anemometers, and 284 gas detection sensors. Inaugurated in 2007, its ventilation control system is being refurbished as the control equipment is reaching the end of its life cycle. In addition to this, the operation of the ventilation system is being analysed and updated, taking into consideration the experience acquired in these years, the current situation of the infrastructure and the capabilities of the new control system.

Updating the ventilation algorithms requires adequate knowledge of the system's capabilities and behavior, as well as a digital model that allows knowing in advance the system's responses to different events or future actions. It is vitally important that the digital model is properly calibrated so that the results obtained accurately predict the behavior that the ventilation will actually have in the tunnel.

Once the capacity and configuration of the ventilation system is adequately known and a properly calibrated simulation model is available, the development of the ventilation algorithms is similar to that of any other tunnel. At this point the difference is only the large number of zones and equipment that must be considered for operation and fire situations.

For the analysis of ventilation and historical records of such a complex, extensive network with so much data, the application of artificial intelligence tools is a vital help. The application of automatic tools that allow comparison of the results of the simulations with those recorded during normal operation or during the various ventilation tests developed is also of great help. It is necessary to take into account the high number of parameters to be considered in the different areas of the infrastructure, in relation to circulation and ventilation itself.

2. DESCRIPTION OF THE INFRASTRUCTURE

The M-30 is the busiest road in Spain: it registers a daily average of 1.3 million trips (vehicles), with peaks of one and a half million journeys in 24 hours. We are talking about 475 million vehicles and 570 million people (users) per year. It is the main ring road of the city of Madrid with a mixed configuration of tunnels and open-air road.

The M-30 is the most extensive network of urban tunnels in Europe (48 kilometers of tunnels, equivalent to an underground lane of 118 kilometers). The tunnels have multiple entrances (21) and exits (22), as well as a wide variety of configurations and number of lanes in their different areas.



Figure 1: Scheme of the M30 tunnels

It also has different ventilation modes in its different areas (longitudinal, longitudinal with specific extractions, semi-transverse and transverse). The complexity of the tunnel network and its ventilation can be seen with some of the figures of its equipment:

- 430 anemometers (347 inside the road tunnels, rest in auxiliary tunnels and portals)
- 75 CO sensors
- 68 NOx sensors
- 141 opacimeters
- 521 jet fans
- 127 smoke extraction shafts for support longitudinal ventilation (normally each of them has two axial fans)
- 85 ventilation shafts with 163 axial fans (part of them are reversible)

3. ANALYSING FIELD DATA RECORDS WITH ARTIFICIAL INTELLIGENCE

3.1. VARIABLES

To analyze the current capacity of ventilation and the influence of the different variables on this system, the records of all relevant elements from the last 12 years (2011-2022) were extracted from the control center. These records included:

- Indoor and outdoor environmental sensors (air velocity, wind, temperature, CO, NO and NO₂, Opacity, etc.)
- Activation of ventilation equipment (jet fans, ventilation shafts, punctual extractions, air filters, dampers information, etc.)
- Traffic data
- Fire alarms and emergency exit sensors.
- Auxiliary variables of the control system

The information collected exceeds 3 TB of database files. Due to the high number of elements for which information is available, the way in which the data is recorded, the great diversity of variables considered and the different scales of the variables, it is practically impossible to process all the records manually or with conventional tools. From the tender stage, it was proposed to process all this information using artificial intelligence.

3.2. PROCESSES, ANALYSIS, REPRESENTATION AND MINING OF DATA

Once all the information received was registered, it was processed and filed homogeneously in a cloud database. In addition, an information viewer was developed with multiple possibilities for filtering and selecting variables, zones and times. This has been of great help to engineers to simultaneously analyze different variables and corroborate the correlations provided by artificial intelligence. It has also allowed us to analyze various specific events that the AI discards because they are not frequent, such as fire drills or real fires.

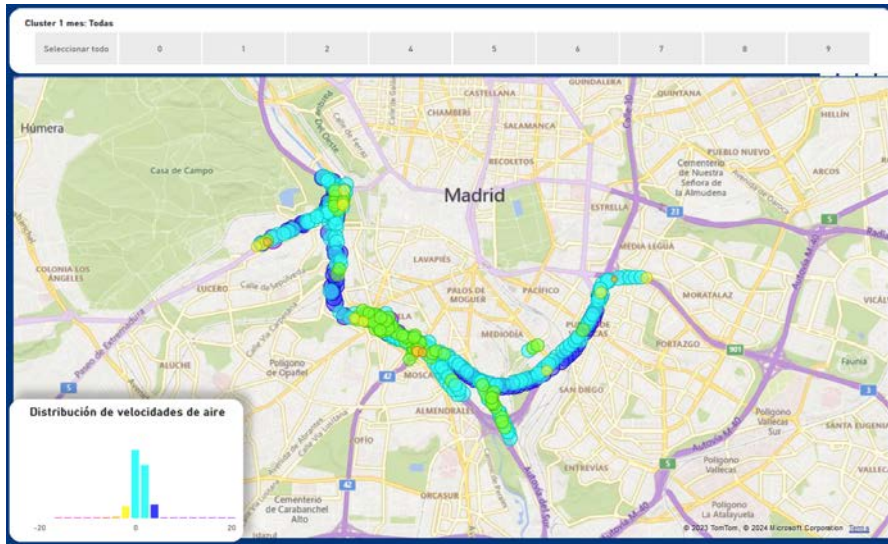


Figure 2: Example of the information viewer. Average air velocity from tunnel anemometers in the period selected.

Once all the information had been stored, the data was processed, filtering all the information that corresponds to specific events or registration failures that do not fit the main correlations that govern the ventilation of the tunnel. This guarantees that the data being analyzed is of quality for the purpose of the study.

To facilitate the analysis of the behavior of the ventilation of the infrastructure, AI techniques have been used to identify the equipment of greatest interest. With this, a large part of the equipment has been grouped into clusters that have similar behaviors or patterns. This allows engineers to see areas where ventilation behavior is similar, as well as greatly reducing the search for physical correlations between events or variables. These clusters have also helped to quickly locate sensors whose measurement is not sufficiently precise (or even incorrect) and have allowed the operator to know which equipment needed to be checked or adjusted. Measurements from devices that belong to clusters with inaccurate measurements are removed from subsequent data analysis and the model calibration process.

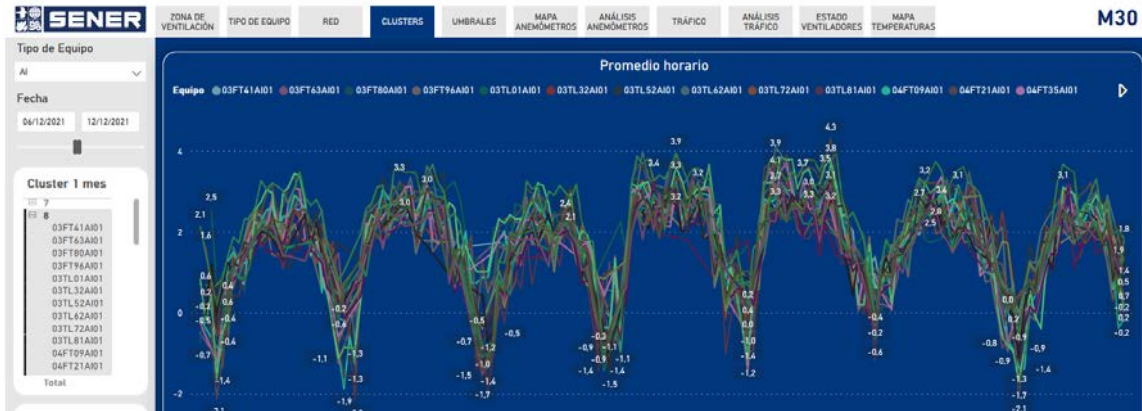


Figure 3: Cluster of anemometers with similar behavior in a given month.

The analysis of traffic data also allows us to obtain correlations in the different areas of the road between traffic intensity and speed and air velocity to analyze the piston effects in the different zones.



Figure 4: Correlation between traffic intensity and speed in the different areas of the tunnel.

Another analysis carried out has been the distribution of temperatures along the tunnel, its variation with time and its relationship to the outside temperatures and air speed. This has allowed us to know its influence on the natural draught during the normal operation of the tunnels. In general, it has been proven that the thermal effects in normal operation are much lower than those of the piston effects. During low traffic hours, thermal effects tend to exhibit repetitive patterns since they occur at the same times every day under very similar thermal conditions. Due to the large air currents in the tunnels caused by traffic, the tunnel temperature quickly adapts to the outside diurnal average. In Madrid, at night, the temperature is always lower than the daily average, so every night the tunnel temperature is higher than the outside temperature and the natural drafts are always the same. Likewise, it is observed that

temperatures tend to be colder in the West area that in the East (TBM tunnel), partly due to the presence of the Manzanares River and partly due to the greater number of connections with the outside of this area.

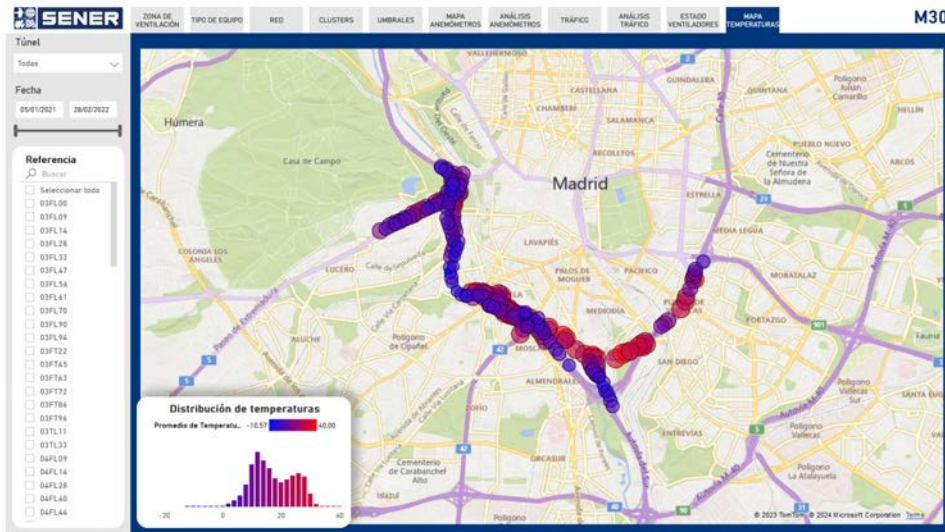


Figure 5: Average temperatures in the different areas of the tunnel in 2021.

Additionally, other artificial intelligence tools developed by Sener have been applied to the data using the Respira® tunnel ventilation control solution that has allowed, among other things, analyze the following:

- Analysis of hours in which the contaminant values are located at the different control thresholds.
- Relationship between traffic intensity and gas concentration.
- Establish homogeneous areas of the tunnels in relation to the different variables of interest.
- Selection of variables that affect tunnel ventilation and categorization in relation to their influence on ventilation.
- Detection of variables whose effect on ventilation overlaps with those of others already considered.

3.3. RESULTS OBTAINED WHEN APPLYING AI

The methodology used by Sener in their AI product Respira® for control the ventilation in tunnels is the next:

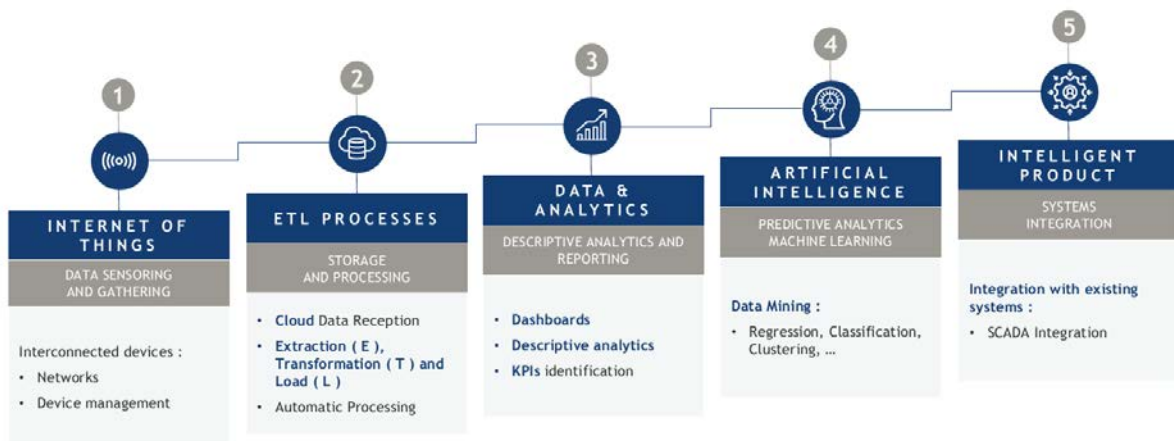


Figure 6: Methodology used by Sener in the tunnel ventilation control system applying IA.

In this project we have used the steps 2, 3 and 4. The most notable results are the following:

- Categorization of the variables that affect ventilation, making it easier to focus on the most important ones for the calibration of the simulation model and mainly discard those whose influence is minimal.
- Provide important tools for visualization and analysis of ventilation in different areas and events.
- Grouping of the different variables into clusters to reduce the number of situations to be analyzed manually.
- Quick obtaining of relevant values in common or specific situations or application of formulas considering the values over time of different variables.
- Detection of equipment with low precision in its measurements or with error.
- Elimination of incorrect or non-representative values of system operation.
- First analysis of the efficiency of the different jet fans and ventilation shafts.
- Obtaining certain correlations between variables (for example piston effect) or interpretation of repetitive events or direct physical relationship (temperature distribution, thermal effects, ...).

Additionally, it has been verified that all the information and tools are available to predict the behavior of the ventilation of the entire infrastructure and carry out control directly through AI assuring algorithms calibrated with real focus on safety and energy efficiency.

4. SIMULATION MODEL GENERATION AND CALIBRATION

The simulation model considered for the ventilation of the tunnel network is a 1-D model. This type of models apply to systems in which longitudinal dimensions are much bigger than transverse dimensions. For this reason, flow variables can be represented varying only along longitudinal coordinates not in the transverse directions. The value of each variable in each point represents the average value of that given variable in the transverse section of the corresponding point. The software used for the 1-D model is IDA-Tunnel, which has been validated for railway and for road tunnel networks. This model can be used to study both normal and fire ventilation scenarios in the tunnel network.

As in any physical model, there are some uncertainties in the definition of the inputs. In order to find values of these inputs that provides a good representation of the actual behavior of the system, a calibration process has been performed. In a first step, the tunnel was modeled without considering the ventilation (what we will call “physical model”); once the geometry and physical parameters of the tunnels were adjusted, the parameters of the different fans and shafts were adjusted, to obtain the “ventilation model” or “digital twin”.

In the input set (input vector) of the physical model, two types of inputs have been considered:

- Model parameters (θ): these are values of inputs of the physical model that are constant in time and have an associated uncertainty in its value.
- State inputs (x): these values are inputs of the model that are variable with time. In the case of the model considered, these inputs are the traffic flows in each of the tunnel segments and the ambient temperature. These inputs are assumed to be measured and part of the field data. For the purpose of the presented study, no uncertainties are considered for these inputs.

The calibration of the model parameters consists of finding the combination of those model parameters (θ) that provides the best fit between the output of the 1D simulation and the field data for different state conditions (traffic vector and ambient temperature). The output variable

that has been used for calibration is the air velocity in the tunnel, measured in each of the anemometers of the infrastructure. For the calibration process, the model parameter space needed to be explored by comparing the outputs of the simulations with the field data for different combinations of the model parameters and state inputs. As will be exposed below, the complexity of the model leads to a great number of parameters to calibrate. With such parameter vector, exploring the parameter space by directly using the simulation model would result in an unaffordable computational time.

In order to solve the computation time issue in the calibration process, a surrogate model of the simulation model has been defined. The surrogate model is a mathematical model that aims to provide (for a given set of inputs) equivalent outputs to the outputs provided by the 1D simulation model, but with a much lower computation time. Once the surrogate model is defined, it can be used in substitution of the simulation model during the calibration process.

Once the physical model has been calibrated, the ventilation is calibrated by adjusting the parameters and variables directly related to the activation of jet fans and shafts. To do this, it is verified that the variation in air velocity over time is accurately reproduced when the different equipment is activated. For this purpose, various tests were carried out in different areas of the tunnels. The complete model (digital twin) was considered adequately calibrated when the simulation results accurately reproduced the measurements of the different tests and the recorded field’s data.

4.1. MODEL BUILDING

In order to build the 1D simulation model, information has been collected from the different project documentation of the infrastructure. The tunnel network uses different ventilation strategies depending on the part of the network considered, with some areas using longitudinal ventilation and others using transverse or semi-transverse ventilation.

In Figure 7, a diagram of the 1D simulation model is represented. The model is composed by 194 tunnel segments. These elements are defined between two air flow bifurcations that can be tunnel bifurcations, connection to ventilation shafts or portals. In order to study situations without mechanical ventilation (used for example in the calibration process), tunnel segments are grouped taking into account only road bifurcations, resulting in 100 groups of tunnel segments.

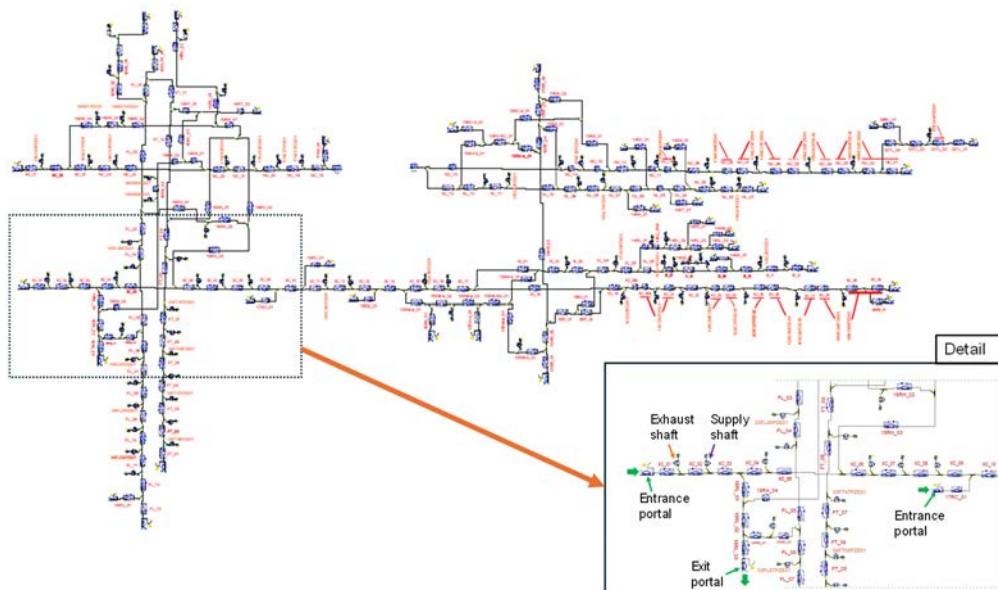


Figure 7: Diagram of the 1D simulation model.

4.2. CALIBRATION OF THE “PHYSICAL MODEL”

4.2.1. PARAMETERS TO CALIBRATE

As it was mentioned above, in any physical model there are some uncertainties in the definition of its inputs.

In the tunnel network considered there are many different vehicle types driving through it. For this reason, there is a considerable uncertainty in the definition of those parameters related to the aerodynamic forces of the traffic (piston effect in the tunnel). In the case studied, these parameters are the front area and the drag coefficient of the vehicles.

The model does not include local geometry changes that generate pressure losses in the tunnel (lay-bys, local height changes, beams, etc.), given the impossibility of including them in the model due to their quantity and complexity. These local pressure losses will be absorbed by the friction coefficient during the calibration process. For the friction coefficient in the model, a unique representative value λ^k is defined for each group of tunnel segments k .

Similarly, there are numerous cross-sectional dimensions for a given tunnel segment, being an unaffordable task to include all of them in the model. For that reason, in the simulation model these have been simplified. Since the tunnel cross sections are approximately rectangular, the simplification used considers a variable width depending only on the number of lanes, but a constant height for each group of tunnel segments. These heights will be also calibrated obtaining a representative value for the whole segments in a group.

The parameters used in the calibration process have been selected with a tradeoff in representing accurately the behavior of the infrastructure, but not increasing the number of parameters in an unreasonable way. In some cases, the parameters selected are not directly inputs of the model, but these inputs need to be calculated from these ones. This is the case of the friction coefficients and the transverse section dimensions.

During the calibration, a steady state approach has been used. Due to this, the tunnel wall temperature evolution is not simulated during the calibration process. To reduce the error due to this effect, an additional parameter (a_{temp}) has been introduced which allows subsequent adjustments of the model for the events in which it intervenes.

For the calibration process, the limits for the parameters need to be defined. In order to obtain realistic calibration results, expert criteria based in experience studying ventilation of tunnel networks is used. In Table 1, the number of parameters and their limits are summarized. The vector of parameters θ , considers the 202 parameters represented in the table.

Table 1: Parameters to calibrate.

Parameter	Number of parameters	Minimum value	Maximum value
Vehicle aerodynamic drag coefficient (c_x)	1	0.3	0.7
Vehicle front area coefficient (A_f)	1	1.9	3.3
Global friction coefficient (λ_{global})	1	0.01	0.035
Local friction coefficient (λ_{local}^k)	100	0	0.035
Tunnel heights (h^k)	98	Different limits depending on the group k	
Wall temperature parameter (a_{temp})	1	0	1
TOTAL	202		

4.2.2. SURROGATE MODEL

As it was mentioned above, the surrogate model aims to provide equivalent outputs to those provided by the 1D simulation model, but with a shorter computation time. The surrogate model that was built represents the air velocity in each of the anemometers, corresponding to a steady state simulation with a constant traffic profile, constant ambient temperature, and without mechanical ventilation. The input set of the surrogate model includes the vector of the parameters to calibrate (θ) and the vector of state inputs (x).

The type of state of the system considered for the calibration is a steady state situation without mechanical ventilation, which is assumed to be reached with a constant traffic flow and ambient temperature for one hour (period that is considered representative and in accordance with the traffic field data available). Therefore, hours of the year in which some of the ventilation was activated (jet-fans or ventilation shafts) have been filtered out and not considered for calibration.

Starting from a complete year of field data (those from the last full year available, which is 2021), after ventilation has been filtered, 3884 hours of data remains to perform the calibration. Looking for the state input, although there are not two hours with the same state input vector (x), the state of the system is repeated periodically along the year in an approximate way, resulting in some groups of state input vectors that are very similar (and would induce similar velocity in the tunnel). To take advantage of this, and to further reduce the computation time, 500 clusters have been defined (regarding the state input data), grouping each of the hours of the year 2021 in one of those clusters. For each cluster of hours j , an average state input vector x_j has been defined.

Surrogate model used has been built by using a gradient boost decision tree regression model [2] [3]. The regression model is fitted with a sample of 3000 simulations performed with the 1D model, varying the input vector (x, θ) in each of the simulations. Input for all these simulations have been generated with a Latin hypercube sampling method (LHS) with the range of variation of inputs limited to the same range that will be considered for calibration (Table 1).

With this set of 3000 simulations, the output of each of the 303 anemometers considered could be evaluated, fitting a surrogate model for each of these anemometers. The complete surrogate model results, therefore, in the combination of these 303 surrogate models.

Performance of the predictions provided by the surrogate model compared with the velocity outputs provided by the 1D model are represented in form of a R^2 score for each of the anemometers. In Figure 8, histogram of the R^2 scores is represented. As it is possible to see in this figure, the surrogate model provides a good prediction of the results of simulations.

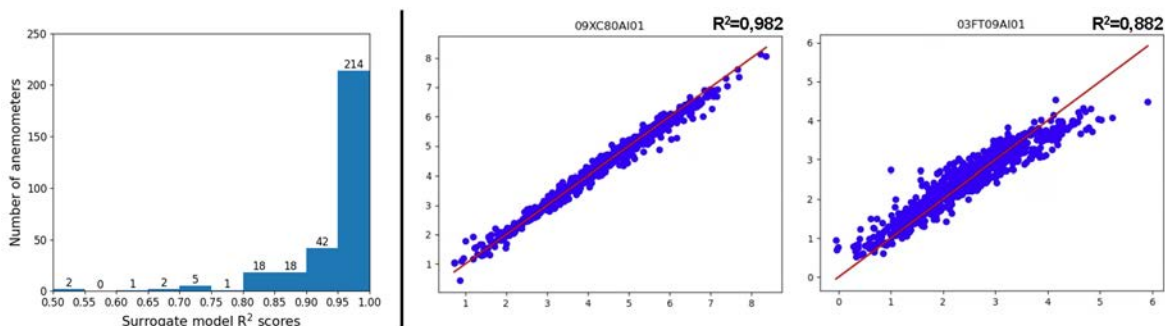


Figure 8: Left - General performance of surrogate model represented as a histogram of R^2 scores of the surrogate models of each of the anemometers. Right - Example of performance of surrogate model of two of the anemometers considered. Predictions of surrogate models compared against result of the simulations.

4.2.3. CALIBRATION OF THE MODEL PARAMETERS

Since the surrogate model has demonstrated to represent with enough accuracy the simulation model (for the conditions of interest) but with a much lower computation time, for the purpose of the calibration process the outputs of the surrogate model have been used substituting the role of the simulation model. With this strategy, an affordable computation time to explore the model parameter space is achieved.

For the field data corresponding to the air velocity measured by each of the anemometers, raw data is considered. This raw data contains measurements of air velocity that are not uniformly distributed in time, being the number of measurements for certain anemometer and certain hour of the year very variable. Measurements are classified in the cluster corresponding to the hour when the measure was taken. Pairs of cluster-anemometer with a low number of measurements (less than 25) are considered not representative enough and have been eliminated from the calibration process. From these filtering there are some anemometers that result with no valid clusters, reducing the number of anemometers usable for calibration from 303 to 289.

For a given value of the parameter vector θ , error functions are defined to measure the difference between simulation results and field data. An error function $e_i(\theta)$ is defined for each anemometer, and from those values a global error function $e(\theta)$ is defined. Equations used in the definition of these error functions are summarized in Figure 9.

$$e(\theta) = \frac{\sum_{i=1}^{N_{anem}} e_i(\theta)}{N_{anem}}, \quad e_i(\theta) = \frac{\sum_{j=1}^{500} w_{ij} \cdot |y_{ij}^{sim}(\theta) - \bar{y}_{ij}^{exp}|}{\sum_{j=1}^{500} w_{ij} \cdot |\bar{y}_{ij} - \bar{y}_{ij}^{exp}|}$$

$$\bar{y}_{ij}^{exp} = \frac{\sum_{k=1}^{N_{ij}} y_{ijk}^{exp}}{N_{ij}}, \quad \bar{y}_i = \frac{\sum_{j=1}^{500} \sum_{k=1}^{N_{ij}} y_{ijk}^{exp}}{\sum_{j=1}^{500} N_{ij}}$$

$$\sigma_{ij} = \sqrt{\frac{\sum_{k=1}^{N_{ij}} (y_{ijk}^{exp} - \bar{y}_{ij}^{exp})^2}{N_{ij}}}$$

$$y_{ijk}^{exp} \longrightarrow k \text{ measurement of anemometer } i, \text{ during hour corresponding to cluster } j$$

$$y_{ij}^{sim}(\theta) = y_i^{sim}(x_j, \theta) \longrightarrow \text{output of surrogate model of anemometer } i \text{ for input vector } (x_j, \theta)$$

$x_j \longrightarrow$ state input vector representative for cluster j

$\theta \longrightarrow$ vector of parameters to calibrate

$N_{ij} \longrightarrow$ total number of measurements of anemometer i , during hours corresponding to cluster j

$e_i(\theta) \longrightarrow$ error between field data and simulation results, for anemometer i and for given parameter vector θ

$e(\theta) \longrightarrow$ global error between field data and simulation results, for given parameter vector θ

$w_{ij} = \frac{N_{ij}}{\sigma_{ij}} \longrightarrow$ weight assigned to each pair of cluster j , and anemometer i

Figure 9: Definition of errors between field data and model results.

The objective of the calibration process is to find the value of θ , that minimizes the global error function. The surrogate model allows to quickly iterate through θ calculating in each step $y_{ij}^{sim}(\theta)$ for all the clusters and anemometers and obtain the corresponding value of $e(\theta)$. Differential evolution algorithm has been used to explore the parameter space finding the value θ that minimizes the value of the error $e(\theta)$.

In **Figure 10** the effect of the calibration on the velocities predicted by the model is represented. In this figure, the air velocity of different anemometers is represented against the value of traffic flow in the tunnel segment where the anemometer is placed. Three data sets are represented for each anemometer, field data (blue dots), outputs of surrogate model before calibration (red dots), and outputs of surrogate model after calibration (green dots).

The field data shows a greater amplitude than those generated by the simulation model, for 2 main reasons: greater variability in the environmental conditions (punctual wind, positive or negative natural draught due to sudden changes in temperature, etc.); and turbulence recorded by the anemometer (three-dimensional effects). It can be seen in the figure, that the calibration of the model improves the prediction of the air speed value and its relation to traffic (piston effect).

In **Figure 11** histograms of the distribution (by anemometer) of errors of the surrogate model in the prediction of field data are represented. Two histograms are represented, by using the parameter vector θ before and after calibration. The figure shows the improvement in the predictions with the calibrated values of the parameters.

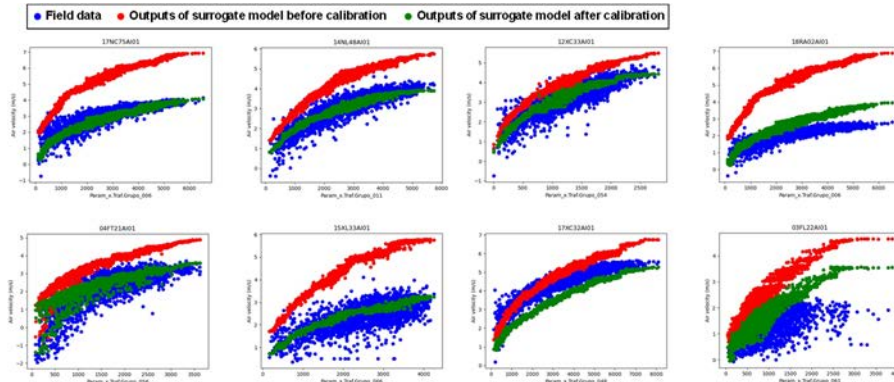


Figure 10: Air velocity (m/s) for different anemometers against the traffic flow (vehicles/hour) in the tunnel segment where the anemometer is placed. Three data sets are represented for each anemometer, field data (blue dots), outputs of surrogate model before calibration (red dots), and outputs of surrogate model after calibration (green dots).

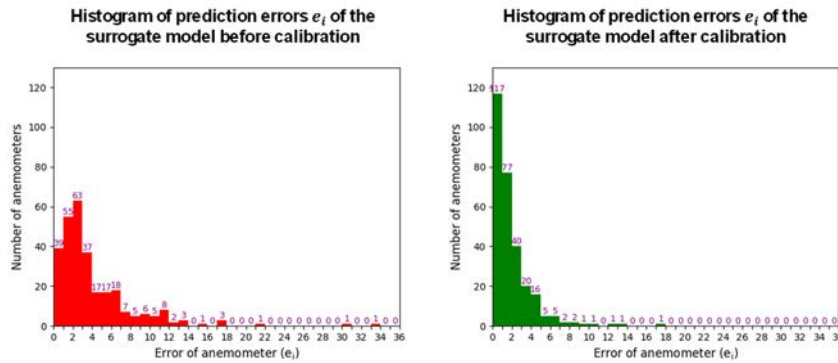


Figure 11: Histograms of the distribution of errors of the surrogate model in the prediction of field data. Left – Before calibration. Right – After calibration.

4.3. CALIBRATION OF THE VENTILATION SYSTEM MODELLING

4.3.1. FIELD AERODYNAMIC TESTS

With the information from the control center records and the equipment data, the necessary parameters of the ventilation system were available, but some uncertainties remained for the simulation model. To minimize these uncertainties, a series of field tests were defined and conducted.

The first round of tests consisted of measuring the air flow of each of the shafts (85) for their different operating regimes (different operating speeds of their axial fans) independently or in combination with nearby ventilation equipment (jet fans or ventilation shafts). From these tests, the most important data has been the current maximum air flow of each shaft. Additionally, first approximations of the efficiency of the jet fans and the influence of each shaft on the adjacent sections were obtained.

Due to the frequency of data recording from the control center, analysis of transient processes when switching ventilation equipment on or off was not possible. For this purpose, 30 aerodynamic tests were defined and carried out. In these tests, 2 anemometer arrays were placed at different points in the tunnel (normally on both sides of a shaft) and 1 additional array in the shaft. Various shaft regimes and nearby equipment (jet fans, shafts and specific

extractions) were turned on, obtaining variations in air flow and velocity throughout the tests. It also allowed knowing the air flow in both directions for the reversible shafts.

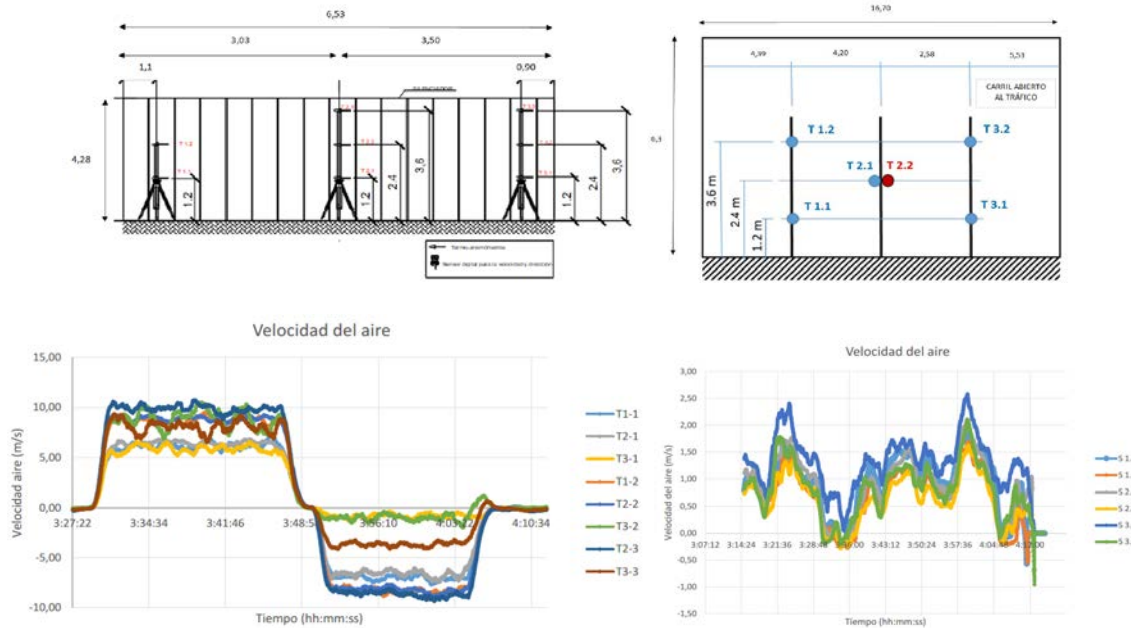


Figure 12: Distribution and measurements of anemometers during aerodynamic testing (left in shaft, right in tunnel).

4.3.2. CALIBRATION OF VENTILATION SYSTEM

Once the model has been calibrated using field data in states without ventilation of 2021, the aerodynamic tests performed in the infrastructure were simulated. With the simulations of these tests, it is verified that the model is able to represent the behavior of the system in the different ventilation regimes tested. In this model, calibration was only necessary to slightly adjust some parameters related to the efficiency of the ventilation equipment, shaft air flow or wall temperature (natural air draught). In Figure 13 comparison of the simulation results and the experimental data from one of the aerodynamic tests is represented.

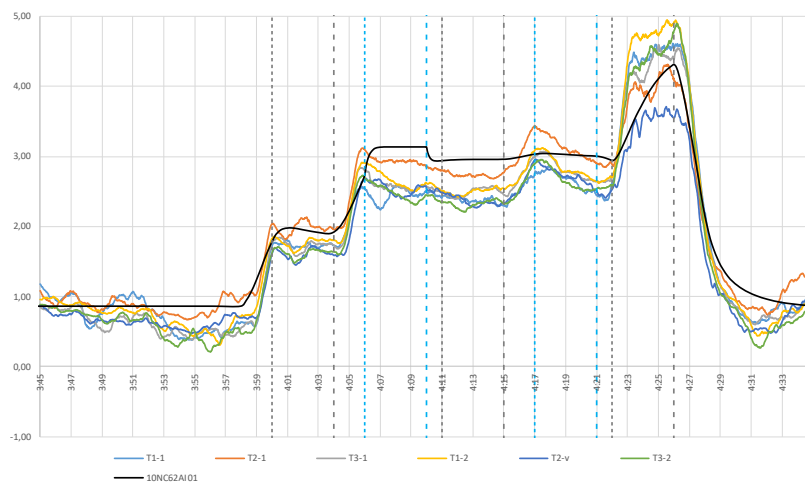


Figure 13. Results of air velocity results obtained in one of the aerodynamic tests. Comparison of simulation results (10NC62AI01) with the measurements of the six anemometers used in the test (T1-1, T2-1, T3-1, T1-2, T2-v, T3-2).

4.4. APPLICATION OF THE MODEL TO THE DEFINITION OF ALGORITHMS

Once the model has been calibrated, the possible ventilation actions required for sanitary and fire ventilation during different events have been simulated. This way, the jet fans and shafts (with their specific regimes) that must be active at all times have been determined, along with the time periods and transitions required for the system to adapt to the potential evolution of the event.

This has made it possible to define in detail the sanitary and fire ventilation algorithms for each position of the infrastructure.

In the next stages of the work, once the ventilation algorithms have been implemented in the control center, it will be verified with aerodynamic and smoke tests that the system response adjusts to what was predicted by the calibrated model.

With the model it has also been possible to analyse the equipment that has the greatest efficiency to achieve the objectives set for each point of the infrastructure, as well as to optimize the exact number of equipment to be turned on and the activation regime required for the ventilation shafts.

5. SUMMARY AND CONCLUSION

The use of new technologies as AI enables engineers to process and analyze a huge amount of information. Madrid Calle 30 Tunnels are a very complex road tunnel network of 43 km inaugurated in 2007. More than 3TB of information related to the ventilation system has been processed and analyzed by an AI system called Respira®. The use of cloud databases and artificial intelligence tools has been demonstrated to be essential in order to characterize the capacity and operation of tunnel ventilation as well as the analysis of certain events of great interest.

With all the information processed, a digital twin of the ventilation system has been created. Once calibrated, it enables the analysis of the optimal response to each event and the definition of the ideal algorithms for both normal operation and fire events.

The calibration process of the digital model has required, given its complexity and extensive recording of verification data, the use of computer tools and artificial intelligence techniques to automate the processes. It should be noted that the calibrated model reproduces with great precision all the field tests carried out both in their global values and their evolution over time (stationary and transient processes).

All this analysis would not be possible without the data collected from the control center since 2011, which remarks the importance of store the information of the facilities of the tunnel through the SCADA system.

6. REFERENCES

- [1] Scipy optimize differential evolution — SciPy v1.12.0 Manual. (n.d.). https://docs.scipy.org/doc/scipy/reference/generated/scipy.optimize.differential_evolution.html
- [2] Scikit-learn: Machine Learning in Python, Pedregosa et al., JMLR 12, pp. 2825-2830, 2011
- [3] 1.11. Ensembles: Gradient boosting, random forests, bagging, voting, stacking. (n.d.). Scikit-learn. <https://scikit-learn.org/stable/modules/ensemble.html#gradient-boosting>

ESTIMATING THE SEASONAL PERFORMANCE OF A SURFACE REFRIGERATION COOLING PLANT FOR AN UNDERGROUND MINE

¹Jolyon Thompson, ¹Mark Gilbey, ²Hugo Dello Sbarba

¹WSP, GB

²Dello Ventilation, CA

DOI 10.3217/978-3-85125-996-4-28 (CC BY-NC 4.0)

This CC license does not apply to third party material and content noted otherwise.

ABSTRACT

Tunnel ventilation and mine ventilation overlap in several areas. One key area is in the analysis of heat and how this can affect processes and people. A range of ventilation and thermal models have developed in parallel to support both industries, with occasional cross-industry use. In this paper we describe the cross-industry use of a mine ventilation model with a transient thermal tunnel ventilation model that WSP developed. The paper describes how the models were used together to answer important questions that could not readily be answered by one of the models alone.

The notional mine used for the case study would have experienced hot conditions at the working faces. A cooling plant at the surface was analyzed as they can be cost effective compared to an underground cooling plant. However, with the working faces a long way from the plant the cooling effect can be compromised by the time the air gets to where it is needed. The accurate evaluation of heat transfer between the rocks and the ventilation air, including seasonal impacts, is therefore important.

Tunnel ventilation models have good capability to model strata heat transfer and can be used in conjunction with the mine ventilation models to understand system performance. In this paper we also report on the performance of a surface cooling plant accounting for such heat transfer from the ground and go on to describe how the position to the cooling plant relative to the surface can have an important impact on how effective the cooling can be.

Keywords: Mine Ventilation, Tunnel Ventilation, Seasonal Performance, SES, Dynamo, Heat transfer

1. INTRODUCTION

Mine and tunnel ventilation analysis and engineering are similar. Both requiring a good understanding of fluid dynamics, network modelling and heat transfer as well as a practical understanding of fan engineering, cooling, flow measurement and flow control. There are, however, several important differences between the two that affect the nature of the modelling tools and approaches they use.

An excellent background into mine ventilation can be found in McPherson's Subsurface Ventilation Engineering [1]. Mines are normally significantly deeper than tunnels and with this comes the need to account for the compressibility of the air at depth which results in a heat input to the air. Just as air cools as altitude increases, it also warms with depth which in the mining industry is referred to as auto-compression. Without other heat transfer this results in approximately 1°C of warming of the air per 100m depth increase, regardless of the air flow rate. Other important differences relate to the complexity of the networks, with many local flow branches and divisions in mines. A considerable amount of practical experience and domain knowledge is needed for mine ventilation to understand the likely hydraulic resistance

of different types of mine walls, conveyances, and stoppings/seals; heat emissions from the ore and processes like blasting; engine emissions for mine vehicles and the control of gases emitted from the strata. Control of gasses and dust contaminants such as silica and diesel particulate matter can also be a consideration. The difference in density and mass between two vertical columns of air will generate a pressure differential that needs to be considered in underground mines, such effect is named the natural ventilation pressure and may have a great impact on the fan selection. The difference in density is a result of geothermal heat as well as heat output of underground machinery.

An excellent background into tunnel ventilation engineering can be found in the Subway Environmental Design Handbook [2]. Road, rail and utility tunnels tend to be shallower than mines and hence factors such as flow compressibility and auto compression can normally be ignored. A good deal of practical experience and domain knowledge is needed for tunnel ventilation to understand rolling stock traction movement, piston effects and heat emissions; pressure comfort; management of air speeds in public areas; transient thermal comfort; fire engineering and practical combined control of multiple ventilation plants, dampers, and systems.

Both mine and tunnel ventilation typically require the use of network modelling. Given the previously mentioned differences, not surprisingly differences emerge in the software used. At WSP we, and the specialists that support us on some projects, have tended to use Howden's VentSim™ for mine ventilation analysis [3]. It is widely used in the mining industry with a good user and support base. It has strong graphics capability, is tailored for the mining industry with pre-populated information and templates specific to mining and, importantly, includes for compressible variable density flow and auto-compression heating. The thermal model for the strata heat transfer is well validated but relies on the application of a semi empirical method to approximate the impact of cyclic and seasonal heat transfer into the ground. Other mine ventilation packages we understand to use a similar approach.

For tunnel ventilation we predominantly use the Subway Environment Simulation (SES) software which we co-developed (in the guise of Parsons Brinkerhoff) and continue to support and update [4]. The programme is well validated, with strong confidence in its aerodynamics results. Thermodynamically, the programme is well validated and, for example, WSP and London Underground [5][6] have used it to model each of the lines on the Underground and found it capable of predicting summer temperatures very well compared to a great deal of temperature validation data that was available on the project. Whilst we have confidence in the software, like VentSim™, it also relies on a semi empirical analytical method to calculate the wall heat transfer. This simplification is usually sufficient, but when there is a need to understand in better detail transient effects such as nighttime cooling and seasonal cooling WSP developed a companion package called Dynamo to model such thermal transient events. The tool was developed for modelling tunnel systems and can manage transient behavior in all inputs to the model.

Dynamo is a flexible energy balance model with a finite difference-based heat sink that can predict in tunnel environments. The tunnel is broken down into segments (normally around 200m long) and for each segment the ground is model as a radial set of finite elements nodes and rings. Inlet conditions are passed through the various segments and heat gains and latent heat transfer can be represented, along with such features as cooling pipes, ventilation shafts and embedded cooling pipes within the tunnel wall. With the right choice of nodal spacing the software was validated to within 0.1K by comparing the predictions of a matching case to an exact analytic solution of the transient cycling heat transfer equations [7][8]. Dynamo can provide transient analysis with continually varying scheduled inputs and outputs. It has been used to model several unorthodox heat transfers in tunnels, including heat waves [9] and

tunnel heat recovery [10]. Flow boundary conditions are input into the software from the 1D network models. Fourier number re-scaling is used to initialize the model and reduce simulation time and thereafter a typical 50-segment model may take around one hour to run on a laptop PC.

2. CASE STUDY – SOFT ROCK UNDERGROUND MINE

Model inputs

For this case study we considered an underground mine in a continental climate. An outside weather file climate was synthesized with an average temperature of 14.7°C and a 1% exceedance temperature of 35.8°C.

The mine was modelled as 750m below ground and with a virgin rock temperature of 40°C at depth. The working faces extended 5 km from the main intake shaft. A single ventilation station was included in the model located below ground 1km into the mine. This ventilation station delivered 125 m³/s of outside air that was shared between the working faces. Inevitably some of that air was modelled as lost due to leakage into the return air gallery at crosscuts mainly for vehicle crossing. The fans positioned on the intake added an additional 800 kW into the air due to compression and inefficiencies. The mine was modelled as a constant 6m by 5m cross-section. The ventilation flow was assumed to branch off after 4 km into the mine to serve working faces. For a given working face, a flow rate of 25 m³/s was assumed. A schematic of the mine ventilation system is shown in Figure 2.

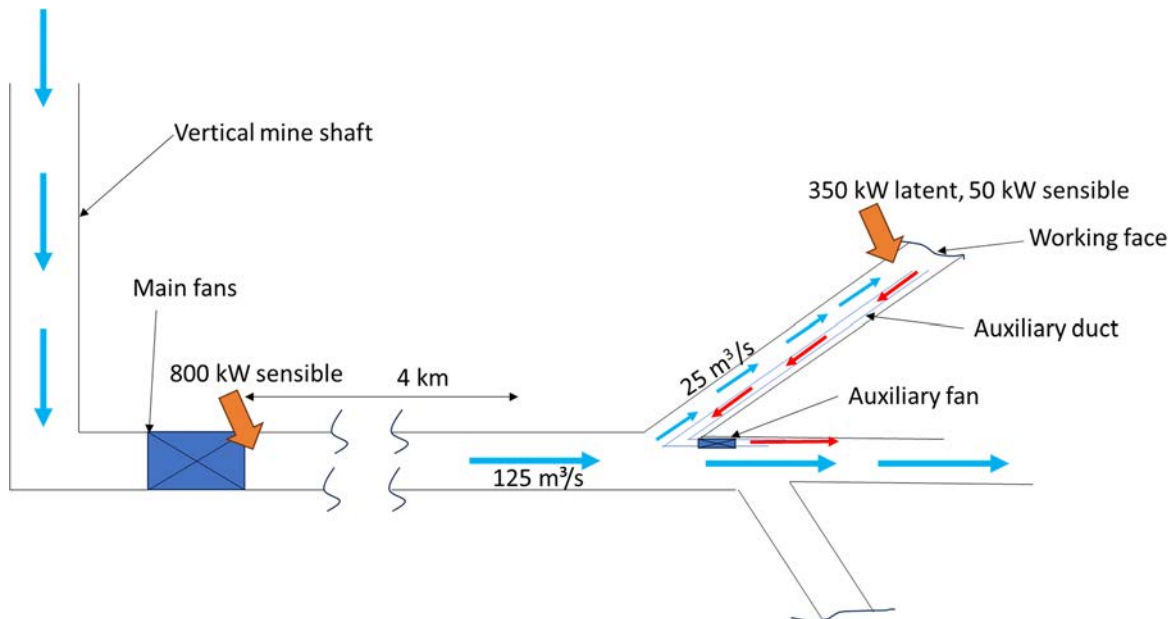


Figure 1: Schematic of test case mine

Each working face was assumed to use an electrically powered continuous panel miner with one to two 25-tonne diesel trucks removing the mined mineral and discharging it into a conveyor in the return air gallery. The working galleries can be up to 350m long and are ventilated with an exhaust auxiliary fan and flexible duct arrangement. The fresh air is supplied and exhausted from the main ventilation gallery and then passed into the return air drift. The fragmentation of the rock by the continuous miner can generate a lot of dust. Water spraying is used both cooling the panel miner and then onwards for dust suppression. Based on our measurements from other mines, the mining process for such mining method with similar sized equipment is estimated to result in an average of 350 kW latent heat emissions

and 50 kW sensible heat emissions. Much of the latent heat emission is caused by direct and then later re-evaporation of the dust suppression water, as well as latent heat from the truck emissions. A working face schematic and the types of equipment can be seen in Figure 2.

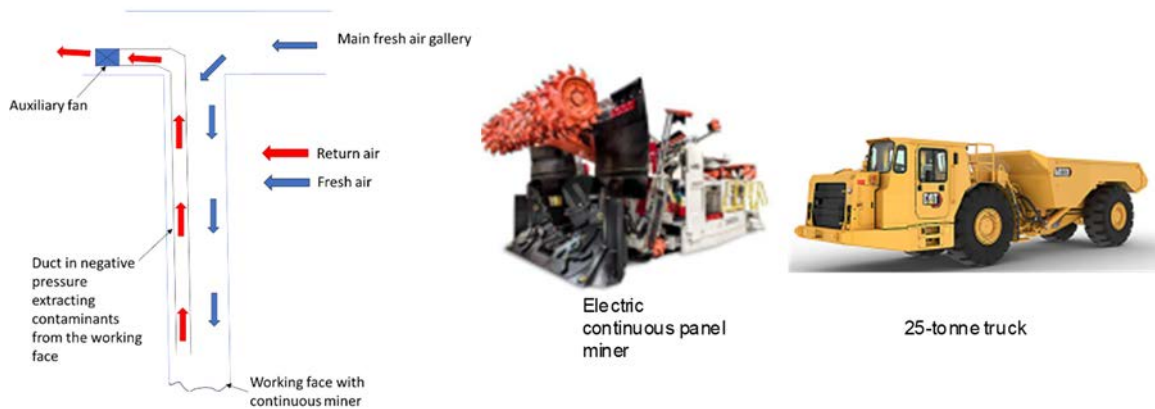


Figure 2: Mine face process

Cooling options

The starting point in managing mine conditions should be maximizing the capacity and effectiveness of the local ventilation at the working face. In practice, this can be challenging, particularly in cases where pillar mining cannot be used, and sinuous drives are used to reach the face. This is due to duct size being limited by the space used by the truck. For this case study the local exhaust capacity was set to a limit of 25 m³/s. To increase this capacity at the working faces the main fans must have enough capacity to provide this airflow at the face while minimizing leakage in crosscuts. If they don't a tradeoff analysis must be conducted to evaluate if it is more feasible to increase the capacity of main fans or install a mechanical refrigeration plant. Mine cooling from the surface is normally more practical for installation and heat rejection purposes. Some or all the intake air is cooled and introduced at, for example, 12°C rather than 30 to 35°C in summer. The cooling will also lower the humidity ratio of the outside air. This method has the major drawback that the cooled air will collect heat from the strata on the way to the working face and become warmed. The alternative is to provide cooling within the mine using air handling units located in excavated side-streams. This limits the heat transfer from the strata but has the cost of installing and maintaining the equipment underground and the challenges to reject the heat in the hot and humid return air stream.

For this study we considered some of the differences between surface and below ground cooling using a case study and a combination of VentSim for airflow and heat generated from the working face and Dynamo for transient heat transfer with strata. The case study was developed to answer the following questions:

1. What is the impact over time of the cooling of air on the strata heat transfer?
2. What is the seasonal performance of the cooling considering the thermal flywheel effect of the ground (the rate at which heat energy is absorbed and released by the surrounding strata during the daily and annual temperature fluctuations)?
3. What peak capacity in-mine plant may have the same effect as a surface plant?

Model results

The results are compared against thermal safety indices. Different countries and mines have different indices that they use to manage worker thermal safety. For this study we report wet bulb globe temperature (WBGT) [11] and Effective Temperature (ET). WBGT can be

calculated as the sum of 70% of the air wet-bulb temperature and 30% of the air dry-bulb temperature (in degrees C). ET can be complex to calculate, but in mining applications can be simplified as the sum of 90% of the air wet-bulb temperature and 10% of the air dry-bulb temperature. Again, different mines and countries set different limits on WBGT or ET. For this application we consider acclimatized workers and eight-hour shifts at the working face with an ET limit of 31°C.

Figure 3 in Appendix 1 shows the results of the base case (i.e no mechanical cooling and ventilation only). The mine was predicted to stabilize thermally after three or four years, a prediction that could not have been ascertained from a mine ventilation model alone. The annual temperature variation at the bottom of the air intake shaft was around 11K dry bulb, less than outside because the shaft moderated the outside air temperature fluctuations of close to 35K. The 11K annual swing in temperatures at the base of the shaft reduced to only 4K at the face. This was as a direct result of the air to wall heat exchange as it passed along the warm mine walls on its way to the working face. Once at the face the daily variation in dry bulb temperature was predicted to be small. There was a higher fluctuation in wet bulb temperature since the strata did not act to buffer the changes in humidity ratio of the air prior to it reaching the face. The WBGT and ET were predicted to be quite stable in summer, with conditions of between 35 and 31°C respectively. The daily range can again be mostly attributed to the changes in humidity ratio rather than dry bulb temperature.

Figure 4 in Appendix 1 shows the impact of 5 MW of surface level cooling with a dew point temperature of 10°C on the coil and a contact factor of 0.9. The system was predicted to be operating at thermal maturity within a year. This was because the strata heat transfer negated most of the sensible cooling effect prior to the air reaching the working face. The system was predicted to reduce the maximum ET by 5K and the average ET by 1.9K. This compares with 4.8K and 2.0K for maximum and average WBGT respectively. The difference in these two metrics can be considered marginal.

Most of this improvement in thermal safety was because of the reduction in wet bulb temperature caused by the coil's dehumidification in summer. Most of the sensible cooling effect was offset by heat transfer from the ground along the length of the mine. An average air temperature increase of over 30K was observed from the cooled supply air to the working face. At the working face the summer dry bulb and wet bulb temperatures were reduced, but the winter temperatures changed little since in that condition the air on-coil conditions were typically close to or cooler than the dew point which resulted in no humidity condensation.

Figure 5 in Appendix 1 shows the impact of 2.5 MW of mine cooling, again with a dew point temperature of 10°C at the coil and a contact factor of 0.9. The contact factor of a coil is defined as the efficiency for dehumidification. In practice it is defined as the ratio between the moisture reduction achieved by the coil and the moisture reduction that would be achieved if the cooling coil could reduce the air to the dewpoint temperature of the coil. The capacity of 2.5 MW was arrived at by iteration until the summer maximum WBGT and ET were like that of the 5 MW surface cooling plant. One immediate conclusion is that a plant within the mine was capable of being only half the capacity of a surface plant for a similar summer peak impact. It is also noteworthy that the underground plant provided a much greater reduction of both dry bulb and wet bulb temperature, and a much greater variation and improvement in WBGT and ET across the whole year (rather than just in summer). This improvement in annual average conditions may be of value in improving worker safety and productivity.

Table 1 shows a summary table of the key results, including the annual average cooling capacity delivered by the plant and the summation of the annual cooling energy delivered by the cooling plant. Whilst the underground plant is lower capacity, annually it delivers more

cooling, or in simpler terms, it is more heavily utilized. This is mainly because the impacts of auto compression heating and fan station warming mean that the on-coil temperature is higher. This could either be seen as a positive in that the investment in the cooling plant is more intensively being capitalized upon, or a negative in that the cooling plant is using more energy. Depending on the value of cooler conditions year-round to the cost of energy, the deep mine plant may be reduced in cooling output in winter and spring.

Table 1: Results comparison for the three cases considered

Case	No Cooling	5 MW Surface Cooling	2.5 MW UG in Mine Cooling
Max / Average Dry bulb (°C)	45.7 / 43.5	41.5 / 40.9	36.5 / 32.6
Max / Average Wet bulb (°C)	31.1 / 29.8	26 / 23.6	27 / 21.7
Max / Average WBGT (°C)	35.4 / 30.8	30.6 / 28.8	29.8 / 24.9
Max / Average ET (°C)	32.5 / 27.2	27.5 / 25.3	27.9 / 22.8
Average cooling (MW)	-	1,200	2,499
Annual cooling (GWh)	-	10,511	21,892

3. CONCLUSION

Mine ventilation models and tunnel ventilation models can be used in combination to deliver more useful results to help guide investment and performance conditions around cooling plant. They allow the seasonal performance of the plant to be appreciated and accounted.

The sensible cooling performance of surface plant can be significantly diminished by the impact of heat gains along the mine walls from the airways before the working faces. The main performance benefits can be in reducing the moisture content of the incoming air. Surface cooling plant is also best suited for reducing peak conditions in summer since in cooler seasons the cooling coils may not deliver significant amounts of cooling.

Whilst cooling plant located within the mine may be more expensive and complex to install, they can potentially be much lower in capacity to deliver a similar cooling effect. They are also able to deliver better annual changes in both tunnel air dry bulb and wet bulb temperatures compared to surface cooling plant. The plant is likely to be more highly utilized (and thus use more energy). This may either be welcome or unwelcome, depending on the mine’s view on the value of cooler conditions year-round compared to the cost of running the cooling plant.

4. REFERENCES

- [1] McPherson, M. J. (1993). Subsurface Ventilation Engineering. Nottingham: MVS Engineering.
- [2] U.S. Department of Transportation. Subway Environmental Design Handbook, Volume I Principles and Applications (2nd Edition), Research and Special Programs Administration John A. Volpe National Transportation Systems Center, Cambridge, MA 02142-1093
- [3] Howden Group, <https://ventsim.com/>
- [4] Parsons Brinckerhoff, 2014, Subway Environment Simulation User’s Manual.
- [5] Bradbury W.M.S, Gilbey M.J, Temperature management on London Underground, 13th International symposium on aerodynamics, ventilation and fire in tunnels, New Jersey, 2009.

- [6] Lightfoot A., Clark G. Hunt K., Tunnel ventilation modelling for normal operations of London Underground, 3th International symposium on aerodynamics, ventilation and fire in tunnels, New Jersey, 2009.
- [7] Thompson J.A., Missenden J.F. Gilbey M.J. and Maidment G.G., Response of wall heat transfer to steady and transient flows along a cylindrical cavity, Int. Symp. Aero. & Vent. Vehicle Tunnels, New Brunswick 2009
- [8] Thompson J.A., Dynamo – Enhancing tunnel ventilation modelling, Network, Issue 78, Parsons Brinckerhoff, December 2014
- [9] Thompson J.A., Kemp S. and Gilbey M.J., Heat waves and their influence on tunnel environments, 15th International Symposium on Aerodynamics, Ventilation and Fire in Tunnels, Barcelona 2013
- [10] Thompson J.A., Gilbey M.J. and Legg M., Application of heat recovery to long tunnels, 16th International symposium on aerodynamics, ventilation and fire in tunnels, Seattle, 2015
- [11] ISO 7243:2017, Ergonomics of the thermal environment Assessment of heat stress using the WBGT (wet bulb globe temperature) index.

5. APPENDIX 1 – RESULTS GRAPHS

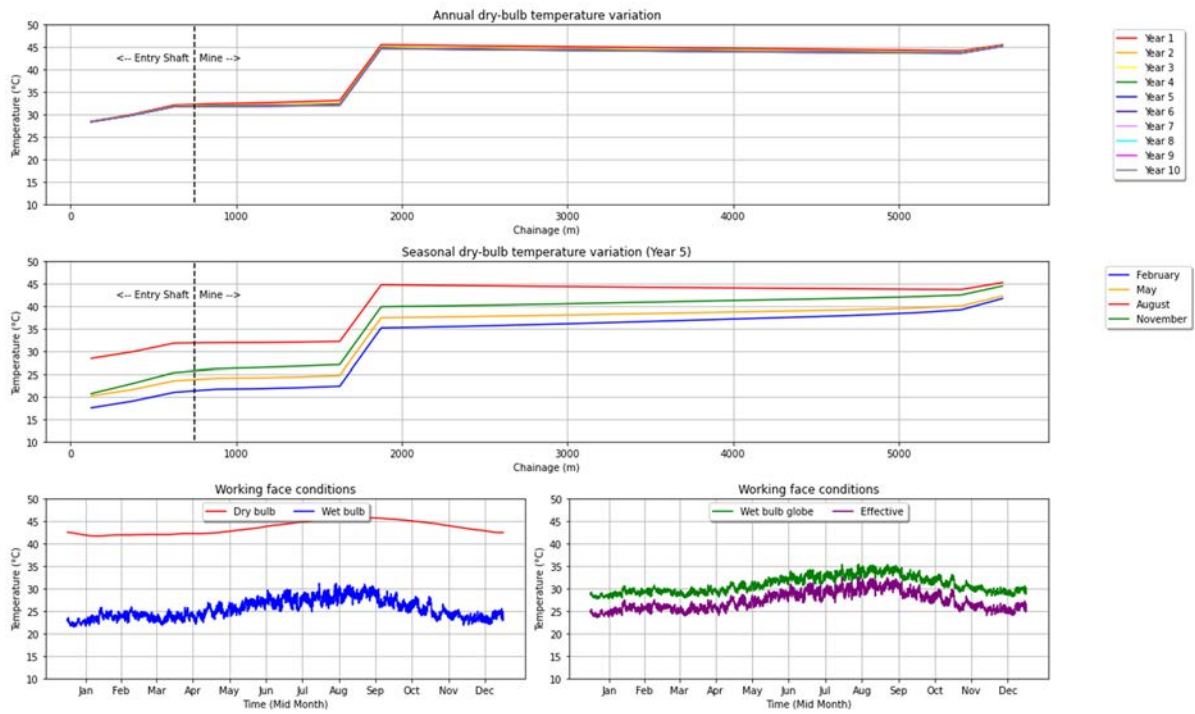


Figure 3: Base case temperature results

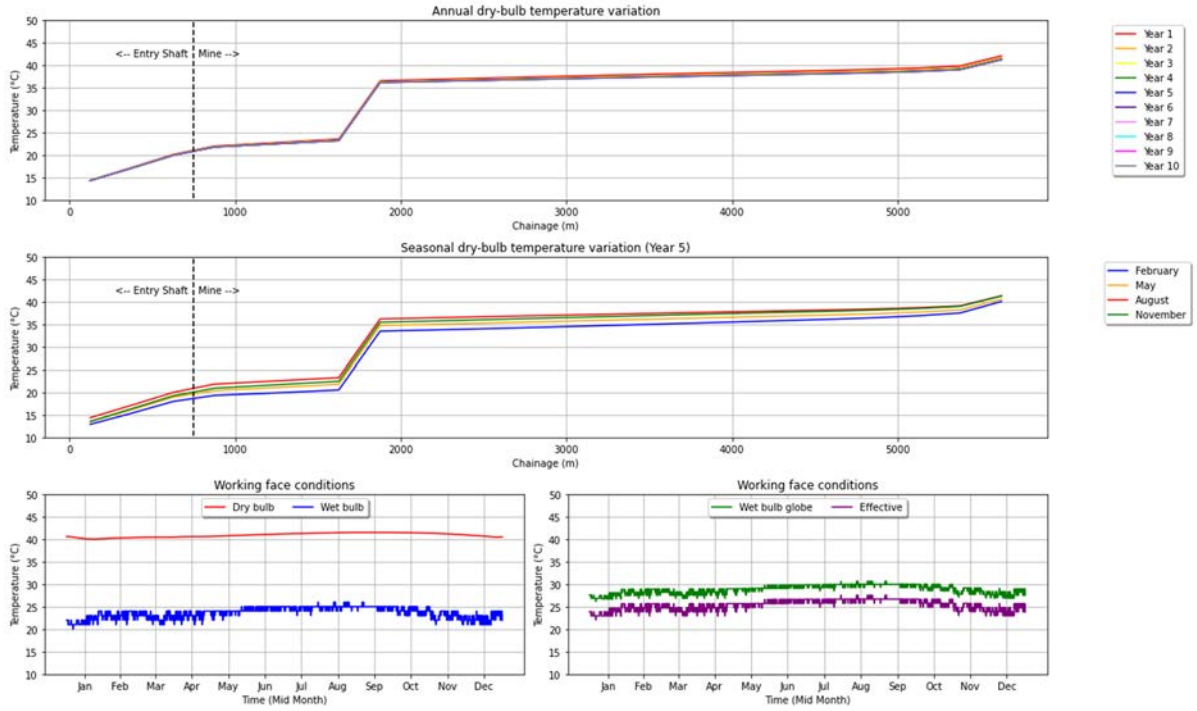


Figure 4: 5 MW Surface cooling temperature results

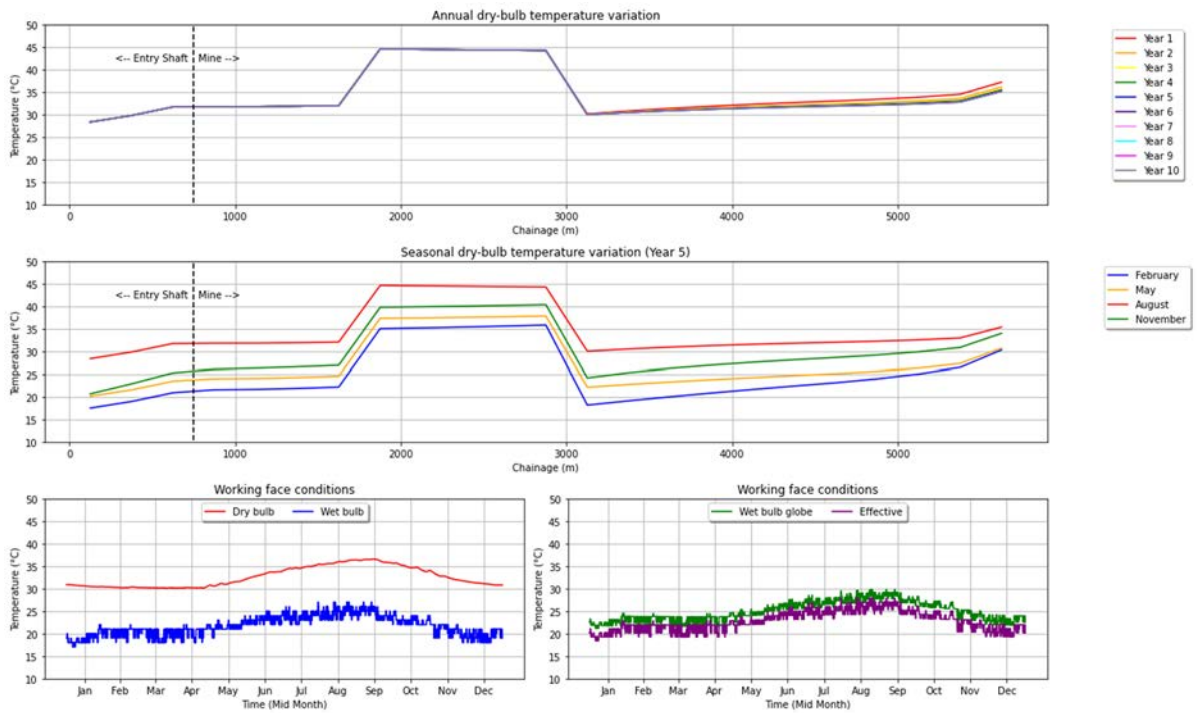


Figure 5: 2.5 MW Deep in mine cooling temperature results

DESIGN OF A VENTILATION SYSTEM IN A TUNNEL BORED WITH A TBM MACHINE IN THE CASE OF METHANE EMISSION FROM A ROCK MASS

Marek Borowski, Klaudia Zwolińska-Gładys, Andrzej Szmuk, Zbigniew Kuczera,
Kamil Piech
AGH University of Krakow, PL

DOI 10.3217/978-3-85125-996-4-29 (CC BY-NC 4.0)

This CC license does not apply to third party material and content noted otherwise.

ABSTRACT

Methane emissions from rock masses pose a significant hazard in underground works, leading to delays and, in the worst case, tragic accidents for workers. Therefore, before beginning mining work, it is necessary to properly design and optimize the ventilation system to ensure safety in the tunnel and prevent possible explosions. This paper presents a case of methane emissions observed before the drilling of the road tunnel. Initially, no emissions problem was expected. However, by preparing drainage wells to reduce water pressure in a rock mass, methane outflow was noticed. The presented analysis covers the design of a ventilation and safety system developed for drilling a tunnel along the S-19 expressway in south-eastern Poland. This two-tubed tunnel is being bored using a TBM and is expected to reach a final length of over 2.2 km. In response to the noticed risk, a ventilation and security system was developed, and a simulation of air dispersion and methane concentration distribution was performed. The developed ventilation and security system is intended to enable the tunnel drilling to continue without interruption, even in the event of significant gas inflows.

Keywords: Ventilation system design; Tunnel Boring Machine (TBM); Methane emission mitigation; Worker safety in tunnels; Environmental impact control, Methane explosion risk.

1. INTRODUCTION

Tunnel Boring Machine (TBM) technology has grown in popularity over the past decades due to significant technological advances. This progress enabled higher tunneling rates, larger drilling diameters (up to 17 m), and lower tunneling costs.

As with all underground works, drilling tunnels may be associated with a risk of methane inflow from rock massifs. Mostly, tunneling at shallow depths is not associated with methane emissions. Nevertheless, the possibility of the presence of methane-air mixtures should be analyzed at the initial stage of the project, especially in the case of rock masses with a complex geological structure. Methane emissions can pose a severe hazard and cause delays in work or even tragic accidents. In the case of a methane threat, it is necessary to design and implement an appropriate ventilation system, which allow to obtain safety working condition.

Due to the impossibility of preventing the simultaneous presence of an explosive mixture of methane with air and ignition sources, TBM machines were not used to drill tunnels in gas rock massifs until 2011, except in cases where the methane hazard was underestimated at the design stage, which consequently led to delays and unexpected costs.

In tunneling, the risk of methane explosions has generally been underestimated, and there have been very few attempts to transfer the vast experience gained in underground coal mining to tunneling. Nevertheless, since the beginning of the 20th century, many studies have been

carried out on the origin and mechanisms of methane inflow in the field of mining engineering. The knowledge gained from this research has contributed to the methods of preventing methane explosions, improving the forecasting and management of such a threat [1].

Despite limited scientific literature on tunneling in gaseous rock masses [2,3], it should be stated that methane may pose a crucial threat during tunneling. Methane occurs in many rock formations, mainly sedimentary ones. Gas emissions are often stochastic and have a non-uniform distribution [4], which makes it difficult to assess the methane risk through preliminary geological surveys. Inappropriate forecasts of the inflow of methane into the tunnel may result in costly delays and, in the worst case, tragic accidents for workers [4-7]. In paper [6], the authors reviewed the world's catastrophic methane explosions during the construction of tunnels.

The article aims to present the design of a ventilation system when drilling a tunnel using a TBM machine in methane-hazard conditions. The paper focuses on the specific case of methane hazard in the S-19 tunnel, presenting modeling of the ventilation system as a method of minimizing the risk associated with the presence of methane during drilling with a TBM machine. The introduction, methane hazard analysis, and ventilation system design with modeling results constitute the structural elements of the article.

2. METHANE HAZARD IN TUNNELS

2.1. Sources of methane emissions in analyzed tunnel

The rate of methane release from the rock formation is contingent on its permeability and could significantly vary based on the rock type and region of its occurrence. The permeability characteristic is significantly influenced by the rock heterogeneity. Permeability is mainly secondary, related to the degree of fracturing, except compressed sediments characterized by primary permeability. Flysch formations generally have permeability ranging from moderately low (sandstones) to very low (shales/mudstones). In the tectonic area (faults and the cracked part of the rock mass), they are characterized by higher values. Clay shales will have very low permeability due to the dominant clay component.

As mentioned above, this paper presents a case study for drilling tunnel on the road S-19 in Poland. At first, the analysis focused on the identification of the methane emission sources and a preliminary assessment of the hazard level. Based on geological reconstruction, several geological structures were selected along the tunnel route and classified as potential localization of methane accumulation or inflow. Such permeable fragments of the rock mass, surrounded by impermeable rocks, may enable gas accumulation and migration due to morphological conditions related to the presence of anticlines and faults. The literature survey also showed that methane can be emitted by geological discontinuities, as shown in Figure 1.

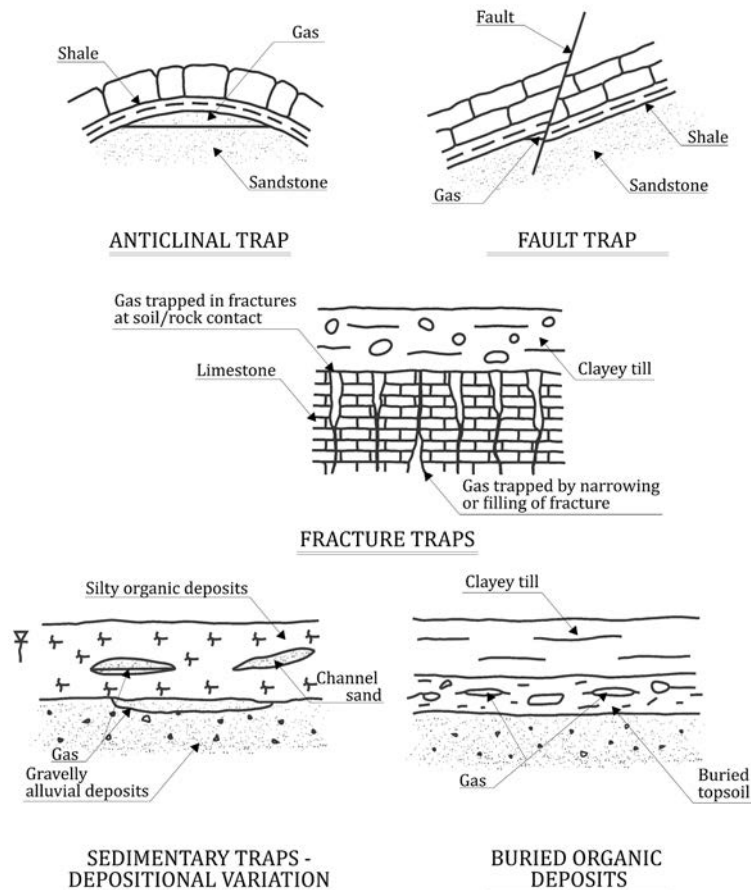


Figure 1: Structural and sedimentary gas traps/deposits. Based on [8].

Based on the analysis of previous observations and the occurrence of methane during the drainage of the S-19 tunnel surrounding area, as well as using tests of chemical origin, it should be concluded that we are dealing with a complex situation due to the occurrence and origin of methane. From the analysis of the structural conditions, it can be concluded that we are dealing with an anticline trap and gas supply related to a fault. As for the origin of the gas, both thermogenic and biogenic gas were found. It may indicate an inflow of gas from deeper layers, e.g., along a fault, and the methane from gas traps in organic sediments. Nevertheless, it should be emphasized that the crucial issue may be connected with the inflow from deeper layers, which was confirmed in the drainage holes. As presented above, determining methane emissions may cause difficulties in predicting the methane flow into the tunnel, which poses a challenge in solving the ventilation method and securing the TBM machine.

2.2. Determination of critical zones in the tunnel and approximate methane inflow

Based on drainage tests, areas associated with the occurrence of methane were identified (Fig. 2). The drawing shows in green the localization of drainage points where no methane was observed, and in red, where methane was noticed. An ellipse frames the zone of expected intense methane inflow into the tunnel during drilling. In the highlighted part, methane hazards may become apparent during TBM drilling. Based on the results of water pumping tests, attempts were made to estimate the methane inflow.

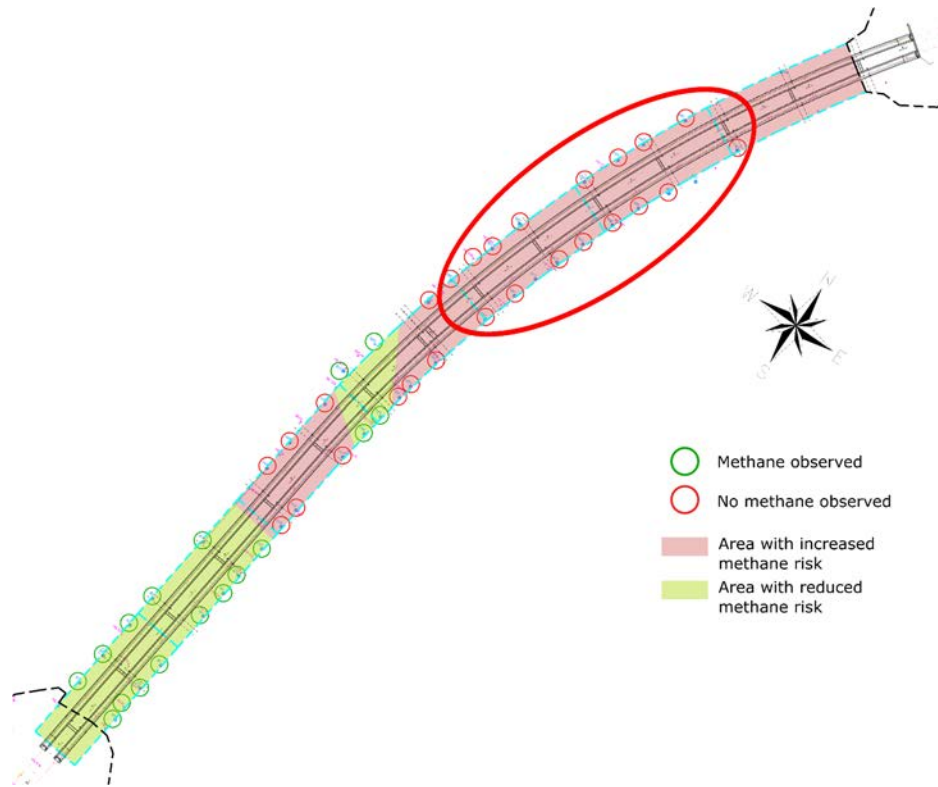


Figure 2: Distribution of methane zones in drainage wells

Figure 3 shows the methane inflow in the drainage wells. In the case of conventional deposits, methane emissions, as on the right side of Figure 3, could be expected. The preliminary analysis indicates that, to some extent, the study case could be characterized by this type of methane inflow. Therefore, if the confirmed water inflow is a maximum of 10 m³/h (0.166 m³/min) to a single well, several times higher methane inflow could be expected in extreme conditions. Assuming up to 10 drainage holes in use during tunnel drilling, and each hole may receive 0.5 m³/min, the maximum methane emission into the tunnel may be 5.0 m³/min. A safety factor of 2 was adopted, so for the calculations of the ventilation system, it was assumed that methane emission into the tunnel would be 10 m³/min.

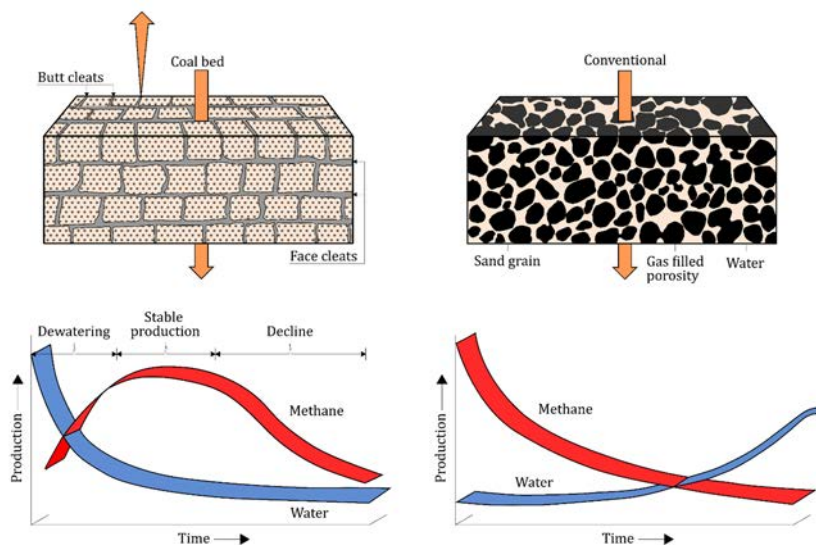


Figure 3: Characteristics of the methane inflow in the drainage well [9]

3. MODELING THE VENTILATION SYSTEM

3.1. Selection of the type of ventilation system for the tunnel

Due to the structure of the TBM, it was proposed to adapt ventilation to two drilling phases (Fig. 4):

- Stage 1 - After starting the TBM machine and drilling a section covering the length of the TBM machine. Then, the ventilation system installed on the TBM machine will work.
- Stage 2 - After entering the TBM machine into the bored tunnel. The main ventilation will be activated with a fan located in the tunnel portal area.

Considering the operation of the TBM machine in methane hazard conditions, it will be necessary to equip the machine with protection consistent with ATEX requirements. Since it is impossible to adapt the entire TBM machine to requirements, only the safety systems of the machine will be ATEX-compliant and fully protected to maintain "vital" functions.

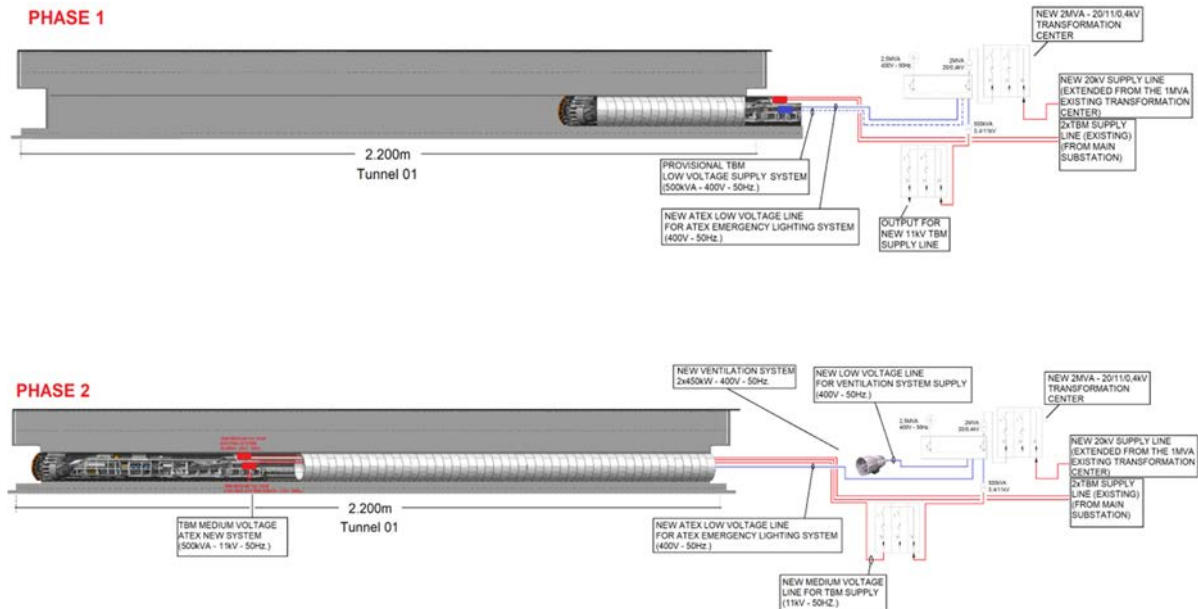


Figure 4: Tunnel drilling phases with ventilation adjustment [10]

Considering the methane hazard, it is necessary to use forced ventilation due to the greater range of the air stream flowing from the duct. It is crucial to ensure appropriate airflow turbulence in the red zone marked in Figure 5.

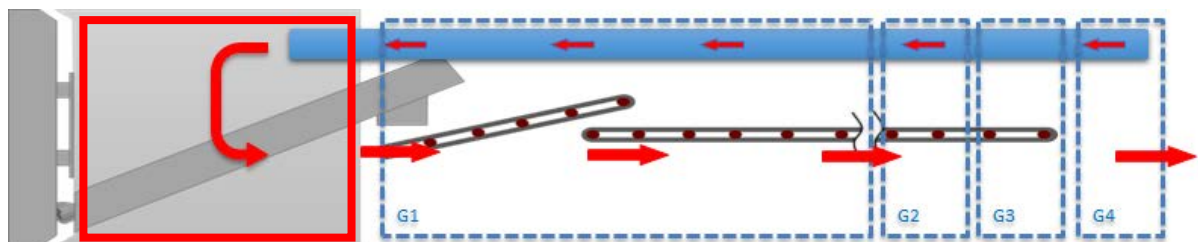


Figure 5 : TBM machine ventilation concept [10]

To calculate the air velocity distribution and volume rate in the tunnel, a 1D ventilation model for the maximum length, based on the tunnel equipment design, was prepared. For this purpose, available engineering software was used that allows for flow analysis of ventilation networks, including mines and tunnels [11]. Calculations were carried out for a single TBM bored tunnel with a length of 2155 m. The model consists of sidings (tunnel sections and a duct between nodes - points) with transverse dimensions and unit resistances appropriate for the designed tunnel in the drilling phase and a pressure duct divided into segments with a diameter of 2500 mm (2070 m) – the principal ventilation and of 1800 mm (85 m) – TBM machine ventilation.

The duct outlet should not be at a distance greater than 20 m from the TBM machine disc. The view of the model is shown in Figure 6. An axial fan is connected 50 m from the tunnel portal inlet (Figure 7) to ensure no recirculation of the exhaust air. from the tunnel.

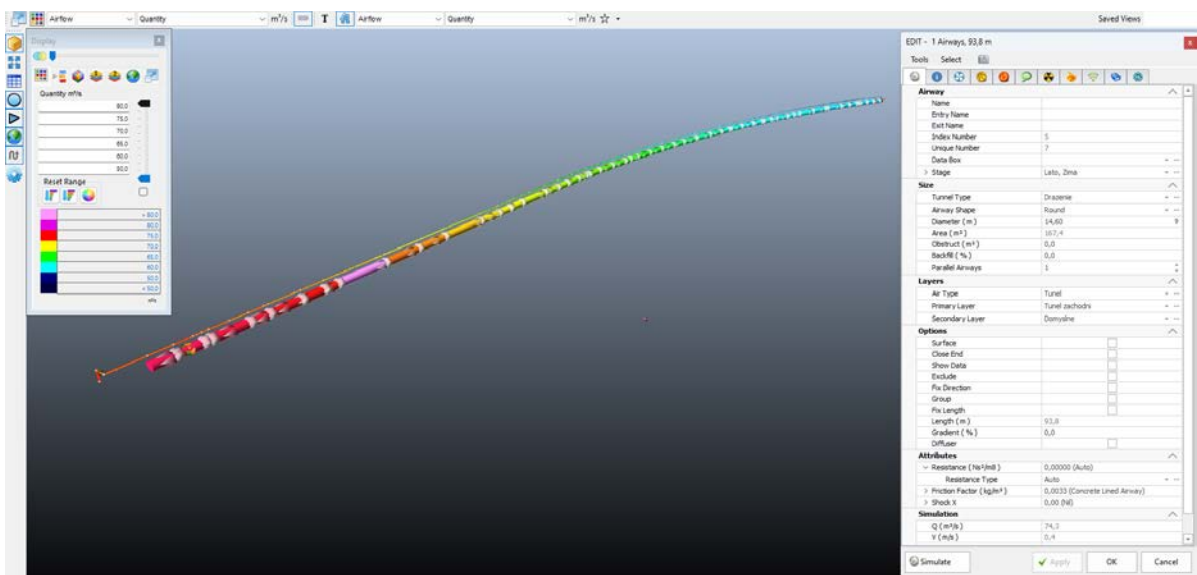


Figure 6: View of the tunnel model and the supply duct

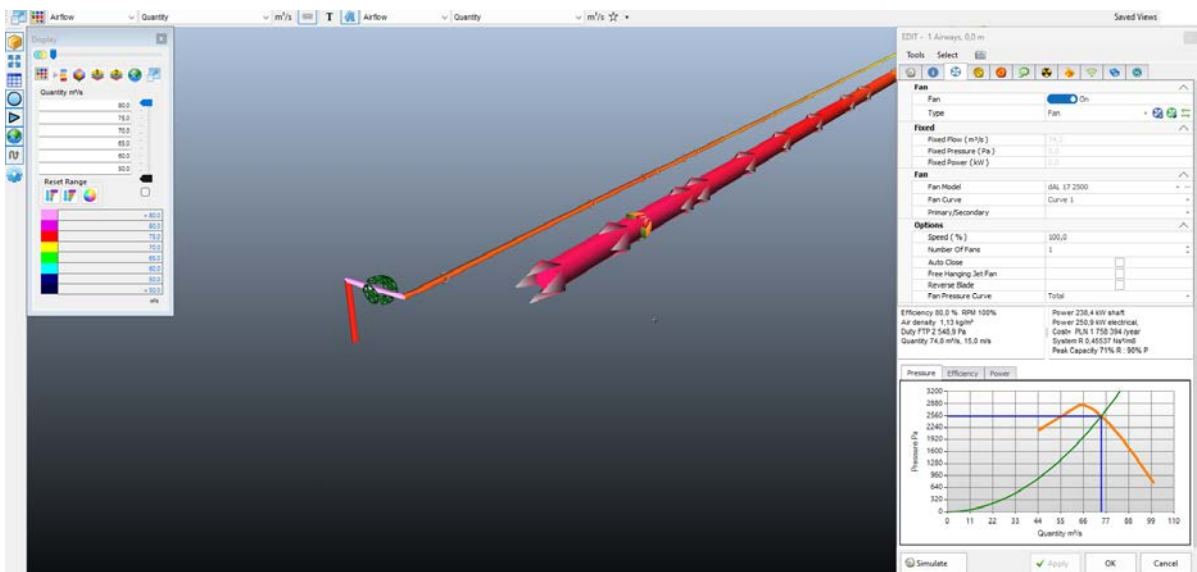


Figure 7: Location of the fan and its characteristics in front of the tunnel inlet

3.2. Results of modeling for the tunnel with the designed ventilation system

The airflow of 53.5 m³/s is supplied to the TBM machine disc via the air duct with an efficiency of 71% (due to leakage along the duct). Distribution of the changes in airflow rate (Fig. 8) and its velocity (Fig. 9) were shown along the length of the tunnel. On the horizontal axis, the point of 0.0 m corresponds to the disc of the TBM machine. As you move away from the heading, the amount of air increases along the length of the tunnel, which results from the air duct leakage and is a phenomenon resulting from the nature of the solution. According to the legal regulation, the provided airflow ensures a minimum air velocity of 0.3 m/s to mitigate the methane hazard.

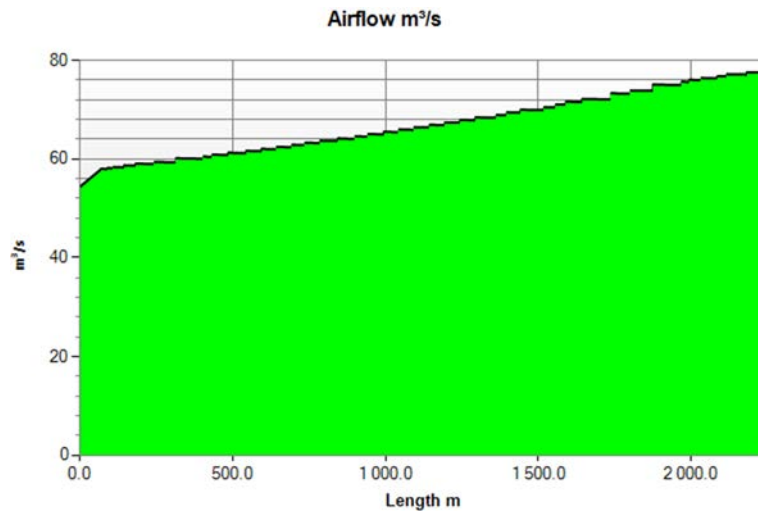


Figure 8: Distribution of the airflow rate (m³/s) in the tunnel cross-section with increasing distance from the heading/disc of the TBM

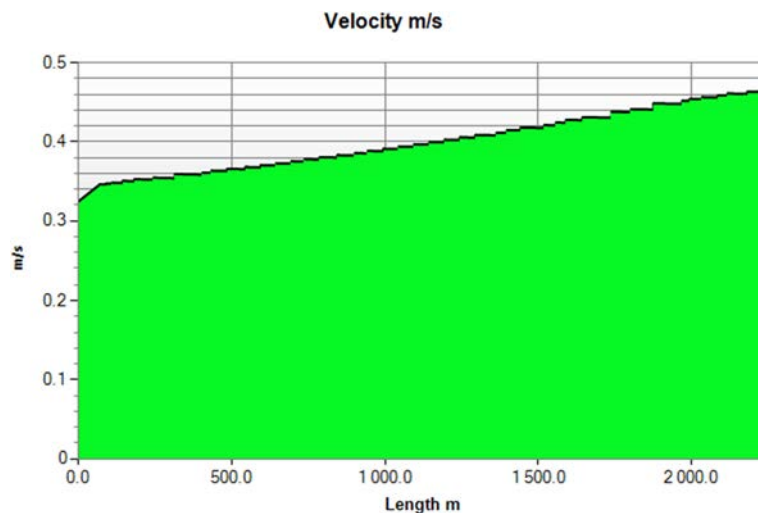


Figure 9: Distribution of the air velocity (m/s) in the tunnel cross-section with increasing distance from the heading/disc of the TBM

Based on the analysis from the previous chapter, the methane flow released into the tunnel was acquired to be 10 m³/min of pure gas. The inflow of methane into the tunnel was assumed to be linear in the roof part (25% of the total outflow) and the bottom part (25% of the total outflow) of the heading, as well as the point inflow of methane (injector) at the outlet from the screw conveyor (50% of the total outflow). The distribution of methane concentration is shown in Figure 10. The analysis shows that with the given amounts of air, the permissible methane concentration of 0.5% will not be exceeded. If the concentration does not exceed

0.5%, the TBM is not required to comply with ATEX requirements but only selected elements of the so-called function support of the TBM. An average concentration of 0.3% is observed at the front of the tunnel heading/shield and 0.2% at the tunnel outlet. Due to possible threats, it is necessary to implement appropriate precautions among additional security measures. Devices and systems such as submersible pumps for emergency drainage, sewage pumps, the fan in the gantry, the vacuum pump of the erector and the segment lift, the lighting and emergency lighting, as well as the gas monitoring system and the evacuation alarm system should be classified at least in category M2 (high level of protection, EU Directive 94/9/EC on equipment and protective systems intended for use in potentially explosive atmospheres). The remaining devices should be classified in category II G2.

In conclusion, the designed ventilation system effectively controls airflow, maintains permissible methane concentrations, and ensures compliance with safety regulations. While ATEX safeguards might not be mandatory for the entire TBM, the implementation of specific security measures is advised to address potential threats and enhance overall safety in the tunneling process.

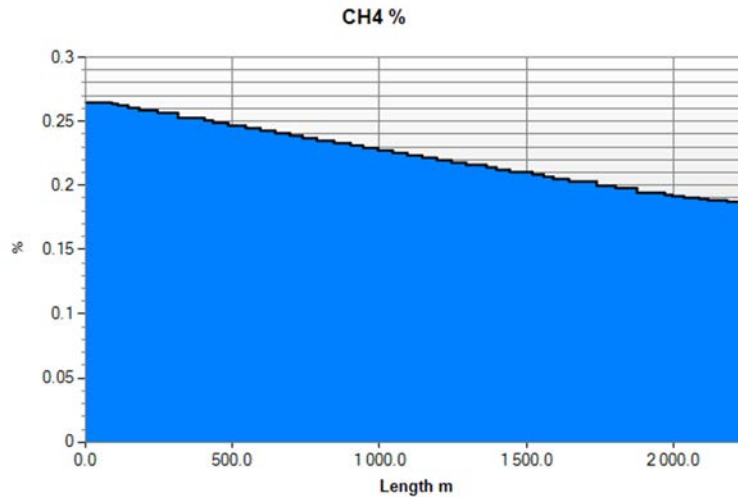


Figure 10: Distribution of methane concentration (%) along the airflow path through a bored tunnel.

4. CONCLUSION

Tunnel drilling in gaseous rock masses carries a severe risk of methane ignition/explosion/explosion, which requires monitoring, preventive measures, and appropriate safeguards. The main goal of the design and ventilation modeling during TBM drilling in methane hazard conditions is to ensure the safety, efficiency, and controlled operation of the TBM machine in the tunnel. The internal environment control in the tunnel is to enable continuous operation of the TBM, thanks to which tunnel drilling can be carried out efficiently, and delays and costs associated with downtime will be minimized.

Based on the analysis of previous observations and the occurrence of methane during the drainage of the surrounding area and using tests of chemical origin, it should be concluded that we are dealing with a complicated situation. From the analysis of the structural conditions, it can be concluded that we are dealing with an anticline trap and gas supply related to a fault. As for the origin of the gas, both thermogenic and biogenic gas were found. It may indicate that there is an inflow of gas from deeper layers, as well as from gas traps in organic sediments. Based on test water pumping, it was assumed that methane emissions into the tunnel would be 10 m³/min.

For methane hazard reasons, it is necessary to use forced ventilation due to the greater range of the air stream flowing from the duct in the area of the TBM shield. To determine air velocity and flow rate distribution, a 1D ventilation model for the maximum length was prepared. Calculations were carried out for a single TBM bored tunnel with a length of 2155 m. The air stream fed to the front of the tunnel behind the TBM machine disc ensures that the minimum air velocity is maintained along the entire length of the tunnel. The analysis of the methane concentration distribution shows that the value of 0.5% will not be exceeded at the given amounts of air (the stream supplied to the air duct is 75.3 m³/s). An average concentration of 0.3% is observed at the front of the tunnel face/shield and 0.2% at the tunnel outlet. For safety reasons, the TBM machine should be equipped with methane measurement sensors.

5. REFERENCES

- [1] Labagnara, D., Maida, L., Patrucco, M., 2015. Firedamp explosion during tunnelling operations: suggestions for a prevention through design approach from case histories. *Chem. Eng. Trans.* 43, 2077–2082. <http://dx.doi.org/10.3303/CET1543347>.
- [2] Doyle, B.R., 2001. *Hazardous Gases Underground. Applications to Tunnel Engineering.* Meyer, M.D. (Ed.), Marcel Dekker Inc, New York.
- [3] Kissel, F.N., 2006. *Handbook for Methane Control in Mining.* In: Kissel, F.N. (Ed.), Department of Health and Human Services. NIOSH, Cincinnati, USA.
- [4] Kang, X.B., Xu, M., Luo, S., Xia, Q., 2013. Study on formation mechanism of gas tunnel in non-coal strata. *Nat. Hazards* 66, 291–301. <http://dx.doi.org/10.1007/s11069-012-0484-y>.
- [5] Borowski, M., Swolkień, J., 2016. *Selected issues related to mining and clean coal technology.* monograph; AGH University of Science and Technology. Faculty of Mining and Geoengineering. Kraków: Agencja Wydawniczo-Poligraficzna ART-TEKST, 2016. 631 s. Bibliogr. przy rozdz. ISBN: 978-83-7783-196-0.
- [6] Copur, H., Cinar, M., Okten, G., Bilgin, N., 2012. A case study on the methane explosion in the excavation chamber of an EPB-TBM and lessons learnt including some recent accidents. *Tunn. Undergr. Space Technol.* 27, 159–167. <http://dx.doi.org/10.1016/j.tust.2011.06.009>.
- [7] Proctor, R.J., 2002. The San Fernando tunnel explosion. *Eng. Geol.* 67, 1–3. [http://dx.doi.org/10.1016/S0013-7952\(02\)00042-X](http://dx.doi.org/10.1016/S0013-7952(02)00042-X).
- [8] Doyle, B.R., Gronbeck, M.P., Rose, J.P., 1991. Construction of tunnels in methane environments. In: *Proceedings of the Rapid Excavation and Tunneling Conference*, USA, pp. 199–224.
- [9] William T. Brown, Jr. *Developing CBM in the Powder River Basin. Coalbed Methane Development in the Intermountain West (April 4-5) 2002.*
- [10] *Technical design for drilling the S-19 tunnel in Poland.*
- [11] *VentSim DESIGN™ – User Guide, version 5.4, Australia: Howden Group.* <https://ventsim.com/files/VentsimManual.pdf> (accessed on 10 December 2023).

RISK ANALYSIS OF ROAD TUNNELS: A QUANTITATIVE RISK ANALYSIS MODEL FOR ASSESSING THE EFFECTS OF FIRE

¹Razieh Khaksari Haddad, ²Zambri Harun

¹London Bridge Associates Ltd, GB

²Department of Mechanical and Manufacturing Engineering
Faculty of Engineering & Built Environment, UKM, MY

DOI 10.3217/978-3-85125-996-4-30 (CC BY-NC 4.0)

This CC license does not apply to third party material and content noted otherwise.

ABSTRACT

The most important factor influencing fire safety in tunnels is the interaction between the fire, tunnel users, traffic, and fire safety measures. A quantitative risk analysis model has been developed to analyse the fire risk, LBA Quantitative risk analysis model (LBAQRA). This paper presents details of this quantitative risk analysis model, consisting of a quantitative consequence analysis model and a quantitative frequency analysis, which was used for this study. The quantitative consequence analysis model includes three sub-models; queue model, distribution model, and egress model to estimate the number of exposed tunnel users, their evacuation times, the extent of damage due to fires, and eventually the number of fatalities and injuries. Frequency analysis is carried out through an event tree which was built on the tunnel fire rate in UK road tunnels. This fire rate is updated considering tunnel length, time of fire incident, traffic condition, accident type, vehicles involved, and location of fire. The study of the impact of various ventilation strategies on the F/N curve showed the positive effect of the activation time of the ventilation system on societal risk. The sensitivity analysis of the model indicates that the number of fatalities increased for longer detection times and the initial fire rate and the probability of congested traffic have a direct influence on the final frequency of fire scenarios.

Keywords: fire safety, quantitative risk analysis, societal risk, road tunnels.

1. INTRODUCTION

In order to reduce congestion in developed areas and improve the connection of regions, road tunnels are one of the most critical systems for daily operation in urban areas. They also raise opportunities for the transportation of individuals and goods. Despite the benefits that road tunnels add to transportation system, their existence leads to an endogenous problem due to the severity of tunnel accidents compared to roads.

The consequence of a fire incident, especially when a heavy good vehicle (HGV) or large good vehicle (LGV) is involved, causes very high temperature, great concentration of toxic gases, and intense smoke. Therefore, disastrous consequences in terms of human losses and structural damage are expected. That is why the fire safety of road tunnels was intensely put in the center of public attention and as it is obliged by CD352 [1], the risk assessment should both inform the design and serve as a check on the adequacy of the design proposals, and identify any risks falling within the 'Tolerable' region that can need further mitigation. There are several methods of risk analysis to determine risks and evaluate the effectiveness of safety measures. One of these methods is quantitative risk analysis (QRA), which has been one of the explicit requirements under the European Union (EU) Directive (2004/54/EC) when the tunnel is opened to dangerous goods [2]. A quantitative risk analysis for road tunnels complying with EU regulations has been presented by Kirytopoulos et al. [3]. Different risk

models exist in the literature, such as the Dutch TUNPRIM, a QRA model for the country’s road tunnels called the QRAFT from Singapore, Austrian TuRisMo, and Italian Risk Analysis Method, IRAM. A project on the transport of dangerous goods through road tunnels was sponsored by PIARC 1995 and the PIARC/OECD/EU QRA model (GRAM) was developed. Thirteen hazardous scenarios are taken in this and was computerized by spreadsheet-based software [4]. The validation of the GRAM model was studied in Austria, France, Netherlands, Norway, Sweden, and Switzerland and various risk reduction measures were examined employing the GRAM software [5].

The societal risk is determined as a combination of event frequency and consequences. Societal risk represented graphically in the form of a frequency/number of fatalities (FN) curve, is the main output of these models. The calculated societal risk must be evaluated by comparison with the risk acceptance criteria, i.e. must be less than a specified minimum and acceptable value (threshold) as presented in the case studies, for instance, Diamantidis [6], Botschek et al. [7] and Kohl and Zibert [8].

Risk assessment of fire incidents in road tunnels includes complicated scenarios as they constitute interactions among the fire, tunnel users, and safety measures such as fire detection, tunnel alarm, or emergency ventilation. Thus, many risk indicators, which affect risks for tunnel users, describe the scenario. Factors affecting tunnel fire risk assessment are influenced by the uncertainty related to the traffic conditions or the environmental conditions, which results in making assumptions adopting a ‘mean’ value or a worst-case scenario.

2. METHODOLOGY

In light of the above considerations, a novel methodology to perform a quantitative fire risk assessment of road tunnels is explained in this paper. A model of quantitative risk analysis concerning safety in road tunnels called LBAQRA has been developed to perform a risk analysis as required by UK regulations. The LBAQRA performs a quantitative risk assessment and includes quantitative frequency analysis and quantitative consequence analysis. The quantitative consequence analysis section of this model was inspired by [9].

Tunnel geometry and its infrastructures, fire safety measures and the interaction between them, as well as equipment and management procedures such as emergency ventilation strategies in addition to the analysis of factors and processes related to human behavior, such as recognition and response to the incident, reluctance to leave the vehicle, interactions between occupants, interactions between occupants and smoke, and how their age and gender affect their evacuation should be considered to evaluate the tunnel fire risk. These aforementioned parameters are taken into account in this model. In this model, the risk assessment analysis is divided into quantitative consequence analysis and quantitative frequency analysis.

2.1. Quantitative frequency analysis

The frequency of defined accident scenarios was calculated via an event tree. The first column of the frequency event tree is initial fire frequency which has been obtained from the historical statistics of fire incidents in England road tunnels. This statistical data has been published in [10]. Then this initial fire rate is updated by considering the length, traffic volume, and gradient of the under-studied tunnel. The second column of the frequency event tree is “The Time of the Incidents”. Since drivers’ eye movement and driving performance are different during day and night, the accident rate and consequently the fire rate are different in day and night. The influence of time on accidents should be considered in the frequency analysis. The third column of the frequency event tree is “Traffic Condition”. As the fire rate is varied by

traffic condition, the effect of traffic condition on fire rate was considered by considering the congested hours of the tunnel under study. Furthermore, two accident types were considered in this model. Incidents that include 1 vehicle are Type 1 and collisions that include more than 1 vehicle are Type 2. The probability of type 1 and 2 incidents is derived from UK road data. The fifth column is “Vehicle Type“. The share of passenger cars, buses, vans, HGV, and trucks involved in fire incidents based on the tunnel fire data in PIARC 1999 is considered. The last column is Fire Source Location. The tunnel is divided into three zones and an average crash rate value was considered to evaluate the safety level of each tunnel zone [11,12].

Table 1: Comparison of tunnel crash rate in different zones

Zone 1	Zone 2	Zone 3
0.23	0.2	0.15

The final fire frequency is calculated by multiplying the initial fire frequency by the below columns:

- Time of fire incident
- Traffic condition
- Accident type
- Vehicle type
- Fire source location

Figure 1 shows a section of quantitative frequency analysis event tree.

Tunnel type	Traffic Condition	AADT		Length		Operation	gradient	Basic frequency		Tunnel length factor	Tunnel traffic factor	Tunnel gradient factor	Basic frequency after influential		Traffic Condition		Accident type		Vehicle type in fire rate	Vehicle type in traffic	Final frequency after influential factors	
		veh/day (Day)	veh/day (Night)	m	km			days	Estimated average fire /100 million veh-km				f_i	f_r	Estimated average fire /100 million veh-km	f_g	Type 1 and Type 2	Estimated average fire rate			Estimated average fire rate	per 100 mill veh-km
uni	678.0	43288.7		490.00	0.49	360.0	0.0	3.875E+00	4.459E+00	4.633E+00	1.0	4.633E+00	non-congested traffic	0.923	Type 1	0.120	PC	0.758	0.700	2.722E-01	2.722E-01	2.722E-01
																0.120		0.758	0.700	2.722E-01	2.722E-01	2.722E-01
																0.120		0.758	0.700	2.722E-01	2.722E-01	2.722E-01
																0.120	BUS	0.029	0.100	1.502E-03	1.502E-03	1.502E-03
																0.120		0.029	0.100	1.502E-03	1.502E-03	1.502E-03
																0.120	HGV	0.089	0.100	4.591E-03	4.591E-03	4.591E-03
																0.120		0.089	0.100	4.591E-03	4.591E-03	4.591E-03
																0.120	VAN	0.123	0.100	6.317E-03	6.317E-03	6.317E-03
																0.120		0.123	0.100	6.317E-03	6.317E-03	6.317E-03
																0.120		0.123	0.100	6.317E-03	6.317E-03	6.317E-03

Figure 1: An example of quantitative frequency analysis event tree

2.2. Quantitative consequence analysis

The number of fatalities is calculated via quantitative consequence analysis which comprises three parts: queue model, distribution model, and egress model.

The queue model calculates the number of vehicles queueing in each lane. The number of vehicles that will enter the tunnel and queue behind the fire (queue length) depends on the time duration subsequent to a fire incident and consequently the tunnel closure time, queue formation speed, stopping distance between vehicles in the queue, fire source location, and the density of stopped vehicles in each lane. The main parameters which should be considered in the queue formation model are the number of vehicles, their percentage and length, and the relative users. Since the average peak traffic density, percentage, and type of vehicles are not uniform between various lanes in a multi-lane tunnel, the traffic flow should be distributed into lanes. Saad Yousif and his colleagues [13] studied the distribution of traffic flow among the available number of lanes and modelled lane utilization. In the absence of tunnel-related

information, the model developed by Yousif et al. [13] is utilized to estimate the lane utilization factor for each lane based on the total traffic flow of vehicles (veh/hr) in two-lane and three-lane tunnels.

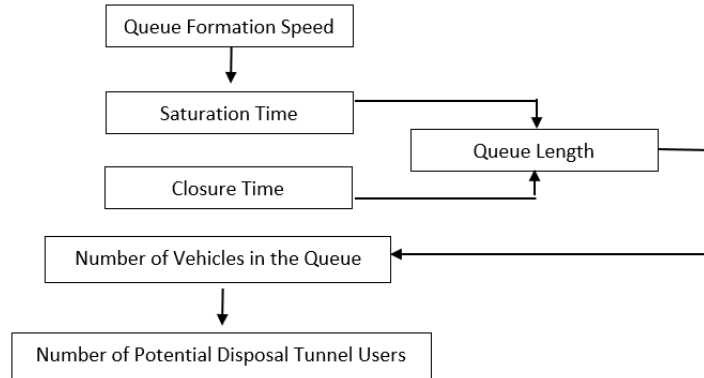


Figure 2: The process sequence of calculating the number of people in the queue

Then the number of vehicles queuing in each lane and consequently the number of exposed tunnel users is estimated by queue length and traffic density as below.

$$N_{veh} = L_q / (\%PC \times L_{PC} + \%BUS \times L_{BUS} + \%VAN \times L_{VAN} + \%TRUCK \times L_{TRUCK} + \%HGV \times L_{HGV} + d_{stop}) \quad 1$$

$$N_i = N_{veh} \times (n_{PC} \times \%PC + n_{BUS} \times \%BUS + n_{VAN} \times \%VAN + n_{TRUCK} \times \%TRUCK + n_{HGV} \times \%HGV), \quad 2$$

Where L_q is the queue length, N_{veh} is the number of vehicles, $L_{PC}, L_{BUS}, L_{VAN}, L_{TRUCK},$ and L_{HGV} are the average lengths of relative vehicles, $\%PC, \%BUS, \%VAN, \%TRUCK,$ and $\%HGV$ are percentage of different types of vehicles in traffic composition, and $n_{PC}, n_{BUS}, n_{VAN}, n_{TRUCK},$ and n_{HGV} are the average occupancy rate respectively of passenger cars, buses, vans, trucks, and HGVs in the i -th lane.

After calculating the number of potentially exposed people, the distribution model is used to divide the queue into cells of the same size and then distribute tunnel users homogeneously. Considering agents' gender, it is assumed that the share of women and men is the same. The gender of cells changes alternatively. Regarding the evacuee's walking speed, the speed calculated in the model is used for cells occupied with men and it is assumed that women's walking speed is 20% lower than men's. The total distance of the evacuation path is calculated by the distribution model taking into account both the longitudinal and lateral shares in the evacuation route. Exposed tunnel users distributed in each cell start the evacuation path from their initial position and they travel cell by cell towards a place of safety i.e., an emergency exit or the tunnel portal.

A timeline model is used for the egress model, which describes the sequence of events as a list of continuous phases. A four-stage evacuation process is considered. The first stage is detection which depends on the safety equipment in the tunnel. The detection times in this model based on the type of detection system are:

- Automatic detection system: 60 seconds
- Automatic detection system + confirmation by an operator: 30+60 seconds = 90 seconds
- Manual fire alarm: 180 seconds

The second stage is the alarm stage which is the time between detection and the time when the alarm system is activated. The alarm time is calculated considering the influence of provided safety systems in the tunnel such as smoke/ fire detection system and video/radar incident detection system.

The third stage is the pre-movement stage including recognition time, response time, and the time to exit the vehicle. Recognition time consists of a period between the activation of the alarm system and when occupants recognise the danger. Once evacuees recognise the fire, they do not start to travel immediately. Time taken between recognition time and leave the vehicle is response time. At this stage, people are strongly influenced by others' reactions. The tunnel length behind the fire is divided into two zones: crash zone and normal zone. Based on the fire size, ventilation velocity in a tunnel under natural ventilation and tunnel dimensions, the backlayering length, which defines the crash zone, is calculated. The people stuck behind the fire in the queue can be divided into three groups:

- Group 1: direct accident witnesses, who are in the crash zone and make the evacuation decision on their own. Their pre-movement time is before detection plus alarm time. They could see the fire and came to a rapid decision to leave their vehicles.
- Group 2: who are out of crash zone and have no knowledge of the situation and have to wait for emergency announcement. Their pre-movement time is more than sum of detection time and alarm time.
- Group 3: a small subgroup of the second group, who made their decision seeing escaping persons from the first group. Their pre-movement time is lower than Group 2 pre-movement time.

People react to extraordinary circumstances in various ways and need different amounts of time to make their decisions. Therefore, the recognition time + response time before evacuation starts is adopted with polynomial trendline with below assumptions:

- The pre-movement time range is from 30 to 300 sec based on real accidents and tunnel experiments.
- The queue length behind the fire source is divided into sections, named cell. The length of the cell influences directly the calculation precision. The smaller the length, the more accurate it is.
- The pre-movement time of the first cell of crash zone is 30 sec (Group 1).
- The pre-movement time of the last cell of crash zone is $t_{det} + t_{alarm} - 30$ (Group 2).
- The pre-movement time of the first cell of normal zone is $t_{det} + t_{alarm} + 30$ sec (Group 2).
- The pre-movement time of the last cell of Group 2 is 300 sec, which is also the pre-movement time of the first cell of Group 3.
- The pre-movement time of the last cell of Group 3 is $(t_{det} + t_{alarm}) + 30$ sec.
- The recognition time + response time graph can be plotted via the centre of each cell as the x-axis values.

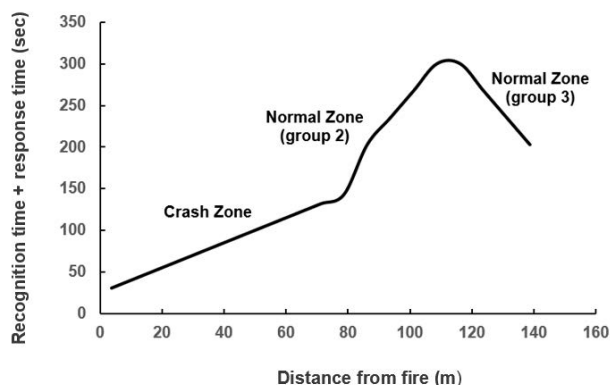


Figure 3: An illustration of the recognition time + response time

A small share of agents in the direct vicinity of the fire, do not leave the fire site, either because of wrong behaviour or because of being unable to evacuate. A share of 3% of all evacuees is assumed to show this behaviour. It is assumed that these people stay at the place of origin and only start evacuation after 15 min.

We assume that the flow capacity of a normal vehicle door is 1 person per 4 seconds. Based on the average occupancy of each type of vehicle, the number of each type of vehicle in the queue, and the number of cells the average time of leaving the vehicle is calculated.

The last stage is traveling which depends on the movement speed and the distance to the emergency exit or portal. In this model, an approach considering a walking speed as a function of local toxic, thermal and visibility conditions is presented in [14]. The proposed approach is based on international work on the fire consequences on people regarding their evacuation capability [14].

The next step is the verification of users' egress process to find out if evacuees can start and then continue the evacuation process based on the considered tenability thresholds. In this section, the evacuation time (RSET) is compared with the time when the tenability thresholds exceed their limits (ASET).

Two indicators are measured at humans' face height at the centre of each cell to assess whether occupants can travel the evacuation path and reach a place of safety.

The tenability criteria used for this model are:

- $FED < 1$,
- $FED_{heat} < 1$.

In addition to considering tenability thresholds to calculate the number of fatalities, fire spread from initial vehicle to neighbouring vehicles causes injuries as well. Radiation, convection, and conduction result in an increase of heating of the skin and consequently skin burns. The pain temperature threshold is 44.8 °C [15,16]. However, skin injury starts to develop when the skin temperature is greater than 44 °C due to the onset of protein breakdown [17,18]. In this model, 44 °C tolerable temperature is measured at the centre of each cell during evacuation to estimate the number of injuries in each quantitative risk analysis scenario as well.

The total number of casualties is defined as the sum of fatalities of each cell where the tenability thresholds are exceeded ($RSET > ASET$). The total number of casualties of the whole tunnel is determined by the sum of fatalities in each lane.

F/N curves of societal risk are provided with the results of quantitative consequence analysis and quantitative frequency analysis. Risk acceptance is obtained using the ALARP criterion in the UK.

The results of one of the case studies implemented by LBAQRA has been published in [19].

3. CASE STUDY

In order to achieve the purpose of this study mentioned in the introduction section, a specific tunnel was investigated. This tunnel, Southwick Tunnel, is located on the A27 between the junction of the Holmbush interchange (A27), portal A and the Hangleton interchange (A293), portal B, UK. The structure is a twin-bore curved unidirectional road tunnel. Each bore is approximately 490 meters long and carries two lanes of traffic. The bores are connected by 3 cross passages, approximately 100 m apart and 100 m from either portal. This tunnel has a positive longitudinal slope of 3% from portal A to B. The tunnel equipped with a longitudinal ventilation system consists of 14 jet fans (7 pairs) installed at the ceiling of each bore.

This tunnel has an annual average daily traffic of about 46900 vehicles/day traffic density in the Eastbound bore with an average percentage of 77% passenger car, 0.2% bus, 19% truck, and 3.8% HGV. Three different traffic conditions, free fluid, congested, and stoppage, were considered. 158 MW, 47 MW, and 30 MW fire scenarios at three locations including 0.3L, 0.5L, and 0.8L (L is tunnel length) are studied.

FN curves as the output of quantitative risk analysis and sensitivity analysis of this model taking into account detection time, fire occurrence rate, and percentage of congested traffic were studied for the scenarios understudied.

4. RESULTS

4.1. F/N Curve

Three different emergency ventilation strategies listed in Table 2 in the case of 158 MW, 47 MW, and 30 MW fire scenarios were studied to investigate the effect of ventilation system strategy on the FN curve. The ALARP limit, acceptable and unacceptable limits, was adopted by Moonis et al. (2008) [20].

FN curve of scenarios without ventilation was located at the unacceptable region which means it could not meet the safety target (Figure 4a). According to FN curves, when the ventilation system was activated at 4 min after ignition, there was no obvious difference between FN curves of $V=0\text{m/s}$ and $V=3.2\text{ m/s}$ with 4 min activation time (Figure 4b, 4c). It means as the ventilation system was activated very late, it could not cope with the influences of fire and smoke. On the other hand, when the ventilation system was activated 2 min after ignition (Figure 4d), the FN curve was lower than in scenarios without ventilation which showed the positive effect of the activation time of the ventilation system. Although it was still in the unacceptable region.

Table 2: Under study ventilation systems

Scenario No.	Ventilation velocity (m/s)	No. Fans	Ventilation activation time after ignition
1	0	-	-
2	3.2	80%	4 min
3	3.2	100%	4 min
4	3.2	80%	2 min

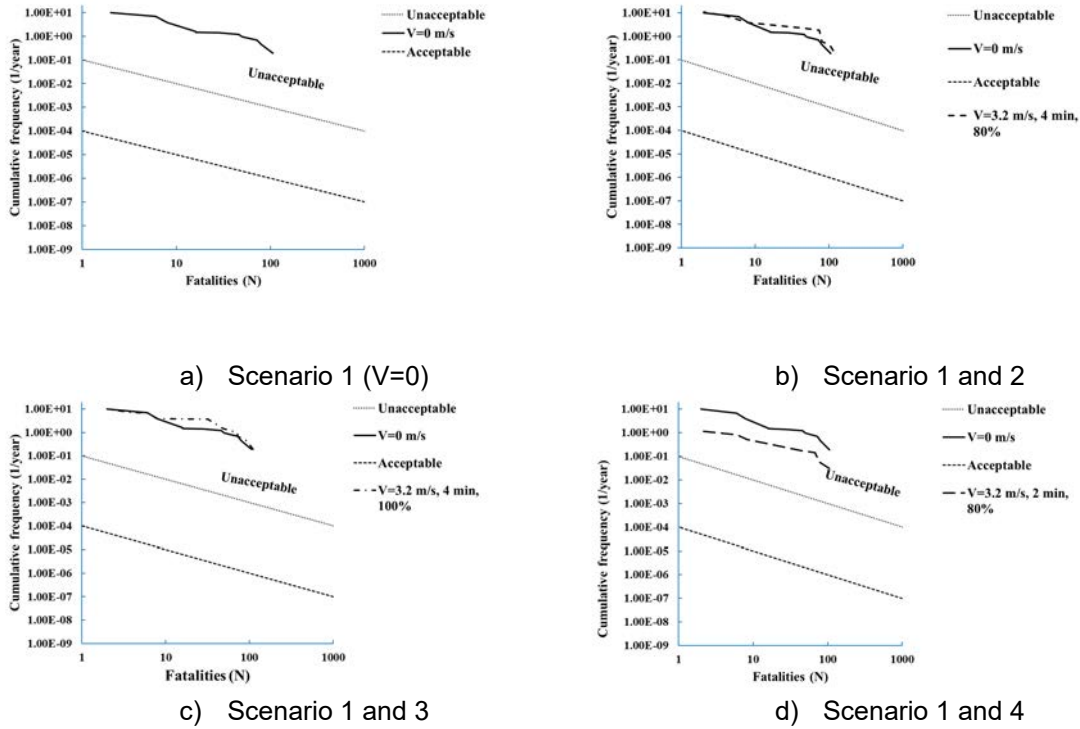


Figure 4: FN curve of different emergency ventilation systems

4.2. Sensitivity analysis

The sensitivity of the LBAQRA model has been analysed by taking into account the impact of key factors including detection time, initial fire occurrence rate, and percentage of congested traffic. These factors have been changed to evaluate their effect on the tunnel safety.

Expected Value (EV), which is the integral of the FN-curve, is used to evaluate the sensitivity of the model to chosen variables. Higher EV means higher level of risk and is defined as below:

$$EDV = \sum N_{Sc} \times F_{Sc}, \tag{3}$$

where N_{Sc} is the number of fatalities for each fire scenario and F_{Sc} is the cumulated frequency of each fire scenario.

4.2.1. Detection time

The risk assessment was carried out for ten cases with two fire sizes, three detection times, three fire source locations, and two ventilation strategies. The activation time of the ventilation system is defined as the time after ignition when the jet fans turn on. These scenarios are defined in Table 3.

Table 3: Scenarios studied to assess the sensitivity of LBAQRA to detection time

Heat Release Rate (MW)	Fire source location (%L)	Ventilation strategy	Detection time (sec)
158	0.8	No ventilation	60
158	0.8	No ventilation	180
158	0.8	Longitudinal ventilation with 3.2 m/s air velocity; 2 min activation time	60
158	0.8	Longitudinal ventilation with 3.2 m/s air velocity; 2 min activation time	180
30	0.3	Longitudinal ventilation with 3.2 m/s air velocity ; 4 min activation time	60
30	0.3	Longitudinal ventilation with 3.2 m/s air velocity; 4 min activation time	180
30	0.5	Longitudinal ventilation with 3.2 m/s air velocity; 4 min activation time	60
30	0.5	Longitudinal ventilation with 3.2 m/s air velocity; 4 min activation time	180
30	0.8	Longitudinal ventilation with 3.2 m/s air velocity; 4 min activation time	60
30	0.8	Longitudinal ventilation with 3.2 m/s air velocity; 4 min activation time	180

Detection time is the time between when the fire starts and when the tunnel safety equipment detects the fire and it is the first stage of evacuation process. The greater this parameter, the greater required safe egress time and consequently the probability that the harmful effects of the fire reach the tunnel user before they leave their vehicle.

Table 4 shows how the EDV varies when the detection time was increased from 60 sec to 180 sec. it can be seen by increasing the detection time to 180 sec, the EDV increases by about 72%. This higher value shows that greater ASET results in more tunnel users cannot start the evacuation process or they cannot finish it after being in the untenable condition for too long. In both cases they die. Consequently, the number of fatalities for scenarios with higher detection time is more than 60 sec detection time scenarios.

Table 4: EDV variation when the detection time varies

	First parameter	Second parameter
Detection time	60 sec	180 sec
EDV	2.403E-02	4.133E-02
Variation		-72.01%

The number of fatalities shown in Figure 5 provides a clear demonstration of 30 MW fire scenarios with the same frequency but different number of fatalities because of different detection times, 60 sec and 180 sec.

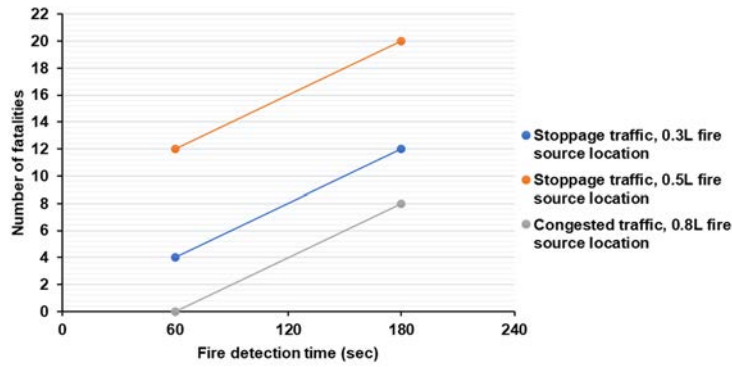


Figure 5: Dependency of number of fatalities on the fire detection time

4.2.2. Fire occurrence rate

The initial fire rate has a direct influence on the final frequency of fire scenarios in the frequency event in this model. Consequently, it has a direct effect on the EDV, which is obtained by multiplying the frequency of each scenario by the number of fatalities. The sensitivity analysis was carried out for fire scenarios with longitudinal ventilation system activated after 2 min and 158 MW and 30 MW fire loads. Three initial fire rates were studied: reference fire rate, halved fire rate, and doubled fire rate. If the initial fire rate is doubled, as it is expected the EDV is doubled and vice versa.

Table 5 illustrates the variation of the EDV for the reference fire rate, halved fire rate, and doubled fire rate.

Table 5: The variation of the EDV for various fire rate.

	Reference parameter	Halved parameter	Doubled parameter
Initial fire rate (/100 million veh-km)	1.511	0.756	3.022
EDV	1.72E+01	8.60E+00	3.44E+01
Variation		-50%	+100%

4.2.3. Probability of congested traffic

Probability of congested traffic is one of influential parameters which the initial fire rate is multiplied by to produce the final fire rate for each scenario considered in the frequency event tree of this model. To evaluate the sensibility of LBAQRA to this parameter, three values were considered, the actual probability of congested traffic for the tunnel under study, and the change of this variable between $\pm 50\%$.

Table 6: The variation of the EDV for various congested traffic probability

	Reference parameter	Halved parameter	Doubled parameter
Congested traffic probability	0.077	0.0386	0.154
EDV	1.72E+01	1.14E+01	2.86E+01
Variation		-33.32%	66.64%

5. CONCLUSION

A model of quantitative risk analysis concerning safety in road tunnels called LBAQRA has been developed to perform a risk analysis as required by UK regulations for complex fire scenarios. LBAQRA consists of two main sections: quantitative frequency analysis and quantitative consequence analysis.

The frequency of each fire scenario has been determined based on the basic fire rate of UK road tunnels per 100 million veh-km which is updated by taking into account the length, traffic, and gradient of the tunnel under study. Then the effect of time of fire incident, traffic condition, accident type, vehicle type, and the fire source location on the updated fire rate is considered through branches of the frequency event tree. The quantitative consequence model comprises three parts, the queue formation model that estimates the number of potential tunnel users for each lane, the distribution model that calculates the evacuation distance in two dimensions, and the egress model that calculates the required evacuation time.

This paper presents a brief description of the sections of this model and how it derives the societal risk. In the second part, an illustrative case study was carried out for the Southwick Tunnel to study the robustness of this model, and the risk reduction potential of different ventilation strategies was assessed.

A study of various emergency ventilation strategies shows that when the ventilation system is activated very late, it cannot cope with the influences of fire and smoke. The sensitivity analysis shows that the number of fatalities increases when the detection time rises and the initial fire rate and the probability of congested traffic have direct influence on the final frequency of fire scenarios.

6. ACKNOWLEDGMENT

We are grateful for the CPU resources possible by Universiti Kebangsaan Malaysia grant GUP-2020-015.

7. REFERENCES

- [1] Highways England. CD 352, 'Design of road tunnels'
- [2] European Parliament and the Council of the European Union. Directive 2004/54/EC of the European parliament and of the council of 29 April 2004 on minimum safety requirements for tunnels in the Trans-European Road Network. Official Journal of the European Union, 167, 39–91, 2004.
- [3] Kirytopoulos, K.A., Rentizelas, A.A., Tatsiopoulos, I.P. and Papadopoulou, G., 2010. Quantitative risk analysis for road tunnels complying with EU regulations. *Journal of Risk Research*, 13(8), pp.1027-1041.
- [4] Organization for Economic Cooperation and Development (OECD). Safety in tunnels transport of dangerous goods through road tunnels. *Int. Transp. Forum* 2001.
- [5] Cassini, P., 1998. Road transportation of dangerous goods: quantitative risk assessment and route comparison. *Journal of hazardous materials*, 61(1-3), pp.133-138.
- [6] Diamantidis, D., 2005. Risk analysis versus risk acceptability in major European tunnel projects. In *Proceedings 1st Asia Pacific conference on risk management and safety*, Hong Kong.

- [7] Kohl, B., Botschek, K. and Hörhan, R., 2006, May. Austrian risk analysis for road tunnels. In 3rd International conference, tunnel safety and ventilation, Graz, Austria.
- [8] Kohl, B. and Žibert, M., 2010. Risk analysis study for Slovenian motorway tunnels. Proceedings of Slovenski Kongres O Cestah in Promeu, Portorož, pp.606-617.
- [9] Borghetti, F., Cerean, P., Derudi, M. and Frassoldati, A., 2019. Road Tunnels: An Analytical Model for Risk Analysis. Springer International Publishing.
- [10] Haddad, R.K. and Harun, Z., 2023. Fire incident data for England road tunnels. Modern transportation, 12(1), pp.e8855-e8855.
- [11] Lemke, K. Road safety in tunnels. Transp. Res. Rec. 2000, 1740, 170–174.
- [12] Yeung, J.S. and Wong, Y.D., 2013. Road traffic accidents in Singapore expressway tunnels. Tunnelling and Underground Space Technology, 38, pp.534-541.
- [13] Yousif, S., Al-Obaedi, J. and Henson, R., 2013. Drivers' lane utilization for United Kingdom motorways. Journal of transportation engineering, 139(5), pp.441-447.
- [14] Milke, J.A., 2000. Evaluating the early development of smoke hazard from fires in large spaces/discussion. ASHRAE Transactions, 106, p.627..
- [15] Buettner, K., 1951. Effects of extreme heat and cold on human skin. II. Surface temperature, pain and heat conductivity in experiments with radiant heat. Journal of Applied Physiology, 3(12), pp.703-713.
- [16] Lawrence, J.C. and Bull, J.P., 1976. Thermal conditions which cause skin burns. Engineering in Medicine, 5(3), pp.61-63.
- [17] Dries, D.J. and Endorf, F.W., 2013. Inhalation injury: epidemiology, pathology, treatment strategies. Scandinavian journal of trauma, resuscitation and emergency medicine, 21, pp.1-15.
- [18] Stoll, A.M. and Greene, L.C., 1959. Relationship between pain and tissue damage due to thermal radiation. Journal of applied physiology, 14(3), pp.373-382.
- [19] Haddad, R.K. and Harun, Z., 2023. Development of a novel quantitative risk assessment tool for UK road tunnels. Fire, 6(2), p.65.
- [20] Moonis, M., Wilday, J., Wardman, M. and Balmforth, H., 2008. Assessing the safety of delivery and storage of hydrogen. Health & Safety Laboratory Report PS/08/01, 14.

SOME QUESTIONS RELATED TO CFD MODELING OF PRESSURIZED TANK BURST IN ROAD TUNNELS

¹Guillaume Lecocq, ¹Laure Heudier, ¹Benjamin Truchot, ²Antoine Mos,
²Christophe Willmann
¹INERIS, FR
²CETU, FR

DOI 10.3217/978-3-85125-996-4-31 (CC BY-NC 4.0)

This CC license does not apply to third party material and content noted otherwise.

ABSTRACT

The current paper focuses on high-pressure reservoirs and the consequences of their potential burst, related to scenarios of thermal or mechanical aggressions, in tunnels.

CFD modeling can be used to account for the effects of such scenarios. An intrinsic advantage of such an approach consists in integrating the specific geometrical effects (tunnel walls, presence of vehicles) on the pressure wave propagation.

To meet such an objective, experimental data are required to offer an opportunity for validation. Data from the literature and new ones from INERIS are detailed in this paper, with their strengths and weaknesses to identify relevant test cases for CFD.

Phenomenological tools are tested against experimental cases of bursting tank in a free field to evaluate their prediction capability for pressure. These tools could be used along with CFD in a global modeling framework.

CFD is tested against fictitious free-field cases, investigating the effect of the thermodynamic model on the results. The numerical method for propagating the pressure wave in realistic tunnels is also studied.

Keywords: tank burst, pressure effects, CFD, phenomenological tools

1. INTRODUCTION

To meet the objective of reducing the transportation impact on the global warming, car manufacturers currently develop new technologies. According to this change, the propulsion of vehicles crossing tunnels is expected to be more and more varied in a next future with Batteries, Fuel Cells or spark-ignition engines using either Natural Gas or Hydrogen. Currently, those two gases, Hydrogen and Natural Gas, are stored at a gaseous state under high pressure, up to 700 bar. The presence of such reservoirs in tunnels raises new risks that should be finely considered by technical experts and regulators.

A first specificity of such burst in confined geometry is the existence of a reflection zone, close to the bursting capacity, leading to the formation of a planar pressure wave. The intensity of this latter decays much more slowly than in free field. Also, vehicles can be present and influence the pressure wave propagation.

As CFD intrinsically accounts for geometrical effects, this method appears attractive for dealing with these scenarios. Nevertheless, confronting CFD computations to reference test cases is needed to define a modeling strategy. Available experimental data are first listed and described. Phenomenological tools are then tested against some points of the database. These tools could be used along with CFD for getting a reference solution for example. CFD computations are also compared with free-field and tunnel burst tank cases.

2. EXPERIMENTAL DATA

2.1. Tunnel cases

The data of the literature produced in the framework of experimental campaigns in tunnels are given in the Table below. They are mainly the measurements from Kudriakov et al. [1] in a disused 507 m long road tunnel. Original data obtained by INERIS in its test tunnel are also supplied. This tunnel cross section is about 10 m² and its length about 80 m.

Table 1: Dataset for the tank burst in tunnel. The tests performed in INERIS are in italics.

Gas	Bottle type	Aggression mode	Volume (L)	Initial pressure (bar)	Rupture pressure (bar)	Brode energy (ideal gas law) (MJ)	Pressure measurements	Ref.
N ₂	<i>IV</i>	<i>Fire</i>	19	700	706	3.3	<i>At 5m: 220mbar</i>	[2]
N ₂	<i>IV</i>	<i>Fire</i>	19	700	715	3.4	<i>At 5m: 287mbar</i>	[2]
N ₂	<i>IV</i>	<i>Fire</i>	36	700	749	6.7	<i>At 5m: 433mbar</i>	[2]
N ₂	<i>IV</i>	<i>Fire</i>	36	700	716	6.4	<i>At 5m: 399mbar</i>	[2]
N ₂	<i>IV</i>	<i>Fire</i>	19	525	585	2.8	<i>At 5m: 399mbar</i>	[2]
N ₂	<i>IV</i>	<i>Fire</i>	19	700	714	3.4	<i>At 5m: 377mbar</i>	[2]
He	IV	Detonation belt	78	650	650	7.7	At 30 m: 98 mbar / 50m: 85 mbar 80 m: 72 mbar / 110m: 68 mbar 140 m: 61 mbar / 170 m: 55 mbar	[1]
H ₂	IV	Detonation belt	78	520	520	10.1	At 30 m: 207 mbar (271 mbar) 50m: 180 mbar (243 mbar) 80 m: 160 mbar / 110m: 205 mbar 140 m: 202 mbar / 170 m: -	[1]
H ₂	IV	Detonation belt	78	610	610	11.9	At 30 m: 187 mbar (218 mbar) 50m: 180 mbar (225 mbar) 80 m: 151 mbar (204 mbar) 110m: 205 mbar (336 mbar) 140 m: 301 mbar / 170 m: 179 mbar	[1]
<i>He</i>	<i>IV</i>	<i>Fire</i>	36	350	378	2.1	<i>At 30 m: 187 mbar</i>	[3]
<i>He</i>	<i>IV</i>	<i>Fire</i>	36	700	703	3.8	<i>At 30 m: 248 mbar</i>	[3]
<i>He</i>	<i>III</i>	<i>Fire</i>	17	718	881	2.3	<i>At 19 m: 140 mbar / 24 m: 159 mbar / 29 m: 152 mbar</i>	[3]
<i>He</i>	<i>IV</i>	<i>Mechanical impact</i>	2.4	698	698	0.25	<i>At 1 m: 150 mbar / 5 m: 50 mbar</i>	[4]
<i>He</i>	<i>IV</i>	<i>Mechanical impact</i>	2.4	693	693	0.25	<i>At 2 m: 142 mbar / 5 m: 67 mbar</i>	[4]

A CFD method for modeling high-pressure tank bursts should be regarded on cases with increasing physical complexity for validation purpose. Then, a modeling work should first address the burst of non-reacting gas tanks. Indeed, the fireball was proved to contribute to the pressure effects [5]. Furthermore, the aggression mode is of importance as it impacts the discharge of the pressure wave. In free field, most reservoirs of the literature contain hydrogen and are thermally aggressed, making these cases hard to address with CFD. A CFD method was nevertheless previously proposed by Molkov et al. for such cases [6].

The results obtained recently by Kudriakov et al. [1] are interesting as the way the pressure discharge is obtained is partially controlled, non-reacting gases are used, and numerous

measuring points were exploited. Nevertheless, there are no pressure measurements around the tank (between the tank and the first wall met by the pressure wave for example). When assessing modeling tools behavior is of interest, it is wished to check the tool could reproduce the pressure field from the source to an observer location.

Some campaigns show only one measurement point, making them difficult to be used for validating tools.

The graph below is built from the data of Table 1. It plots the peak pressure versus the reduced distance λ , which writes: $\lambda = r/m_{TNT}^{1/3}$. r is the distance between the pressure source and the sensor and m_{TNT} is the TNT equivalent. This latter is deduced from E , the explosion energy, closed with the expression of Brode [7]. An ideal gas behavior is assumed. A free-field decay is computed with the PROJEX tool [8], relying on the Multi-Energy method abacus [9]. The severity is then set to 10 and the explosion energy is calculated with the Brode formula. The comparison shows that for a given explosion energy, the available experimental data describe either the spherical pressure wave expansion or the planar wave propagation, but not the whole propagation process.

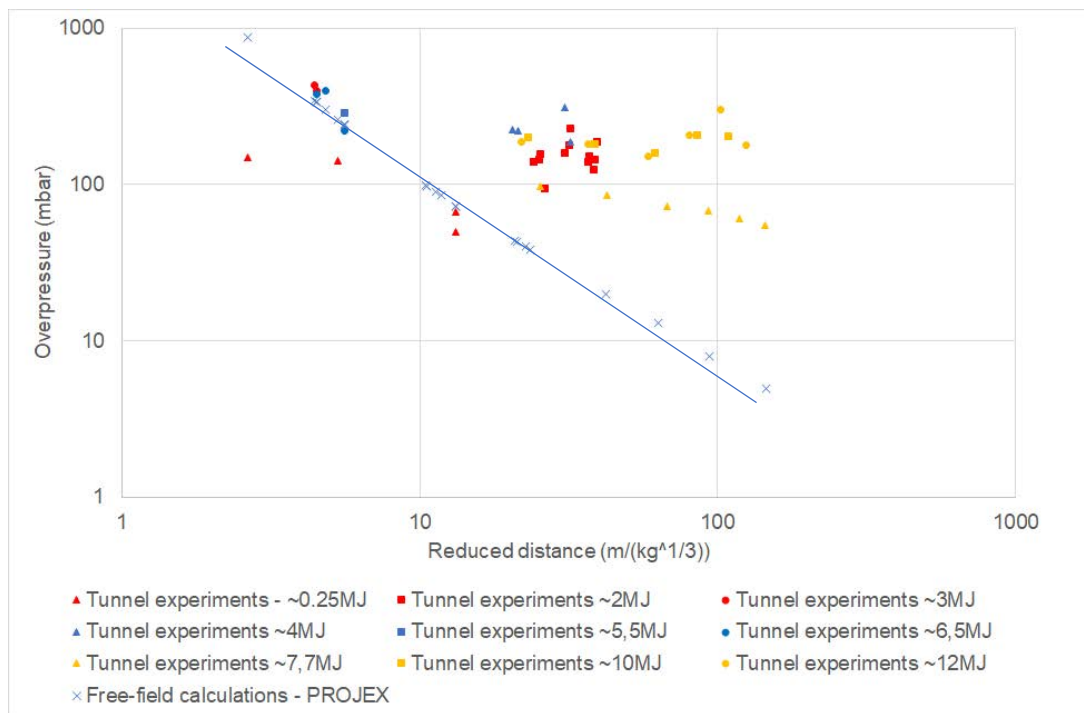


Figure 1: Overpressure peaks in case of tank burst in tunnel (experiments) and in free field (calculations). The blue line approximates the PROJEX results.

The database is not sufficient for testing CFD. Tank burst cases in free field are then regarded in the next section.

2.2. Free-field cases

The data found in the literature related to tests of high-pressure tanks bursting in free field are detailed in Table 2. This latter contains also original data produced by INERIS.

The overpressure measurements in Figure 2 show that several values of overpressure peaks can be retained, depending on the analysis of the measured signal. That's why, in Table 2, for some tests, several values of overpressure peaks are indicated for the same sensor. For this reason, it is preferable to have the overpressure signals and not only the peak values when

trying to assess the performance of modeling tools such as phenomenological or CFD based ones.

Table 2: Dataset for the tank burst in free field. For the data⁽¹⁾, the bottle was surrounded by four concrete walls that could have impacted the measured value. Furthermore, the bottle moved when bursting making it difficult to know the real distance between the sensor and the bottle. The tests performed in INERIS are in italics.

Gas	Bottle type	Aggression mode	Volume (L)	Initial pressure (bar)	Rupture pressure (bar)	Pressure measurements	Ref.
H ₂	IV	Fire	72.4	343	357	On the bottle axis, at 4.2m: 650 mbar On the normal axis, at 1.9m: 3 bar / 4.2 m: 830 mbar, 6.5m: 410 mbar	[10]
H ₂	III	Fire	165	350	440	No pressure measurement. Bottle projected 200 m away	[11]
H ₂	IV	Fire	35	700	945	At 5 m: 1.1 bar / 10 m: 234 mbar	[12]
H ₂	III	Fire	36	700	995	At 5 m: 743 mbar / 10 m: 234 mbar	
H ₂	<i>N/A</i>	<i>Detonating cord</i>	9	700	700	<i>Axis 1, at 10 m: 96 mbar / 15 m: 58 mbar Axis 2, normal to axis 1: at 10 m: 110 mbar / 15 m: 64 mbar</i>	[13]
H ₂	<i>IV</i>	<i>Fire</i>	2.4	481	600	<i>At 5 m: 58-68 mbar / 10 m: 30-36 mbar</i>	[14]
H ₂	<i>IV</i>	<i>Fire</i>	2.4	525	673	<i>At 5 m: 58-75 mbar / 10 m: 32 mbar</i>	
H ₂	<i>IV</i>	<i>Fire</i>	2.4	700	827	<i>At 5 m: 61-69-78 mbar / 10 m: 38 mbar</i>	
H ₂	<i>IV</i>	<i>Fire</i>	2.4	700	854	<i>At 5 m: 71-80-104 mbar / 10 m: 41-53 mbar</i>	
N ₂	<i>IV</i>	<i>Fire</i>	19	700	722	<i>At about 1 m: 1 bar⁽¹⁾</i>	[2]
N ₂	<i>IV</i>	<i>Fire</i>	19	467	488	<i>At about 1 m: 2.5 bar⁽¹⁾</i>	
He	<i>IV</i>	<i>Fire</i>	19	700	730	<i>At about 1 m: 4.5 bar⁽¹⁾</i>	
He	<i>IV</i>	<i>Fire</i>	19	467	506	<i>At about 1 m: 2.5 bar⁽¹⁾</i>	
H ₂	<i>IV</i>	<i>Fire</i>	19	700	713	<i>At about 1 m: 450 mbar⁽¹⁾</i>	
H ₂	<i>IV</i>	<i>Fire</i>	19	467	483	<i>At about 1 m: 6-7 bar⁽¹⁾</i>	

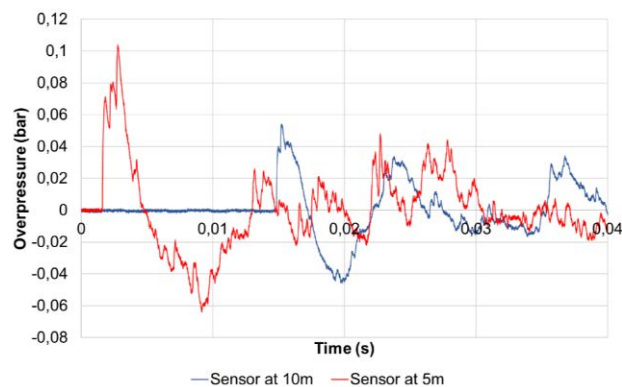


Figure 2: Pressure signals measured for the burst of a 2.4 L bottle containing 700 bar of hydrogen. Red: at 5 m. Blue: at 10 m.

Again, a campaign only supplies a single measurement, which is not enough for testing the codes. This measurement can also be disturbed by the surrounding walls. The data coming from [14] present several tests and two measuring points. The first pressure rise is followed by several pressure peaks. This may notably be explained by a progressive pressure discharge, which is tricky to address through numerical modelling. The first part of the signals of Zalosh [10] and Tamura [12] (not shown) is closer to the typical shock wave shape, with a single peak

followed by a pressure decay. Some data obtained for non-reacting gases could greatly improve the database, when thinking to modeling tool assessment.

3. MODELING BURST TANK CASES

3.1. Phenomenological tools for free-field bursting tanks

As experimental data appear to miss to provide a complete validation database for CFD dedicated to bursting tanks, some phenomenological tools are regarded. Indeed, if they are accurate enough, they could be used to complete experimental dataset with extra points.

The considered tools are PROJEX, the TNT equivalent [15] and the Baker methods [16]. Also, the Brode energy upon which rely PROJEX and the TNT equivalent method can be quantified with the ideal gas law and with a real gas law, such as the Able-Nobel one [5]. The dataset provided by Zalosh and Tamura is used to test the phenomenological approaches (see Tables 3 and 4). All approaches are employed for a charge located on the ground and do not account for chemical effects related to a fireball generation.

Table 3: Phenomenological tools results compared to Zalosh measurements [10]. The Baker method results are from [5]. Computations made for a TNT equivalent of 4,57 MJ/kg.

Location	Exp. data	PROJEX (6,46 MJ)	PROJEX A-N (5,33 MJ)	TNT Eq. (1,41 kg)	TNT Eq. A-N (1,16 kg)	BAKER A-N (9,4 MJ)
at 1.9 m orthogonally to the bottle axis	3 bar	2,35 bar	2,05 bar	4,2 bar	3,6 bar	3,19 bar
at 4.2 m on the bottle axis	650 mbar	441 mbar	403 mbar	740 mbar	650 mbar	608 mbar
at 4.2 m orthogonally	830 mbar					
at 6.5 m orthogonally	410 mbar	222 mbar	205 mbar	336 mbar	302 mbar	284 mbar

Table 4: Phenomenological tools results compared to Tamura measurements [12].

	Location	Exp. data	PROJEX (8,3 MJ)	PROJEX A-N (5,8 MJ)	TNT Eq (1,81 kg)	TNT Eq. A-N (1,27 kg)
35 L type IV bottle	at 5 m orthogonally to the bottle axis	1,1 bar	390 mbar	320 mbar	618 mbar	500 mbar
	at 10 m orthogonally to the bottle axis	234 mbar	138 mbar	116 mbar	196 mbar	165 mbar
		Exp. data	PROJEX (8,95 MJ)	PROJEX A-N (6,3 MJ)	TNT Eq (1,96 kg)	TNT Eq. A-N (1,37 kg)
36 L type III bottle	at 5 m orthogonally to the bottle axis	743 mbar	402 mbar	331 mbar	650 mbar	520 mbar
	at 10 m orthogonally to the bottle axis	234 mbar	142 mbar	120 mbar	204 mbar	172 mbar

For the Zalosh database, all the methods recover the proper orders of magnitude. Nevertheless, the most accurate methods seem to be the TNT Equivalent method with a real gas law and the Baker method. Concerning the Tamura cases, PROJEX and the TNT equivalent method underestimate the peak about 1 bar, 5 m from the first bottle. Overall, the best results are obtained with the TNT equivalent method.

According to the results, the phenomenological methods give most of the time the proper orders of magnitude when compared with the chosen experiments but are not necessarily

accurate. These methods can help to assess a result obtained with CFD but do not give strict reference results.

3.2. CFD

The CFD approach is regarded in modeling the fictitious case of the burst of a 78 L reservoir containing air at a pressure of 610 bar. The CFD tool is OpenFoam [17]. The solver *rhoCentralFoam* is chosen. It solves the Euler equations with the convective numerical scheme of Tadmor ad Kurganov. The time derivatives are discretized with the Euler scheme. The basic solver does not account for transport equations for the chemical species, meaning the gas in the bottle and in the environment is the same. By default, also, the user can only rely on an ideal gas law. The specific heat at constant pressure can be set to a constant or a JANAF table can be used to introduce a law $C_p = C_p(T)$.

Developments were carried out to add the transport equations for chemical species and enable to account for a real gas law such as the Peng-Robinson one. A recent work [18] gives elements to perform the coding.

Several CFD computations are performed for a regular mesh, the cell width being 5 cm. In a volume equal to the tank one, a pressure of 610 bar is initially imposed. The discharge is then implicitly modeled as the instantaneous disappearance of the tank walls. The results of the CFD computations for several parametrizations are given in the Table below, as well as results obtained with phenomenological tools. It can be seen these latter tools provide the same orders of magnitude from 5 to 30 m from the pressure source, the TNT equivalent overpredicting the PROJEX results. In the previous part, the TNT equivalent gave the best results for similar bursting cases. The CFD computation based on a resolution of the chemical species transport equations and a real gas law gave the closest results to the TNT equivalent ones. It should be nevertheless noted that in the previous part, the regarded cases involved a fireball, that potentially contributed to pressure effects and not the current one.

Table 5: Pressure effects at several distances related to a fictitious case of a bursting 78 L reservoir containing 610 bar of air. Several computing methods are used.

Modeling method	Distance (m)					
	5	10	15	20	25	30
PROJEX (E=12,2 MJ)	472mbar	162 mbar	93 mbar	65 mbar	51 mbar	41 mbar
TNT equivalent (m=2,67 kg)	795mbar	238 mbar	133 mbar	91 mbar	70 mbar	55 mbar
CFD with ideal gas law and constant Cp coefficients	168 mbar	69 mbar	38 mbar	25 mbar	21 mbar	19 mbar
CFD with transport equations for chemical species, an ideal gas law and JANAF tables	1550 mbar	320 mbar	189 mbar	154 mbar	124 mbar	90 mbar
CFD with transport equations for chemical species, a real gas law (Peng-Robinson) and JANAF tables	823 mbar	237 mbar	155 mbar	109 mbar	94 mbar	84 mbar

Finally, first CFD computations of a case of the Kudriakov et al. campaign is performed. The Helium case is addressed as it is theoretically the simplest as no fireball is generated at the tank rupture. The computational domain is 3D and 120 m long and decomposed into cubic cells with a characteristic width of 5 cm. It was chosen to work with relatively small cells instead of using an Automatic Mesh Refinement (AMR) method. Indeed, the criterion that is used by default is the normalized pressure gradient meaning only the first pressure wave will be refined. This may be fine for dealing with free field cases but not necessarily tunnel cases for which the reflection zone involving numerous pressure waves is of importance.

Two CFD are performed, both with the transport of the chemical species and JANAF tables for computing the Cp coefficients. The first CFD relies on the ideal gas law, the other on the Peng-Robinson law. The Figure below shows the results obtained 30 m away from the pressure source and the measured pressure signal. It should be pointed out the experimental signal has been treated with a low-pass filter and a cut-off frequency of 100 Hz in order to suppress acoustic effects. It explains why a shock is not visible on the experimental signal. The CFD results are very similar between them. The impact of the gas law can be noticed, as the real gas law leads to lower pressure magnitude but remains moderate. The CFD pressure waves have a higher intensity than the experimental one and are quicker. These computations are first attempts in order to assess their potential but extra work is needed to address properly free field cases.

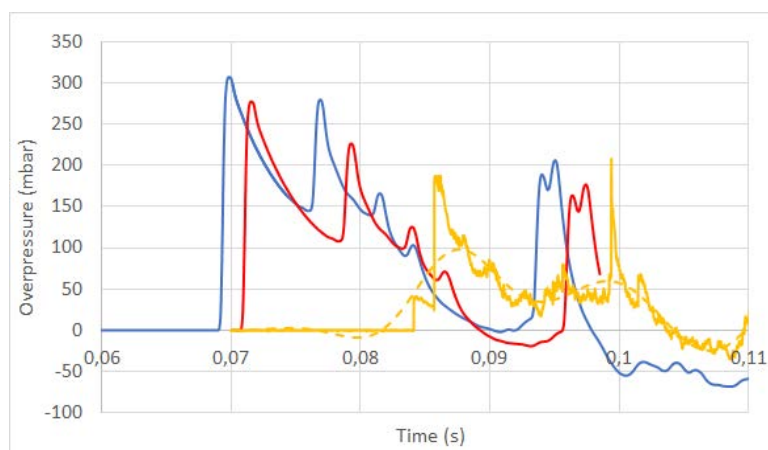


Figure 3: Experimental (yellow) raw (line) and filtered (dash line) signal measured at 30 m after bursting of a 78 L Helium bottle under 650 bar in the Mortier tunnel [7]. CFD modeling with an ideal gas law (blue) and a real gas law (ref).

4. CONCLUSION

A CFD approach is studied for dealing with high-pressure tank burst in tunnels. Reference tests are needed to propose a CFD strategy. Most tests are physically complex as they correspond to a thermal aggression of a hydrogen tank. These tests do not permit to quantify the part of pressure effects related to the fireball and the other one related to gas expansion.

Tests in tunnels were performed but the available data remain too limited to design and validate step by step a CFD modeling strategy. A promising experimental campaign could consist in provoking tank burst in free field for one or two non-reacting gas and for hydrogen, for the same tank volume and the same initial pressure. Burst could be generated by a detonating cord to control the discharge mode (initial pressure and surface discharging pressure). Repeatability tests would be needed. The same tests could be performed in a gallery or in a tunnel. Pressure probes locations should be the same in both types of tests and chosen in order to detect in tunnel, the reflection zone, the planar zone and the transition between the two.

Phenomenological tools were tested against some free field results. These models recover orders of magnitude for the pressure magnitude but their accuracy may vary. The way the pressure energy is quantified for high pressure cases may impact the results.

Some CFD was performed in free field and in tunnel. Some modeling choices for thermodynamics seem to be preferable nevertheless, the results obtained in the tunnel overestimate the experimental results. Extra work is needed based on the analysis of the projected experimental campaign mentioned above. This latter could also be beneficial for

checking the behavior of already existing CFD strategies for modeling hydrogen tank bursts [6].

5. REFERENCES

- [1] S. Kudriakov et al. (2022) Full-scale tunnel experiments: Blast wave and fireball evolution following hydrogen tank rupture. *Int. J. Hydrogen Energy* 47(43), pp. 18911-18933
 - [2] P. Blanc-Vannet et al. (2019) Fire tests carried out in FCH JU Firecomp project, recommendations and application to safety of gas storage systems, *Int. J. of Hydrogen Energy* 44(17), pp. 9100-9109
 - [3] S. Ruban et al (2012) Fire risk on high-pressure full composite cylinders for automotive applications, *Int. J. of Hydrogen Energy* 37 pp. 17630-17638
 - [4] INERIS test campaign (2012)
 - [5] V. Molkov et al. (2015) Blast wave from a high-pressure tank rupture in a fire: Stand-alone and under-vehicle hydrogen tanks, *Int. J. of Hydrogen Energy* 40, pp. 12581-12603
 - [6] V.V. Molkov et al. (2021) Dynamics of blast wave and fireball after hydrogen tank rupture in a fire in the open atmosphere. *Int. J. Hydrogen Energy* 46(5), pp. 4644-4665
 - [7] H.L. Brode (1959) Blast waves from a spherical charge. *Phys Fluids* 2, pp. 217-29
 - [8] L. Heudier (2013) Les éclatements de capacité. Phénoménologie et modélisation des effets. Rapport Omega 15. www.ineris.fr.
 - [9] A.C. Van den Berg (1984) The Multi-Energy method – a framework for vapour cloud explosion blast prediction, TNO-PML Report 1984-C72
 - [10] R. Zalosh et al. (2005) Hydrogen Fuel Tank Fire Exposure Burst Test. SAE 2005-01-1886
 - [11] C. Shen et al. (2018) Consequence assessment of high-pressure hydrogen storage tank rupture during fire test. *J. Loss Prev. in the Process Ind.* 55, pp. 223-231
 - [12] Y. Tamura et al. (2006) Fire exposure burst test of 70MPa automobile high-pressure hydrogen cylinders. Society of Automotive Engineers of Japan Annual Autumn Congress
 - [13] J. Chaineaux et al. (2000) Sécurité des dispositifs de stockage de l’hydrogène sous haute pression équipant des véhicules routiers. Final report. EURO-QUEBEC HYDRO-HYDROGENE Project.
 - [14] INERIS test campaign (2010)
 - [15] TM5. 1300 (1969) Department of the Army, the Navy and the Air Force. Structures to resist the effects of accidental explosions. Technical Manual, NAFVAC-P397 / AFM88
 - [16] W.E. Baker, P.A. Cox, J.J. Westine, R.A. Kulesz, P.S. Strehlow (1983) *Explosion hazards and evaluation*, Elsevier editions.
 - [17] www.openfoam.org
- K.A. Ghasemi (2020) Release of high-pressure hydrogen into the air, Master’s Thesis, University of South-Eastern Norway

INTEGRATION OF NEW ENERGY CARRIERS IN FRENCH SPECIFIC HAZARD INVESTIGATIONS: OVERVIEW OF PRINCIPAL ISSUES

Christophe Willmann, Pauline Charles
CETU, French tunnel study centre, FR

DOI 10.3217/978-3-85125-996-4-32 (CC BY-NC 4.0)

This CC license does not apply to third party material and content noted otherwise.

ABSTRACT

A national work group comprising specialists in specific hazard investigations has been set up by the CETU with the aim of adapting specific hazard investigations to the new energy carriers vehicles. Two main adaptations have been made. The first concerns the adaptation of the criticality matrix ranking, so as to take into account the specificities of gas dangerous incidents in terms of frequency and severity. The second concerns the adaptation of the detailed scenario analysis to take account of two dangerous incidents involving gas, kinetic vapour cloud and tank rupture explosions, which are more instantaneous than fires (the dangerous incident that is the most feared in tunnels).

Keywords: risk analysis, new energy carriers, adaptation.

1. INTRODUCTION

The French Centre for Tunnel Studies (CETU) has been working on the impact of new energy carriers (NEC) in underground space for many years. A joint research project with INERIS has enabled a quantitative assessment of the additional risks of these vehicles.

As they are already present in traffic, it was necessary to integrate them into the safety management system. The approach used began with adapting the risk analysis conducted for French tunnels (known as the specific hazard investigation) so as to take into account these new vehicles.

To handle this topic, CETU set up a work group of national specialists in specific hazard investigations. The work is still in progress but almost finalized. The main issue was to find a work methodology and ways to integrate quantitative risk assessment results (from the CETU-INERIS study [3]) into the specific hazard investigation methodology which is scenario-based ([1]). After a short reminder of the specific hazard investigation methodology, the paper will explain how the main difficulties related to the specificities of NEC vehicles were overcome in the adaptation process.

2. SPECIFIC HAZARD INVESTIGATION METHODOLOGY

A specific hazard investigation is a French methodology for analysing risks related to user safety in road tunnels. In this method, the tunnel is considered as a system, which includes the users, equipment, environment, operator, maintenance and emergency services. The approach is scenario-based [1]. Unlike a system-based approach, only a few relevant scenarios are chosen and analysed in detail. The main goal is to identify potential hazards related to the tunnel, analyse in detail how the system mitigates them, and, if necessary, propose improvements to address the weaknesses identified.

A specific hazard investigation is divided into five phases, which will be presented overleaf (details can be found in [2]).

2.1. The tunnel and its environment

This section of the investigation describes the tunnel and its environment. In general, the following aspects are relevant:

- tunnel characteristics;
- location of the operating centres and emergency centres in relation to the tunnel;
- natural environment (geology, hydrogeology, meteorology, etc.);
- human environment (population and nearby activities including temporary ones);
- roads: main routes and their usual traffic conditions;
- traffic composition;
- any other aspects considered relevant.

2.2. Functional description of the tunnel

This section highlights the link between the safety functions and the principal structural elements, equipment and operating arrangements to ensure their effective performance.

2.3. Identification of hazards and choice of scenarios

The first step of this section is the identification of hazards and dangerous incidents that they may entail. An exhaustive inventory of potentially dangerous incidents is drawn up, for example LV fire or HGV fire. They are then ranked in a criticality matrix, combining their presumed frequency and severity. The matrix has five columns, for five classes of severity. For example, class I corresponding to “Minor or none” means there is only material damage, class II “Significant”, implies slightly injured persons and class III “Critical”, could lead to seriously injured persons or less than 5 fatalities.

The matrix resulting from the above severity and frequency classes is shown in Figure 1.

	I Minor or None	II Significant	III Critical	IV Catastrophic	V Major Catastrophe
A Very frequent					
B Frequent					
C Occasional					
D Rare					
E Very rare					
F Extremely rare					

Figure 1: Criticality matrix

Fires incidents are more numerous in this matrix than those related to other hazards (accidents, breakdowns) because they are more impacted by the vehicle type (HGV, LV, dangerous goods vehicle). Moreover, they are of greater interest for the objectives of the specific hazard investigation as they provide better knowledge of how the system is able to address and mitigate the danger and how this system can be improved.

The second step is the choice of scenarios. This begins with the choice of dangerous incidents, based on the matrix. Dangerous incidents are then combined with contextual parameters to

define a scenario. These contextual parameters are for example the location of the incident, the traffic conditions and the initial air flow velocity. In general, only between 4 and 8 scenarios are selected for detailed analysis, which would not be possible if the number of scenarios is too high. This set of scenarios must be representative and instructive.

2.4. Analysis of the scenarios

Each scenario starts with the dangerous incident chosen previously, and continues with sequences of events until the end of users’ evacuation.

In the case of fire, the first step in this analysis is to choose the hypothesis related to user behaviour (walking speed related to visibility, influence of temperature and toxicity, etc.) and fire modelling. The analysis is then conducted by using a space-time graph that illustrates the fire’s development and the users’ trajectory which are influenced by air opacity, temperature, heat radiance, and toxicity.

2.5. Summary

This section of a specific hazard investigation contains a summary of what has been learned from the scenarios and a summary of their consequences. It also evaluates the system’s level of safety especially by qualitatively assessing its ability to address the hazards. Then, if necessary, proposals for improvement are made.

3. ADAPTING THE METHODOLOGY TO THE SPECIFICITIES OF NEC-RELATED DANGEROUS INCIDENTS

As explained in [3], new propulsion energies that raise the most concern for user safety are gases: hydrogen, compress natural gas (CNG) and liquid natural gas (LNG)¹. They can cause specific dangerous incidents in addition to classic incidents that also occur with vehicles powered by petrol or diesel (accident and fire). These dangerous incidents specific to gas are jet fires or VCE (vapor cloud explosions) both resulting from a collision, a malfunction during tank filling, or tank rupture following fire². They will be called “gas dangerous incidents” in the following sections of the present article.

Because of their specificities, gas dangerous incidents can’t be treated in a specific hazard investigation methodology in the same way as accidents and fires. These specificities also provide new opportunities in terms of risk assessment. The following sub-sections explain these specificities and how the steps of the methodology can be adapted to integrate them.

3.1. Adaptation of the ranking in the criticality matrix to the frequency and severity of gas dangerous incidents

The first step in the methodology significantly impacted by the specificities of gas dangerous incidents is the identification of hazards and choice of scenarios. Both frequency and severity of gas dangerous incidents have specificities that need to be analysed to determine if it is possible to integrate them in the criticality matrix presented in 2.3 or if another approach should be developed.

¹ Apart from a very specific batteries, the only specific incident related to Li-ion batteries (assuming a battery capacity of 80 kWh), is thermal runaway, which has a non-significant impact on user safety, even if it would be difficult to extinguish by firefighters.

² A jet fire following a fire doesn’t have a significant additional impact on users’ safety apart if the gas vehicle is a bus. A tank rupture following a collision was assumed to be very unlikely given the shield effect of the other part of the vehicles and the strong resistance of the tanks required by regulation.

Frequency specificities and related issues

The frequencies of classic dangerous incidents (accident and fire) and gas dangerous incidents are calculated based on occurrence rates. However, the occurrence rates of classic dangerous incidents are based on a dangerous incidents data base, whereas the occurrence rates of gas dangerous incidents are calculated with formula. Although the proportion of gas vehicles in French traffic has seen a significant increase over the past few years, it remains very low. Therefore, the gas dangerous incidents data base isn't large or reliable enough to base occurrence rates on.

The occurrence rate of fire is 0.9 per 10⁸ *veh.km* for light vehicles and 3 per 10⁸ *veh.km* for heavy goods vehicles [4], and the occurrence rate of CNG tank rupture is given by the formula below.

$$R_{Burst} = \tau_{penetration} * \tau_{type_veh} * \tau_{veh_fire} * P_{malfunction_TPRD} \quad (1)$$

where: τ_{type_veh} is the existence rate of the type of vehicle considered in the traffic, $\tau_{penetration}$ is the proportion of CNG vehicles in the car population, τ_{veh_fire} is the occurrence rate of fires in the type of vehicle considered, $P_{malfunction_TPRD}$ is the probability of a malfunction of the TPRD. More details can be found in [3].

Because of a totally different approach in term of occurrence rate calculation, the uncertainties of frequencies are significantly different between gas dangerous incidents and classic dangerous incidents. This therefore raises the question of the integration of these two frequency types in the same matrix.

Severity specificities and related issues

The severity of classic dangerous incidents, especially fires, is expressed in the number of users losing their self-evacuation capacity by applying the principles outlined in [5]. In the context of a fire in a tunnel, which is the dangerous incident that is mainly investigated in the methodology (see. 2.3), a user losing self-evacuation capacity will quickly die if not helped. Hence, because of the arrival time of rescue services (up to 30 min after the loss of self-evacuation capacity), the number of users losing their self-evacuation capacity is often converted by practitioners into the number of deaths.

In line with French regulations [6], the severity of gas dangerous incidents is expressed as the number of users subjected to significant lethal effects. A user subjected to significant lethal effects is a user that has a certain probability of dying, but death is not certain. For instance, the significant lethal effect threshold of an overpressure is 200 mbar, as stated in [6], whereas the overpressure that kills by lung rupture is between 900 and 1500 mbar, depending on the medical sources. At 200 mbar, lung disorder resulting in death could happen to people who already have health problems or poor physical condition (direct effect) or users could get killed by falling on the ground or being hit by flying pieces from tunnel equipment or vehicles (indirect effect). There are various direct and indirect effects and their impact on the body is complex given the huge variety of health conditions. Therefore, [6] doesn't provide the possibility of deducing a number of deaths from a number of users subjected to significant lethal effects.

As the severity of gas dangerous incidents is not expressed in the same unit as for classic dangerous incidents, they cannot be directly ranked in the same matrix.

Overcoming the issues by a specific integration of gas dangerous incidents into the matrix

To resolve the two issues previously mentioned, two options were investigated.

The first consists in having two separate criticality matrixes: one for classic dangerous incidents and a second for gas dangerous incidents. This will avoid ranking dangerous

incidents that have frequencies with different uncertainties (first issue) and severities with different units (second issue) within the same matrix. However, this has two strong disadvantages. Firstly, the selection of dangerous incidents will be made more difficult and subject to more mistakes. Secondly and principally, the overview of risks offered to stakeholders by a unique dangerous incidents matrix will be lost.

A second option is to find a solution to integrate the gas dangerous incidents into the single matrix.

Concerning frequency, as explained in 2.3, the criticality matrix is organized with frequency classes and severity classes. That means that two events of the same matrix cell belong to the same frequency class and are considered equivalent in term of frequency for the dangerous incidents selection. Generally, the difference between the lower value of a frequency class and the higher one is an order of magnitude (for example between 1 event in one year and 10^{-1} event in one year for class “B”). Even uncertainties higher than 100% are thus unlikely to change the frequency ranking of a dangerous incident³. Therefore, the difference in terms of uncertainty between classic dangerous incidents and gas ones is unlikely to change the ranking of these dangerous incidents in frequency classes. Hence, it was eventually stated that it is acceptable to rank classic and gas dangerous incidents together in the frequency classes.

Concerning severity, as explained before, the severity of gas dangerous incidents is expressed as the number of users subjected to significant lethal effects. The probability that such users will die is non-negligible but unknown, which means that the only possible assumption is that this probability is between 0 and 1. Therefore, if n users are subjected to lethal effects of a given gas dangerous incident, the number of deaths will be between 0 and n . It is likely that the users still alive after being subjected to significant lethal effects will be seriously injured. Therefore, to rank this gas dangerous incident in the severity classes together with the classic dangerous incidents, it is possible to consider that it belongs to the classes between the critical one (seriously injured persons or less than 5 fatalities) and the one including n deaths. For example, according to [3], a CNG vapour cloud explosion (VCE) will subject up to 9 users to significant lethal effects, so it belongs to both critical class and catastrophic class (between 5 and 50 deaths) as illustrated in green in Figure 2.

I Minor or none	II Significant	III Critical	IV Catastrophic	V Major catastrophe
			CNG VCE HGV fire	

Figure 2: Example of gas dangerous incident ranking in the criticality matrix

This second option was therefore chosen by the work group.

3.2. A possible calculation of generic severities that provides the opportunity to have a generic risk assessment of gas dangerous incidents

In the step dedicated to hazard identification and scenario choice, the severity of classic dangerous incidents is only estimated based on expert judgement in a generic way, independent of the tunnel characteristics. Therefore, this estimation is a wide range of possible values rather than a precise one, which is enough to classify the dangerous incident in a

³ Only uncertainties close to 1000% are likely to do so.

severity class that covers an order of magnitude. Of course, by using a quantitative approach (see. 2.4), the scenario analysis enables this first estimation to be more accurate.

[3] gives results from modelling, with a reasonable worst-case geometry (60 m² section, 6 m high, 10 meters wide) that enable a far more precise estimate of the severity of gas dangerous incidents by taking into account certain tunnel characteristics (for example the number of lanes). [3] also enables the frequency of each gas dangerous incident to be calculated. Thus, it is possible to have a more precise risk assessment of gas dangerous incidents (see. Table 1) than the one given by the criticality matrix (see 2.3).

Table 1: Extract of the risk assessment table of hydrogen dangerous incidents

Energy	Dangerous incident	Vehicle type	Frequency (penetration rate ⁴ of 2%)	Number of users subjected to significant lethal effects
H ₂	VCE	LV	8,32E-05	15 to 25
		HGV	5,80E-06	15 to 25
		Bus	4,47E-07	15 to 25 + bus passengers
	Tank rupture	LV	1,12E-06	15 to 25
		HGV	2,52E-07	15 to 25
		Bus	1,94E-08	15 to 25+ bus passengers

3.3. A detailed scenario analysis that has to be adapted to gas dangerous incident kinetics

The choice of scenarios

Gas dangerous incidents follow a collision or a fire. Therefore, the collision scenarios and the fire scenarios chosen for all vehicles types will be used as a basis to study gas dangerous incidents. Indeed, as explained in [3], apart from these gas dangerous incidents that can occur, there is no significant differences between a collision or a fire involving a classic vehicle and these same incidents with a gas-powered vehicle.

Kinetic issues

A fire takes from minutes to tens of minutes to develop. This enables an analysis of the progressive impact of the fire and safety measures on users (see 2.4). The order of magnitude of the kinetics of VCE and tank ruptures is up to the second, so very little can be expected from such analysis. This raises the question of the added value of such an analysis in case of VCE or tank ruptures, as these dangerous incidents are already assessed in a generic way (see 3.2).

To address this issue, VCE and tank ruptures were handled differently. Indeed, even if their kinetics have nearly the same order of magnitude, their occurrence time is significantly different. A VCE is likely to happen from few seconds to one or two minutes after the collision, whereas a tank rupture is likely to happen from 8 to 20 minutes after a collision [3].

The added value of a detailed analysis for a VCE

When a VCE occurs, nearly all the users will still be in their vehicle when impacted by the effects, maybe in a vehicle that is still running. This is very different from the fire scenario in which, unless in rare cases, most users affected by the fire would be outside their vehicles trying to evacuate. For a fire it makes sense to perform the analysis based on the space-time graphic described in chapter 2.4. However, such an analysis is obviously not relevant if all

⁴ proportion of the NEC energy in the car population

users are in their vehicle when impacted by an explosion. Nevertheless, it could be interesting to analyse the actual location of the vehicles in the significant lethal area of the VCE when it occurs and the consequences for their passengers. In this analysis, vehicles already stopped and vehicles still running have to be distinguished, as the distance between stopped vehicles is far lower than the distance between vehicles still running. The generic severity assessment of VCE (see 3.2) is based on the worst-case scenario in which the significant lethal effect area is full of vehicles stopped. This type of detailed analysis will therefore give a more accurate perspective of the possible results for a representative scenario.

The added value of a detailed analysis for a tank rupture

As reminded in 3, it was assumed in [3], that a tank rupture will only be triggered by a fire. As indicated above, this will happen between 8 to 20 minutes after the gas vehicle catches fire, which means that users would already have started the evacuation process because of the fire. It is therefore of interest to investigate the impact of the tank rupture on the self-evacuation process. To do so, the significant lethal effect area should be integrated into the space time graph presented in 2.4, as illustrated in Figure 3. Then, the specific impact of this area should be analysed, especially to assess if it increases the severity of the initial fire or not. The generic severity assessment of a tank rupture is based on the worst-case scenario in which all the passengers of the vehicles in the significant lethal effect area don't evacuate, so are all subjected to these effects. This type of detailed analysis will give a more accurate perspective of the possible results for a representative scenario.

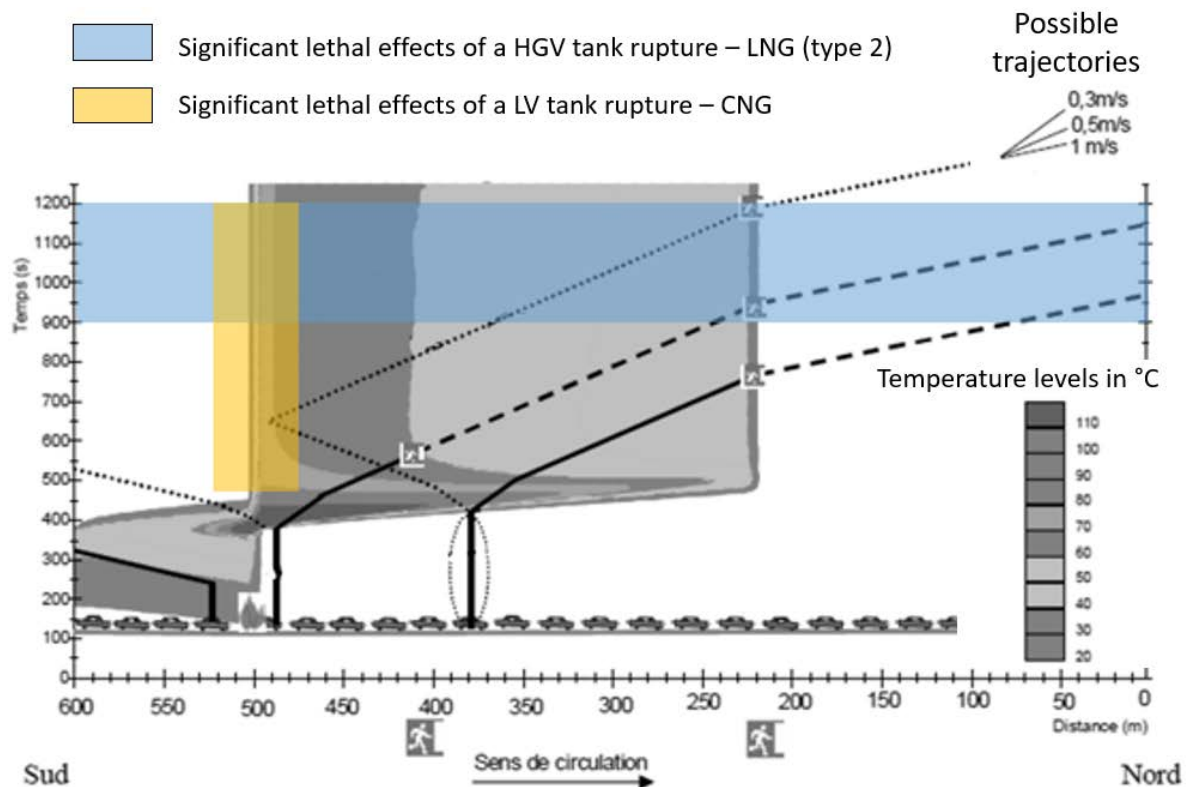


Figure 3: Example of gas dangerous incident integration in the space time graph of a scenario

In the analyses, one should be cautious to not overestimate the impact of the tank rupture. Indeed, in Figure 3, the significant lethal effects represented by the blue and yellow rectangles correspond to all possible time occurrences of the rupture. However, if this happens, it would happen only once. For instance, an LNG tank rupture could happen between 900s and 1200s. The users that may be subjected to lethal effects are the ones on the three trajectories that cross the blue rectangle, whereas if the tank rupture happens at 1150s, only one trajectory would be impacted, as the users on the two others will have evacuated.

4. SUMMARY AND CONCLUSION

Two main issues were identified and solved when adapting the French specific hazard investigation methodology to NEC.

The first concerned an apparent incompatibility of the frequencies and severities of gas dangerous incidents with the criticality matrix. Concerning frequencies, this issue was solved by stating that the difference in terms of uncertainties between classic dangerous incidents and gas ones are non-significant in terms of frequency ranking because this ranking is done in classes that each cover an order of magnitude. Concerning severity, n users subjected to significant lethal effects⁵ means that at best there are seriously injured users and at worst n deaths. This makes it possible to rank gas dangerous incidents in one or more classic severity classes that are based on injuries and deaths.

The second issue involved taking into account the specific kinetics of gas dangerous incidents in the detailed scenario analysis. For a VCE, that could occur very quickly after a collision, the detailed analysis should consist in studying the location of the vehicles in relation to the gas-powered vehicle, taking into account that certain vehicles would have stopped and others would still be running. For a tank rupture, that would occur a certain time after a fire, the significant lethal effects area of this gas incident will be integrated into the space-time graph used to analyse the fire. The detailed analysis of the impact of the tank rupture on users should then be performed and take into account their self-evacuation.

Moreover, the quantitative results from the CETU-INNERIS study (see [3]) offered the opportunity of adding a somewhat systemic approach to the scenario-based approach of the specific hazard investigation in sense of [1].

These main adaptations now need to be consolidated and backed up by a document that will clearly explain how the steps of the methodology have to be adapted.

5. REFERENCES

- [1] “Risk analysis for road tunnels”, PIARC technical committee C3.3 Road tunnel operation, 2008
- [2] « Fascicule 4 des Guides des dossiers de sécurité des tunnels routiers », CETU publication, 2003
- [3] Willmann, C, Truchot B, “New energy carriers and additional risks for user’s safety in tunnels”, ISTSS 2020 Munich
- [4] “Pannes, accidents et incendies en tunnel routier, éléments statistique”, reference document, CETU publication, February 2022, 25 pages,
- [5] ISO 13571, « Life-threatening components of fire – Guidelines for the estimation of time available for escape using fire data », 2012.
- [6] Arrêté du 29 septembre 2005 relatif à l'évaluation et à la prise en compte de la probabilité d'occurrence, de la cinétique, de l'intensité des effets et de la gravité des conséquences des accidents potentiels dans les études de dangers des installations classées soumises à autorisation.
NOR: DEVP0540371A - Version consolidée au 08 décembre 2017, 2005

⁵ meaning that there is a non-negligible probability that they will die but their death is not certain

INNOVATIVE APPROACH TO IMPROVE THE SAFETY OF TUNNELS AND TUNNEL CONTROL CENTRES

¹Harald Kammerer, ²Anne Lehan, ¹Bernhard Klampfer

¹ILF Consulting Engineers Austria GmbH, AT

² Federal Highway Research Institute, DE

DOI 10.3217/978-3-85125-996-4-33 (CC BY-NC 4.0)

This CC license does not apply to third party material and content noted otherwise.

ABSTRACT

Developments in the field of digitalization of the road and its infrastructure are strongly aimed at connected and automated driving. The collection of vehicle mobility data and its use for traffic monitoring and control can make a significant contribution to preventive event detection and the early initiation of protective measures in tunnels. By using real-time risk assessment in tunnels, it is possible to intervene in a controlling manner before the event occurs and thus mitigate or even completely avert negative effects. The potentials arising from mobility data are faced with major challenges, e.g. how to check the integrity of these large volumes of data, and how to select, merge, analyse and evaluate them systematically. Here, the application of Artificial Intelligence is considered as a very promising method. With that in mind, the research project KITT investigated for the first time the possibility of carrying out a risk assessment in tunnels in real time by using weak AI. Furthermore, it was investigated which additional vehicle data from C-ITS could be available in the future in tunnels. It is expected that their targeted use will contribute to a significant increase in tunnel safety and to maintain the availability of tunnels.

Keywords: tunnel safety, real-time risk assessment, artificial intelligence, C-ITS

1. INTRODUCTION

Tunnel control centres play a crucial role in ensuring the availability of the road network. In normal operation, they monitor and control the traffic in tunnels; thus ensure safe and efficient traffic flow. In the event of an incident or emergency, tunnel operators initiate measures to protect road users and the structure as well as support the emergency and rescue services in a coordinating manner. Dealing with incidents in tunnels requires special attention because, unlike on the open road, road users are in a structure that restricts smoke-propagation as well as rescue options. Therefore, events in tunnels have a serious impact on user safety compared to the open route and cause damage to the structure and tunnel equipment. The refurbishment usually leads to long traffic restrictions and often causes considerable additional travel times due to the use of low-performance alternative routes. Therefore, strategies and technical solutions to avoid and mitigate the effects of these events are important for maintaining the availability and safety of tunnels and tunnel control centres.

As a consequence of the big tunnel fires in the Montblanc, Tauern and Gotthard tunnel around 2000 extensive regulations and guidelines have been implemented on European and national level. However, as a result of the introduced minimum safety requirements relevant for road tunnels [1] and the increasing traffic volume, the implementation as well as the complexity of tunnel monitoring and tunnel control systems are steadily increasing. In order to counter this complexity, there has been a trend in recent years for operators to centralize tunnel monitoring and control. Due to the increase in information and communication technologies (ICT), the

number of digital points of attack is growing and with it the challenge of ensuring operational safety and the resulting safety of road users.

Nevertheless, digitization harbours great potential for significantly improving tunnel safety and availability. Developments in the field of digitization of the road and its infrastructure are strongly aimed at connected and automated driving. The field of Mobility 4.0 opens up a new possibility: the use of the traffic collective as a fully digitized mobility, information and communication platform. This technology, known as Cooperative Intelligent Transport Systems (C-ITS) is to be regarded as an extension of driving assistance systems. In future, it will make additional information available to infrastructure operators and road users to assess the current traffic or safety situation in the tunnel [2].

On the other side, the potentials arising from the additional information from C-ITS are faced with major challenges, e.g. how to check the integrity of these large volumes of data, and how to select, merge, analyse and evaluate them systematically. Moreover, the additional information should not lead to a further increase in the workload of the operating personnel in tunnel control centres. If, in the medium term, additional data from C-ITS should be used to improve tunnel safety, concepts must be developed to use them in an appropriate manner. The use of (weak) Artificial Intelligence (AI) offers a promising approach. Potentially it can be used to support operators in assessing the overall situation and making decisions in the event of an incident, as well as in predicting exceptionally dangerous situations. With that in mind, the research project KITT (“Artificial Intelligence to Improve the Safety of Tunnels and Tunnel Control Centres”) is investigating for the first time the possibility of utilizing AI to reduce reaction times in event detection and management, mitigate events or prevent them entirely by proactive implementation of real-time safety measures, provide emergency services and tunnel users with targeted information and secure the interfaces of C2I and the communication in the entire network by means of anomaly detection. The main objective is to further increase tunnel safety and to maintain the availability of tunnels. This paper will present the final findings of the KITT project.

2. UTILIZATION OF NEW C-ITS DATA

C-ITS allows to exchange information continuously between vehicles and the road infrastructure. Various hardware components are required to enable a wireless communication between individual vehicles and traffic infrastructure. Triggering a message in a vehicle, various kinds of safety equipment, often standard in modern cars, are necessary. This might be rain and light sensors, ESP (Electronic Stability Program) or ABS (Anti-lock Brake System), to name just a few of them. The actual communication then happens via the OBU (On Board Unit). This unit enables the vehicle to communicate with its surrounding environment.

The central elements of C-ITS on the infrastructure are the Road Side Units (RSU), receiving information from the vehicles and transmitting information to the vehicles. Thus, the RSU serves as information transfer point between control centres, traffic infrastructure and vehicles. The networked communication usually takes place via WLAN, in order to establish short-term connections between vehicles and the infrastructure.

In order to enable an efficient data flow and data processing standardization of message formats and interfaces is crucial. The European Telecommunications Standards Institute (ETSI) issues technical standards in the field of ICT. It defines in detail the format of C-ITS-messages. There is a rough classification of message types which provide information continuously or just event-based. In this context, the Cooperative Awareness Messages (CAM) and Decentralised Environmental Notification Messages (DENM) formats used to

transmit information are considered particularly relevant in the context of tunnel safety. CAMs contain static and dynamic information on the vehicle status, such as position, direction, speed, vehicle type (car, truck, etc.), propulsion system (battery, gas, etc.), etc. and are transmitted continuously, approx. every second. DENMs are notifications of road users or infrastructure systems sent only in case of safety-critical events with specific event information. Corresponding messages can be e.g. accident type, emergency braking, traffic jam, road works or tunnel closure. Almost all events can be indicated according to the requirements defined in the corresponding standards, except of fire. However, a direct coupling with ambient temperatures of the vehicle can be optionally sent in a DENM, for instance in case of a vehicle breakdown. The available message types are listed in the corresponding ETSI standards for CAM [3] and DENM [4].

At this point, a distinction between mandatory and optional information has to be made. Mandatory information are basic sets which must be made available in accordance with the ETSI standard. They allow a prompt implementation in tunnel operation, as all C-ITS equipped vehicles transmit this data. Nevertheless, the rapidly advancing technologies in the field of digitization with regard to connected and automated driving call for considering not yet mandatory information at an early stage. Furthermore, detailed definitions already exist in the standards, so that applications already can be built on it.

The collection of vehicle mobility data and its use for traffic monitoring and control can make a significant contribution to preventive event detection and the early initiation of protective measures by tunnel control centres. In contrast to conventional detection systems, which just react to effects of incidents, C-ITS technology allows detecting its causes directly [5]. Furthermore, the additional information source can be merged with other conventional sensor data, i.e. to check plausibility and reduce false alarms respectively. Moreover, the dissemination of additional information to other involved actors, such as emergency services, but also road users, was assessed as having great potential.

3. THE ROLE OF ARTIFICIAL INTELLIGENCE

Processes from the field of Artificial Intelligence (AI) have been the subject of research for many years. Artificial intelligence is understood to be the constructed replica of intelligence that is orientated on the intelligent abilities of humans. In this replication of intelligence, two types of AI have to be distinguished: weak and strong AI.

The weak Artificial Intelligence has no creativity and no explicit ability to learn independently. Its learning skills are mostly reduced to training recognition patterns or comparing and searching through large amounts of data. It can be used to deal with clear defined tasks with a set of predefined methodologies in order to solve more complex but recurring and well-specified problems. The special advantages of weak AI lies in the automation and controlling of processes, but also in speech recognition and processing. Popular examples are text and image recognition, speech recognition, translation of texts, navigation systems, etc. Digital assistance systems such as Alexa, Siri and Google Assistant also belong to this category. The most significant successes have been celebrated with methods based on Machine Learning, which is an approach to achieve Artificial Intelligence by learning from experience in order to find patterns in a range of data.

The second type is the strong Artificial Intelligence. However, the realization of a strong AI in practice is not yet within reach. A strong AI can independently recognize and define tasks and autonomously develop and build up knowledge of the corresponding application domain. It examines and analyses problems in order to find an adequate solution – which can also be new or creative.

In KITT the weak AI was developed to support in the following tasks: First, the AI should improve the detection of (potential) critical traffic situations (e.g. slowly driving or stopping vehicles, dangerous driving, congestion, etc.) at an early stage. The improved knowledge about these events can be used to warn the tunnel operators or to adapt the results of the real-time risk assessment by varying the probability of events. Moreover, in this step the AI was used to cope with the big amount of data transmitted by vehicles via C-ITS technology. In particular the continuously transmitted CAMs generate a flood of information that cannot be processed meaningfully and in a reasonable time without machine-supported procedures.

In addition, a major advantage can be seen in sensor fusion, i.e. to meaningfully merge the information from innovative C-ITS with conventional information from tunnel sensors and check its plausibility. On the one hand, a benefit can be expected due to the increased information density. On the other hand, it can be assumed that false alarms can be reduced by plausibility checks from different systems. Overall, this is seen as increasing the efficiency of traffic monitoring and control. However, this step was not (yet) implemented within the project.

Furthermore, AI methods were used to detect security-relevant events (tunnel security and security of the IT systems), i.e. anomalies, at an early stage in time series of sensor and log data.

Finally, a concept for on-the-job learning was developed in KITT. In the future, the experience of operators can be used to continuously improve the performance of the AI modules by learning from the reactions of the operators. However, the improvement of AI components through further learning during operation is a major challenge, especially in safety-relevant application scenarios. It must be ensured that further learning does not lead to a deterioration in the overall system and thus to critical situations.

4. REAL-TIME RISK ASSESSMENT

The main objective of KITT is the improvement of safety of road users. In general, this is achieved through an adequate protection against collisions and fires as well as the optimised handling of self-rescue and emergency response measures. In KITT, however, innovative tools like C-ITS and AI were used to extend common risk assessment methods and investigate the possibility of carrying out a risk assessment of the overall safety situation in road tunnels in real-time and implement fast mitigation or protection measures.

Currently, quantitative risk assessment studies are based on static tunnel parameters (e.g. tunnel length, gradient, cross section dimensions, etc.) as well as on average values of dynamic parameters (e.g. for traffic volume, truck share, driving speed, congestion hours, vehicle occupancy, etc.), leading to annual average risk values. Currently, these risk values are used for example to design the required tunnel equipment, like the ventilation system, or to define consistent operational measures, like the maximum speed limit.

In a real-time risk analysis dynamic data (real-time data) will be used in addition to standard values, leading to a better understanding of the current safety situation in the tunnel. This real-time data originates on the one hand from C-ITS data transmitted from vehicles, on the other hand from existing tunnel sensor systems (see Table 1). This allows for a real-time assessment of safety in road tunnels and an intervention in a controlling manner before the event occurs and thus mitigate or even completely avert negative effects.

Table 1: Overview of different input parameters for the real-time risk analysis and their sources

	Static tunnel parameter	Tunnel sensor systems	C-ITS	Processed by AI
Structural tunnel data	X			
Traffic data		X	X	X
Vehicle data			X	X
Environmental data		X	X	X
Event information		X	X	X
Tunnel equipment status		X		
Incident probabilities	X		X	X
...

For the real-time risk analysis existing quantitative risk assessment tools are used and expanded to include additional safety-related information and functionalities (see Figure 1). Both, in Austria [6] and Germany [7] [8] sufficient flexible methodologies for risk assessment are available for this purpose.

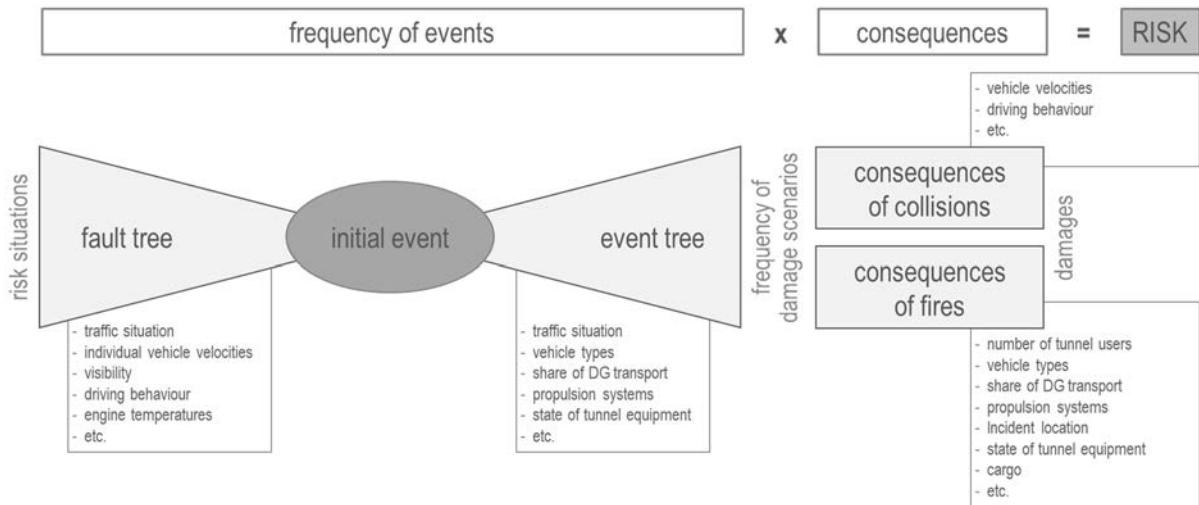


Figure 1: Major elements of a risk analysis extended by real-time information

In the following chapters the process is explained in detail including the potential where C-ITS data can be implemented and where AI can be of support.

4.1. Fault tree analysis to estimate the probability of initial events

When assessing safety in road tunnels using quantitative risk analysis tools, the safety assessment is based on triggering initial events: vehicle breakdowns, collisions, fires. The probabilities of initial events are usually determined using basic statistical data. In the real-time risk analysis the basic probabilities are continuously determined based on the current traffic situation and vehicle data.

A similar approach has been realized in the research project ESIMAS [9]. In the course of this, numerous fault trees were developed illustrating which initial events can be deduced from risk situations. In KITT, the ESIMAS-concept was expanded by data derived from C-ITS communication. Such data was treated as an additional sensor system included in the fault trees. In addition, the AI can enable the early detection of risk situations and thus provide real-time probabilities for the initial events required in the risk analysis. This allows to detect additional causes of events and to recognize initial events or risk situations better and faster.

4.2. Event tree analysis to estimate the frequency of incident scenarios

In the event tree analysis, the frequency of a series of predefined damage scenarios is estimated. Starting from an initial event (for which the frequency is known) various possible chains of events leading to different damage scenarios are developed in several steps (branches of the event tree). Possible branching points are, on the one hand, failure probabilities of tunnel safety equipment and, on the other hand, traffic parameters (e.g. traffic situation), share of vehicle types (e.g. cars, trucks, buses), existing vehicle propulsion systems, share of dangerous goods transport, etc. By quantifying the event tree (absolute probability of initial event and relative probabilities of different branches), the frequency of each individual consequence scenario can be estimated.

4.3. Consequence analysis to estimate the consequences of collisions and fires

In the consequence analysis the effects of the individual damage scenarios are estimated. The basis for the consequence analysis for tunnel collisions is provided by statistical data of tunnel incidents. In many countries statistical values for general tunnel types or individual tunnels are existing. Real-time traffic data can be used to dynamically adapt the standard values based on current traffic data, like vehicle velocities or driving behaviour.

The consequence analysis for tunnel fires is determined by using complex simulation models for fire development, smoke propagation and evacuation behaviour. Thereby, the impairment of tunnel users during evacuation is determined. The fire model implemented in FDS allows for a realistic reproduction of specific energy and smoke releases and determine the effects of a fire by calculating the smoke distribution, the visibility, the CO-concentrations, the temperature and the longitudinal flow velocities in the tunnel over time. Real-time data, like existing vehicle types, the share of Dangerous Goods transport vehicles, the existing propulsion systems or the incident location were used to influence the smoke-propagation results. Due to the complexity and the computational cost of these three-dimensional simulations it was necessary to pre-calculate a representative set of damage scenarios, which are used during the real-time process.

The results of the smoke-propagation simulations were combined with an evacuation simulation. Thereby, the accumulated effect of the noxious substances and the visibility were determined for each time step, resulting in survival rates for each tunnel user. With that, parameters like the number and position of tunnel users, the evacuation time, the walking speeds or the escape route lengths can be assessed. Real-time data like vehicle position, traffic volume, bus share or vehicle occupancy can be used to estimate the number and position of people in the tunnel and influence the results of the evacuation simulation.

4.4. Risk evaluation and visualisation

The risk in the tunnel is the combination of the estimated consequence and frequency of each individual damage scenario. In the risk assessment the collective risk of all tunnel users is estimated, represented by the statistical number of fatalities in the tunnel per year. The real-time risk is evaluated by using a relative approach: The real-time risk value of the tunnel is

compared to the risk value of an idealised reference tunnel exactly fulfilling the relevant guidelines and standards. If the risk of the assessed tunnel is below or equal to the risk of the reference tunnel, the tunnel is considered to be sufficiently safe. If the risk of the assessed tunnel exceeds the risk of the reference tunnel, additional risk-mitigation measures are required.

The real-time risk and appropriate risk-mitigation measures are visualised to the tunnel operator on a specific platform. A similar graphical user interface has been realized in the research project ESIMAS [9] and was further developed in KITT.

5. LEGAL AND ETHICAL ASPECTS

The current legal situation with regard to the above-mentioned range of topics is already very extensive. The equipment and operation of road tunnels are covered in Austria [10] and Germany [11] by special safety regulations, which also implement European requirements. The Austrian Road Tunnel Safety Act [12] also contains specifications for tunnel surveillance using video surveillance, and therein already specifications for data minimization. In the area of cyber and information security the extensive European requirements (NIS Directive) have also been implemented nationally. In the area of data protection law and privacy, the legal framework is largely specified by the European legal framework (especially GDPR) and is also specified and implemented in the national DSG (Austria) and BDSG (Germany).

However, due to the technical development in the field of automation and networking in traffic an evaluation and possibly an adaptation of the current legal situation may be required. C-ITS provides for an extensive data exchange between vehicles, but also between vehicles and infrastructure. The collection and aggregation of a large amount of individual data, but also the additional communication channel that is opened up as a result, which can result in new security gaps, require not only technical innovation but also a legal framework that is dynamic on the one hand, in order to be able to take technical progress into account, and on the other hand, sufficiently specific to comply with fundamental rights and the rule of law and to ensure legal certainty.

A major objective of KITT was a review of all relevant legal as well as ethical aspects arising from new developments within this project. For that, two Universities from both, Austria and Germany, each specialised in privacy, liability law and legal informatics conducted extensive analyses in this area.

6. CONCLUSION AND OUTLOOK

At the time of the preparation of this paper, the project is almost finished and a final demonstration of the KITT modules in a German road tunnel is planned in the near future. At the current stage of the project, it is clear that this project is to be designed with great perspective, but the relevance requires this early step due to the rapidly advancing digitization in the area of connected and automated driving. The requirements from the point of view of tunnel safety must be formulated at an early stage, as they may well deviate from those of the open road. This addresses infrastructure operators for the development of the necessary technical infrastructure and integration into existing monitoring and event management concepts as well as the development of competences of system users and vehicle manufacturers who include safety aspects and the requirements derived from them in their design when providing information to the infrastructure. This opens up potentials that can contribute to improving road safety. For tunnel monitoring, concepts for targeted data fusion and plausibility checks can be expected to provide opportunities for better incident prevention.

For the interpretation of the large amounts of data, methods such as AI are needed that make them manageable. At the same time, it can be assumed that improvements in the case of incident management and explicitly for self-rescue can be achieved through the possibility of individualised responses.

7. ACKNOWLEDGEMENT

The project was funded by the German Federal Ministry of Education and Research (BMBF) within the framework of the call "Artificial Intelligence in Civil Security Research" and by the Austrian Federal Ministry of Agriculture, Regions and Tourism (BMLRT) within the framework of the funding programme for security research KIRAS and was handled by the VDI Technology Centre and the Austrian Research Promotion Agency (FFG). The project started on 01 April 2021 and will end on 31 December 2023.

8. REFERENCES

- [1] European Union, „*Directive 2004/54/EC of the European Parliament and of the Council on minimum safety requirements for tunnels in the trans-European road network*“, 29.04.2004
- [2] Lehan, A., „*Influence of digital transformation on the interaction between tunnel infrastructure and road user - opportunities and risks*“, „*Proceedings from the Ninth International Symposium on Tunnel Safety and Security*“, Munich, Germany, March 11-13, 2020, S. 13-22
- [3] ETSI TS 102 637-2: „*Intelligent Transport Systems (ITS); Vehicular Communications; Basic set of applications; Part 2: Specification of cooperative awareness Basic Service*“, v1.4.1, 2019
- [4] ETSI TS 102 637-3: „*Intelligent Transport Systems (ITS); Vehicular communications; Basic set of applications; Part 3: Specification of decentralized environmental notification basic service*“, v1.3.1, 2019
- [5] Mayer, G., Badocha, C., Norkauer, A., „*Potentials of Integrating C2X Communication into Tunnel Operations Control Technology*“, Tunnel Safety and Ventilation Conference, Graz, 2018.
- [6] Österreichische Forschungsgesellschaft Straße-Schiene-Verkehr, „*RVS 09.03.11 Tunnel-Risiko-Modell (TuRisMo)*“, 2015.
- [7] Bundesanstalt für Straßenwesen, „*Bewertung der Sicherheit von Straßentunneln (Heft B66)*“, 2009.
- [8] Bundesanstalt für Straßenwesen, „*Bewertung der Sicherheit von Straßentunneln, Überprüfung der Annahmen und Parameter für Risikoanalysen (Heft B138)*“, 2022.
- [9] ESIMAS consortium, „*Einsatz eines Echtzeit-Sicherheitsmanagement-Systems in Tunnelleitzentralen – Einsatzmöglichkeiten, Systembestandteile und Integration*“, Bundesanstalt für Straßenwesen, Bergisch Gladbach, Germany, December 2015
- [10] Österreichische Forschungsgesellschaft Straße-Schiene-Verkehr, RVS 09 Tunnel Guidelines.
- [11] Forschungsgesellschaft für Straßen- und Verkehrswesen – Arbeitsgruppe Verkehrsführung und Verkehrssicherheit, „*Richtlinien für die Ausstattung und den Betrieb von Straßentunneln (RABT)*“, 2006.
- [12] Austrian Straßentunnel Sicherheitsgesetz (STSG), 14.2.2011.

CFD-ASSISTED FLOW RATE MEASUREMENTS IN VENTILATION DUCTS OF LONG ROAD TUNNELS

¹Diego Angeli, ²Paolo Levoni, ¹Elisabetta Salerno, ³Gioivanni Sebastiano Barozzi,

⁴Paolo Verraz, ⁴Cedric Petitcolin

¹DISMI – University of Modena and Reggio Emilia, IT

²mimesis s.r.l., Modena, IT

³DIEF – University of Modena and Reggio Emilia, IT

⁴TMB-GEIE, Courmayeur (AO), Italy and Chamonix, FR

DOI 10.3217/978-3-85125-996-4-34 (CC BY-NC 4.0)

This CC license does not apply to third party material and content noted otherwise.

ABSTRACT

Large-size air ducts with irregular cross section, such as the ventilation channels of road tunnels, offer formidable difficulties in the measurement of the flow rate. Despite a large bulk of experiences, the measurement techniques developed so far are not completely satisfactory in terms of accuracy or repeatability. Moreover, technical standards only consider very simple cross-section shapes, and prescribe the adoption of a prohibitive amount of measurement points. This motivated the development of an alternative technique for the reconstruction of the air flow rate, where the signals from a custom-built, multi-point measurement rig composed of 16 Pitot-Prandtl tubes are supported and integrated with Computational Fluid Dynamics (CFD) predictions. The technique was tested on two cross-sections of the extraction line in service at the Mont Blanc Tunnel (TMB). Preliminarily, CFD analyses were performed over a range of Reynolds numbers typical for that application. These were used to post-process the point-velocity data collected on field and to reconstruct the flow rate. Results of the testing campaign are presented here, along with a general description of the technique. Preliminary outcomes of the tests are encouraging and indicate that the present approach could be applicable to a larger variety of case studies.

Keywords: tunnel ventilation; smoke extraction; flow rate measurement; CFD; Pitot tubes.

1. INTRODUCTION

The development of an original technique for multi-point velocity rigs was imposed by the demand of measuring with sufficient accuracy the air flow rate in the extraction circuit of the Mont Blanc Tunnel (TMB) in case of fire. The TMB extraction line consists of a channel, with variable and irregular cross-section, running along the entire tunnel under the road deck, consisting of two branches, on the French and the Italian sides, respectively, joining near the half of tunnel length. Vitiated air is extracted from a series of on/off extraction vents, located each 100 m on the tunnel ceiling. In the case of an event, 7 extraction vents open, for a total length of 600 m centered on the fire, and the channel is depressurized by a couple of centrifugal fans at each end. The airflow extracted through the vents from the tunnel ceiling splits in two once in the channel, a certain percentage flowing towards the French station and the rest towards the Italian one (Fig. 1), depending on the atmospheric conditions and on the position of the event. The strategic importance of this safety line does not need to be stressed and for this reason TMB-GEIE, the concessionary binational company of the infrastructure, commits periodical checks of the extraction rate to specialized companies.

The problem of detecting the air flow rate in irregular ducts of large size dates to the XIX century, in the context of mine excavation safety rules [1]. In the case of large and irregular sections only techniques falling in the class of the “velocity-area methods” are practically

viable. These techniques can be classified as: (i) single-point methods, where the flow rate is retrieved from a single velocity signal to be multiplied by the section area; (ii) continuous traversing methods, where a single velocity probe is moved through the duct section, and velocity values are averaged to give the mean air-velocity; and, (iii) multi-point methods, where the duct area is subdivided into a number of sub-areas at the centers of each the air velocity is measured. The volumetric flow rate in the duct is built-up by summation of all the (velocity x area) contributions.

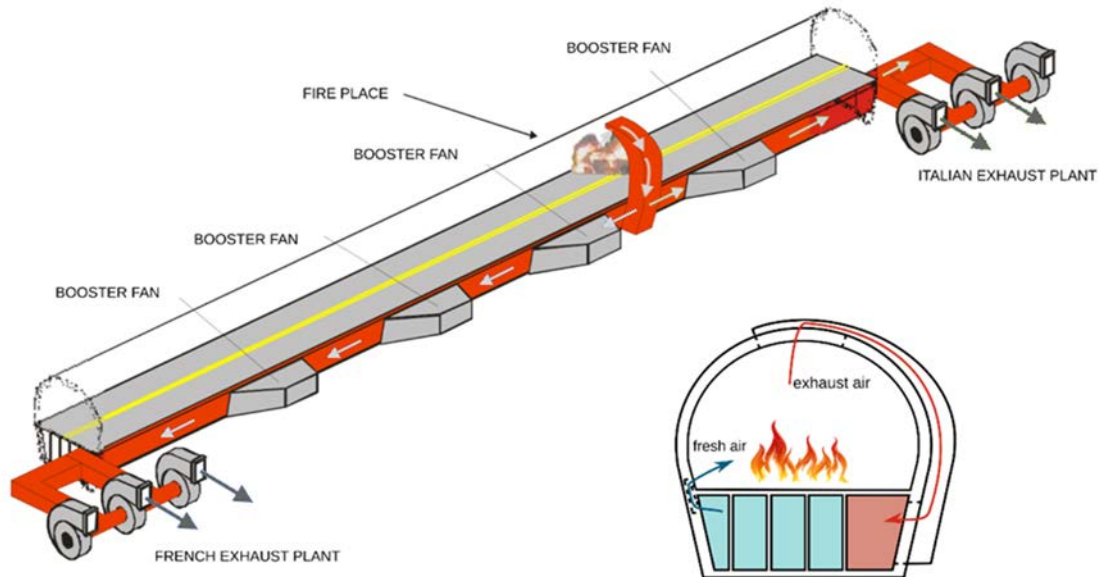


Figure 1: Schematic of the TMB extraction system (courtesy of TMB-GEIE) and typical cross-section of the tunnel and ventilation channels

In single-point measurements a correction factor must preliminarily be determined, to account for the non-uniform velocity distribution along the duct section [2]; such a factor may depend on the type of velocity probe, the presence of an operator, the data collection technique, but also depends on the total flow-rate, i.e. the Reynolds number, and, most of all, on the specific duct geometry. Continuous traverse methods are expected to be more accurate than static single-point measurements in the experimental reconstruction of the mean velocity in non-standard shape tunnels. Since the complete sweeping of a large section takes time, the method reliability decays if unsteady conditions affect the flow [3].

Multi-point methods are generally considered to be superior, in terms of accuracy and reliability, to single-point and continuous traverse methods. In this context, the problem arises of optimizing the number and the positions of the velocity probes over the duct section. Two schemes for determining the grid of locations where measurements should be taken have been credited for rectangular ducts in the context of HVAC systems. These are the Equal Area and Log-Tchebycheff distributions. In the latter case, the grid-points are unequally spaced with the external points close to the walls to account for the wall-friction effects, as opposite to the Equal area distribution, where the section is subdivided into equal square or rectangular sub-areas. The experimental comparison of the two methods carried out by Klaassen and House [4] however demonstrates that the two distributions are, in general, equally consistent.

On the other hand, no technical directions are available relative to the number of velocity sensors and their relative positioning on a section of irregular shape: ISO Standard n.7194 [5] only considers circular ducts; ISO Standard n.5802 [6] includes square, rectangular, annular, elliptical, oval, octagonal, and trapezoidal sections. The number of probes needed for an accurate estimate of the flow rate in a non-circular duct is in any case very high. For example,

for a rectangular section, a 49-point rake is prescribed over a properly distributed 7x7 grid [6]. It is therefore obvious that sections of irregular shape would demand clusters of 100 probes or more. In practical terms, numbers of velocity probes of that order imply the risk of blockages, high costs, and excessively long times of setting-up of the experiments, often incompatible with the operational constraints of a tunnel. For the above reasons, a limited number of measuring points has been used in all the cases considered in the literature [7-10].

Despite such a considerable number of experiences, the methods developed so far appear as not completely satisfactory, either in terms of accuracy or of repeatability. This motivated the development of an alternative technique of reconstruction of the air flow rate, where the signals from a multi-point measurement rig are post-processed by means of CFD predictions. In the case of concern here, the use of multi-point procedures was dictated not only by the need of accuracy and repeatability of the measurements, but also by the impossibility of accessing the ducts under operative conditions. To overcome the drawbacks of the classic velocity-area methods an accurate pre-analysis was carried out to verify the possibility of integrating the point-velocity data with numerical predictions by CFD. This gave rise to the design and realization of two 16-probe clusters. As detailed below, a large CFD-prediction data set was created and this was used to build-up the entire axial velocity profile over the section, based on the measured velocity values. In this way, using a relatively low number of sensors, it was possible to account for the complexity of the velocity distribution and to derive more reliable estimates of the flow rates. The technique was finally tested in the two branches of the extraction line of TMB, and results from one of the first testing campaign are presented here and discussed.

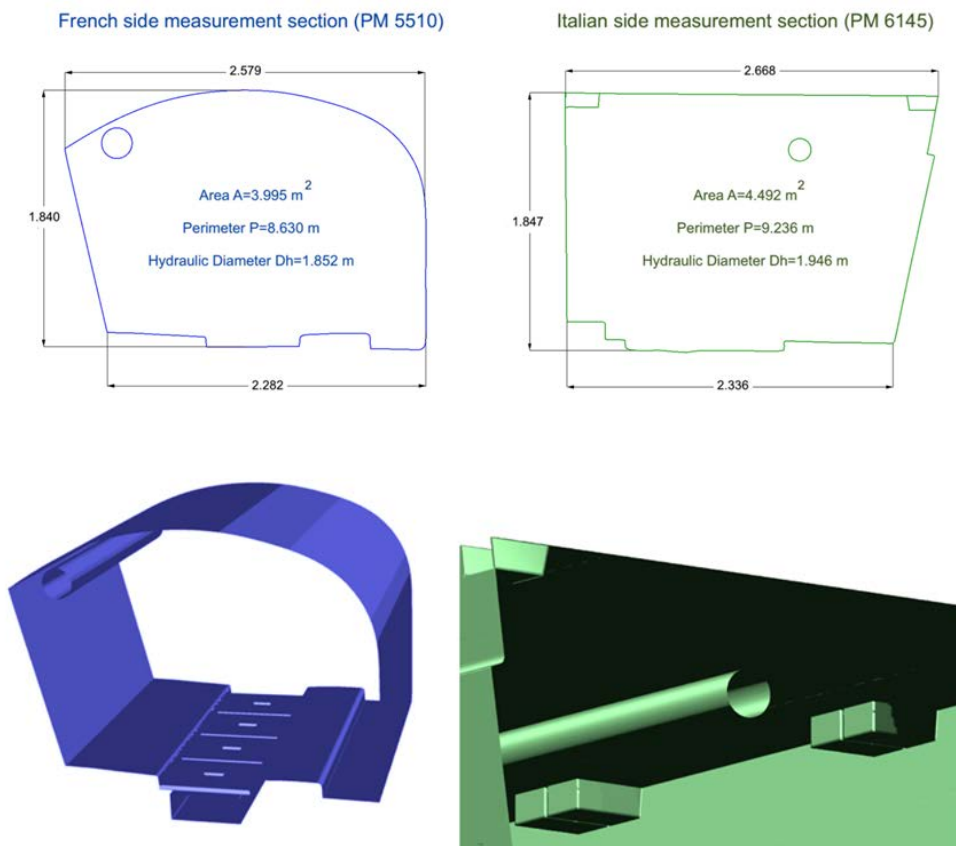


Figure 2: (above) measurement sections in the TMB extraction channel: French side (left) and Italian side (right); reconstruction based on laser scanner data; (below) details of the 3D model showing service pipes, drains and other structural elements.

2. CASE STUDY

In addition to practical issues due to measuring in such an infrastructure, the operative difficulties the task presents are formidable and demand specific solutions to be developed.

One first problem is given by the large size and the variable geometry of the dimensions of the duct section. Assuming an event at the mid-point of the tunnel, two sections were identified immediately outside of the extraction area where the channel geometry is sufficiently regular, with approximately constant cross section, and far away from any important upstream obstacle, to avoid possible wake effects.

The two sections, located at metric points PM5510 and PM6145 (considering as origin PM0 the French portal) are irregular, different in shape and size and result to be multi-connected due to the presence of a longitudinal drainage pipe, as represented in Fig. 2.

3. NUMERICAL ANALYSIS

The numerical activity relied upon the use of the CFD Finite Volume code OpenFOAM v7. The flow was assumed to be incompressible and steady state. The flow-field was assumed to be fully turbulent, and the RANS (Reynolds Averaged Navier-Stokes) approach enforced. Three alternative turbulence models were selected among the most popular and validated for this type of applications. In particular, the $k-\omega$ SST (Shear Stress Transport) model, the realizable $k-\varepsilon$ model, and the Reynolds Stress Model (RSM) were tested and compared.

Two series of preliminary simulations were carried out: the first on a simplified geometry but with similar flow structures (square section) to validate the numerical procedure and to derive general guidelines for grid convergence, the second on real sections (Fig. 3) with increasing level of detail for final assessment of the numerical procedure on the real case.

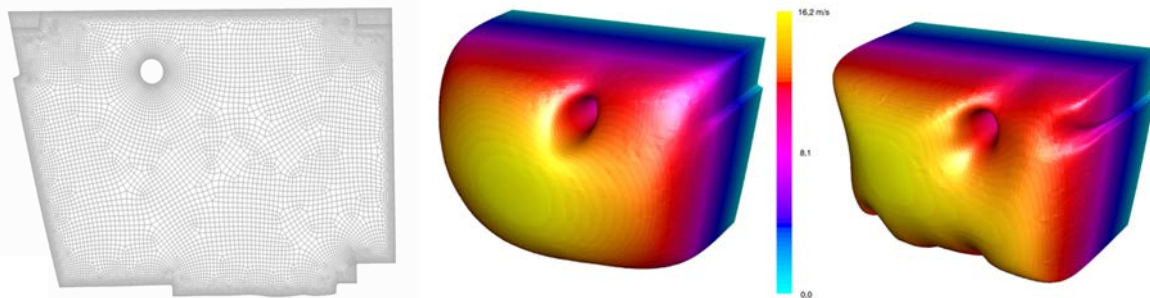


Figure 3: (left) final mesh adopted for the cross section of the Italian side (the French one is qualitatively similar); longitudinal velocity profile on the Italian measurement section with the $k-\omega$ (center) and RSM (right) models.

4. EXPERIMENTAL FACILITY AND DATA REDUCTION

4.1. Choice of the measurement points

Previous experiments had been carried out over the two sections of the extraction line described above. In those cases, an array of 10 Pitot-tubes was used, arranged on two parallel vertical rows. The volumetric flow-rate values were derived by the crude average of the local velocity signals times the section area. Based on CFD analyses, it was decided to increase to 16 the number of probes on each section, complementing the 10 original positions, that were conserved for the sake of comparison, with 6 additional probes located on a single horizontal row. The geometry of the two probe-arrays is shown in Fig. 4.

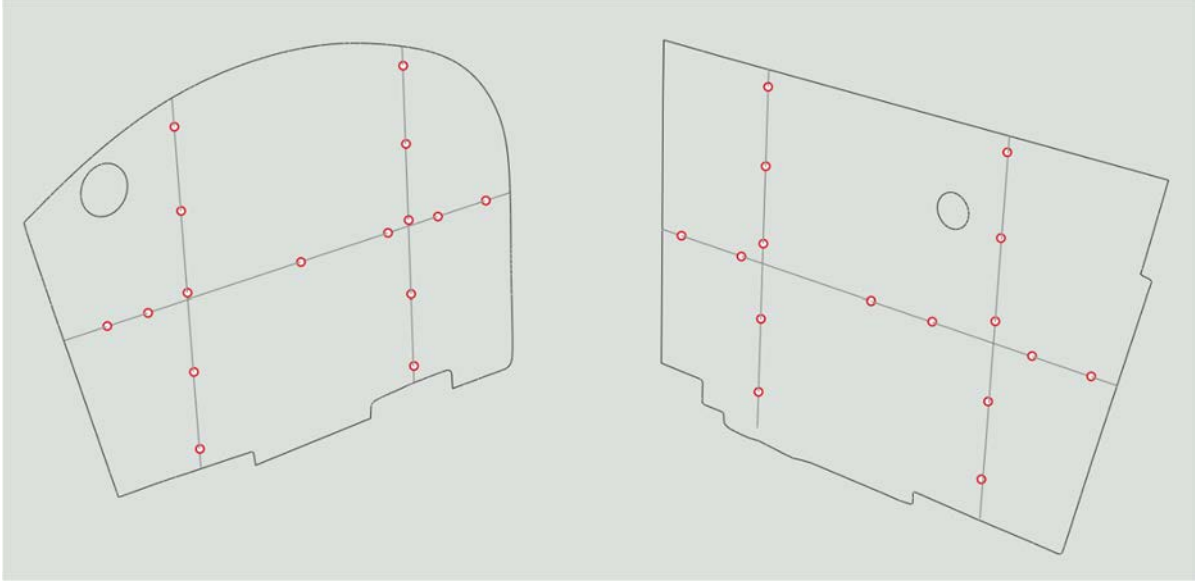


Figure 4: qualitative distribution of the measurement points on the French (left) and Italian (right) sections.

4.2. Experimental rig

8 mm NPL-type Pitot probes were adopted for velocity measurements in accordance with ISO3966, Annex A [5]. The design of the two arrays was directed to minimize as much as possible the aerodynamic influence of the rigs, while ensuring accurate and repeatable measurements. Extruded aluminum alloy hollow beams with low aerodynamic impact (NACA0009 profile) were adopted for the holding structures and the 32 pressure lines pass inside the beams, sort out at the foot of the vertical bars, and connect to the pressure scanner, positioned several meters downstream. Each pressure scanner is equipped with two series of 8 differential pressure transducers with different full-scale value (250 Pa was chosen for the central probes and 160 Pa for the peripheral probes, closer to walls) with an accuracy of $\pm 1.75\%$ of the full scale. The dynamic pressure data are complemented with the measurement of local temperature, absolute pressure, and relative humidity, needed for an accurate estimation of the local air density. The sampling frequency for all the measurements was set at 1 Hz. Some geometrical details of the probe and its connection to the support structure are shown in Fig. 5.

4.3. Data reduction

The database provided by the numerical experiments was used to correlate the axial velocity values, as measured at the 16 sampling points, with the mean velocity over the section area, and the total flow rate. The procedure is based on the following equation:

$$\bar{v} = \frac{\sum_{i=1}^N f_i(v_i)}{N} \quad (1)$$

Here, \bar{v} and N are the mean velocity and the number of the measuring points over the section ($N = 16$ for each of the two sections), and $f_i(v_i)$ is a function correlating \bar{v} to the local velocity value, v_i . The correlating functions are derived by the numerical predictions, and as expected, they change with the position of the sampling point and the mean-velocity value itself. The accurate estimate of the f_i - functions is a crucial point of the procedure. For example, Fig. 6 presents the 16 functions for the French section with reference to the RSM model. It is immediate to observe that, over the interval of interest for the experiments, all the local velocities correlate linearly with the mean values. Similar trends were obtained with all the three models for both sections.

For the i -th sensor the linear trend can be expressed as:

$$v_i = m_i \bar{v} + q_i \quad (2)$$

By dividing by \bar{v} one obtains

$$\frac{v_i}{\bar{v}} = m_i + \frac{q_i}{\bar{v}} \quad (3)$$



Figure 5: details of the Pitot-probes system (above) and general view (below) as installed on the French side.

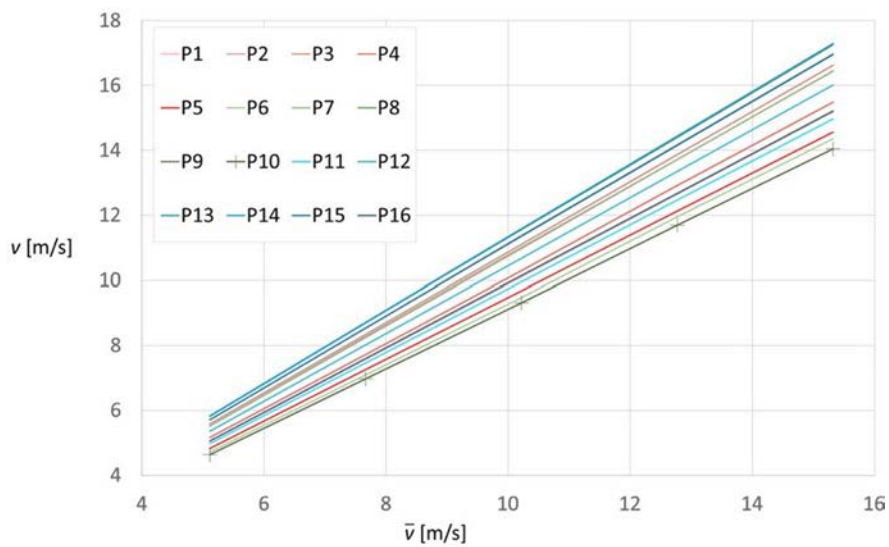


Figure 6: axial velocity vs. mean velocity at the 16 measurement points for the French section (CFD - RSM model).

It is convenient to recast eqn. (3) by introducing into it the Reynolds number, Re

$$Re = \frac{\rho \bar{v} D_h}{\mu} \quad (4)$$

Here, D_h is the hydraulic diameter of the section, and ρ and μ are the air density and viscosity under the actual operative conditions. It is useful to remind that the thermodynamic properties of air encountered in the experiments can differ substantially from the standard values employed in the numerical simulations. Eqn. (3) becomes:

$$\frac{v_i}{\bar{v}} = m_i + \frac{k_i}{Re} \quad ; \quad k_i = \frac{q_i \rho D_h}{\mu} \quad (5)$$

Solving back for \bar{v} we get the final form of the f_i - function to be inserted into eqn. (1):

$$\bar{v} = f_i(v_i) = \frac{v_i}{m_i} - \frac{k_i \mu}{m_i \rho D_h} \quad (6)$$

It is appropriate to point out that the \bar{v} - value estimate differs from one measuring point to the other, due to two main reasons: (i) the f_i 's are based on numerical predictions, and these can just approximate the real flow-fields; (ii) the local velocity data are affected by uncertainties inherent to the use of the Pitot-probes as well as to the positioning of the sensors and the accuracy of the transducing chain. The final value of the mean velocity, i.e. the one we assume to be the most reliable, is therefore the result of the averaging of the 16 independent estimates of \bar{v} , as from eqn. (1).

5. FIRST RESULTS

The technique described above was applied so far 6 times to reconstruct the extraction flow rate at TMB. Results of a testing campaign which took place on July 7th, 2023, are reported in Table 1, in terms of relative deviation with respect to a reference value of the reconstructed flow rate. In this case, the reconstruction using the CFD results obtained with the k- ω SST model is chosen as the reference, since it determined the lowest percentage standard deviation on the reconstructed flow rate among the three turbulence modelling approaches.

It can be observed that the three estimates are characterized by extremely low relative deviations. Obviously, the single reconstructed velocity is crucially dependent on the adopted turbulence model, and significant differences could arise between different models (see again Fig. 2); nevertheless, even using a moderate number of points, the reconstructed values already appear as insensitive of the adopted turbulence model. This corroborates the consistency of the present approach, especially if this is compared to a simple averaging procedure (as reported in Table 1). As a matter of fact, the mean value obtained by averaging is systematically higher than the reconstructed value, indicating the need for a weighting of the values on the different measurement points to account for points in the boundary layer or local anomalies due to the presence of elements like the service pipe in the two sections considered here. Furthermore, standard deviations of the CFD-assisted reconstructions do not substantially deviate from those of the simple averaging procedure, suggesting that the uncertainties linked to potential discrepancies between the numerical and experimental profiles are anyway restrained.

Table 1: results from a sample testing campaign

Model	Flow rate French side (% deviation from ref.)	Standard deviation French side	Flow rate Italian side (% deviation from ref.)	Standard deviation Italian side
k- ω SST (ref.)	-	10.93%	-	14.45%
realizable k- ϵ	0.10%	11.21%	0.06%	14.96%
RSM	0.00%	10.47%	1.10%	16.24%
mean value	3.55%	9.95%	2.84%	10.25%

6. CONCLUSION

A technique for the reconstruction of the air flow rate in large ducts of irregular size was developed and tested on two cross-sections of the vitiated air extraction channel of the Mont Blanc Tunnel. A custom-built, multi-point rig with 16 Pitot-Prandtl tubes provided velocity measurements which were subsequently processed using correlations derived from CFD. Preliminary results of the testing campaigns performed so far highlight the consistency of the technique and its potential adaptability to other duct geometries. Further analyses will entail a deeper analysis of the error propagation and a finer characterization of the experimental profiles in light of CFD results.

7. REFERENCES

- [1] Unwin ID 1998, “The Measurement of Air Flow in British Coal Mines: A Historical Review”, The Northern Negros State College of Science and Technology, Philippines.
- [2] Kohler JL and Thimons ED 1987, An analysis of air volume-flowrate determinations for mines, *Mining Science and Technology* 6, 17-29.
- [3] Jamróz P 2014, Effect of the continuous traverse trajectory and dynamic error of the vane anemometer on the accuracy of average velocity measurements at the cross-section of the mine heading – model-based testing, *Arch. Min. Sci.* 59(4), 1051–1060.
- [4] Klaassen CJ and House JM 2001, Equal area vs. Log-Tchebycheff, *HPAC Engineering* 2021, 31-35.
- [5] ISO 3966: 2020, Measurement of fluid flow in closed conduits - Velocity area methods using Pitot static tubes.
- [6] EN ISO 5802:2008, Industrial fans - Performance testing in situ.
- [7] Parra MT, Villafruela JM, Castro F and Méndez C 2006, Numerical and experimental analysis of different ventilation systems in deep mines, *Build. Environ.* 41, 87–93.
- [8] Król M, Król A, Koper P, Wrona P 2019, The influence of natural draught on the air flow in a tunnel with longitudinal ventilation, *Tunn. Undergr. Sp. Tech.* 85, 140–148.
- [9] Levoni P, Angeli D, Stalio E, Agnani E, Barozzi GS and Cipollone M, 2015, Fluid-dynamic characterization of the Mont Blanc tunnel by multi-point airflow measurements, *Tunn. Undergr. Sp. Tech.* 48, 110-122.
- [10] Levoni P, Angeli D, Cingi P, Barozzi GS and Cipollone M, 2021, An integrated approach for the analysis and modelling of road tunnel ventilation. Part I: Continuous measurement of the longitudinal airflow profile, *Transport. Eng.* 3, 100039.

JET FAN INSTALLATION FACTOR CORRELATIONS FOR CONVENTIONAL JET FANS AND MOJETS

¹Fathi Tarada, ¹Pier Bertacche, ²Luca Stantero

¹Mosen Ltd, GB

²Risk Design Engineering SRL, IT

DOI 10.3217/978-3-85125-996-4-35 (CC BY-NC 4.0)

This CC license does not apply to third party material and content noted otherwise.

ABSTRACT

This paper presents the results of nearly 1,000 CFD calculations undertaken with two jet fan diameters, two jet fan installations, two different surface roughness values, for a range of tunnel velocities, with various jet fan spacings, with varying clearances between the jet fan and the tunnel surface and with two types of jet fans (conventional and MoJet). The CFD calculations were undertaken with the ANSYS Fluent code and were validated by reference to the full-scale tunnel measurements reported by Tarada et al [5]. The calculations modelled a 2-lane road tunnel with hard shoulder - 9.6 m wide, 6 m high and 500 m long, along with its associated jet fans (including their rotating blades). Cell counts for each CFD simulation ranged from 20 to 35 million, using polyhedral and prism cells for maximum accuracy.

The results of our CFD calculations were correlated in the form of mathematical expressions, which account for each of the considered influencing parameters (jet fan diameter, type of installation, surface friction factor, tunnel velocity, jet fan spacing and clearance, and jet fan type). We report on the open provision of these correlations via web tools, to facilitate their use by designers and researchers in this field.

Keywords: Jet fan, thrust, installation factor, CFD, measurements, correlations

1. INTRODUCTION

Following PIARC [1], the jet fan installation factor η_i is used to calculate the in-tunnel value of thrust (T) using the following equation:

$$T = \eta_i \rho A_j v_j (v_j - v_t) \quad (\text{Equation 1})$$

where A_j is the cross section of the jet fan, v_j the average axial velocity of the discharge jet and v_t the velocity in the tunnel beyond the direct influence of the jetfan intake and discharge. There is an expectation that η_i should be below unity, although it is theoretically possible for values slightly above unity to be obtained (Meidinger [2] and Truckenbrodt [3]). Although Equation 1 was developed for conventional jet fans, the same formulation can be used for jet fans with shaped silencers (MoJets), with cross-sectional areas and axial velocities based on equivalent conventional jet fans. This on the basis that any thrust lost due to the reduction of jet velocity within the shaped discharge silencer would be recovered through an increase in the local static pressure (by reference to the Bernoulli equation).

As previously reported by Tarada and Bertacche [6], previous correlations for jet fan installation factors suffer from a range of limitations, including being based on low model-scale Reynolds numbers, the lack of discharge swirl in the physical tests and their applicability to only a single jet fan, rather than relating to multiple jet fans in a series. This study was undertaken to address these limitations, and to provide a more reliable set of jet fan installation factor correlations for designers.

2. CFD METHODOLOGY AND VERIFICATION

In order to estimate the jet fan installation factors for a variety of geometrical and tunnel flow conditions, we used the same CFD modelling approach as that employed by Tarada et al [5]. This comprised using ANSYS Fluent version 2022 R1 for models that incorporated both the jet fans (including the rotating blades) and the tunnel in a single CFD run. Turbulence effects were simulated using the $k-\omega$ shear stress transport model of Menter [4], in order to accurately capture aerodynamic separation and reattachment effects. The computational mesh comprised polyhedral cells refined with prism layers on all solid surfaces, with y^+ values less than 25 on blade surfaces, and less than 60 on the internal jet fan surfaces. Cell counts for each CFD simulation ranged from 20 to 35 million, with higher cell counts being required to resolve the aerodynamics around bellmouths for MoJet simulations. Tarada et al [5] reported that calculated bench thrust values were within 3% of measurements, and calculated in-tunnel thrust values were within 2% of measurements.

For each CFD run, three jet fans separated by a defined longitudinal spacing were simulated within the tunnel. In order to economise on mesh sizes and run times, the last jet fan (in the downstream direction) was set up as a “master” jet fan, while the other two were defined to be “slave” jet fans. The flow, pressure and turbulence profiles in the upstream and downstream mixing planes either side of the rotor were regularly copied from the master to the slave jet fans during the CFD runs. Within the master jet fan, a single rotating blade was modelled, with periodic boundary conditions set at the end faces of the rotating domain to simulate a full ring of blades. Steady-state calculations were undertaken. Jet fan installation factors were post-processed from the CFD results based on the procedure described in Tarada et al [5].

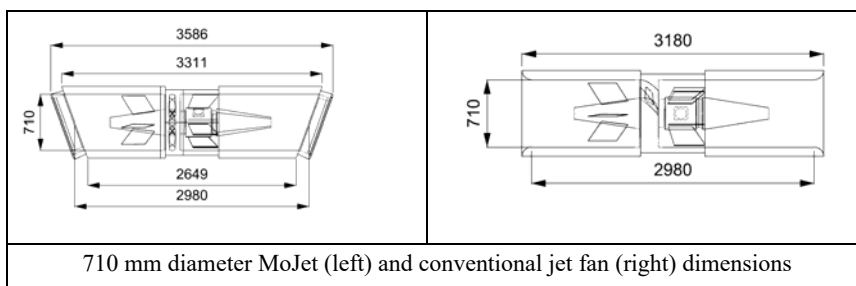
3. TUNNEL AND JET FAN GEOMETRIES

The tunnel and jet fan geometries considered in this study were the same as those reported by Tarada and Bertacche [6], and are briefly reproduced below for completeness. A description of the shape and function of MoJet silencers is provided by Tarada et al [7].

Two jet fan diameters were selected for the study: 1250 mm and 710 mm (Table 1). The range encompassed by these diameters corresponds to the majority of jet fan sizes currently installed in tunnels worldwide. The bench thrust values for the MoJet were approximately the same as those for conventional jet fans, when the vector sum of both the vertical and horizontal components of thrust are considered.

Table 1: Jet fans considered in this study

Jet fan internal diameter (mm)	Number of blades	Blade pitch angle	Bench thrust (N)
710	10	34.6°	782
1250	10	32°	1695



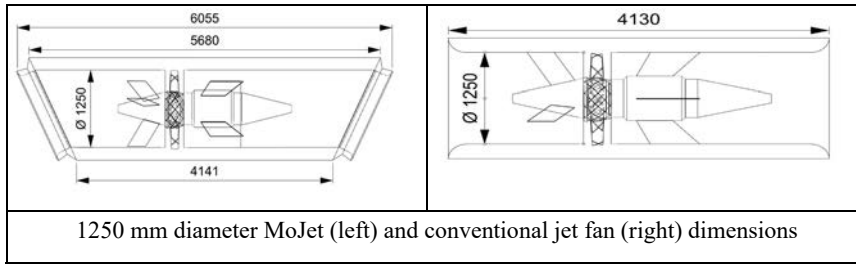


Figure 1: Jet fan dimension (all dimensions in mm)

A rectangular tunnel with 9 m width and 6.6 m height and which corresponds to 2-lane road tunnel with a hard shoulder. Fans were placed in the vicinity of a corner or under a soffit (Figure 2).

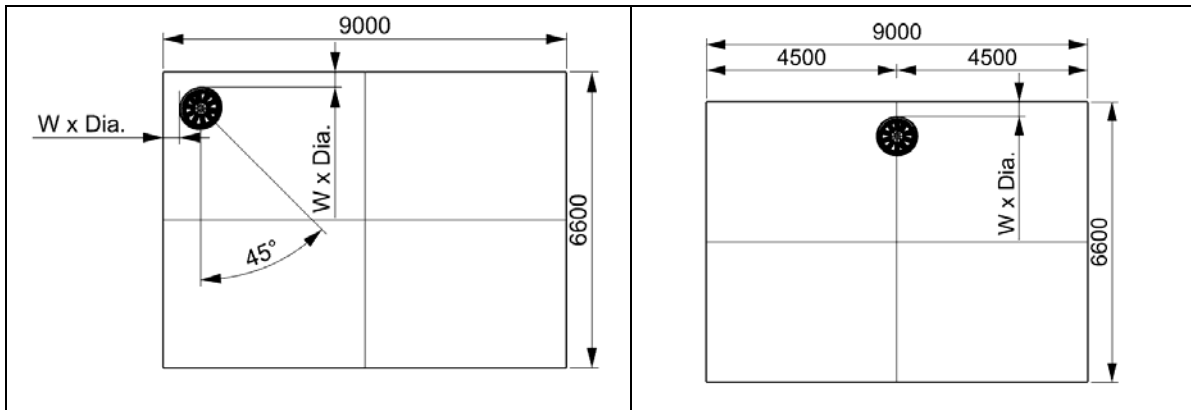


Figure 2: Tunnel cross-section, with a fan at a corner (left) and below the soffit (right) - all dimensions in mm

Three sets of clearances between the outer silencer and the wall (or soffit) were simulated, denoted by “POS 01” (only 50 mm clearance), “POS 03” (0.3×1250 mm fan diameter) and “POS 05” (0.5×1250 mm fan diameter). Table 2 summarises the clearances adopted in this study.

Table 2: Clearances employed between jet fans and tunnel

	“POS 01” clearance (mm)	“POS 03” clearance (mm)	“POS 05” clearance (mm)
710 mm fan	50	375	625
1250 mm fan	50	375	625

In order to model the potential aerodynamic interactions between the jet fans, three fans were modelled in each CFD run, with longitudinal spacings set at approximately 5, 10 and 15 tunnel hydraulic diameters (40 m, 80 m and 120m). Two sand-grain roughness heights were applied to the tunnel surfaces in our study: 8 mm which produces a Darcy friction factor of 0.02140, and 80 mm roughness height, which produces a Darcy friction factor of 0.02838. Tunnel air velocities between 1 to 6 m/s were simulated.

4. CFD RESULTS

A selection of results of our CFD analyses are presented below. These indicate the behaviour of the installation factor with the major variables considered in our study, as well as their predicted trends based upon our proposed correlations (which are presented in section 5). The symbols within the plots below indicate our CFD results, while the lines represent our

correlations. It can be seen that there is generally a close correspondence between the CFD results and the correlations.

We observed that the general trend is for the installation factors to reduce with increasing tunnel velocity (Figure 3), which is due to the stretching of the “friction patch” downstream of the jet fans, on the neighbouring tunnel surfaces. However, some recovery of the installation factor was observed for the highest velocities, particularly with the MoJet, due to more intensive mixing of the jet with the tunnel air.

As can be reasonably expected, increasing the clearance between the jet fans and the tunnel surfaces leads to improvements in the installation factor (Figure 4), although the trend is influenced by the jet fan diameter – smaller diameter conventional jet fans tend to have smaller installation factors. This is possibly due to the effects of the tunnel boundary layer and due to the higher discharge velocities associated with smaller tunnel jet fans driven by two-pole motors, which cause higher shear on the neighbouring tunnel surfaces.

Figure 5 demonstrates the “unloading effect” of the loss of thrust when jet fans are installed at short longitudinal spacing, as previously reported by Costeris [8]. In particular, Figure 5 shows that the conventional rule of designing conventional jet fans with ten hydraulic diameter spacing appears to deliver significantly lower jet fan installation factors than would be expected for a single jet fan. Although the mass flow through downstream jet fans is slightly increased through the ingestion of jets, a significant proportion of the upstream jets may be captured through such ingestion, leaving a smaller proportion of longitudinal momentum to exchange with the tunnel air. MoJets are less sensitive to jet fan spacing, due to the deflection of the jet away from the downstream fans.

Figure 6 shows a trend of reducing installation factors with increasing tunnel friction factors for conventional jet fans, due to the increased friction between the jet and the tunnel surfaces. MoJets are less sensitive to changes in tunnel friction factors.

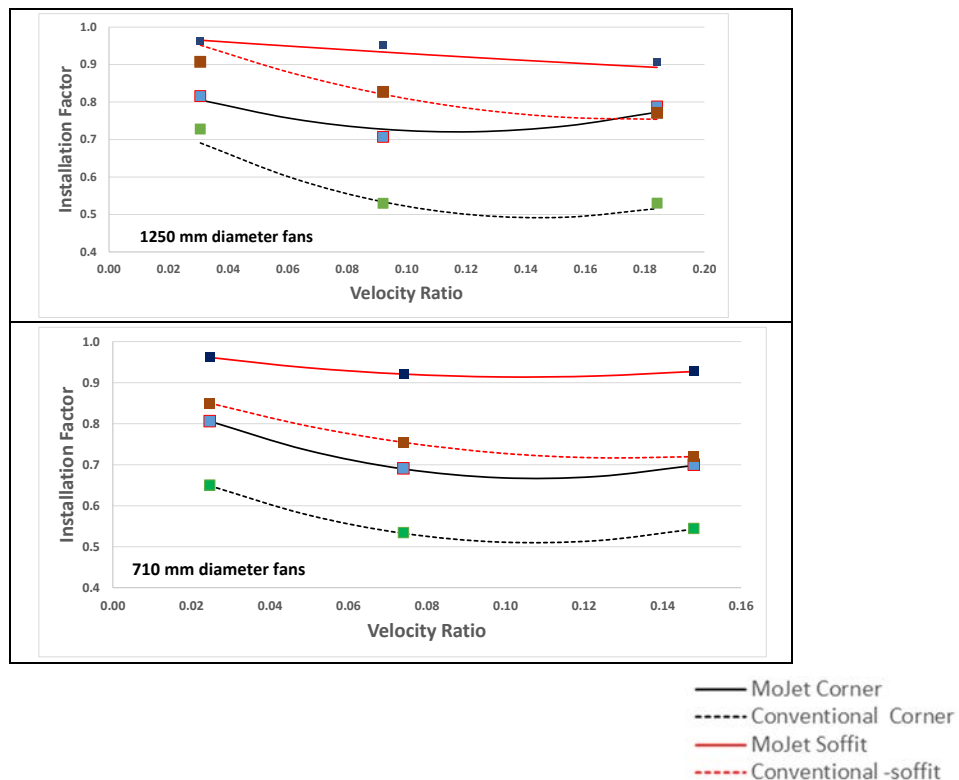


Figure 3: Variation of installation factor with velocity ratio for the 1250 mm fan (left) and the 710 mm fan (right), for 3 m/s tunnel air velocity and 8 mm tunnel surface sand-grain roughness

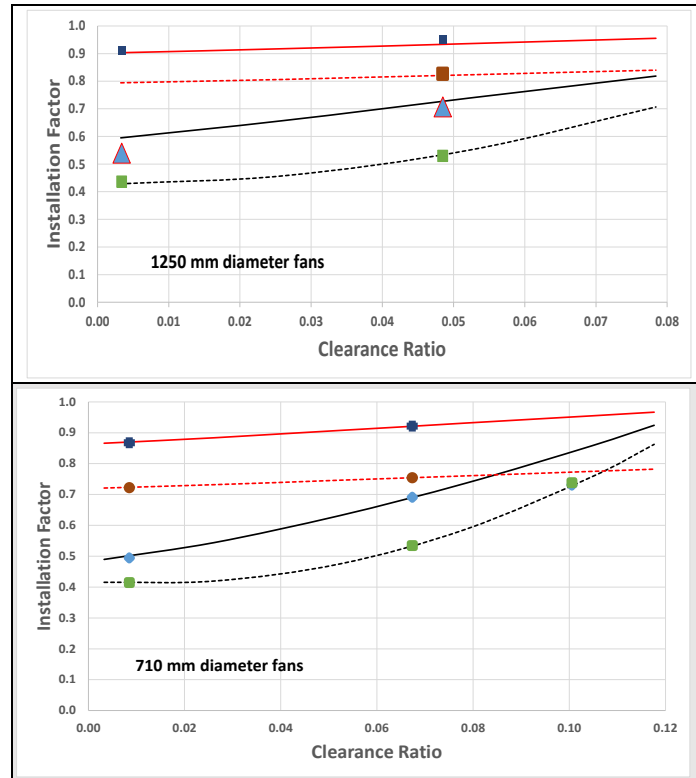


Figure 4: Variation of installation factor with clearance ratio for the 1250 mm fan (left) and the 710 mm fan (right), for 3 m/s tunnel air velocity and 8 mm tunnel surface sand-grain roughness

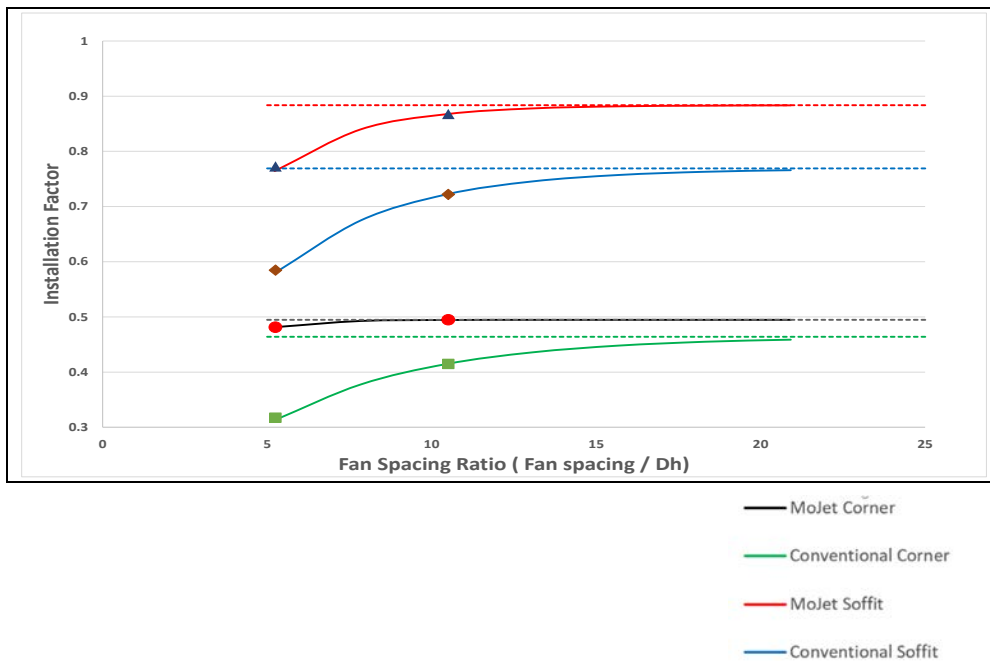


Figure 5: Variation of installation factor with fan spacing ratio for 710mm Fan at 3m/s, 8mm sand-grain roughness, POS 01 for soffit and POS 03 for corner

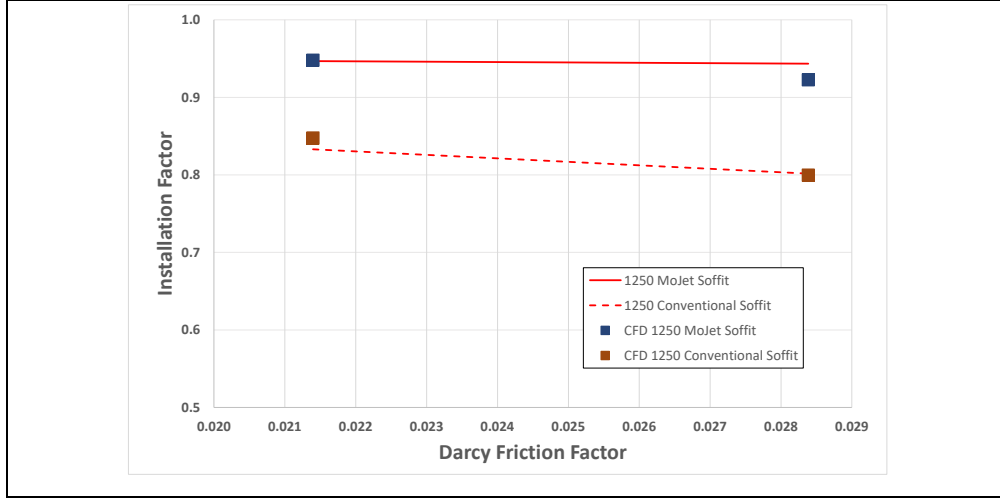


Figure 6: Variation of installation factor with Darcy friction factor ratio for the 1250 mm fan at POS 03 for 3 m/s tunnel air velocity

5. INSTALLATION FACTOR CORRELATIONS

Definitions

$v_r = \frac{v_t}{v_j}$ = velocity ratio between tunnel velocity (v_t) and jet velocity (v_j)

c_{fr} = fan clearance ratio = $\frac{(\text{clearance to silencer} + \text{silencer thickness})}{\text{Tunnel hydraulic diameter } (D_H)}$

$f_{dr} = \frac{D_f}{D_H}$ = fan diameter ratio

D_f = fan diameter

f_s = fan spacing correction ratio

f_f = friction Factor correction ratio

F_{fcr1}, F_{fcr2} and F_{fcr3} = fan diameter correction ratios

F_f = Darcy friction factor for the tunnel

Installation Factor Calculation

Installation Factor $\eta_i = (a_{v1} v_r^2 + b_{v1} v_r + c_{v1}) f_s f_f$

The velocity coefficients a_{v1} , b_{v1} and c_{v1} are corrected based on the fan diameter and on the clearance ratio.

Calculation of the velocity coefficients

$$\begin{pmatrix} a_{v1} \\ b_{v1} \\ c_{v1} \end{pmatrix} = \begin{pmatrix} m_{a1} & q_{a1} \\ m_{b1} & q_{b1} \\ m_{c1} & q_{c1} \end{pmatrix} \begin{pmatrix} f_{dr} \\ 1 \end{pmatrix}$$

f_{dr} = correction for fan diameter ratio (D_f/D_H)

$$\begin{pmatrix} a_{1|fr} \\ b_{1|fr} \\ c_{1|fr} \end{pmatrix} = \begin{pmatrix} a_a & b_a & c_a \\ a_b & b_b & c_b \\ a_c & b_c & c_c \end{pmatrix} \begin{pmatrix} c_{fr}^2 \\ c_{fr} \\ 1 \end{pmatrix} \text{ for the 710 mm fan diameter}$$

$$\begin{pmatrix} a_{1ufr} \\ b_{1ufr} \\ c_{1ufr} \end{pmatrix} = \begin{pmatrix} a_{1lfr} \\ b_{1lfr} \\ c_{1lfr} \end{pmatrix} \begin{pmatrix} F_{fcr1} \\ F_{fcr2} \\ F_{fcr3} \end{pmatrix} \text{ for the 1250 mm fan diameter}$$

$$\begin{aligned} m_{a1} &= \frac{a_{1ufr} - a_{1lfr}}{0.0706} & q_{a1} &= a_{1lfr} - 0.0928m_{a1} \\ m_{b1} &= \frac{b_{1ufr} - b_{1lfr}}{0.0706} & q_{b1} &= b_{1lfr} - 0.0928m_{b1} \\ m_{c1} &= \frac{c_{1ufr} - c_{1lfr}}{0.0706} & q_{c1} &= c_{1lfr} - 0.0928m_{c1} \end{aligned}$$

Fan spacing correction ratio

R_{fs} = Fan spacing ratio for a particular fan, which is the ratio of the installation factor at user fan spacing divided by the installation factor at 80m fan spacing (approximately 10 times the hydraulic diameter of our simulated tunnel) for a reference velocity ratio of 0.092 and a reference clearance ratio of 0.081.

$$R_{fs} = \frac{1 - e^{(-\delta F_{SP})}}{1 - e^{(-\delta 80)}}$$

δ = fans spacing correlation factor that depends on the type of fan and installation position
 F_{SP} = fan spacing in metres

$$f_s = \frac{R_{fs1250} - R_{fs710}}{0.0706} f_{dr} + R_{fs710} - 1.3144(R_{fs1250} - R_{fs710})$$

The subscript in R_{fs} denotes the diameter of the reference fans used in the correlation.

Friction Factor Correction Ratio

Corner Position

For MoJet: $f_f = -8.37922 F_f + 1.17929$

For Conventional Jet Fan: $f_f = -20.70549 F_f + 1.4430$

Soffit Position

For MoJet: $f_f = -0.52625 F_f + 1.01126$

For Conventional Jet Fan: $f_f = -5.40106 F_f + 1.11556$

Variation of Velocity Coefficients vs Clearance

MoJet Corner

$$\begin{pmatrix} a_a & b_a & c_a \\ a_b & b_b & c_b \\ a_c & b_c & c_c \end{pmatrix} = \begin{pmatrix} -1605.3000 & 122.9000 & 20.4740 \\ 777.4700 & -72.8750 & -3.4844 \\ -36.4110 & 6.7807 & 0.5900 \end{pmatrix}$$

Conventional Jet Fan Corner

$$\begin{pmatrix} a_a & b_a & c_a \\ a_b & b_b & c_b \\ a_c & b_c & c_c \end{pmatrix} = \begin{pmatrix} 996.8000 & -128.6200 & 24.1150 \\ -167.5500 & 14.6600 & -4.4434 \\ 48.6440 & -2.6283 & 0.6406 \end{pmatrix}$$

MoJet Soffit

$$\begin{pmatrix} a_a & b_a & c_a \\ a_b & b_b & c_b \\ a_c & b_c & c_c \end{pmatrix} = \begin{pmatrix} 0 & -8.7932 & 8.0717 \\ 0 & 5.6151 & -1.9977 \\ 0 & 0.5398 & 0.9516 \end{pmatrix}$$

Conventional Jet Fan Soffit

$$\begin{pmatrix} a_a & b_a & c_a \\ a_b & b_b & c_b \\ a_c & b_c & c_c \end{pmatrix} = \begin{pmatrix} 0 & 0.7277 & 11.8340 \\ 0 & 1.8226 & -3.2575 \\ 0 & 0.4078 & 0.8866 \end{pmatrix}$$

Fan Diameter Correction Ratios

$$\begin{matrix} \textit{MoJet Corner} \\ \begin{pmatrix} F_{fcr1} \\ F_{fcr2} \\ F_{fcr3} \end{pmatrix} = \begin{pmatrix} 0.55793 \\ 0.58652 \\ 0.98222 \end{pmatrix} \end{matrix}$$

$$\begin{matrix} \textit{Conventional Corner} \\ \begin{pmatrix} F_{fcr1} \\ F_{fcr2} \\ F_{fcr3} \end{pmatrix} = \begin{pmatrix} 0.77196 \\ 1.04373 \\ 1.13734 \end{pmatrix} \end{matrix}$$

$$\begin{matrix} \textit{MoJet Soffit} \\ \begin{pmatrix} F_{fcr1} \\ F_{fcr2} \\ F_{fcr3} \end{pmatrix} = \begin{pmatrix} 0.05719 \\ 0.35816 \\ 0.98995 \end{pmatrix} \end{matrix}$$

$$\begin{matrix} \textit{Conventional Soffit} \\ \begin{pmatrix} F_{fcr1} \\ F_{fcr2} \\ F_{fcr3} \end{pmatrix} = \begin{pmatrix} 0.77196 \\ 1.04373 \\ 1.13734 \end{pmatrix} \end{matrix}$$

Fan Spacing Correction Factor Data

For Corner Position

Correlation Variable	1250 Fan Diameter		710 Fan Diameter	
	MoJet	Conventional	MoJet	Conventional
δ	0.033	0.02	0.09	0.028

For Soffit Position

Correlation Variable	1250 Fan Diameter		710 Fan Diameter	
	MoJet	Conventional	MoJet	Conventional
δ	0.09	0.04	0.05	0.035

6. SUMMARY AND CONCLUSION

Our 3D CFD calculations have indicated the variation of jet fan installation factor with variables including tunnel velocity, clearance to tunnel surfaces, spacing between jet fans, tunnel friction factor and jet fan diameter. We have developed correlations of our CFD results for both conventional jet fans and MoJets. The latter type of fans are designed to deflect the flow away from the bounding tunnel surfaces and enhance the installation factor, without compromising the jet fan bench thrust. To facilitate the use of our correlations, these have been implemented via Excel via a website [9] and independently checked via Matlab. The correlations provide a much better basis for the estimation of jet fan installation factors than previous guidance (Ref. [6]), although engineering judgment and caution are always advised in the design of longitudinal tunnel ventilation via jet fans. The current paper does not address installation factors for banks of jet fans installed at the same tunnel chainage, nor does it address arched tunnel soffits. Further full-scale tunnel testing of our CFD predictions and correlations, in particular related to the effect of jet fan spacing, banks of jet fans and arched tunnel soffits, are currently underway and will be reported in future publications.

7. REFERENCES

- [1] PIARC (1995), Vehicle Emissions, Air Demand, Environment - Longitudinal Ventilation, Committee on Road Tunnels.
- [2] Meidinger U. (1964), “Längslüftung von Autotunneln mit Strahlgebläsen”, Schweizerische Bauzeitung, Heft 28, 82. Jahrgang, 9th July.
- [3] Truckenbrodt E. (1980), Fluidmechanik I, Springer.
- [4] Menter, F. R. (1994), "Two-Equation Eddy-Viscosity Turbulence Models for Engineering Applications," AIAA Journal, Vol. 32, No. 8, August 1994, pp. 1598-1605, <https://doi.org/10.2514/3.12149>.
- [5] Tarada, F., Lehmann, L. and Bertacche, P. (2022), Measurements and CFD Calculations with a MoJet and a Conventional Jet Fan, 11th International Conference ‘Tunnel Safety and Ventilation’, Graz.
- [6] Fathi Tarada and Pier Bertacche, “Jet Fan Installation Factors”, 19th International Symposium on Aerodynamics, Ventilation & Fire in Tunnels, Brighton, 2022.
- [7] F. Tarada, K. Else, A. Domoney, P. Hendrick, A. Tarhach, A. Mugisha, A. Kabuya, B. Sermeus, “MoJet Tunnel Ventilation – Full-Scale Testing and CFD Analysis”, 18th International Symposium on Aerodynamics, Ventilation and Fire in Tunnels, Athens, Greece, 25th – 27th September 2019.
- [8] Costeris, N. (1991), Impulse fans, Aerodynamics and Ventilation of Vehicle Tunnels, pp. 827-846.
- [9] <https://mojet.global/jet-fan-installation-factor-calculations/> (accessed on 12/12/2023)

CFD INVESTIGATION OF THE IMPROVEMENT OF SMOKE CONTROL IN A TUNNEL EQUIPPED WITH A LONGITUDINAL AND A TRANSVERSE VENTILATION SYSTEM

¹Gabriel Remion, ¹Antoine Mos, ²Pietro Salizzoni, ²Massimo Marro, ²Stefano Lanzini

¹Center for Tunnel Studies (CETU), FR

²Laboratoire de Mécanique des Fluides et Acoustique (LMFA), FR

DOI 10.3217/978-3-85125-996-4-36 (CC BY-NC 4.0)

This CC license does not apply to third party material and content noted otherwise.

ABSTRACT

Smoke control in the case of a tunnel fire is vital to ensure an atmosphere allowing tunnel users to evacuate. Depending on the type of ventilation, namely the longitudinal or the transverse ventilation system, the aim is respectively either to push the smoke longitudinally towards a tunnel exit or to evacuate the smoke transversally by the tunnel ceiling. In France, the regulation imposes a sufficient mechanical airflow to prevent any smoke back-layer and to ensure an efficient smoke exhaust.

Previous experiments implemented in a small-scale tunnel have shown the potential of solid barriers, or containment screens, attached to the tunnel’s ceiling. The shape of dampers of the transverse ventilation strategy was also questioned. Wide rectangular dampers appeared to be significantly more efficient than narrower or square dampers, which are commonly installed. Both technical propositions increased significantly the robustness of both ventilation systems by reducing the airflow required to prevent any smoke back-layer from occurring. Reducing the required airflow goes along with reducing the power need of the ventilation system. It tackles the issues of energy consumption and the improvement of the robustness of existing ventilation systems. It also eases the dimensioning and cost of ventilation systems installed in new tunnels.

In the present work, a numerical Computational Fluid Dynamics model of those experiments has been validated by comparison with experimental data measured in both tunnel configurations. The StarCCM+ software was used. It allowed verifying numerically significant benefits of solid barriers for the longitudinal ventilation system. Regarding the transverse ventilation system, it also verified its increased robustness allowed by rectangular dampers compared to commonly used square dampers. The validation of this numerical model is a first step in a wider work aiming at numerically testing the equipment in other configurations.

Keywords: Tunnel, ventilation system’s optimization, dampers’ shape, containment screens, CFD

1. INTRODUCTION

In France, fire safety regulations impose every new tunnel longer than 500 m, or 300m in urban areas, to have a smoke exhaust ventilation system. Smoke exhaust is either achieved thanks to a longitudinal or a transverse ventilation system. Both systems should meet minimum performance requirements in order to ensure a safe auto-evacuation.

The first strategy is based on inducing a longitudinal airflow thanks to fans installed in the cross section of the tunnel, usually near the ceiling. The smoke is evacuated following the airflow towards the tunnel exit. The effectiveness of this strategy depends on the speed of the

longitudinal airflow. Below a threshold value, namely the critical velocity, there is a risk that a part of the smoke layer moves against the airflow. This phenomenon is called smoke back-layering. When the smoke back-layer is still near the fire, its temperature is still high and buoyancy forces maintain the smoke back-layer near the ceiling. The self-evacuation is not perturbed. However, after some distance from the fire, the smoke back-layer starts to decrease in temperature, and buoyancy forces become weaker. The smoke reaches lower zones of the cross section, which may prevent the auto-evacuation. Smoke back-layering may occur over long distances from the fire, which may significantly alter the safety level of the tunnel. An effective longitudinal smoke exhaust strategy relies on the absolute absence of the so-called smoke back-layer provided by a sufficiently high airflow (greater than the critical velocity).

The second strategy uses dampers located on the tunnel ceiling near the fire location to exhaust the smoke. Dampers are distributed all along the tunnel at specific interval (usually 50 to 100 m). The air is extracted thanks to fans that are located in a specific ventilation facility. Fans are then connected to dampers by a ventilation duct. The air is usually extracted through the closest 5 to 7 dampers from the fire location. The objective is to confine the smoke between the two extreme dampers from which the smoke is expected to be extracted. Similarly to the longitudinal strategy, a back-layer can occur. In this case, the back-layer is defined as a smoke layer moving upwind the confinement zone. To prevent the back-layer, the airflow flowing inside the tunnel (or similarly the airflow extracted by dampers) has to be higher than a threshold value called the confinement velocity.

Previous experiments implemented in a small-scaled tunnel located at the Fluid Mechanics and Acoustics Laboratory, in Centrale Lyon France, have tested several configurations to improve the efficiency of both aforementioned ventilation systems [1], [2]. Chaabat et al. [1] questioned the interest of implementing solid barriers, also called containment screens, in the cross section of the tunnel near the ceiling to improve the robustness of longitudinal ventilation systems. They found that containment screens allowed to significantly decrease the critical velocity up to 45%, i.e. the velocity which prevents smoke back-layering in longitudinal ventilation systems. Regarding transverse ventilation systems, Chaabat et al. [2] questioned the shape of dampers. A wide, “slit-like” rectangular damper appeared to be a lot more efficient than the usually implemented square damper located at the ceiling corner. The confinement velocity was decreased by 80%. Thus, significant robustness improvements were identified for both ventilation strategies. Those results are interesting because they allow to ease the dimensioning and the cost of new tunnels. It would also allow to improve the efficiency of already installed ventilation systems without replacing fans that can be very costly.

This paper presents a CFD model of these experiments. A comparison of results obtained experimentally and numerically is systematically performed. The aim is to give more credits to interesting results found experimentally. Section 2 presents the method. Section 2.1 describes configurations that were tested experimentally and reproduced numerically, and section 2.2 focuses on the implementation of the CFD model. Then, results are presented in section 3, first focusing on the contribution of barriers (section 3.1), and then on the influence of damper shapes (section 3.2).

2. METHODS

2.1. Tested configurations

Configurations that were tested experimentally, and that are reproduced numerically here, are presented in this section. Figure 1 shows a picture of the experimental set up of the transverse ventilation system. The small-scaled tunnel, which hosted experiments, is 8.4 m long, 0.18 m

high (H) and 0.36 m wide, around 1/25 of a real tunnel. The fire-induced smoke is reproduced by the injection of a light gas composed by a mixture of air and helium. This technique intends to simulate the smoke buoyancy while bypassing the influence of heat transfer, which is complicated to account for. Densimetric plumes have already been shown reliable in describing the behavior of fire-induced smoke in tunnels [3]. The buoyant source is located in the center of the tunnel, and is released through a circular hole 10 cm in diameter (D). The density ratio ρ_0/ρ_i between the ambient air, and the light gas was set to 0.7. Its influence was shown to be negligible by Salizzoni et al. [4]. Varying the speed of injection of the light gas (W_i), several heat release rates could be simulated, which can be characterized by the plume Richardson number (Γ_i):

$$\Gamma_i = \frac{5}{16} \frac{(\rho_0 - \rho_i) g D}{\alpha W_i^2}$$

With $\alpha = 0.12$, the reference entrainment coefficient [5]. Richardson numbers of 2, 4, 6, 8 and 10 were tested, characterizing plumes more and more dominated by buoyancy forces instead of momentum.

The Froude number is introduced, and represents a dimensionless form of the longitudinal velocity. The Froude number is defined as the ratio between inertia forces induced by the longitudinal airflow, and buoyancy forces introduced by the buoyant source (with Bi the buoyancy flux).

$$Fr_{cr} = \frac{U_{0cr}}{\left(\frac{Bi}{H}\right)^{1/3}}$$

A similarity analysis developed in several articles [2], [4] concluded that the critical or the confinement Froude number did not show any dependence on single buoyant source parameters for highly buoyant sources, meaning for high values of Γ_i . In other words, conclusions are independent from the heat release rate for highly buoyant sources.

Both ventilation systems were implemented. A fan was used to impulse the airflow of the longitudinal ventilation system. The transverse ventilation system was realized thanks to two dampers located symmetrically from the buoyant source, at a distance of $5H$. Dampers were connected to an extraction fan located outside of the tunnel section. Extracting the air through these dampers induces a convergent airflow entering the tunnel symmetrically by both exits.

Barriers were implemented in the cross section of the tunnel, attached to the ceiling. Their width are equal to the width of the tunnel. Different heights were considered: two large barriers with a height of $H/3$ and $H/4$, and a small barrier with a height of $H/10$. Large barriers were located just upstream the source of the fire. In configurations testing small barriers, one was also placed just upstream of the source but several other barriers were distributed all along the tunnel, with a fixed spacing of H between each other. Figure 2 shows those two configurations (schematics a. and b.).

Regarding the transverse ventilation system, three different shapes were tested: the usual square shape (0.104 m x 0.104 m) located in the center of the ceiling (SSD – PC), the square shape located in a corner of the ceiling (SSD – PS), and a narrow rectangular shape (0.32 m x 0.034 m) whose width is almost equal to the width of the tunnel (RSD). Figure 2 also presents these configurations (schematics c.).



Figure 1: Picture of the experimental set up for the transverse SSD - PC ventilation system

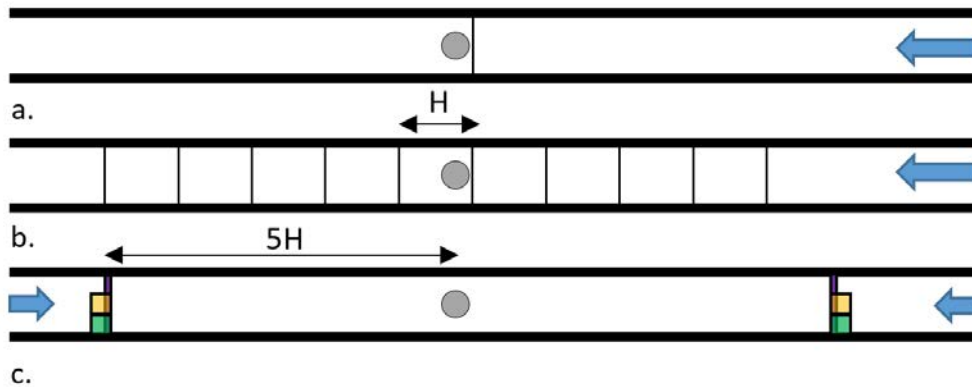


Figure 2: Schematics of configurations: a. longitudinal system with large barriers; b. longitudinal ventilation system with small barriers; c. transverse ventilation system with SSD - PC (yellow squares), SSD - PS (green squares), RSD (purple rectangles)

2.2. CFD model

The experimental set up presented in the previous section was modelled using the StarCCM+ CFD software. An isothermal steady RANS realizable k-epsilon closure model was implemented. Regarding the longitudinal ventilation system, the inlet of the tunnel was imposed as a constant velocity inlet on the cross section of the tunnel. The turbulence intensity and the turbulent length scale were defined in accordance with standard values for rectangular ducts. The exit was defined as a pressure outlet.

The air extracted from dampers of the transverse ventilation system was done by a mass flow inlet boundary condition. Both tunnel's exits from which the convergent airflow enters the tunnel were defined as pressure outlets, meaning that a reversed flow occurs. Those boundary conditions were expected to be the most representative of the real physics.

For both configurations, the buoyancy source was introduced as a mass flow inlet of the same mixture of Air and Helium. Authors made sure that the length between tunnel's exits and the zone of interest allowed a well-established boundary layer.

The mesh is generated by the trimmed mesher provided by StarCCM+, which is particularly suited to tunnel applications with longitudinal airflows. Prismatic layers were defined on walls and barriers to ensure the low-Reynolds resolution ($y^+ \sim 1$). The mesh grid represents 100k to 1 million cells depending on configurations. Authors made sure that results were independent from a mesh refinement.

3. RESULTS & DISCUSSION

3.1. Effect of barriers on the performance of longitudinal ventilation system

To obtain critical velocities, the inlet velocity was iteratively reduced until Helium was detected upstream of the extremity of the buoyant source (or upstream of the barrier). Figure 3 shows a smoke back-layer, which occurred in the configuration with a large H/3 barrier. The critical velocity found for a Richardson number $\Gamma_i = 2$ is about 0.155 m/s.

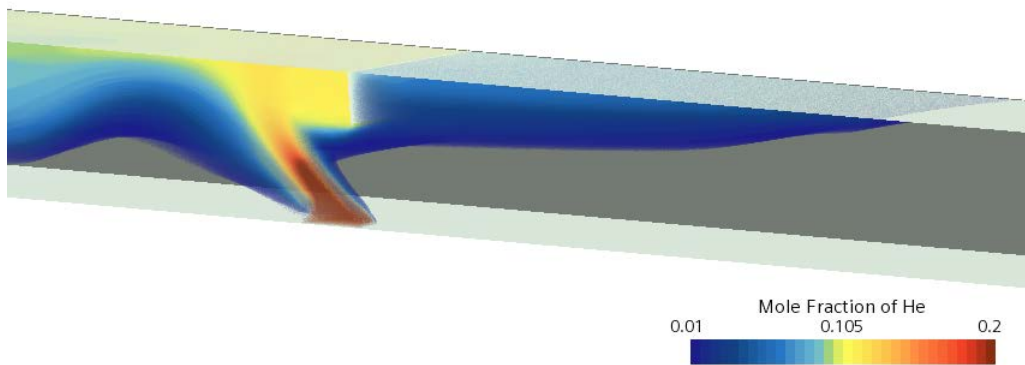


Figure 3: Configuration with barrier H/3 with a smoke back-layer occurring for critical velocity of 0.155 m/s, and Richardson number of 2

Figure 4 shows the dimensionless critical velocity in the form of the critical Froude number. It is plotted against the Richardson number for each configuration. Triangles, solid and dashed bars refer respectively to simulation results, experimental and simulation best fits. Best fits (experimental and simulation) were applied on critical Froude numbers obtained for $\Gamma_i > 8$, as the behavior of the Froude number seem to be different on both sides of this threshold value. As was stated on section 2.1, the critical Froude number is expected to be independent from buoyant source parameters as long as the buoyant source is buoyant enough. Yet, for small Γ_i ($\Gamma_i < 8$) the critical Froude number seems to increase with increasing Γ_i , whereas for higher values of Γ_i ($\Gamma_i > 8$), it becomes constant. It was already observed experimentally [2], and this is consistent with findings presented in ref. [2], [4], that show a constant critical Froude number for high values of Γ_i . It can be noted that, even for small values of Γ_i , the evolution of the critical Froude number with Γ_i is quite similar for each configuration. Benefits allowed by barriers are, thus, independent from the heat release rate of the fire.

Before focusing on benefits allowed by barriers, it is interesting to compare experimental and simulation results. Indicative 10% error bars were added to simulation results. The reference configuration with no barriers shows an underestimation of simulation results. The deviation decreases as Γ_i increases, and lies below 10% from $\Gamma_i = 20$. The average underestimation is about 8% (0.017 m/s). Small barriers H/10 show good correlations. Finally large barriers lead to an overestimation compared to simulation results. The average deviation of large barriers H/4 and H/3 is respectively 13% (0.012 m/s) and 10% (0.017 m/s). In general, deviations

between experimental and simulation results are all within 13% (0.017 m/s), which demonstrates a rather good correlation.

We now focus on benefits brought by barriers. As critical Froude number and velocity are proportional, benefits observed on critical Froude numbers are equivalent to those on critical velocities. Focusing on simulation results, small barriers allow a small benefit of 3%. Considering the confidence interval, this benefit is insignificant. However, large barriers allow a significant reduction of the critical velocity. Large barriers $H/4$ and $H/3$ allow to reduce the critical velocity by respectively 22%, and 33% on average.

Experimental results showed also a rather small benefit of small barriers, but greater benefits of large barriers. Barriers $H/4$ and $H/3$ led to a reduction of the experimental critical velocity of respectively 35% and 45% (compared to 22% and 33% numerically). Those results show that both investigation techniques demonstrated significant benefits of large barriers in reducing the velocity that prevents any smoke back-layer to occur.

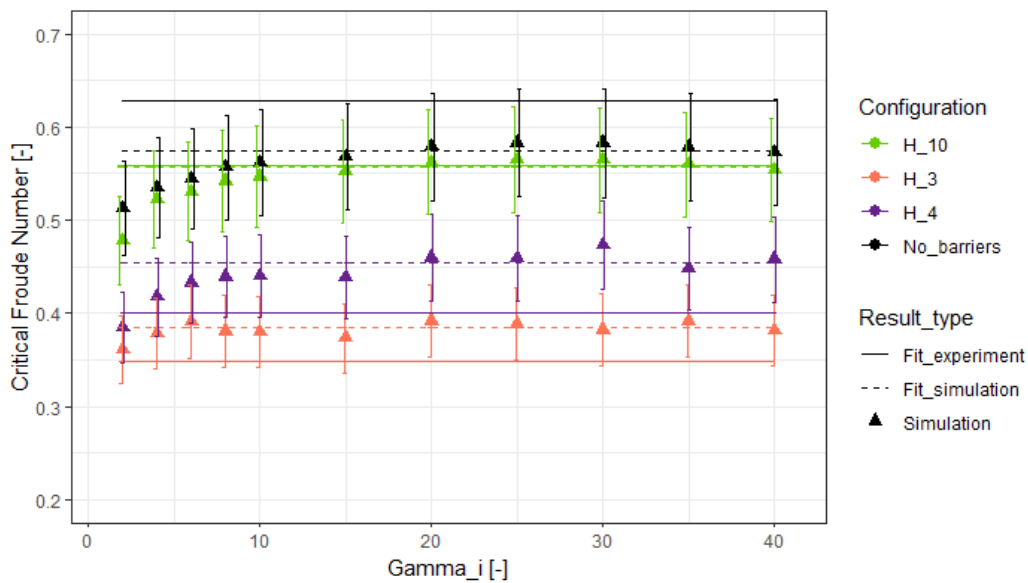


Figure 4: Froude number plotted against the Richardson number for each configuration

3.2. Effect of dampers' shape on the performance of transverse ventilation system

The influence of dampers' shape is questioned in this paragraph. The confinement velocity was assessed by iteratively reducing the extracted air flow rate until helium was detected upstream of the dampers (the flow is symmetrical). Figure 5 shows a smoke back-layer, which occurred for rectangular dampers (RSD), a confinement velocity of 0.08 m/s and a Richardson number of 2.

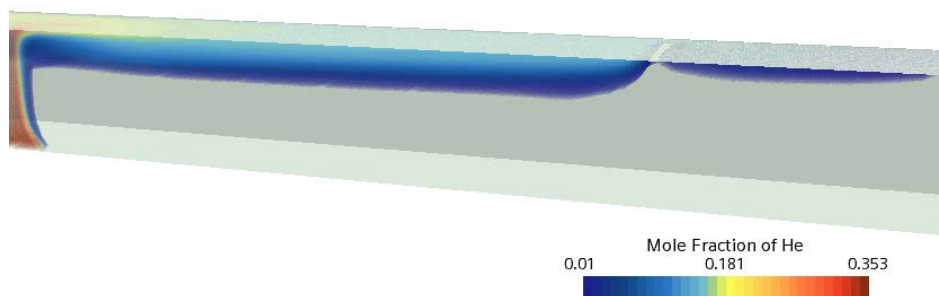


Figure 5: Configuration with rectangular dampers RSD, with a smoke back-layer occurring for $U_{0cr} = 0.08$ m/s and $\Gamma_i = 2$

Figure 6 shows confinement Froude number plotted against the Richardson number for each damper shape. Similarly to Figure 4, best fits of experimental results (solid bars) are given for the comparison. Dashed bars represent best fits of the simulation results. The regression was applied on Froude number obtained for $\Gamma_i > 4$ for the reason stated on section 3.1. However, unlike Figure 4, the confinement Froude number induced by centered square dampers (SSD PC) and rectangular dampers (RSD) do not seem to show any dependence at all on Γ_i (even for $\Gamma_i < 4$). Indicative 10% error bars have been added to simulation results.

It is first interesting to question the consistency between experimental and simulation results. All configurations show good correlations between experiment and simulation results. The reference configuration of sided square dampers (SSD_PS) lead to deviations within 10%. Its average deviation is about 6% (0.03 m/s). Centered square dampers (SSD_PC) simulation results are on average 9.7% (0.02 m/s) lower than experimental results. Finally, rectangular dampers (RSD) are 17% lower on average than experimental results. However, in view of its smaller absolute value compared to other configurations, its absolute deviation remains very low (0.01 m/s).

Figure 6 show that the most common configuration (sided square dampers) is clearly the worst situation, leading to significantly higher confinement Froude number. Locating square dampers in the center of the ceiling allows to increase significantly the smoke exhaust effectiveness. The confinement Froude number is reduced by 52% compared to the reference configuration. Wide and slim rectangular dampers (transverse slits) are the most effective dampers. They allow to reduce the confinement Froude number by 84%. Experimental results led to quite similar benefits of the centered square dampers and rectangular dampers of respectively 44% and 80%.

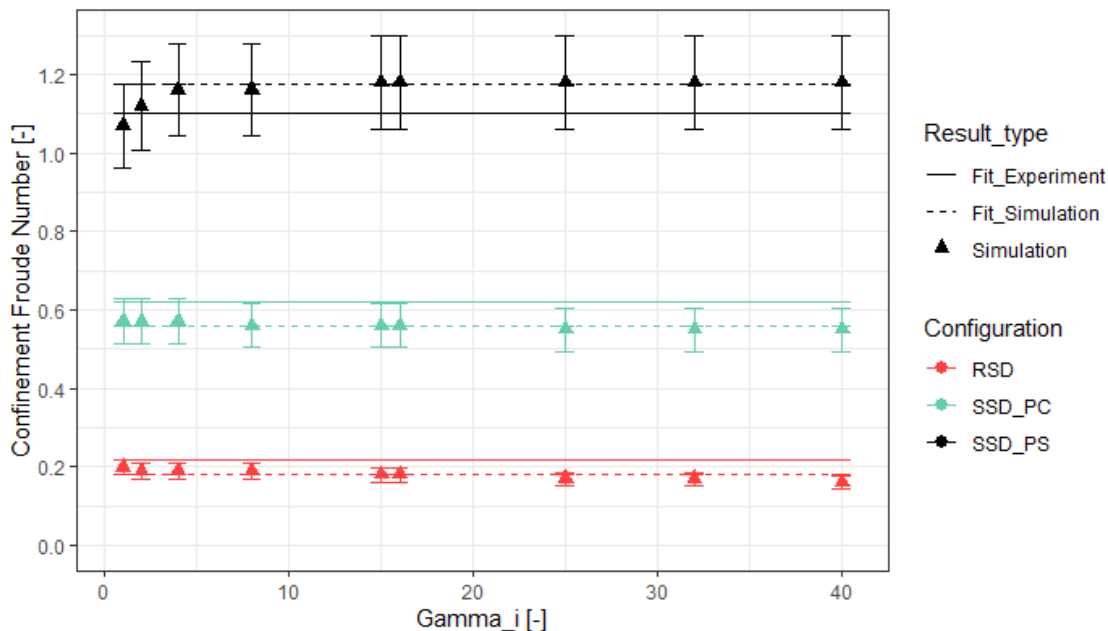


Figure 6: Critical Froude number plotted against the Richardson number for each damper shape

4. CONCLUSION

In this article, a reduced-scale tunnel CFD model was elaborated. It reproduced experiments that have previously been implemented. Those experiments questioned benefits of different configurations aiming at improving the robustness of the smoke exhaust by a longitudinal

and a transverse ventilation system. They showed that solid barriers attached to the ceiling appeared effective in reducing critical velocities involved in longitudinal ventilation systems. They also showed that the shape of dampers used in transverse ventilation systems has a significant influence on the confinement velocity.

Numerical results presented here allowed to verify significant improvements allowed by these passive geometrical optimizations. Large solid barriers led to a reduction of the critical velocity up to 33%, slightly weaker than experimental results that showed an even greater benefit of up to 45%. Regarding the transverse ventilation system, numerical and experimental results showed that narrow and wide rectangular dampers were way more efficient than usually installed square dampers. Both investigation techniques showed a reduction of the confinement velocity by around 80% compared to usually-installed sided square dampers. Locating the square damper in the center of the ceiling allows a reduction of around 50%.

The sensitivity of conclusion towards heat release rates has been assessed. As long as the buoyant source was buoyant enough (high Richardson number), the critical or the confinement Froude number was conserved for each HRR. It means that conclusions of the present paper are independent from the HRR.

The overall consistency between experimental and simulation results gives credit to those findings. Passive optimizations may, thus, have a great influence on the performance of ventilation systems. It is interesting to keep those findings in mind for the dimensioning and retrofitting of ventilation systems. It should however be taken into consideration that the implementation of those passive implementation may come with some technical difficulties that were not questioned in this paper. Also, vertical barriers proposed to improve the robustness of the longitudinal ventilation system may increase the wall friction. The energetic gain provided by the lower critical velocity as to be put in perspective of the energetic loss due to an increased wall friction. A following research will aim at questioning those results with the consideration of heat transfers among the tunnel's envelope.

5. REFERENCES

- [1] F. Chaabat *et al.*, « The effects of solid barriers and blocks on the propagation of smoke within longitudinally ventilated tunnels », *Build. Environ.*, vol. 160, p. 106207, août 2019, doi: 10.1016/j.buildenv.2019.106207.
- [2] F. Chaabat *et al.*, « Smoke control in tunnel with a transverse ventilation system: An experimental study », *Build. Environ.*, vol. 167, p. 106480, janv. 2020, doi: 10.1016/j.buildenv.2019.106480.
- [3] L. Jiang, M. Creyssels, A. Mos, et P. Salizzoni, « Critical velocity in ventilated tunnels in the case of fire plumes and densimetric plumes », *Fire Saf. J.*, vol. 101, p. 53-62, oct. 2018, doi: 10.1016/j.firesaf.2018.09.001.
- [4] P. Salizzoni, M. Creyssels, L. Jiang, A. Mos, R. Mehaddi, et O. Vauquelin, « Influence of source conditions and heat losses on the upwind back-layering flow in a longitudinally ventilated tunnel », *Int. J. Heat Mass Transf.*, n° 117, p. 143-153, 2018.
- [5] G. R. Hunt et N. B. Kaye, « Lazy plumes », *J. Fluid Mech.*, vol. 533, p. 329-338, juin 2005, doi: <https://doi.org/10.1017/S002211200500457X>.

AN ANALYSIS OF THE 3D CRITICAL REGION LENGTH IN LONGITUDINALLY VENTILATED TUNNELS DURING FIRE EVENTS

^{1,2}Ayala, Pablo, ²Amo, Luis, ^{1,2}Cantizano Alexis

¹Institute for Research in Technology, ICAI, Comillas Pontifical University, ES

²ICAI School of Engineering, Comillas Pontifical University, ES

DOI 10.3217/978-3-85125-996-4-37 (CC BY-NC 4.0)

This CC license does not apply to third party material and content noted otherwise.

ABSTRACT

Computational models are valuable tools for designing fire ventilation systems in tunnels. However, these models can be very complex and computationally expensive. Moreover, smoke behavior depends on many factors, such as tunnel geometry, ventilation velocity, fire intensity, tunnel slope, etc. Hybrid or multiscale models are alternatives that can lower the computational demand and still produce trustworthy results. These models combine regions with different levels of detail: one-dimensional (1D) and three-dimensional (3D). The 1D regions offer simpler results through faster computation, while the 3D region provides greater realism and detail, albeit at the cost of increased computational resources and time. Defining the 3D region is critical and challenging, as it significantly influences the model's accuracy and efficiency. Its length, i.e., critical length, can be determined by employing various criteria, mainly based on relevant parameters such as the hydraulic diameter or the heat release rate (HRR). In this study, the downstream critical length of a fire in a longitudinally ventilated tunnel is analyzed through a numerical study comprising 108 simulations conducted with FDS 6.8.0. The assessment considers the impact of HRR, tunnel cross-sectional area, and ventilation velocity on the critical length. As HRR increases, downstream critical length grows, expanding the simulation domain and computational cost. Similarly, the critical length slightly rises as the cross-sectional area decreases, but further studies needed for quantitative analysis. These conclusions are drawn from defining critical length based on the tunnel's longitudinal temperature gradient. Furthermore, various models are introduced to illustrate the dimensionless relationship between the critical length and HRR, confirming that a linear relationship is not suitable when longitudinal ventilation is present. The dependency of the critical length on ventilation velocity is quite significant, greatly improving the model's fit when taken into account.

Keywords: CFD, Multiscale, Coupled hybrid modeling, Tunnel fire ventilation, FDS, 3D Region

1. INTRODUCTION

According to several studies, smoke inhalation is the primary cause of death in fires, making its study highly relevant in the field of fire safety, particularly in tunnels [1]. Numerous tunnel ventilation studies have been conducted to assess smoke behaviour based on factors such as fire location, wind influence, vehicle blockage effects, or tunnel temperature distribution, among others [2–4]. Additionally, various full-scale tests have been conducted [5–8], but these come with high costs and environmental impacts. As an alternative, reduced-scale tests with ratios of 1/6 to 1/50 have also been used [9]. However, the inability to maintain complete similarity in dimensionless numbers reduces the precision of their results compared to full-scale tests. With technological advancements, Computational Fluid Dynamics (CFD) models for fire simulation have become widespread in the industry, supporting classic prescriptive designs for assessing smoke and flame behaviour [10–12].

One of the main challenges in CFD models with large domains is the high computational cost, limiting the number of simulations for design optimization. Strategies like Design of Experiments (DoE) are employed to predict potential behaviour [13,14]. Particularly in long tunnels, the use of hybrid models or multiscale models for tunnel fires has become more common due to their reduced computational cost [15–18].

The definition of the 3D-CFD region in hybrid or multiscale models is critical, as it affects both model accuracy and computational cost. A larger 3D domain enhances precision but also increases computational cost. Recent studies have explored the critical length for non-ventilated tunnels, quantifying dimensionless relationships between critical length and HRR. They include analyses using dimensionless methods to assess various tunnel phenomena, such as backlayering length, critical velocity [19], or smoke stratification [19, 20].

This work examines the downstream critical length of a fire in a longitudinally ventilated tunnel through a numerical assessment, involving 108 simulations using FDS 6.8.0 [22]. The influence of HRR, cross-sectional tunnel characteristics, and ventilation velocity is evaluated. Additionally, different models are presented to quantify the downstream critical length.

2. THEORETICAL APPROACH – DIMENSIONAL ANALYSIS

In the case of longitudinally ventilated tunnels, the critical length of the tunnel can be evaluated using a dimensionless model [18, 22, 23]. In these studies, the critical length (L_{ds}) generally depends on the HRR (\dot{Q}), ambient temperature (T_0), gravity (g), air specific heat capacity (c_p), air density (ρ_0), and tunnel hydraulic diameter (\bar{H}). However, in this work, unlike the previous ones, the bulk velocity of longitudinal ventilation is also included. Thus, the downstream critical length of the fire can be expressed as:

$$L_{ds} = f(Q, T_0, g, c_p, \rho_0, \bar{H}, u_0)$$

Thus, we obtain the following relationship of dimensionless groups:

$$\frac{L_{ds}}{\bar{H}} = f\left(\frac{Q}{\rho_0 c_p T_0 \bar{H}^2 g^{\frac{5}{2}}}, \frac{u_0}{(g\bar{H})^{\frac{1}{2}}}\right) = f(Q^*, V^*)$$

For scenarios without ventilation, a linear model between the dimensionless critical length (L^*) and HRR ($Q^{*1/3}$) is proposed by Wang [24]:

$$L^* = 95Q^{*1/3}$$

In this study, we will analyze the fitting of simulation data with three different models.

Linear model: $L^* = c_1 Q^{*1/3}$

Potential model: $L^* = c_1 (Q^{*1/3})^{c_2}$

Linear model with velocity dependency: $L^* = c_1 Q^{*1/3} + c_2 \ln(c_3 V^*)$

3. CASES OF STUDY

3.1. Numerical models

Different numerical models have been developed in FDS 6.8.0, an open-source software commonly used by the industry. This software employs the Eddy Dissipation Concept (EDC) with a thermal extinction model to simulate combustion. Turbulence is simulated using the Deardorff model ($C_v=0.1$), and radiation is considered using the radiation transport equation with 100 angles. Additionally, the maximum number of iterations has been set to 100, compared to the default value of 10, defined by FDS, to solve the Poisson equation. This will avoid numerical instabilities due to the extensive domain length of FDS and the high HRR in some cases.

A total of 108 numerical simulations have been conducted to evaluate the influence of various parameters. In Table 1, a summary of the fire scenarios is provided, encompassing scenarios with different HRR and longitudinal ventilation velocities. Furthermore, different cross-sectional areas have been assessed by varying both the width and height of the tunnel.

The tunnel's overall length spans 2,000 meters, with the fire source positioned at 500 m from the upstream portal at a height of 1.2 meters. A HRR per unit area ranging from 1,300 kW/m² to 1,800 kW/m² has been established, adjusted based on the mesh size. The specific configurations are as follows:

- HRR: 5 MW. Fire area: 2.4 x 1.6 m²
- HRR: 30 MW. Fire area: 6.4 x 3.2 m²
- HRR: 50 MW. Fire area: 8.8 x 3.2 m²

Temperature and velocity measurements are conducted at 0.5-meter intervals throughout the entire tunnel, at 0.4 meters from the ceiling, and at a distance of 0.4 meters from the wall.

Table 1: Summary of the values considered for the different parameters

Simulations	HRR (MW)	Velocity (m/s)	Tunnel width (m)	Tunnel height (m)
1-36	5	0 / 1.5 / 3 / 5	6 / 8 / 12	4 / 6 / 8
37-72	30	0 / 1.5 / 3 / 5	6 / 8 / 12	4 / 6 / 8
73-108	50	0 / 1.5 / 3 / 5	6 / 8 / 12	4 / 6 / 8

3.2. Mesh sensitivity analysis

A mesh sensitivity analysis has been conducted with the 8 m wide and 4 m high tunnel model, with 1,000 m length, a longitudinal ventilation velocity of 1.5 m/s and a 5 MW fire centrally positioned. The choice of the mesh size (Δ) has taken into account the characteristic fire diameter (D^*) with a spatial resolution analysis $R=D^*/\Delta$, that should be maintained between 1/16 and 1/4 [22]. For this reason, the lowest HRR has been selected since it requires the smallest mesh size. Four mesh sizes have been studied: 0.2 m, 0.2/0.4 m, 0.4 m, and 0.8 m, corresponding to resolutions within the required range. The numerical model with 0.2/0.4 m is divided in such a way that a length of 50 m, centered on the fire, have a mesh size of 0.2 m, and 0.4 m in the rest of the tunnel.

Figure 1 shows the vertical temperature profile and temperature evolution under the ceiling at the centerline of the tunnel, at 20 m (Figure 1a and Figure 1b) and 100 m (Figure 1c and Figure 1d) downstream the fire. At 20 m, vertical temperature profiles exhibit differences between the models. However, these discrepancies decrease as the distance from the fire increases, i.e., being less than 10 °C at 100 m downstream, which corresponds to an 11% error compared to the finest mesh.

Table 2 shows the relative errors at different downstream locations, with respect to the finest mesh values. It is observed that differences under the ceiling decrease significantly, always staying below 11.2% from 100 m downstream onwards.

Finally, the backlayering length is also influenced by mesh size for the different cases: 18.5 m (0.8 m), 42 m (0.4 m), 44.5 m (0.2/0.4 m), and 49.5 m (0.2 m). It is observed that backlayering length increases as the mesh size becomes smaller, but with differences less than 7 m between the 0.4 m and 0.2 m meshes. These results are similar to those found by McGrattan and Bilson [25], emphasizing how the sensitivity of smoke backlayering length significantly depends on the mesh size and definition criteria applied.

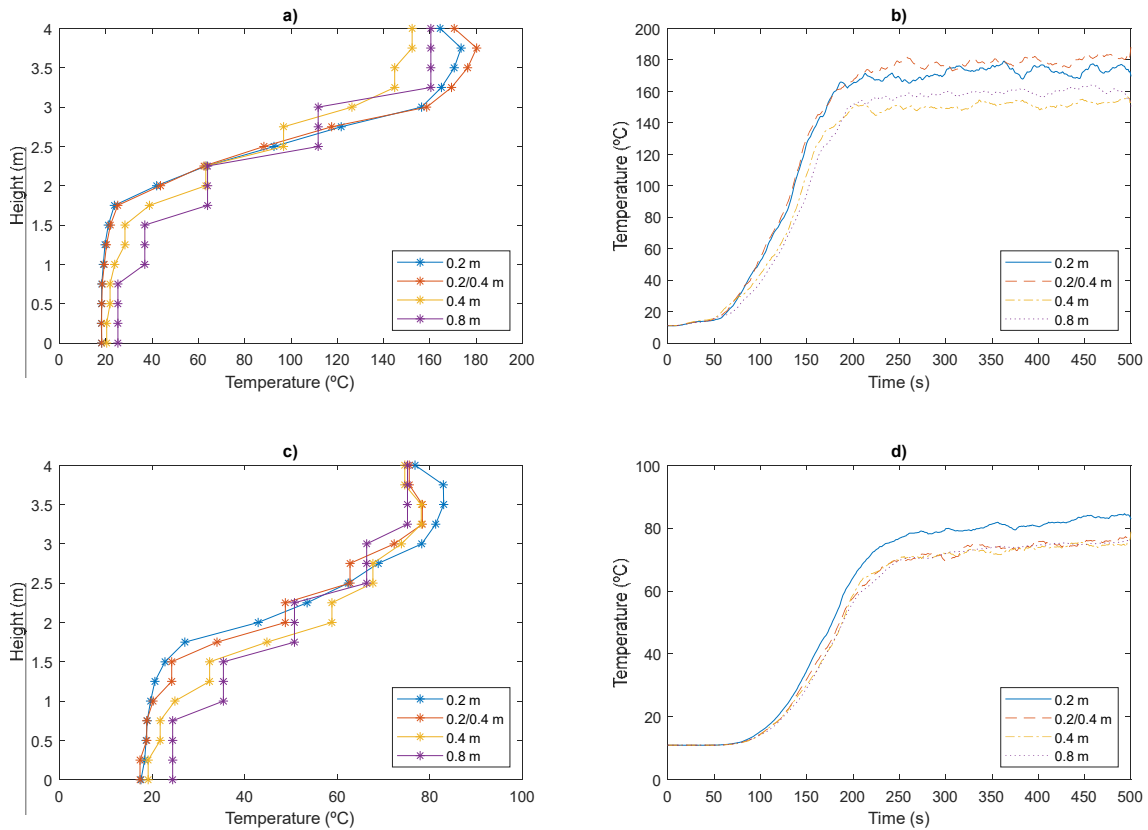


Figure 1: Vertical temperature and temperature evolution under the ceiling in the centerline of the tunnel: at 20 m (a-b) and 100 m downstream the fire (c-d).

Table 2: Relative errors (%) of temperature under the ceiling along the centerline of the tunnel.

Δ (m)	Downstream distance from fire source (m)									
	50	100	150	200	250	300	350	400	450	500
0.2/0.4	6.2	8.9	11.2	10.5	9.9	9.4	8.5	8.9	8.6	8.3
0.4	15.2	10.0	7.4	5.8	3.8	2.6	1.1	1.8	1.9	2.9
0.8	11.7	9.3	8.4	6.2	4.0	2.2	0.9	0.7	1.8	2.2

Based on these results, this study has been conducted with a mesh size of 0.4 m. This mesh configuration not only maintains good accuracy in the distant fire field but also reduces computational costs, requiring only 13.7 hours compared to the 82 hours needed for the simulation with a 0.2 m mesh size. Despite the mesh size not being sufficiently fine for detailed analysis, it is adequate for conducting a qualitative study to analyze the critical length.

3.3. Critical length downstream the fire

Smoke flow characteristics are defined through different regions: near region, one-dimensional flow region, and turbulent mixing region [23,24,26]. These are analyzed based on the temperature distribution along the tunnel. Different methodologies can be found in the literature to define the critical length. This work uses the methodology presented by Wang et al. [24] by calculating a parameter 'k' derived from the temperature difference between two adjacent positions:

$$k = \frac{1}{n} \sum_{i=1}^n \frac{T(x_1) - T(x_0)}{x_1 - x_0}$$

The number of data points 'n' depends on the region under consideration and 'k' is close to 1 in the turbulent zone. Here, 'k' is estimated by calculating the average thermal gradient every 10 meters.

Figure 2a illustrates the evolution of the mean temperature under steady-state conditions (during the last 100 seconds of simulation). In Figure 2b, the profile of the 'k' parameter is depicted. This is computed as the average temperature gradient every 0.5 meters over a 10-meter tunnel section. Finally, the critical length is calculated as the position where a 1°C variation, for every 10 meters of the tunnel, equivalent to a 'k' value of 0.1, as can be seen in the figure with a red mark.

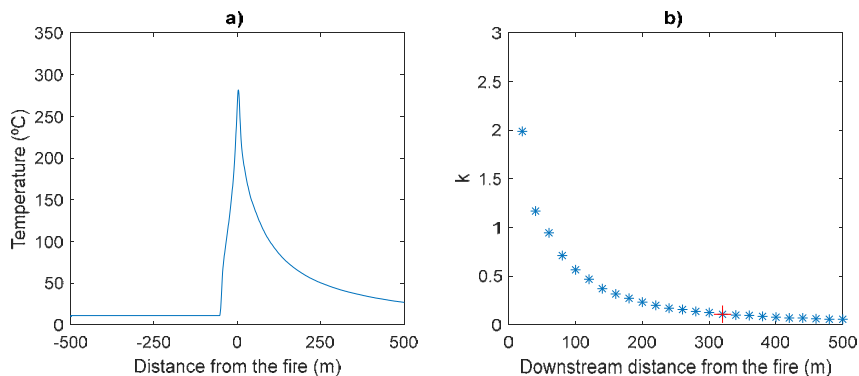


Figure 2: a) Temperature distribution along the centerline of the tunnel; b) k distribution.

4. RESULTS

4.1. HRR and tunnel cross-sectional area influence

The influence of the HRR and the tunnel cross-sectional area on the critical length for different longitudinal ventilation conditions can be observed in Figure 3. Firstly, the influence of the HRR is significant, regardless of the tunnel's cross-sectional area and ventilation. As the HRR rises, the critical length also increases. Nevertheless, the increase in critical length does not correlate proportionally with the rise in HRR. Notably, the disparity within the rise 5-30 MW is significantly larger than in the rise 30-50 MW, particularly at velocities up to 3 m/s. In unventilated scenarios, the average difference of critical lengths for rise 5-30 MW amounts to 330 m, whereas it is only 20 m for rise 30-50 MW. At a ventilation rate of 1.5 m/s, the average difference for both 5-30 MW and 30-50 MW, remains substantial (330 m and 85 m, respectively). This trend persists at 3 m/s, where the average difference for rise 5-30 MW is 490 m, contrasting with 160 m for rise 30-50 MW. Lastly, the average increments at 5 m/s are comparable for both rises: 290 m (5-30 MW) versus 260 m (30-50 MW). In summary, the average differences for rise 5-30 MW seem insignificant at any ventilation speed. However,

for rise 30-50 MW, there is a pronounced dependency on velocity, with differences escalating notably with velocity.

Considering every value of HRR, for a 5 MW fire, it is observed that as the ventilation velocity increases, the critical length decreases. This reduction ranges from an average of 288 m for models without ventilation to 64 m for a ventilation speed of 5 m/s. This could be explained as ventilation facilitates the attainment of uniform temperature conditions over a shorter distance downstream of the fire. In the 30 MW scenario, for ventilation velocities up to 3 m/s, the average values of critical length are approximately 600 m, with a difference of less than 50 m depending on the ventilation rate. However, at 5 m/s velocity, the average critical length reduces to 350 m. Ultimately, the 50 MW scenarios are the least influenced by ventilation velocity, as their average lengths range between 610 and 750 m for any ventilation rate.

Regarding the influence of the tunnel cross-sectional area, despite the inability to draw direct conclusions from the graph, a trend emerges: the critical length slightly increases as the tunnel width decreases, particularly for higher HRR values and lower ventilation speeds. Similarly, for a given width, the critical length slightly decreases as the height increases. However, the differences in critical lengths do not follow a fixed pattern, indicating the need for further analysis to draw more precise conclusions.

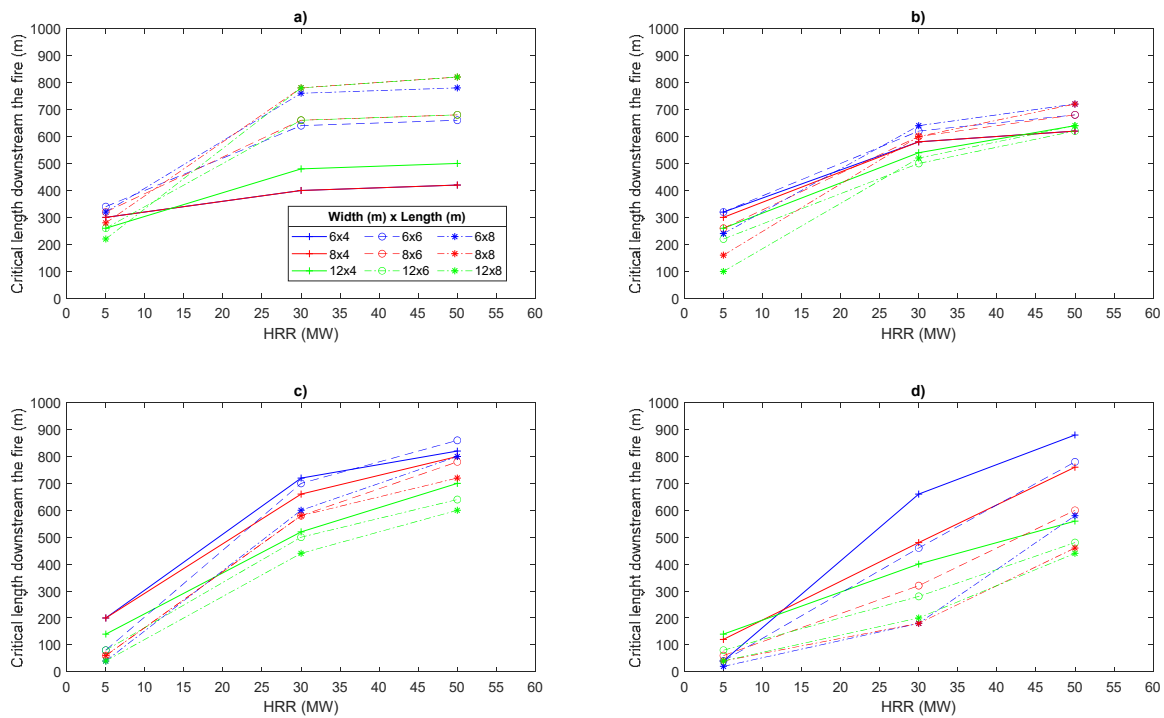


Figure 3: Critical downstream length for different longitudinal velocities: a) 0 m/s, b) 1.5 m/s, c) 3 m/s, and d) 5 m/s.

4.2. Dimensionless model

Figure 4 illustrates various fitting curves between the downstream critical length of the fire and the dimensionless HRR for different scenarios of longitudinal ventilation: 0 m/s, 1.5 m/s, 3 m/s and 5 m/s. In each scenario, simulation data is represented in different colours: 5 MW (blue), 30 MW (red), and 50 MW (green). It is evident that there is a clear relationship between $Q^{*1/3}$ and L^* at low HRR values. As mentioned in the previous section, the data has been fitted to three types of curves: linear, potential, and linear with velocity dependency.

For the scenarios without longitudinal ventilation, the coefficients obtained for linear and potential models are:

Linear	Potential
$L^* = 130 Q^{*1/3}$	$L^* = 114 (Q^{*1/3})^{0.7}$
$R^2 = 0.85$	$R^2 = 0.82$

Secondly, for the scenario of longitudinal ventilation at 1.5 m/s, Figure 3b includes linear and potential fits as well as linear fit with velocity dependency. In this case, it is observed that the predictions made by all three models are accurate. The coefficients obtained are:

Linear	Potential	Linear with velocity
$L^* = 137 Q^{*1/3}$	$L^* = 147 (Q^{*1/3})^{1.2}$	$L^* = 155 Q^{*1/3} + 32 \ln(3.7 V^*)$
$R^2 = 0.92$	$R^2 = 0.94$	$R^2 = 0.96$

For the scenario of a ventilation velocity of 3 m/s, Figure 3c shows that the potential model fits well and is comparable to that considering velocity. However, the linear fit deviates considerably from the previous ones. The coefficients obtained are:

Linear	Potential	Linear with velocity
$L^* = 145 Q^{*1/3}$	$L^* = 204 (Q^{*1/3})^{1.9}$	$L^* = 254 Q^{*1/3} + 3.7 \ln(10^{-8} V^*)$
$R^2 = 0.78$	$R^2 = 0.96$	$R^2 = 0.97$

Finally, the results obtained with a longitudinal ventilation of 5 m/s are similar to those obtained for the ones of 3 m/s, as shown in Figure 3d. Similarly, the linear fit is less accurate. The coefficients obtained are:

Linear	Potential	Linear with velocity
$L^* = 112 Q^{*1/3}$	$L^* = 214 (Q^{*1/3})^{2.9}$	$L^* = 225 Q^{*1/3} + 40.2 \ln(0.3V^*)$
$R^2 = 0.63$	$R^2 = 0.92$	$R^2 = 0.90$

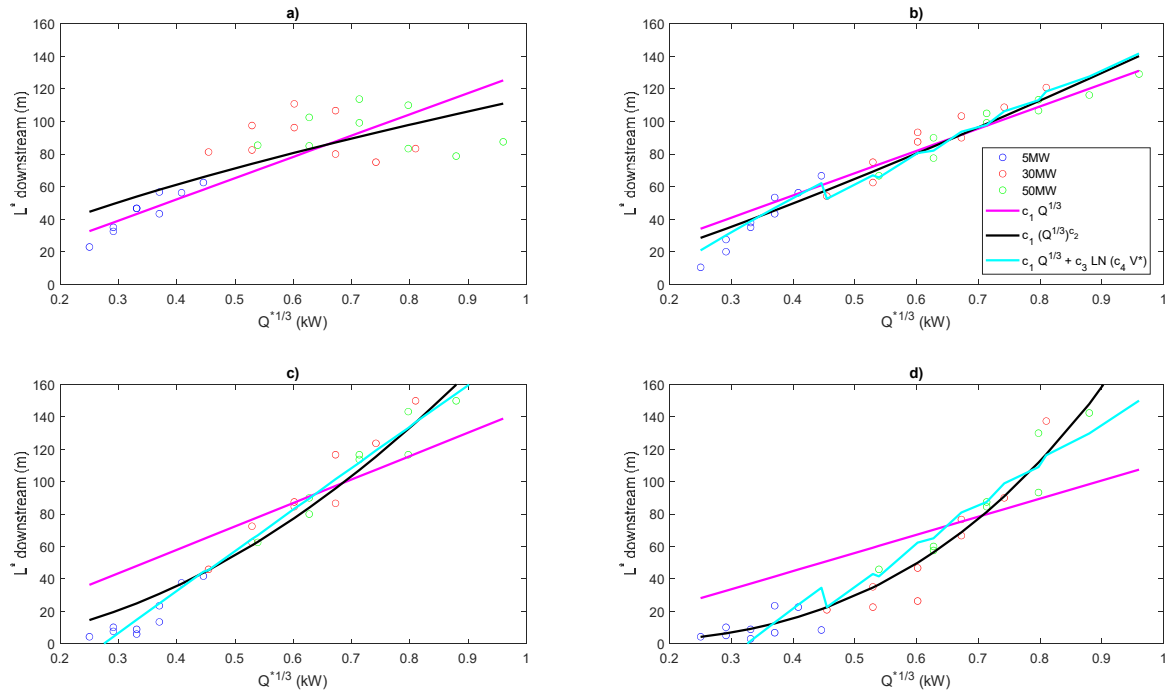


Figure 4: Fitting curves between dimensionless critical length and dimensionless HRR for different ventilation velocities: a) 0 m/s, b) 1.5 m/s, c) 3 m/s, and d) 5 m/s.

5. CONCLUSION

The study presented investigates the downstream critical length of a fire in a tunnel under various ventilation conditions. A total of 108 numerical models are developed, incorporating three different heat release rates (5 MW, 30 MW, and 50 MW), four different ventilation velocities (0 m/s, 1.5 m/s, 3 m/s and 5 m/s), three different widths (6 m, 8 m, 12 m), and three different heights (4 m, 6 m and 8 m). The objective is to assess the influence of HRR and tunnel cross-sectional area on the critical length under different longitudinal ventilation speeds.

It has been observed that a higher HRR leads to an increase in the downstream critical length, resulting in a larger 3D domain, with consequently, higher computational costs. Additionally, the critical length slightly increases as the cross-sectional area decreases. However, for a quantitative analysis, further studies are required. These conclusions are derived from defining the critical length based on the spatial gradient of the tunnel's longitudinal temperature.

Furthermore, adjustments of the data to different fitting models are presented. These models aim to illustrate the dimensionless relationship between the critical length and HRR. It is noted that the linear relationship between HRR and critical length becomes inadequate in the presence of longitudinal ventilation. Notably, the influence of ventilation velocity on the critical length is substantial, significantly enhancing the model's accuracy when appropriately considered.

This study is based on a definition of a critical length through the tunnel's longitudinal temperature gradient, but further analysis on its definition should be studied, for example, through velocity, transverse velocity and temperature distributions, or smoke stratification analysis, among other options, given the vital importance of this parameter in such studies. Additionally, there should be an emphasis on proposing models that allow for the quantification of this critical length under different ventilation conditions.

6. REFERENCES

- [1] A review of tunnel fire research from Edinburgh - ScienceDirect, (n.d.). <https://www.sciencedirect.com/science/article/abs/pii/S0379711216300273> (accessed January 11, 2024).
- [2] L. Yi, D. Luan, L. Yang, T. Chen, H. Tao, Z. Xu, C. Fan, Flow field and fire characteristics inside a tunnel under the influence of canyon cross wind, *Tunnelling and Underground Space Technology* 105 (2020) 103575. <https://doi.org/10.1016/j.tust.2020.103575>.
- [3] A. Król, M. Król, Numerical investigation on fire accident and evacuation in a urban tunnel for different traffic conditions, *Tunnelling and Underground Space Technology* 109 (2021) 103751. <https://doi.org/10.1016/j.tust.2020.103751>.
- [4] M. Weng, I. Obadi, F. Wang, F. Liu, C. Liao, Optimal distance between jet fans used to extinguish metropolitan tunnel fires: A case study using fire dynamic simulator modeling, *Tunnelling and Underground Space Technology* 95 (2020) 103116. <https://doi.org/10.1016/j.tust.2019.103116>.
- [5] Memorial Tunnel Fire Ventilation Test Program. Interactive CD-ROM and Comprehensive Test Report, Massachusetts Highway Department, 1996., (n.d.).
- [6] A. Haack, Fire protection in traffic tunnels: General aspects and results of the EUREKA project, *Tunnelling and Underground Space Technology* 13 (1998) 377–381. [https://doi.org/10.1016/S0886-7798\(98\)00080-7](https://doi.org/10.1016/S0886-7798(98)00080-7).
- [7] T. Yan, S. MingHeng, G. YanFeng, H. JiaPeng, Full-scale experimental study on smoke flow in natural ventilation road tunnel fires with shafts, *Tunnelling and Underground Space Technology* 24 (2009) 627–633. <https://doi.org/10.1016/j.tust.2009.06.001>.
- [8] Runehamar tunnel fire tests - ScienceDirect, (n.d.). <https://www.sciencedirect.com/science/article/abs/pii/S0379711214001660> (accessed February 28, 2020).
- [9] P. Lin, Y.-Y. Xiong, C. Zuo, J.-K. Shi, Verification of Similarity of Scaling Laws in Tunnel Fires with Natural Ventilation, *Fire Technol* 57 (2021) 1611–1635. <https://doi.org/10.1007/s10694-020-01084-9>.
- [10] W. Wang, Z. Zhu, Z. Jiao, H. Mi, Q. Wang, Characteristics of fire and smoke in the natural gas cabin of urban underground utility tunnels based on CFD simulations, *Tunnelling and Underground Space Technology* 109 (2021) 103748. <https://doi.org/10.1016/j.tust.2020.103748>.
- [11] A. Cantizano, P. Ayala, E. Arenas, J.R. Pérez, C. Gutiérrez-Montes, Numerical and experimental investigation on the effect of heat release rate in the evolution of fire whirls, *Case Studies in Thermal Engineering* (2022) 102513. <https://doi.org/10.1016/j.csite.2022.102513>.
- [12] P. Ayala, A. Cantizano, G. Rein, C. Gutiérrez-Montes, Factors affecting the make-up air and their influence on the dynamics of atrium fires, *Fire Technology* 54 (2018) 1067–1091.
- [13] P. Ayala, A. Cantizano, E.F. Sánchez-Úbeda, C. Gutiérrez-Montes, The Use of Fractional Factorial Design for Atrium Fires Prediction, *Fire Technol* 53 (2017) 893–916. <https://doi.org/10.1007/s10694-016-0609-z>.
- [14] M. Król, A. Król, Multi-criteria numerical analysis of factors influencing the efficiency of natural smoke venting of atria, *Journal of Wind Engineering and Industrial Aerodynamics* 170 (2017) 149–161. <https://doi.org/10.1016/j.jweia.2017.08.012>.
- [15] F. Colella, G. Rein, R. Borchiellini, J.L. Torero, A Novel Multiscale Methodology for Simulating Tunnel Ventilation Flows During Fires, *Fire Technology* 47 (2011) 221–253. <https://doi.org/10.1007/s10694-010-0144-2>.

- [16] M. Pachera, X. Deckers, T. Beji, Capabilities and Limitations of the Fire Dynamics Simulator in the Simulation of Tunnel Fires with a Multiscale Approach, *J. Phys.: Conf. Ser.* 1107 (2018) 042016. <https://doi.org/10.1088/1742-6596/1107/4/042016>.
- [17] C. Xu, Y. Li, X. Feng, J. Li, Multi-scale Coupling Analysis of Partial Transverse Ventilation System in an Underground Road Tunnel, *Procedia Engineering* 211 (2018) 837–843. <https://doi.org/10.1016/j.proeng.2017.12.082>.
- [18] D. Álvarez-Coedo, P. Ayala, A. Cantizano, W. Węgrzyński, A coupled hybrid numerical study of tunnel longitudinal ventilation under fire conditions, *Case Studies in Thermal Engineering* 36 (2022) 102202. <https://doi.org/10.1016/j.csite.2022.102202>.
- [19] Y.Z. Li, B. Lei, H. Ingason, Study of critical velocity and backlayering length in longitudinally ventilated tunnel fires, *Fire Safety Journal* 45 (2010) 361–370. <https://doi.org/10.1016/j.firesaf.2010.07.003>.
- [20] J.S. Newman, Experimental evaluation of fire-induced stratification, *Combustion and Flame* 57 (1984) 33–39. [https://doi.org/10.1016/0010-2180\(84\)90135-4](https://doi.org/10.1016/0010-2180(84)90135-4).
- [21] H. Nyman, H. Ingason, Temperature stratification in tunnels, *Fire Safety Journal* 48 (2012) 30–37. <https://doi.org/10.1016/j.firesaf.2011.11.002>.
- [22] K. McGrattan, R. McDermott, S. Hostikka, J. Floyd, FDS (Version 6) user’s guide, Technical report, NIST, 2013.
- [23] Z. Wang, X. Jiang, H. Park, L. Wang, J. Wang, Numerical Investigation on the length of the near-field region of smoke flow in tunnel fires, *Case Studies in Thermal Engineering* 28 (2021) 101584. <https://doi.org/10.1016/j.csite.2021.101584>.
- [24] Z. Wang, X. Jiang, F. Tang, J. Li, Study on critical length for simulation in tunnel fires, *Tunnelling and Underground Space Technology* 115 (2021) 104013. <https://doi.org/10.1016/j.tust.2021.104013>.
- [25] K. McGrattan, M. Bilson, Modeling longitudinal ventilation in tunnels using fire dynamics simulator, *Fire Safety Journal* 141 (2023) 103982. <https://doi.org/10.1016/j.firesaf.2023.103982>.
- [26] J. Ji, F. Guo, Z. Gao, J. Zhu, J. Sun, Numerical investigation on the effect of ambient pressure on smoke movement and temperature distribution in tunnel fires, *Applied Thermal Engineering* 118 (2017) 663–669. <https://doi.org/10.1016/j.applthermaleng.2017.03.026>.

LONGITUDINAL VENTILATION SYSTEM FOR A LONG ROAD-TUNNEL: OPTIMAL DESIGN WITH BATTERIES OF JET FANS AND CHALLENGES TO OVERCOME EXTREME FOGGY WEATHER CONDITION

Sunit Kanti Dhar

Freelance Consulting Engineer - Tunnel Ventilation & Fire Safety and E&M Services, IN

DOI 10.3217/978-3-85125-996-4-38 (CC BY-NC 4.0)

This CC license does not apply to third party material and content noted otherwise.

ABSTRACT

An optimal design solution for a long road-tunnel mechanical ventilation system with an application of batteries of jet fans at a location where extreme foggy weather conditions prevails for a third of the year. The main purpose is to make it practically feasible, by applying the concept of longitudinal ventilation system, as well as optimizing the design to keep the vehicular pollutants under control and fully functional to high standard of international design parameters and criterion, even during heavy fog and rainfall, for normal mode ventilation, particularly during congestion and slow-moving traffic, as well as to cater to an effective smoke management at any probable locations of the fire scenarios.

The design will be innovative for application for such a long road-tunnel with heavy traffic profile, and very practical for application that will harmonize with good engineering practices and international codes and guidelines with an objective to achieve highest standards of safety criteria, both during normal and emergency situations.

Keywords: Design, Foggy, Longitudinal, Road-Tunnel, Ventilation, Extinction Coefficient Fire, Smoke.

1. INTRODUCTION

The purpose of this paper is to identify and address the challenges faced to overcome the extreme foggy weather condition that prevails during rainy climatic conditions for a third of the year in the location of this long road tunnel at a medium altitude hilly terrain.

The longitudinal mechanical ventilation system design philosophy with batteries of jet fans being adopted for this 8.67 km long unidirectional rural parallel twin tube road tunnel with four traffic lanes in each tunnel-bore, because of the terrain and inaccessibility for an intermediate ventilation shaft(s), as well as for the protection of the wildlife and the forest, specifically in the region where these twin tunnels are passing through.

The main purpose is to make it practically feasible, as well as optimizing the design to keep the vehicular pollutants under control and fully functional to high standard of international design parameters and criterion, even during heavy fog and rainfall, for normal mode ventilation, particularly during congestion and slow-moving traffic, as well as to cater to an effective smoke management at any probable locations of the fire incident.

The detailed design of the ventilation system has been independently carried out with both PIARC [1] and RVS [2] guidelines for the vehicle emission and fresh air demand for ventilation calculations. However, in this paper the design with PIARC the methodology, design aspects and details with calculations are discussed here in this paper.

2. DESIGN

2.1 Design parameters under consideration for this case study

2.1.1 Physical design parameters and geometry of unidirectional rural parallel twin tunnels.

Table 1: Physical Parameters and Geometry of the Tunnels

Parameters	Dimensions
Length of the Tunnels:	8.67 Km
Number of Tunnel Bore:	2 tunnels
Number of Lanes per Tunnel:	4 lanes
Maximum Tunnel Altitude above sea level (@ East Portal):	700 m
Tunnel Slope / Gradient:	± 2.0 %
Tunnel Cross-sectional Area:	202 sqm
Tunnel Perimeter:	60 m
Maximum Height at the Tunnel Crown:	9.5 m
Tunnel Width at the Pavement Level:	23.5 m

2.1.2 Traffic Input Data

Table 2: Traffic Profile and Density and Designed Vehicle Speed

Parameters	Dimensions
Annual Average Daily Traffic (AADT)	65,000 vehicles/day
Peak Hour Traffic Volume @ 10% of AADT	6,500 vehicles/day
Therefore, Peak Hour Traffic Volume per Tunnel	3,250 vehicles/hour/tunnel
Henceforth, Peak Hour Traffic Volume per Lane	813 vehicles/hour/lane
Maximum Design Speed of the Vehicles	130 Km/hour

Table-3: Traffic Composition

Category:	Passenger Cars (PC)		Light Commercial Vehicles (LCV)			Heavy Goods Vehicles (HGV)				
	Car	Taxi	LMV	LCV	Mini Bus	Std. Bus	2 Axle	3 Axle	MAV (4-6 Axle)	MAV (>6 Axle)
Percentage:	39%	15%	5%	10%	2%	5%	5%	4%	10%	5%
Fuel Type Composition:										
Gasoline:	23%		1%			-				
Diesel:	31%		16%			29%				

2.1.3 Traffic Output Profile: Calculated [1] for the Peak Hour Traffic with the Data of Table-1, 2 & 3 above

Table 4: Fleet Composition in Both Tunnel at Different Traffic Vehicular Speed [for Down-Hill / Up-Hill Tubes]

Vehicle Speed (Km/hour)	No. of Vehicles in Tunnels	No. of Cars		No. of LCV		No. of HGV		
		Gasoline	Diesel	Gasoline	Diesel	15t	23t	32t
0	3292	764	1013	22	537	165	296	494
10	1536	357	473	10	251	77	138	230
20	1409	327	434	10	230	70	127	211
30	939	218	289	6	153	47	85	141
40	704	164	217	5	115	35	63	106
50	564	131	173	4	92	28	51	85
60	470	109	145	3	77	23	42	70
70	403	93	124	3	66	20	36	60

80	352	82	108	2	57	18	32	53
90	313	73	96	2	51	16	28	47
100	282	65	87	2	46	14	25	42
110	256	59	79	2	42	13	23	38
120	235	55	72	2	38	12	21	35
130	217	50	67	1	35	11	20	33

2.1.4 Basis of Emission criteria being considered for estimation of the vehicular emission and pollution dilution by standard approach [1].

Table-5: Design Emission Criteria

Description	Data
Base Year for the Emission Rates:	2018
Technology Standard Group / Class:	C
Design Year:	2030
Corresponding Time Shift Applicable:	10 years
Therefore, Year of Base Emission Rates for Class C:	2020

Table 6: Design Threshold Values for Emissions

Pollutants	Design Parameters	Equivalent in g/m ³
Carbon Monoxide, CO (ambient)	5 ppm	5.716 mg/m ³
Carbon Monoxide, CO (admissible)	70 ppm	80.031 mg/m ³
Nitrogen Dioxide, NO ₂ (ambient)	0.1 ppm	0.188 mg/m ³
Nitrogen Dioxide, NO ₂ (admissible)	1 ppm	1.878 mg/m ³
Percentage of NO ₂ in NO _x	20%	
Extinction Coefficient (Admissible), K (admissible)	0.005 m ⁻¹	
Extinction Coefficient (Ambient), K (ambient)	0.000 m ⁻¹	

2.2 Fresh Air Flow Rate Demand and Visibility Condition During Dense Foggy Weather

2.2.1 Determination of fresh air demand for standard operation

Fresh Air Flow Rate Demand Calculated [1] for the Peak Hour Traffic at every 10 km/hour intervals from standstill traffic (0 Km/hour) to maximum design vehicular speed of 130 km/hour, for both down-hill and up-hill tunnels by adopting standard approach for the emission estimation [1] along with the Data of Table-4, 5 & 6 above.

Table 7 & 8: Fresh Air Flow Rate Demand for Down-Hill Tunnel & Up-Hill Tunnel

Vehicle Speed (Km/hour)	Table-7: Down-Hill Tunnel				Table-8: Up-Hill Tunnel			
	CO (m ³ /s)	NO ₂ (m ³ /s)	Opacity (m ³ /s)	Max Air Demand (m ³ /s)	CO (m ³ /s)	NO ₂ (m ³ /s)	Opacity (m ³ /s)	Max Air Demand (m ³ /s)
0	29	538	130	538	29	538	130	538
10	44	1077	257	1077	59	1342	311	1342
20	45	1006	295	1006	72	1378	359	1378
30	29	680	236	680	48	1003	302	1003
40	23	486	210	486	44	871	285	871
50	20	371	193	371	39	767	271	767
60	16	312	182	312	38	869	268	869
70	16	273	177	273	41	950	273	950
80	15	250	177	250	43	1053	280	1053

90	14	250	174		250		44	1033	284		1033
100	15	248	177		248		45	1021	282		1021
110	17	282	179		282		56	1051	282		1051
120	21	327	184		327		75	1080	283		1080
130	32	388	190		388		117	1142	290		1142
Max FA Demand	@ Down-Hill Tunnel			1077 m³/s @ 10 Km/h due to NO ₂		@ Up-Hill Tunnel:			1378 m³/s @ 20 Km/h due to NO ₂		

2.2.2 Fresh air demand with respect to foggy weather situations

Also, to evaluate the visibility situations due to extreme foggy weather conditions during monsoon season, fresh air flow rate demand has been calculated for the same peak hour traffic at various vehicular speeds as in sl. no. 2.2.1 above, with enhanced visibility extinction coefficient values – ranging from design value of 0.005 m⁻¹ up to 0.001 m⁻¹. The detailed effects on the fresh air demand at various extinction coefficient values has been summarized in Table-9 below. It has been observed that the maximum fresh air demand requirement in both the down-hill and up-hill tunnels has little or no changes up to extinction coefficient value of 0.002 m⁻¹. However, at extinction coefficient value of 0.001 m⁻¹ there is a significant change in the maximum fresh air demand requirement in both the down-hill tunnel (increases by 37%) and up-hill tunnel (increases by 30%) than that of with the design extinction coefficient value of 0.005 m⁻¹. The effects due to this aspect has been analyzed, for various factors having potential toward affecting visibility inside the tunnel, with detailed study on the optimal design length of light beam, in the subsequent clauses 2.2.3 to 2.2.6, below.

Table 9: Fresh Air Flow Rate Demand Summary for Multiple Extinction Coefficients to Evaluate the Visibility Situations due to Extreme Foggy Weather during Monsoon for Normal Mode Ventilation

Fresh Air Demand with Design Extinction Coefficient:			0.005 m ⁻¹		0.003 m ⁻¹		0.002 m ⁻¹		0.001 m ⁻¹	
Vehicle Speed (Km/hour)	*CO (m ³ /s)	*NO ₂ (m ³ /s)	Opacity (m ³ /s)	Max Air Demand (m ³ /s)	Opacity (m ³ /s)	Max Air Demand (m ³ /s)	Opacity (m ³ /s)	Max Air Demand (m ³ /s)	Opacity (m ³ /s)	Max Air Demand (m ³ /s)
Down-Hill (LHS) Tunnel										
0	29	538	130	538	217	538	325	538	651	651
10	44	1077	257	1077	428	1077	642	1077	1283	1283
20	45	1006	295	1006	492	1006	738	1006	1477	1477
30	29	680	236	680	394	680	591	680	1182	1182
40	23	486	210	486	349	486	524	524	1048	1048
50	20	371	193	371	322	371	483	483	966	966
60	16	312	182	312	303	312	454	454	908	908
70	16	273	177	273	296	296	444	444	887	887
80	15	250	177	250	295	295	442	442	884	884
90	140	250	174	250	290	290	435	435	871	871
100	15	248	177	248	294	294	442	442	883	883
110	17	282	179	282	298	298	446	446	893	893
120	21	327	184	327	307	327	461	461	921	921
130	32	388	190	388	316	388	474	474	949	949
Max Fresh Air Demand @ Down-Hill Tunnel:			1077 m³/s @ 10 Km/h due to NO ₂		1077 m³/s @ 10 Km/h due to NO ₂		1077 m³/s @ 10 Km/h due to NO ₂		1477 m³/s @ 20 Km/h due to Opacity	
Up-Hill (RHS) Tunnel										
0	29	538	130	538	217	538	325	538	651	651
10	59	1342	311	1342	518	1342	777	1342	1553	1553
20	72	1378	359	1378	598	1378	896	1378	1793	1793
30	48	1003	302	1003	503	1003	755	1003	1509	1509
40	44	871	285	871	476	871	714	871	1427	1427
50	39	767	271	767	452	767	678	767	1356	1356
60	38	869	268	869	447	869	671	869	1341	1341

70	41	950	273	950	454	950	681	950	1363	1363
80	43	1053	280	1053	467	1053	701	1053	1402	1402
90	44	1033	284	1033	474	1033	711	1033	1421	1421
100	45	1021	282	1021	470	1021	705	1021	1411	1411
110	56	1051	282	1051	470	1051	704	1051	1409	1409
120	75	1080	283	1080	472	1080	707	1080	1415	1415
130	117	1142	290	1142	483	1142	725	1142	1450	1450
Max Fresh Air Demand @ Up-Hill Tunnel:	1378 m³/s @ 20 Km/h due to NO ₂		1378 m³/s @ 20 Km/h due to NO ₂		1378 m³/s @ 20 Km/h due to NO ₂		1793 m³/s @ 20 Km/h due to Opacity			
Note: * Fresh Air demand remains unaffected for CO & NO ₂ with various Design Extinction Coefficients.										

2.2.3 Determination of Extinction Coefficient

Comparative study of the extinction coefficient with respect to percentage of intensity of the light at the receiver vis-s-vis intensity of the light source, according to extinction coefficient expressed by equation (1), below.

	$K = -\frac{1}{L} \cdot \ln \left\{ \frac{I}{I_0} \right\}$	(1)
--	---	-----

L = Beam length between source and receiver, I_0 = Intensity of the Light Source, I = Intensity of the Light at the Receiver

2.2.4 Dense Fog Analysis

- The mass concentration of PM_{2.5} ($\mu\text{PM}_{2.5}$) is ranged from 121–375 $\mu\text{g}/\text{m}^3$, and the interaction between fog droplets and fine particles is analyzed [3].
- And with the equation 5 [1]: Extinction Coefficient, $K = f_{\text{vis}} \cdot \mu\text{PM}_{2.5}$
Where, f_{vis} is a conversion factor = 0.0047 m^2/mg
 $\mu\text{PM}_{2.5} = 375 \mu\text{g}/\text{m}^3 + 15\%$ (in excess for more safety) = 430 $\mu\text{g}/\text{m}^3$
- Therefore, due to dense fog in the atmosphere the Extinction Coefficient at ambient is, $K_{\text{amb}} = 0.002 \text{ m}^{-1}$

Table 10: Comparative of Visibility Condition & Fog Analysis Visibility Condition vis-à-vis Extinction Coefficient

Parameters	Design Criteria	Comparisons of Visibility Condition						Fog Analysis Visibility Condition		
Extinction Coefficient (Admissible), K_{adm} (m^{-1})	0.005	0.003		0.002		0.001		0.005		0.007
Extinction Coefficient (Ambient), K_{amb} (m^{-1})	0	0		0		0		0.002		0.002
Extinction Coefficient (Difference), $K = K_{\text{adm}} - K_{\text{amb}}$ (m^{-1})	0.005	0.003		0.002		0.001		0.003		0.005
Percentage of Intensity of the Light at the Receiver (I) w.r.t. Source (I_0), I/I_0 (%)	20%	20%	38%	20%	52%	20%	72%	20%	38%	20%
Length of Light Beam, L (m)	322	536	322	805	322	1209	322	536	322	322
Remarks / Observations	More Light beam length @ design I/I_0 ratio & Better I/I_0 ratio @ design Light beam length									

2.2.5 Impact on Fresh air demand vis-à-vis extinction coefficient

The comparative study of Table-10 vis-à-vis Table-9 above reflects that by enhancing the extinction coefficient, resulting considerable enhancement of either the length of light beam or the percentage of intensity of the light at the receiver, the fresh air demand has very little or no changes up to an extinction coefficient value of 0.002 m^{-1} . Therefore, preliminary review and study could be conclusive that during extreme foggy weather conditions in the region the estimated fresh air demand can meet the visibility parameters comfortably up to an extinction coefficient value of 0.002 m^{-1} (i.e., having at least 805 m long light beam with 20% intensity [1] of the light at the receiver or safe design light beam length of 322 m with 52% intensity of the light at the receiver) without any modification in the normal ventilation design criteria adopted, even though quantum of fresh air requirement increases for pollution dilution due to opacity, by considering enhancing admissible extinction coefficient and zero ambient extinction coefficient. But, the fresh air requirement for dilution of NO_2 still governs here in the design criteria of this particular case study, except for certain higher vehicular speed at enhanced extinction coefficient in the down-hill tunnel where fresh air demand is governed due to opacity dilutions. Nevertheless, these have an insignificant impact in the design as the ventilation system been designed for maximum fresh air demand requirement at congested slow traffic movement.

Furthermore, the results of the extinction coefficients with dense fog analysis in Table-10 above indicates that with $K = 0.003 \text{ m}^{-1}$ or 0.005 m^{-1} it shall still be within the acceptable limit of visibility (i.e., having at least 536 m long light beam with 20% intensity of the light at the receiver or safe design light beam length of 322 m with 38% intensity of the light at the receiver or at least 322 m long light beam with 20% intensity of the light at the receiver even when considering in the design with hazy extinction coefficient of 0.007 m^{-1} prevailing inside the tunnel) without any modification in the normal ventilation design criteria adopted, even though quantum of fresh air requirement increases with decreasing differences of extinction coefficient between admissible and ambient for pollution dilution due to opacity, but the fresh air requirement for dilution of NO_2 still governs here in the design criteria of this particular case study.

2.2.6 Visibility Analysis for a Safe Stopping Sight Distance

Safe Stopping Sight Distance (SSSD) is the distance required for a driver to bring the vehicle to a stop after observing any object on the road. It is calculated based on the design speed of the road and the reaction time of the driver. Following formulas [4] are adopted to calculate the SSSD:

$$SSSD = LD + BD$$

LD = Lag or Reaction Distance = $V \cdot tR$

BD = Braking Distance = $V^2 \cdot \left[\frac{1}{2 \cdot g \cdot f + s} \right]$

V = Design Vehicle Speed in metre per second

tR = Reaction Time in seconds

g = Acceleration due to Gravity = $9.81 \text{ metre/second}^2$

f = Coefficient of Longitudinal Friction = $0.35 \sim 0.40$ [5]

s = gradient in %

Table 11: Effects of Visibility Condition due to Safe Stopping Sight Distance (SSSD)

Design Vehicle Speed, V (Km/h)	10	20	30	40	50	60	70	80	90	100	110	120	130
Safe Stopping Sight Distance, SSSD (m)	8	19	32	47	65	85	107	132	159	189	221	255	292
Light Level (i.e., I/I ₀ in %) @ Extinction Coefficient, K = 0.005 m ⁻¹	96%	91%	85%	79%	72%	66%	59%	52%	45%	39%	33%	28%	23%

Note: Therefore, Table-11 vis-à-vis Table-10 above concludes that since the Length of Light Beam, L = 322 m [@ Minimum Acceptable Visibility or Light Level (i.e., I/I₀ = 20%) and Design Extinction Coefficient, K = 0.005 m⁻¹] is Greater than SSSD as well as I/I₀ Ratio at all Design Speed, the adopted Design Basis is safe and holds good.

2.3 Jet Fan Calculation Procedure for Longitudinal Ventilation

2.3.1 Total Pressure and Thrust in the Tunnel

To determine the quantities / number of jet fans required for the longitudinal road tunnel ventilation system it is pertinent to determine the total thrust required to overcome the gross total pressure drops / losses in the tunnel [6].

The total pressure loss and thrust in the tunnel defined by the following equations:

$$\Delta P_{Total} = \Delta P_{ent} + \Delta P_{exit} + \Delta P_{wf} + \Delta P_w + \Delta P_{veh} + \Delta P_{ce} + \Delta P_{fire} + \Delta P_{met} \dots\dots\dots (1)$$

$$T_{Total} = \Delta P_{Total} \times A_{Tunnel} \dots\dots\dots (2)$$

- ΔP_{Total} = total pressure drops (in Pa)
- T_{Total} = total thrust required (in N)
- A_{Tunnel} = tunnel cross-sectional area (in m²)
- ΔP_{ent} & ΔP_{exit} = pressure drops due to tunnel entrance and exit
- ΔP_{wf} = pressure drops due to tunnel wall friction
- ΔP_w = pressure drops due to adverse wind
- ΔP_{veh} = pressure drops / gains due to vehicles / piston effects
- ΔP_{ce} = pressure drops due to chimney effect / fire buoyancy
- ΔP_{fire} = pressure drops due to fire blockage (in fire scenario only)
- ΔP_{met} = pressure drops due to meteorological conditions

2.3.2 Jet Fan Estimation

Number of operating jet fans required for the longitudinal road tunnel ventilation system [6] is calculated by the following equations:

$$N_{Jet\ Fan} = \{T_{Total}\} \div \{T_{Jet\ Fan} \times (\eta_i \times \eta_v \times \eta_\rho)\} \dots\dots (3)$$

- $N_{Jet\ Fan}$ = number of operating jet fans
- T_{Total} = total thrust required (in N)
- $T_{Jet\ Fan}$ = nominal jet fan thrust (in N)
- η_i = installation efficiency
- η_v = velocity derating factor
- η_ρ = density derating factor

2.3.3 Longitudinal Tunnel Ventilation Summary

With the above equations in clauses 2.3.1 & 2.3.2 the results [6] are summarised and tabulated below in Table-12 for the fresh air flow rate demand and visibility condition during dense Foggy weather, as designed at clause 2.2 above, for normal mode tunnel ventilation, as well as for the fire mode ventilation.

Table 12: Battery of Jet Fans for Longitudinal Tunnel Ventilation

Ventilation Parameters	Normal Mode		Emergency (Fire) Mode	
	Down-Hill Tunnel	Up-Hill Tunnel	Down-Hill Tunnel	Up-Hill Tunnel
Maximum Fresh Air Demand (m^3/s) @ Dense Foggy Weather with 0.002 m^{-1} Ext. Coeff.	1077	1378	-	-
Critical Velocity @ Fire size of 200 MW (m/s)	-	-	3.30	3.55
Total Thrust Required (N)	141058	198507	131230	133287
Selected Jet Fan Thrust (N)	2200	2200	2200	2200
Installation Efficiency, $\eta_i =$	0.8	0.8	0.8	0.8
Velocity Derating Factor, $\eta_v =$	0.83	0.79	0.90	0.89
Density Derating Factor, $\eta_p =$	0.87	0.87	0.79	0.82
Total Number of Operating Jet Fans	111	165	105	104
Number of Jet Fans mounted in each location	3	3	3	3
Max equal distance between Jet Fans sets (m)	228	155	241	243
Min recommended distance between Jet Fans sets [7] is $10 \times$ tunnel hydraulic diameter (m)	135	135	135	135

2.3.4 Smoke Management Consideration

In the above Table-12 vis-à-vis explanations given in the above clauses 2.2.2, 2.2.5 & note @ 2.2.6, along-with 1-D Simulation [6] with a Fire size of 200 MW HRR, the number of Jet Fans batteries, required for a design criteria and dense foggy condition for a normal mode longitudinal ventilation system, shall be sufficient for an effective smoke management at the worst probable locations of the fire scenarios. Furthermore, the recommended distance between jet fan sets [7][8] and the economics of the optimization on the design for the installation of these jet fans near the portals [9] are also adhered to.

3. SUMMARY AND CONCLUSION

The above analysis and study with detailed calculations of the longitudinal mechanical ventilation system designed, with batteries of jet fans mounted at the crown of the tunnels, for normal mode operation reflects that even during extreme foggy weather condition the basic acceptable limit of visibility will be achievable without any modification to the system for the selected normal mode ventilation basic design criterion.

Even though the quantum of fresh air requirement increases with decreasing differences of extinction coefficient between admissible and ambient for pollution dilution due to opacity, the fresh air requirement for dilution of NO_2 still governs here in the design because of a very high standard of international design criterion being adopted for nitrogen dioxide.

Furthermore, the longitudinal mechanical ventilation system for normal mode shall also cater to an effective smoke management, up to a fire size of 200 MW HRR, at any probable locations of the fire scenarios, with the selected jet fans specifications and quantities.

It can be concluded that the adopted design is optimized with a very reliable functional requirement achievability for all weather conditions and stringent safety standards.

4. REFERENCES

- [1] PIARC 2019R02EN – Road Tunnels: Vehicle Emissions and Air Demand for Ventilation
- [2] RVS 09.02.32 June 2010 – Tunnel Equipment Ventilation Systems Fresh Air Demand: Air Demand Calculation
- [3] Paper: “*Fog Droplet Size Distribution and the Interaction between Fog Droplets and Fine Particles during Dense Fog in Tianjin, China*” – by Qing Liu, Bingui Wu, Zhaoyu Wang and Tianyi Hao [Read full-text or Download full-text PDF at: https://www.researchgate.net/publication/339761583_Fog_Droplet_Size_Distribution_and_the_Interaction_between_Fog_Droplets_and_Fine_Particles_during_Dense_Fog_in_Tianjin_China]
- [4] Paper: “*Sight Distances: Lecture Notes in Transportation Systems Engineering*” – by Prof Tom V. Mathew [https://www.civil.iitb.ac.in/tvm/nptel/303_SigDst/web/web.html]
- [5] Highway Engineering Design Data Hand Book (Geometric Design & Pavement Design) Compiled by Dr. P. Nanjundaswamy / IRC
- [6] Detailed calculation procedures, 1-D simulation and results are incorporated under a separate design head / volume of this paper. Not able to submit as a part of this paper because it is quite extensive and voluminous to restrict within the stipulation of not exceeding 8 pages. However, if permitted, I can include the same in this paper or submit separately.
- [7] PIARC 05.02.B – 1995: Vehicles Emissions Air Demand Environment Longitudinal Ventilation: *Article IV.2.1 (c) @ page-51 – Longitudinal distance (η_3)*
- [8] 2011 ASHRAE Handbook – HVAC Applications: Chapter-15: Enclosed Vehicular Facilities: Equipment – Fans – Number & Sizes of Fans @ 15.33
- [9] PIARC 05.05.B – 1999: Fire and Smoke Control in Road Tunnels: *Article V.1.2.1; last para @ page-145 – Longitudinal system*

ADVANCED CHARACTERISATION OF A FAN SUBMITTED TO PISTON EFFECT

¹Elisa Béraud, ¹Benoit Houseaux, ²Sydney Tekam

¹Eiffage Énergie Systèmes, Ventilation of tunnel & underground spaces, FR

²Tech'am Ingenierie, FR

DOI 10.3217/978-3-85125-996-4-39 (CC BY-NC 4.0)

This CC license does not apply to third party material and content noted otherwise.

ABSTRACT

In the frame of the "Grand Paris Express" network, Eiffage designed a test cell to test the behaviour of a model fan to the train piston effect. The test cell has already been presented in the last TSV conference. In this paper, it is proposed to focus on the model fan.

The model fan has been first tested by manufacturer in the unexplored area of negative pressure and negative flowrate both in forward and reverse mode. Then it has been operated on the Eiffage test cell with successive negative and positive forced pressure on hundreds of thousands of cycles.

Aeraulic, electric and mechanical parameters recording have been conducted on the model fan during these tests.

The behaviour of the fan in wind milling mode has also been tested in insufflation and extraction mode when submitted to a flow generated by train passage and piston effect.

In parallel, CFD simulations have been conducted on the model fan in steady mode to determine the velocity profile on the blades and to illustrate the passage of air through the impeller with a negative airflow. It has also been carried out for an unsteady case.

Keywords: metro tunnel, train piston effect, model fan, CFD, test cell

1. INTRODUCTION

The piston effect created by train passing in the 200 km of tunnels of the new "Grand Paris Express" network [1] ("GPE") has been estimated to create a variation of + 900 Pa / - 1400 Pa in a few seconds. These pressure fluctuations will be transmitted in the stations and in the service structures where the ventilation equipment is installed.

The fans that will allow the "push-pull" type ventilation and smoke extraction system [2] of the metro will also be operated for normal mode of ventilation.

At reduced speed, the study of operating curves [3] has demonstrated the fans will be passed through with a negative airflow and also operated in negative pressure. Therefore, they will be operated in areas that are not usually defined by the usual.

People involved were aware that the consequences could be dramatic for operation: the fans could be damaged in operational shortly after commissioning and would cause restrictions (or closure) of lines while operating.

2. THE PISTON EFFECT ON FAN

The fans that are installed by Eiffage in the ventilation service structures and train stations of lines 15 South, 16 and 17 of GPE are from Howden. The model ANR-2371/1122 will allow an operation for both fire extraction mode (operating point 1) and normal mode of ventilation (operating point 2).

In case of fire, the fan will generate a flowrate of 150 m³/s and face a network resistance of 1,200 Pa. In normal mode, the fan will work half speed and will generate a flowrate of 75 m³/s for a total pressure of 300 Pa.

The study of operating curves at this reduced speed raised many questions [3]. First it revealed the need for anti-stall treatment. Then it has allowed to investigate how the piston effect will influence the operation of the fan. The effect of train arriving (overpressure of + 900 Pa in the tunnel experienced as decrease of 900 Pa for the fan) suggests that the fan will face negative pressure. This implies *a priori* the operation of the motor as a generator (negative mechanical power). And the effect of train leaving (depression of – 1,400 Pa in the tunnel) suggests the fan will be passed through with a negative airflow even though the fan is still running the same direction.

It appeared the fans would be experienced in operating zones never encountered. As a consequence, they have to be characterized in these zones and have their resistance and durability tested with strong pressure variations.

3. THE MODEL FAN

The consequences of piston effect (both in the thresholds and in the pressure gradients) can be characterized on a model fan. [3] Scale consideration led Eiffage to carry out the tests on a fan with a diameter of 1,000 mm. The model fan is ANR-1000/473.

The ratio between the real size fan diameter and the model fan diameter is 2,371.

In order to have the same blade loading, the tip speed had to be the similar. With a speed of 490 rpm, the model fan had to be performed with a speed of around 1,150 rpm.

With a speed of 1,150 rpm, the Reynolds number calculated on the tip speed and tip diameter is $4 \cdot 10^6$ that is superior to $3 \cdot 10^6$ as recommended by AMCA 802 to avoid scale effect.

The tip speed Mach parameter of the real size fan at 490 rpm is 0.181. The tip speed Mach parameter of the model fan should be inferior to 0.35 in accordance with AMCA-802, which corresponds to a speed of 1,670 rpm.

The requirements for dynamic similarity were respected.

The following table gives the scaling and operating points of the model fan.

Table 1: Real size and model fan characteristics

	Real size	Model
Impeller diameter	2,371 mm	1,000 mm
Hub diameter	1,122 mm	473 mm
	Operating point 1	
Airflow	150 m ³ /s	26.7 m ³ /s
Total pressure	1,200 Pa	1,200 Pa
Rotation speed	980 rpm	2,324 rpm
	Operating point 2	

Airflow	75 m ³ /s	13.3 m ³ /s
Total pressure	300 Pa	300 Pa
Rotation speed	490 rpm	1,162 rpm

4. THE MODEL FAN CHARACTERIZATION

4.1. Aerodynamic test by manufacturer

The test fan had to be characterized by manufacturer for the specified operating points in smoke extraction mode and normal mode. It had also to be tested at negative pressure and negative flow, both in forward and reverse direction. In total, 6 tests had to be conducted.



Figure 1: The tests at manufacturer facilities – Howden Denmark on the left, Howden France on the right

First the model fan has been characterized by manufacturer in Howden facilities (Denmark) in accordance with AMCA 802. The operating curves at 1,150 rpm is presented below:

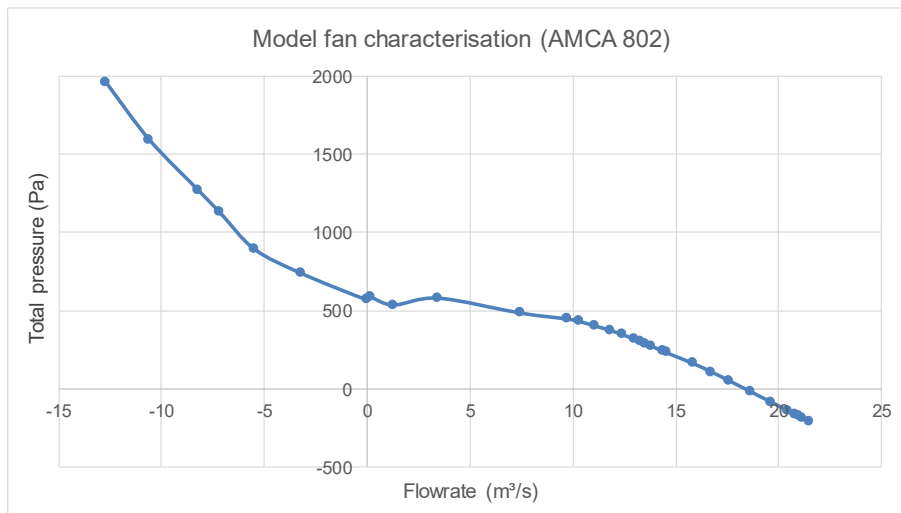


Figure 2: The characterization of model fan according to AMCA 802

Then the model fan has been characterized in accordance with standard ISO 5801 (ex NF X 10-200) in Howden France facilities. The tests have been realized at the speed of 1,470 rpm with many diaphragms that allowed to determine total pressure for a flowrate from 20 to 0.01 m³/s in both directions.

The transposed operating curve is presented on the figure below:

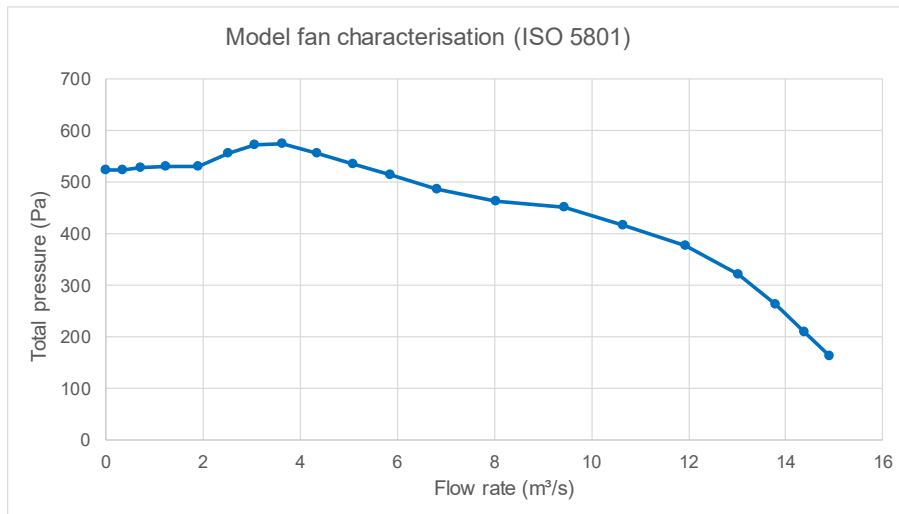


Figure 3: The characterization of model fan according to ISO 5801

The model fan has been tested by two methods: the first one (in Denmark) has allowed to characterize the operating curve in negative airflow and negative pressure; the second one (in France) carried out in a second time has allowed to refine the “stall” zone of the operating curve. Both measurements series are complementary. Even if some differences can be noticed on the curve, the results present a quite satisfactory matching.

4.2. Tests at Eiffage

Then the model fan has been installed and operated on the test cell designed by Eiffage to simulate the train piston effect. Pictures can be found in [4] and below.

The test cell is equipped by many sensors. On each upper and lower ducts of the circuit, there at least two means of airflow determination which could be:

- Vane anemometers;
- Static pressure probes;
- Measurement wings.

There are 3 anemometers: one is placed in the upper duct to measure airflow upstream the fan when operated in negative direction (equivalent to train leaving) and the two others are in the lower duct to measure airflow upstream and downstream the fan when operated in positive direction (equivalent to train arriving).

Flow is also measured with pressure probes in the area of the model fan impeller and the flow straighteners. Moreover, a measurement damper (a classic damper whose blades are fitted with pressure taps [5]) was placed in the upper duct that allow to determine the flow through the duct.

The bench has been calibrating with Pitot probe measurement on 36 vertical and horizontal points on a section with log-Tchebycheff distribution (according to NF EN ISO 5802). All the sections close to anemometers have been tested. In parallel, the “dzeta” or pressure drop coefficient of the grid (or “flow straightener disposal”) that has been added in the duct has been determined.



Figure 4: The model fan with anemometers and pressure probes

The fan is also equipped with vibration sensors. Temperature bearings and windings are also measured. Voltage, intensity, torque, power, etc. are recorded too.

The model fan has been tested on the test platform for several months. More than 400,000 cycles have been performed, corresponding to 400,000 train passing with maximum overpressure and depression, which can be equivalent to an operation over more than 10 years.

Aeraulic data

The flow rates measured are those expected according to the operating curve of the fan. The variation takes place around a nominal flow of 13 m³/s to reach 19.5 m³/s when operated in positive direction and – 8 m³/s when operated in negative direction.

The total pressure maximum and minimum that were measured correspond to those expected. The variations reach a peak around 1,200 Pa in negative flow and another peak around – 200 Pa with flow in the same direction than fan airflow generation.

An example of the model fan total pressure variation is represented below:

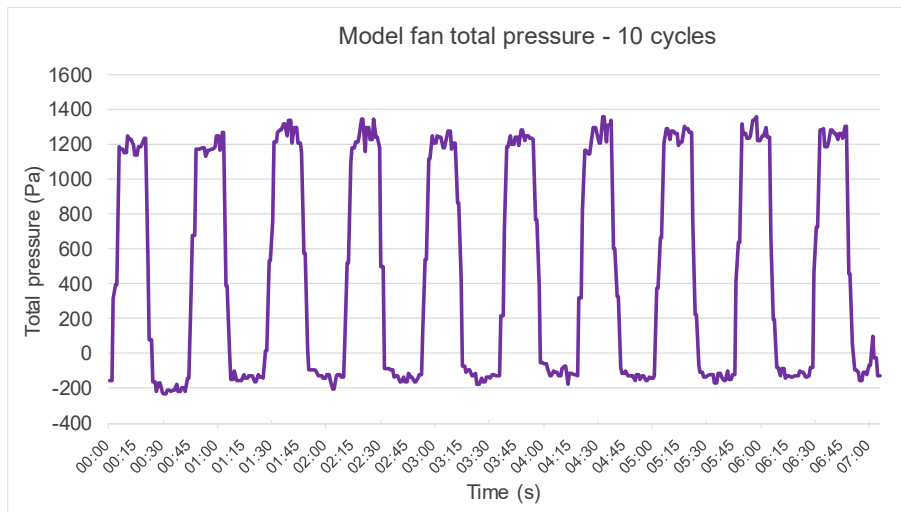


Figure 5: Total pressure variation of model fan

Electric data

This variation is faced by the inverter which accelerates or brakes the motor to meet its parameter settings.

In negative direction, the model fan is facing high pressure. Despite a slight decrease in speed rotation, the motor runs in the same direction (driven by inverter). From an electric point of view, the engine torque increases significantly.

In positive position, the limit of driving by the centrifugal fan (corresponding to an almost zero pressure) is reached. From an electric point of view, the mechanical power at the shaft is then negative. The fan works as a generator.

There is a significant increase in the level of vibration during a complete cycle, while remaining within the acceptable limits defined by standards for this type of fan.

During the 400,000 cycles, no warm-up in the windings or the bearings were measured. The temperatures of the windings were stabilized at 50 °C and those of the bearings at 45 °C.

Mechanical data

Strain gauge measurement have been recorded on 2 blades of the model fan in order to investigate blade stress at train passage. The strain gauges were mounted on both side of one blade and one side another blade.

Stress blade has been measured during a complete cycle from negative air flow under high pressure to negative pressure. The level of stress measured on the blades is of the order of 4 / 5 MPa. A comparable stress level is expected on the real size blades.



Figure 6: Strain gauge on blade

The finite element analysis report provided by manufacturer for the real size fan indicated values of the order of 3.5 / 4 MPa (at the exact position of the gauges). These tests therefore made it possible to conclude to the validity of the calculation note carried out on the real-size blades and to validate the limit of 22.9 MPa for an infinite number of cycles.

5. CFD

The pressure and speed sensors distributed across the test cell allow to determine the air flow rates in the different ducts and on either side of the model fan propeller. However, they do not allow to measure and represent what is happening at the propeller.

The aim is to study, using numerical simulation, the flow in the vicinity of the propeller and particularly between the blades. The profiles on “common” operating points are generally well known; on the other hand, a visualization of the counter-current speed profiles is not well known. To better define the later, a dedicated study of the speed profiles on the blade (from the hub to the tip of the impeller) as well as in the spaces between the blades was performed.

5.1. Mesh and methodology

The mesh is produced in ANSYS MESHING.

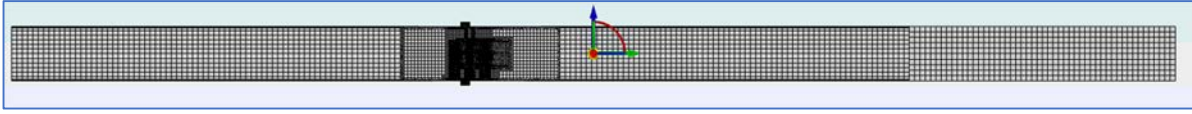


Figure 7: Mesh of platform

Numerous tests were carried out to define the meshing methodology. The latter was chosen as a result from a compromise between accuracy and size of the model. The optimal number of meshes used to model the Ivanov ring was defined to have precise results without generating models that are too large and difficult to use.

The turbulence model k- ω SST was used to account for the flow around the impeller. Wall law is modeled using low y^+ model.

Boundary limits are “mass-flow inlet” to the left of the domain and “pressure outlet” to the right of the domain.

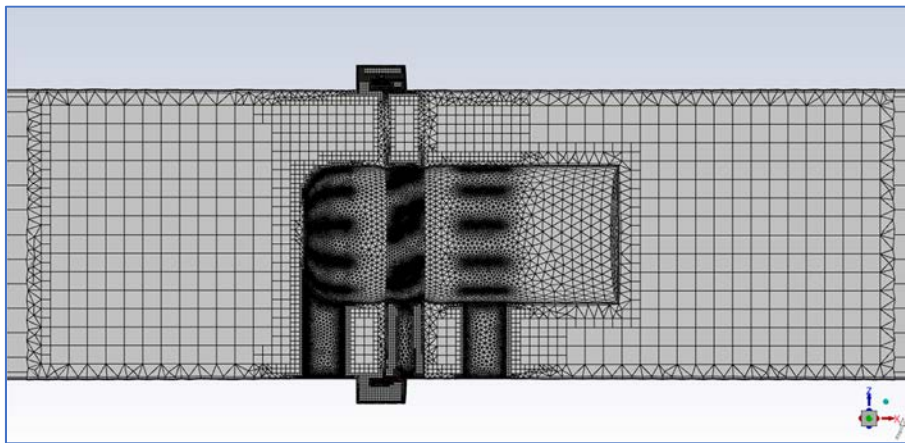


Figure 8: Mesh of model fan

Fan rotation is simulated. It is taken into account in two ways:

- with Multi Reference Frame: the impeller is stationary, and a drive speed is applied in the fluid domain containing the impeller;
- with Sliding Mesh: the impeller physically rotates; the simulation is therefore by definition unsteady.

The simulations and post-processing are produced in ANSYS FLUENT.

5.2. Results

First, steady cases were considered. Six cases with flowrate as input and total pressure difference as output were studied:

Table 2: Steady cases

	Q_v	P_t		Q_v	P_t
Case 1	- 5 m ³ /s	840 Pa	Case 4	11 m ³ /s	410 Pa
Case 2	0 m ³ /s	570 Pa	Case 5	13 m ³ /s	320 Pa
Case 3	6 m ³ /s	510 Pa	Case 6	20 m ³ /s	- 100 Pa

The figure below summarises the results for the 6 cases. It shows the speed at the trailing edge of the blade from the hub to the tip of the impeller. The normal mode ventilation operating point is represented by Case 5.

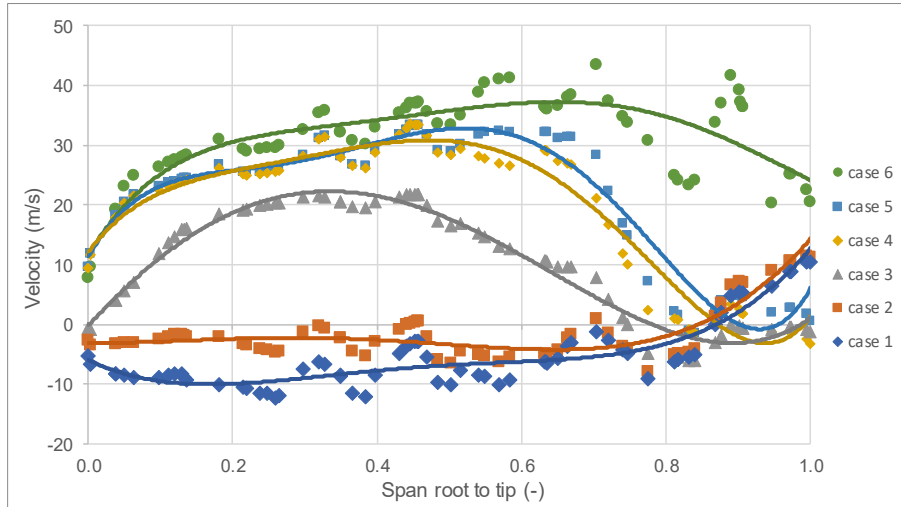


Figure 9: Profiles of axial speeds at the trailing edge of a blade of model fan

It can be noted that for all cases the maximum flow rate through the impeller moves from the root of the blades towards the tip as the flow rate increases.

For the Case 1 and 2, a shear flow is observed at the tip of the blade. As expected for an axial fan with such a blade angle, the negative flow simulated in Case 1 is observed close to the hub. It could be explained also by the presence of Ivanov ring at the periphery.

Other results as streamlines between the blades or velocity vectors in Ivanov ring were recorded for further analysis.

Then unsteady case has been studied. The signal of pressure has been used as input for a flow rate range $[-10 \text{ m}^3/\text{s}; 25 \text{ m}^3/\text{s}]$. Unsteady results will be presented during the conference.

6. CONCLUSION

The test cell has allowed to test the resistance and the durability of the fan submitted to pressure variations with very strong pressure gradients both positive and negative over a very short time interval. Tests with pressure gauges have proven the blade to be compliant to resist millions of cycles.

All these tests have allowed to characterize the behaviour of the fan with significant airflow disturbances in operation. This test cell has confirmed the project stakeholders and especially the owner, Société des Grands Projets, on the resistance and durability of the fans subjected to the piston effect of the trains.

The CFD study has highlighted the flow patterns. It could be kept in mind that maximum flow through the impeller moves from the root of the blades towards the tip and that vortices in the Ivanov ring change from transverse to longitudinal as the flow increases.

7. ACKOLEGEMENT

We would like to thank Aurelien Auzias who conducted the CFD simulations.

8. REFERENCES

- [1] <https://www.societedugrandparis.fr>
- [2] Ventilation et désenfumage des réseaux de métro, P. Carlotti, J.-F. Burkhart, A. Mos, A. Dusserre and J.-M. Passelaigue, Techniques de l'Ingénieur, March 2022
- [3] A model fan to test the train piston effect at Grand Paris Express metro, E. Béraud, B. Houseaux, F. Duet, FAN 2022, Senlis (France), June 2022
- [4] The piston effect test bench for the Grand Paris Express metro, E. Béraud, F. Jouve, B. Houseaux, TSV 2022, Graz (Austria), May 2022
- [5] The measurement damper tested and validated in the B5 ramp, E. Béraud, B. Houseaux, J-Ph. Margrita, ISAVFT 2022, Brighton (UK), September 2002

OPTIMIZING SAFETY IN SHORT HIGH-SLOPE ROAD TUNNELS: SMOKE PROPAGATION AND VENTILATION SYSTEM RESPONSE

¹Krešimir Ivanek, ²Robert Keser, ¹Miodrag Drakulić, ³Željko Špiljar

¹CTP PROJEKT d.o.o., Zagreb, HR

²IN SILICO d.o.o., Zagreb, HR

³INVENTO VENTILACIJA d.o.o., Zagreb, HR

DOI 10.3217/978-3-85125-996-4-40 (CC BY-NC 4.0)

This CC license does not apply to third party material and content noted otherwise.

ABSTRACT

This study focuses on fire protection in short, steep road tunnels, with an emphasis on ensuring passenger safety during evacuation. It introduces a ventilation system designed to address the challenges posed by rapid smoke flow. The system includes a reversible ventilation system in the traffic tunnel tube, accommodating bi-directional traffic, and an overpressure ventilation system in the pedestrian evacuation tunnel.

An early smoke detection feature is integral, rapidly activating the tunnel and the overpressure-protected evacuation gallery ventilation systems, ensuring early warning and passenger safety. The study employs advanced numerical simulations using the OpenFOAM software [1], focusing on a fire scenario with a heat-release rate of 120 MW within the initial 10 minutes, a critical evacuation period. Simulations consider traffic congestion and vehicle shapes.

The findings provide insights into 3D time-dependent smoke propagation within the tunnel, accounting for its unique structure, vehicular obstructions, and buoyant effects from thermal energy release. Results also offer information on the stack effect progression and smoke propagation velocities, crucial for the effective operation of the ventilation system, ultimately enhancing passenger safety during evacuation.

Keywords: road tunnel, steep tunnel, tunnel ventilation, fire, smoke propagation.

1. INTRODUCTION

The focus of this paper is the ventilation system of the Dugi Rat Tunnel, situated on a state road on the Croatian coastline. This tunnel complex consists of two tunnel tubes, each serving distinct functions. The traffic tube spans 852.46 m and facilitates two-way traffic with a single lane for each direction. The evacuation tunnel, spanning 540.2 m, is primarily designated for passenger safety during unforeseen incidents. These two tunnel tubes are interconnected through three cross passages, specifically designed to accommodate pedestrians.

In the process of designing the ventilation system for the Dugi Rat Tunnel, the project team adhered to rigorous safety standards and guidelines. A notable reference point in this endeavor was the application of Swiss guidelines, specifically ASTRA 13002 [2], which addresses ventilation of safety corridors (galleries) in road tunnels. The significance of these guidelines lies in their incorporation of overpressure ventilation for the evacuation tunnel, a critical component for passenger safety. Additionally, ASTRA 13004 [3], focusing on fire detection

in road tunnels, played a pivotal role in shaping the design and implementation of the tunnel's safety measures.

This paper deals with the specific details of the ventilation system's design, with a particular emphasis on how to ensure user safety and efficiency of the tunnel ventilation system. Furthermore, the paper discusses how the designed tunnel ventilation system and the number of fans for a fire scenario were rigorously validated and optimized through comprehensive CFD (Computational Fluid Dynamics) modeling and simulations.

2. MANAGEMENT OF THE VENTILATION SYSTEM OPERATION

2.1. Regular work regime

During the regular work regime, the planned longitudinal ventilation system operates in automatic mode and consists of 8 reversible axial jet fans, organized into 4 pairs (batteries). The intensity of ventilation is determined by the level of pollution, with carbon monoxide (CO) as the predominant gas pollutant, and the reduction of visibility due to the emission of smoke and soot. The ventilation system must adhere to the stricter of the two mentioned criteria. The measurement of CO concentration and visibility is conducted at 2 measuring points using combined visibility and CO sensors.

For reliable velocity measurement and as a precaution against potential damage, 3 combined velocity and flow direction sensors are installed. Airflow speed in the tunnel is kept within a specified range, typically under 10 m/s, regulated by the ventilation SCADA system.

Due to the increased risk of rapid smoke propagation in the tunnel, caused by the high longitudinal slope of 4%, 8 sensors for early smoke detection will be installed. These sensors play a crucial role in controlling the ventilation system during fire incidents (more details in Section 2.2). The measurement data generated by these sensors is remotely transmitted to the control and monitoring center. Based on the measurement data, individual fans, batteries, or groups of batteries are automatically activated, utilizing specialized software that manages the operation of the ventilation system.

Operating criteria for ventilation system were selected according to the Austrian guidelines RVS 09.02.31 [4].

2.2. Fire regime

During the fire regime, two points of interest will be discussed: the traffic tunnel tube and parallel evacuation tunnel tube for pedestrians.

When a fire occurs in the traffic tunnel tube and the alarm is confirmed, the overpressure ventilation system of the evacuation tube is activated, and the ventilation system operates depending on which of the 3 action zones the fire occurred in (see Fig. 1).

If a fire occurs in the 1st operating zone (from 0 to 190 m), the ventilation system automatically activates the farthest jet fans - specifically, fan batteries no. 4 and 3 - directing air flow towards the lower portal. The precondition for this is that their neighboring smoke sensors, SS-7, and SS-5, are not triggered by smoke. This strategy is known as the "Fire-eject" [5] from the tunnel, designed to prevent smoke from spreading by buoyancy towards the higher portal, which would fill a large part of the tunnel and in this way achieve a "chimney effect" with a high buoyancy smoke flow. This flow can pose danger or even entirely prevent

the evacuation of passengers. In the smoke-free section of the tunnel tube, the airflow speed should be greater than or equal to the critical flow velocity, v_c . For the given conditions of an undeveloped fire and the tunnel’s geometry, the critical flow velocity, v_c , is 2.9 m/s.

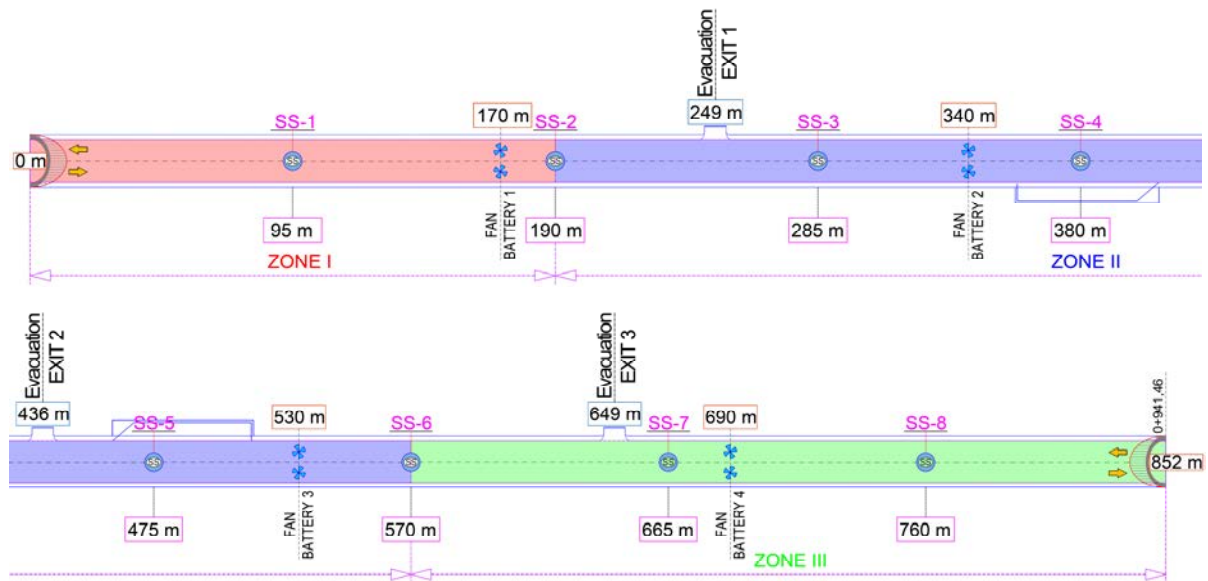


Figure 1: Diagram of the action zones of the ventilation system and sensors for early fire detection
Source: CTP Projekt d.o.o.

If a fire occurs in the 2nd operating zone (from 190 to 570 m), the ventilation system is automatically switched off and does not participate in the smoke control process. Insights from fires in similar tunnels [6], along with the results of the CFD analysis of fire and smoke development made for Dugi Rat Tunnel, revealed high velocities of smoke propagation towards the higher portal of the tunnel. Specifically, the buoyant smoke propagation velocities, as per the results of CFD modeling, reached up to 4.7 m/s for fires with a heat release rate (HRR) of 20 to 120 MW, as detailed in Section 3. Given this data, the designer believes that involving ventilation during rapid smoke propagation could only contribute to additional smoke turbulence and expedite the filling of the tunnel tube with smoke across its entire cross-section. Moreover, the ventilation management system is too slow to be able to efficiently handle ventilation in fire conditions in a short tunnel with a relatively large longitudinal slope, such as the Dugi Rat Tunnel.

If a fire occurs in the 3rd operating zone (from 570 to 852 m), the ventilation system automatically activates the fans of battery no. 1, and then battery no. 2, with the flow directed towards the higher portal, provided that their neighboring smoke sensors, SS-2 and SS-4, are not triggered by smoke. This sequential activation aims to align the operation of the ventilation system with the natural direction of smoke flow towards the higher portal, with the goal of containing smoke within the shorter part of the tunnel. The airflow velocity, maintained by the ventilation system, should range from 1.5 to 2.0 m/s towards the upper portal. This setup is designed to counteract the potential influence of the wind, which might otherwise direct the airflow towards the lower portal, potentially causing smoke to accumulate in the longer part of the tunnel. If the air flow velocity in the initial phase of the fire exceeds 2 m/s towards the upper portal, the ventilation system will not be activated.

The implementation of overpressure ventilation in the evacuation tube is a crucial measure for active fire protection in the Dugi Rat Tunnel. This measure is designed to ensure the safety of passengers throughout the entire evacuation process to a secure open space. The overpressure

ventilation system’s primary objective is to prevent smoke infiltration from the fire-endangered tunnel tube into the evacuation tunnel. By doing so, it maintains a safe passage for the evacuation of passengers, even in conditions of rapidly expanding smoke buoyancy toward the higher portal of the traffic tunnel tube, influenced by the fire.

Figure 2 illustrates a cross-section of an emergency exit featuring two partitions. The first partition is fireproof, situated between the traffic tunnel and the crosswalk (exit) for pedestrians, which maintains a 25 Pa overpressure. The second partition is positioned between the crosswalk and the evacuation tube, which maintains a higher overpressure of 50 Pa. Each partition within the three crosswalk exits is equipped with two pressure relief dampers. Additionally, the fireproof partition is fitted with smoke dampers, designed to open exclusively during the activation of the overpressure system.

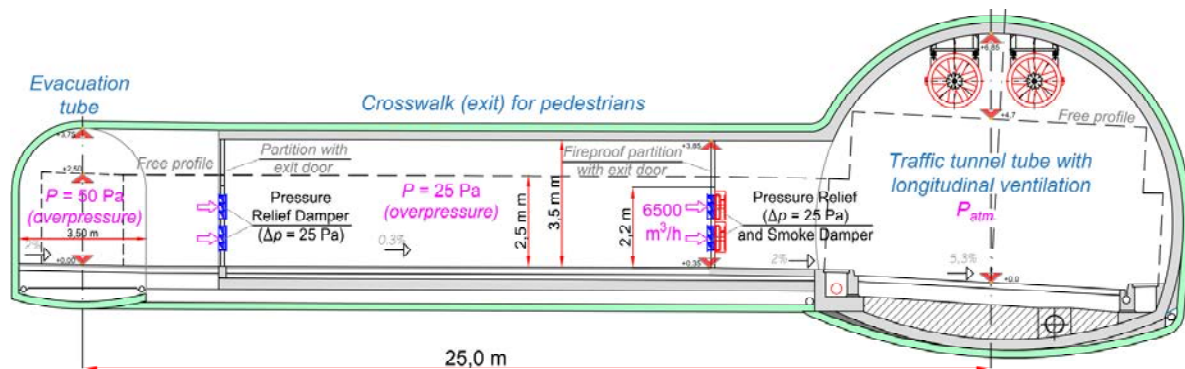


Figure 2: Cross-section of the traffic tunnel tube and the evacuation tunnel for pedestrians

Source: CTP Projekt d.o.o.

A mechanical ventilation system, designed to provide a high-capacity and reliable supply of fresh air in fire conditions, is employed to establish an overpressure condition along the entire length of the evacuation tunnel. The primary components of this system are two ventilation units situated in the engine room above the air-lock room (smokeproof enclosure) at the exit of the evacuation tube. One ventilation unit functions as the primary unit, while the other serves as a stand-by unit, activated only in the event of a failure or error in the primary ventilation unit. The role of the primary ventilation unit can be programmatically altered as part of the ventilation management system.

3. NUMERICAL SIMULATION OF SMOKE PROPAGATION AND VENTILATION SYSTEM RESPONSE

3.1. Numerical model

The numerical simulations were conducted using the OpenFOAM (v2112) open-source simulation toolbox [1], primarily utilized for solving problems in the field of continuum mechanics, particularly in computational fluid dynamics. The simulations utilized a transient model for buoyant, turbulent flows of compressible fluids. The fire scenario within the tunnel was simulated as a variable source of both heat and smoke. The model does not consider the chemical reactions due to combustion; instead, it treats the smoke as a passive scalar represented by carbon dioxide concentration levels. The carbon dioxide is propagated through the computational domain using a standard transport equation that incorporates the effects of both advection and diffusion.

In the context of fire modeling, the study adopts a strategy where a specified fraction of the total heat generated is assumed to escape into the environment via radiation without affecting the gas within the tunnel (approx. 30%). The remaining energy is transferred to the surrounding gas. Figure 3 presents the employed HRR curve, in the initial phase of fire, where the thermal power increases quadratically. The used scenario of 120 MW primarily defines the fire growth coefficient (α) for the HRR calculation. However, within the scope of interest of this study, which is the initial 10 min., the fire does not reach the full fire load of 120 MW.

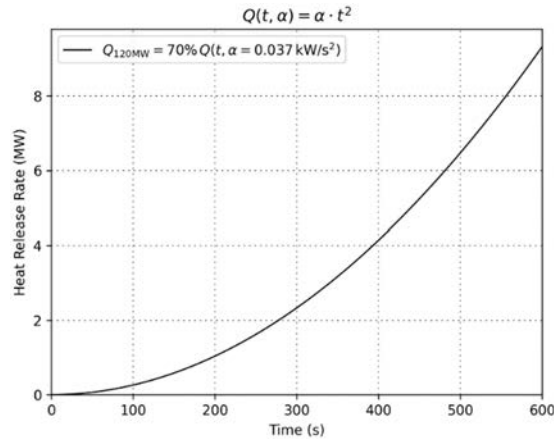


Figure 3: HRR curve - thermal power increase

Figure 4 depicts the simplified geometry of the traffic tunnel, serving as the base for creating the computational mesh. The mesh consists of approx. 2.5 million cells, each with a mean dimension of 0.3 m. The volumetric heat source is positioned 230 m from the tunnel's lower entrance. Table 1 presents the temporal behavior of the heat source, i.e., volume of the fire as a function of time. Additionally, the simulations account for the impact of traffic congestion. To mirror the bidirectional traffic, vehicles are strategically placed at 15-meter intervals in both directions relative to the fire's origin, with 15% of lorries in total vehicle volume.

In the simulation of the Fire-eject strategy, axial fans were modeled as volumetric sources of momentum. This involved assigning specific velocity values to the computational cells within the fan regions, based on specifications provided in the manufacturer's datasheet.

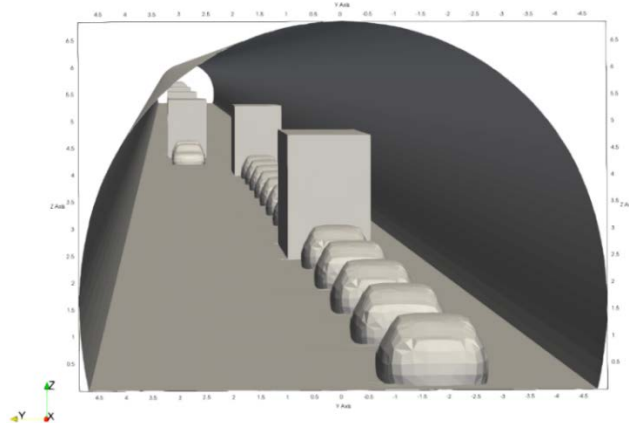


Figure 4: Simplified geometry of the traffic tunnel

Table 1: Behavior of the volumetric heat source

	$0 < t \leq 200$	$200 < t \leq 400$	$400 < t \leq 600$
$V(t)$	12 m^3	36 m^3	60 m^3

3.2. Ventilation-off strategy

This analysis provides insights into smoke propagation and the progression of the stack effect within the tunnel for the previously defined 120 MW fire scenario when the ventilation system does not participate in the smoke control process. Figure 5 illustrates the regions impacted by smoke along the longitudinal section for various time intervals (100, 200, 300, 400, 500, and 600 seconds). Zones with a carbon dioxide concentration exceeding 0.1% are indicated in black. Results at 400 and 500 s suggest that the stack effect is becoming powerful enough to push the already propagated smoke (from the lower section) towards the upper portal.

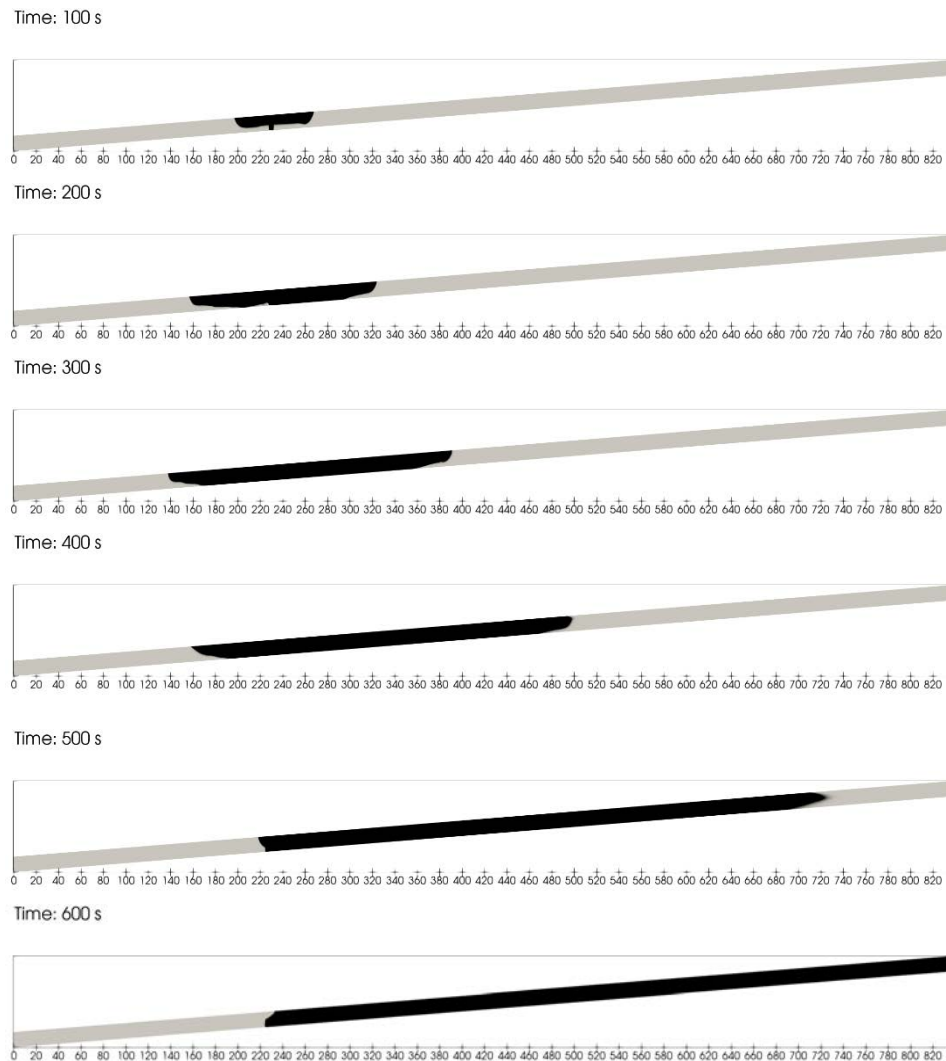


Figure 5: Smoke propagation and progression of the stack effect within the tunnel for a 120 MW fire scenario

3.3. Fire-eject strategy

To compare the smoke behavior between the Fire-eject strategy and the Ventilation-off strategy, we utilize the same fire setup, maintaining consistency in terms of location and Heat Release Rate (HRR) curve. Despite the chosen location being situated outside the 1st zone of action as illustrated in Figure 1, where the Fire-eject strategy would typically be activated, this is a deliberate choice aimed at demonstrating the ventilation system's capability to manage slightly greater distances when ejecting smoke.

However, when smoke reaches the closest sensors, SS-2 and/or SS-3, approximately 140 s, in accordance with the management strategy outlined in Section 2, the control system activates

fan batteries 3 and 4. These fans start to push the smoke towards the lower portal. To ensure an adequate safety margin, the simulation incorporates a 20 s delay, and a 10 s ramp-up time for the axial fans.

Figure 6 illustrates the smoke distribution at 160, 200 and 250 s, showcasing the capability of the selected ventilation system to successfully stop the development of the stack effect and push the already accumulated smoke within the tunnel towards the lower portal. Furthermore, Figure 7 presents the sampled longitudinal velocity at 271 m from the lower portal, the location of the combined velocity and air flow direction sensor. The solid red line represents the sampled velocity for the Ventilation-off strategy, and the dashed blue line depicts the velocity for the Fire-eject strategy. Both curves have identical behavior until the activation of axial fans. Shortly after the activation, the flow direction sensor would detect a change in the air-flow direction, as demonstrated by the smoke distribution images.



Figure 6: Smoke distribution in the Fire-eject strategy

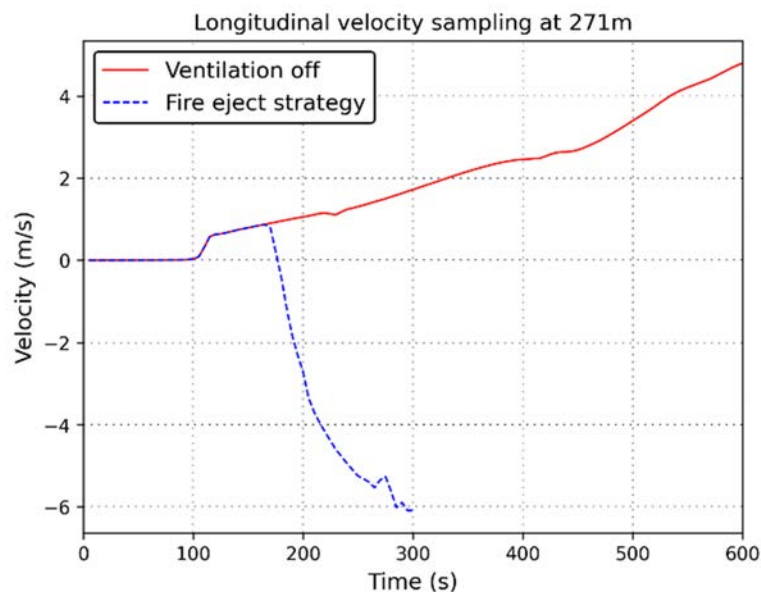


Figure 7: Longitudinal velocity at 271 m from the lower portal

4. SUMMARY AND CONCLUSION

The role of the ventilation system in fire conditions in short steep tunnels is very delicate, primarily due to the rapid propagation of smoke towards the higher portal caused by intense thermal buoyancy. In the Dugi Rat Tunnel, velocities of buoyant smoke flow, determined through Computational Fluid Dynamics (CFD) simulations, can reach up to 4,7 m/s in the observed interval of time (600 s) and corresponding heat release rate. These high velocities of smoke propagation highlight the need for a fast and efficient evacuation of passengers. Active operation of the ventilation system becomes essential when it can justifiably contribute to a better and safer evacuation.

The results presented in this paper demonstrate that, in the initial fire phase with a reliable system for fast smoke detection, the ventilation system can successfully expel smoke from the tunnel using a "Fire-eject strategy." This strategy proves particularly effective when the fire occurs in the lower third of the tunnel tube, representing the most dangerous fire scenario. In other fire scenarios, the potential for the ventilation system to positively contribute to the evacuation process is minimal (e.g., the upper third of the tunnel) or even counterproductive (e.g., the central part of the tunnel). Unrealistic expectations should not be placed on the ventilation system due to its inherent aerodynamic inertia and the limited ventilation resource in short tunnels. Therefore, a reliable passenger protection system should be provided throughout the evacuation process. The overpressure ventilation system of the evacuation tunnel, described in this paper, effectively combines passive and active protection measures for tunnel users.

To fully confirm the described ventilation strategy in short steep tunnels, the effects of surrounding factors, notably the influence of wind on the tunnel portals, must be considered. This requires further numerical simulations that incorporate local climatological parameters and terrain characteristics. Complete validation depends on operational experiences with this relatively complex tunnel tube ventilation system and the overpressure ventilation of the evacuation corridor for passengers, including rapid smoke detection.

5. REFERENCES

- [1] OpenFOAM v2112, ESI-OpenCFD. Available from: <https://www.openfoam.com/news/main-news/openfoam-v2112>
- [2] ASTRA 13002: Lüftung der Sicherheitsstollen von Strassentunneln. 2008
- [3] ASTRA 13004: Branddetektion in Strassentunneln, 2007
- [4] RVS 09.02.31: Tunnel equipment, Ventilation, Basic principles, 2014
- [5] Zumsteg F., Steinemann U., Berner M.: Ventilation and Distance of Emergency Exits in Steep Bi-Directional Tunnels, Conference “Tunnel Safety and Ventilation”, Graz 2012
- [6] Viamala tunnel in Switzerland: *Tunnel fire death toll rises*. (2006, September 18). SWI swissinfo.ch, <https://www.swissinfo.ch/eng/tunnel-fire-death-toll-rises/5452828>

HOW INFORMATION SECURITY CAN BE ENSURED IN TUNNEL SYSTEMS

Gerhard Hudecek

ASFINAG Maut Service GmbH, AT

DOI 10.3217/978-3-85125-996-4-41 (CC BY-NC 4.0)

This CC license does not apply to third party material and content noted otherwise.

ABSTRACT

Based on Directive (EU) 2016/1148 of the European Parliament, the European Cyber Security Strategy [1] was transposed into Austrian law (NIS Act) at the end of 2018. The aim was to ensure a high level of security of network and information systems. The requirement was to take appropriate and proportionate technical and organisational security precautions and to report security incidents.

ASFINAG, as the Austrian motorway operator, was identified as the operator of elementary services by notice dated 12.11.2019. One of these essential services is tunnel control. By 11.11.2022, proof of NIS conformity had to be provided to a so-called qualified body.

A tunnel system is now equipped with a large number of IT and OT systems and components. These are connected with each other and connected to remote monitoring centres for control and monitoring. This creates a multitude of potential security risks, which can lead to an impairment of the function of safety equipment and to a reduction in the availability of the tunnel.

Until the establishment of the NIS Act (NIS-G) [2], ASFINAG very successfully pursued the strategy "never touch a running system". I.e. it was well planned, well built and well maintained. Software changes were avoided as far as possible. In order to comply with the NIS-G, this strategy had to be completely changed to "keep the system up-2-date", which means very frequent software changes. ASFINAG currently operates 167 tunnel systems, so the NISFIT © programme was developed on how to make these systems "cybersecure". In order to achieve a sufficient level of information security, the following key points must be addressed: A seamless IT asset management in order to know where which systems and components are installed and in operation, as well as to be able to assess potential risks.

Another important element is physical security on site as well as remote access management. Only those persons who are authorised to do so should be allowed secure access. Thirdly, active monitoring of the systems, including regular virus scans and penetration tests, is required. To make all this possible, as well as the requirement to report security incidents within the specified time, a Security Operation Centre (SOC) has been implemented.

In the end, ASFINAG succeeded in proving to the auditing authority in due time that all necessary measures for network and information system security (NIS) had been implemented.

Keywords: Information Security, Cybersecurity.

1. INTRODUCTION

Apart from artificial intelligence, there is hardly any other topic in information technology that is more prominent in the media of all kinds than information security, also often referred to as cybersecurity. The reason for this is the rapid progress of digitalisation, which affects all

areas of life, especially the economy in all its sectors. Every use of hardware and software increases the risk of external attacks, while digitalisation leads to increasing networking, which increases the variety of attack vectors. Attack vectors include phishing emails, malware infections, vulnerabilities in software that enable malware to be executed, but also insecure networks that allow attackers to penetrate hardware and software or spy on data traffic - a colourful bouquet of possibilities.

Cybersecurity affects every system. Pure IT systems - there are constant reports of successful attacks on companies and authorities that have been affected by successfully introduced ransomware with fully encrypted and therefore no longer usable data. But also, OT systems - probably the most famous case is the successful attack on the Iranian nuclear programme back in 2010. Stuxnet was specially developed to attack a monitoring and control system (SCADA system) that uses Siemens Simatic S7 programmable logic controllers.

It is clear from this that all systems that support our lives and processes are potential targets, regardless of the technology used. Such systems are also referred to as critical infrastructure and as such also affect road transport facilities as a whole and tunnels in particular.

2. CRITICAL INFRASTRUCTURE – ESSENTIAL SERVICES

The European Union has defined a cybersecurity strategy based on Directive (EU) 2016/1148 of the European Parliament. The aim was to ensure a high level of security of network and information systems. The requirement is to take appropriate and proportionate technical and organisational security precautions and to report security incidents. At the end of 2018, this directive was also transposed into Austrian law, the so-called NIS Act. As NIS2 is now specifically dealt with, we refer to it here as NIS1.

The Austrian authorities had to determine who is an operator of essential services in Austria and which critical infrastructure is declared as an essential service. Sectors were defined that must achieve a high level of security for network and information systems. These include:

- Energy
- Banking
- Financial market infrastructure
- Health sector
- Drinking water supply and distribution
- Digital infrastructure
- and transport!

In November 2019, ASFINAG, as the operator of all Austrian motorways and highways, was therefore sent a notice in which the following two essential services were defined as particularly worthy of protection:

- Traffic control on highways
- Traffic control in tunnels!

ASFINAG now had 36 months from receipt of the notice to prove that these two essential services meet the high cyber security requirements. The fulfilment of these requirements was checked by an auditor, a so-called qualified body. The fact that 36 months is very short can be explained by the fact that the authority assumed that these services would be operated with

appropriate security precautions anyway and that 36 months is therefore sufficient to provide evidence.

This review of the suitability of the security measures in place was divided into four areas and eleven categories:

Table 1: Categories of security

#	Area	#	Category
A	Governance and ecosystem	1	Governance and Risk management
		2	Dealing with service providers, suppliers and third parties
B	Protection	3	Security Architecture
		4	System Administration
		5	Identity and Access Management
		6	System Maintenance and Operation
		7	Physical Security
C	Defence	8	Incident Detection
		9	Incident Management
D	Resilience	10	Business Continuity
		11	Crisis Management

In contrast to many other standardisations, there are no concrete specifications for NIS1 as to which exact security precautions must be implemented in which way in order for the qualified body, i.e. the auditor, to give a positive assessment. There is no helpful checklist. There are three ratings for the review regarding the effectiveness of measures:

- **effective**, i.e. the auditor determines that the implemented measures are effective
- **partially effective**, i.e. improvements are required
- **not effective** i.e. the implemented measures are not effective > The objective has not been achieved.

The special challenge is that only a **single ineffective** measure in a category leads to the entire category being **not effective**; this applies analogously to partially effective. Consequently, each individual measure must be effective in each category in order to achieve an effective rating in all categories.

3. THE PROGRAMME

Although ASFINAG has placed a special focus on information security for many years, it quickly became clear after the NIS Act and the notice were issued: the goal to provide positive evidence to a qualified body could only be achieved with a concentrated effort, as a whole range of measures had to be implemented. In addition, many of these measures were interdependent and could only be implemented on time and with sufficient quality with overall control, meaning that multi-project management was required. Based on this recognition, the **programme NISFIT © - Network and Information System Security Fitness** - was launched.

The aim of the programme was to centrally manage all measures, from the risk analysis of essential services to ensuring all documentation Furthermore to regularly report progress to ASFINAG management, as well as to identify essential obstacles and bring about the necessary decisions via a ASFINAG-Group-wide steering committee.

In order to implement information security to a suitable extent, the following must be considered essential:

- ISMS - Information Security Management System
 - Review and revision of emergency concepts, emergency manuals and emergency plans
 - Review and revision of the existing crisis handbook
 - Creation of information security implementation concepts for each service in the scope
- Process analysis
 - Analysing which processes require adjustments in order to be able to establish information security sustainably.
- Scope definition
 - Determining what the scope is: Which associated services make up the essential services
- Risk analysis
 - Using a GRC tool (Governance, Risk and Compliance)
 - Business impact analysis
 - Gap analysis of the affected services based on previous modelling
 - Project definitions derived from this in order to close the gaps in the services in the scope in a targeted and timely manner.
- Asset management
 - Which components make up the services in the scope, both hardware and software. In order to be able to assess a risk or take protective measures in a given case, it must be known what is being used and where.
- Physical access protection
 - Premises in which the components from services in scope are installed must be secured against unauthorised access - development of a zone concept.
 - Derived from this, project definition for establishing access protection in order to establish physical access protection in a targeted and timely manner.
- Dealing with third parties
 - Contractors must be involved. Complete authorisation must be ensured with regard to access and access by third parties.
 - It must be made clear to suppliers and service providers that information security is given special attention.
- Remote access
 - It must be ensured that networks, systems and services are accessed via controlled and secure channels. This also includes secure file transfer to prevent malware from being introduced into the ecosystem.
- User administration
 - Regardless of whether it is your own staff or third parties, every single user must be known and authorised - Physical Identity and Access Management PIAM. The personal handling of information security must be trained in a sustainable manner.
- Protective measures
 - Centrally controlled virus protection on all systems, log management, monitoring
- Defence
 - The establishment of a Security Information and Event Management (SIEM) and a Security Operation Centre (SOC) is necessary to ensure the highest possible level of protection for the network and services. This is the only way to achieve 24/7 detection and defence against attacks.

It is clearly that many projects and measures must be implemented in parallel in order to be able to successfully provide evidence of information security in accordance with the NIS Act

to the qualified body in time - the need for programme management can be clearly derived from this.

4. IMPLEMENTATION OF THE NISFIT © PROGRAMME

In parallel to the countless measures and projects that secure ASFINAG's overall system externally, both technically and organisationally or procedurally, all tunnel facilities were analysed in depth. It was clear from the beginning that ASFINAG's previous very successful strategy "never touch a running system", that means it was well planned, well built and well maintained, and software changes were avoided as far as possible, would have to be completely changed to "keep the system up-2-date", which force frequent software changes.

First, the so-called target state had to be achieved, following a clear priority: ASFINAG operates almost 90 tunnels that are subject to the STSG (Road Tunnel Safety Act). The control systems of these tunnels, specifically the SCADA systems, and, where applicable, the local control systems (PLC) were comprehensively renewed or brought up to the latest technical standard. This means that the server infrastructure was replaced with Hyper Converged Infrastructure systems, which are high-performance and redundant server infrastructures that enable very high availability and simple manageability with several virtual machines. The applications and databases themselves were migrated to the latest version to achieve the best possible security. The local PLCs whether hardware or software PLCs, were also replaced where necessary or at least upgraded to the latest software version. In addition, centralised virus protection was implemented, and the prerequisites were created to enable regular software updates (patch management) to be carried out with the least possible effort.

These migration projects were not only a technical challenge, but they also had to be tested extensively, as tunnel safety naturally has top priority. Both required full tunnel closures or at least partial closures. The need for very high availability of the tunnel facilities in order to minimise disruption to traffic was no less of a challenge than the technical aspects. This is because, regardless of the establishment of NIS1 compliance, other ASFINAG renovation projects also cause traffic-impairing measures, which required complex and time-consuming coordination with various ASFINAG organisational units.

Clarification works also had to be carried out in advance with the tunnel administration authority to make clear, that these migration projects would not change the functionality approved by the authority during the construction or latest renovation of the tunnel.

A major effort, which was always carried out in advance of the migration works, was checking the installed assets and updating the asset information in the Configuration Management Database (CMDB).

Part of the migration projects was the creation of the so-called information security implementation concepts, which help to ensure that the necessary measures were also implemented in a comprehensible manner.

5. THE PROOF

All measures from the 11 categories were reviewed in 4 partial audits by the so-called qualified body and the reports were sent to the Austrian DSN (Directorate of State Security and Intelligence). The audits were also carried out on site, primarily to be able to check the requirements for property protection and access protection. Ultimately, the measures in all 11 categories were assessed **positive** by the authority.

6. THE CHALLENGES

Protection of buildings was particularly challenging, as the necessary measures went beyond all the partial responsibilities of different organisational units at ASFINAG. In addition, the geographical distribution of the properties - and these are not just the tunnels, but all premises that host components that are in the scope of the essential services - also contributed to the complexity. The realisation of the construction measures was not only costly, but also difficult in terms of time. Here, the programme management raised awareness accordingly and brought about decisions with the necessary consistency.

The time resources and information security expertise of the individual employees responsible for the individual services in the scope had to be supported. These support resources were also procured and provided and managed by the programme management.

7. CONCLUSION

Only by deciding to launch the NISFIT © programme was ASFINAG able to successfully implement all measures on time. In addition, the programme management initiated the long-term safeguarding of the level of information security achieved by making information security part of ASFINAG's day-to-day business in all processes and planning procedures.

Mission accomplished!

8. REFERENCES

- [1] <https://eur-lex.europa.eu/legal-content/DE/TXT/?uri=CELEX%3A32016L1148>
- [2] <https://www.ris.bka.gv.at/GeltendeFassung.wxe?Abfrage=Bundesnormen&Gesetzesnummer=20010536>

ONE-DIMENSIONAL CRITICAL VELOCITY FORMULATION – AN ASSESSMENT OF THE DEFICIENCY OF THE CURRENT MODELS, AND THE INTRODUCTION OF A NEW CONCEPT

J. Greg Sanchez
TYLin International, US

DOI 10.3217/978-3-85125-996-4-42 (CC BY-NC 4.0)

This CC license does not apply to third party material and content noted otherwise.

ABSTRACT

A review of the most classic set of critical velocity (V_c) equations in the tunnel ventilation industry is presented. Assumptions, and limitations in the derivation of V_c are explained. A new methodology is presented, which takes into account the fundamental laws of physics described in the conservation of mass, momentum, energy, and combustion. Simple, but robust enough to capture the different velocities, temperatures and mixing of gases to calculate the minimum velocity that is required to control the backlayer of smoke in the event of a tunnel fire. The results presented are in agreement with expectations – lower fire heat release rate, lower V_c ; higher fire heat release rate, higher V_c . The new methodology results do not asymptote to 3.5 m/s, as the classic V_c set of equations point, but progressively increases V_c as the fire heat release rate increases. Geometrical aspects of the tunnel are taken into account to provide a proper set of results.

Keywords: critical velocity, tunnel ventilation, fire modelling

1. INTRODUCTION

The classic critical velocity (V_c) was developed in the mid 1970’s as part of the SES Handbook [1]. Danziger and Kennedy [2] presented its application for the first time in 1982; and Kennedy, Gonzalez, and Sanchez [3] presented the derivation of these equations in 1996 at ASHRAE for the first time. The following year, Kennedy [4] edited the paper outlining the derivation [3] and added information about the Memorial Tunnel Fire Test Program. After being published in 1996, these equations were implemented as an Annex into NFPA 502 for information. Up until 2014, NFPA 502 used the formulation presented in the 1996 publication by Kennedy et al. [3]. In 2017, NFPA 502 Annex included a revision to the equations varying the Froude Number (Fr) as a function of the Fire Heat Release Rate (FHRR). Y.Z. Li, and H. Ingason [5] presented a discussion where they found some problems with the critical Fr_c . In 2020, NFPA 502 issued a revised set of equations that were very controversial, which led NFPA 502 to pull out all calculation methods for V_c . Stacey and Beyer [6] presented an argument that researchers have not yet captured the physics and geometry. In 2022, NFPA 502 issued an Annex that did not endorse any method, but called out the 2014, 2017 versions, and CFD, and described the subject open to research.

Shi, De Los Rios and Lopez [7] presented an argument that modifying Fr as a function of the FHRR would increase the ventilation capacity by 50%, and they called it “a penalty”. But the fact is that physics is not politics, and we should focus on the physics that would give us the right answer first. We need the facts before we assess the risk.

2. CLASSIC CRITICAL VELOCITY

Kennedy et al. [3] presented the derivation of the SES V_c equations in 1996. A summary of the derivation is presented as a review here to lay the foundation for discussion.

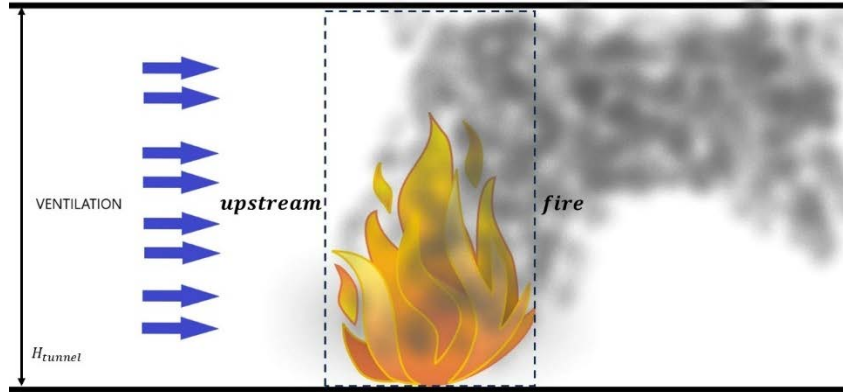


Figure 1: Classic V_c control volume.

The starting point was based on a Fr a scale modeling approach, defined as:

$$Fr = \frac{\text{gravitational force}}{\text{inertial force}} \quad (1)$$

Density, ρ , was introduced to address buoyancy effects

$$Fr = \frac{gH(\rho_{upstream} - \rho_{fire})}{\rho_{upstream}V^2} = \frac{gH}{V^2} \left(1 - \frac{\rho_{fire}}{\rho_{upstream}} \right) \quad (2)$$

which was converted into temperature relationships derived from the gas laws

$$Fr = \frac{gH}{V^2} \left(1 - \frac{T_{upstream}}{T_{fire}} \right) \quad (3)$$

Based on the control volume shown in Figure 1, using only the Convective FHRR (\dot{Q}_c), the temperature rise is calculated to be

$$\dot{m}C_p T_{upstream} + \dot{Q}_c = \dot{m}C_p T_{fire} \quad (4)$$

Assuming constant properties - ρ , mass flow rate (\dot{m}), and specific heat (C_p), the approaching temperature is formulated as a function of the \dot{Q}_c

$$T_{upstream} = \frac{\dot{m}C_p T_{fire} - \dot{Q}_c}{\dot{m}C_p} \quad (5)$$

which is then introduced into Equation 3 and a Fr as a function of \dot{Q}_c and T_{fire} is formulated.

$$Fr = \frac{gH\dot{Q}_c}{\dot{m}C_p T_{fire} V^2} \quad (6)$$

Assuming ρ constant, the mass flow rate is converted in terms of air velocity and tunnel area (A), yielding,

$$Fr = \frac{gH\dot{Q}_c}{\rho C_p A T_{fire} V^3} \quad (7)$$

For all practical purposes, the critical Fr (Fr_c) is now correlated with V_c

$$Fr_c = \frac{gH\dot{Q}_c}{\rho C_p A T_{fire} V_c^3} \quad (8)$$

Introducing a constant, K_{grade} , to address the slope effect on the fire, the V_c is formulated as

$$V_c = K_{grade} \left(\frac{gH\dot{Q}_c}{\rho C_p A T_{fire} Fr_c} \right)^{1/3} \quad (9)$$

Kennedy et al. [3], recommended the conservative value for Fr_c be 4.5. This leads to

$$V_c = 0.61 K_{grade} \left(\frac{gH\dot{Q}_c}{\rho C_p A T_{fire}} \right)^{1/3} \quad (10)$$

To calculate T_{fire} , still assuming constant properties, the following is carried out.

$$\rho A C_p V_c T_{upstream} + \dot{Q}_c = \rho A C_p V_c T_{fire} \quad (11)$$

$$T_{fire} = \frac{\dot{Q}_c}{\rho A C_p V_c} + T_{upstream} \quad (12)$$

Equations 10 and 12 constitute the classic V_c equations used since 1975.

3. FROUDE NUMBER DERIVATION

Based on a traditional fluid mechanics theory definition, as shown in Szirtes [8],

$$Fr = \sqrt{\frac{\text{inertial force}}{\text{gravitational force}}} \quad (13)$$

Under this definition,

$Fr < 1$ is subcritical and waves move upstream,

$Fr = 1$ is critical and waves moves with the bulk fluid,

$Fr > 1$ is super critical and waves move downstream.

First, let us review what “inertial force” (ma) is. It is the force that a mass has to maintain its motion or rest position. Second, let us review what “gravitational force” (mg) is. Quite often confused with buoyancy force, gravitational force is the force that pulls all masses downwardly towards the center of the earth, while buoyancy force is the force that pushes any mass upwardly (against the gravitational vector direction) and keeps this mass afloat fluids.

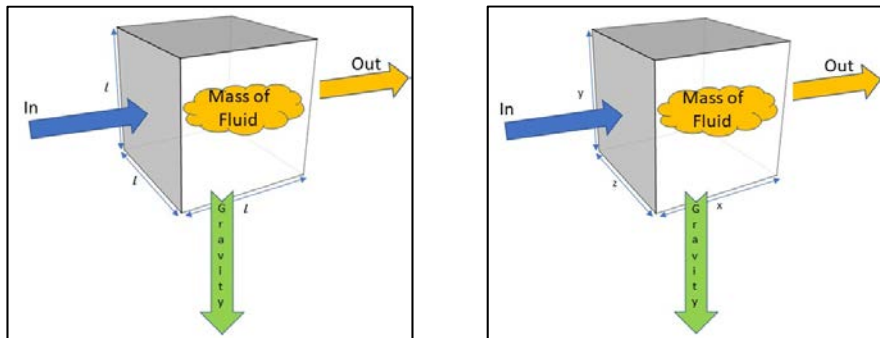


Figure 2: (a) left schematic assumes all dimensional length are l ; (b) right schematic assumes dimensions following the coordinate system x,y,z .

Let us examine a small fluid control volume of dimensions x , y , and z , and a horizontal velocity u that travels from *in* to *out*, to evaluate the terms for Fr (Equation 13). If we assume a uniform length scale for all dimensions, l , as shown in Figure 2(a), we lose directionality, as shown in Equation 14, and l can take either x , y , or z .

$$Fr = \sqrt{\frac{ma}{mg}} = \sqrt{\frac{\rho l^3 a}{\rho l^3 g}} = \sqrt{\frac{\rho l^3 V \frac{V}{t}}{\rho l^3 g}} = \sqrt{\frac{\rho l^3 V \frac{V}{l}}{\rho l^3 g}} = \sqrt{\frac{\rho V^2}{\rho l g}} = \sqrt{\frac{V^2}{l g}} = \frac{V}{\sqrt{l g}} \quad (14)$$

If we consider the planes where the forces act upon - y , and z for direction of motion, and x , and z for direction of the gravitational pull, following Figure 2(b), the correct Fr is thus derived. The fluid is moving along the, as in tunnel ventilation. The inertial force acts perpendicular to the gravitational force. This leads Equation 15 to define the Fr with the length scale being the x direction, parallel to the motion. William Froude derived Fr to quantify the resistance of floating objects when navigating at a given speed. Under his application, the length scale was the length of the ship, with water and ship travelling in parallel in the x -axis, thus the length scale is in the length of the ship. Furthermore, the formulation presented in Equation 16 becomes the correct form.

$$Fr = \sqrt{\frac{ma}{mg}} = \sqrt{\frac{\rho xyz a}{\rho xyz g}} = \sqrt{\frac{\rho xyz V \frac{V}{t}}{\rho xyz g}} = \sqrt{\frac{\rho xyz V \frac{V}{x}}{\rho xyz g}} = \sqrt{\frac{\rho yz V^2}{\rho xyz g}} = \sqrt{\frac{V^2}{x g}} = \frac{V}{\sqrt{x g}} \quad (15)$$

$$Fr = \frac{V}{\sqrt{x g}} \quad (16)$$

4. FIRE HEAT RELEASE RATE, REACTANTS, AND PRODUCTS

Figure 3 outlines the split of the masses, velocities, and temperatures in simplicity: upstream, into the fire and out to the fire chamber, the annular bypass, and the downstream mixture chamber. The total fire heat release rate (\dot{Q}_t) is a result of the combustion of the reactants. Sanchez [9] described in detail the non-stoichiometric effect fires have. There are three regions of the combustion process: lean, stoichiometric, and rich. This is assessed via the equivalence ratio, ϕ , which is defined to be:

$$\phi = \frac{AFR_{stoich}}{AFR_{actual}} \quad (17)$$

$$\phi < 1 \text{ lean (lighter blue color, no CO, no soot, no radiation)} \quad (18)$$

$$\phi = 1 \text{ stoichiometric (dark blue color, no CO, no soot, no radiation)} \quad (19)$$

$$\phi > 1 \text{ rich (orange color, CO, soot, radiation)} \quad (20)$$

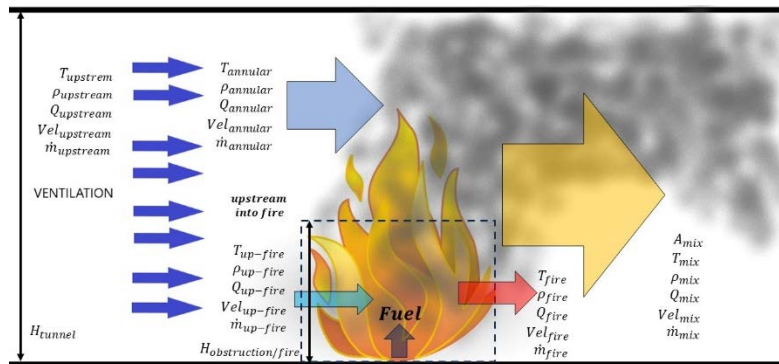


Figure 3: Full V_c Fire Control Volume

Sanchez identified the effect ϕ has on \dot{Q}_t and its properties. For tunnel fire applications, the fires are classified as rich because they generate a flame orange in color, generate soot, CO, and radiation. Fresh air comes down the tunnel from the inlet (upstream), the upstream airflow will split into airflow to sustain the fire and the rest will be bypass airflow to push the fire plume. Using Equation 21, the products of combustion are calculated. For this one-

dimensional analysis, it assumed that all products of combustion are fully mixed and all together represent the smoke from the fire. In a similar way, when the annular airflow mixes with the fire smoke, it is assumed that the mixture is fully mixed and this one body of mass will be the smoke plume the tunnel ventilation system is trying to control.

$$1 \text{ kg fuel} + AFR \text{ kg air} = (1 + AFR) \text{ kg products} \quad (21)$$

Prescribing the design \dot{Q}_t , the fuel consumption rate is calculated.

$$\dot{m}_{fuel} = \frac{\dot{Q}_t}{\chi \Delta H_c} \quad (22)$$

χ is defined to be the fuel burning efficiency for the fire process. It shall be noted that \dot{Q}_t is composed of two components – convection and radiation.

$$\dot{Q}_t = \dot{Q}_c + \dot{Q}_r \quad (23)$$

For the time being, we shall prescribe the percentage radiation fraction. Only the convective term will be used to derive the critical velocity. The upstream mass flow rate is calculated by defining the upstream velocity and ρ , while the annular velocity is derived from the upstream mass flow rate minus the mass flow used to sustain the fire.

$$\dot{m}_{upstream} = (\rho VA)_{upstream} \quad (24)$$

$$\dot{m}_{up-fire} = (AFR_{actual})\dot{m}_{fuel} \quad (25)$$

$$\dot{m}_{annular} = (\rho VA)_{annular} = \dot{m}_{upstream} - \dot{m}_{up-fire} \quad (26)$$

$$\dot{m}_{fire} = (1 + AFR_{actual})\dot{m}_{fuel} \quad (27)$$

$$\dot{m}_{mix} = (\rho VA)_{mix} = \dot{m}_{annular} + \dot{m}_{fire} \quad (28)$$

$T_{annular} = T_{upstream}$ are known. T_{flame} is the actual temperature of the flame and calculated based on ΔH_c , \dot{Q}_t , and kinetics (not discussed in this paper, but it is a needed parameter). T_{flame} has to be converted into the effective convective temperature, T_{fire} , that mixes with the annular mass flow by multiplying it by the ratio of \dot{Q}_c to \dot{Q}_t . Therefore, the temperature of the fire gases after mixing the fire plume with the upstream annular mass flow is calculated as follows:

$$T_{mix} = \frac{(\dot{m}c_p T)_{annular} + \left[(\dot{m}c_p T_{flame} \left(\frac{\dot{Q}_c}{\dot{Q}_t} \right))_{fire} \right]}{(\dot{m}c_p)_{mix}} \quad (29)$$

It should be noted that C_p has to be the corresponding values at the local temperature of the various mass flows. As a result of the conservation of mass and energy, ρ is computed as follows:

$$\rho_{upstream} = \frac{101325}{RT_{upstream}} \quad (30)$$

$$\rho_{annular} = \frac{101325}{RT_{annular}} \quad (31)$$

$$\rho_{fire} = \frac{101325}{RT_{fire}} \quad (32)$$

$$\rho_{mix} = \frac{101325}{RT_{mix}} \quad (33)$$

And consequently, the velocities are calculated as follows:

$$V_{upstream} = \frac{\dot{m}_{upstream}}{\rho_{upstream} A_{upstream}} \quad (34)$$

$$V_{annular} = \frac{\dot{m}_{annular}}{\rho_{annular} A_{annular}} \quad (35)$$

$$V_{fire} = \frac{\dot{m}_{fire}}{\rho_{fire} A_{fire}} \quad (36)$$

$$V_{mix} = \frac{\dot{m}_{mix}}{\rho_{mix} A_{mix}} \quad (37)$$

These lay out all the parameters derived for the fire scenario. It should be noted that for fires, V , ρ , and C_p are not constant due to the conservation equations of mass and energy. They vary as a function of local temperature.

5. CLASSIC CRITICAL VELOCITY DEFICIENCIES

The following are deficiencies in classic critical velocity derivation:

1. The definition of Fr used by Kennedy et al. [3] is not consistent with the standard fluid dynamics definition [8]. As it can be seen, Equation 1 is the inverse of Equation 13, and already squared. Furthermore, following Equation 13 convention, and taking the square root of 4.5, the value for Fr_c would have been 2.1213, which then inverting this value to concur with Equation 13, it would yield $Fr_c = 0.4714$, which indicates that the value is a subcritical value that would allow the wave (backlayer) move upstream. The value desired should be >1.0 .
2. The tunnel height is used as the length scale (Equation 2). But Equation 15 shows that Fr depends on the length scale parallel the motion of the fluid, x .
3. Fr is not a function of the buoyancy force; ρ does not appear in its standard definition (Equation 16). Equation 2 introduced density ratios to address buoyancy effects, but as shown on Equation 16, Fr is a function of the gravitational force (mg); not the buoyancy force (ρg). Moreover, Fr is not a function of any fluid density ratio. Kennedy et al. added an extra term K_{grade} to address the effect the slope has on the buoyancy forces. Fr does not depend on slope. In a similar way, it should be pointed out that Fr is not a function of any \dot{Q}_c .
4. Equation 4 is not correct. ρ and C_p vary with temperature. It does not account for the mass of the fire, which leads to miscalculate the velocity.

Fr should not be used to derive the critical velocity as Kennedy et al. [3] so derived it. Li and Ingason [5] identified problems with the critical value of $Fr_c=4.5$. The above description presents evidence why Li and Ingason were having problems validating $Fr_c=4.5$.

In 2017, NFPA 502 presented values for Fr based on \dot{Q}_c . But \dot{Q}_c is not part of the Fr fundamentals. The Fr_c values are presented in the Table 1 below. These values are misleading. They are all subcritical.

In 2020, NFPA 502 presented a curve fit trying to match a plot from the Memorial Fire Test. Such correction was not based on any physics, and thus the controversy was created.

Table 1: NFPA 502 -2017 Annex D – Range of K₁ values for various \dot{Q}_c

\dot{Q}_c (MW)	K ₁	Fr_{cSES}	$\sqrt{Fr_{cSES}}$	Fr_{fluid} mech	Flow Regime
>100	0.606	4.493	2.120	0.472	Subcritical
90	0.620	4.196	2.048	0.488	Subcritical
70	0.640	3.815	1.953	0.512	Subcritical
50	0.680	3.180	1.783	0.561	Subcritical
30	0.740	2.468	1.571	0.637	Subcritical
<10	0.870	1.519	1.232	0.811	Subcritical

6. NEW CRITICAL VELOCITY FORMULATION

A new critical velocity methodology is presented in this paper founded on the conservation of mass, momentum, energy, and combustion in a simple one-dimension. Equations above (17 through 37) show how to calculate the various mass flow rates, velocities, temperatures. Equation 39 represents the conservation of momentum. Many researchers and engineers have focused on the buoyancy component. Ingason and Li [10] has expressed that the slope effects are overestimated using NFPA 502. That is correct. Based on Equation 39, that component is very small. The component that is missing is the throttling effect the temperature rise has on the flow. Adding this factor into Equation 39 makes all the difference. Equation 39, in conjunction with Equations 17 through 37, represent the final critical velocity equation.

$$(\rho AV^2)_{annular} = (\Delta P_{throttle} A)_{annular} + \sin(\alpha) F_{buoyancy} \quad (38)$$

$$(\rho AV^2)_{annular} = \left(1 - \frac{T_{annular}}{T_{mix}}\right) \left(\frac{g\rho HA}{2}\right)_{annular} + \sin(\alpha) g m_{mix} \left(\frac{\rho_{annular} - \rho_{mix}}{\rho_{mix}}\right) \quad (39)$$

Where m represents mass, g the gravitational constant, and $\sin(\alpha)$ the sine function of the angle of the slope.

7. SAMPLE CALCULATIONS

Calculations were performed with the following assumptions: $\dot{Q}_t = 20$ MW, $\dot{Q}_c = 0.7\dot{Q}_t$, $\chi = 0.7$, $\Delta H_c = 20$ MJ/kg, $\phi = 1.25$, $AFR_{stoich} = 12.9$, $T_{annular} = T_{upstream} = 25$ C, and $T_{fire} = 1153$ C (This value has been calculated based on ΔH_c , \dot{Q}_t , and kinetics; not discussed in this paper, but submitted as an input parameter). The area of the fire obstruction = 3.38 m² (Height=1.5m, Width=2.25m). The tunnel area is as the Height and Width shown in the figures.

Figure 4 plots the V_c for various \dot{Q}_t (10, 20, 30, 50, 75, and 100MW) as a function of various slopes (-10%, -5%, 0%, +5%). The plot shows that V_c increases both as \dot{Q}_t increases, and as the slope increases downward; not like the classic V_c equation, which leads to a limit of 3.5 m/s for all slopes and \dot{Q}_t . The increase of \dot{Q}_t as the upstream tunnel ventilation rate increases is in agreement with Li et al. [11], which states that “the fire growth rate increases with the ventilation velocity”. But I would like to restate the statement – to sustain a higher \dot{Q}_t , the upstream airflow rate must be increased; otherwise, there will not be enough air and \dot{Q}_t cannot increase more than the upstream airflow rate can support.

Figure 5 plots the variation of V_c at various tunnel H/W aspect ratios. The results show that V_c increases as the tunnel becomes narrower, and as the tunnel height increases.

Figure 6 plots the variation of V_c as a function of the radiation factor. The results are as expected. As the radiation fraction increases, the convective fraction decreases, and the V_c decreases as well. Between 0% to 40% radiation factor, the V_c decreases by 0.5 m/s.

8. CONCLUSION

This paper has identified that the classic V_c set of equations derived by Kennedy et al. [3] in 1996, and used throughout the world since, have some fundamental limitations due to the way Fr was defined, the value for Fr_c , and the implementation of constant properties. The new methodology presented in this paper has demonstrated how to account for all the physics involved in the determination of the critical velocity. The new methodology is consistent with expectations – low \dot{Q}_t , low V_c is required; high \dot{Q}_t , high V_c is required. Although still a one-dimensional approximation, the effect of properties as a function of temperature helps identify that the velocities downstream are greater because of lower ρ , and higher temperature. This paper brings the tunnel ventilation industry to a closer understanding on how to determine ventilation requirements based on a one-dimensional V_c approximation.

9. ACKNOWLEDGEMENTS

The author would like to thank Engineer Justo Suarez for his listening, long discussions, and encouragement during the development of this paper.

10. REFERENCES

- [1] Subway Environmental Design Handbook, Volume II, Subway Environment Simulation (SES) Program, Version 3.0, Part I, User’s Manual, Chapter 16 – Fire Model, Technical report No. UMTA-DC-06-0010-75-1, Transit Development Corporation, Inc. October 1975
- [2] Danziger, N.H., Kennedy, W.D., “Longitudinal Ventilation Analysis for the Glenwood Canyon,” 4th International Symposium on the Aerodynamics and Ventilation of Vehicle Tunnels, BHRA, 1982 York, UK.
- [3] Kennedy, W.D., Gonzalez, J.A., Sanchez, J.G., “Derivation and Application of the SES Critical Velocity Equations”, ASHRAE Summer Meeting, paper 3983, San Antonio, TX, 1996
- [4] Kennedy, W.D., “Critical Velocity: Past, Present, and Future”, Independent Technical Conference, 1997
- [5] Li, Y.Z. and Ingason, H., “Discussions on Critical Velocity and Critical Froude Number for Smoke Control in Tunnels with Longitudinal Ventilation”, Fire Safety Journal, Volume 99, July 2018.
- [6] Stacey, C., and Beyer, M., “Critical of Critical Velocity – An Industry Practitioner’s Perspective, 10th International Conference on Tunnel Safety and Ventilation, 2020, Graz, Austria
- [7] Shi, Y.S., De Los Rios, N., Lopez, K., “The Critical Penalty”, ISAVFT 2022, BHR, Brighton, UK, 2022
- [8] Szirtes, Thomas, “Applied Dimensional Analysis and Modeling”, 2nd Edition, Butterworth-Heinemann, 1997
- [9] Sanchez, J.G., “Non-Stoichiometric Fire Modeling Predictions with Applications to Train Fires in Tunnels”, International Congress on Fire Computer Modeling, University of Cantabria, Santander, Spain, October 2012.

[10] Ingason, H, and Li, Y.Z., “Understanding of critical velocity in Memorial Tunnel Fires Tests Using Longitudinal Ventilation:”, paper about slope not influential.

[11] Li, Y.Z., Ingason, H., and Lonnermark, A, “Effect of longitudinal ventilation on fire growth rate and flame length in a tunnel fire”, 14th International Symposium on Aerodynamics and Ventilation of Tunnels, BHR Group, Dundee, Scotland, 2011

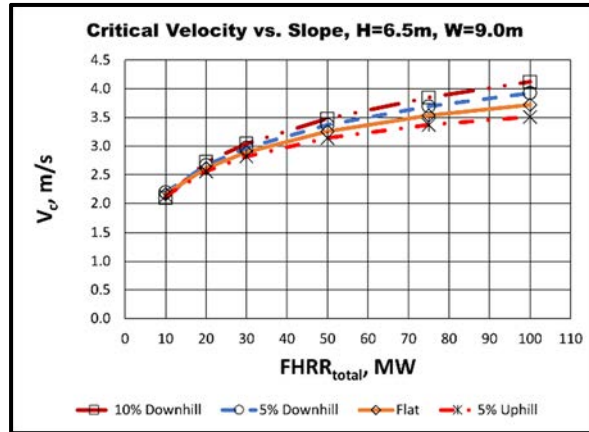


Figure 4: V_c as a function of \dot{Q}_t and slope.

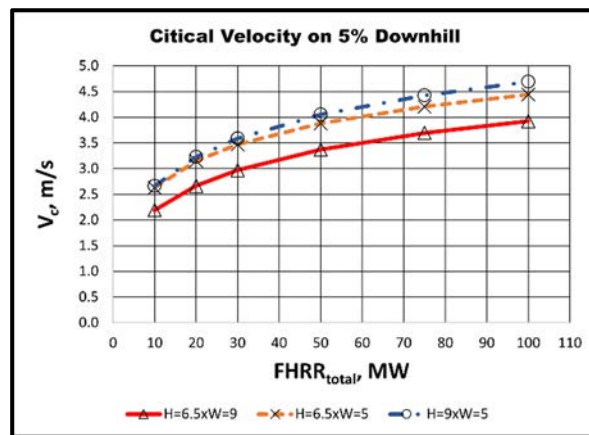


Figure 5: V_c as a function of \dot{Q}_t and various tunnel H/W aspect ratios.

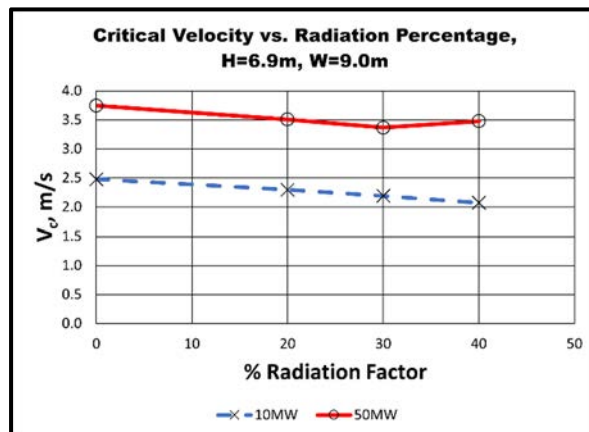


Figure 6: V_c as a function of % radiation factor.

CONFINEMENT VELOCITY FOR SMOKE IN TUNNELS – HOW TO POKE A STICK AT IT

¹Michael Beyer, ^{1,2}Conrad Stacey

¹Stacey Agnew Pty Ltd, AU

²Delve Stacey Agnew LLC, US

DOI 10.3217/978-3-85125-996-4-43 (CC BY-NC 4.0)

This CC license does not apply to third party material and content noted otherwise.

ABSTRACT

In 2023, NFPA 502 changed from the absolute prevention of backlayering (critical velocity) to allowing some backlayering (confinement velocity). That made sense for tunnel safety. However, it is not clear how to design for that. NFPA 502 does not provide any guidance on how to determine such a confinement velocity and there is no reliable calculation method that can be used for real (full-scale) tunnels. The complexity of determining confinement velocity and the parameters that influence backlayering are explored. Those influences are quantified via a CFD model validated for critical velocity, also understanding the importance of parameters like wall roughness, wall temperature etc. Surprisingly, in some circumstances, confinement velocity is no less than critical velocity. Guidance on how to approach confinement velocity for real projects is also offered.

Keywords: Smoke control, smoke propagation, confinement velocity, critical velocity

1. INTRODUCTION

Strategies for smoke control during tunnel fires vary considerably. Different countries have different approaches through their national standards. One of the philosophies is to prevent smoke propagation upstream of the fire by achieving critical velocity. Other philosophies acknowledge the adverse effects of higher airspeeds on smoke layer mixing, fire growth rates and peak heat release rates (HRR), and apply a lower velocity, accepting some upstream propagation of a hot smoke layer. That can be specified as a fixed velocity that is lower than critical velocity (e.g. 1.0 to 2.0 m/s) or allowing smoke backlayering up to a fixed length (e.g. 30 m). The low velocity approach minimises the risk of adversely affecting the egress conditions during the self-rescue phase, but, depending on the actual fire scenario and tunnel parameters, the smoke layer can propagate upstream for distances of several metres up to a couple of hundred metres. The maximum allowable backlayer approach is a compromise between low velocity, with the risk of having ‘uncontrolled’ upstream propagation of a smoke layer, and achieving high velocities for an absolute prevention of upstream smoke propagation. A tunnel air velocity that confines upstream smoke propagation to a specific distance is termed a confinement velocity. A more comprehensive discussion on the different smoke management philosophies can be found in [1] and [2].

NFPA 502, the national standard in the US, historically proposed a ‘critical velocity’ approach, but with the 2023 edition [3], changed its terminology from preventing backlayering to controlling backlayering, and now refers to a confinement velocity. However, even if such an approach is desired, no guidance on how to achieve confinement velocity is offered in the standard. Also, the literature does not provide information that can reliably be used for design purposes. Full-scale fire tests are rare, expensive and usually designed for a particular purpose, where it is often not possible/reasonable to draw conclusions outside of the test purpose. The Memorial Tests [4], [5], [6], for example, were designed (among other purposes) for analysing critical velocity over a wide range of fire heat release rates. So, the focus was on identifying

the condition where the thermal force generated by the fire was balanced by the pressure force of the longitudinal airflow approaching the fire [4]. Beyond that point, no steady state backlayering length in combination with almost constant air velocity and fire heat release rate were explicitly documented in the test reports. Also, the instrument loops upstream of the fire beyond the first loop were too widely spaced to observe either the backlayering distance accurately or the steadiness of a backlayer.

Full-scale tests were also performed in the Koralmtunnel, again with fire pans, but with smaller fire heat release rates, up to 20 MW. The purpose of those tests was to analyse smoke ingress into cross passages with the focus on measuring temperature distribution and analysing smoke propagation downstream of the fire. Based on observations during the field tests, a smoke backlayering length for selected tests are documented with an uncertainty of several metres [7]. The stated backlayering length (in [7]) occurred just before reaching peak-HRR, with no indication whether either the smoke propagation or the HRR were stable at that time. Also, the upstream air velocity was not kept constant during the fire tests (as stated in [7]), and therefore a conclusion on confinement velocity (backlayering length vs. upstream air velocity) can't be made reliably.

There are numerous small-scale tests based on Froude scaling [8], [9], [10], [11], [12], [13], [14], [15] with the objective to analyse critical velocity and/or backlayering length for different fire settings. However, as discussed in [16] and [17], the Froude number widely used for Froude scaling misses the buoyancy term that is very important for the backlayering flow regime. There is no evidence that the data produced in small-scale tunnels can be scaled up to a real tunnel by any parameter, and therefore it is unclear if the flow regime established in the small-scale tunnels represents the situation in a real tunnel. Any proposed equation for calculating a backlayering length, confinement velocity, or critical velocity derived from such small-scale tests needs to account for all relevant physics before it could be considered for use for real tunnels. To date, attempts to find non-dimensional relations to allow appropriate scaling of the relevant physics have fallen short.

As discussed above, there is not much guidance available on how to approach confinement velocity for fires in real tunnels. So, as designers, how do we poke a stick at it?

Beyer, Stacey & Brenn [17] recently proposed a mixed convection model for estimating critical velocity for smoke control in road tunnels. As the flow regimes relevant to critical velocity and confinement velocity are expected to be very similar, the important aspects that influence critical velocity according to [17] will likely also influence the confinement velocity. Before addressing confinement velocity, the main findings on critical velocity provided by [17] will be summarised.

2. CHARACTERISTICS OF FLOW REGIME

When achieving critical velocity or confinement velocity, the buoyancy force relevant for developing a backlayer of hot smoke is in the order of the inertial force relevant for pushing the smoke downstream. Such a flow regime can be defined as mixed convection and characterised by the Richardson number $Ri = Gr/Re^2$ (strength ratio between natural convection and forced convection). Interestingly, a similar definition of the Richardson number is sometimes quoted as ‘critical Froude number’ in the tunnel community and fire engineering field [18], [19], [20]. However, it is important to note that the ‘critical Froude number’ is very different to the Froude number behind the so-called Froude-scaling of such flows. The number that has been used for scaling represents the ratio of the inertial force to the gravity force and neglects the buoyancy term. Froude number is central for any isothermal fluid flow which can be significantly influenced by the body force due to gravity (e.g. water

waves in open channel flows), but it does not characterise buoyancy driven flows and therefore should not have been used for scaling attempts [16], [17].

In the Richardson number, the Grashof number Gr is a measure of the natural convection and the Reynolds number Re a measure of the forced convection. Using the tunnel hydraulic diameter D_h as the relevant length scale for the forced convection and the tunnel height from the fire base L_n as relevant for the natural convection, the velocity relevant for upstream smoke propagation U can be expressed [17] as:

$$U = K_F K_g \left(\frac{g L_n^3}{D_h^2} \frac{1}{Ri} \frac{\Delta T}{T_a + \Delta T} \right)^{1/2} \quad (1)$$

The temperature T_a refers to the ambient temperature of the approaching air. Appropriate definition of the parameters K_F , K_g , Ri and ΔT for estimating critical velocity will be summarised in the following section. For a more comprehensive discussion refer to [17].

3. CRITICAL VELOCITY

The following section provides a short summary of the physical model for estimating critical velocity as presented in [17]. The intention here is to discuss the essential parameters that influence critical velocity as they will also be relevant for the even more complex flow regime around confinement velocity.

For critical velocity it is assumed that the strength of forced convection is of the same order as the strength of natural convection, which requires that the Richardson number in equation (1) is unity.

One of the challenges is, to identify an appropriate temperature difference ΔT relevant for the buoyancy term. As discussed in [17], the first aspect that is important for estimating the effective temperature difference is the fire intensity (heat release rate per unit area). The more heat that gets released per unit area, the higher is the density deficit and thus the buoyancy force. That is, the relevant buoyancy force for establishing a backlayering is not necessarily a function of the fire heat release rate. This was also observed during the Memorial Tunnel tests where the fire heat release was increased by adding fire pans (same fire intensity) in the longitudinal direction with the result that the observed critical velocity value was essentially unchanged between 20 MW and 100 MW [4]. The second important aspect is how much of the front bit of the fire contributes to the buoyancy force relevant for creating a backlayer. When increasing the fire heat release rate by extending the fire in the longitudinal direction but keeping the fire width and fire intensity the same, the contribution of the downstream bit of the fire to the density deficit at the front of the fire becomes less important the longer the fire gets. According to [17], the contribution of the fire front in the effective temperature difference ΔT was found to be a function of the ratio between fire length and the length scale relevant for natural convection.

The mixing of the approaching air with the hot plume gases is the final important factor that influences the effective temperature difference. In [17] it is acknowledged that some of the approaching air passes the fire front without interacting with the hot plume. With a smaller plume frontal area, the hot plume gases are mixed with less of the approaching ambient air and the initial smoke layer temperature is reduced less. Along with the fire width influence below, this addresses the aspect ratio correction that was seen to be required on all methods that evaluated temperature rise using the total flow.

The influence of the plume frontal area on the approaching flow is another effect of the width scales of the fire and the tunnel, also detailed in [17]. If the plume frontal area is small compared to the tunnel area (wide tunnels), a bigger fraction of the flow avoids the rising

plume, with the plume less affected by the air slipping easily around it. For a wider fire with a plume area nearly as big as the tunnel area, a higher fraction of the flow momentum is ‘opposing’ the plume so that the velocity required to prevent backlayering goes down. The influence of the plume width on critical velocity in [17] was found to be a function of the ‘free area’ around the plume and is considered by the factor K_F in equation (1).

The final interesting outcome in the study provided in [17] is that the influence of the tunnel grade on the critical velocity can be neglected for tunnels with typical gradients ($\pm 6\%$). That is, the grade factor K_g in equation (1) becomes unity. When critical velocity is achieved and backlayering prevented, the gravity vector in the Grashof number that is relevant for the natural convection stays nearly the same for small tunnel slopes and so it is plausible that the critical velocity is not influenced by typical tunnel slopes. However, while a typical tunnel slope does not influence the critical velocity, it still has huge implications in the required ventilation power to achieve/maintain the required critical velocity, due to the buoyancy effects related to the hot smoke gases downstream of the fire.

With considering the essential effects on the relevant temperature difference for the buoyancy force and the influence of the fire width, together with the conclusion on the grade factor, the physical model for estimating critical velocity as proposed in [17] is able to predict critical velocity values for the relevant full-scale test as well as the measured dimensional values in small scale tunnels, all within an acceptable accuracy. As the physics relevant for upstream smoke propagation for fires in tunnels seems to be adequately captured with those equations, it appears to be an appropriate starting point for discussing confinement velocity.

4. CONFINEMENT VELOCITY

4.1. Influence on Local Fire Plume Dynamics

For confinement velocity (lower than critical velocity) the inertial force reduces relative to the buoyancy force so that the two forces are not in the critical velocity equilibrium, and hot smoke starts propagating upstream. This refers to a Richardson numbers >1 in equation (1). It is pretty straightforward how a change in the velocity upstream of the fire changes the inertial force, but it is difficult to estimate what it does to the effective temperature difference relevant for the buoyancy force ΔT and the fire width dependency as discussed in Section 3. We explore this a bit further.

The fire intensity influence on ΔT will be similar to the ‘critical’ case, but as smoke starts propagating upstream more of the fire length may contribute to the plume front that influences the buoyancy force. That potentially requires an adjustment of the relevant empirical parameters derived in [17]. The backlayering restricts the free flow area upstream of the fire, and potentially lowers the height at which the plume enters the smoke layer. That reduces the fraction of the fresh air mass flow that mixes with the plume, likely causing a higher ΔT . However, as the backlayering restricts the area for the approaching flow, there is less space for the air to get around the plume and that seems likely to cause a higher deflection of the plume (higher momentum onto the plume front) and more mixing into the plume (relative to the free upstream velocity). Consequently, the factor K_F might increase or stay the same. Both effects (plume front area definition for mixing and plume deflection) of course depend on the thickness of the backlayering (e.g. frontal area of the backlayering versus tunnel area) and potentially offset each other. Based on that rationale, it seems likely that the buoyancy force stays more or less the same between critical velocity and confinement velocity if the backlayering is stable and the length is limited (e.g. 20 to 50 m). Figure 1 and Figure 2 compare the temperature and velocity distributions resulting from a simulation of a 50 MW pool fire at some confinement velocity, and without upstream smoke propagation (critical velocity).

Any differences in the relevant/effective buoyancy force between critical velocity and confinement velocity for small backlayering distances could be tied into a modified Richardson number $Ri_B = Ri \cdot f_B$ required for restricting backlayering. According to equation (1) that would lead to following relation of confinement velocity U_B .

$$U_B = K_F K_g \left(\frac{gL_n^3}{D_h^2} \frac{1}{Ri_B} \frac{\Delta T}{T_a + \Delta T} \right)^{1/2} \quad (2)$$

4.2. Influence on Backlayer Dynamics

Equation (2) above may describe the initial momentum of the backlayering once backlayering starts to grow due to the imbalance of buoyancy and inertia force, but it does not address the physics relevant for the resulting backlayering length based on that imbalance. As an example, for the same tunnel air velocity (< critical velocity), the backlayering extent for a very rough tunnel wall will be lower than the backlayering extent for a very smooth tunnel wall. So, wall roughness likely is important as it reduces the resulting momentum of the backlayer, applying a retarding shear on the layer to supplement the shear from the flow underneath the layer. There are other effects related to heat transfer, thermal radiation, shear layer between the backlayering and approaching flow and tunnel slope that influence the resulting momentum and propagation of the backlayer. The heat transfer between the backlayering and the cooler tunnel wall, the thermal radiation between the underside of the backlayering and the cooler surroundings, and the mixing within the shear layer, all reduce the temperature of the hot smoke layer while moving upstream. That temperature reduction, as well as the interaction with the approaching air in the shear layer, reduces the resulting momentum of the backlayering and thus the upstream propagation of the hot smoke. The effect of the heat loss due to thermal radiation is assumed to be minor. Part of the cooler smoke in the shear layer flows against the backlayering and back to the fire front. That counterflow insulates the hot smoke layer adjacent to the tunnel ceiling and reduces heat loss by thermal radiation. If the tunnel is sloped, the gravity component in the longitudinal direction would have an additional effect on the resulting momentum of the backlayering due to the buoyancy force, and likely on the shear layer. Even if a typical tunnel slope does not affect critical velocity [17], it intuitively seems likely to affect the propagation of the backlayering.

The upstream smoke propagation stops, and is perhaps stable, once all the effects are in equilibrium. However, the backlayering may still slowly creep upstream while the tunnel wall adjacent to the backlayering gets hotter over time and so slowly reduces the heat transfer from the backlayer into the tunnel wall. A first estimation of the time-dependent temperature rise in the tunnel lining based on a one-dimensional transient heat transfer calculation (see Figure 9) shows that the wall heat flux adjacent to the backlayering decreases by 15% after 10 minutes, by 20% after 20 minutes and by 40% after 120 minutes. That suggests that the wall heat flux in the first 20 minutes reduces as much as in the following 100 minutes. With an important timescale of 20 minutes, there is only a slim chance of wall heating being important to egress. Tunnel shape and profile is a further aspect that likely influences the backlayer thickness and propagation (e.g. curved ceiling vs. flat ceiling, or horseshoe profile vs. rectangular profile with lower air velocity at the corners).

All of the above would be required to be appropriately implemented in a physical model, and possibly incorporated into equation (2), to be able to estimate a backlayering distance. In a further step, the empirical model would need to be adequately validated against a systematic parameter study or preferably, against full-scale test data. However, while full-scale test data are preferred, it will be very difficult to achieve a steady flow field with a backlayer of any significant length.

4.3. CFD study

To explore the influences on the propagation of the backlayering a bit further, a CFD model was created based on the proposed methodology used for evaluating critical velocity by Beyer & Stacey [21]. The overall methodology, mesh type and resolution as well as boundary conditions were kept the same. The simulation software ANSYS Fluent [22], [23], [24, 25] was used. The modelled tunnel has a typical 3-lane TBM profile with a cross section area of 93 m² with a hydraulic diameter of 9.9 m and a height from floor to ceiling of 8.92 m. The tunnel domain has a total length of 500 m. The fire source was placed 300 m downstream of the inlet portal on the floor in the middle of the tunnel. Adopted design fire parameters as proposed in [17] for a 50 MW fire, and other input parameters, are listed in Table 1.

Table 1. Input parameters used for the CFD model.

Parameter	Value
Tunnel air temperature	30°C
Wall temperature (constant)	30°C
Wall roughness height Ks	0.0015 m
Tunnel slope	Flat (0%)
Total Fire HRR	50 MW
Radiative fraction	0.2
Fire width	2.5 m
Fire intensity	2.25 MW/m ²
Fire length	8.889 m
Fuel	Fuel-oil (C ₁₉ H ₃₀)
Combustion efficiency based on total HRR (relevant for additional CO ₂ and H ₂ O source)	0.95

Based on the initial CFD model as described above, the critical velocity (no backlayer) and the confinement velocity for a backlayer length of 30 m was analysed to understand the variation in velocity between the two conditions.

In a further step, the influence of the tunnel slope, wall roughness and wall heating on the backlayer length were analysed. In all simulations, the confinement velocity (that was necessary in the base case to maintain the backlayer distance to 30 m) was kept the same and the variation in backlayering length compared to the base case CFD model. For the tunnel slope sensitivity, the results of the flat tunnel were compared to tunnels with 4% and 8% downgrade. The wall roughness influence was analysed by increasing the wall roughness height by a factor of 5, and also by simulating a smooth wall. Regarding wall heating, the initial simulation with a constant wall temperature (equal to approaching air temperature) was compared to a simulation where the wall temperature was increased in the upstream region where the smoke layer interacts with the tunnel wall. The wall temperature in the remaining upstream section and downstream of the fire front (between front of the fire and exit portal) was kept constant, as before. The wall temperature was estimated based on a one-dimensional transient heat transfer calculation (see Figure 9). Appropriate values for smoke temperature adjacent to the wall, and a heat transfer coefficient within the smoke affected region upstream of the fire were evaluated based on the initial simulation (30 m smoke backlayer). The surface wall temperature after 60 minutes resulting from the one-dimensional calculations was used as the wall boundary condition for the simulation with the heated wall. The comparison of the

simulations should provide information about the variation on backlayering length due to the wall heating effect for a fire that lasts approximately 60 minutes.

In a final step, critical and confinement velocities for a train fire in a rail tunnel with 3% downgrade were analysed. The train has a frontal area of approximately 8.4 m² and was stationary in the tunnel. The head of the train is positioned 300 m downstream of the entry portal. The fire source (1.8 m wide and 22 m long) is sitting on the floor of the second carriage and has a total HRR of 15 MW. As a “worst case” scenario (less train blockage and smoke/heat can more easily escape the carriage), it is assumed that the glass of all the windows was broken and that the doors at one side of the fire carriage were opened. The TBM tunnel profile has a free flow area of approximately 27.2 m², a hydraulic diameter of approximately 3.9 m and a total height of 5.4 m. The floor of the carriage is 1.13 m off the tunnel floor. With those parameters, the average annular velocity over the train is 1.446 times the average upstream velocity. The train wall was assumed to be adiabatic with a wall roughness height of 0.25 mm. Also, the walls of the installations (e.g. cable trays) were assumed to be adiabatic. The tunnel wall was simulated with a constant temperature of 21.4°C (same as ambient upstream air temperature) and a wall roughness height of 1.5 mm. All other input parameters and simulation settings were according to Table 1 and [21].

4.3.1. Results of the CFD Study

Critical velocity versus confinement velocity: The established critical velocity in the first simulation was slowly reduced until a steady state backlayering distance of 30 m was established. For the assessed tunnel and fire parameters, the critical velocity and confinement velocity are 3.54 m/s and 3.28 m/s respectively. Figure 1 and Figure 2 compare the temperature and velocity distributions at critical and confinement velocities. As discussed in Section 4.1, the comparison of the temperature field around the fire confirms that the plume shape and temperature distribution is very similar between critical and (30 m) confinement velocity. In the critical velocity simulation, the fire is spread downstream a bit more, as the velocity onto the flame front is slightly higher (see Figure 2) compared to the case with confinement velocity. Also, the temperature at the upper part of the plume close to the ceiling is slightly higher with the lower confinement velocity airspeed.

Figure 2 indicates that while the average upstream velocity in the case of a 30 m backlayer is less than critical velocity, the velocity under the smoke layer and onto the fire is nearly as high as for the critical velocity case. This of course is related to the smoke layer thickness reducing the free area for the upstream flow. Figure 3 illustrates the temperature profile for the case with smoke backlayering, and the velocity profile for both cases (50 MW in a flat tunnel). The temperature profile provides information on the shear layer thickness (approximately 2.5 m in this case) and the velocity profile gives information on the velocity gradient in the shear layer (from -1.5 m/s to 4.2 m/s in this case). It is interesting to see that, below the smoke layer, the approaching velocity at the front of the fire pans for the lower confinement velocity case is higher than for the critical velocity case. However, while hard to see in Figure 2, the velocity onto the flame front is still slightly higher with critical velocity.

When assuming that the overall fire plume dynamics can still be described by equation (1) (Ri at critical velocity is 1.0) the modified Richardson number Ri_B required for maintaining a backlayer distance of 30 m would be 1.25 according to equation (2) ($U_B = U_c / \sqrt{Ri_B}$). That implies that the model assumptions (e.g. tunnel profile, wall roughness, tunnel slope, wall temperature etc.) and the subsequent influences on the backlayer and fire plume dynamics are included in the modified Richardson number. Any difference in the model assumptions would either result in a different backlayer distance (if a steady state layer still arises) or in a different modified Richardson number to achieve the same backlayer distance of 30 m.

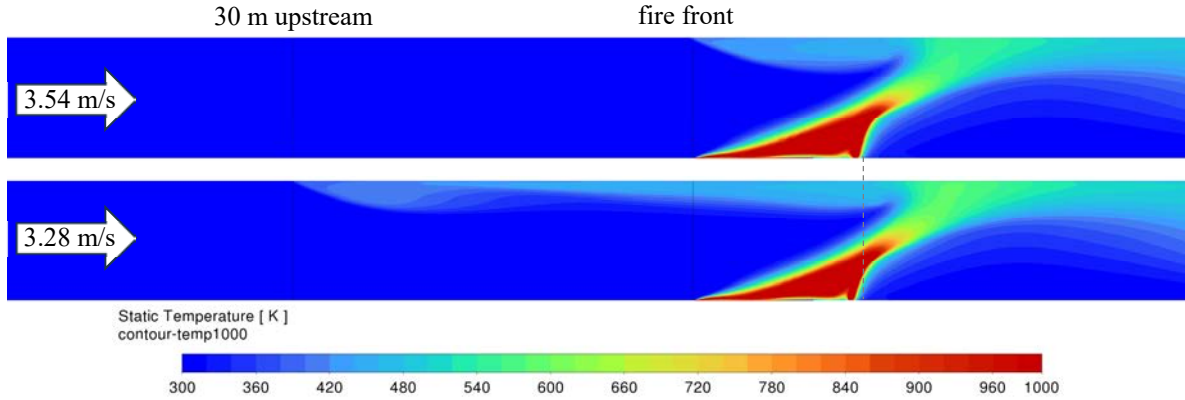


Figure 1: Contour plot of temperature distribution through the middle of the tunnel for critical velocity (top) and confinement velocity (bottom) – Initial CFD model. Temperature is clipped to 1000 K for better presentation.

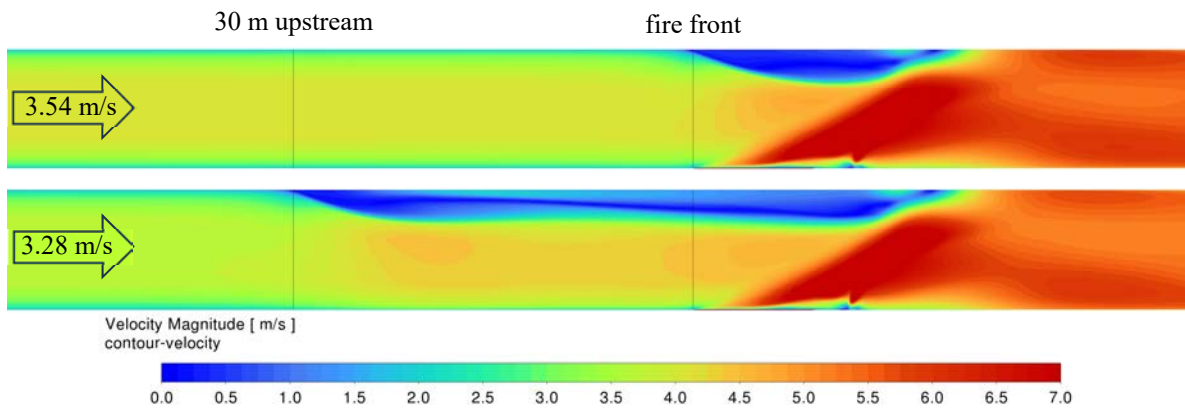


Figure 2: Contour plot of velocity distribution through the middle of the tunnel for critical velocity (top) and confinement velocity (bottom) – Initial CFD model. Velocity is clipped to 7 m/s for better presentation.

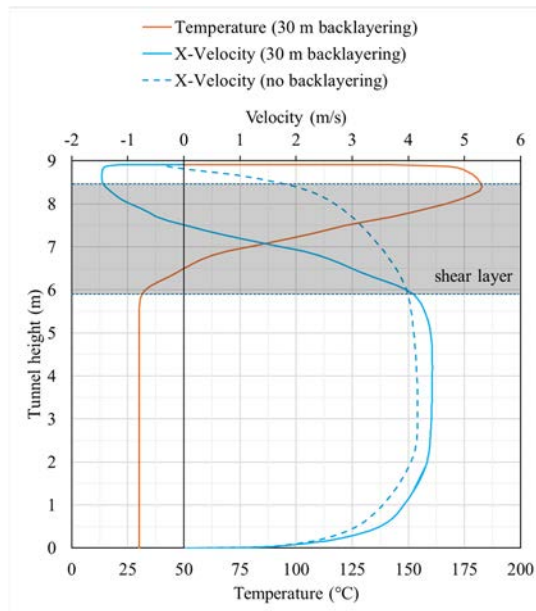


Figure 3: Velocity and temperature profile at the fire front for confinement velocity, and velocity profile for critical velocity. The profiles were taken on a vertical line from tunnel floor to ceiling in the symmetry plane of the tunnel profile.

Tunnel slope influence: To explore the slope influence on the upstream smoke propagation, the initial simulation with confinement velocity in a flat tunnel was repeated for a 4% and 8% downgrade. All the other parameters were kept the same, including the oncoming airspeed. The results at 4% downgrade were surprising. Instead of getting the expected increase in smoke backlayering distance, the smoke backlayer length was reduced by approximately 50% and oscillated between 10 m and 15 m. The simulation with the 8% downgrade tunnel showed a similar outcome. Figure 4 compares the temperature distribution in the flat tunnel with that in the sloped tunnel (4% downgrade) and depicts the amplitude of the smoke layer oscillation (transient behaviour) observed in the sloped tunnel. Temperature and velocity distribution for the tunnel with the 8% downgrade are shown in Figure 5, at nearly the maximum extent of the smoke advance, before the smoke backlayer moved backwards again. Based on that flow field, the velocity and temperature profile at the fire front were compared in Figure 6 to the profiles obtained for the flat tunnel (according to Figure 3). Examination of the flow field and the profiles confirmed that the additional buoyancy force in the smoke backlayer increases the velocity in the backlayer. That results in more smoke volume propagating upstream (higher smoke mass flow), creating a thicker smoke backlayer. The higher speed and the thicker backlayer increase the shear layer and the shear stress onto the backlayer (relative velocity between smoke backlayer and approaching air). That also seems to create instability in the flow, which of course increases mixing. It may be a moot point whether the extra shear or the instability cause the effect seen, as they are causally linked, but the effect is clear; that the smoke layer can’t propagate further upstream. In the unstable behaviour, the smoke layer increases in thickness and finally gets caught by the approaching air, mixed down and pushed back towards the fire, before it starts over again. While the smoke layer increases in thickness, the velocity onto the fire increases as well so that the fire plume behaviour and the generated buoyancy force likely change in favour of pushing the smoke layer back (assisting the oscillation). Figure 6 shows that the peak velocity of the smoke propagating upstream in the tunnel with 8% downgrade is almost twice as high as in the flat tunnel. Also, the smoke layer thickness increases by approximately 1 m. Despite these factors that would be expected to increase the backlayering length, the backlayer is much smaller.

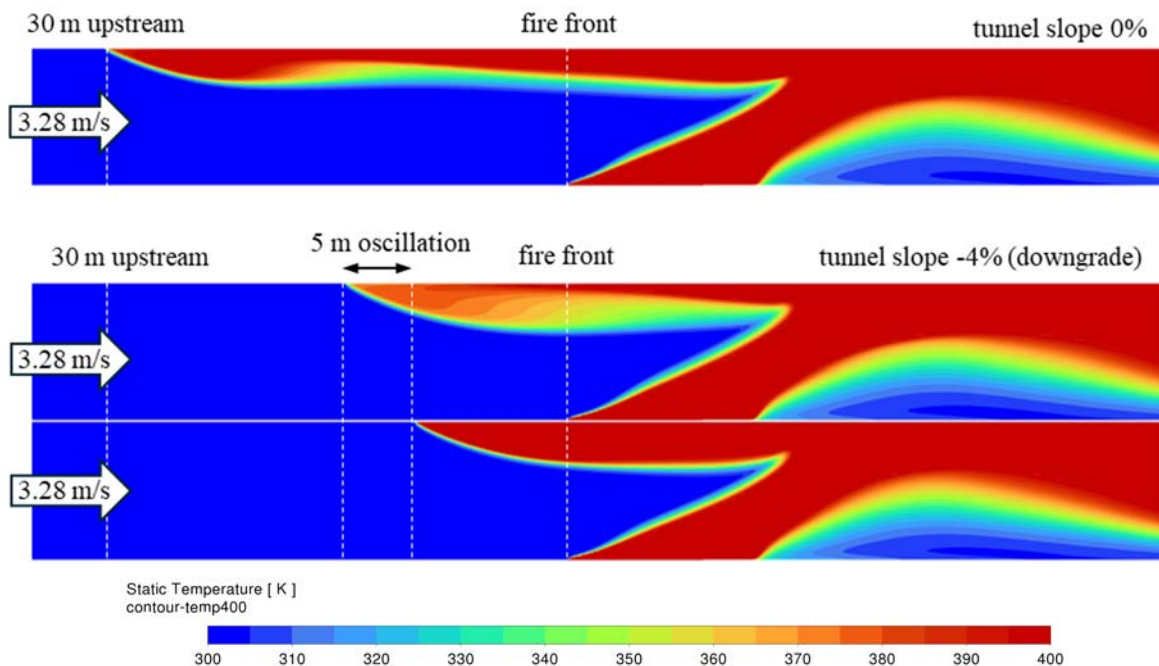


Figure 4: Contour plot of temperature distribution through the middle of the tunnel for confinement velocity in a flat tunnel (top) and a tunnel with 4% downgrade (bottom). The comparison in the bottom picture indicates the amplitude of the smoke backlayer oscillation. Temperature is clipped to 400 K for better presentation.

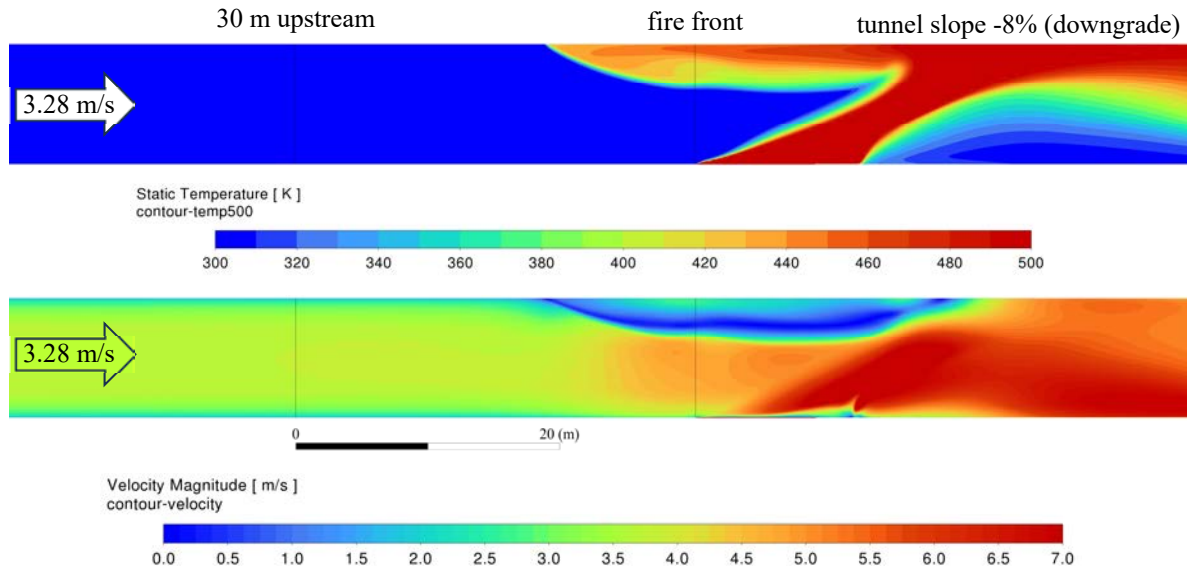


Figure 5: Contour plot of temperature (top) and velocity distribution (bottom) through the middle of the tunnel for confinement velocity and a tunnel with 8% downgrade. Temperature is clipped to 500 K and velocity is clipped to 7 m/s for better presentation.

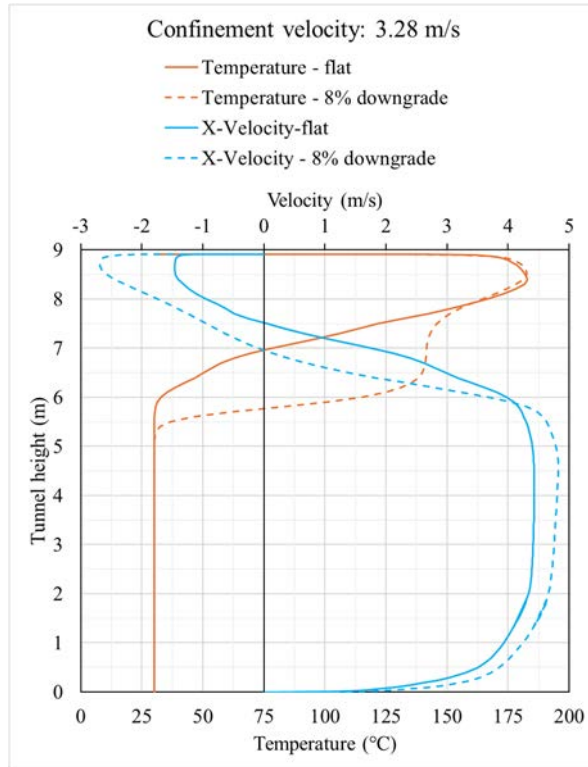


Figure 6: Velocity and temperature profile at the fire front for confinement velocity in a flat tunnel and a tunnel with 8% downgrade. Profile was created on a vertical line from tunnel floor to ceiling in the symmetry plane of the tunnel profile.

Wall heating influence: The wall temperature adjacent to the smoke backlayer was estimated based on a one-dimensional transient heat transfer calculation (results are shown in Figure 9). According to the initial simulation with confinement velocity (backlayer distance of 30 m) the smoke temperature adjacent to the wall and the heat transfer coefficient in the upstream smoke layer were evaluated to be 367 K and 10.3 W/m²K respectively. These values were used as boundary conditions for the one-dimensional transient heat transfer calculation. The estimated wall surface temperature after 60 minutes of 324 K (increase of approximately 21°C) was used as a wall boundary condition in the smoke affected region upstream of the fire, and the simulation repeated. As indicated in Figure 7, the backlayer distance increased from 30 m to 35.4 m (18%) within 60 minutes, due to the wall heating. Figure 8 compares the velocity and

temperature profile at the fire front and shows that the initial velocity and temperature distribution of the upstream smoke layer stays almost the same. That indicates that the initial momentum of the smoke layer decays slightly less with less wall heat transfer when propagating upstream. The increase in backlayering length by 18% for a fire duration of 60 minutes might be acceptable and therefore wall heating may not be an essential inclusion in calculations for estimating confinement velocity. That assumes that the accepted backlayer length is in the range assessed here. The influence on a backlayer distance much higher than 30 m may have a bigger impact on the extra length due to wall heating and so wall heating may then become essential.

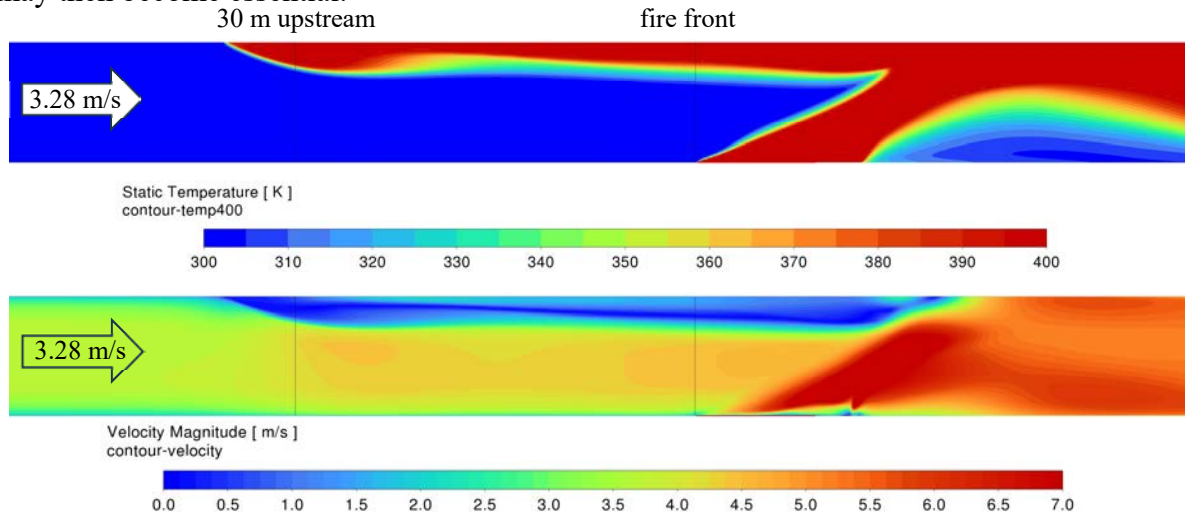


Figure 7: Contour plot of temperature (top) and velocity distribution (bottom) through the middle of the tunnel for confinement velocity with heated wall (heated wall for fire duration of 60 minutes) in the smoke affected wall region upstream of the fire. Temperature is clipped to 400 K and velocity is clipped to 7 m/s for better presentation.

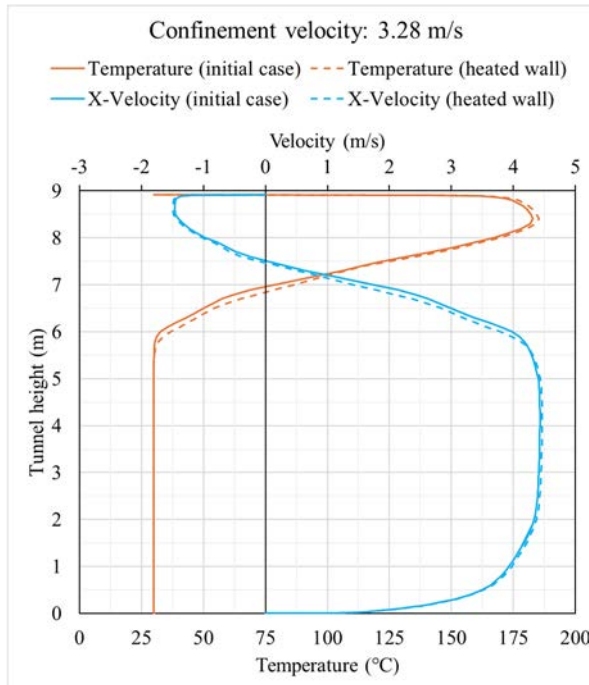


Figure 8: Velocity and temperature profile at the fire front for confinement velocity with constant wall temperature and increased wall temperature (heated wall for fire duration of 60 minutes). Profile was created on a vertical line from tunnel floor to ceiling in the symmetry plane of the tunnel profile.

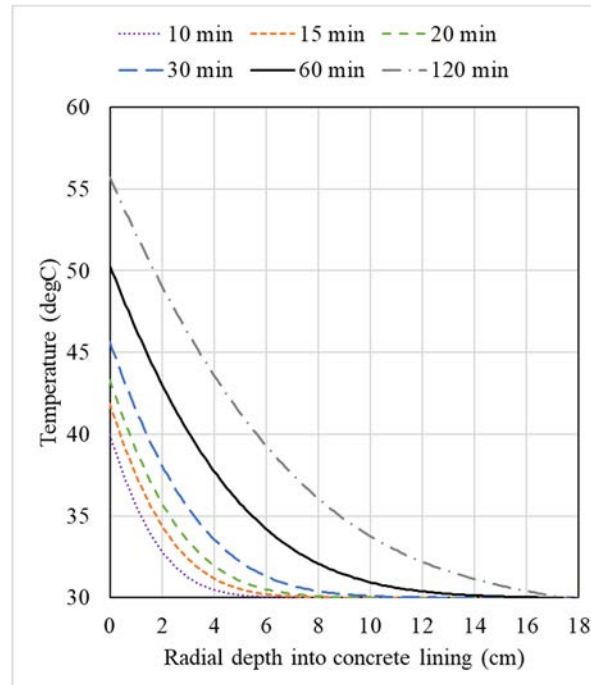


Figure 9: Temperature distribution in concrete lining over time. The radial depth of 0 cm refers to the smoke adjacent wall surface with an inner radius of 4.96 m. Calculations are based on one-dimensional (radial) transient heat transfer.

Wall friction influence: Based on the initial simulation, the typical wall roughness height of $K_s = 0.0015$ m, was increased by a factor of 5 to $K_s = 0.0075$ m and the simulation repeated. A further simulation with smooth wall was also conducted. All other parameters were kept the same. Figure 10 depicts the temperature and velocity distributions of the steady state backlayering with both the increased wall roughness and a smooth wall. With the rougher wall, the backlayer went back from an initial 30 m to a length of 7.8 m (reduction of 75%). For a smooth wall, backlayer length increased by 5.7 m (increase of 19%). Interestingly, the relative reduction in backlayer length for the rougher wall is almost as much as the wall roughness increase. The maximum upstream velocity in the smoke layer at the fire front was reduced by 20% due to the much higher wall roughness (Figure 11) and slightly increased for the smooth wall condition. When considering that a wall roughness height of 0.003 m [26] already refers to a very rough concrete surface, the simulation results likely show the maximum variation in backlayer distance related to wall roughness for any usual concrete tunnel wall. Of course, high effective roughness can also be created by fittings in the tunnel ceiling. No design response for that is offered here.

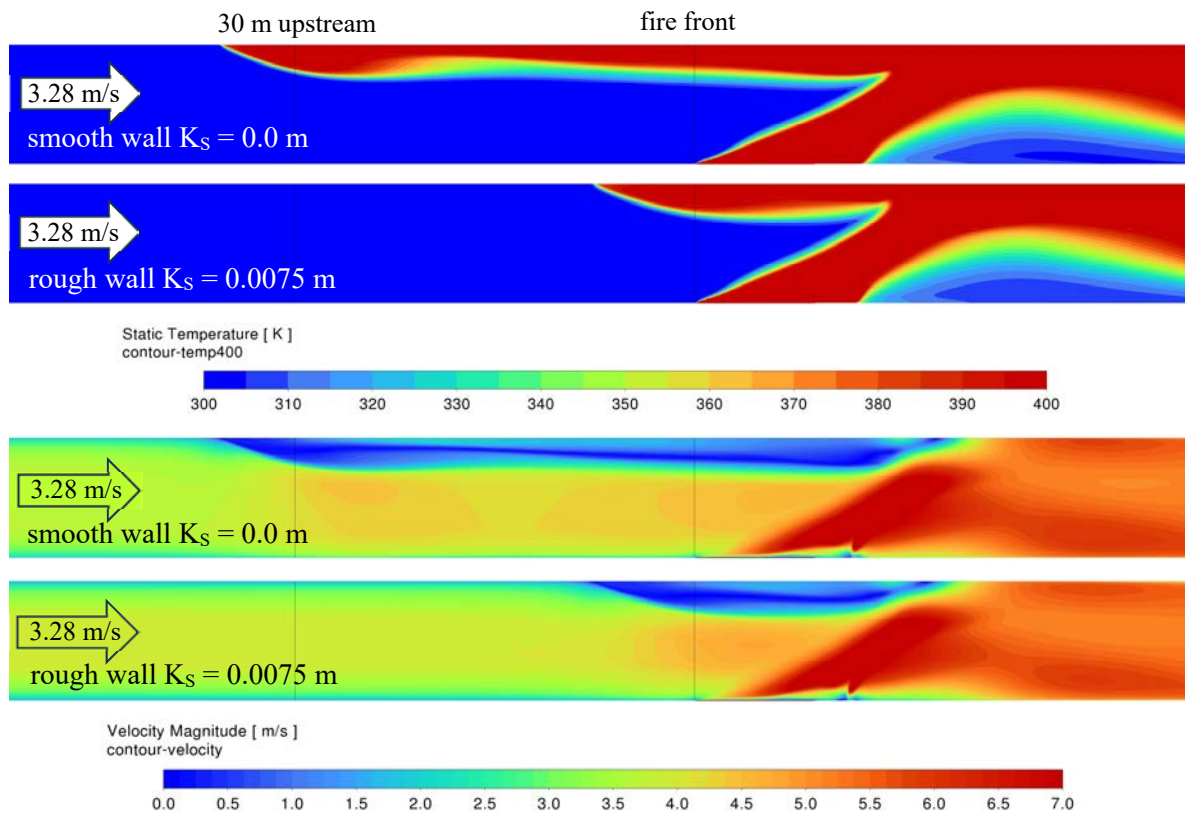


Figure 10: Contour plot of temperature (top) and velocity distribution (bottom) through the middle of the tunnel for confinement velocity with smooth wall and with increased wall roughness (5 times higher compared to initial case). Temperature is clipped to 400 K and velocity to 7 m/s for better presentation.

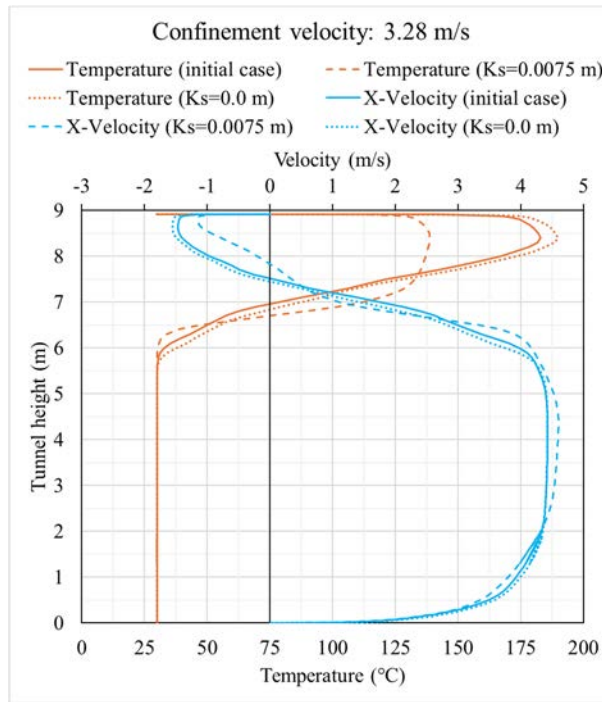
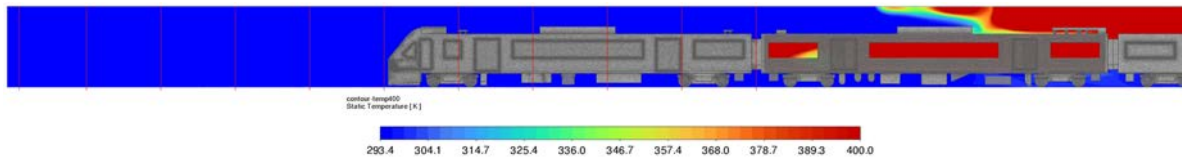


Figure 11: Velocity and temperature profile at the fire front for the initial case with confinement velocity and for the case with increased wall roughness. Profile was created on a vertical line from tunnel floor to ceiling in the symmetry plane of the tunnel profile.

Rail tunnel (high blockage ratio): Using a previously established model of a real case, the air velocity onto the fire was slightly decreased until smoke started propagating upstream. The train in the tunnel restricts the free flow area so that the annular air velocity over the train is higher (here 1.446 times higher) than the average velocity upstream of the train. Once smoke starts propagating upstream and passes the head of the train, the approaching air velocity is much lower and so the smoke starts spreading more readily upstream. Figure 12 illustrates the smoke propagation as the temperature distribution, for the case where upstream propagation of the smoke was just prevented (annular velocity of 1.8 m/s) and the case where smoke was propagating freely upstream (annular velocity of 1.7 m/s). Just a small change in the annular velocity (0.1 m/s) was enough for a change between controlled and uncontrolled conditions. That behaviour might be related to the low velocity values (approximately 1.2 m/s upstream of the train) and the associated low dynamic pressure (stagnation pressure). As soon as the buoyancy force overwhelms the inertia force, the resulting forces on the smoke backlayer are too small to stop their continued upstream propagation. At such low velocities, the mixing that cools the smoke shear layer and assists to blow it downstream, is much reduced.

Annular velocity: 1.8 m/s (1.25 m/s upstream)



Annular velocity: 1.7 m/s (1.18 m/s upstream)



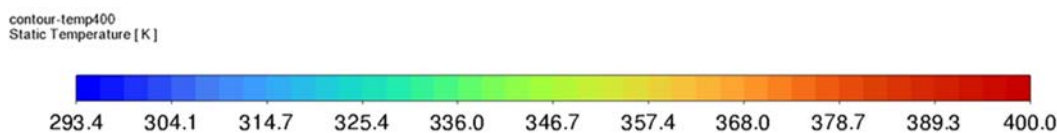


Figure 12: Contour plot of temperature through the middle of the tunnel (long section) for a 15 MW fire and an annular velocity of 1.8 m/s (top) and 1.7 m/s (bottom). Temperature is clipped to 400 K for better presentation. Grid marks (red lines) are at 5 m intervals.

4.4. Practical Approach for Estimating Confinement Velocity

If the typical wall roughness height of the concrete lining is not much less than assumed for the CFD investigation (see Table 1), then the influence due to wall roughness may be less relevant. Something similar can be concluded on the wall heating effect. If a typical fire scenario in a tunnel does not last longer than 30 to 60 minutes, the slow upstream propagation of the smoke backlayer due to the tunnel wall heating over time may still provide acceptable conditions during egress. For conservatism, a tunnel slope could be neglected. Based on that discussion and accepting some variation in the backlayer distance, equation (2) in combination with a modified Richardson number of 1.25 (see Section 4.3.1) could be used for a first guess of confinement velocity (backlayer distance of approximately 30 m). That assumes that the resulting confinement velocity is still sufficiently high (say >2.5 m/s but may need to be higher for sloped tunnels), that the neglected effects on the fire plume and backlayering dynamics do not drastically affect the balance of the counteracting forces and cause an upstream propagation of hot smoke without bounds (see discussion around Figure 12).

However, this proposal to use a modified Richardson number is based on a limited CFD study where a broader range of parameters was not systematically explored. It is not clear how a smaller tunnel area, a different tunnel shape, different tunnel height etc. affect the conclusions made for sloped tunnels. Further, the relationship between confinement and critical velocities may also be a function of the critical velocity. The lower the required critical velocity, the more unlikely it is that a smoke backlayer length can be controlled (kept stable). That also influences the sensitivity and variation of a backlayer length to wall roughness, wall heating etc. Finally, the sensitivities of backlayer distance as discussed in Section 4.3.1 have been explored based only on a 30 m long smoke backlayer. The conclusions made are likely to be different for longer backlayer distances (lower confinement velocity) especially if wall heating is considered.

For now, it seems that the only reliable guide for evaluating confinement velocity is to use a CFD method validated for critical velocity (as proposed in [21]), hoping that the additional physics involved in the backlayer doesn't compromise the CFD model too seriously when allowing significant backlayering.

There are two aspects that may demand adjustment to the proposed CFD model for analysing confinement velocity.

The first is related to thermal radiation between the backlayering smoke and the surroundings. Considering the thermal radiation in the computational domain would supersede the applied radiative fraction approach in the proposed CFD model [21] and thus require a re-validation of the critical velocity cases first. Solving the additional transport equations for thermal radiation would add model complexity and notably increase the computing time. As discussed in Section 4, the influence on the backlayering of the radiative heat loss is assumed to be minor. Including radiation would likely lead to a shorter backlayering distance. Adding the extra complexity just for a minor correction is not seen to be a practical approach.

The second aspect is related to wall heating adjacent to the backlayering and how it affects the backlayering length over time. The proposed model methodology for modelling critical

velocity [21] suggests a steady state solver with constant wall temperature. That seems to be an acceptable approach for analysing critical velocity but needs to be reconsidered for analysing confinement velocity for reasons discussed in Section 4.2.

To include heat flow into the concrete tunnel lining over time would require a transient simulation and drastically increase the computation time. As an alternative, the tunnel wall upstream of the fire could be changed to an adiabatic wall (no heat exchange) to add conservatism, but that would overestimate the required confinement velocity. To still have a reasonably accurate outcome, the smoke propagation can be analysed with a constant wall temperature (same as approaching air) first. After establishing a desired steady state backlayer distance, the simulation could be run again, with an adjusted wall temperature within the region of the upstream smoke layer adjacent to the wall, as described in Section 4.3.

5. COMMENTARY AND CONCLUSION

From a fire life safety perspective, it makes sense to reduce the tunnel air velocity onto the fire so far as is reasonably practicable [27] [28] to optimise conditions for egress. This approach has been common practice especially in Europe via the PIARC [29] and national standards [28], [27], [25] but is also acknowledged in the 2023 version of NFPA 502 [3]. Instead of having a fixed design velocity depending on ventilation system and traffic conditions as usually adopted in Europe [29], [28], [27], [25], NFPA 502 [3] permits a design velocity (confinement velocity) that controls upstream smoke propagation to within a limiting length (e.g. 30 m).

As there is no guidance on how to establish confinement velocity, the essential physics on smoke propagation and confinement velocity were re-visited. Based on the mixed convection model for estimating critical velocity for smoke control in road tunnels [17], the local fire plume dynamics relevant to establishing or preventing upstream smoke propagation were summarised. Once smoke is propagating upstream, additional parameters and effects become relevant. The most important parameters influencing the backlayer dynamics were discussed, and their influences on the backlayer distance explored by means of a CFD model validated for critical velocity. The outcomes of that study, based on the fire and tunnel characteristics investigated were that:

- For a typical high arched road tunnel, the difference between critical velocity and confinement velocity with a 30 m smoke backlayer was found to be approximately 7%.
- Confinement velocity is actually lower in downgrade tunnels. For the same airspeed confining smoke to 30 m upstream in a flat tunnel, backlayer distance was reduced by 50% for the 4% and 8% downgrade tunnels.
- The heat transfer from the upstream smoke layer to the tunnel wall increases the wall surface temperature over time which causes the smoke layer to slowly propagate upstream and increases the backlayer length by 18% over a period of 60 minutes.
- Compared to a typical tunnel wall roughness (roughness height of 0.0015 m), a smooth wall increased backlayer length by 19%. Backlayer length was reduced by 75% for a wall roughness that was 5 times higher than the typical value.
- Especially in highly blocked tunnels (e.g. rail tunnels), once critical velocity value is already very low (<2 m/s), confinement velocity is no different to critical velocity.

However, those outcomes are based on a limited CFD study, with only one fire scenario in each example tunnel. It is unclear how the effects that were explored might impact the upstream smoke propagation for different fire scenarios, tunnel geometries or different confinement velocity definitions (e.g. accepted backlayer length). For the time being, it is recommended to use a CFD model validated against critical velocity (as proposed in [21] and

discussed in this paper), with the hope that the additional physics involved in the backlayer are still captured well enough to not invalidate the outcome.

6. REFERENCES

- [1] P. Sturm, M. Beyer and M. Rafiei, "On the problem of ventilation control in case of a tunnel fire event," *Case Studies in Fire safety, CSFS 22, Elsevier publishing*, doi: 10.1016/j.csfs.2015.11.001, 2015.
- [2] M. Beyer, C. Stacey and A. Dix, "Critical velocity and tunnel smoke control Part 2, Filling the NFPA 502 void," *Australian Tunnelling Society*, p. 6, 2021.
- [3] NFPA 502, "Standard for Road Tunnels, Bridges, and Other Limited Access Highways," The National Fire Protection Association, US, 2023.
- [4] G. W. Kile and J. A. Gonzalez, "The Memorial Tunnel Fire Ventilation Test Program: The Longitudinal and Natural Tests," *ASHRAE Transactions 103, ProQuest Science Journals*, p. 701, 1997.
- [5] MTFVTP, "Memorial Tunnel Fire Ventilation Test Program - Comprehensive Test Report," Bechtel/Parsons Brinckerhoff, Boston, 1995a.
- [6] MTFVTP, "Memorial Tunnel Fire Ventilation Test Program - Memorial Tunnel Test Data Report incl. 9 discs of raw data," Bechtel/Parsons Brinckerhoff, Boston, 1995b.
- [7] D. Fruhwirt, P. Sturm, M. Bacher and H. Schwingenschlögl, "Smoke Propagation in Tunnels - Comparison of In-Situ Measurements, Simulations and Literature," in *10th International Conference "Tunnel Safety and Ventilation"*, Graz, 2020.
- [8] S. R. Lee and S. Ryou, "An Experimental Study of the Effect of the Aspect Ratio on the Critical Velocity in Longitudinal Ventilation Tunnel Fires," *Journal of Fire Sciences*, no. 23, pp. 119-138, 2005.
- [9] Y. Oka and G. T. Atkinson, "Control of Smoke Flow in Tunnel Fires," *Fire Safety Journal*, no. 25, pp. 305-322, 1995.
- [10] G. T. Atkinson and Y. Wu, "Smoke Control in Sloped Tunnels," *Fire Safety Journal*, no. 27, pp. 335-341, 1996.
- [11] Y. Wu and M. Z. A. Bakar, "Control of smoke flow in tunnel fires using longitudinal ventilation system – a study of the critical velocity," *Fire Safety Journal*, no. 35, pp. 363-390, 2000.
- [12] Y. Li and H. Ingason, "Study of critical velocity and backlayering length in longitudinally ventilated tunnel fires," *Fire Safety Journal*, no. 45, pp. 361-370, 2010.
- [13] Y. Li and H. Ingason, "Effect of cross section on critical velocity in longitudinally ventilated tunnel fires," *Fire Safety Journal*, no. 91, pp. 303-311, 2017.
- [14] Y. Li and H. Ingason, "Corrigendum to "Effect of cross section on critical velocity in longitudinally vent-lated tunnel fires" [Fire Saf. J. 91 (2017) 303-311]," *Fire Safety Journal*, no. 110, 2019.

- [15] Y. Li and H. Ingason, "Discussions on critical velocity and critical Froude number for smoke control in tunnels with longitudinal ventilation," *Fire Safety Journal*, no. 99, pp. 22-26, 2018.
- [16] C. Stacey and M. Beyer, "Critical of critical velocity - An industry practioner's perspective," in *10th International Conference 'Tunnel Safety and Ventilation'*, Graz, 2020a.
- [17] M. Beyer, C. Stacey and G. Brenn, "A Mixed Convection Model for Estimating the Critical Velocity to Prevent Smoke Backlayering in Tunnels," *Springer Fire Technology*, no. prepring, p. 50, 2024.
- [18] P. Thomas, "The Movement of Smoke in Horizontal Passages Against an Air Flow," *Fire Research Station*, no. Fire Research Note No 723, 1968.
- [19] P. Thomas, "The Movement of Buoyant Fluid Against a Stream and the Venting of Under-ground Fires," *Fire Research Station*, no. Fire Research Note No 351, 1958.
- [20] W. Kennedy, "Critical velocity: Past, Present and Future," *Seminar of Smoke and Critical Velocity in Tunnels*, pp. 305-322, 9-11 March 1996.
- [21] M. Beyer and C. Stacey, "CFD Validation for Tunnel Smoke Control Design," in *11th International Conference Tunnel Safety and Ventilation*, Graz, 9th and 10th May 2022.
- [22] Ansys, Inc, "ANSYS Fluent Theory Guide, Release January 2023 R2," USA, 2023b.
- [23] Ansys, Inc, "ANSYS Fluent User's Guide, Release January 2023 R2," USA, 2023a.
- [24] Ansys, Inc, "ANSYS Fluid Dynamics Verification Manual, Release January 2023 R2," USA, 2023c.
- [25] RABT, "Richtlinie für die Ausstattung und den Betrieb von Straßentunnel (RABT)," Richtlinie, Forschungsgesellschaft für Straßen- und Verkehrswesen , Arbeitsgruppe Verkehrsführung und Verkehrssicherheit, Germany, 2016.
- [26] J. Raposo, E. Cavaco, L. Neves and E. Julio, "A novel roughness parameter for more precise eztimation of the shear strength of concrete-to-concrete interfaces," *Elsevier ScienceDirect*, vol. 410, no. Construction and Building Materials 410, p. 12, 2024.
- [27] ASTRA, "Lüftung der Strassentunnel - Systemwahl, Dimensionierung und Ausstattung (2008 V2.03)," Richtlinie, Bundesamt für Strassen ASTRA, Bern, CH, 2008.
- [28] RVS 09.02.31, "Tunnel / Tunnel Equipment / Ventilation Systems - Basic Principles," Richtlinie, Österreichische Forschungsgesellschaft Straße - Schiene - Verkehr, Wien, AT, 2014.
- [29] PIARC (C3.3), "Operational Strategies for Emergency Ventilation (P. C. (C3.3), Ed.)," World Road Association (PIARC), 2011.

DESIGN, REFURBISHMENT AND OPERATION OF THE VENTILATION IN THE ROAD TUNNEL COMPLEX IN PRAGUE

Jiří Zápařka, Jan Pořízek, Ludvík Šajtar
Satra spol. s r. o., CZ

DOI 10.3217/978-3-85125-996-4-44 (CC BY-NC 4.0)

This CC license does not apply to third party material and content noted otherwise.

ABSTRACT

In this article we would like to present the history of the ventilation system of the city tunnel complex in Prague. We will focus on fire ventilation, ventilation to reduce the environmental impact and also on the operation of the tunnel complex.

The existing part of the tunnel complex is 8.7 km long and was commissioned in stages between 1997 and 2015 and is in operation today. The project of the last section in the eastern part of the city circuit, 7.1 km long MO-LS "Eastern link", is currently in the phase of documentation for planning permission. When the last section of the city circuit is completed, 16 km of tunnels will be in operation.

Keywords: tunnel complex, ventilation, fire, environment, tunnel operation

1. INTRODUCTION

The first tunnel on the City Ring Road was the 2 km long Strahov tunnel, opened in 1997, designed in the 1970s and replicating the Alpine tunnel system with full transverse ventilation aimed at ensuring clean air during normal operation. Another concept for the 1.2 km long Mrázovka, opened in 2004, and the 5.5 km long Blanka, opened in 2015, was longitudinal ventilation with the transfer of polluted air from the exiting tube into entry tube and exhaust by nearest machine room, in order to reduce pollution outside the portal.

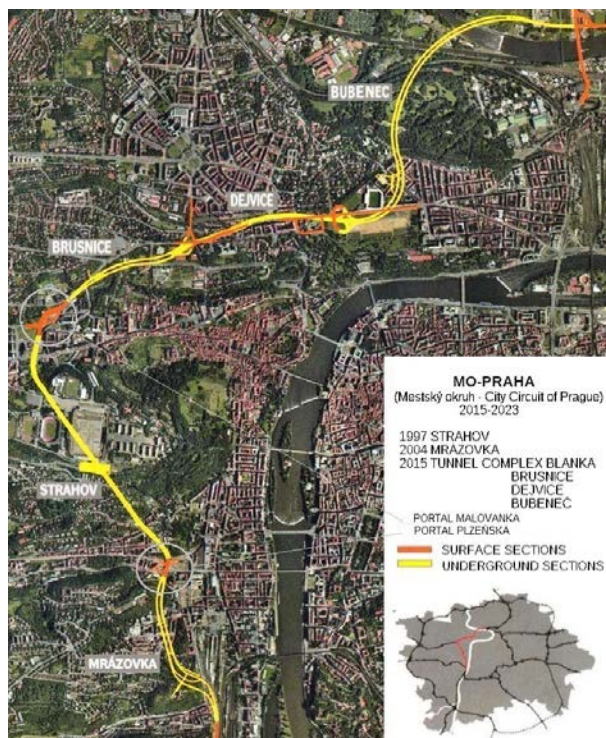


Figure 1: Location of tunnels including sensitive locations

2. TRAFFIC AND VENTILATION OF CITY CIRCUIT TUNNELS

2.1. Two rings traffic concept in Prague

The traffic concept in Prague after 1989 was decided as having 2 circuits. Highway outer circuit for transit and inner city circuit for local transportation. The functionality is limited because only part of the traffic system is completed.

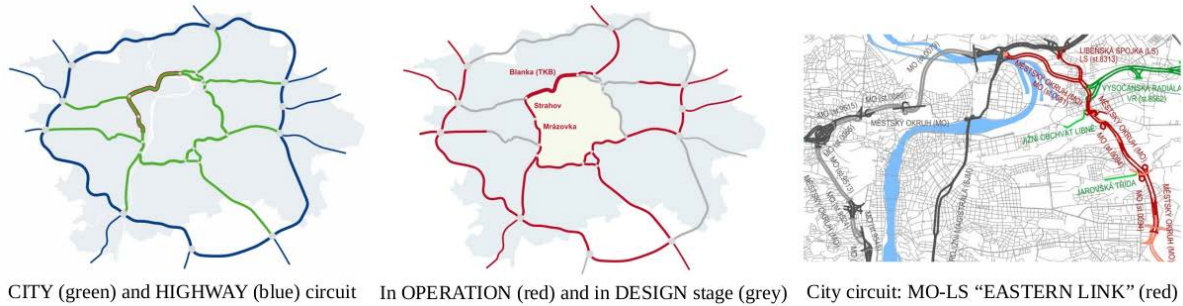


Figure 2: City and highway circuits in Prague

2.2. Traffic

Traffic intensity is 50 000 vehicles/1lane with traffic composition 96-97 % personal cars and 3-4 % trucks up to 12t.

2.3. Ventilation

Fire ventilation has been upgraded to the extent that the longitudinal speed can be controlled in all the tunnel. The critical condition in the Strahov tunnel has been corrected, but the upgrades in Strahov and Mrázovka are not yet complete.

In normal operation, the tunnels are ventilated naturally. The Blanka tunnel complex is equipped with an expert system that is used when exhaust protection is switched on.

The tunnels are in the center of Prague and close to Prague Castle, so the choice of locations for the ventilation stacks was limited. In both cases, the location was about 600-700 m from the portal, so an additional machine room was designed near the portal (about 50 m before the end) to transfer the polluted air from the outgoing tube to the inlet section of the second one (similar to the M5 in Australia or partly Engelberg in Germany).

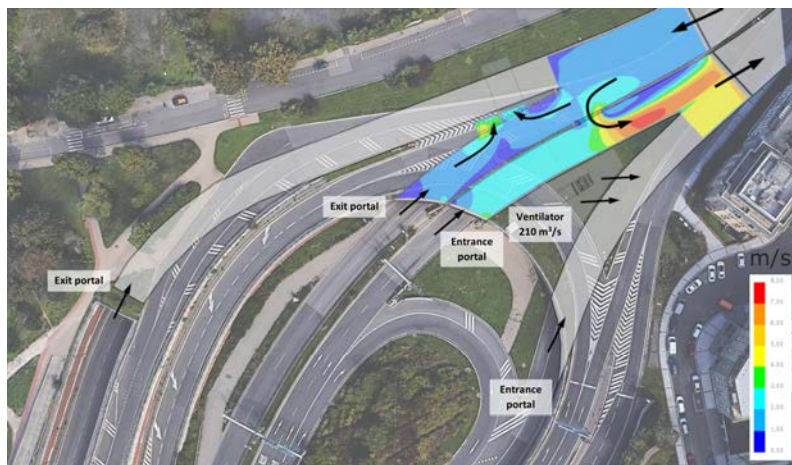


Figure 3: Malovanka portal

3. PARTIAL UPGRADE OF FIRE VENTILATION IN STRAHOV

First, a major reconstruction was necessary in the oldest Strahov tunnel with transverse ventilation due to the longitudinal slope of the tunnel. The ventilation system was converted to longitudinal ventilation with extraction at the end of the tunnel instead of extraction along the entire length of the tunnel. Jet fans were installed for longitudinal smoke control.

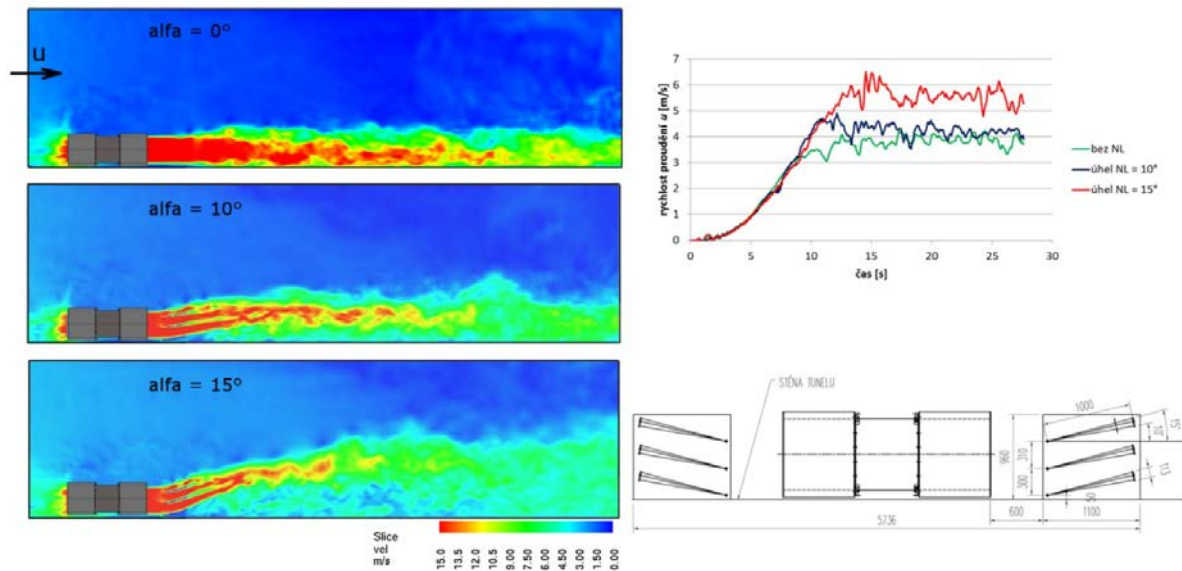


Figure 4: Jet fans with outlet blades were installed.

4. OPERATIONAL EXPERIENCE WITH VENTILATION REGARDING ENVIRONMENT

At the time of the design for the building permit of the Mrázovka tunnel (1997-2001), the objective was to reduce the critical short-term NO_x value to $200 \mu\text{g}/\text{m}^3$ outside the tunnel (Law 309/1991)[1]. At the design stage, traffic in the portal area of the proposed Mrázovka tunnel was congested for most of the day and based on the 1998 model (ATEM; 2000), after the opening of the Strahov tunnel, even without emissions from Mrázovka, the short-term NO_x concentration in the vicinity of the "Portal Plzeňská", was $865 \mu\text{g}/\text{m}^3$. The limit was exceeded at least twice at all selected locations in the vicinity of the portal. This was confirmed by measurements in 1998-9, when the maximum was more than $900 \mu\text{g}/\text{m}^3$.

All other pollution limits were met, but the short-term limit for NO_x was exceeded at 10-24% compared to the 5% maximum required by law. This led the City Council to require a method of ventilation to ensure that no polluted air exits the portal.

Since 2006, the focus has turned from NO_x to NO_2 and the annual concentration of $\text{IHR} = 40 \mu\text{g}/\text{m}^3$ has become an issue as the (ATEM; 2006) indicates that background concentrations were higher in 2006.

The annual average concentration at the Plzeňská and Malovanka portals in 2006 was $47\text{-}63 \mu\text{g}/\text{m}^3$. The requirements of the municipality for Blanka remained the same as for Mrázovka.

..

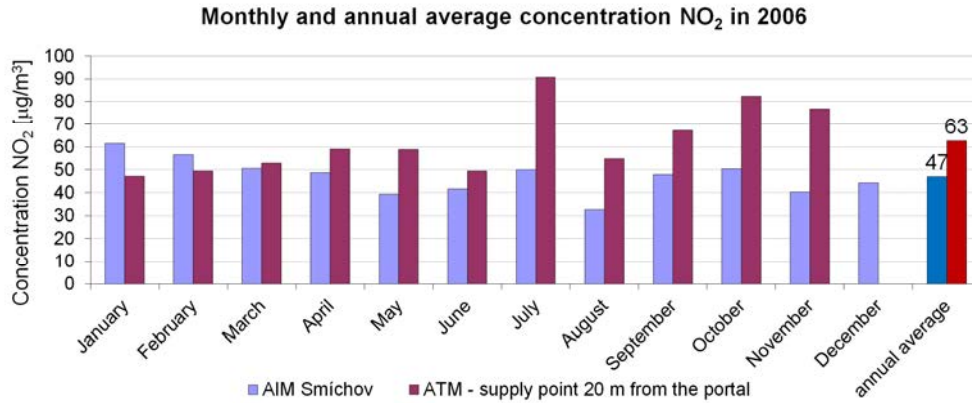


Figure 5: Plzeňská portal monthly and annual average NO₂ (µg/m³) in 2006

The effectiveness of the measure is illustrated in the following figure, which shows how the flow from the outlet portal is stopped when this environment mode is used:

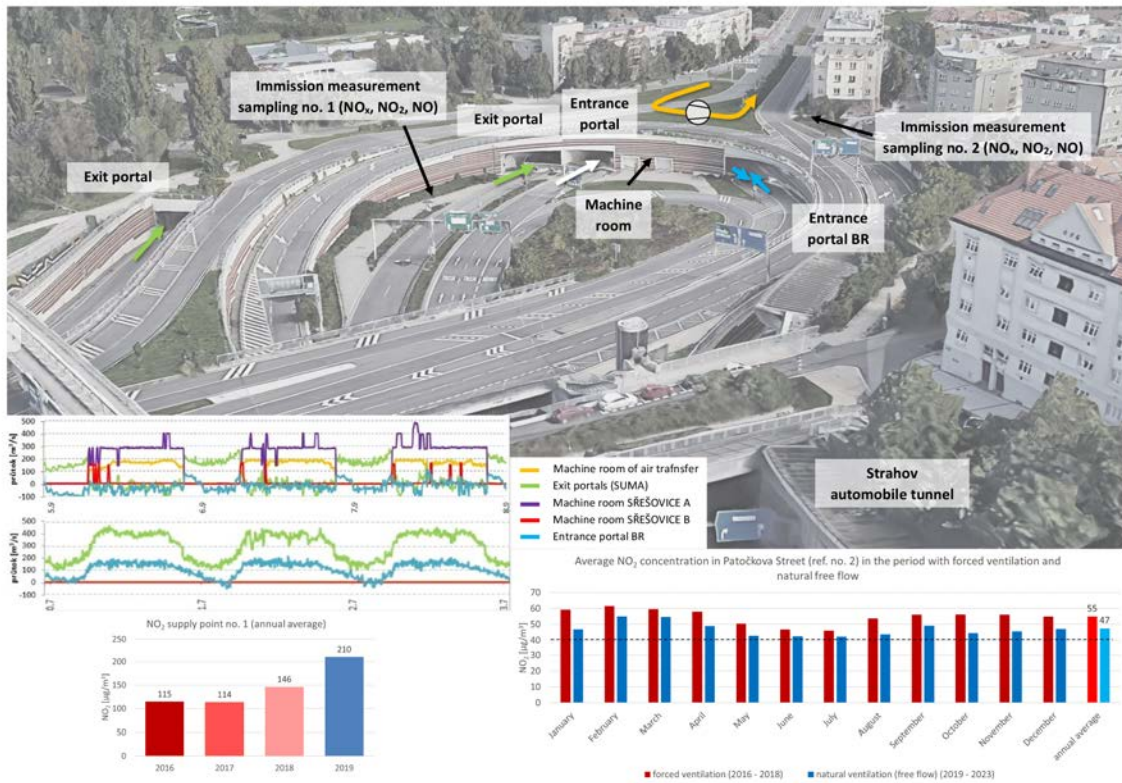


Figure 6: Malovanka portal: environmental mode 2016-2018 vs. natural airflow 2018-2023

The example of three days with portal protection vs. natural flow shows how the airflow from the exit portal, which is normally around 400 m³/s, drops to 0.

In 2016-2018, the concentration at point 1 was lower with ventilation than with natural flow.

Interestingly, at point 2 (further away from the portal), the measured concentrations are lower during natural flow and not during the environmental regime.

This can be explained by missing airflow near the portal, that would more dilute the pollution during environmental mode. During natural flow 400 m³/s emits out of the exiting portal and 300 m³/s is sucked in through entry portal.

In 2020, work started on the zoning decision of the last section of the city circuit MO-LS "Eastern link". Based on the modeled results, the annual NO₂ concentration levels in 2015 are still close to the limit. In 2030 they are at least 10 µg/m³ lower than that, not exceeding 30 µg/m³.

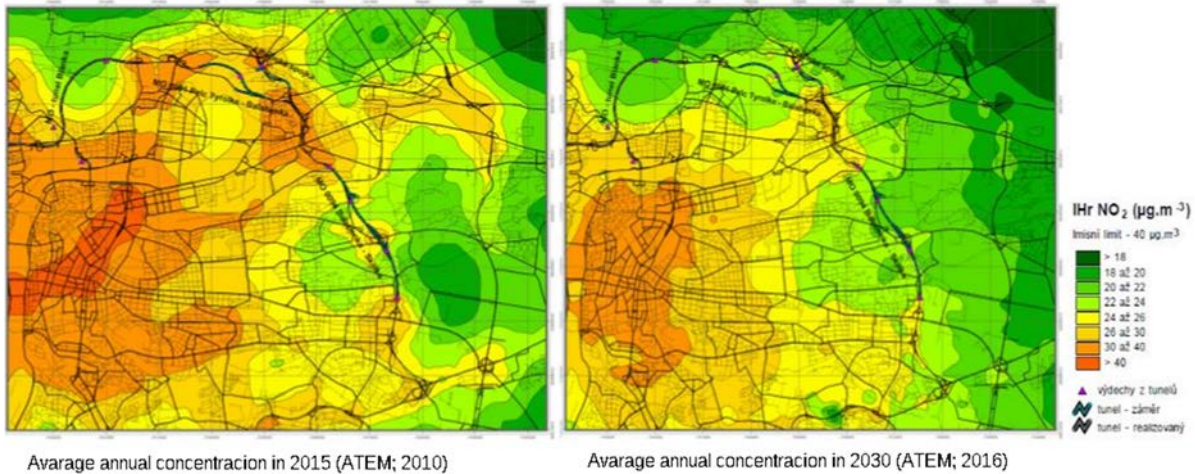


Figure 7: Annual NO₂ concentrations in 2015 and 2030

Figure 8 shows the difference between the environmental mode and natural airflow, without background pollution. During natural airflow, there is only an increase of 1-3 µg/m³ near the portal.

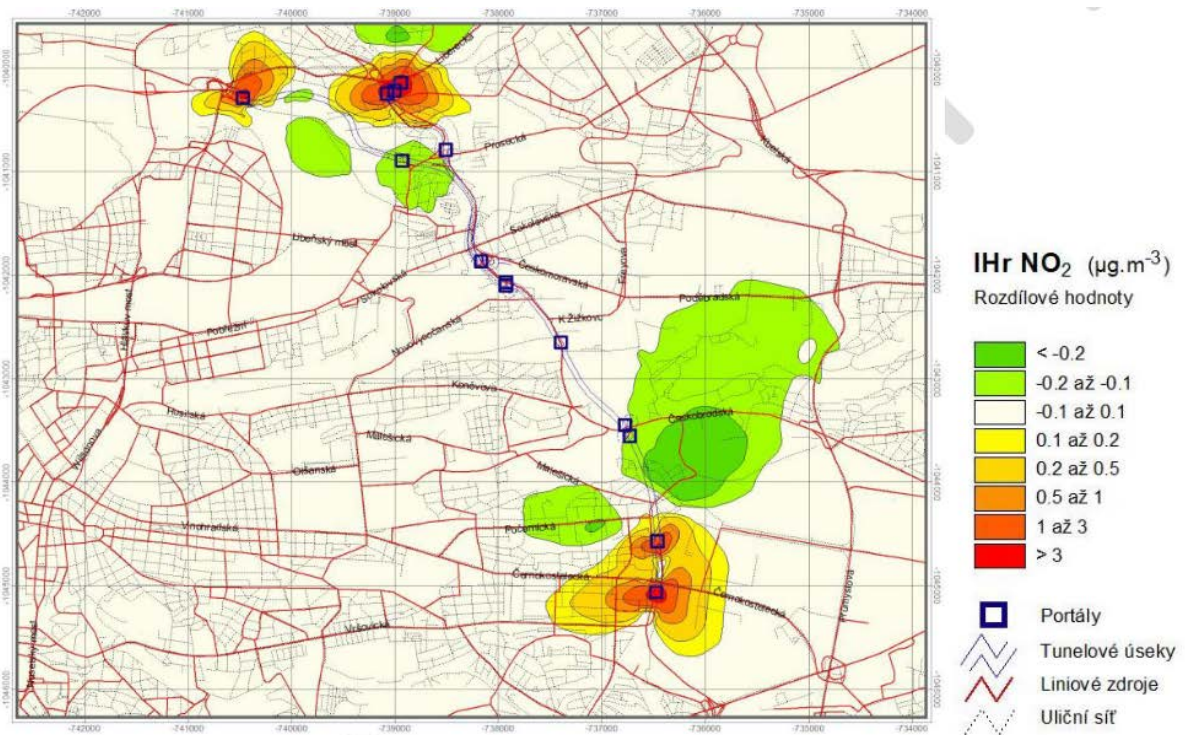


Figure 8: NO₂ difference values between environmental mode and natural flow

5. OPERATION, TRAINING, TESTING

The operation is so far controlled from two centers. One is the police which controls the traffic and the other is tunnel operator which controls the technology. The process is now underway to unify traffic and technology control in a new control center called MOS, which is under construction. This will also improve communication with the emergency services (integrated rescue system such as firefighters, paramedics...).

The different age and corresponding “state of art” of the tunnel control system places greater demands on the operators. In addition to their repeated training and testing, the control system and operator interface are gradually being unified.

Repeated tests of the ventilation system, operators and exercises of the firefighters and all rescue systems are carried out. During some of these tests and exercises, the smoke effects have proved to be very useful. For more on fire ventilation see [2].



Figure 9: Tunnel Blanka



Figure 10: Rescue system exercise in tunnel Blanka

6. SUMMARY AND CONCLUSION

Longitudinal airflow control is now possible in all tunnels.

Traffic control for environmental reasons in Prague is based on NO₂ levels. Previously, NO_x was the target pollutant and the short-term limit (1 hour) was decisive for the design. Since the change in legislation in 2006, when the limit was changed to NO₂, compliance with the long-term limit (1 year) is critical.

The "ecological mode", if operated at all, should therefore be based on an algorithm with a long-term target value and not on the actual measured concentration outside the tunnel.

In the latest MO-LS "Eastern Link" tunnel project for 2030, no environmental technology or mode of operation is needed anymore.

7. REFERENCES

- [1] Act number 309/1991 about air pollution (Zákon o ovzduší č. 309/1991)
- [2] 8th International Conference “Tunnel Safety and Ventilation”

HYDROGEN POWERED VEHICLES IN A TUNNEL INCIDENT – RISKS AND CONSEQUENCES

¹Martin Aggarwal, ²Daniel Fruhwirt, ³Patrik Fößleitner, ⁴Oliver Heger, ¹Patrick Pertl,
⁴Regina Schmidt, ¹Alexander Trattner
¹HyCentA Research Ltd., AT
²Graz University of Technology, AT
³FVT Ltd., AT
⁴ILF Consulting Engineers., AT

DOI 10.3217/978-3-85125-996-4-45 (CC BY-NC 4.0)

This CC license does not apply to third party material and content noted otherwise.

ABSTRACT

The mobility sector is subject to a massive transition from fossil fuels to new energy carriers. The driving force is the reduction of greenhouse gas emissions in order to minimize the impact on global climate. Hydrogen represents a promising fuel as it can be used in combination with internal combustion engines as well as fuel cells. However, due to its physical and chemical properties it potentially poses high risks in an incident scenario. This mainly refers to its wide flammability limits as well as the common way of storage at nominal pressures of 350 bar (busses and trucks) and 700 bar (passenger cars). This paper presents the findings of the Austrian research project “HyTRA” that aimed at an evaluation of potential hazards in tunnel incident scenarios involving hydrogen powered vehicles. Five scenarios with a high potential risk have been identified and investigated related to the consequences for tunnel users and the tunnel facility. Ultimately, a comparison to incident events with conventional vehicles gives information about the consequences for the level of tunnel safety.

Keywords: hydrogen, tunnel safety, incident scenarios, consequence evaluation, risk assessment

1. INTRODUCTION

Tunnel safety represents a topic of special concern, as past tunnel incident events [1] have shown the hazard potential of such scenarios. Thus, it is inevitable to investigate new factors, which might have an impact on the safety level. The transition from fossil fuel powered vehicles to alternatively powered vehicles represent such a new factor. Battery electric vehicles have already penetrated the market and hydrogen powered vehicles (H_2 vehicles) are expected to become relevant in the future. The latter use either combustion engines or fuel cells to convert the chemically stored energy of hydrogen into kinetic energy for the vehicle. The storage system probably is the most critical part of today’s hydrogen technology. This is due to the physical and chemical properties of hydrogen, which require hydrogen to be stored liquid at very low temperatures or pressurized at a high-pressure level. The latter represents the more common way of hydrogen storage. The nominal storage pressure for busses and trucks is 350 bar. For passenger car application this value increases to 700 bar. Obviously, in an incident situation both, the mechanical energy due to high pressure as well as the chemical energy of hydrogen may cause severe harm.

Due to the importance of this topic, a variety of experimental and/or analytical and numerical investigations with respect to different hydrogen scenarios have been carried out in past research projects. This includes investigations on jet-flames, hydrogen cloud explosion as well as tank ruptures. In recent years several research projects have been funded by the European

Union [2][3][4]. These projects covered safety strategies, the evaluation of risk and the development of powerful tools, which can be used for risk assessment in future tunnel projects. Further research output was published by [5] where analytical calculations that aimed at quantifying temperatures, pressures and heat fluxes caused by incidents of vehicles powered by gaseous and liquified fuels were conducted.

However, there are still many uncertainties and the transfer of knowledge to tunnel operators, tunnel users and emergency services must be promoted. In order to reduce the uncertainties, the Austrian research project HyTRA aimed to evaluate incident scenarios with hydrogen-powered vehicles and to determine the consequences for human health and the tunnel infrastructure in the specific context of Austrian road tunnels. For this reason, extensive literature and data collection, analytical and numerical investigations as well as a detailed risk assessment have been conducted. Finally, technical and organizational measures to avoid hydrogen scenarios or to mitigate the consequences were listed and evaluated in terms of efficiency, range of influence and implementation effort. This paper provides a brief overview of the main findings of the project. The final report of the HyTRA project including detailed explanations is available via [6].

2. HYDROGEN POWERED VEHICLES

2.1. Technology Overview

H_2 vehicles operate by converting the chemically stored energy of H_2 into kinetic energy for vehicle propulsion. There are two primary types of powertrains: H_2 internal combustion engine vehicles (H_2 ICEVs) and Fuel Cell Electric Vehicles (FCEVs).

H_2 ICEVs employ internal combustion engines akin to those found in traditional gasoline-powered cars. However, instead of burning gasoline, these vehicles combust H_2 gas within the engine to generate mechanical power, propelling the vehicle forward. They serve as a transitional solution between conventional ICEVs and FCEVs, capitalizing on existing infrastructure and manufacturing capabilities.

On the other hand, FCEVs utilize H_2 by generating electricity via a chemical reaction with oxygen, powering electric motors. The powertrain of a FCEV comprises H_2 tanks for energy storage, a battery serving as an energy storage and converter, a fuel cell acting as an energy converter, several voltage converters, an electric motor, transmission and mechanical drive for the wheels. FCEVs have higher efficiencies than combustion technologies and are classified as zero-emission vehicles, emitting solely water vapor and air through the exhaust. Additionally, these vehicles offer rapid refueling times and long driving ranges. Figure 1 illustrates examples of serial vehicles on the road.



Figure 1: Selected applications of FCEVs [7][8][9][10][11][12]

H_2 ICEVs have yet to enter series production, contrasting with the availability of several models of FCEVs designed for road use. While there is notable interest in medium and heavy-duty FCEVs, the production of light-duty FCEVs, such as the Toyota Mirai 2 and the Hyundai Nexo, is already underway. By 2022, the global stock of FCEVs surged by 40% compared to 2021, surpassing 72,000 vehicles. Among these, approximately 80% are cars, while 10% trucks and nearly 10% buses. Notably, in 2022, the fuel cell truck segment experienced a rapid 60% growth rate, outpacing the expansion seen in cars and buses [13].

2.2. Hydrogen Storage System

H_2 vehicles utilize H_2 as an energy carrier. H_2 is a colorless and odorless gas, possessing the lowest density among all elements and being approximately 14 times lighter than air. However, due to its low density, storage and transportation with sufficient energy density pose significant technical and economic challenges. Common methods of H_2 storage include:

- Gaseous compressed hydrogen (CGH_2) stored in pressure vessels at pressures ranging from 350 to 700 bar,
- Liquid cryogenic hydrogen (LH_2) stored at temperatures below $-252.85\text{ }^\circ\text{C}$ (20.3 K) in cryogenic containers,
- H_2 stored in chemical or physical compounds, primarily in or on solids or liquids, which are currently in the laboratory stage. [14]

The state-of-the-art storage technology for on-road applications is CGH_2 , currently utilized in all series vehicles. In this method, H_2 is compressed to pressure levels up to 700 bar. Other storage technologies are still in a prototype phase and exhibit a low technology readiness level. Gaseous storage constitutes a closed system, enabling the storage of H_2 over extended periods without loss. Pressure vessels typically adopt a cylindrical shape for favorable stress distribution. For mobile applications, type 3 (aluminum liner wrapped in carbon fiber) and type 4 (plastic liner wrapped in carbon fiber) tanks are predominantly used due to their lightweight design, as depicted in Figure 2. Type 5 tanks (linerless, solely carbon fiber) are currently under development and not yet ready for serial application.

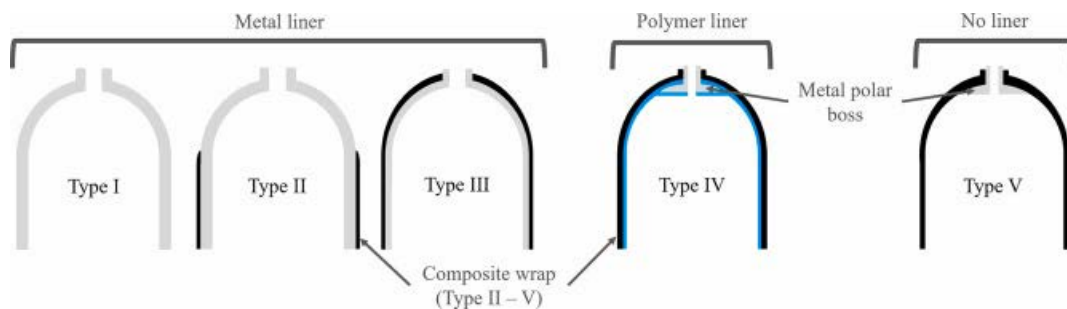


Figure 2: Types of hydrogen storage tanks for CGH_2 [15]

Compared to diesel, the gravimetric energy density of H_2 is about 3 times higher with a value of 33,33 kWh/kg. To meet the usual driving range of a passenger car, a H_2 storage capacity of up to 6.5 kg is needed for passenger cars. Due to the fact, that the well-to-wheel efficiency of a FCEV is about twice of an ICEV, the total stored chemical energy in a FCEV is about 2 times lower.

Typical specification of CGH_2 storage systems for various road transport applications are defined in Table 1 and are used for the subsequent damage analysis in section 4.

Table 1: Vehicle types and tank parameters considered in the subsequent damage analysis (see section 4)

Vehicle Type	Details	Single Tank	Total Storage System
Passenger Car	3 tanks at 700 bar	52 Liter and 2,1 kg	157 Liter and 6,3 kg
Heavy duty truck	7 tanks at 350 bar	192 Liter and 4,6 kg	1342 Liter and 32,6 kg
Bus	5 tanks at 350 bar	313 Liter and 7,5 kg	1563 Liter and 37,5 kg

In a hydrogen storage system (HSS) multiple tanks can be interconnected. Alongside the tanks themselves, various components such as valves, pipework, couplings, screw fittings, and sensors are employed to monitor pressure, temperature, and tightness, as depicted in Figure 3.

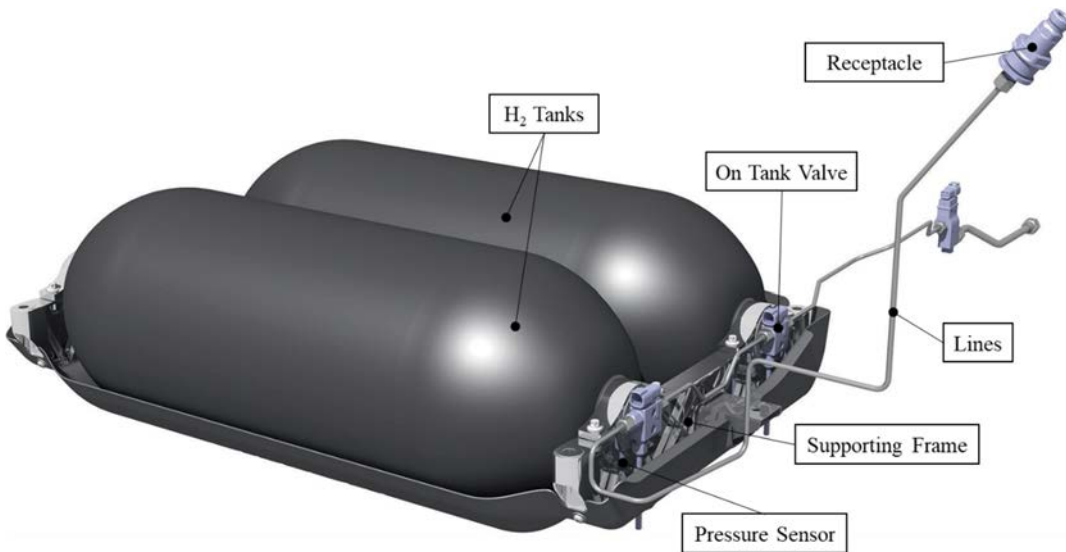


Figure 3: Automotive 700 bar compressed gaseous hydrogen storage system [16]

H_2 vehicles have additional hazards like fire and explosion hazards due the onboard stored H_2 . The most critical component in terms of chemical and pressure energy is the H_2 tank. To ensure safe operation and approval for road traffic, these components must undergo design, manufacturing, testing, and maintenance in compliance with relevant codes and standards.

Within the European Union (EU), regulations such as (EU) 2019/2144, (EU) 2021/535 and UN Regulation No 134 govern the type-approval process of H_2 vehicles and their components, focusing on safety-related functions. Here is a summary of the most crucial test procedures for tank approval [17]:

- **Fire test:** The tank should vent through the Thermally-activated Pressure Relief Device (TPRD) and withstand exposure to an engulfing bonfire without failure.
- **Hydrostatic burst test:** This test determines the burst pressure, which should be at least 2.25 times the nominal working pressure for a duration of at least three minutes.
- **Ambient pressure cycling test:** H_2 tanks must not leak or rupture before undergoing 11,000 fill cycles, representing a 15-year life of use.

These rigorous testing procedures ensure the reliability and safety of tanks, contributing to the overall safety of H_2 vehicles on the road.

In the event of a thermally induced rupture of the tank in a H_2 vehicle incident, there is a risk of harmful and potentially lethal overpressures in the vehicle's vicinity and along the tunnel. To mitigate this risk and prevent intolerable pressure buildup within the tank during a surrounding fire, it is imperative to equip the tank with a TPRD.

The TPRD is designed to activate thermally, typically triggered at around 110°C, and remains non-closable once activated. Upon activation, hydrogen is released through a defined opening cross-section within the TPRD, typically with a diameter ranging from 2 to 5 mm. The released H_2 flows into the environment in a controlled manner via a vent line. It is crucial that the opening of the vent line is not directed towards any ignition sources, the passenger compartment, the wheel housing, the front, the sides, or horizontally towards the floor of the vehicle [17].

Under UN Regulation R134, the functionality of the tank equipped with the TPRD must be verified through the bonfire test, as depicted in Figure 4. During this test, the tank is pressurized to the nominal working pressure (NWP) and subjected to fire exposure. Initially, the tank endures a 10-minute localized fire before progressing to an engulfing fire stage. The diameter of the TPRD is chosen so that the storage pressure drops below 10 bar before tank failure due to fire exposure. Importantly, there should be no additional release resulting from leakage (excluding release through the TPRD) that leads to a flame exceeding 0.5 m beyond the circumference of the applied flame. [17]

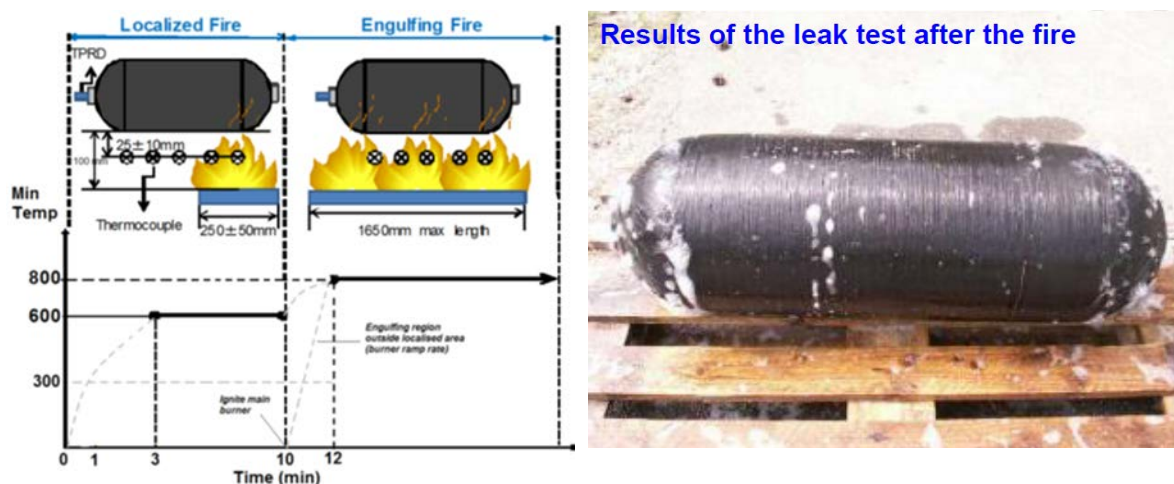


Figure 4: Bonfire test of the tank and valve in accordance with UN Regulation No 134 (left) and the tank after the test (right) [18]

In the event of a TPRD malfunction, combined with sufficient external heat, the pressure within the tank may exceed its burst pressure, potentially resulting in a tank rupture. This rupture can unleash a blast wave that propagates along the tunnel, causing severe damage to tunnel equipment and posing serious threats to human safety, potentially resulting in lethal effects. Furthermore, a tank rupture can also lead to thermal effects, manifesting in the form of a fireball, in addition to the mechanical stresses exerted.

Conversely, if the TPRD functions properly and prevents tank bursting, H_2 is released with high velocities due to the high storage pressure and the small opening of the relief device. This rapid release can result in the formation of a jet flame if the released H_2 ignites. Given the low ignition energy required for H_2 (only 0.017 mJ) and the presence of an underlying fire that triggered the TPRD, ignition of the H_2 jet is highly likely. Such H_2 jet fires pose a distinct hazard, with direct contact causing severe injuries and intense pain, as the stoichiometric combustion temperature of H_2 (2130°C) far exceeds the temperatures of typical hydrocarbon fires. Additionally, H_2 flames are challenging to detect due to the lack of electromagnetic radiation in the visible spectrum.

In instances where H_2 is released unignited from the pressure relief device or any other part of the storage system, a gas cloud forms, propagating along the tunnel. With a lower flammability limit of 4 Vol.% and an upper flammability limit of 76%, there is a significant

risk of such a gas cloud forming a flammable or explosive mixture within the tunnel. [19] If exposed to a sufficient ignition source, this cloud can trigger a vapor cloud explosion, further escalating the hazard.

In summary, three hazardous scenario types are associated with H_2 incidents in tunnels: tank rupture, H_2 jet flame, and H_2 vapor cloud explosion. Each presents unique risks and requires careful consideration in tunnel safety planning and mitigation strategies.

3. RISK SCENARIOS

The criticality of such events in terms of passenger safety strongly depends on the boundary conditions, and in particular the scenario timeline, under which such incidents are most likely to happen. To work out the relevant scenario boundary conditions as well as incident timelines, a simplified event-tree analysis has been applied. In this analysis an incident scenario has been defined by a set of relevant scenario parameters that contribute to the accident outcome. For the purpose of identification and analysis these parameters are categorized into three groups – accident initiators (e.g. incident type), consequence factors (e.g. type of release and time of ignition), tunnel factors (geometry, operational parameters) and vehicle factors (vehicle size, H_2 storage parameters).

To work out the relevant scenario conditions, a simplified event-tree analysis has been applied. All resulting scenarios have been assessed qualitatively with respect to their probability of occurrence and their potential consequences on tunnel users. A quantitative assessment of the probability of occurrence was not carried out as no statistical data is available on these events. Twelve scenarios are identified as relevant for tunnel safety. Five of these twelve relevant scenarios have been categorized with high priority. For comparison, a conventional scenario (gasoline vehicle) of a full vehicle fire (vehicle body and energy carrier) and a vehicle-body fire have been added, see Table 2.

Table 2: Basic scenarios for further consideration in the quantitative consequence analysis

No.	Scenario Name	Scenario description
0.1	Conventional fire	Full conventional vehicle fire (vehicle body and energy carrier)
0.2	Vehicle body only	Vehicle body only (no energy carrier)
1	H_2 tank rupture (mechanically triggered)	Collision of a H_2 vehicle with immediate tank rupture
2	Gas cloud explosion (leakage)	Unignited release of H_2 through a leakage of the tank system with delayed ignition
3	Gas cloud explosion (TPRD)	Vehicle-body fire of a H_2 vehicle with unignited H_2 release through the TPRD and delayed ignition of the H_2 cloud
4	H_2 jet-fire	H_2 release through TPRD and immediate ignition of the H_2 cloud and the vehicle body
5	H_2 tank rupture (thermally triggered)	Vehicle body fire of a H_2 vehicle and tank rupture due to a malfunction of the TPRD

4. CONSEQUENCE ANALYSIS

Aforementioned scenarios relate to three different hazards: hydrogen jet-flames, tank burst and a hydrogen cloud explosion. Each of these hazards has been investigated in detail. In a first step, an extensive literature study provided available information. In case of missing

information, analytical and numerical calculations were performed to fill the gaps. In the subsequent risk assessment, the comparison to a conventional fire provided information about the potential consequences and allowed to estimate the overall risk.

4.1. Harm criteria

To analyze potential consequences to tunnel users caused by H_2 incidents harm distances, representing the minimum separation of a person from a hazard origin to avoid negative consequences, were estimated. Harm to people may be caused by high temperatures, (radiative) heat fluxes or a mechanical impact (pressure wave). In literature, different information exists about the consequence of certain temperature, heat flux or pressure levels. In HyTRA harm criteria according to Table 3 have been taken into account when defining the above-mentioned harm distances.

Table 3: Harm criteria related to high temperatures, heat fluxes and pressure impact.

Temperature	70°C	No harm
	114°C	Severe pain, exposure no longer than 5 min
	149°C	Loss of escape capability due to breathing issues
Heat flux	1.58 kW/m ²	No harm
	4.73 kW/m ²	Severe pain, loss of escape capability after some minutes
	35.0 kW/m ²	Fatal effect after 10 sec.
Pressure	8 kPa	no harm criterion
	13.8 kPa	threshold for eardrum rupture
	103.4 kPa	threshold for lung hemorrhage

4.2. Jet-flames

In case of a thermal impact on the hydrogen tank system that would cause an impermissible pressure and lead to tank bursting, hydrogen should be released via thermally triggered safety valves (TPRD). This represents some kind of intended scenario in a fire event. The hydrogen released is most likely ignited by the frictional heat or the heat input from the fire. This leads to the formation of a hydrogen jet-flame, which for two reasons represents a hazard. On the one hand combustion temperatures above 2,000°C lead to massive burns in a direct exposure. Furthermore, the (radiative) heat flux may as well cause severe or fatal harm. Both criteria must be taken into account when determining the harm distances caused by a hydrogen jet-flame. The calculations of the flame length and the heat flux were done by HYRAM+ software [20] and an analytical tool developed in the course of HyTunnel-CS project [4] was employed. Both quantities were determined for different combinations of storage pressure and TPRD sizes. When comparing harm criteria for fatality, it turned out that the temperature criterion is decisive if an undisturbed horizontal release is assumed. Table 4 shows the comparison of harm distances for both criteria.

Table 4: Harm distances (fatal consequences) caused by a hydrogen jet-flame. [6]

Hydrogen storage system	Temperature (> 149 °C)	Heat flux (> 35 kW/m ²)
350 bar / 2.25 mm TPRD	20.2 m	7 m
350 bar / 5.00 mm TPRD	34.3 m	15 m
700 bar / 2.25 mm TPRD	28.3 m	9 m
700 bar / 5.00 mm TPRD	43.9 m	18 m

4.3. Tank burst

In case of an unacceptable mechanical impact due to a collision or a malfunction of the TPRD in a thermal event, a tank burst may occur. Such a scenario leads to a disruptive pressure wave propagating throughout the tunnel and causing severe harm to people. Because of the severity of this scenario, it was deeply investigated in the HyTunnel-CS project. Figure 5 shows the decay of overpressure in a tunnel for distances of 0 m to 1,500 m from the point of tank rupture [7]. Moreover, harm distances according to criteria defined in Table 3 are added in red.

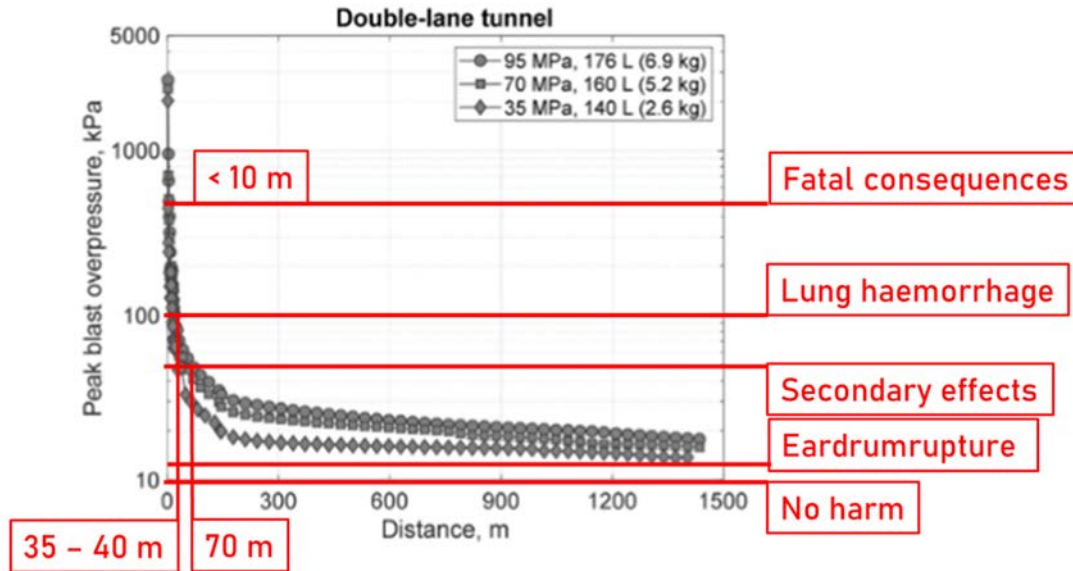


Figure 5: Peak overpressure as a consequence of a hydrogen tank rupture and harm distances on basis of harm criteria according to Table 3. [4]

4.4. Hydrogen cloud explosion

Although hydrogen is characterized by a very low activation energy, it cannot be ruled out that hydrogen will also be released unignited. In such a case it is most likely that, due to strong buoyancy forces, hydrogen will accumulate beneath the tunnel ceiling and form a hydrogen cloud. Within a range of 4 - 76 Vol.% hydrogen in the air, one can speak of a flammable cloud. This flammable cloud moves driven by the tunnel air flow and will ignite when getting in contact with an ignition source. A small electric impulse (fans) or a hot surface (non-LED bulbs) is sufficient to ignite the hydrogen cloud. However, due to the movement of the hydrogen cloud, the point of ignition is not necessarily identical to the release point. Hence, the definition of harm distances is quite complex.

The more effective way to investigate the hydrogen cloud scenario, is to put the focus on the hydrogen cloud formation and to determine whether critical hydrogen concentrations are reached under realistic tunnel operation conditions. For this reason, a series of numerical investigations were conducted. These simulations mainly covered the release from a passenger car at different tunnel air speeds (no ventilation, 1 m/s and 2 m/s according to the Austrian guideline RVS 09.02.31 [21]). Traffic induced airflow characterized by a transient air speed profile was also taken into account in another simulation run. In addition, one single simulation considered the release from a hydrogen driven bus. This simulation aimed at determining maximum hydrogen concentrations in a tunnel, as the entire hydrogen inventory was released in a short period of time.

Figure 6 illustrates the hydrogen cloud formation at different longitudinal air speeds. Apparently, there is a strong impact of the longitudinal air flow on the extension of the hydrogen cloud. An air speed of 2 m/s significantly reduced the hydrogen concentration at the

ceiling and led to concentrations below the lower flammability limit apart from the direct vicinity of the release point.

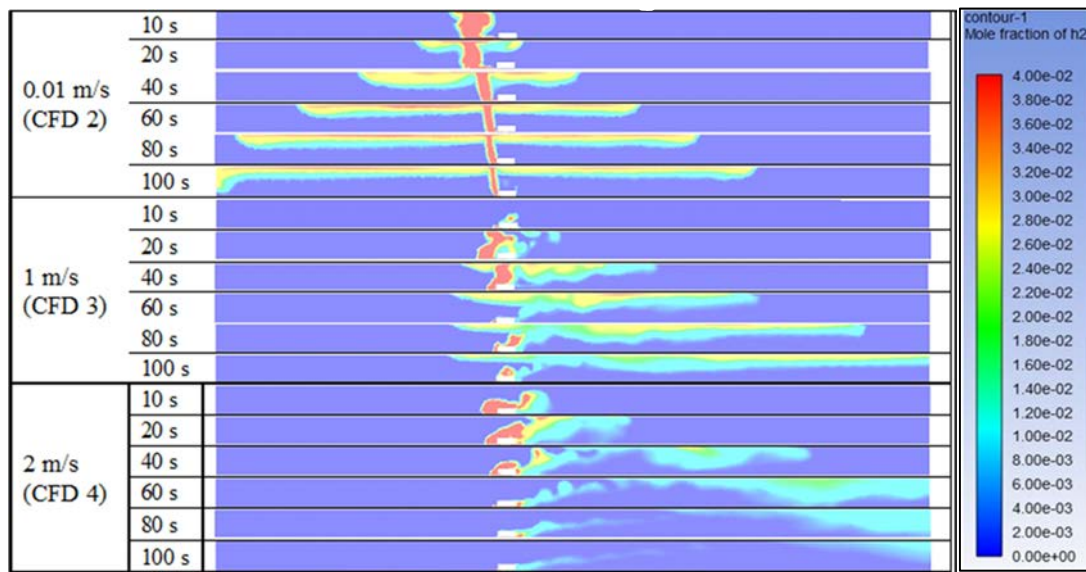


Figure 6: Impact of longitudinal airflow on hydrogen cloud formation after an unignited release. [6]

4.5. Consequence assessment

In the next step the models and findings from the consequence analysis were combined with an evacuation model usually used in quantitative tunnel risk assessments according to the Austrian tunnel risk assessment methodology TuRisMo [22]. The results demonstrated that the consideration of the evacuation procedure is essential for estimating the overall risk, as the impact of time is even more relevant than in conventional tunnel fire scenarios. Several parameters, as time of TPRD activation, TPRD orientation or the number of involved hydrogen tanks, important for the assessment, are either related to large uncertainties or were needed to be estimated based on expert judgment, as precise data for these parameters does simply not exist. The account for this uncertainty in some of the input parameters related to hydrogen scenarios, the quantitative consequence assessment of hydrogen scenarios was performed with varying scenario parameters and the most optimistic (Optimistic approach) and most conservative result (Conservative approach) for each hydrogen scenario, stemming from these parameter variations, are presented in Figure 7 (passenger cars) and Figure 8 in order to show the potential bandwidth of possible results. Figure 7 (passenger cars) and Figure 8 (buses) depict the number of fatalities for conventional fire scenarios (no bandwidth since scenario parameters are generally better known due to decades of experience with such events), in comparison to consequences for the quantitatively investigated hydrogen scenarios S1, S4 and S5 from Table 2.

Scenarios S2 and S3 (hydrogen cloud explosion) are not included in the comparison, as their potential consequences were not assessed quantitatively.

The results demonstrate the propagation of the uncertainty in the input parameters to the consequence outcome, showing potentially significantly larger consequences for hydrogen scenarios compared to conventional fire scenarios in unidirectional well-ventilated tunnels. This result must, however, be interpreted with great care. The potentially significantly larger consequences do not necessarily refer to an increased risk for hydrogen vehicles. First, because the results refer only to consequences, while incident probabilities (the second dimension of risk) were not quantified and are indeed likely to be significantly smaller for

specific hydrogen scenarios than for conventional fires. If this is the case, potentially larger consequences could be relativized by smaller probabilities for hydrogen scenarios.

Second, as experience from real world incidents is missing, the exact development of hydrogen scenarios is uncertain (even more uncertain than for conventional fire scenarios). To account for this uncertainty, scenario parameters such as time of TPRD activation or the number of involved hydrogen tanks have been varied and the smallest and largest consequence numbers resulting from all the variations are presented for each hydrogen scenario (Optimistic approach vs. Conservative approach for S1, S4 and S5). Larger values for consequence numbers in Figure 7 (passenger cars) and Figure 8 (buses) must therefore be seen as upper boundaries of very broad consequence intervals, which are due to combinations of conservative assumptions (like early TPRD activation or unfavorable TPRD orientation) to reflect parameter uncertainties and model limitations, and are unlikely to manifest in reality.

However, what these large upper boundaries for consequence intervals are qualified to demonstrate is that without actual knowledge and experience from real world operation of hydrogen vehicles inside road tunnels or alternatively, extensive additional experimental investigations under realistic tunnel operation conditions, catastrophic tunnel incidents, even though potentially extremely unlikely, cannot be excluded with certainty, as proper measures to mitigate consequences are presently not available. Despite the potentially larger consequences of hydrogen scenarios compared to conventional fire scenarios and the broad bandwidth of potential consequences of hydrogen scenarios, the results indicate that accidental scenarios involving buses are much more critical than incidents involving only passenger cars. This is true for conventional cars but seems to amplify for hydrogen vehicles as more persons (i.e. all bus passengers) are located in close vicinity to the hydrogen tank.

The situation for bus passengers is in particular critical in case of fast incident development, as is the case for an immediate tank rupture following a collision (S1 – optimistic approach and conservative approach) and a jet fire with an early TPRD activation, (S4 – conservative approach). In these situations, the hydrogen scenario (explosion or jet fire) is triggered before bus evacuation, which takes significantly longer than evacuation of a passenger car, has been completed successfully.

For a thermally triggered tank rupture (S5) the number of involved tanks and thus the severity of the explosion is an important factor. Under conservative assumptions, where all hydrogen tanks are supposed to rupture and burst simultaneously, the large amount of hydrogen stored on a bus leads to a further extending fatality zone (zone where the fatality overpressure threshold is exceeded), extending to areas to which bus passengers have managed to egress between start of the evacuation and detonation of the tanks, leading to more than 60 fatalities in the considered scenarios.

In particular the last two consequence number results mentioned before – S4 conservative approach and S5 conservative approach, demonstrate the conservativity of the assumptions leading to the upper boundaries of the resulting hydrogen consequence number intervals. In case of early TPRD activation (S4 conservative approach) TPRD activation was assumed at the time a gas temperature of 110° was reached, neglecting the time needed to actually heat the TPRD to the activation temperature. In case all tanks are involved in the thermally triggered tank rupture (S5 conservative approach) all hydrogen tanks are assumed to rupture simultaneously without any time delay. The time delay, which is in fact likely to occur in reality as not all of the tanks will rupture exactly at the same instant, would lead to a less enhancing superposition of the resulting pressure waves from the individual tanks and thus to lower consequences. In this regard, the upper boundaries of the presented consequence

number intervals for hydrogen scenarios must again be put into perspective and interpreted with care.

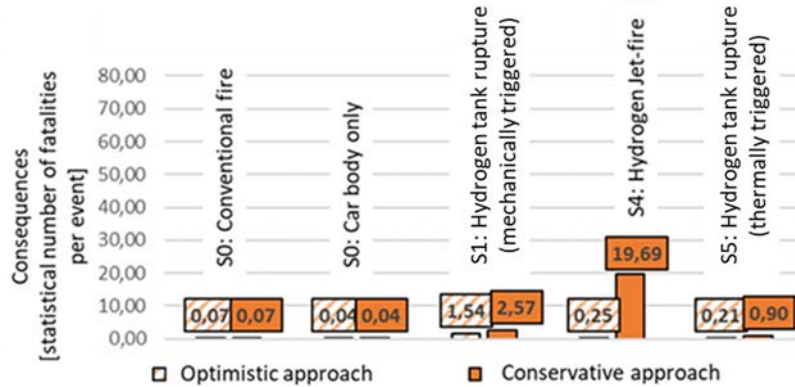


Figure 7: Comparison of risk for different incident scenarios of passenger cars. [6]

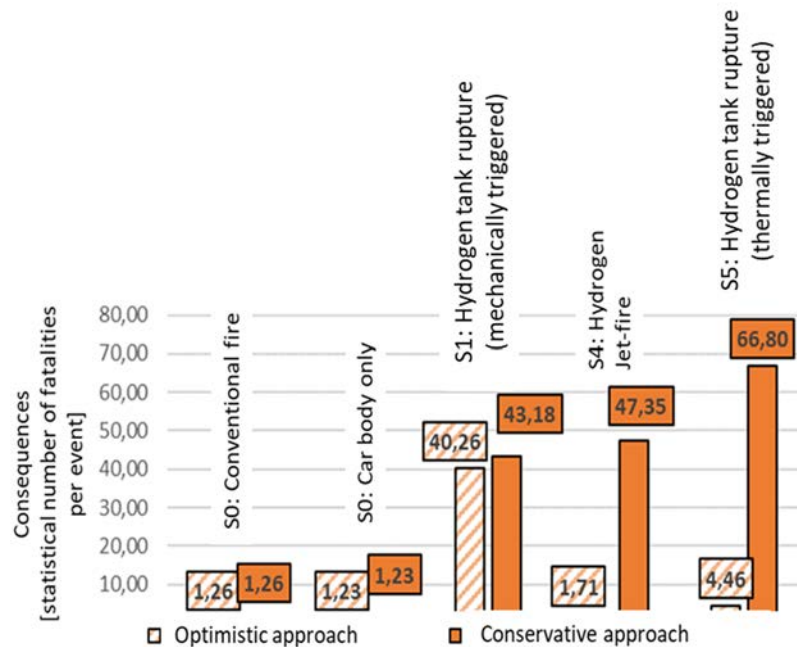


Figure 8: Comparison of risk for different incident scenarios of passenger buses. [6]

5. PREVENTIVE AND MITIGATION MEASURES

As indicated by Figure 8 H_2 vehicles pose new risks in a tunnel incident situation. In particular, explosion scenarios may lead to a disruptive pressure wave that cause severe harm to humans. Thus, measures to prevent such scenarios or to mitigate their consequences are potentially needed in the future. In HyTRA a list of technical and organizational measures has been developed. In addition, measures were prioritized on basis of their range of influence, effectiveness and required effort for implementation. In the present paper only measures with high priority are explained in more detail.

Identification of hydrogen powered vehicles

The identification of a hydrogen powered vehicle in order to be aware of the potential risk is essential in an emergency situation. Different concepts exist that enable the identification.

These range, for instance, from visual elements on the car body to allow for video detection, a monitoring at the portals using transmitters and receiver (e.g. GO box) to a dedicated vehicle-infrastructure communication. However, it is very important to keep the identification simple, as in an emergency situation, emergency services have to decide quickly on the intervention strategy. Today, legal requirements hinder the implementation of a monitoring system due to privacy rules. Thus, there is the urgent need of starting the process of implementation that starts with the adaptation of laws.

Early detection of congestion and primary events (e.g. fire)

Results of HyTRA show the time (to evacuate) being one of the key elements in the emergency response. For this reason, it is essential to enable an early detection of emergency events or events that may trigger a tunnel incident. These include heat detection wires to detect thermal events such as a tunnel fire, and systems (e.g. automatic video detection or acoustic detection – “AKUT” [23]) to detect congestion. While the latter aims to prevent an immediate tank burst due to a massive mechanical impact, the early detection of thermal events extends the time available for evacuation and intervention.

TPRD orientation towards the road surface (passenger cars) or the ceiling (busses and trucks), optimization of TPRD size or self-venting tanks

Hydrogen jet-flames are characterized by high temperatures. An exposure leads to severe harm to people that may result in the loss of escape capability. The hydrogen release through a TPRD most likely results in a hydrogen jet-flame characterized by a certain length, which depends on the storage pressure as well as the TPRD size. In order to keep flame lengths short and decrease the possibility of an exposure, a rapid reduction of momentum should be aspired. This can be realized by the optimization of the release orientation, which should be towards (angle of 45°) the road surface (passenger cars) or the ceiling (busses and trucks).

Furthermore, the TPRD size needs to be optimized as two opposing requirements have to be met. On the one hand, the TPRD diameter has to be large enough to prevent from thermally triggered, unacceptable storage pressures. On the other side, smaller TPRDs reduce the hydrogen flame length due to a limited outlet momentum.

A new tank technology has been described by Molkov V. et al. [24] which does not require any TPRD. Instead, the gas-tight wall of the tank becomes permeable when exposed to high temperatures, allowing H_2 to escape around the circumference of the tank. This prevents dangerous flashbacks or other pressure peaks. This new technology can massively increase the safety of H_2 vehicles. However, this technology is still at the research stage.

General measures that increase traffic safety

General measures to increase traffic safety lower the risk of incidents involving hydrogen powered vehicles. One among a variety of measures are speed limits. The efficiency of speed limits is significantly increased if mechanisms to enforce the speed limit are in place. As an example, Section control has proven to be very effective in encouraging drivers to reduce their driving speed. In addition, distance control is effective as well, as sufficient time for action is available if a sufficient distance to the car in front is kept.

It is worth noting that some low priority measures may need to be upgraded to the high priority category in the future as the number of H_2 vehicles on European roads might increase.

6. SUMMARY AND CONCLUSION

The presented study aimed at a detailed analysis of hydrogen incident scenarios. Such scenarios pose additional risk in a tunnel incident. In an event-tree analysis, five hydrogen related scenarios could be identified to be characterized by a potential high risk. This included:

- Collision of a hydrogen powered vehicle with massive mechanical impact
- Accidental hydrogen release with delayed ignition
- Thermally triggered activation of TPRD with delayed ignition of hydrogen
- Thermally triggered activation of TPRD with immediate ignition of hydrogen
- Malfunction of TPRD in a thermal event

Three different hazards can be associated with these scenarios. These include a hydrogen jet-flame, a tank rupture and a hydrogen cloud explosion. In an extensive literature study as well as analytical and numerical calculations, harm distances were determined based on harm criteria taken from literature. The applied criteria accounted for the impact of high temperatures, heat fluxes as well a mechanical impact due to a pressure wave. Subsequently, the obtained harm distances were taken into account in a detailed consequence assessment that was part of an overall semi-quantitative risk assessment. A quantitative comparison of conventional vehicle fires and hydrogen incidents provided information about the statistical number of fatalities per event. It was observed that boundary conditions such as the activation time of TPRD, TPRD orientation, or the number of involved hydrogen tanks have a significant impact on the accident consequences. Compared to a conventional passenger vehicle fire in a tunnel, the number of fatalities are around 3 (optimistic) to 280 (conservative) times higher. For a bus, the number of fatalities compared to a conventional fire is approximately 1.4 to 53 times higher. However, as the probability of occurrence has not been taken into account, no assumption regarding the overall risk can be made. Even though such accidents are very unlikely to happen these days due to the low penetration rate of hydrogen vehicles, significant consequences in case of hazardous hydrogen scenarios cannot be excluded with certainty unless more knowledge from real-world tunnel incidents or experiments under realistic tunnel operation conditions are available.

Ultimately, measures to prevent hydrogen scenarios and to mitigate their consequences were listed and prioritized on basis of criteria that refer to the range of influence, effectiveness and implementation effort. Measures with highest priority are:

- Identification of H_2 vehicles in an emergency event
- Early incident detection (fires and congestions)
- Optimized TPRD and/or tank design
- Measure which generally increase the traffic safety level

Acknowledgments

The HyTRA project was funded by the Austrian Research Promotion Agency FFG. Financial resources were provided by the Austrian Federal Ministry for Climate action, Environment, Energy, Mobility, Innovation and Technology as well as by ASFINAG.

7. REFERENCES

- [1] Leitner, A., 2001. The fire catastrophe in the Tauern Tunnel: experience and conclusions for the Austrian guidelines. *Tunnelling and Underground Space Technology* 16, 217–223. [https://doi.org/10.1016/S0886-7798\(01\)00042-6](https://doi.org/10.1016/S0886-7798(01)00042-6)
- [2] Bertau, S.; Li, Z.M; Tretsiakova-McNall, S.; Molkov, V.; Makarov, D.; 2016. *European Emergency Response Guide (Final report)*.
- [3] The EC Network of Excellence for Hydrogen Safety “HySafe,” n.d. URL <http://www.hysafe.org/> (accessed 10.03.22).
- [4] Molkov, V.; Makarov, D.; Cirrone, D.; 2022. *HyTunnel-CS*. URL <https://hytunnel.net/> (accessed 10.03.22).
- [5] Li, Y.Z., 2019. Study of fire and explosion hazards of alternative fuel vehicles in tunnels. *Fire Safety Journal* 110, 102871. <https://doi.org/10.1016/j.firesaf.2019.102871> (accessed 05.02.2024)
- [6] Institute of Thermodynamics and sustainable propulsion systems at Graz University of Technology et.al., 2023 , *Hydrogen Tunnel Risk Assessment – HyTRA; final report*; <https://projekte.ffg.at/projekt/4091428> (accessed 16.01.2024)
- [7] Official Hyundai Nexo safety rating (2024). Available online at <https://www.euroncap.com/en/results/hyundai/nexo/33731>, updated on 12.02.2024, checked on 12.02.2024.
- [8] Chatelain, Dominique (2019): *Hyundai Hydrogen Mobility gewinnt den Truck Innovation Award 2020 - aktuell*. Available online at <https://aktuell.hyundai.ch/hyundai-hydrogen-mobility-gewinnt-den-truck-innovation-award-2020/>, updated on 27.11.2019, checked on 12.02.2024.
- [9] Toyota DE (2024): *Der Toyota Mirai. Mehr als emissionsfrei | Toyota DE*. Available online at <https://www.toyota.de/neuwagen/mirai>, updated on 12.02.2024, checked on 12.02.2024.
- [10] HONDA Ladekabel | Stecker | Mobile Ladestationen | Wallbox | Ladestation | evmotions.at (2024). Available online at <https://evmotions.at/evcars/honda/>, updated on 12.02.2024, checked on 12.02.2024.
- [11] Mercedes-Benz kombiniert Strom und Wasserstoff im Zeichen von EQ Power - Mercedes-Benz | Online Presse-Center (2024). Available online at <https://presse.mercedes-benz.at/news-mercedes-benz-kombiniert-strom-und-wasserstoff-im-zeichen-von-eq-power?id=53809&menueid=10733&tab=1&imageid=147323>, updated on 12.02.2024, checked on 12.02.2024.
- [12] *Modellbus.info Aktuelles* (2014). Available online at http://www.modellbus.info/akt_12_10.htm, updated on 07.10.2014, checked on 12.02.2024.
- [13] *Global EV Outlook 2023, Catching up with climate ambitions. 2023*. International Energy Agency.
- [14] Klell, M.; Eichlseder, H.; Trattner, A.; 2023, *Hydrogen in Automotive Engineering*. Springer, Wiesbaden. <https://doi.org/10.1007/978-3-658-35061-1> (accessed 05.02.2024)

- [15] Air, Alexander; Shamsuddoha, Md; Gangadhara Prusty, B. (2023): A review of Type V composite pressure vessels and automated fibre placement based manufacturing. In: Composites Part B: Engineering 253, S. 110573. DOI: 10.1016/j.compositesb.2023.110573.
- [16] Müller, H.; Bernt, AO.; Salman, P.; et. al.; 2017, Brennstoffzellen-Range-Extender-Fahrzeug FCREEV Große Reichweiten ohne Emissionen. ATZ Automobiltech Z 119, 62–67; <https://doi.org/10.1007/s35148-017-0033-9> (accessed 05.02.2024)
- [17] UNECE. Regulation No 134. Uniform provisions concerning the approval of motor vehicles and their components with regard to the safety-related performance of hydrogen fuelled vehicles. HFCV; 2019.
- [18] Tretsiakova-McNally S., Makarov D.: LECTURE - Safety of hydrogen storage. HyResponse Grant agreement No: 325348
- [19] Trattner, A., Aggarwal, M.; 2020, Safety aspects related to Fuel Cell BEVs; in Proceedings of the 10th International Conference on Tunnel Safety and Ventilation, virtual
- [20] Hydrogen Plus Other Alternative Fuels Risk Assessment Models (HyRAM+), National Technology and Engineering Solutions of Sandia, LLC. URL: <https://energy.sandia.gov/programs/sustainable-transportation/hydrogen/hydrogen-safety-codes-and-standards/hyram/> (accessed 04.02.2024)
- [21] RVS 09.02.31 – Tunnel, Tunnelausrüstung, Belüftung, Grundlagen. 2008. Forschungsgesellschaft Straße - Schiene – Verkehr.
- [22] FSV (Austrian Society for Research on Road, Rail and Transport), “Guideline RVS 09.03.11 Methodology of Tunnel Risk Analysis”, Vienna, 2015
- [23] AKUT - Acoustic Incident Detection in Tunnels (2024). Available online at <https://www.akut-tunnel.com>, updated on 12.02.2024, checked on 12.02.2024.
- [24] Molkov V., Kashkarov S., Makarov D., Safety technology of explosion free in fire self-venting (TPRD-less) tanks: The concept and validation of the microleaks-no-burst technology for carbon-carbon and carbon-glass double-composite wall hydrogen storage systems, International Journal of Hydrogen Energy, Volume 48, Issue 86, 2023, Pages 33774-33785, ISSN 0360-3199, <https://doi.org/10.1016/j.ijhydene.2023.05.148>.

LEANTECH IN ROAD TUNNELS

¹Simon Frey, ¹Rune Brandt, ²Jean-Paul Schnetz

¹HBI Haerter AG, CH

²jps-conseils, CH

DOI 10.3217/978-3-85125-996-4-46 (CC BY-NC 4.0)

This CC license does not apply to third party material and content noted otherwise.

ABSTRACT

Due to historical developments and the desire to provide road users with the safest possible infrastructure, today's practice results in complex and cost-intensive electromechanical equipment in road tunnels. The Swiss Federal Roads Office (FEDRO) initiated the LeanTech research project aiming at reducing the system and operating costs by streamlining the specifications without reducing noticeably aspects relating to safety, availability, and maintenance.

The currently applicable requirements on the operating and the electromechanical equipment in road tunnels were critically examined in a systematic process. In terms of LeanTech, the question was whether and how requirements can be optimised with neither reducing the safety of the road users nor the availability of the infrastructure.

A total of 2182 requirements were identified that could be optimised without affecting compliance with the minimum requirements for tunnel safety. The applied multiple-step analysis concluded that the optimisation potentials of 2113 requirements were too small to allow for an in-depth investigation in this research project. From the remaining requirements, 41 were examined in detail. This resulted in 9 adaptation proposals with major impacts in terms of LeanTech, which can be implemented easily and promptly. In addition, 12 recommendations for action were proposed for more thorough investigations.

Keywords: LeanTech, requirements on electromechanical equipment, cost reduction,

1. INTRODUCTION

Due to historical developments and the desire to provide road users with an infrastructure that is as safe as possible, road tunnels today are characterized by complex and cost-intensive electromechanical installations. The constantly increasing cost pressure (investment, maintenance, and replacement) and the changing socio-legal-economic context make it necessary to critically scrutinize the existing requirements on road-tunnel equipment as well as current practice in planning and implementation. Therefore, the LeanTech research project [1] was initiated by the Swiss Federal Roads Office (FEDRO). LeanTech is aiming at streamlining the current specifications with only marginal impact on safety, availability, and maintenance. To do so, the following tasks had to be performed:

- Recording and presenting the reference system (existing requirements).
- Analysis and evaluation of the reference system (existing requirements).
- Identify recommendations and implementation strategies for improvements, considering usual European standards [2].
- Develop specific suggestions for improvement and demonstrate their feasibility.

One of the difficulties in implementing the project objective is to reduce the requirements on the equipment without compromising the required level of safety. This applies both to road

users (the public) and stakeholders within the FEDRO and emergency services (police, fire-fighters, etc.).

To achieve the project objectives, the following four steps were performed:

1. systematic processing of the current requirements
2. selection of requirements with optimization potential
3. detailed analysis of the selected requirements with optimization potential
4. assessment of the remaining requirements with optimization potential

The approach was transparent and comprehensible. Consequently, it was deliberately refrained from developing a multi-dimensional model of the interaction between requirements, technical implementation variants and results in terms of safety, availability, and maintenance, including all dependencies.

Parallel to the systematic analysis and processing of the requirements, the opinions of international experts on the topic were obtained. This allowed the topic of LeanTech to be expanded and enriched from an international perspective.

2. STATE OF RESEARCH AND NEEDS

The currently valid standards, FEDRO guidelines and technical manuals to be used for the design and implementation of electromechanical equipment are driven on one hand by research findings and on the other by major fire incidents. The desire for safety is a major factor and tends to result in increased complexity and costs of the electromechanical systems.

From the point of view of the Swiss Tunnel Research Working Group, the time has come to critically review and, if necessary, revise the requirements on the electromechanical equipment in road tunnels. In this way, the systems can be reduced to what is strictly necessary and less effective systems as well as redundancies that are not sensible or insufficiently thought through can be modified or even eliminated.

The current guidelines and specifications regulate the requirements on individual systems and components. These can and should be scrutinized (e.g. need of redundant power supply, and optical guidance lighting versus safety lighting). The interaction between the individual systems and the superordinate relationships between several systems must also be considered. In this respect, for example, both the emergency exits, and the ventilation of the traffic space have a direct influence on self-rescue in the event of a fire. Nevertheless, there is currently no direct dependency between the relevant requirements. However, it is prescribed that deviations from the core requirements in the FEDRO guidelines must be assessed in a cost-benefit context by means of a risk analysis [7], [8].

By critically scrutinizing the meaningfulness, usefulness, and timeliness of the applicable requirements, it seems possible to make substantial savings regarding investment, operation, and maintenance without causing a noticeable reduction in the safety level or availability of the system.

The basic questions for the selection and evaluation of the possibilities for simplifications of the equipment in road tunnels are the following:

- Which functions are to be fulfilled and to what extent?
- How efficiently are the requirements implemented by the equipment?
- What mutual influences are there between the individual functions and the associated systems?
- What redundancies are necessary and how are these implemented?

- What is the possible/acceptable scope for simplification?
- What are the consequences (advantages and disadvantages in terms of safety, availability, maintenance, and costs) of the simplifications?
- How can the simplifications be implemented?

In principle, the questions are aimed at new installations to be built. However, there is also potential for simplification in forward-looking replacement planning (e.g. standardized open communication systems).

It makes sense to compare and review the design philosophy and/or the equipment standard with international standards (guidelines, planning manuals, etc.) and international research results to determine the minimum equipment required. This can also provide more clarity as to where redundancies are necessary or appropriate. In addition, the assessments of optimization potential by international experts should be obtained and used in the project.

3. METHODOLOGY

Two distinct approaches are available for the elaboration of requirements: top-down and bottom-up. The top-down approach is based on a high degree of abstraction or a global view. Step by step, the problem is increasingly concretized. An overall problem is divided into sub-problems, which may then be subdivided into further sub-problems. In the bottom-up approach, delimited, detailed sub-problems are solved first. These are then used to tackle the next larger problems above them and so on until the overall problem can be solved at the end.

Within the LeanTech project, both approaches were applied in parallel, the interviews with the international experts can be regarded as top-down, whereas the systematic classification and analysis of the requirement framework was a bottom-up approach.

3.1. Systematic classification and analysis

The hierarchy of guidelines, standards, etc. defined by FEDRO was used for this purpose. This ranking and the considered project perimeter are shown in Figure 1. Requirements of higher priority than FEDRO guidelines (e.g. the FEDRO instructions) were considered a priori to be irrevocable, as these are outside the sphere of influence of the research activities. Consequently, the FEDRO instruction [1], which defines the minimum safety requirements for tunnels in the national road network, was excluded from the project perimeter. This implicitly means that the requirements stated in the EU directive on minimum safety requirements for road tunnels [2] must be complied with.

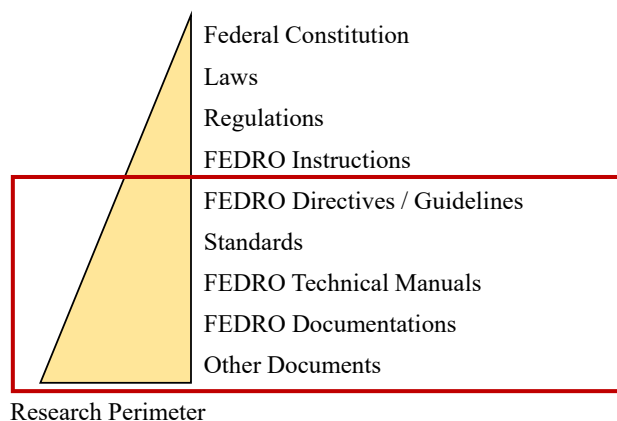


Figure 1: LeanTech Research Perimeter

The bottom-up approach based on existing regulations was considered advantageous, as the research perimeter is clearly defined. The requirements to be scrutinized are clearly structured and prioritized. Moreover, the analysis and any optimizations relate directly to existing requirements.

The systematic analysis revealed requirements relevant to the LeanTech project contained in

- 18 FEDRO directives and guidelines
- 5 national standards
- 69 FEDRO technical manuals and documentations

In order to determine the requirements that have the most potential in terms of LeanTech, the following sequential steps were applied:

- Step 1: Compliance with minimal safety requirements
- Step 2: Complexity- and/or cost-driving
- Step 3: Preliminary evaluation
- Step 4: Detailed evaluation
- Step 5: Selection for LeanTech

As a results of the first step, it was concluded that 2182 requirement could be optimized in terms of LeanTech without violating compliance with the minimum safety requirements.

In the second step, the impact on system complexity and/or cost (installation and maintenance) was analysed (minimal influence, relevant influence, uncertain influence). 366 of the initially identified 2182 requirements were judged to have adequately large influence on the system complexity and/or costs. Requirements with minimal influence were discarded.

The third step evaluated three aspects of the impact of any modification (simplification) of the requirement i.e. in terms of:

- tunnel safety (safety for the tunnel user),
- availability of the infrastructure (for the tunnel user), and
- maintenance (maintenance effort, maintenance intervals)

For each aspect, the impact was assessed potentially to be:

- positive (increase in terms of tunnel safety, increase of the availability, eased maintenance),
- neutral, or
- negative (reduction of tunnel safety, decrease of availability, increased maintenance).

If two of the above-mentioned aspects were judged to have a negative impact, it was decided not to pursue adjustments of the requirement. 265 requirements remained for subsequent scrutiny.

In step 4, it was concluded that 102 of the 265 remaining requirements had adequate financial potential to justify a more detailed analysis. Moreover, it was assessed if the details of the requirements could depend on tunnel length and/or traffic (type and quantity), as this could either allow for more general adjustments or more simplifications based on specific tunnel characteristics.

For the final selection, the results of the methodology were considered together with specialist and expert assessments also taking the suggestions and proposals of the international experts (see chapter 3.2) into account. This resulted in a selection of:

- 41 requirements for detailed analysis, and further,
- 28 requirements for an overall potential assessment.

3.2. Expert survey

The international experts were asked the following question:

Which requirements for electromechanical equipment in road tunnels should be adapted and in what way to reduce costs (or complexity) without having to accept any real negative impact on safety, availability, and maintenance?

An open question was deliberately posed to allow for a variety of feedback. No reference to the conditions in Switzerland was requested. The expert's feedback was analysed considering the constituency of each expert and therefore the expert's natural frame of reference.

This question was asked at the beginning of the research project. The feedback was therefore useful for the detailed analysis of the requirements with optimization potential.

4. RESULTS

4.1. Expert survey

A total of 38 international experts were consulted, and the feedback received exceeded expectations. The feedback can be summarized as follows:

- 23 specific adaptation proposals for individual equipment types or installations,
- 12 specific adaptation proposals based on considerations of multiple installations,
- 3 high level adaptation proposals.

The full list of proposals can be found in [1]. The proposals are deliberately not affiliated to a certain expert, as it was desired to obtain honest and perhaps controversial responses. Specific proposals are for example: reduction of requirements on material qualities, renouncement of cross-passage ventilation, simplification of the surveillance (anemometers, CO-measurements) and detection equipment (incident detection) or general simplification of control systems (general renouncement of touch panels, limitation of data points and limitation of PLCs). The proposals based on consideration of multiple installations are mainly aimed at simplifications according to the principle of "one system for one purpose".

In addition, the opinion was also expressed that no adjustments to the current requirements are possible or appropriate.

4.2. Systematic classification and analysis

As presented in chapter 3.1, the full number of catalogued requirements were processed. From the total number of 2182 requirements having passed evaluation step 1 (compliance with minimal requirements), a total of 41 requirements emerged as being interesting in terms of LeanTech (optimisation possible, sufficient impact in terms of cost, specific optimization proposal possible) and were examined in depth. For each FEDRO equipment type, Table 1 presents number of requirements with LeanTech potential after each evaluation step.

Table 1: Summary of the number of requirements with LeanTech potential per evaluation step and equipment type

Evaluation step	Total number	Superordinate requirements	Energy supply	Lighting	Ventilation	Signalization	Surveillance and detection	Communication & Controls	Cables	Auxiliary installations
Step 1: Compliance with minimal requirements	2182	7	183	254	519	291	179	333	222	194
Step 2: Complexity- and/or cost-driving	366	4	17	42	262	10	14	8	0	9
Step 3: Preliminary evaluation	265	3	7	26	190	10	14	8	0	7
Step 4: Detailed evaluation	102	0	4	10	55	10	14	8	0	1
Step 5: Selection for LeanTech	41	0	4	10	14	5	6	1	0	1
Requirements for further analysis	28	0	0	0	17	1	6	4	0	0

In the end, 9 specific adaptation proposals were elaborated, which can easily and promptly be implemented whilst still having a major impact in terms of LeanTech. In addition, 12 recommendations for action were made for more in-depth investigations and further 28 requirements with optimisation potential were subjected to a higher-level analysis.

The 9 specific adaptation proposals concern the following:

- 1) Power supply from two independent power grids,
- 2) Determination of the total required energy supply,
- 3) Life-time requirements on batteries for uninterrupted power supply (UPS),
- 4) Reduce the temperature requirement on axial fans,
- 5) Lower minimal permissible under-pressure in ventilation ducts along the traffic space,
- 6) Permit to determine anti-recirculation measures at tunnel portals using a detailed analysis and not simply require a certain staggering in direction of the road axis,
- 7) Omit the requirement for fixed installed control panels locally for intervention on site of control units. However, certain local control panels are required to activate tunnel closure,
- 8) Increase the required minimum lifetime of LED in traffic signals,
- 9) Constrain video detection (CCTV) to halted vehicles, wrong direction vehicles and occupation of laybys.

The 12 recommendations for further in-depth analysis relate to:

- 1) Base the dimensioning of the UPS on the estimated required power requirement and duration and not on the nominal power of each consumer,
- 2) Combination of optical guidance lighting and safety lighting,
- 3) Increase of the required maintenance factor of luminaries from 0.80 to 0.85,
- 4) Requirements on luminaries to increase efficiency and longevity; reduce maintenance,
- 5) Reduce the requirements on material quality according to the findings in the soon to be published research project AGT 2014/004,
- 6) Refine requirements on civil measures to minimise flow short circuit at tunnel portals,

- 7) Detailed method to determine the minimum distance between two following tunnels to ensure that they are aerodynamically independent,
- 8) Rethink the redundancy requirements on the ventilation of egress tunnels so that one ventilation station is basically deemed adequate,
- 9) Re-define the necessity and functionality requirements on air locks in egress tunnels,
- 10) Maintain local HMI for equipment enabling cross overs at tunnel portals,
- 11) Consider if linear heat detectors can be omitted in certain (typically short) tunnels and/or be replaced with temperatures sensors in smoke detectors,
- 12) Maintain the currently specified bundling of equipment to different local control units.

4.3. Exemplary optimisation proposal

According to [4], [5] and [6], tunnels in general and especially the traffic space respectively escape-route ventilation equipment needs to be powered (medium voltage level) by two independent local power grids. Furthermore, an uninterruptable power supply (UPS) must be installed (no need to account for ventilation equipment).

For certain tunnels, a supply from two independent power grids is only possible at great expense (tunnels in remote areas or city tunnels). In addition, grid outages have become a rarity these days. Currently, the most common cause of grid interruptions is maintenance work; disruption-related grid outages that cannot be predicted or immediately compensated have become rare events. Interruptions are usually rectified by the energy supplier/grid operator within less than 60 minutes. The probability of a simultaneous failure of the two independent grids is very low. The UPS system cannot fully compensate for a power failure; it only supplies parts of the installations such as the control systems, emergency lighting and signalization.

If a tunnel would be powered by only one power grid, this would mainly impact the availability. However, the effects are highly dependent on the tunnel length and amount of equipment. For a network-wide coherent implementation (standardization of the considerations to be carried out), it may be advantageous to introduce a form of tunnel classification that clearly defines under which conditions two independent, local power supplies are mandatory or when deviations from this are possible.

Therefore, the following proposal was formulated:

For tunnels which have a traffic-space ventilation system and/or an escape-route ventilation system, power supply from two independent sources must be provided.

- Normally, power should be provided by two independent, local power grids.
- If this is not practical for economic reasons, power must be provided by at least two supplies from the medium-voltage grid.

For all other tunnels, energy supply from only one power grid is permitted, provided the following conditions are met:

- Due to safety considerations, it is admissible to continue operating the tunnel despite a complete blackout (normal network and UPS system); with or without additional measures such as traffic-speed reduction, personnel on site, etc.
- In the event of planned interruptions to the power supply (e.g. during maintenance work on the power grid), the tunnel's power supply can be guaranteed.

5. SUMMARY AND CONCLUSION

Due to historical development and the desire to provide road users with the safest possible infrastructure, today's practice results in complex and cost-intensive installations (electromechanical equipment) in road tunnels.

The research project LeanTech in road tunnels was initiated and financed by the Swiss Federal Roads Office FEDRO. It addresses this issue and aims at reducing both the system costs and the operating costs (costs on the part of the operators for maintenance and operation) for road tunnels by streamlining the specifications without having to reduce noticeably aspects relating to safety, availability, and maintenance.

Using a systematic approach, the existing requirements on electromechanical equipment were catalogued, categorized, and evaluated in terms of their LeanTech potential. A grand total of 2182 requirements were identified that could be optimised without affecting compliance with the minimum requirements for tunnel safety. From those, a total of 41 requirements were examined in depth. This resulted in 9 specific adaptation proposals, which can be implemented easily and promptly whilst having a major impact in terms of LeanTech. In addition, 12 recommendations for action were made for more in-depth investigations and further 28 requirements with optimisation potential were subject to a high-level analysis.

6. REFERENCES

- [1] ASTRA Research Project AGT 2016/005, LeanTech in road tunnels, March 2022
- [2] Bundesamt für Strassen ASTRA, Weisung 74001 Sicherheitsanforderungen an Tunnel im Nationalstrassennetz, V1.02, 2010
- [3] European Parliament and Council of the European Union, Directive 2004/54/EC on minimum safety requirements for tunnels in the Trans-European Road Network
- [4] Schweizerischer Ingenieur- und Architektenverein SIA, SN 505 197/2 Projektierung Tunnel – Strassentunnel, 2023
- [5] Bundesamt für Strassen ASTRA, Richtlinie ASTRA 13001 Lüftung der Strassentunnel - Systemwahl, Dimensionierung und Ausstattung, V3.01, 2021
- [6] Bundesamt für Strassen ASTRA, Richtlinie ASTRA 13002 Lüftung der Sicherheitsstollen von Strassentunneln, V1.06, 2008
- [7] Bundesamt für Strassen ASTRA, Richtlinie ASTRA 19004, Risikoanalyse für Tunnel der Nationalstrassen, Richtlinie, V1.10, 2014
- [8] Bundesamt für Strassen ASTRA, Dokumentation ASTRA 89005, Methodik zur Ermittlung und Bewertung der Risiken in Tunneln, V1.10, 2014

LOOKING TO THE FUTURE FROM PIARC'S PERSPECTIVE

Ingo Kaundinya

Federal Highway Research Institute (BAST),
Chairman of PIARC TC 4.4 Tunnels, DE

DOI 10.3217/978-3-85125-996-4-47 (CC BY-NC 4.0)

This CC license does not apply to third party material and content noted otherwise.

ABSTRACT

This paper presents the new topics which PIARC’s road tunnel committee (TC4.4) will address in the current work cycle 2024-2027. TC4.4 will deliver in total 13 outputs until the end of 2027. Current topics include: Sustainability of Tunnel Operation, Active Modes of Transport (walking, cycling, wheelchair) in Road Tunnels, Digitalization of Road Tunnel Design and Management, Road Tunnel Operation and Safety Issues related to the Usage of New Energy Carriers (NEC) in Road Vehicles, update of the online Road Tunnel Manual, dissemination and possible update of the DG-QRAM Software, organization of the 3rd International Conference on Road Tunnels Operation and Safety and organization of two International Seminars in Low- and Medium-Income Countries (LMIC).

Keywords: Tunnel operation, sustainability, digitalization, tunnel safety, Online Tunnel Manual, transport of dangerous goods, New Energy Carriers (NEC).

1. INTRODUCTION

The World Road Association PIARC is an international, non-political, non-profit organization, established in 1909. The mission of PIARC is to promote international cooperation on issues related to roads and road transport. Since more than 100 years PIARC continues to foster and facilitate global discussion and knowledge sharing on roads and road transport. The Association now boasts 127 government members worldwide and retains consultative status to the Economic and Social Council of the United Nations. The main objective of PIARC is to facilitate exchange of knowledge on roads and road transport policy and practices within the context of integrated, sustainable transport. PIARC is worldwide acknowledged for the quality of its outputs. The work within PIARC is organized in Technical Committees (TC) which are regularly nominated for a working period of 4 years (so-called work cycles). PIARC’s tunnel committee is one of the oldest and one of the largest committees in PIARC. During the past decades the TC Tunnels has produced

- a total of approximately 51 technical reports, covering all matters relating to the operation of road tunnels: geometry, equipment and maintenance, operating, safety, sustainability and resilience,
- numerous articles in PIARC’s quarterly magazine Routes/Roads,
- a comprehensive Online Tunnel Manual and
- many more contributions to international events.

Work topics for the TC’s are defined in the 4-years Strategic Plan (SP) [1]. The SP for the cycle 2024-2027 includes a new structure of PIARC Technical Committees and task Forces (Figure 1). TC 4.4 Tunnels is part of the Strategic Theme 4 “Resilient Infrastructure” (similar to last work cycle).

Strategic Theme 1 Road Administration	Strategic Theme 2 Road Mobility	Strategic Theme 3 Safety and Sustainability	Strategic Theme 4 Resilient Infrastructure
Technical Committees			
TC 1.1 Performance of Transport Administrations	TC 2.1 Roads for Accessibility and Mobility in Urban and Peri-urban Areas	TC 3.1 Road Safety	TC 4.1 Pavements
TC 1.2 Contribution of Roads to Economic and Social Development	TC 2.2 Roads for Equity, Accessibility and Mobility in Rural and Interurban Areas	TC 3.2 Winter Service	TC 4.2 Bridges
TC 1.3 Finance and Procurement	TC 2.3 Sustainable Freight	TC 3.3 Asset Management	TC 4.3 Earthworks
TC 1.4 Planning the Resilience of Road Networks - Climate Change and other Hazards	TC 2.4 Road Network Operations and ITS for Sustainability	TC 3.4 Environmental Impacts of Road Infrastructure and Transport	TC 4.4 Tunnels
TC 1.5 Disaster management	TC 2.5 Road infrastructure for Connected and Automated Mobility	TC 3.5 Road infrastructure for road transport decarbonization	TC 4.5 Decarbonization of road Construction and Road Maintenance
Task Forces			
TF 1.1 HDM-4 (postponed)			TF 4.1 Road Design Standards
Cross-cutting committees			
Terminology Committee			
Road Statistics Committee			

Figure 1: New PIARC Structure according to 2024-2027 Strategic Plan (SP) [1]

The TC 4.4 Tunnels has currently 120 members representing 36 countries around the world. The work is organized in biannual TC meetings, 6 thematic working groups (WG) and 1 Task Forces (TF) (Figure 2).

Working Groups (WG) cycle 2024-2027	Responsible for Topic (according to the SP)
WG 1 “Sustainable Operations and Maintenance”	4.4.1
WG 2 “Safety”	4.4.2
WG 3 “Digitalization”	4.4.3
WG 4 “New Propulsion Technologies & Ventilation”	4.4.4
WG5 “Road Tunnel Manual”	4.4.5
WG6 “3 rd International Conference”	4.4.6
Task Force “DG-QRAM”	4.4.7

Figure 2: Working Groups and Task Forces in TC4.4 Tunnels

2. TOPICS FOR THE 2024-2027 PIARC WORK CYCLE

In the following subchapters the planned activities in the 2024-2027 work cycle are summarized. For detailed information and the free download of already published TC4.4 outputs please refer to the PIARC website [2].

2.1. Sustainability of Tunnel Operation: new Approaches (topic 4.4.1)

The activities and outputs in relation to the topic “Sustainability of Tunnel Operation: new Approaches” focus on an update of the existing report “First steps to a sustainable approach [3]” with new aspects regarding reduction of energy consumption and use of renewable energy sources for tunnel operation. The topic of sustainability is fast evolving and has a major impact for road tunnel operators. Main questions related to this topic include:

- Energy efficiency and sufficiency (e.g. ventilation, lighting) including self-supplying of energy at tunnels (Figure 3),
- Monitoring of energy consumption,
- Impact of thresholds on energy consumption (e.g. required air quality, lighting level),
- Tools and methods for assessing the sustainability in the planning & design phase (LCA, SD indicators),
- Tools and methods for constraining operation and maintenance cost in both soft and hard aspects; e.g. the former is to set the frequency of daily/ periodical inspection,
- Lifetime related design and optimization of tunnel equipment, operation & maintenance, condition monitoring of tunnel equipment,
- Reduction of operational costs.

As a first output a comprehensive Case Studies Collection with worldwide examples and good practices will be produced in 2025. The publication of the final Full Technical Report is foreseen for 2027.



Figure 3: PV-modules on noise protection tunnels (photo: left: BASt, right: Autobahn GmbH, NL Nordbayern)

2.2. Active Modes of Transport (walking, cycling, wheelchair) in Road Tunnels (topic 4.4.2)

The purpose of this work is to summarize international experiences and good practices regarding pedestrians (including reduced mobility users, e.g. in wheelchairs) and cyclists in road tunnels. The focus will be on tunnels with separate galleries for active mobility users as well as on tunnels with mixed traffic, i.e. pedestrians and cyclists in the same tunnel tube as motorized vehicles. Main topics to be addressed include:

- Roadway sharing issues (coexistence of road traffic (including buses) and cycles, road traffic and cycles and pedestrians) / separate tubes (Figure 4),
- Geometric considerations, necessary cross sections, design aspects (Figure 4),
- Possibilities for retrofitting of existing road tunnels regarding active modes of transport,

- Safety measures to protect road users (like pedestrians, cyclists, reduced mobility users e.g. using wheelchairs) including evacuation issues, smoke ventilation strategies and air quality issues (sanitary ventilation),
- Intermodal aspects (e.g. bus stops in underground facilities),
- Impact on risks for safety and how to take them into account in risk analyses and in the safety documentation.

The existing Report “General principles to improve Accessibility for Persons with Reduced Mobility in Road Tunnels [4]” will be considered. As first outputs two Briefing Notes based on a collection of worldwide examples and good practices for the 2 application cases (one tube or separate tube for non-motorized traffic) will be produced in 2025 und 2026. The publication of the final Full Technical Report is foreseen for 2027.



Figure 4: Road tunnel with mixed traffic (photo: left: Henning Koepke, right: CETU)

2.3. Digitalization of Road Tunnel Design and Management (topic 4.4.3)

The purpose of this work is to investigate the impact of the Digital Transformation on different aspects of road tunnel design, operation, safety and maintenance/inspection. Main topics to be addressed include:

- Digitalization of operation, maintenance and inspection (e.g. IoT sensors for tunnel equipment like e.g. emergency call stations),
- Handling and digitalization of data from new ways of inspecting tunnels, such as the use of drones and robots,
- Project development using BIM methodology and experiences acquired (Figure 5),
- Digital twins for life cycle management, the support of fast and smooth commissioning of a new or renovated tunnel and its equipment or the use of digital twins in the training of tunnel control centre staff, first responders and stakeholder’s management,
- Centralization of documentation and easy access,

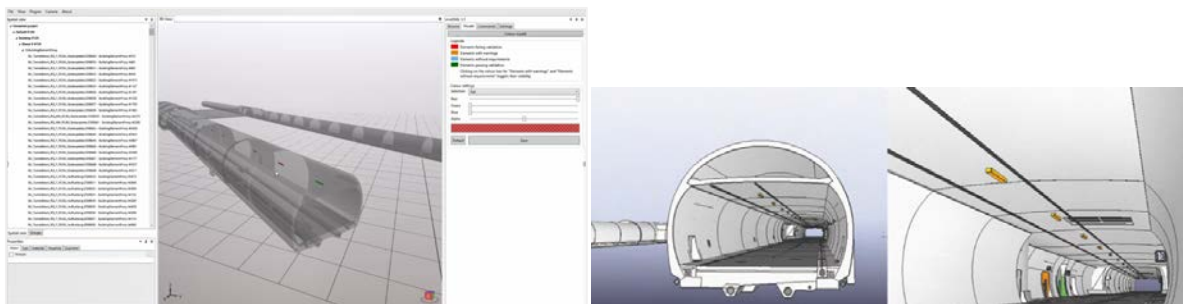


Figure 5: BIM model of a road tunnel (photos: BAST)

A first deliverable on this topic will be a Case Studies report about international experience and technologies already used in 2025 followed by a workshop with stakeholders in 2026. The final output will be a Briefing Note to be published at the end of 2026.

2.4. Road Tunnel Operation and Safety Issues related to the Usage of New Energy Carriers (NEC) in Road Vehicles (topic 4.4.4)

New Energy Carriers (NEC), including battery-electric vehicles, are becoming more prevalent. Whilst such vehicles remain a small overall proportion of the vehicle fleet, the combination of impacts of government policy and technological advances in alternative fuels is expected to accelerate their increase in numbers on the road and in tunnels in coming years.

As a result of these changes, the nature of tunnel safety risk (including from fire) is expected to change with time, and detailed consideration of the risk of significant incidents involving such vehicles is required. This should include the evaluation of incident consequences with particular attention paid to fire characteristics and toxic emissions and their impact on tunnel users and on emergency intervention strategies.

The purpose of this work is to further investigate this fast-emerging topic by collecting and sharing international experiences. There are some relevant open questions after the work done in the 2020-23 work cycle [5] which should be addressed in the 2024-2027 work cycle:

- Incidents with NEC vehicles, collection of data internationally, probability of incidents,
- Intervention / incident management, implications of incidents (e.g. with busses, Figure 6),
- Impact of NEC powered HGV vehicles,
- Impact of NEC vehicles on existing regulation,
- New developments in battery technologies, e-fuels (hydrogen, synthetic fuels) vehicles,
- Pollution and health impact during burning,
- Technologies / solutions to recognize / detect NEC vehicles.

Due to the currently still small number of NEC vehicles on the roads, there is still far too little experience with problems with these vehicles - especially commercial vehicles - in road tunnels. The expected results of the work on this topic will foster the knowledge base for safe operation and incident management of road tunnels.

A first deliverable on this topic will be a Case Studies report about international experience and good practices in 2025. The final output will be a Full Technical Report to be published at the end of the work cycle (2027).



Figure 6: Fire tests and intervention by firefighters (photos: TU Graz / BRAFA project)

2.5. Update of the Online Road Tunnels Manual (topic 4.4.5)

During the last cycles the TC on Road Tunnel Operations has produced a total of approximately 51 technical reports plus many Routes/Roads-Magazine articles and special issues. The main added value of the Online Tunnel Manual is to incorporate and disseminate this information through an electronic document, so as to reach the widest possible audience.

The current version of the online Tunnel Manual is available in English, Spanish and French. The update of the Tunnel Manual will be managed by a Working Group with the support of all Working Groups of TC 4.4. The Tunnel Manual is accessible at <https://tunnels.piarc.org/>.

2.6. Preparation of the 3rd International Conference on Road Tunnel Operation and Safety (topic 4.4.6)

The previous two International conferences in Lyon, France (October 2018) and Granada, Spain (October 2022) were very successful events. The 3rd PIARC International Conference on Tunnels will be held in October 2026 in Cracow, Poland. A Working Group with participation of members of TC4.4 is responsible for the preparation of the technical program in closed collaboration with the Polish National PIARC Committee and other relevant international organizations in the field of Road Tunnels. More information about the event, and the exact date will be posted soon on PIARC website (www.piarc.org).

2.7. Dissemination and possible update of DG-QRAM (topic 4.4.7)

The Dangerous Goods Quantitative Risk Assessment Model, known as “DG-QRAM” is a software tool, which enables its users to perform a specific risk analysis for dangerous goods transport.

Numerous road agencies are using the DGQRAM software and/or have set up risk analysis methodologies that are based on this software. They recommend or require that these analyses are included in the safety documentation of operating tunnel bodies or, at least justify some of its content. The improvements make the software more accurate or more user friendly (reducing risk of mistakes) which enhance the quality of the risk analyses. Many improvements have been made in the last work cycle which lead to the publication of the current software version V.10. The software could be ordered at PIARC website.

The following works are planned for the coming 4 years:

- Organize further training sessions with users of the DGQRAM software,
- Collect feedback of users of Version 4.10,
- Implement improvement tasks within phase 3 (continuation of phase 2 from last cycle, depending on funding),
- If relevant (enough improvement tasks implemented within phase 3), organize a Worldwide Webinar to share the advances in the software with users,
- Possible release of a new updated software version (depending on funding).

3. SUMMARY AND CONCLUSION

Since 1957, date of creation by PIARC of the "Committee on Road Tunnels", the Association has conducted an ongoing activity on all matters relating to the operation of road tunnels: geometry, equipment and maintenance, operating, safety and environment. All outputs are available online (free download) on the PIARC website.

There will be continuous publications on the PIARC website during the next years because not only Full Technical Reports will be published but also intermediate deliverables like Collection of Case Studies or Briefing Note. Please visit the PIARC website regularly to stay updated. Anyone interested in contributing to the topics mentioned above is cordially invited to participate in TC 4.4.

4. REFERENCES

- [1] PIARC (2024). *Strategic Plan 2024-2027*. <https://www.piarc.org/en/PIARC-Association-Roads-and-Road-Transportation/strategic-plan>.
- [2] PIARC Technical Committee 4.4: *List of all Technical Reports Road Tunnel Operations*. <https://www.piarc.org/en/PIARC-knowledge-base-Roads-and-Road-Transportation/Resilient-Road-Infrastructure/Road-Tunnels-Operations/Technical-Reports-Road-Tunnels>
- [3] PIARC Technical Committee 3.3 (2017). *Road tunnel operations: First steps towards a sustainable approach*. PIARC Ref.: 2017R02EN, <https://www.piarc.org/en/>.
- [4] PIARC Technical Committee D.5 (2019). *General principles to improve Accessibility for Persons with Reduced Mobility in Road Tunnels*. PIARC Ref.: 2019R20EN, <https://www.piarc.org/en/>.
- [5] PIARC Technical Committee 4.4 (2023). *Impact of New Propulsion Technologies on Road Tunnel Operations and Safety*. PIARC Ref.: 2023R34EN, <https://www.piarc.org/en/>.

**Reports of the
Institute of Thermodynamics and Sustainable Propulsion Systems
(formerly: Institute of Internal Combustion Engines and Thermodynamics)**

HEFT NR.	VERFASSER	TITEL	ERSCHIENEN	PREIS in €
85	STURM P.J.	Verkehr und Umwelt Transport and Air Pollution Tagung/Symposium 1.-3. June 2005	2005	50,--
86	EICHLSEDER et.al.	Der Arbeitsprozess des Verbrennungsmotors The Working Process of the Internal Combustion Engine Tagung / Symposium 22. und 23. September 2005	2005	70,--
87	STURM P.J.	Sicherheit und Belüftung von Tunnelanlagen Tunnel Safety and Ventilation Tagung/Symposium 15.-17. Mai 2006	2006	50,--
88	EICHLSEDER et.al.	1 st International Symposium on Hydrogen Internal Combustion Engines 28. und 29. September 2006	2006	50,--
89	EICHLSEDER et.al.	Der Arbeitsprozess des Verbrennungsmotors The Working Process of the Internal Combustion Engine Tagung / Symposium 20. und 21. September 2007	2007	70,--
90	STURM P.J.	Sicherheit und Belüftung von Tunnelanlagen Tunnel Safety and Ventilation Tagung/Symposium 21.-23. April 2008	2008	60,--
91	HAUSBERGER St.et.al.	Verkehr und Umwelt Transport and Air Pollution Tagung/Symposium 16.-17. June 2008	2008	60,--
92	EICHLSEDER et.al.	Der Arbeitsprozess des Verbrennungsmotors The Working Process of the Internal Combustion Engine Tagung / Symposium 24. und 25. September 2009	2009	70,--
93	STURM P.J.	Sicherheit und Belüftung von Tunnelanlagen Tunnel Safety and Ventilation Tagung/Symposium 3.-4. Mai 2010	2010	70,--
94	EICHLSEDER et.al.	Der Arbeitsprozess des Verbrennungsmotors The Working Process of the Internal Combustion Engine Tagung / Symposium 22. und 23. September 2011	2011	100,--
95	STURM P.J.	Sicherheit und Belüftung von Tunnelanlagen Tunnel Safety and Ventilation Tagung/Symposium 23.-25. April 2012	2012	70,--

12th International Conference 'Tunnel Safety and Ventilation' 2024, Graz

96	EICHLSEDER et.al.	Der Arbeitsprozess des Verbrennungsmotors The Working Process of the Internal Combustion Engine Tagung / Symposium 24. und 25. September 2013	2013	100,--
97	STURM P.J.	Sicherheit und Belüftung von Tunnelanlagen Tunnel Safety and Ventilation Tagung/Symposium 12.-13. Mai 2014	2014	100,--
98		Inter-Regional Air Quality Assessment Bridging the Gap between Regional and Kerbside PM Pollution Results of the PMinter Project Authors: U. Uhrner, B.C. Lackner, R. Reifeltshammer, M. Steiner, R. Forkel, P.J. Sturms	2014	30,--
99	EICHLSEDER et.al.	Der Arbeitsprozess des Verbrennungsmotors The Working Process of the Internal Combustion Engine Tagung / Symposium 24. und 25. September 2015	2015	100,--
100	STURM P.J.	Sicherheit und Belüftung von Tunnelanlagen Tunnel Safety and Ventilation Tagung/Symposium 25.-26. April 2016	2016	100,--
101	EICHLSEDER et.al.	Der Arbeitsprozess des Verbrennungsmotors The Working Process of the Internal Combustion Engine Tagung / Symposium 28. und 29. September 2017	2017	100,--
102	STURM P.J.	Sicherheit und Belüftung von Tunnelanlagen Tunnel Safety and Ventilation Tagung/Symposium 12.-14. Juni 2018	2018	100,--
103	EICHLSEDER et.al.	Der Arbeitsprozess des Verbrennungsmotors The Working Process of the Internal Combustion Engine Tagung / Symposium 26. und 27. September 2019	2019	100,--
104	EICHLSEDER et.al.	Nachhaltigkeit in Mobilität, Transport und Energieerzeugung (vormals: Der Arbeitsprozess des Verbrennungsmotors) Sustainable Mobility, Transport and Power Generation (formerly „The Working Process of the Internal Combustion Engine”) Tagung / Symposium 23. und 24. September 2021	2021 -	100,-
105	STURM P.J.	Sicherheit und Belüftung von Tunnelanlagen Tunnel Safety and Ventilation Tagung/Symposium May 09 – 10, 2022	2022	100,--
106	EICHLSEDER et.al.	Nachhaltigkeit in Mobilität, Transport und Energieerzeugung (vormals: Der Arbeitsprozess des Verbrennungsmotors) Sustainable Mobility, Transport and Power Generation (formerly „The Working Process of the Internal Combustion Engine”) Tagung / Symposium 28. und 29. September 2023	2023 -	160,-
107	BACHER M.	Sicherheit und Belüftung von Tunnelanlagen Tunnel Safety and Ventilation Tagung/Symposium April 16 – 17, 2024	2024	100,--